Probabilistische Erdbeben-Gefährdungs-Analyse für KKW-StandOrte in der Schweiz (PEGASOS)

Probabilistic Seismic Hazard Analysis for Swiss Nuclear Power Plant Sites (PEGASOS Project)

Final Report
Volume 4
Elicitation Summaries
Seismic Source Characterisation (SP1)

prepared for the
Unterausschuss Kernenergie (UAK) der Ueberlandwerke (UeW)

by the
Nationale Genossenschaft für die Lagerung radioaktiver Abfälle (Nagra)

Wettingen, 31 July 2004

nagra   PEGASOS

TABLE OF CONTENTS

Part I:

SP1 Seismic Source Characterisation, Elicitation Summary

Expert Team EG1a

Dr. Nicolas Deichmann

Schweizerischer Erdbebendienst /
Institut für Geophysik ETHZ
Zürich – Switzerland

Dr. Dario Slejko

Istituto Nazionale di Oceanografia
e di Geofisica Sperimentale
Trieste – Italy

Prof. Dr. Stefan Schmid

Geologisch-Paläontologisches Institut
der Universität Basel
Basel – Switzerland

Probabilistische Erdbeben-Gefährdungs-Analyse für die KKW-Stand Orte in der Schweiz
(PEGASOS)

SP1 Seismic Source Characterisation

Elicitation Summary

Expert Team EG1a

Nicolas Deichmann

Schweizerischer Erdbebendienst / Institut für Geophysik ETHZ
Zürich – Switzerland

Dario Slejko

Istituto Nazionale di Oceanografia e di Geofisica Sperimentale
Trieste – Italy

Stefan Schmid

Geologisch-Paläontologisches Institut der Universität Basel
Basel – Switzerland

TABLE OF CONTENTS

LIST OF TABLES

LIST OF FIGURES

1   SEISMOTECTONIC FRAMEWORK

The definition of the seismogenic sources is generally based on evidence coming from geology and seismicity. In rare cases a direct correlation between the two pieces of information leads to the identification of tectonic structures with documented seismic activity. More frequently, geology identifies tectonic structures which were, and perhaps still are, active and seismicity depicts earthquakes scattered in a broad area where many faults exist. Furthermore, the deep geometry of the faults is unknown and cannot be inferred from surface geology. Upon these unfavourable clues available, a different way to establish a link between geology and seismicity is needed: The definition of a general kinematic framework. Seismotectonic regions with homogeneous behaviour will be identified, based on this kinematic framework. Finally, the definition of these regions will lead to mapping seismogenic zones which collect one fault, or alternatively, fault populations with their associated earthquakes.

1.1   Large-scale kinematic framework

The large-scale kinematic framework of the entire area, which is depicted in Figure 1, was the first step towards the definition of the seismogenic sources for Switzerland and neighbouring regions. This kinematic framework primarily follows Meletti et al. (2000) regarding N Italy, and Schmid & Kissling (2000) regarding the Western Alps. The establishment of a conceptual model for the study area is feasible because the large-scale kinematic framework is fairly well known, particularly regarding the motion of the Adria plate (Fig. 5 in Meletti et al. 2000). Regarding northern Switzerland, the work of Müller et al. (2001) played a key role, particularly their figure 3.13 on p. 120.

Late Miocene to recent tectonic processes are proposed also to control the present and future seismicity, as many, but not all, elements of this kinematic framework are applicable to contemporary seismicity. The Friuli and Valais earthquake areas are good examples for this.

The motion and "push" of the Adria microplate towards the WNW, associated with dextral transpression along its northern margin, i.e. the Central Alps, lead to the identification of the 6 neotectonic and kinematic provinces labelled A to F in Figure 1. Province A corresponds to the Apennine, characterised by young to recent deformation, but being very distant from the area of interest. Province B, the Adria plate, plays a crucial role for contemporary tectonics and associated seismicity. It acts as an indenter in respect to the "European" foreland (Alps and their northern and western foreland, respectively). The indenter moves WNW and simultaneously undergoes counter-clockwise rotation (Meletti et al. 2000; Schmid & Kissling 2000). To the east, mainly compressive movement is taken up in the Friuli area (just off the map of Fig. 1) which extends westwards with a transpressive character along the boundary between zones B (Adria plate) and D (Central and Eastern Alps).

Further to the west, this dextrally transpressive movement zone produces two deformation zones which were active in the recent geological past and which are, in parts, also active at the present time: (1) the Canavese line, situated between provinces A (Adria plate) and C (Western Alps), and (2) the Simplon-Rhone line, situated between provinces C (Western Alps) and D (Central and Eastern Alps). Eventually, this Simplon-Rhone line swings around and into a N-S-orientation, which leads to W-directed thrusting of province C (Western Alps) onto province E (Proximal Alpine foreland). This thrusting is well documented along the Pennine frontal thrust, active during late Oligocene to Early Miocene times (Ceriani et al. 2001; Schmid & Kissling 2000). However, deformation since propagated further into the foreland. The front of the Western Alps (province C) propagated further to the west and in front of the external massifs during younger geological periods, i.e. the Late Miocene to Pliocene (Fügenschuh and Schmid,

in press). Its suspected present-day position (see position of province boundary between C and E) is largely drawn after Grellet et al. (1993).

The front of the Alps in Switzerland (boundary between provinces D (= Central and Eastern Alps) and E (= Proximal Alpine foreland) is an important province boundary regarding the geological past (front of the Central and Eastern Alps). More importantly, it also represents a marked boundary regarding the focal depth distribution of present-day earthquakes and regarding the seismotectonic regime (Deichmann 2002), as will be discussed later. However, there is evidence that the deformation front of the Central Alps migrated further to the N from the Late Miocene onwards (Burkhard & Sommaruga 1998, Müller et al. 2001, Schmid homepage). Hence, another province boundary between provinces E (Proximal Alpine foreland) and F (Distal Alpine foreland) was introduced. While the former is relatively strongly affected by deformation in the northern Alpine foreland, still related to the indentation of the Adria plate (province B), the latter is characterised by weaker deformation which does not more appear to be related to this indentation everywhere. The boundary between provinces E and F was largely drawn after Müller et al. (2001) and Grellet et al. (1993).

The establishment of this framework represents step 1 in defining seismic source areas. In two further steps, these neotectonic and kinematic provinces will be subdivided into smaller areas (see chapters 1.7 and 2.6). These two further steps will also take into account seismotectonic evidence and present-day seismicity, respectively. Below follows a brief definition and description of the map depicted in Figure 1.

1.2   Map of neotectonic and kinematic provinces

The following units were defined and mapped (Fig. 1):

A = Apennines. This unit is bounded by the presently active northern front of the Apennine to the north (Adria plate) and by a sinistrally transpressive western limit (contact with the Western Alps).

B = Adria plate. Rigid plate which moves to the WNW relative to a fixed European framework and which rotates counter-clockwise around a pole situated in western Liguria (Meletti et al. 2000).

C = Western Alps. Part of the Alps, which is at least partially displaced towards the WNW, together with the Adria plate. However it absorbs part of the WNW directed translation of Adria with respect to Europe. Kinematically, the Friuli convergent zone is linked with the Centovalli-Simplon-Rhone faults, although the neotectonic evidence for this direct link is weak. However, the limit between provinces C and D may conveniently explain dextral strike-slip motion and/or the abrupt change of the stress regime along and across the Rhone valley, respectively (Maurer et al. 1997).

D = Central and Eastern Alps. The southern boundary is defined by the Valais-Simplon-Garda movement zone, which extends into the Friuli active area situated just outside the SE edge of the map. The northern limit corresponds to the northern front of the Alps. This northern front of the Alps is characterised by two features. Firstly it corresponds to the southern limit of the zone of deep crustal earthquakes characteristic for the European foreland (provinces E and F; Deichmann 2002). Secondly, it corresponds to the northern limit of significant present-day thrusting activity (seismotectonic evidence provided by Deichmann et al. 2000 and Kastrup 2002). Towards the SW (limit between province C and E) at least the second of the above mentioned characteristics is also valid (province C represents the front of the Western Alps). In this sense provinces D and C have similarities.

Fig. 1:   Map of neotectonic and kinematic provinces

                Legend:

                A: Apennines
                B: Adria plate
                C: Western Alps
                D: Central and Eastern Alps
                E: Proximal Alpine foreland
                F: Distal Alpine foreland

E = proximal European foreland. Provinces A and B are proposed to push onto the European foreland, as suggested by the kinematic model of Meletti et al. (2000). Provinces C and D ("Alps") are very strongly deformed by this ongoing collision while "European foreland" (provinces E and F) is less affected by this collision. The subdivision of the European foreland into provinces E and F is inspired by the concept that the Alpine front migrated northward during the last 13 Ma (Jura folding, Burkhard & Sommaruga 1998) and present-day tectonic activity (Müller et al. 2001). The northern boundary of province E starts to branch off the front of province D near lake of Konstanz (Bodensee) and then follows the northern rim of the ENE-WSW-striking Permo-Carboniferous trough (Müller et al. 2001 and references cited therein). It

also delimits a region of recent relative uplift of province E from a region of relative subsidence at the southern limit of province F within the NAGRA precision levelling network (see Beil. 3.3 and Fig. 3.13 in Müller et al. 2001). WSW-wards the limit was drawn along the Rhine-Bresse transform corridor and north of a small basement uplift (massif de la Serre), across the northern-most part of the Bresse graben and into the northernmost Central massif, mostly according to Grellet et al. (1993).

F = Distal European foreland. This province is still affected by collision, but to a weaker extent and less directly. Additionally, this region is affected by young volcanic activity. Processes, such as deep crustal and/or mantle flow, have been invoked by many authors for this and for a multitude of other reasons (e.g. Laubscher 1992). This region is also characterised by strong recent uplift (parts of the Black Forest, Rheinisches Schiefergebirge) for which mantle up-welling rather that a direct effect of compression in front of the Alps in terms of thrusting may be invoked (Müller et al. 2001). However, the stress field exerted by plate collision in the Alps is here proposed to be still felt during the Neogene and at present.

1.3 Pre-existing faults in the Alpine foreland of Northern Switzerland, potentially controlling the present and future seismicity

As no single seismogenic discontinuity, such as a major plate boundary, can be identified in the investigated area, deformation is considered as diffusely distributed. Also, identifiable line sources are exceedingly rare. Hence, most of the seismicity is proposed to be associated with the reactivation of pre-existing faults which are situated within source areas, and which were generated during past tectonic events. Their reactivation is governed by the present-day stress regime.

The following fault systems, affecting the basement, and formed in the geological past, are prone for present-day reactivation:

Fault System 1. "Rhinish" system (strike NNE-SSW), essentially formed during Oligocene Rhine and Bresse graben formation. Suitable for sinistral reactivation, given present day stress field as revealed from seismotectonics (Kastrup 2002).

Fault System 2. "Hercynic" system (strike NW-SE, such as Vorwald or Neuhausen faults), formed and reactivated during a series of geological periods (i.e. Variscan orogeny, formation of Permo-Carboniferous troughs, Miocene; e.g. Müller et al. 2001). Suitable for tensile and/or dextrally transtensive ractivation, given the present day stress field as revealed by seismo-tectonics.

Fault system 3. "Permo-Carboniferous trough" system (strike ENE-WSW), formed during Variscan orogeny, but predominantly during Late Carboniferous to Permian graben formation in a dextrally transtensive regime (Schumacher 2002). Suitable for thrust reactivation only, given the present-day stress field. However, most fault plane solutions of recent low magnitude earthquakes do not provide evidence for presently active thrusting by reactivating this Permo-Carboniferous through system: the appropriate nodal planes are missing (Deichmann et al. 2000). Also, the resolved shear stress on this system might be too low in a transtensive stress field, dominated by NE-SW extension, such as deduced from seismotectonics. On the other hand, some of the new seismotectonic and local tomography data from the French part of the southern Rhine Graben (Lopez Cardoso, pers. comm.) do suggest presently ongoing inversion of the fault system 3 by thrusting.

1.4   Thick vs. thin-skinned present-day tectonic activity in the northern Alpine foreland

This topic is of fundamental importance for PSHA in northern Switzerland and adjacent areas. Choosing between thin- and thick-skinned scenarios has severe implications regarding the potential reactivation of basement faults situated below the "thin skin" of sediments. Moreover, the earthquake potential of faults situated in the upper "skin" is expected to be significantly higher in case of a thin-skinned scenario.

With <u>thick-skinned tectonics</u> it is intended that basement and cover are shortened by equal amounts at any given locality. Decoupling between basement and cover may occur, but would be of minor importance.

With <u>thin-skinned tectonics</u> it is intended that the sediments ("thin skin" of the earth's crust) are totally detached from the basement. When applied to the Alps-Jura system, this implies that shortening in the sediments, as observable in the Jura mountains, does not affect the basement underneath these Jura folds. The corresponding shortening within the basement takes place much further to the south, i.e. at the front of the Alps. This model demands a "distant push" (*"Fernschub"*) and decollement in a ductile horizon near the basement-cover interface (Triassic evaporites and/or shales).

In case of thin-skinned deformation, the geologically observable deformation of the sediments may not conform to the seismogenic activity observable within the deeper basement. In case of thick-skinned deformation, however, the deformation of the sediments observable at the earth's surface is directly linked to movements within the basement. In the foreland of an orogen, such as the Alps, such movements within the basement are usually related to the inversion or reactivation of former normal faults and/or their reactivation as transtensive or transpressive faults.

Regarding present-day tectonics, the following options do exist within the scientific community:

<u>Thesis 1 (Thin-skinned model)</u>. Most authors (e.g.: Müller et al. 2001) do favour present-day tectonic activity in terms of thin-skinned tectonics. The proponents of this model do argue that thin-skinned deformation, accepted to have been active by most authors (see discussion in Burkhard 1990) during "classical" Jura folding (which took place at about 13 to 5 Ma ago), is still ongoing. This view is additionally supported by evidence from seismotectonics. Thrusting appears to be restricted to the northern rim of the Alps, while the basement of the foreland deforms by strike-slip motion and/or normal faulting. Hence, the type of deformation is different in basement (transtension) and cover (transpression or thrusting). Also. it is reasonable to assume that thin-skinned Jura-folding (starting at about 13 Ma ago) is still ongoing at the present day.

<u>Thesis 2 (Thick-skinned model s.str.)</u>. Data from the Ajoie (Giamboni et al., in press), as well as evidence from underneath the Molasse basin ("Fribourg" fault; see offset of basement in Meier 1994a, 1994b and corresponding alignment of epicentres according to the Swiss earthquake catalog), do indicate, that thrusting and/or transpression in the Northern Alpine foreland also affects the basement underneath the "decollement" horizon. Hence, deformation observable in the sediments at the earth's surface also affects the underlying basement. This is strong evidence that present-day deformation may be thick-skinned according to the definition given above. Thrusting reactivation of system 3 cannot be excluded based on the seismotectonic evidence alone.

<u>Thesis 3 (Thick-skinned model s.l. or "Pavoni-model")</u>. This scenario may be regarded as thick-skinned s.l., and it was originally proposed by Pavoni (1961) in order to explain Jura tectonics. This model proposes that strike-slip motion in the basement induces folding of the sediments situated above a decoupling horizon (i.e. Triassic evaporites). Hence, this model is thick-skinned because deformation of the cover directly roots in the basement below this cover (no

"Fernschub"). On the other hand, the style of deformation is different in cover and basement: Folding, i.e. distributed deformation in the cover, is taken up by discrete slip in the basement. The only principle objection to this model is that folding of the cover alone is not compatible with pure strike-slip in the basement (extension parallel to fold axis would be needed as well!). However, if the motion in the basement is assumed to be transpressive, the model appears more likely. In fact, flower structures have been observed in connection with the "Fribourg" fault (Meier 1994b). Hence, this model, perhaps in a somewhat modified form, has to be very seriously considered. It is thick-skinned in the sense that no "distant push" is needed and thin-skinned in the sense of decoupling between basement and cover (for which there is also evidence from in situ stress data obtained in drillhole Schafisheim, Müller et al. 1987).

From the analysis of all seismotectonic data available, it is the authors' opinion that all three theses are plausible, although thesis 3 seems the most convincing. Regarding the definition of seismic sources for hazard assessment, the decision in favour of one or the other of the theses discussed above is not crucial as seismicity is documented to occur also below the "thin skin". In fact, there is no evidence for a higher seismic activity in the upper plate, situated above the "decollement" horizon, as opposed to the basement below this horizon, which argues against thesis 1. In case of theses 2 and 3, this activity in the basement would be directly coupled to Alpine shortening (hence crustal shortening would have to be suspected, although it is not convincingly documented by the seismotectonic evidence). In case of thesis 1 the Alpine foreland would be subjected to transtension only. In this respect, the uncertainty regarding the 3 theses discussed above will flow into the decision as to whether the Permo-Carboniferous troughs may be reactivated or not by presently active thrusting (first bifurcation in the logic tree regarding the definition of seismic sources, see Fig. 3).

1.5 How representative are the seismotectonic data derived from low magnitude (M < 5) earthquakes for assessing seismic hazard at a very low probability level?

Seismotectonic data (obtained on low magnitude earthquakes) indicate that there is no, or only very little, thrusting activity north of the front of the Alps. On the other hand geologists report post-2.6 Ma folding activity (Ajoie data on Sundgau gravels reported by Giamboni, in press; activity of Mandach thrust after deposition of 2 Ma old Quarternary gravels reported in Müller et al. 2001). This leads to the conclusion that thrusting activity could possibly be restricted to high magnitude earthquakes with a very long return period. Because the latter accumulate more strain over geological times (compared to large numbers of small earthquakes) they could possibly have remained undetected by the seismotectonic analysis based on seismicity of the last years only.

This leads to the conclusion that reactivation of fault system 3 by thrusting, associated with large earthquakes, cannot be excluded. The question, as to how well seismotectonic data represent the stress field, remains open. This uncertainty is taken into account by the first bifurcation in the logic tree regarding seismic sources (Fig. 3).

1.6 The Basel earthquake and the "Reinach Fault"

Recently, Meghraoui et al. (2001) provided evidence that the presently active "Reinach Fault" has to be associated with the historical high-magnitude Basel earthquake of 1356. Based on numerous visits to the trench across the Reinach fault (by S. Schmid), and based on its re-interpretation as a gravitationally induced slide by Schmid (2. Workshop of SP 1), the evidence provided by Meghraoui et al. (2001) is considered rather unlikely. Location and orientation of the causative fault of the Basel 1356 earthquake remain, therefore, unknown. Because the Basel

area is dominated by long segments of fault systems 1 and 3, the most likely orientation is that of fault system 1 or 3. By also taking the seismotectonic evidence into account, the Reinach fault, or another system 1 fault, are the most likely candidates. These considerations led to a series of bifurcations regarding the logic tree associated with our source definition (see logic tree in Fig. 3, bifurcations associated with the topics "Reinach Fault" and "Basel Geometry").

Activity along fault system 3 (northern boundary of the Permo-Carboniferous fault) cannot be excluded based on the geological evidence, as discussed earlier. In this case, however, such thrusting events could have a very long return period (such as the strong Basel earthquake), hence they could remain undetected by present seismicity. This uncertainty was taken into account by the first bifurcation in the logic tree associated with source definition.

1.7   Map of the seismotectonic regions (see Fig. 2)

The map of Figure 2 represents a second step towards mapping seismic sources. This map of seismotectonic regions was constructed with the following "philosophy": The boundaries drawn in the first map are maintained, but a new set of boundaries now further subdivides the neotectonic and kinematic provinces mapped out in Figure 1. The criteria for these new boundaries are:

a)   seismotectonic evidence (Deichmann 2002, Deichmann et al. 2000, Kastrup et al. 2004, Sue et al. 1999), and,

b)   pre-dominant orientation of pre-existing sets of faults.

The seismotectonic regions depicted in Figure 2 were defined as follows:

Provinces A and B remained un-subdivided. Their large distance to the area of interest does not warrant further subdivision. Most of province A is constituted by the Alps-Apennines transfer zones (Meletti et al. 2000) with expected sinistral strike-slip focal mechanisms in the shallow crust and dip-slip mechanisms in the deep crust. Province B is constituted by the Po plain and can be considered as a stable aseismic sector.

Province C was further subdivided according to the work of Sue et al. (1999) and Eva et al. (1997) into:

C1: Western "compressional" region (strike-slip to thrusting);

C2: Central extensional area region (normal faulting);

C3: Eastern "compressional" region (strike-slip to thrusting).

Regions C1 and C3 are characterised by strike-slip to thrusting fault plane solutions, and they absorb relative WNW-directed movements between the two provinces A and B in respect to province E. Region C2, characterised by normal dip-slip fault plane solutions, is currently in extension due to gravitational forces ("overthickened" crust). These gravitationally induced stresses interfere with the far-field stress pattern and they dominate within C2, at least within the shallow crust.

Province D was further subdivided into:
D1: Northern "compressional" region (strike-slip and subordinate thrusting)
D2: Central dome region (no fault plane solutions)
D3: Austroalpine extensional region (normal faulting and subordinate strike-slip)
D4: Southern "compressional" region (no seismotectonic evidence)

Fig. 2:   Map of seismotectonic regions

                 Legend:

                 Province and region A: Apennines
                 Province and region B: Adria plate

                 Province C: Western   Region C1: Western compressional belt of Western Alps
                             Alps   Region C2: Central extensional belt of Western Alps
                                           Region C3: Eastern compressional belt of Western Alps

                 Province D: Central and   Region D1: Northern compressional area
                             Eastern   Region D2: Central dome
                             Alps   Region D3: Austroalpine extensional area
                                           Region D4: Southern compressional area:

                 Province E: Proximal   Region E1: Massif Central
                             Alpine   Region E2: Bresse – Jura – Western Molasse basin
                             foreland   Region E3: Eastern Molasse basin

                 Province F: Distal   Region F1: Paris basin
                             Alpine   Region F2: Upper Rhine Graben
                             Foreland   Region F3: Black Forest – Schwäbische Alb

<u>D1 (Northern "compressional" region)</u> is characterised by the present-day coexistence of all three types of focal mechanisms, including mostly shallow thrusting events. On the whole the region is best characterised as being dominated by strike-slip motion with subordinate thrusting. The southern limit of D1 is diffuse. The northern limit (D-E province boundary), however, is well defined and coincides with a change regarding the depth distribution of earthquake foci (Deichmann 2002). The area south of this D-E province boundary is characterised by the absence of earthquakes deeper than about 15 km. North of this boundary earthquakes do occur all the way down to the Moho: 65% of them are located in the 0-15 km range, 35 % of them below 15 km and above the Moho.

<u>D2 (Central dome region)</u> is a "quiet" region, possibly due to the persistence of a thermal anomaly associated with the Tertiary (Lepontine) metamorphic dome. The outlines of this region D2 are drawn parallel to the isograds of Lepontine metamorphism, although a genetic link remains speculative. The term "dome" is chosen since this area also structurally represents a dome. The stress regime remains unknown.

<u>D3 (Austroalpine extensional region)</u> is again a region where the far field stress field interferes with gravity forces (similar to C2) but extension is oblique (rather than orthogonal as in C2) to the strike or the Alpine orogen (Kastrup 2002). The fault plane solutions point to the predominance of normal faulting with subordinate strike-slip motion.

<u>D4 (Southern "compressional" region)</u> represents the continuation of the Friuli compressional realm onto the map. Note, however, that the very intense present-day deformation associated with the Friuli area stops near the SE border of our map. The Friuli area and D4 do not exhibit identical seismicity. This region is interpreted as being characterised by a compressional stress regime based on geological arguments only.

<u>Provinces E and F</u> were further subdivided according to the pre-dominance of certain sets of pre-existing faults into:

E1: Massif Central region (reactivation mode unknown)
E2: Bresse-Jura-Western Molasse basin region (reactivated in strike-slip)
E3: Eastern Molasse basin region (reactivated in strike-slip to normal fault motion)

and likewise into:

F1: Paris basin region (reactivated in strike-slip to normal fault mode)
F2: Rhine graben region (reactivated in strike-slip mode)
F3: Black Forest and Schwäbische Alb (reactivated in strike-slip to normal fault mode)

<u>Regions E1 and F1</u> are characterised by the predominance of fault system 3. However, in these regions this fault system predominantly strikes SW-NE (Grellet et al. 1993). Hence its orientation slightly departs from that of fault system 3 in northern Switzerland where a WSW-ENE strike predominates. No seismotectonic data (except for one normal fault plane solution, Grellet et al. 1993) are available for region E1 (Massif Central). The pre-existing faults in region F1 (Paris basin) are presently reactivated in strike-slip to normal fault mode (Grellet et al. 1993).

<u>Regions E2 and F2</u> represent areas that are heavily affected by pre-existent faults formed during Rhine and Bresse Graben formation, hence these regions are pre-fractured by fault system 1. This is evident from surface geology (see GIS-map provided by PROSEIS) and from subsurface information (Meier 1994b). According to these data, system 1 faulting seems to be associated with a very diffuse and broad transform area situated within the entire Western molasse basin. A nice alignment of recent epicentres can be observed parallel to fault system 1 in an area near Fribourg (the so-called Fribourg Fault). Presently, region E2 is characterised by strike-slip fault motions and the same holds for region F2 (Plenefisch & Bonjer 1997, Kastrup 2002).

<u>Regions E3 and F3</u> are dominated by the predominance of fault system 2, while system 1 faults are either absent or rare in these areas (GIS-map provided by PROSEIS, subsurface data provided by Meier 1994a and Birkhäuser et al. 2000). Seismotectonic evidence points to a predominance of strike-slip to normal faulting motions in region E3 (Kastrup 2002) and the same holds for region F3 (Plenefisch & Bonjer 1997).

2   SEISMIC SOURCE DEFINITION

The distribution of present-day seismicity, as based on the historical and instrumental catalogs, is now also taken into account. This will directly lead to an additional set of boundaries. These new boundaries, together with the boundaries characterised so far, will define the seismic source zones (see Figs. 4 and 5). The boundaries of these seismogenic zones largely (but not every-where) follow the boundaries defined in Figures 1 and 2. The most severe modification regards the possible reactivation of the Permo-Carboniferous troughs (fault system 3). This issue will be treated after having discussed a few fundamental questions regarding seismic source definition in general.

2.1   Basic considerations regarding a zone-less approach

The zone-less approach, with spatial smoothing, was taken seriously into consideration and finally rejected on the following reasons.

a) Stationarity of seismicity. The Swiss seismicity does not seem to be stationary in time and space: therefore the use of earthquake data alone is seriously limited. An example for the lack in stationarity in time is provided by the area around Vierwaldstättersee. While this area appears as very active in the pre-instrumental period, post-1975 instrumental data do not indicate this area to be particularly seismogenic.

b) Low-probability events. The strong events with a low probability, such as events with a magnitude > 6, are particularly relevant for the task of PEGASOS. Yet, such earthquakes occur very rarely. For example, the Basel event with an estimated moment magnitude of around 7 is the only one in this range of high magnitudes to be found in the earthquake catalog. This seriously limits the use of the catalog and favours "geological" arguments. Consequently, as discussed in chapter 1.5, rare events such as the Basel event may represent "characteristic earthquakes".

c) Quality of geophysical and geological data in the area of investigation. The quality of the available seismotectonic data is very high for the Swiss region (see chapter 1). Also, the kinematic framework, as described in chapter 1.1, is believed to be reasonably well constrained. Although there are open questions regarding apparent (?) contradictions between "geological" and "seismotectonic" activity (see discussion at the end of chapter 1.4 regarding potential thrusting events in Northern Switzerland), the use of a zone-less approach would not be helpful in addressing these uncertainties.

2.2   Characterisation of area versus line sources

After ruling out the zone-less approach as a viable alternative, area and line sources were investigated. The only line sources considered in addition to the zones presented below (see Figs. 4 and 5) are the "Reinach Fault" (RF) and the Fribourg Fault (FF). The Reinach Fault is considered as a line source based on the evidence given by paleoseismic investigations (Meghraoui et al. 2001), although this evidence is far from conclusive. The Fribourg Fault is well documented by post-1975 instrumental data. However, in the future this "post-1975 activity" may not be stationary in space and hence the "Fribourg" line source may be one of several within the area source surrounding this line source. As a consequence, both line sources will only be considered along certain bifurcations along the logic tree (see Fig. 3).

2.3   Source boundary properties

Since the area of interest is not characterised by a still active subduction zone, and, as the precision of focal depths does not allow for an appropriate 3-D-resolution, all the area source boundaries are taken as vertical and hard, i.e. no uncertainty is taken in their geometry. Nevertheless, in a few cases some epicentres will be associated to a different seismogenic zone than the one where they are located on the basis of specific seismological considerations. Furthermore, when evaluating b-values, some areas will have to be lumped together in order to gather sufficient information from the earthquake catalog (see chapter 4).

Generally, seismicity was taken to be homogeneous within all source areas. This procedure is justified since very small seismogenic zones characterise the model proposed here. In any case, smoothing within certain areas was envisaged (for example in source area C2), particularly in the vicinity of the power plants.

No background seimogenic zones were introduced since the entire map was subdivided into source areas. Source areas decrease in size when approaching the sites of the power plants. Some of the sources are very small in order to justify that seismicity is homogeneously distributed over the entire area.

Ruptures that are longer that the source's dimensions, are allowed to extend beyond the source boundaries. Hence, earthquake ruptures from earthquakes occurring within a seismic source are allowed to spread across source boundaries. This allows for a very detailed zonation by the use of small areas (such as will be proposed in Figs. 4 and 5) without making large ruptures a priori impossible.

2.4   Potentially seismogenic structures

As discussed in chapter 1.4, seismotectonics do not provide evidence for presently active thrusting by reactivating the Permo-Carboniferous through system (fault system 3), while some of the new seismotectonic and local tomography data from the French part of the southern Rhine Graben do suggest inversion of fault system 3 (Lopez Cardoso, pers. comm.). Also, the geological evidence does suggest presently ongoing inversion of the fault system 3 by thrusting. Furthermore, the possibility that some of the unidentified sources corresponding to fault system 3 might be associated with earthquakes with a very long return period (characteristic earthquakes) cannot be ruled out (see discussion in chapter 1.5). This uncertainty was taken into account by introducing a first bifurcation of the logic tree (Fig. 3: "inversion of PC troughs yes" and "inversion of PC troughs no"; also see alternative zonations given in Figs. 4 and 5, respectively).

The Reinach Fault was considered as a line source, but its existence as a seismogenic feature is given a low probability (0.1), based on the results of on-site observations (Schmid 2002). The only other seimogenic line source considered is the Fribourg Fault, whose existence as a discrete and unique line source was given a probability of 0.5.

Most of the potentially seismogenic line sources are associated with the reactivation of one or several of the pre-existing fault systems 1, 2 or 3 (see discussion in chapter 1.4). However, the exact location of these line sources remains unknown and in most cases they were assumed as homogeneously spread out over the entire seismogenic zone.

Unfortunately, the fault associated with the 1356 Basel historical earthquake remains unknown (see discussion in chapter 1.6) although this seismogenic structure is expected to produce high magnitude earthquakes with a long return period. This uncertainty led to the introduction of a series of alternative zonations for the Basel area (see source areas F2d, F2e and F2f, as well as line source RF).

2.5 The logic tree associated with seismic source definition

The logic tree presented in Figure 3 has a number of bifurcations briefly described below.

1. Bifurcation ("PC-Existence"). This first bifurcation has to do with the epistemic uncertainty associated with the potential reactivation of fault system 3 ("Permo-Carboniferous troughs"). As previously discussed, most of the seismotectonic evidence argues against a reactivation of these structures, while there is substantial geological evidence regarding their reactivation in thrusting mode during the geological past. The potential for thrust-mode reactivation in the future was given a probability of only 0.3, because we decided to put more weight on the seismotectonic evidence which perhaps better reflects the present and future tectonic activity than the geological record. However, we feel uneasy in assigning an exact value to an epistemic uncertainty. This bifurcation led to two alternative source maps depicted in Figure 4 ("Permo-Carboniferous troughs reactivated") and Figure 5 ("Permo-Carboniferous troughs not reactivated")

2. Bifurcation ("Reinach-Fault"). This bifurcation only exists for the case that the Permo-Carboniferous troughs are not inverted in thrust mode (Fig. 5). This is because the Reinach Fault, whose orientation is parallel to fault system 1, cannot be considered a viable alternative in case that the 1356 Basel earthquake is associated with thrust-mode reactivation of fault system 3 (implicit assumption behind choosing the option "Permo-Carboniferous troughs reactivated"). The low weight (0.1) given to the option "Reinach Fault yes" reflects our great scepticism regarding the evidence provided by Meghraoui et al. (2001) that the Reinach fault is indeed the seismogenic source of the famous Basel earthquake.

3. Bifurcation ("Basel geometry"). In case of the option "Permo-Carboniferous troughs reactivated" no further bifurcation is introduced and the seismogenic zone F2e is proposed. Thereby it is implicitly assumed that the 1356 Basel earthquake reactivated fault system 3 somewhere within area F2e. In case of the option ("Permo-Carboniferous troughs not reactivated"), line source RF is active within area F2b when choosing the option "Reinach fault yes". In case of "Reinach fault no" and "2PC-existence no" we assigned a probability of 0.7 to the likelihood that area F2d hosted the Basel earthquake. This is because we regard it more likely that the seismogenic fault linked to the Basel earthquake was parallel to fault system 1, oriented parallel to the long side of the rectangle defining area F2d. However, we did not want to exclude the possibility that the Basel earthquake might be due to an intersection effect between fault systems 1 and 3 meeting and crossing each other in the Basel area (weight of 0.3 given to square-shaped area F2f).

4. Bifurcation (Fribourg-Fault). This bifurcation was applied to all branches, except for the option "Permo-Carboniferous troughs reactivated". The latter branch does not consider the Fribourg fault as an important seismogenic structure, because the Fribourg fault reactivates fault system 1 (and not fault system 3, i.e. the Permo-Carboniferous through). All other branches contain a bifurcation with 0.5 probability for either branch because we could not decide on which branch might be more likely. Either the Fribourg Fault FF represents an important line source within a larger source area consisting of E2c, E2d and E2e lumped together, or alternatively, FF is not treated as a line source and areas E2c, E2d and E2e are treated as separate source areas.

5. Bifurcation (further subdivision of parts of province D). Alternatives regarding areas D1b, D1c, D1d and D1e have been treated with branches in the logic tree as follows:

a) branch (0.2): D1b, D1c, D1d and D1e are grouped into 1 area;
b) branch (0.4): (D1b + D1c + D1d) is separated from D1e;
c) branch (0.4): D1b is separated from D1c and from (D1d + D1e).

These alternatives are independent of all previously mentioned alternatives and they were applied to every previously defined branch of the logic tree. Two possibilities were regarded as twice more likely than the third one, and were hence given a weight of 0.4.

PC_Existence	Reinach_Fault	Basel_Geometrie	Fribourg_Fault	Ds
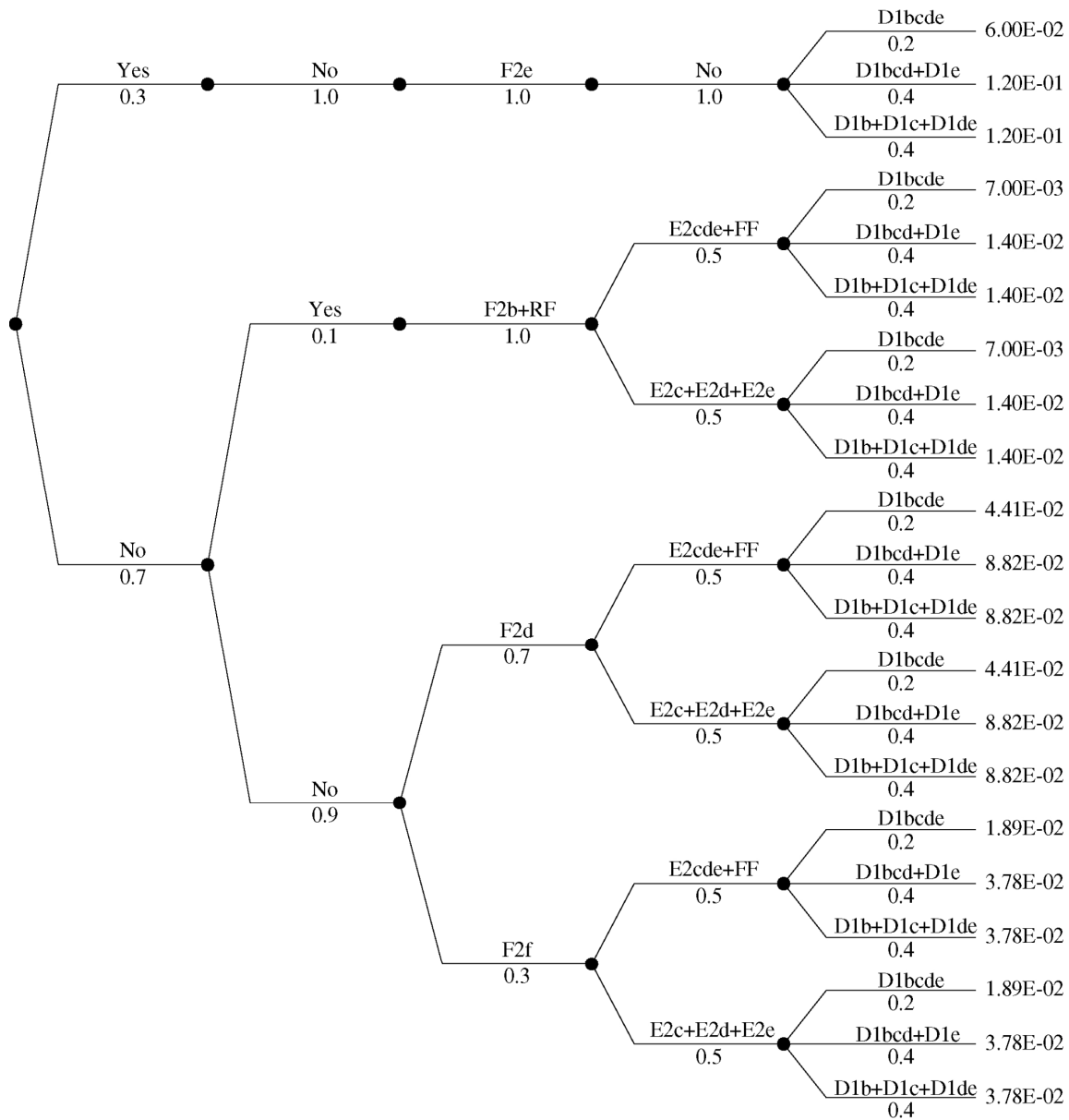
Fig. 3:   Logic tree for seismic source definition

2.6   Seismic source zonation (see Figs. 4 and 5)

Two alternative seismic zonations were performed (see first bifurcation in Fig. 3) and these are depicted in Figures 4 and 5. Note that the zonations only differ in parts of the provinces E and F, i.e. in the area of Central and Northern Switzerland. Below, a short description of each of these areas is given.

2.6.1 Province A (Apennines)

Province A (Apennines) was not subdivided further since it is too distant from the sites to warrant further subdivision. No assumptions are made concerning orientation of faults and type of faulting.

PC Yes:
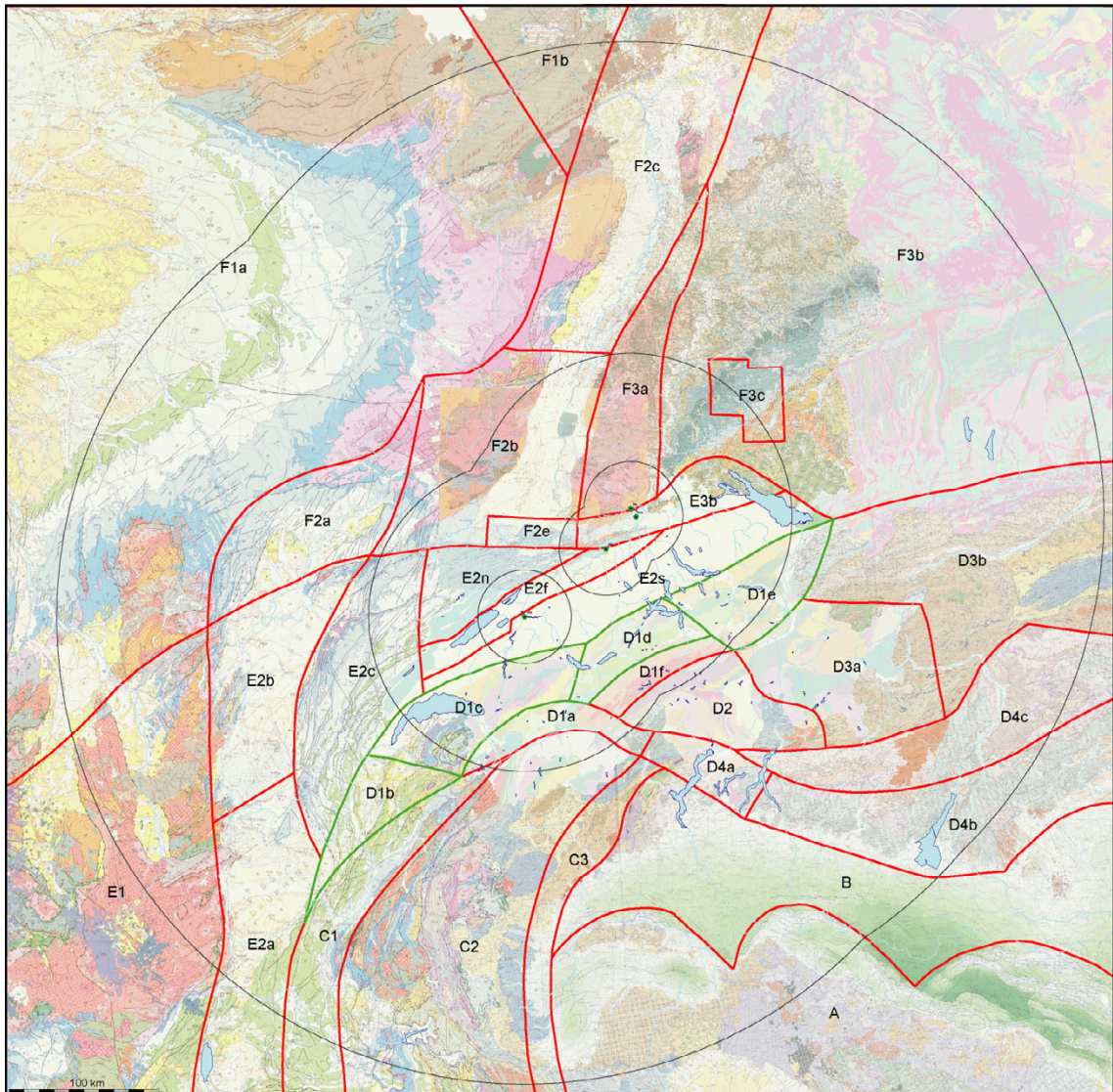
Fig. 4:   Scenario "Permo-Carboniferous troughs reactivated"

For legend, see text in chapter 2.6.

PC No:
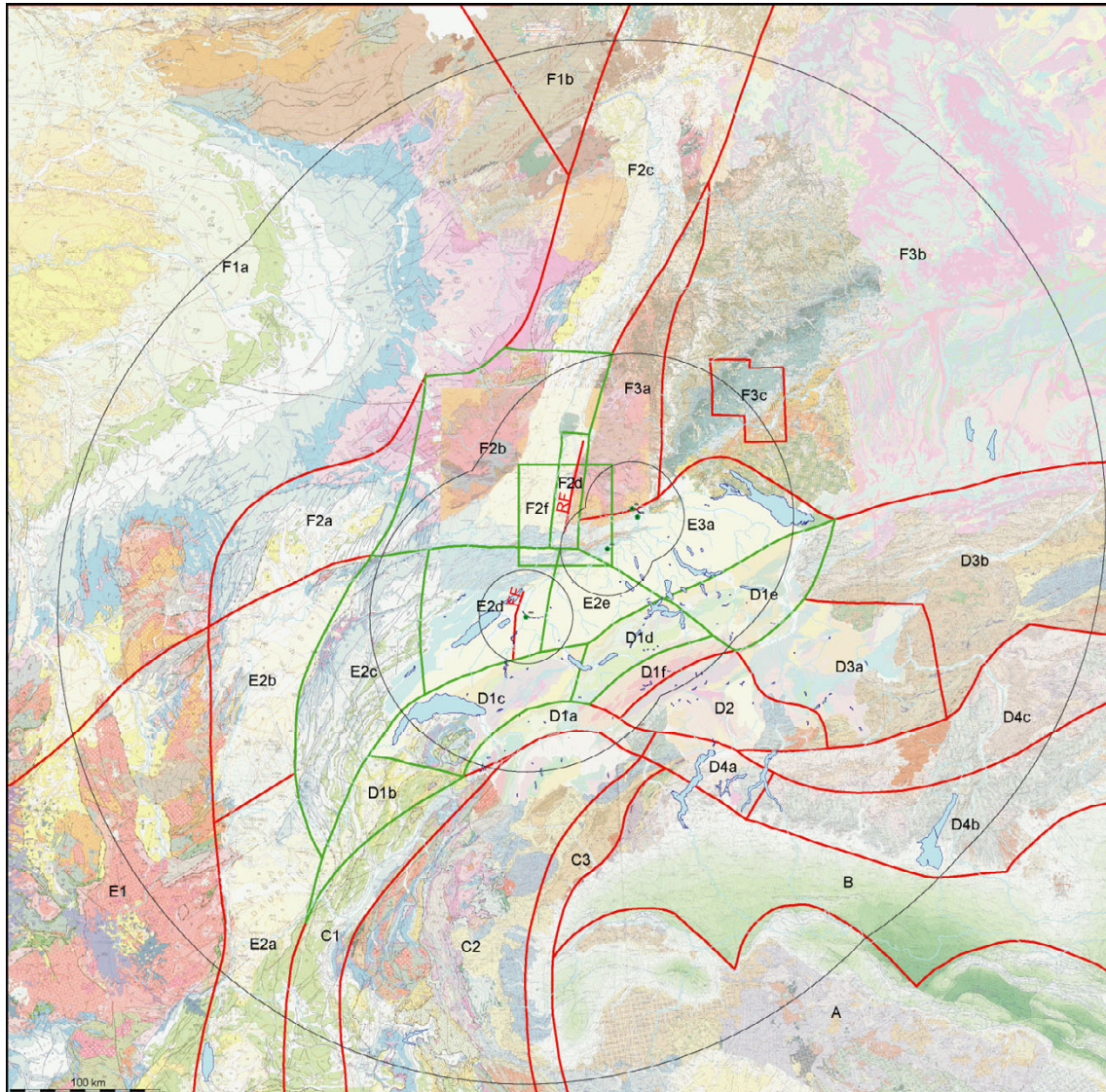
Fig. 5:　　　Scenario "Permo-Carboniferous troughs not reactivated"

　　　　　　For legend, see text in chapter 2.6.

2.6.2　　　Province B (Adria plate)

Province B (Adria plate) was not subdivided further since it is too distant from the sites to warrant further subdivision. The few main neotectonic structures seem to be almost aseismic. No assumptions on orientation of faults and type of faulting.

2.6.3　　　Province C (Western Alps)

Region C1 (Western compressional belt) was not subdivided further and represents a source area. No a-priori orientation of active faults is assumed; expected sense of slip is strike-slip to thrusting.

Region C2 (Central extensional belt) was not subdivided further and represents a source area. Orientation of active faults is assumed to be orogen-parallel, i.e. N-S to NE-SW oriented, expected sense of slip is normal faulting.

Region C3 (Eastern compressional belt of Western Alps) was not subdivided further and represents a source area. No a-priori orientation of active faults is assumed; expected sense of slip is strike-slip to thrusting.

2.6.4   Province D (Central and Eastern Alps)

Subsequent changes in respect to Figs. 1 and 2): The D1 vs. D3 boundary, as depicted in Figure 2, was subsequently slightly modified according to seismicity criteria. The boundaries of province D with E, as well as those with C and B also had to be slightly modified in respect to the previously established maps depicted in Figures 1 and 2. Changes to these major boundaries were made according to the following considerations: (1) Near Lake Geneva the northern boundary of D with area E was moved away from the front of the Alps by a small distance into the Molasse basin in order to capture badly located epicentres around Geneva within area D (instead of area E). (2) The discrete southern boundary of D with areas C and B (Valais-Simplon-Garda movement zone) was replaced by series of elongated areas (D1a, D4a and D4b). Particularly area D4a overrules former boundaries drawn on the map of seismotectonic regimes, which were removed.

Alternatives incorporated into the logic tree of Figure 3: areas D1b, D1c, D1d and D1e have been treated with the logic tree approach considering the following 3 branches:

1. Branch (0.2): D1b, D1c, D1d and D1e are grouped into 1 area (area D1bcde);
2. Branch (0.4): (D1b + D1c + D1d), refered to as D1bcd, is separated from D1e;
3. Branch (0.4): D1b is separated from D1c and from (D1d + D1e), referred to as D1de.

Areas within seismotectonic region D1:

Area D1a   (Westernmost part of the Valais – Simplon – Garda movement zone): This is an E-W trending belt of enhanced seismicity, which includes the northern part of the Valais active area, situated in the southernmost Helvetic nappes. Fault-orientation is roughly E-W and parallel to the elongated shape of the area. Sense of slip is predominantly dextral strike-slip.

Area D1b   (Savoy part of northern margin of the Alps): This part is located in an area were Alps and Jura meet. The area is transitional to area C1 (external part of Western Alps) and it is relatively quiescent compared to the more active D1c area. No a-priori fault orientation is assumed and sense of slip is strike-slip with subordinate thrusting.

Area D1c   (Western Switzerland part of northern margin of the Alps): Relatively high density of epicentres. In terms of high seismicity the boundary with area D1a (= northern part of Valais active zone) appears transitional. No a-priori fault orientation is assumed and dominant sense of slip is strike-slip (with subordinate thrusting or normal faulting).

Area D1d   (Central Switzerland part of northern margin of the Alps): area which includes the seismically very active area (mostly based on historical information) around Lake Lucerne, including thrusting quakes. No a-priori fault orientation is assumed and dominant sense of slip is strike-slip (with subordinate thrusting).

Area D1e   (Eastern Switzerland part of northern margin of the Alps): part of the northern margin of the Alps, which might be kinematically linked via E3 and E3b (Eastern Molasse basin) to the northward propagation of foreland deformation across the Molasse basin, causing increasing amounts of recent uplift in the area west of Lake Constance (Müller et al. 2001). No a-priori fault orientation is assumed and dominant sense of slip is strike-slip (with subordinate thrusting).

Area D1f   (Aar massif): Quiescent zone. No assumptions regarding fault orientation and/or sense of slip.

Only area within seismotectonic region D2:

Area D2   (Central dome): Quiescent zone, adjacent to D1f and corresponding to the Lepontine metamorphic dome. No assumptions regarding fault orientation and/or sense of slip.

Areas within seismotectonic region D3:

Area D3a   (Mittelbünden – Engadine – Alta Valtellina area): No assumptions regarding fault orientation. Enhanced seismicity with predominantly normal faulting and subordinate strike-slip.

Area D3b   (Western Austria): Generally moderate seismicity, but including quite active areas such as the Inntal line. Seisimicity is unequally distributed and spatial smoothing needs to be applied. Fault orientation is ENE-WSW and sense of slip is sinistral strike-slip.

Areas within seismotectonic region D4:

Area D4a   (Insubric part of Valais-Simplon-Garda movement zone): Relatively quiet part of this important movement zone. No assumptions can be made regarding fault orientation and sense of slip.

Area D4b   (Southern Alps part of Valais-Simplon-Garda movement zone): Relatively active and directly connecting with the Friuli area, situated immediately east of the margin of the map. There is good agreement between the outlines of our map with those provided by with the data of Meletti et al. (2000). Reverse faults strike N70E.

Area D4c   (Trento area): Relatively quiescent block. No assumptions can be made regarding fault orientation and sense of slip.

2.6.5   Province E (Proximal Alpine foreland)

Subsequent changes in respect to Figures 1 and 2: The boundary of E with F2 was modified in the Basel area in order to properly take account of the Basel source area.

The former subdivision E2 vs. E3 (boundary between eastern and western Molasse basin) was only kept as an option. Also, the location of this E2/E3 boundary was modified.

Alternatives incorporated into the logic tree of Figure 3: Alternatives have been considered concerning areas E2c, E2d, E2e and line source FF (Fribourg fault) and put into the form of a logic tree considering the following 2 branches:

1. Branch (0.5): area (E2c + E2d + E2e) and separate line source FF;
2. Branch (0.5): separate areas E2c, E2d and E2e, but no line source FF.

Alternatives concerning the exact shape of areas within E2 and E3 which depend on the choice of the "Basel source geometry" (see below): Minor adjustments are necessary near the northern border of these areas in case F2f is chosen for the Basel source geometry. Areas modified accordingly will carry the suffix "F2f". E3a, for example, will be referred to as "E3aF2f" in that case.

Only area within seismotectonic region E1:

Area E1   (Massif Central): No further subdivision was necessary in view of the large distance to the power plants. No assumptions can be made regarding fault orientation and sense of slip

Areas within seismotectonic region E2:

Area E2a   (Basse Dauphinée): Relatively higher seismic activity, as compared to E2b. Fault-orientation is that of fault system 1 (NNE-SSW), sense of slip is strike-slip.

Area E2b   (Bresse): Relatively quiescent area. Fault-orientation is that of fault system 1 (NNE-SSW), sense of slip is sinistral strike-slip.

Area E2c   (Western Jura): Relatively quiescent area, when compared to E2d, and area with very narrow or no Molasse basin. Fault-orientation is that of fault system 1 (NNE-SSW), predominant sense of slip is sinistral strike-slip.

Area E2d   (Western Molasse basin): This area is only activated in the option "Permo-Carboniferous troughs not reactivated" (Fig. 5). The area is heavily pre-fractured by Rhinish faults (NNE-SSW), of which line source FF (situated within this area) is a particularly active example. Pre-fracturing also occurred by fault system 3 (Permo-Carboniferous troughs), particularly near the Molasse-Jura border. Fault orientation is taken as NNE-SSW and sense of slip is sinistral strike-slip.

Line source FF (Fribourg Fault): This line source is only activated in the option "Permo-Carboniferous troughs not reactivated" (Fig. 5) and only as an alternative in one of the "Fribourg fault" bifurcation. It is situated within area E2d. Documented offsets of base Mesozoic coinciding with line source FF (see Meier 1994b). Good candidate for thick-skinned reactivation of former faults: sinistral strike-slip parallel fault system 1 (geological and seismotectonic evidence). However, inversion of fault system 3 by thrusting (geological evidence only from seismic sections) was also envisaged (in case of the option "Permo-Carboniferous troughs reactivated", where FF is de-activated, however).

Area E2e   (Central Molasse basin): This area is only activated in the option "Permo-Carboniferous troughs not reactivated" (Fig. 5). The area is situated east of the former E2/E3 boundary (eastern limit of existence of fault system 1). The E2/E3 boundary was slightly modified later, however, according to seismological criteria. Relatively quiescent area. No assumptions can be made regarding fault orientation and sense of slip.

Only Area within seismotectonic region E3:

Area E3a   (Eastern Molasse): This area is only activated in the option "Permo-Carboniferous troughs not reactivated" (Fig. 5). The area is characterised by recent uplift and represents a neotectonically active zone according to Müller et al. (2001). Area of increased seismicity, as compared to E2e. The area is pre-fractured by fault systems 2 and 3, particularly at its northern margin. Given the option "Permo-Carboniferous troughs not reactivated" chosen when activating this area present-day tectonic activity is expected to be primarily thin skinned. Within the basement, sense of slip is expected to be a combination of dextral strike-slip and normal faulting, primarily reactivating fault system 2 (NW-SE strike).

Areas which span seismotectonic regions E2 and E3:

The following areas span both regions E2 and E3 (Western and eastern Molasse basin), and they are only activated in the option "Permo-Carboniferous troughs reactivated" (Fig. 4). This option with a probability of 0.3 in the first bifurcation of the logic tree (Fig. 3) assumes that fault system 3 (Permo-Carboniferous troughs) is presently reactivated, as suggested by geological evidence. Hence this scenario proposes inversion of normal faults by thrusting. It also infers that the Basel earthquake corresponds to such an inversion of a Permo-Carboniferous trough in the Basel area (see description of area F2e).

Area E2n   (Eastern Jura): This area is situated in between the Northern Permo-Carboniferous trough (areas F2 and E3b) and the Southern Permo-Carboniferous trough (area E2s). It is pre-fractured by fault system 1 (NNE-SSW-strike); expected sense of slip is sinistral strike-slip.

Area E2f   (Southern Permo-Carboniferous trough): Area corresponding to the southern Permo-Carboniferous trough, joining the northern one in the NE (boundary with area E3b). Area pre-fractured by ENE-WSW-striking normal faults. These faults are at present reactivated by thrusting. In addition, the area is also pre-fractured by fault system 1 (NNE-SSW-strike) which is reactivated in sinistral strike-slip mode.

Area E2s   (Southern Molasse basin): Rest of the Molasse basin situated south of area E2f. The area is pre-fractured by fault systems 1, 2 and 3. Sense of slip is expected to be sinistral strike-slip (fault system 1, NNE-SSW-strike), a combination of dextral strike-slip and normal faulting (fault system 2, NW-SE strike) and minor thrusting (fault system 3, ENE-WSW-strike).

Area E3b   (eastern part of Northern Permo-Carboniferous through): Elongated strip containing the eastern part of the Northern Permo-Carboniferous trough, linking to Basel source area F2e (= western part of Northern Permo-Carboniferous). This area is only activated in scenario "Permo-Carboniferous troughs yes". In this scenario inversion of fault system 3 (ENE-WSW-strike) by thrusting is expected ("characteristic" earthquake), although the expected recurrence rate is lower than that expected in area F2e (Basel area). In addition, but of subordinate importance, fault system 3 is expected to be reactivated in a combination of sinistral strike-slip motion and (e.g. "Neuhauser" Störung). This area contains an area which is extremely well documented by 3D seismics (Birkhäuser et al. 2000).

2.6.6   Province F (Distal Alpine Foreland)

Subsequent changes in respect to Figures 1 and 2: The boundary between F and E has been modified, as well as the boundary between F2 and F3.

Alternatives incorporated into the logic tree of Figure 3: The Basel area, and particularly the Basel 1356 earthquake play a key role in area F. Concerning the Basel area, several alternatives have been considered. Thereby, questions about the Reinach fault are of great importance. If the Reinach fault is indeed the surface expression of the seismogenic fault associated with the 1356 earthquake, this Reinach fault has to be treated as a line source (line source RF). This line source would have originated the Basel earthquake and can originate events with very high magnitude in the future (see RF-bifurcation in the logic tree of Fig. 3). For the more probable case that RF is not a seismogenic feature, some possible seismic zones have been defined for the Basel area. Three alternative area sources (F2d, F2e and F2f) were chosen large enough in order to include a potentially seismogenic fault which is long enough for accommodating the Basel 1356 earthquake, whatever its exact orientation and location was. These considerations led to the following features in the logic tree:

In case of the option "Permo-Carboniferous troughs reactivated" RF is not activated, and area is F2e is the only source area activated around Basel.

In case of the option "Permo-Carboniferous troughs not reactivated" there is a first bifurcation (probability 0.1) with a branch Reinach fault (RF), treated as a line source placed within a very large "Basel area" F2b, and a branch (probability 0.9) leading to the following additional bifurcation:

1. Branch (0.7): establish area F2d;
2. Branch (0.3): establish area F2f.

Areas within seismotectonic region F1:

Area F1a   (Paris basin): Includes most of the F1 region and is characterised by very moderate seismicity. Orientation of faults variable, sense of slip is strike-slip to normal fault mode.

Area F1b   (Lower Rhine Graben area): Contains pre-existing fault sets which are mostly NW-SE-oriented (Lower Rhine Graben, extending into the Netherlands), but also fault sets which are NE-SW-oriented. Sense of slip is strike-slip to normal faulting.

Areas within seismotectonic region F2:

Area F2a   (western part of Bresse-Rhine transfer area): seismically less active (as compared to F2b) area of the Rhine-Bresse transfer zone. Pre-fractured by fault system 1 (NE-SW-oriented in this area), sense of slip is strike-slip and subordinate normal faulting.

Area F2b   (eastern part of Bresse-Rhine transfer area): this seismically more active area of the Rhine-Bresse transfer zone is adjacent to the alternatives concerning the zonation of the Basel area, i.e. adjacent to sources F2d, F2e, F2f and line source RF. The area is primarily pre-fractured by fault system 1 (NNE-SSW-strike). Reactivation is by strike-slip to normal faulting. Subordinate normal faulting also occurs on fault system 2 and thrusting on fault system 3 cannot be excluded. The exact size of area depends on the choices regarding the first 3 bifurcations in the logic tree: F2bpcy denotes its size in case of "PC troughs activated". In case of "PC troughs not activated" F2b_Rf denotes the size of F2 when it is considered to contain the RF line source; F2bF2f denotes its size when F2f is chosen; F2b without a suffix is used if F2d is chosen for the Basel source geometry.

Area F2c   (Upper Rhine Graben): Less active part of the Upper Rhine Graben. Dominated by fault system 1 (NNE-SSW-strike). Expected sense of slip is strike-slip. Minor normal faulting reactivating fault system 2 is also expected.

Line source RF (Reinach fault): Assumes that past and future quakes, similar to the 1356 Basel earthquake, all took and will take place along the seismogenic Reinach fault which acts as a line source. Sense of slip is sinsistrally oblique normal faulting.

Area F2d   (Basel quake re-activates fault system 1): Assumes that past and future quakes, similar to the 1356 Basel earthquake, took and will take place near to and parallel to the Reinach fault (fault system 1, NNE-SSW-strike). Sense of slip is sinisitrally oblique normal faulting.

Area F2e   (Western part of Northern Permo-Carboniferous trough): Assumes that past and future quakes, similar to the 1356 Basel earthquake, took and will take place along faults which have the orientation of the Permo-Carboniferous trough (W-ward extension of E3a, but more seismogenic than E3a). Fault orientation is E-W, sense of slip is dextrally oblique thrusting.

Area F2f   Basel quake due to interference effects between fault systems 1 and 3): Does not make an assumption about the orientation of faults responsible for that past and future quakes, similar to the 1356 Basel earthquake. However, this alternative assumes that strong earthquakes do indeed concentrate in an area around Basel where fault systems 1 and 3 do intersect. The Basel high seismicity is caused by an interference between fault systems 1 (ENE-WSW) and 3 (E-W). However, activity on fault system 2 (NW-SE) is also expected. Expected sense of slip is sinistrally oblique strike-slip to normal fault motion (fault system 1), dextral oblique strike-slip to normal fault motion (fault system 2) or oblique thrusting (fault system 3).

<u>Areas within seismotectonic region F2:</u>

Area F3a   (Eastern flank of Upper Rhine Graben): Area of relatively high seismicity within former area F3. Predominance of fault systems 1 (NNE-SSW) and 2 (NW-SE). Sinistral transtension on fault system 1, normal faulting on fault system 2. Note that the size of this area is altered when area F2f is chosen for the Basel source geometry (it will be denoted area F3aF2f in that case).

Area F3b   (SW Germany): Bulk of former F3, characterised by low seismicity. Predominance of fault system 2 (NW-SE) with normal faulting.

Area F3c   (Schwäbische Alb): Contains the enigmatic seismically active Hohenzollern area. The Hohenzollern area is characterised by intersections between fault systems 1 and 2. Activity could be due to intersection effects between fault systems 1 and 2. In this case sinistral transtension on fault system 1 and normal faulting on fault system 2 is expected. Present-day activity is sinistral strike-slip parallel fault system 1, but this presently active source may not be stationary in time and space. Alternatively, the earthquakes in this area could also be due to magmatic processes (mantle upwelling!). In view of all these uncertainties no assumptions regarding fault orientation and/or sense of slip are made.

2.7   Summary of seismic zonation used for hazard analysis

During our evaluation of recurrence rates and M_{max} a number of modifications had to be made to the following zonations discussed so far:

1. Neotectonic and kinematic provinces (Fig. 1);
2. Seismotectonic regions (Fig. 2);
3. Seismic source zonation (2 alternative versions, i.e. Figs. 4 and 5).

For further evaluations described in chapter 3 we additionally introduced:

4. "Macro-zones". These were defined for evaluating b-values and M_{max}. The Macro- zones (Fig. 6) are a simplified version of the Seismotectonic regions of Figure 2.

5. "National catalog zones". These zones (Fig. 7) have been defined for investigating catalog-related effects on b-values.

6. "Swiss zones". These zones (Fig. 8) have also been defined for investigating catalog-related effects on b-values.

2.8   Final zonation used for seismic hazard assessment

This chapter is an updated version of the Hazard Input Document (HID) for Sensitivity Hazard Analysis, dated January 30, 2003.
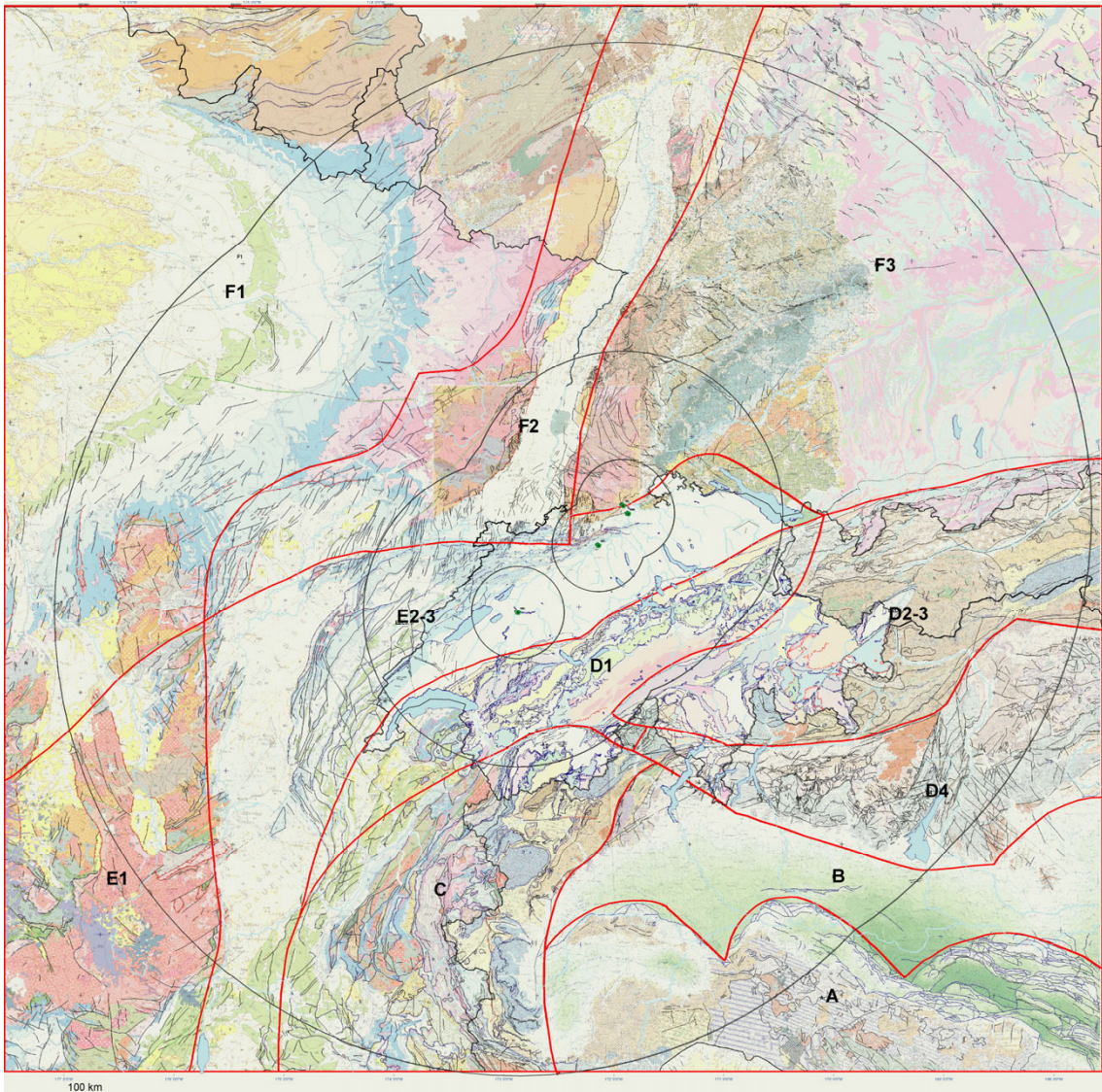
Fig. 6:   Macro-zones

2.8.1   Seismic zonation

The master logic tree that defines alternative seismic source area mapping is shown on Figure 9. Further details concerning the logic tree and its different branches, including the justifications for giving particular weights to all the branches are found in chapter 2.5. Here follows a brief summary regarding all the different branches, and particularly, a series of figures depicting the alternative source area maps used (Figs. 10 – 13).
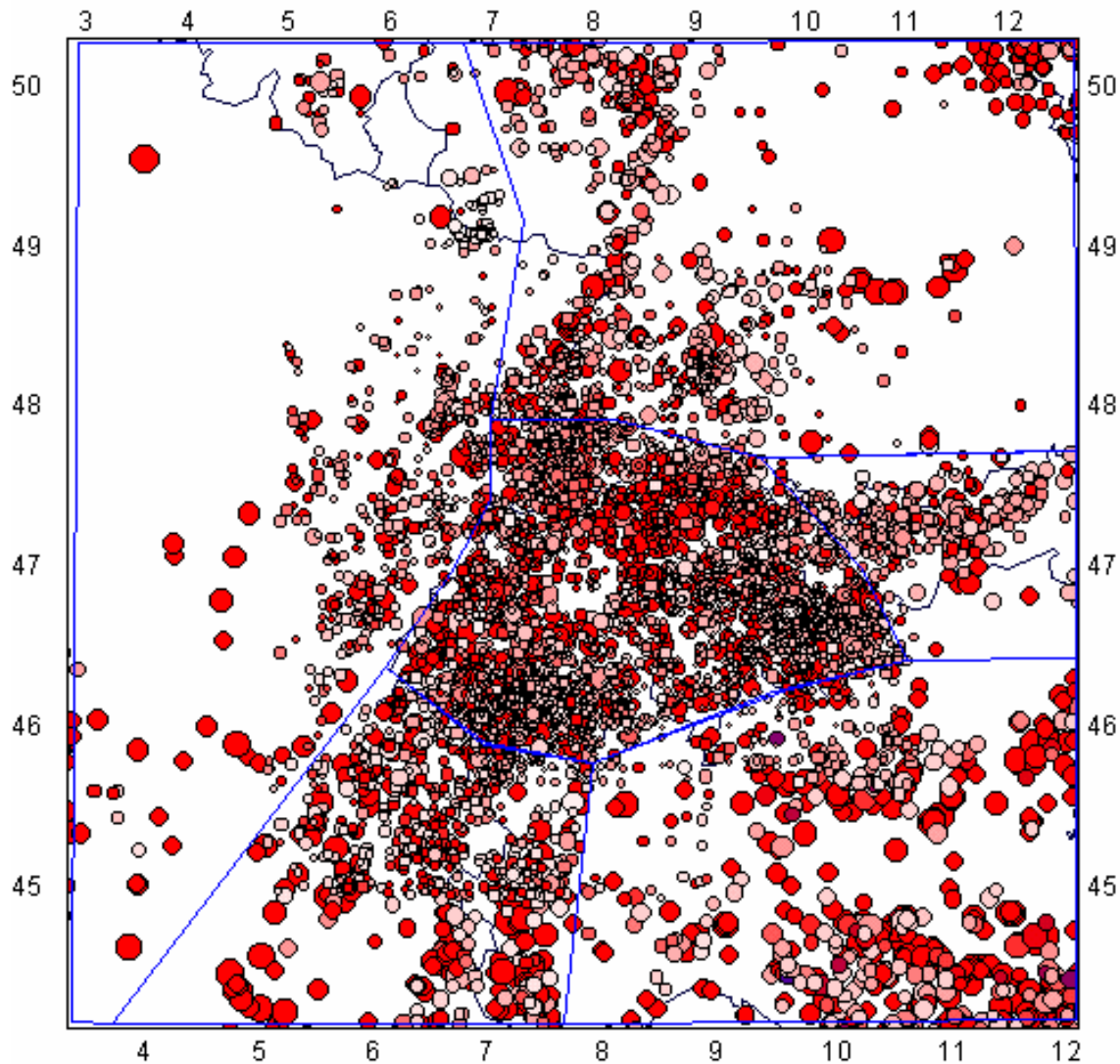
Fig. 7:   National catalog zones

The first node addresses whether or not the Permo-Carboniferous troughs are an active source. Figure 10 shows the seismic source zonation of the Alpine foreland for the case when the Permo-Carboniferous troughs are an active source ("PC YES" case). If the Permo-Carboniferous troughs are not active ("PC NO" case), a number of alternatives for Basel and the Alpine foreland are included.

The second node address whether or not the Reinach fault is modeled as active fault-specific source localizing seismicity and the third node addresses the source. For the PC YES case, the fault is not considered to be a localizer of seismicity, and the Basel source is an east-west trending zone F2e (Fig. 10). For the PC NO case, Figure 11 shows the alternative seismic sources. If the Reinach fault (RF) is considered a line source, then it lies within a larger zone, source F2b_RF. If not, then the Basel region is modeled as a narrow, north-south trending zone (F2d), or as a large zone representing the intersection of north-south and east-west structures (F2f). In the case that source F2f is used, the surrounding source zones have modified boundaries (e.g. zone F3a is changed to zone F3aF2f).
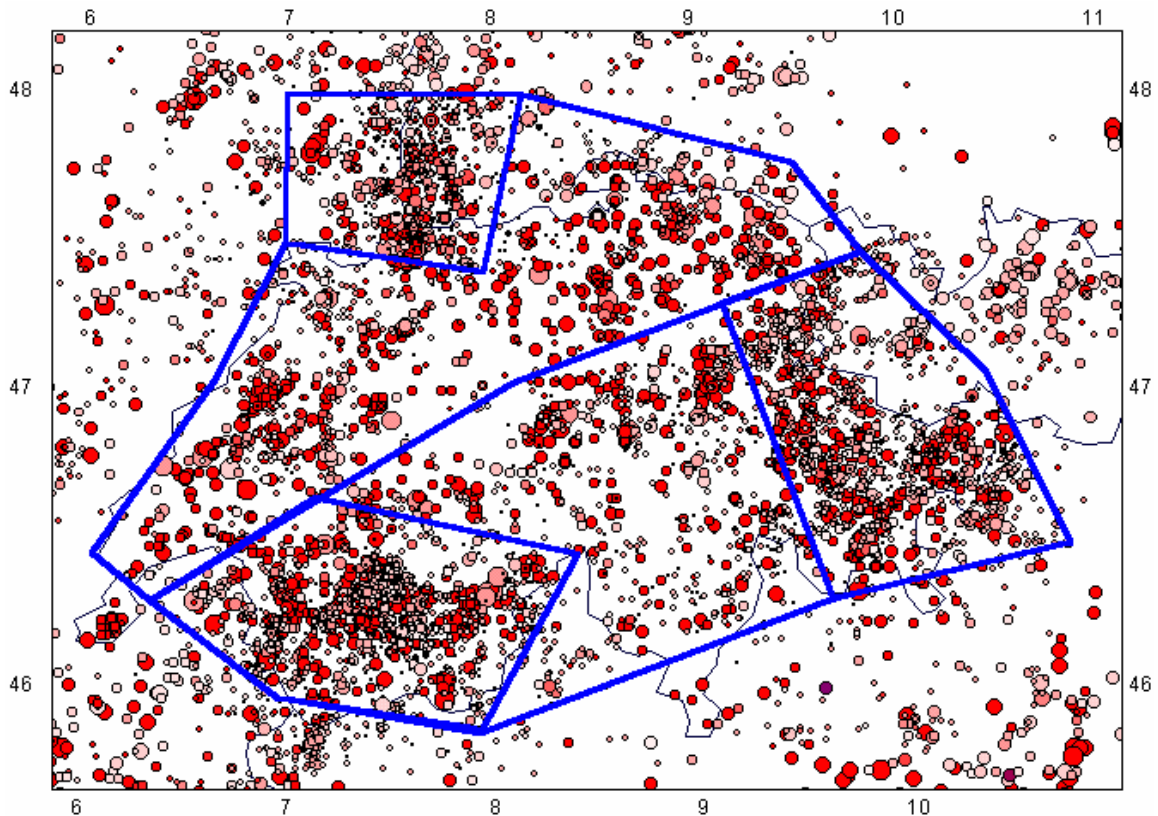
Fig. 8:   Swiss zones (zone "Swiss Alps" encompasses all three Alpine zones)

The next node of the logic tree addresses the source zonation in the Alpine foreland and the Fribourg area. The alternative source models are shown on Figure 12 for the PC NO case. If the Fribourg fault (FF) is considered to be an active fault localizing seismicity, it is modeled as a line source within a large Alpine foreland source E2cde (lower left plot of Fig. 12). If not, then the Alpine foreland is modeled by the three zones E2c, E2d, and E2e (upper left plot of Fig. 12). The right-hand plots on Figure 12 show the modifications to the Alpine foreland zones in the case that the Basel source is represented by zone F2f.

The final node of the logic tree (Fig. 9) shows the source zonation for the Alps (regional zone D1). Three alternatives are considered, as shown on Figure 13. The remaining portion of the study region is modeled by a number of source zones whose geometry does not change with the alternative zonations described above. Figure 14 shows these source zones.

The right-hand column in Figure 9 indicates the various source sets produced by the logic tree. The source zones comprising these source sets are listed in Table 1.

PC Active	Reinach Fault Source	Basel Source Geometry	Fribourg Fault Source	Alps Zone D1	Source Set

Yes (0.3) — No (1.0) — F2e (1.0) — No (1.0)
- 1 subzone (0.2) — Set 1
- 2 subzones (0.4) — Set 2
- 3 subzones (0.4) — Set 3

No (0.7)

Yes (0.1) — RF (1.0)

Yes (0.5)
- 1 subzone (0.2) — Set 4
- 2 subzones (0.4) — Set 5
- 3 subzones (0.4) — Set 6

No (0.5)
- 1 subzone (0.2) — Set 7
- 2 subzones (0.4) — Set 8
- 3 subzones (0.4) — Set 9

No (0.9)

F2d (0.7)

Yes (0.5)
- 1 subzone (0.2) — Set 10
- 2 subzones (0.4) — Set 11
- 3 subzones (0.4) — Set 12

No (0.5)
- 1 subzone (0.2) — Set 13
- 2 subzones (0.4) — Set 14
- 3 subzones (0.4) — Set 15

F2f (0.3)

Yes (0.5)
- 1 subzone (0.2) — Set 16
- 2 subzones (0.4) — Set 17
- 3 subzones (0.4) — Set 18

No (0.5)
- 1 subzone (0.2) — Set 19
- 2 subzones (0.4) — Set 20
- 3 subzones (0.4) — Set 21

Fig. 9:   Logic tree for EG1a seismic source zonation

Fig. 10:   The Alpine foreland zones for the "PC YES" case (Permo-Carboniferous troughs
             are an active source)
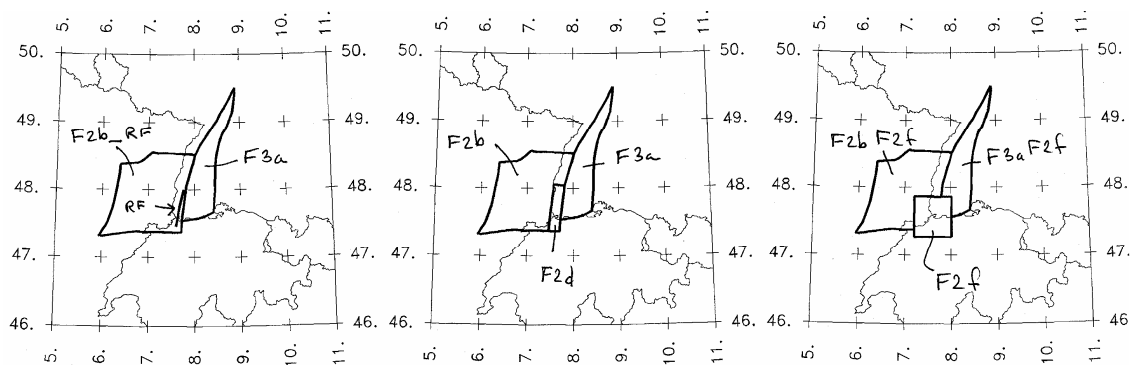
Fig. 11:   Alternative source zonations for Basel area for the "PC NO" case (Permo-Carboni-
             ferous troughs are not an active source)
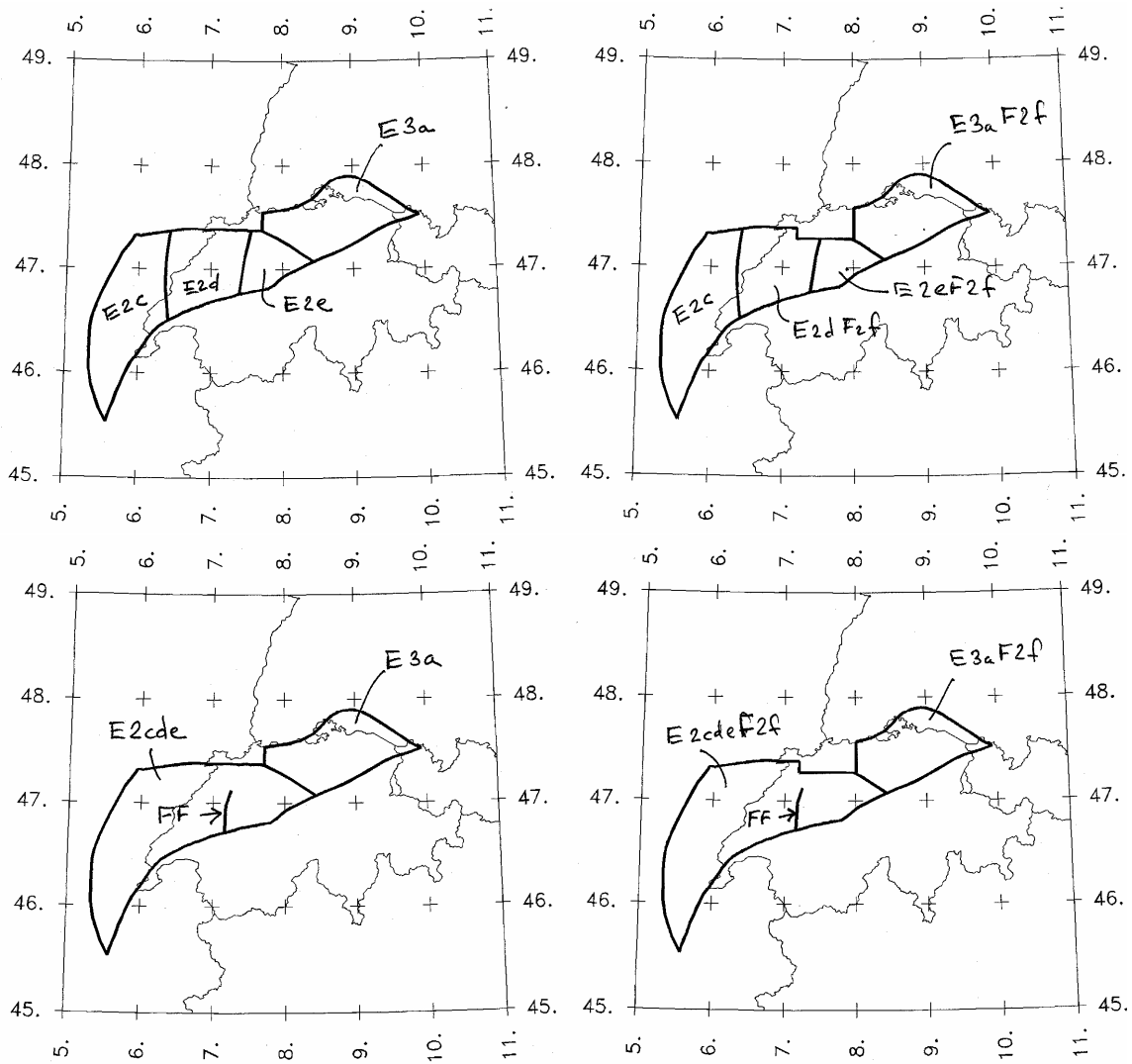
Fig. 12:   Alternative source zonations for Alpine foreland for the "PC NO" case (Permo-Carboniferous troughs are not an active source)
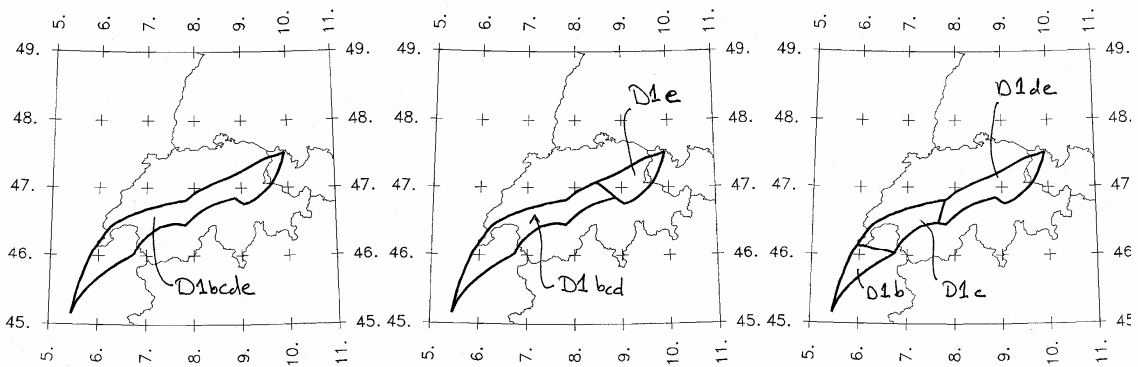
Fig. 13:   Alternative source zonations for the Alps
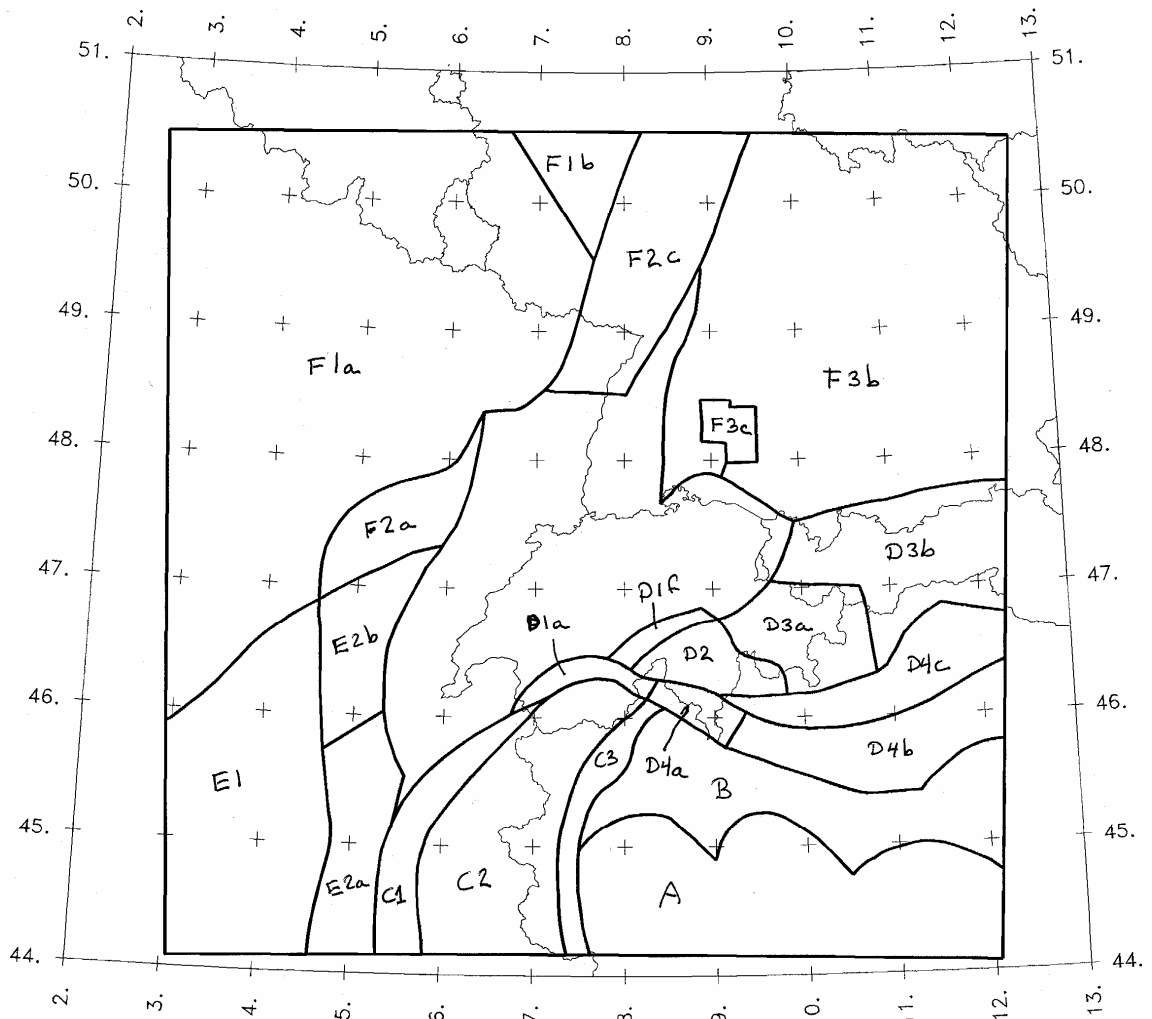
Fig. 14:   Source zones whose boundaries do not change as a function of alternative zona-
            tions

2.8.2   Earthquake rupture geometry

The size of earthquake ruptures is defined by the relationship:

$$\text{Mean } \log_{10}(\text{rupture area}) = M\text{-}4$$
$$\sigma_{\log10(\text{rupture area})} = 0.24.$$

Using the relationship for the expectation of a lognormal distribution, the mean rupture area is
given by the relationship:

$$\log_{10}(\text{mean rupture area}) = M\text{-}3.934$$

We assume an aspect ratio of 1:1 until the maximum rupture width for a source is reached. This
width is defined on the basis of the maximum depth and fault dip, as defined below. For larger
ruptures, the width is held constant at the maximum width and the length is obtained by dividing
the rupture area by this width.

Tab. 1:   Source Sets for EG1a

Source Set	Sources
Set 1	F2bpcy, F2e, F3a, E2c, E2n, E2f, E2s, E3b, D1bcde + UC*
Set 2	F2bpcy, F2e, F3a, E2c, E2n, E2f, E2s, E3b, D1bcd, D1e + UC
Set 3	F2bpcy, F2e, F3a, E2c, E2n, E2f, E2s, E3b, D1b, D1c, D1de + UC
Set 4	F2b_RF, RF, E2cde, FF, E3a, D1bcde, F3a + UC
Set 5	F2b_RF, RF, E2cde, FF, E3a, D1bcd, D1e, F3a + UC
Set 6	F2b_RF, RF, E2cde, FF, E3a, D1b, D1c, D1de, F3a + UC
Set 7	F2b_RF, RF, E2c, E2d, E2e, E3a, D1bcde, F3a + UC
Set 8	F2b_RF, RF, E2c, E2d, E2e, E3a, D1bcd, D1e, F3a + UC
Set 9	F2b_RF, RF, E2c, E2d, E2e, E3a, D1b, D1c, D1de, F3a + UC
Set 10	F2b, F2d, E2cde, FF, E3a, D1bcde, F3a + UC
Set 11	F2b, F2d, E2cde, FF, E3a, D1bcd, D1e, F3a + UC
Set 12	F2b, F2d, E2cde, FF, E3a, D1b, D1c, D1de, F3a + UC
Set 13	F2b, F2d, E2c, E2d, E2e, E3a, D1bcde, F3a + UC
Set 14	F2b, F2d, E2c, E2d, E2e, E3a, D1bcd, D1e, F3a + UC
Set 15	F2b, F2d, E2c, E2d, E2e, E3a, D1b, D1c, D1de, F3a + UC
Set 16	F2bF2f, F2f, E2cdeF2f, FF, E3aF2f, D1bcde, F3aF2f + UC
Set 17	F2bF2f, F2f, E2cdeF2f, FF, E3aF2f, D1bcd, D1e, F3aF2f + UC
Set 18	F2bF2f, F2f, E2cdeF2f, FF, E3aF2f, D1b, D1c, D1de, F3aF2f + UC
Set 19	F2bF2f, F2f, E2c, E2dF2f, E2eF2f, E3aF2f, D1bcde, F3aF2f + UC
Set 20	F2bF2f, F2f, E2c, E2dF2f, E2eF2f, E3aF2f, D1bcd, D1e, F3aF2f + UC
Set 21	F2bF2f, F2f, E2c, E2dF2f, E2eF2f, E3aF2f, D1b, D1c, D1de, F3aF2f + UC
*Set UC	A, B, C1, C2, C3, D1a, D1f, D2, D3a, D3b, D4a, D4b, D4c, E1, E2a, E2b, F1a, F1b, F2a, F2c, F3b, F3c

Earthquake epicenters are assumed to be uniformly distributed within the source. Earthquake ruptures are located symmetrically on the epicenters (the epicenter is at the midpoint of the rupture). For those epicenters located closer than L/2 rupture length to the source zone boundary, the ruptures are allowed to extend beyond the source boundary.

Table 2 defines the relative frequency of the style of faulting and rupture orientations for the individual sources. Three specific styles of faulting are considered, normal, strike-slip and reverse. For each style of faulting, there is a preferred fault dip that should be used to model ruptures.

The depth distribution of earthquakes for the sources is defined by the following three distributions. For the northern Alpine foreland sources (FF, E2d, E2e, E2cde, E2cdeF2f, E2n, E2f, E2s, E3a, E3aF2f, E3b) the distribution is triangular over the depth range of 1 to 30 km, with the mode at a depth of 10 km (Fig. 15). For the southern Alpine foreland and southern Germany sources (C3, D4a, D4b, D4c, F3a, F3aF2f, F3b, F3c) the depth distribution is triangular over the depth range of 1 to 25 km, with the mode at a depth of 10 km (Fig. 16). For the remaining zones

and RF, the distribution is trapezoidal over the depth range of 1 to 20 km, with the upper uniform region extending over the depth range of 1 to 10 km (Fig. 17).

For larger earthquakes, a magnitude-dependent depth distribution is assumed, based on the weighted model outlined in Toro (2003, PEGASOS TP1-TN-0373), using a value of T = 0.5 (hypocenter in the lower half of the rupture). Consequently, earthquakes with sufficiently large fault planes are allowed to rupture the surface. This applies in particular to the Reinach (RF) and Fribourg (FF) fault sources.

Tab. 2:   Style of Faulting and Rupture Orientation for EG1a Sources

Sources	Relative Frequency for Style of faulting			Orientation of Ruptures		
	SS*	NF*	TF*	SS*	NF*	TF*
A, B, D1f, D2, D4a, D4c, E1, E2e, E2eF2f, F3c	0.33	0.33	0.33	Random	Random	Random
C1, C3	0.75		0.25	N20E		N20E
C2		1.0			N20E	
D1a	1.0			N90E		
D1b, D1d, D1e, D1bcde, D1bcd, D1de,	0.75		0.25	Random		Random
D1c	0.8	0.1	0.1	Random	Random	Random
D3a	0.25	0.75		Random	Random	
D3b	1.0			N70E		
D4b, E2f			1.0			N70E
E2a, E2b, E2c, E2d, E2dF2f, E2n, E2cde E2cdeF2f, F2c	1.0			N15E		
E3a, E3aF2f, F1b	0.5.	0.5		N45W	N45W	
F2a	0.75	0.25		N15E	N15E	
F2b, F2bpcy, F2b_RF, F2bF2f	0.5	0.5		N15E	N15E	
F1a	0.5	0.5		Random	Random	
E2s	0.7	0.2	0.1	Random	Random	Random
E3b			1.0			N90E
F2d	0.3	0.7		N15E	N15E	
F2e	0.3		0.7	N90E		N90E
F2f	0.4	0.4	0.2	Random	Random	Random
F3a, F3aF2f	0.25	0.75		N15E & N45W	N15E & N45W	
F3b		1.0			N45E	
RF	0.3	0.7				
FF	1					

*SS – strike slip, dip 80°, NF normal slip, dip 60°, TF thrust, dip 30°.

Fig. 15:   Earthquake depth distribution for sources FF, E2d, E2dF2f, E2eF2f, E2e, E2cde, E2cdeF2f, E2n, E2f, E2s, E3a, E3aF2f, and E3b
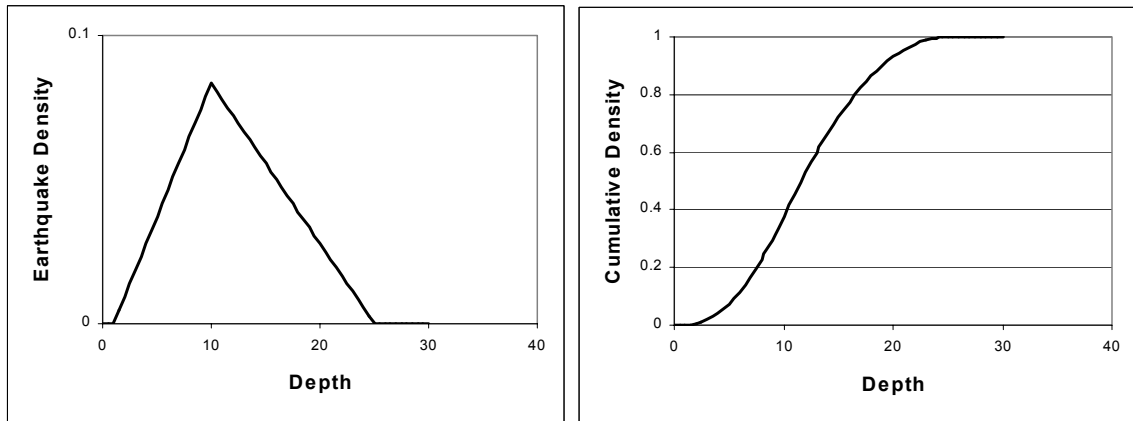
Fig. 16:   Earthquake depth distribution for sources C3, D4a, D4b, D4c, F3a, F3aF2f, F3b, and F3c
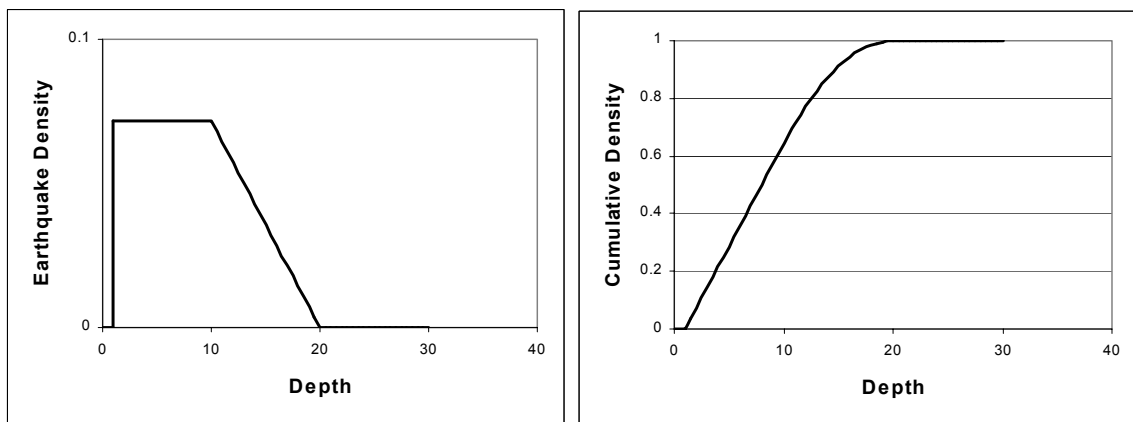
Fig. 17:   Earthquake depth distribution for all other sources except those listed for Figures 15 and 16

3   EARTHQUAKE RECURRENCE RELATIONSHIPS

3.1   Earthquake catalog analysis

As is explained in the accompanying report (PEGASOS EXT-TB-0043) to the PEGASOS (ECOS) Earthquake Catalog (TP1-CAT-0004), each event in the PEGASOS catalog has been classified according to certainty (cc = certainty code) and according to type (ty = type code; see catalog report pp. 12-13). The catalog was searched for questionable and fake events (c = 2 and cc > 2) and for events of unknown type, induced events and explosions (type = 0, 1 and 2). Based on the results given below, the catalog used for subsequent analyses was modified accordingly. In the lists included in the text below, the first three parameters given are: ag = catalog source, cc = certainty code, ty = type code.

a)   cc = 2, questionable events: 609 events found

These are events located mainly within Switzerland and they span the entire range in time and magnitude. It is debatable whether they should be included in our hazard evaluation or not. Upon consultation with the catalog compilers, it was decided to remove these events from the catalog. The events classified as questionable and removed fall into the following time periods:

```
250 - 1878:  61 events,
1879 - 1899: 262 events,
1900 - 1974: 277 events,
1975 - 2000: 9 events.
```

b)   cc > 2, fake events: 0 events found

c)   type = 0, unknown events: 275 events found

The following event is misclassified (confirmed by the data compilers):

```
ag cc ty year mo dy hr mi  sec    lat     lon    Z  Mw  Io  Ix
-------------------------------------------------------------
10  1  0 1823 12 13 03 00  .00   45.82    5.68   0 4.3  55   0
```

The type of this event was changed to 4 (mainshock or single earthquake). This leaves 274 "unknown" events. All of them have been classified as unknown based on information from the BGR catalog. They are either located in the mining area of the Saarland or in the far NE, beyond the area of interest to our study. All of these unknown events have been removed from the catalog.

d)   type = 1, induced events: 30 events found

The following two events are misclassified (confirmed by the data compilers):

```
ag cc ty year mo dy hr mi  sec    lat     lon    Z  Mw  Io  Ix
-------------------------------------------------------------
 1  1  1 1665 04 10 00 00  .00   46.98    6.92   0 3.2  40   0
10  1  1 1837 11 12 22 00  .00   47.88    7.47   0 3.9  50   0
```

The type of the two events listed above were changed to 3 (earthquake). This leaves 28 "induced" events, which where removed from the catalog. Amongst these events, 9 have been classified as such by the LED and these are associated with injection procedures at the Soultz-sous-Foret geothermal site in summer 2000 (incidentally, most of these events are flagged by all the de-clustering algorithms except with the Uhrhammer de-clustering parameters − see chapter 3.2). The rest are classified as such based on the BGR catalog and they mostly lie outside the area of concern.

e) <u>type = 2, explosions: 52 events found</u>

The following event is misclassified (confirmed by the data compilers):

```
ag cc ty year mo dy hr mi  sec    lat    lon    Z  Mw  Io  Ix
-----------------------------------------------------------
10  1  2 1757 01 18 05 52  .00  47.77   6.73  0 4.7  60   0
```

The type of this event was changed to 3. This leaves 51 events identified as explosions. All of these have been contributed by foreign catalogs and they mostly lie within Switzerland. Particularly irksome is a Mw 2.9 event in northern Switzerland (1994/11/30 14:49) and the Mw 3.2 explosion of the ammunitions cavern near the Sustenpass (1992/11/02 15:13). All of these 51 explosions have been removed from the catalog.

f) <u>explosions erroneously listed as earthquakes: 23 events found</u>

23 events, which have been classified as explosions by the SED (see table given below), have crept into the catalog from foreign agencies. However these were not identified as such in the PEGASOS catalog. Most of them lie in the border region between northern Switzerland and southern Germany. Although of small magnitude and probably statistically insignificant, they were changed into type 2 and removed from the final catalog.

```
ag cc ty year mo dy hr mi   sec    lat   lon    Z  Mw Io Ix location
--------------------------------------------------------------------
 4  1  3 1977 02 25 07 32 33.40  47.47  9.97 10 2.8  0  0 ?
 4  1  3 1977 07 14 13 37 20.30  47.73  8.21  0 2.5  0  0 Villigen?
 4  1  3 1977 10 21 08 06 22.90  47.48 10.20 10 2.6  0  0 ?
 7  1  3 1981 04 23 06 28 16.00  47.43  9.90 10 2.2  0  0 ?
 7  1  3 1981 09 16 04 30 20.00  47.70  8.00  0 2.1  0  0 ?
 5  1  3 1983 06 06 14 22 38.00  47.59  8.22  2 2.2  0  0 Villigen?
 5  1  3 1983 08 18 09 42 41.00  47.07  8.51  6 2.0  0  0 ?
 5  1  3 1983 12 07 15 28 34.00  47.35  7.25  2 2.0  0  0 ?
 7  1  3 1984 01 19 00 45 56.80  47.61  7.69 10 1.8  0  0 Refr. shot Nagra
 7  1  3 1985 06 05 07 53 57.00  47.13  9.63 15 2.1  0  0 Walenstadt
 5  1  3 1991 06 13 07 52 23.00  47.14  9.33  6 2.1  0  0 Walenstadt
11  1  3 1991 10 23 12 10  7.10  47.81  8.05  2 2.0  0  0 Feldberg
 5  1  3 1992 09 19 10 40 39.00  47.70  7.80  0 1.5  0  0 Wies?
 5  1  3 1992 11 30 15 00 17.00  47.86  8.50 10 1.9  0  0 ?
 5  1  3 1993 09 02 09 00 40.00  47.54  7.79 10 2.1  0  0 Reckingen
 6  1  3 1994 08 30 09 10 36.70  47.85  7.92  5 2.1  0  0 Feldberg
 7  1  3 1994 10 07 15 38  3.39  47.63  8.30 12 1.4  0  0 Uehlingen?
 4  1  3 1994 10 24 11 44 55.80  47.82  7.95  4 2.2  0  0 Feldberg
 5  1  3 1994 11 15 10 28 50.00  47.53  8.17  0 1.9  0  0 Villigen
 7  1  3 1994 11 18 10 20  2.10  47.83  8.05  1 1.7  0  0 Feldberg
 6  1  3 1995 09 07 12 16 37.10  47.82  8.02  1 2.1  0  0 Feldberg
 6  1  3 1995 10 09 12 57  9.60  47.69  8.28  0 1.9  0  0 Uehlingen?
 6  1  3 1995 11 25 12 31  5.70  47.81  8.00  1 2.1  0  0 Feldberg
```

3.2   Catalog de-clustering

In the following, we discuss two alternative approaches for evaluating different de-clustering methods. This discussion will serve as a basis for choosing a particular method for removing dependent events from the catalog.

3.2.1   Performance of de-clustering methods regarding earthquake statistics

The catalogs obtained by de-clustering the PEGASOS catalog according to the four approaches described in the Wiemer (2002) report have been considered for further elaborations and comparisons. All the earthquakes considered as main (i.e. independent) events with a magnitude

larger than, or equal to, 0 have been considered. De-clustering according to the methods of Reasenberg (1985: "RE" in Table 3; first pair of columns of the PEGASOS cataolgue modified by Wiemer), Gardner & Knopoff (1974: "GK" in Table 3, second pair of columns of PEGASOS modified by Wiemer) with original parameters, Gardner & Knopoff (1974) with parameters for central Europe as suggested by Grünthal (1985) ("GR" in Table 3 third pair of columns of ECOS modified by Wiemer), and, Gardner & Knopoff (1974) with parameters for California according to Uhrhammer (1986: "UH" in Table 3; fourth pair of columns of PEGASOS modified by Wiemer) yielded the following numbers of main events: 12327 (RE), 11897 (GK), 10506 (GR), and, 15478 (UH), respectively.

Tab. 3:   Seismicity rates (annual number of earthquakes) calculated with the Albarello & Mucciarelli (2002) approach

Mag	RE	GK	GR	UH
1.5	23.61811	22.05366	19.50332	26.61851
1.8	30.36671	30.40698	29.48510	37.88504
2.1	35.22528	35.16383	29.75845	41.10890
2.4	17.93747	16.78552	15.27489	18.54763
2.7	8.28355	8.21628	6.53959	9.88694
3.0	7.68385	6.71911	5.93608	8.32996
3.3	5.83699	5.36949	4.79729	6.63173
3.6	4.09687	3.44349	3.11624	4.33272
3.9	3.09999	2.79738	2.59319	3.16072
4.2	1.40943	1.28259	1.22678	1.38190
4.5	0.70272	0.65200	0.62586	0.68217
4.8	0.50043	0.45591	0.43922	0.48399
5.1	0.29159	0.24773	0.24773	0.27618
5.4	0.12781	0.10981	0.10997	0.11488
5.7	0.06442	0.06442	0.06442	0.06442
6.0	0.02305	0.01867	0.01867	0.02305
6.3	0.01596	0.01596	0.01596	0.01596
6.6	0.00090	0.00090	0.00090	0.00090
6.9	0.00097	0.00097	0.00097	0.00097

The Albarello & Mucciarelli (2002) approach has been applied to all these four de-clustered catalogs in order to compute seismicity rates (see Table 3).

The following parameters have been used for these four catalogs:
Minimum magnitude considered: 1.5;
Magnitude step: 0.3;
Time span: from 200 A.D. to 2000;
Time step: 5 years.

The parameters chosen imply that all the four types of de-clustered catalogs were investigated for the time period 200 A.D. to 2000 with an analysis step of 5 years. Seismicity rates were computed by starting at magnitude 1.5 and with a step of 0.3. The results obtained (Table 3) are expressed in terms of annual number of earthquakes per magnitude class. As can be easily seen,

the rates are very similar and almost identical for magnitudes larger than 5.1. Concerning magnitudes larger than 6 they remain exactly the same.

Table 3 also shows that the magnitude classes lower than 2.1 must be incomplete. Consequently, they should not be considered for further elaborations. All the other classes have been used for subsequent b-value computations.

The b-value computations based on all the data contained in the four types of de-clustered catalogs have been performed by two different approaches: (1) by the maximum likelihood method and (2) by the least squares method (Table 4). As can be seen from Table 4 the values are very similar amongst the four types of de-clustered catalogs, both in terms a- and b-values. However, both a- and b-values strongly differ when comparing the two alternative fitting approaches: the least squares method gives b-values close to 1, while the maximum likelihood method gives much lower values at around 0.7.

Tab. 4:   b-values for the four de-clustered catalogs

Cat	max. likelihood			least squares			
	a	b	σb	a	σa	b	σb
RE	3.33	0.66	0.04	4.39	0.26	0.98	0.06
GK	3.33	0.68	0.05	4.33	0.25	0.98	0.05
GR	3.23	0.66	0.05	4.25	0.26	0.96	0.05
UH	3.41	0.68	0.04	4.44	0.25	0.99	0.05

Figure 18a shows cumulative annual rates and best fit obtained by the maximum likelihood and the least squares methods, respectively, when the catalog is de-clustered according to the Reasenberg (1985) algorithm. The numerical differences between the two fitting procedures are very pronounced, as was pointed out above. The maximum likelihood method is strongly conditioned by the low magnitude data and almost "forgets" high magnitudes. This is caused by the huge number of earthquakes with low magnitudes. The application of the least squares method is formally wrong, since the data (cumulative annual rates) are not independent, as is requested by the method itself. Nevertheless, the fit obtained may appear more adequate for our needs. We are interested in assessing recurrence of high magnitudes, and hence, although the uncertainty is larger at high magnitudes, the low weight given to these large quakes by the maximum likelihood method might not be justified. In case of the least squares method, all data points are equally weighted, while the confidence we have in the frequency of the high magnitude events is certainly worse when compared to that of the small events. It must be pointed out, furthermore, that the low magnitude classes (lower than 4.8) are very probably incomplete (see their low number in Fig. 18) in our sample and, consequently, should be omitted from the fit.

The fits have been re-done for a new data set, which only takes magnitudes larger than 3.8 events from Table 3, and these results are shown in Table 5 and Figure 18b, again for the catalog de-clustered according to the Reasenberg (1985) method. Now the two fits are much closer each other and, probably, represent the information more adequately.
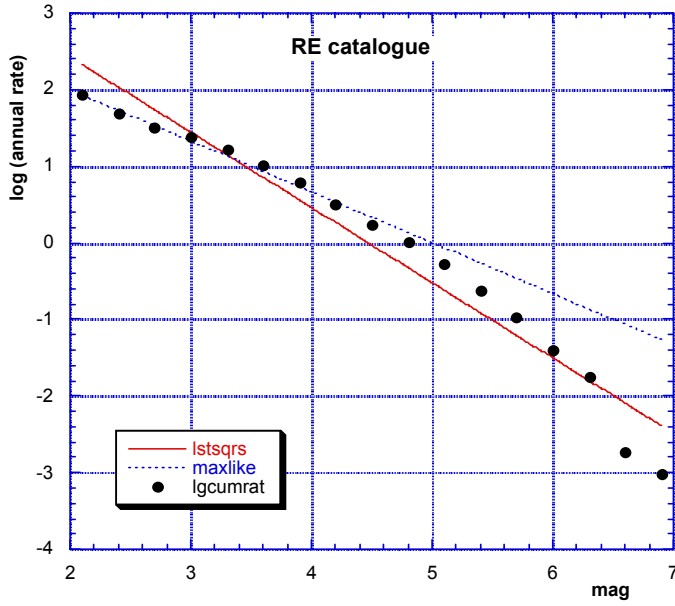
a)
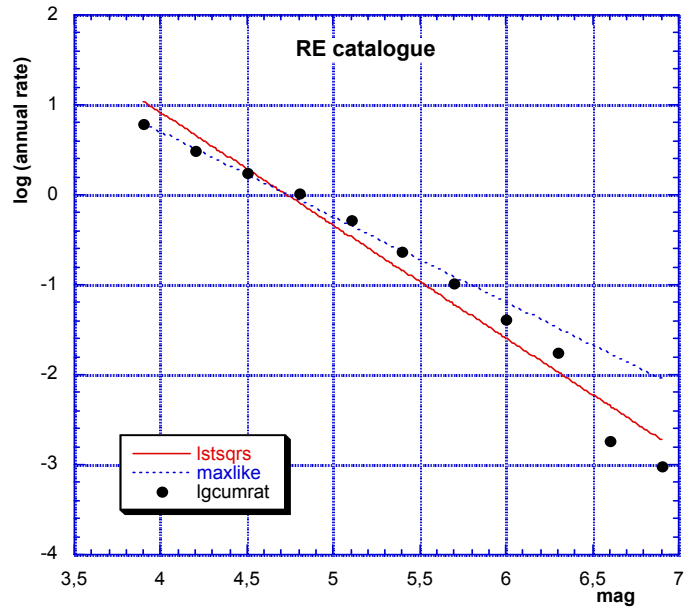
b)

Fig. 18:   Annual rates, maximum likelihood and least squares fits for the de-clustered (Reasenberg method) PEGASOS catalog: a) all data; b) considering medium to large magnitudes only

Tab. 5:   b-values for the four de-clustered catalogs for rates related to magnitudes larger than 3.8, taken from Table 3

cat	max. likelihood			least squares			
	a	b	σb	a	σa	b	σb
RE	4.49	0.95	0.27	5.93	0.43	1.25	0.08
GK	4.46	0.95	0.29	5.81	0.42	1.24	0.08
GR	4.38	0.93	0.29	5.77	0.43	1.23	0.08
UH	4.54	0.96	0.28	5.90	0.43	1.25	0.08

At this point it is interesting to investigate the influence of the de-clustering method on the values of maximum possible magnitude, as calculated by the Kijko & Graham (1998) approach. This approach computes the maximum magnitude with two different formulae: the Tate-Pisarenko (T-P) and the Kijko-Sellevol (K-S). For both of them Kijko & Graham (1998) give also their Bayesian formulation (T-P-B, and K-S-B). In particular, the K-S-B estimate is considered to be the most robust by Kijko & Graham (1998).

The input parameters requested for the maximum magnitude assessment are: maximum observed magnitude in the considered catalog, minimum magnitude that is complete in the catalog, standard deviation of the magnitude estimates, b-value and its standard deviation, annual seismicity rate for the minimum magnitude, and finally, the time period for which the catalog is considered complete. All requested values have been taken from the maximum likeliood estimates in Table 5. A value of 0.2 has been arbitrarily given to the magnitude standard deviation, and, the last 1000 years of the catalog have been considered complete for magnitudes exceeding 3.9. This last choice is justified by the method by which the seismicity rates have been computed: with the Albarello & Mucciarelli (2002) method the entire catalog contributes to the rate assessment. Some tests which were performed have shown the dependence of the results on the completeness period considered.

The results of these maximum magnitude calculations are displayed in Table 6: the differences are very small and deviate very little from the maximum observed value (6.9).

Tab. 6:   Maximum magnitude computed for the four de-clustered catalogs

type	RE		GK		GR		UH	
	max_mag	σ	max_mag	σ	max_mag	σ	max_mag	σ
T-P	7.00	0.23	7.02	0.23	7.01	0.23	7.01	0.23
T-P-B	6.90	0.20	6.90	0.20	6.90	0.20	6.90	0.20
K-S	6.99	0.22	7.00	0.22	6.99	0.22	6.99	0.22
K-S-B	6.95	0.21	6.95	0.21	6.95	0.21	6.95	0.21

Conclusion: in case of the PEGASOS catalog, the effect of the de-clustering method plays a very minor role on the characterisation of the seismicity, both in terms of a- and b-values, as well as regarding expected maximum magnitudes.

3.2.2   Performance of de-clustering methods regarding selected earthquake sequences

There seems to be consensus, that there is no single best way for de-clustering earthquake catalogs. The performance of the four de-clustering schemes proposed by Wiemer (2002) were examined by de-clustering a few well-known earthquake sequences. It was mainly investigated as to how the proposed schemes deal with sequences (either aftershocks or swarms) that contain several strong events, each having their own aftershocks.

When abbreviations (UH = Uhrhammer, RE = Reasenberg, GK = Gardner and Knopoff, and GR = Grünthal) appear next to an event in the lists given below, this means that the corresponding algorithm did identify that event as a mainshock.

```
Sierre 1946 (all events found in the PEGASOS Catalog)

1946 01 25 17 32   .00  46.35     7.40  12 6.1  80  80    UH RE GK GR
1946 01 26 03 15   .00  46.28     7.43  12 5.2  60  60
1946 02 04 04 11 28.00  46.30     7.52  12 5.1  50  50        RE
1946 05 30 03 41   .00  46.30     7.42  12 6.0  70  70    UH RE
```

Comment: the second and third events can be considered as aftershocks of the first event: RE probably does not agree because of the difference in location. Whether the last event should be regarded as a main shock or as another after-shock event dependent upon the first event (4 months later!) remains uncertain.

```
Sarnen 1964 (only the two main events)

1964 02 17 12 20   .00  46.88    8.27   5 5.0  70  70
1964 03 14 02 39   .00  46.87    8.32   0 5.7  70  70   UH RE GK GR
```

Comment: these two events are part of a sequence of hundreds of events that lasted for several months (typical swarm activity). All four algorithms evidently regard the first event as depenent upon the second stronger one.

```
Fribourg 1987-1999 (only the stronger events)

1987 09 20 11 53 57.80  46.76    7.22   7 3.7   0   0   UH RE GK GR
1987 09 23 13 09  1.60  46.76    7.20   7 2.8   0   0

1995 09 17 16 29 24.60  46.78    7.18   7 3.5  40  40   UH RE GK GR
1995 10 07 01 37 31.40  46.79    7.18   7 3.3   0   0   UH RE

1999 02 14 05 57 54.30  46.78    7.21   7 4.0  50  50   UH RE GK GR
1999 02 17 16 07 22.60  46.78    7.21   7 2.2   0   0
1999 02 24 09 36 18.10  46.78    7.22   7 2.1   0   0   UH RE
1999 04 16 10 37 15.30  46.80    7.21   7 2.1   0   0   UH RE GK
```

Comment (see Fig. 19): among the Fribourg events there are three distinct clusters that occurred over a short period each in the years 1987, 1995 and 1999. The hypocenters of the 1995 and 1999 events are all located within 1 km from each other, while the 1987 events are located 2 – 3 km further south. The signals of the events in each cluster are identical to each other. It is suggested to consider only the strongest event in each cluster as an independent main shock, in agreement with the Grünthal algorithm.

```
Bormio 1999-2000 (only the strongest events)

1999 12 29 20 42 33.70  46.53   10.31  12 4.9   0   0   UH RE GK GR
1999 12 31 04 55 53.50  46.55   10.32  12 4.2   0   0
2000 04 06 17 40 36.80  46.54   10.33  15 4.1   0   0   UH RE
2000 05 28 11 22 19.90  46.53   10.35  15 2.8   0   0   UH RE GK
2000 06 09 05 06  6.40  46.54   10.30  15 3.0   0   0   UH RE GK
```

Comment (see Fig. 20): the Bormio activity started at the end of 1999 and persisted well into 2002 with about 200 events. It features several events of intermediate size, each of them followed or accompanied by a temporary increase in the rate of activity. Hence, it is debatable whether all these stronger sub-events are to be considered as aftershocks of the first event, or alternatively, as separate and independent events, each of them with its own aftershock sequence.

Conclusion: as was to be expected from the analysis of Wiemer (2002), the Grünthal scheme does the most rigorous job of de-clustering in the case studies discussed above.

3.2.3   Choice of de-clustering method

Based on the fact that the algorithm of Gardner & Knopoff (1974) with the parameters suggested by Grünthal (1985) based on European data does the most rigorous job of de-clustering the earthquake sequences chosen for analysis, we decided to use this procedure for de-clustering the whole catalog. We believe that a rigorous de-clustering is desirable, because it ensures the largest possible statistical independence of the events remaining in the catalog.
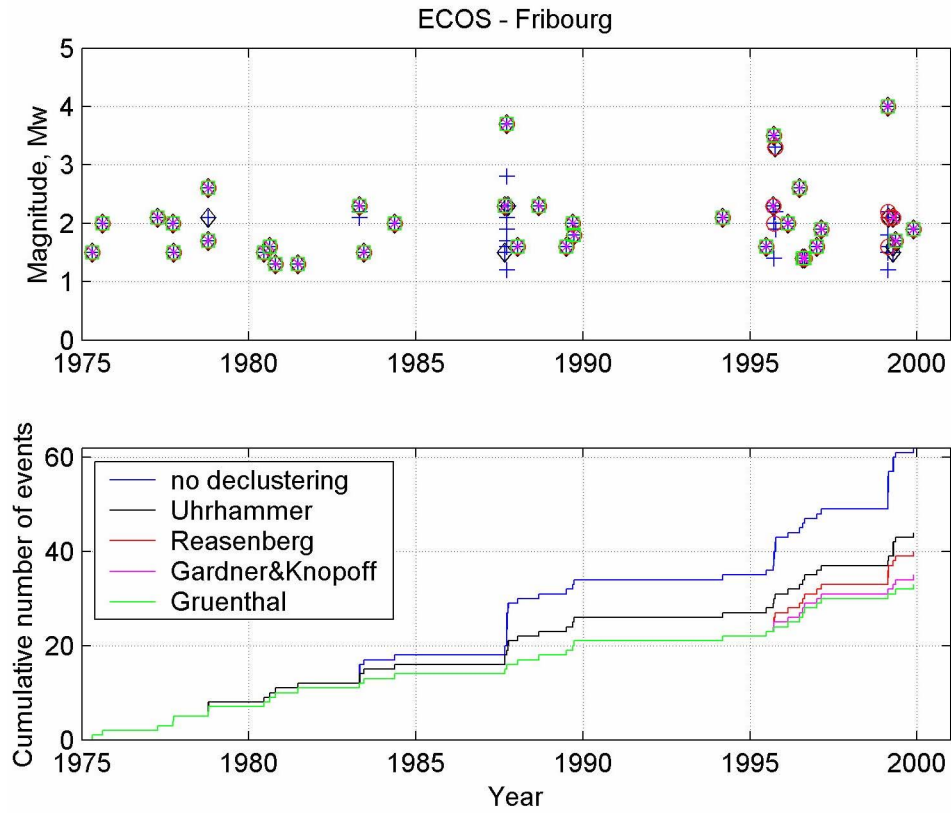
Fig. 19:   Fribourg events (1975-2000; 7.15E-7.25E / 46.65N-46.95N)
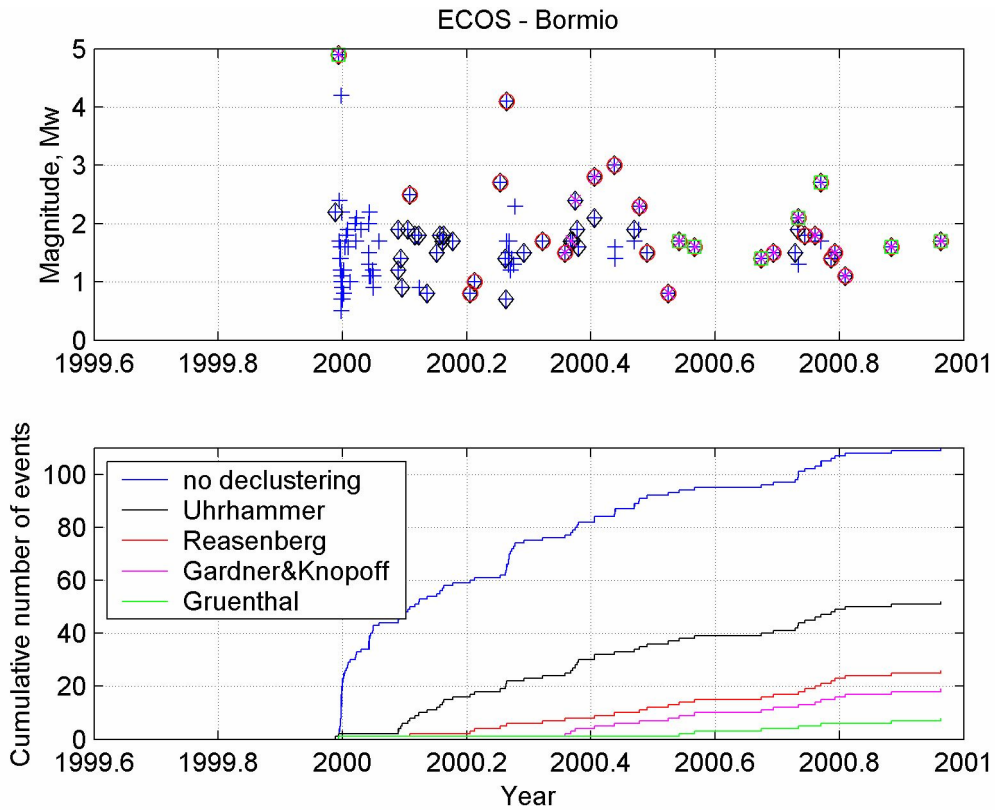
Fig. 20:   Bormio events (1999-2000; 10.2E-10.4E / 46.5N-46.6N)

3.3   Catalog completeness

One of the prerequisites for an evaluation of recurrence relationships based on earthquake catalogs is that such an analysis be restricted to regions, time periods and magnitude ranges for which the catalog is complete. In the following two sections, we review the available information concerning completeness of the PEGASOS earthquake catalog. This compilation subsequently will serve as the basis for the actual completeness assumptions used and documented for the individual recurrence assessments in Section 3.5.

Since the PEGASOS earthquake catalog was assembled from a fusion of several different national catalogs (see the national catalog zones, mapped in Fig. 7), the completeness information based on the documentation supplied with the individual national catalogs will be compiled in a first step (Section 3.3.1). Subsequently (Section 3.3.2), the analysis will consider the completeness of catalog subsets corresponding to the macro zones defined in Figure 6.

3.3.1   Completeness assessment of national catalogs

This section summarizes information about catalog completeness for the individual national catalogs that form part of the PEGASOS catalog. It is based on information from the catalog compilers and from so-called Stepp-plots (see document "Assessment of Catalog Completeness Using Stepp Plots", distributed by Bob Youngs, and Stepp 1972). Figures 21 to 23 illustrate the catalog content as a function of magnitude for national catalog zones shown in Figure 7. The Stepp-plots, referred to in this section (Figs. 24 – 30), were calculated by Geomatrix Consultants, based on the catalog, which was de-clustered with the Reasenberg method (see document "Assessment of Earthquake Recurrence for Seismic Sources", distributed by Bob Youngs).
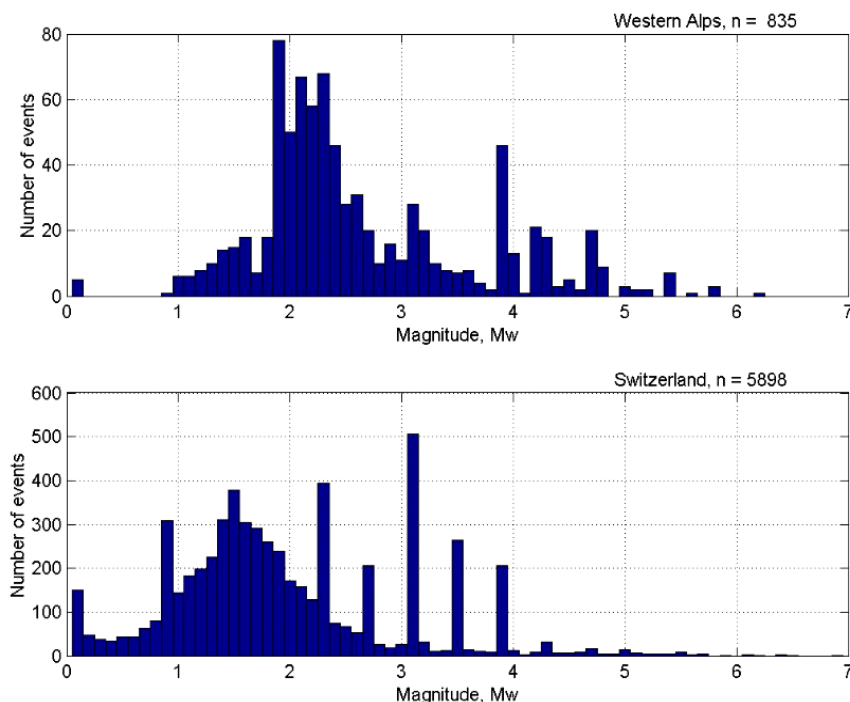
Fig. 21:   Analysis of the catalog contents

The fact that the Stepp-plots (Figs. 26 – 30) referred to in this section are based on a catalog declustered by the Reasenberg algorithm rather than using the more rigorous Gardner & Knopoff method with the Gruenthal parameters, could result in estimates of catalog completeness that are somewhat too optimistic. As discussed in Section 3.5.1.2, an examination of the actual Gutenberg-Richter plots as well as additional considerations regarding the compilation of

the catalog suggest that in some cases more conservative completeness assumptions are more appropriate. For compatibility with the Swiss catalog, which is the dominant part of the PEGASOS catalog, the period after 1975 is regarded as instrumental for all sub-regions, even though the catalog also includes earlier instrumental data in some cases. In what follows we list for each zone individual periods of completeness, giving the beginning year and the minimum magnitude for each period, followed in most cases by a comment regarding the basis of the assessment.
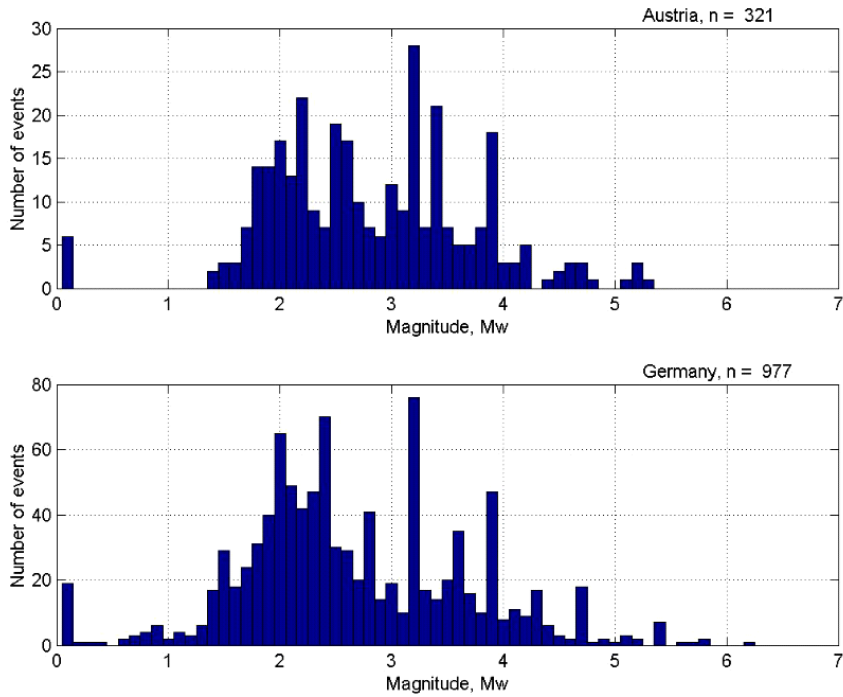
Fig. 22: Analysis of the catalog contents
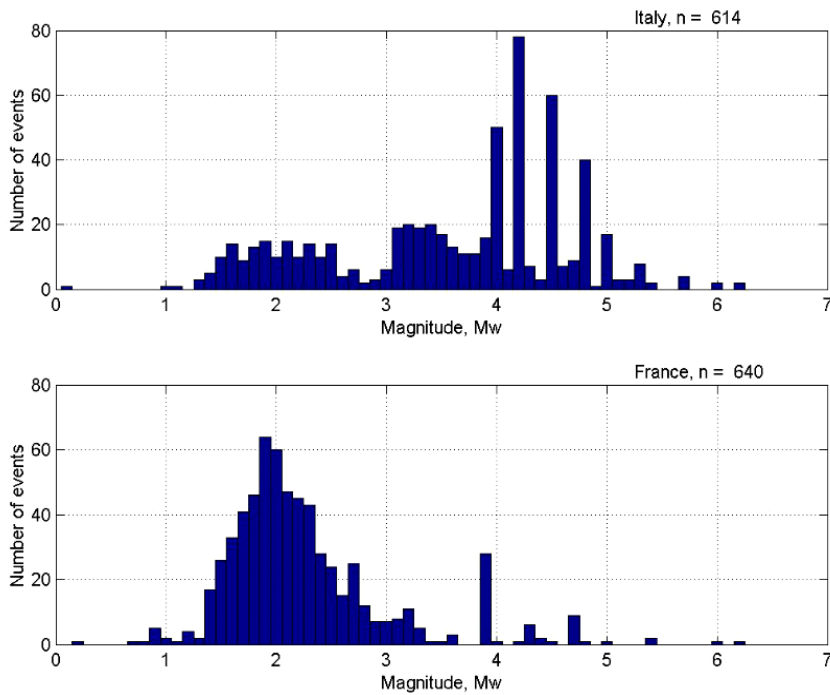
Fig. 23: Analysis of the catalog contents
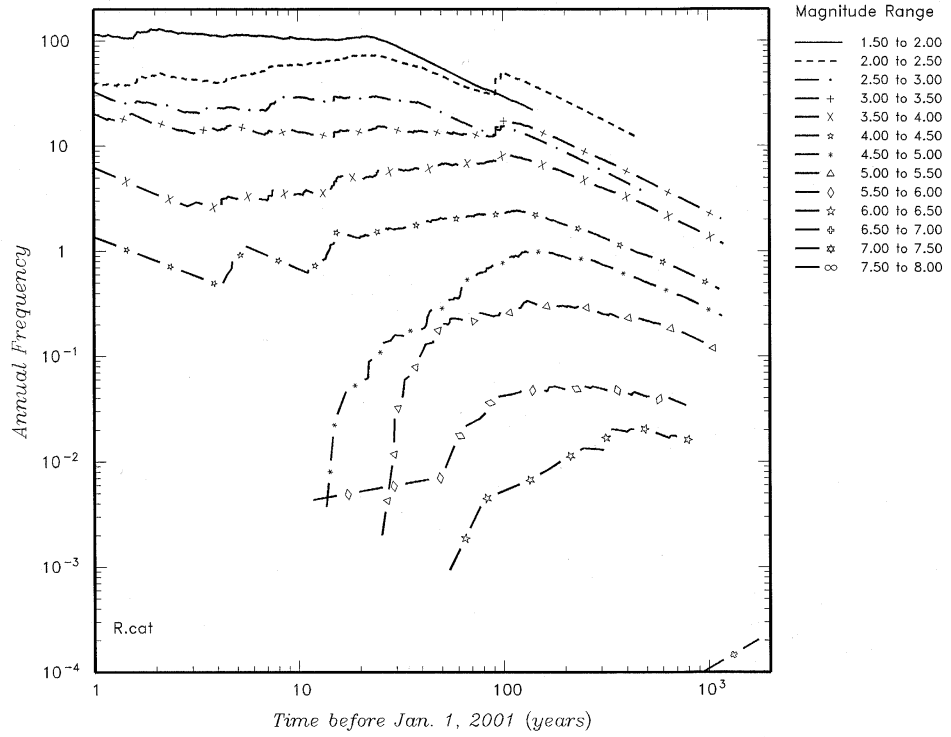
Fig. 24: Completeness plot for PEGASOS catalog de-clustered using the Reasenberg approach
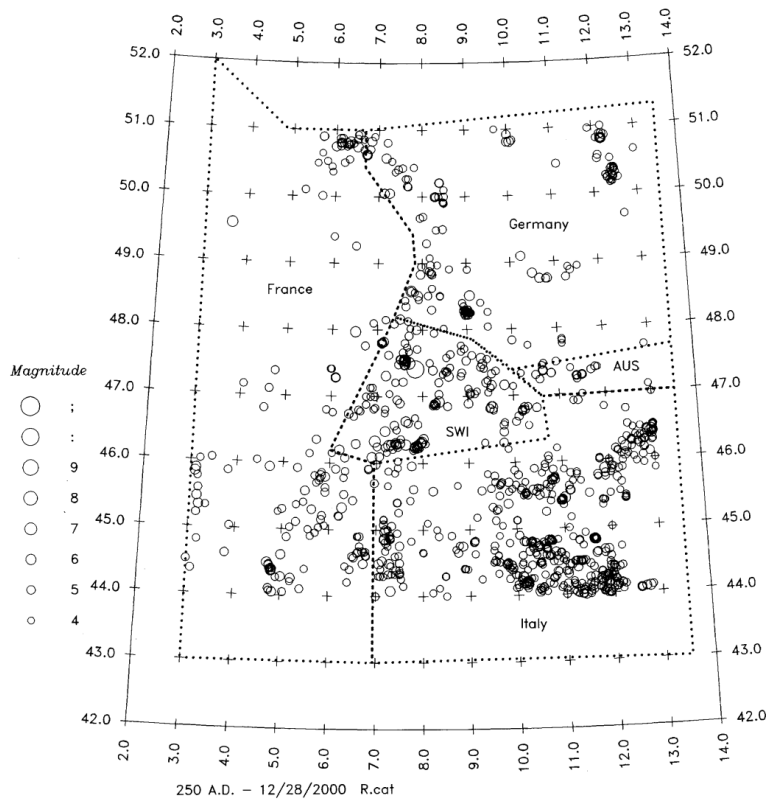
Fig. 25: Map of earthquakes in the PEGASOS catalog identified as independent events by the Reasenberg de-clustering approach
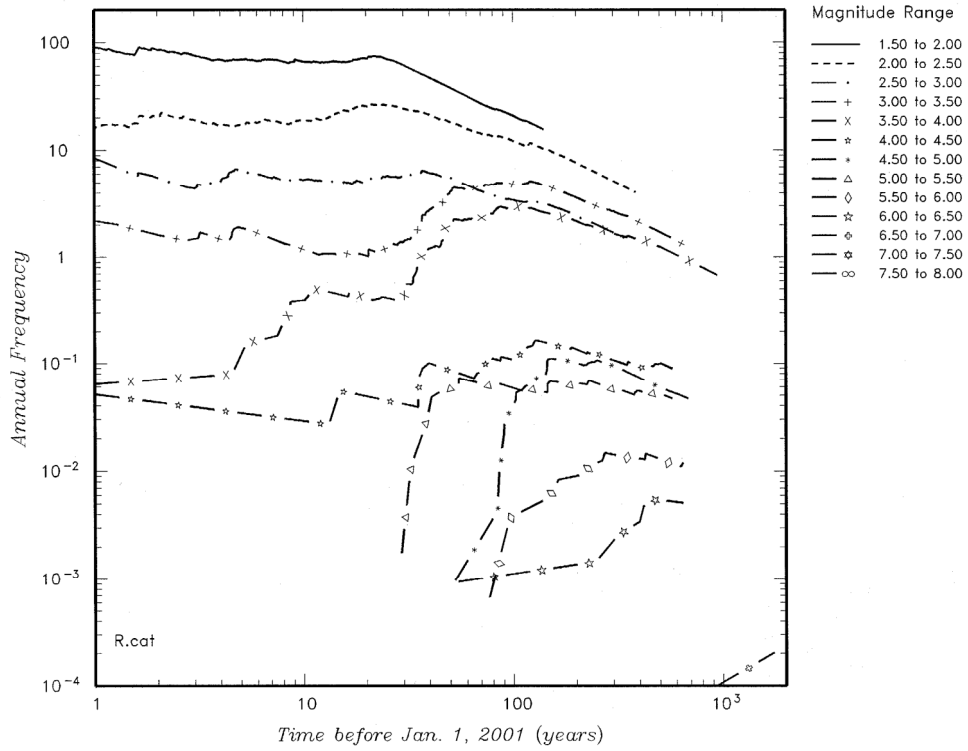
Fig. 26: Completeness plot for Switzerland region (see Fig. 25)
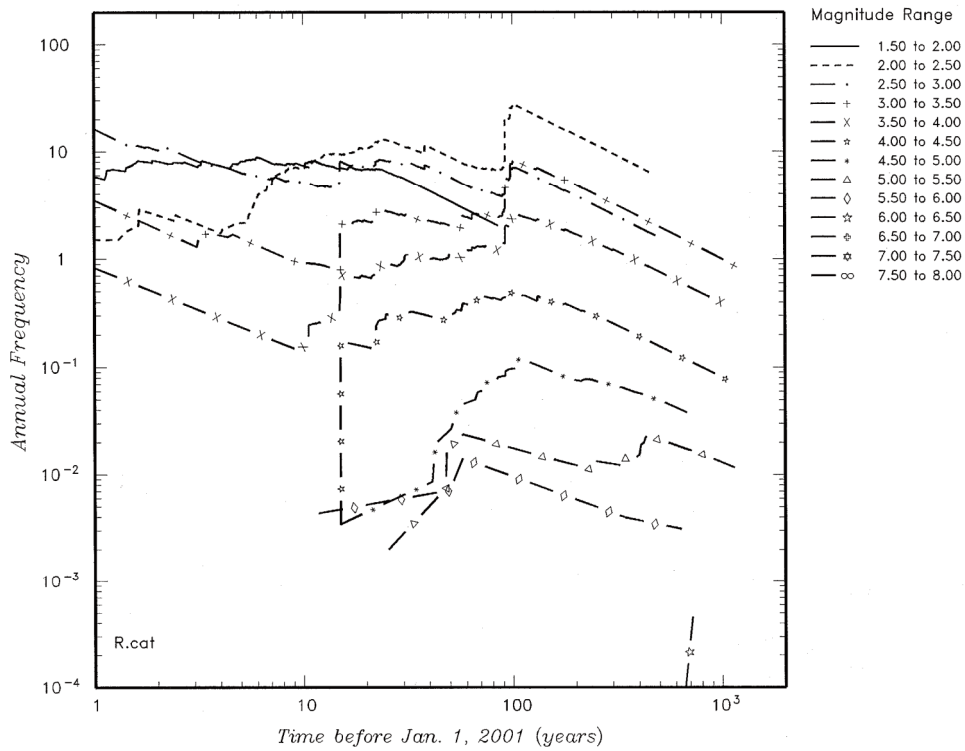
Fig. 27: Completeness plot for Germany region (see Fig. 25)
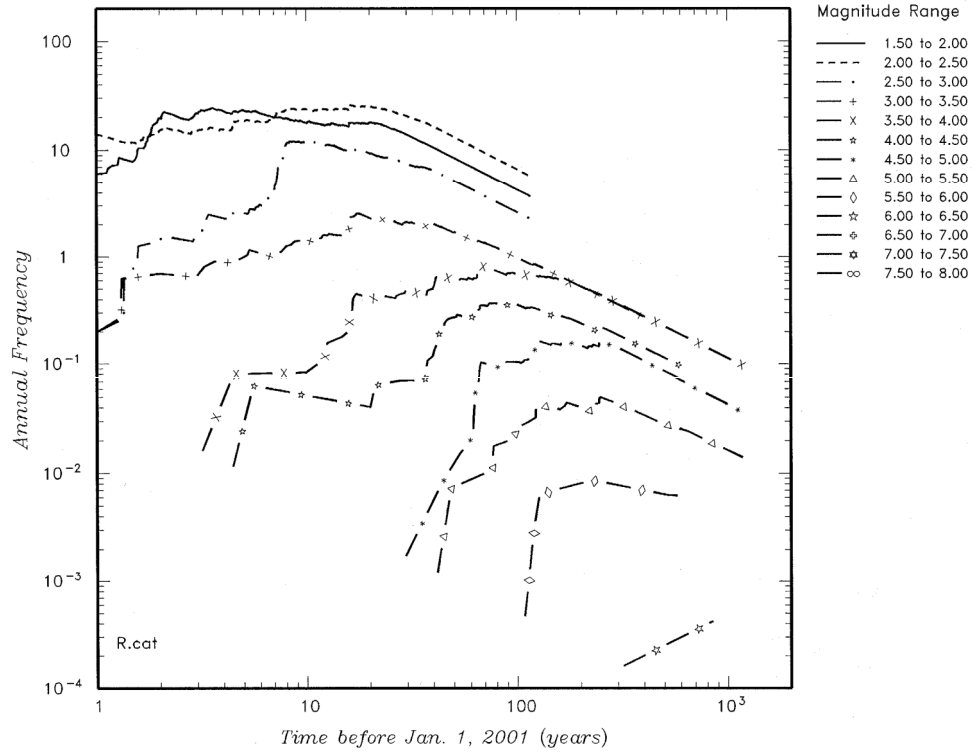
Fig. 28:   Completeness plot for France region (see Fig. 25)
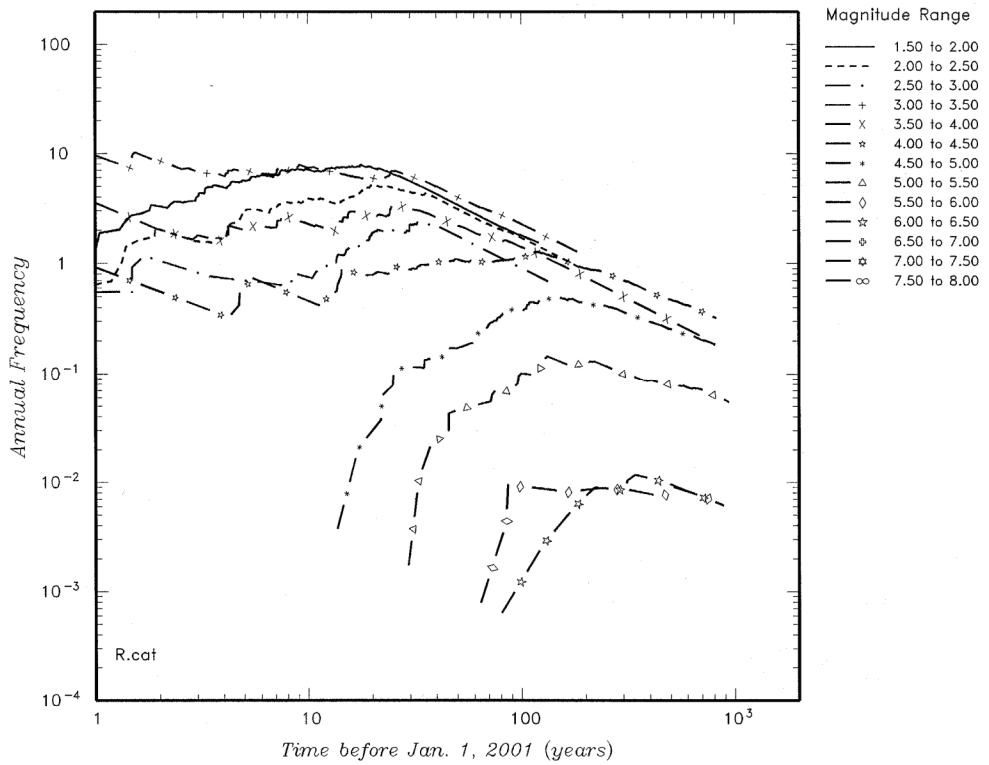
Fig. 29:   Completeness plot for Italy region (see Fig. 25)
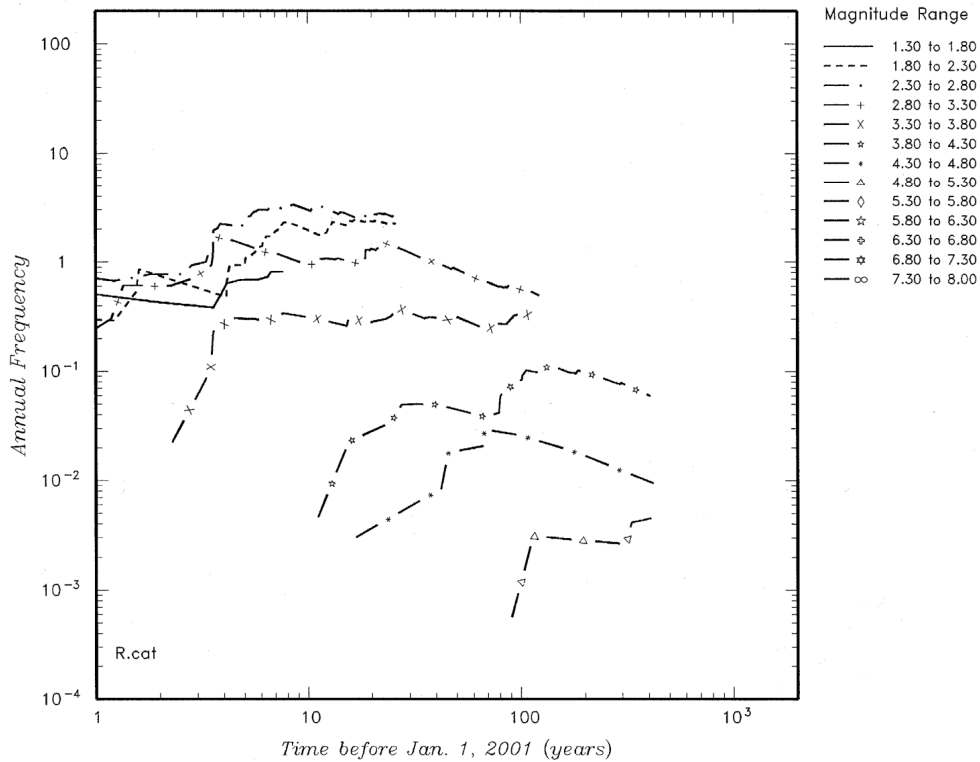
Fig. 30:   Completeness plot for Austria region (see Fig. 25)

Switzerland (Figs. 21 and 26)

Instrumental data:
1984 Ml=1.8   Mw=1.6   digital, high station density
1975 Ml=2   Mw=1.8   analog, lower station density

Macroseismic data (ECOS Table 4.3 and Table 4.7):
1964 Io=IV   Mw=3.1   some instrumental, reevalution in ECOS
1879 Io=V   Mw=3.9   first yearly rep. of Swiss Seismological Comm.
1750 Io=VI   Mw=4.7   except Wallis (1850) and Ticino (1800)
1680 Io=VII Mw=5.4   Wallis and Ticino (1750)

Basel and Alpine foreland:
1300 Io=VIII Mw=6.2
1200 Io=IX   Mw=6.9

Alps:
1500 Io=VIII Mw=6.2
1200 Io=IX   Mw=6.9

Austria (Figs. 22 and 30)

Instrumental:
1975 Ml=3.0 Mw=3.0

Macroseismic:
1900 Io=V   Mw=3.4 from Austrian catalog and Stepp-plot
pre-1900 unknown

Italy (Figs. 23 and 29)

Instrumental:
1975 Mw=3.0 from Stepp-plot

```
Macroseismic:
1900 Mw=4.0 from Stepp-plot
pre-1900 unknown
```

France (E of 5 deg.**)** (Figs. 23 and 28)

```
Instrumental:
1975 Mw=2.5 (given that M(LDG)-Mw = 0.6)
```

```
Macroseismic:
1900 Mw=4.0 from Stepp-plot
pre-1900 unknown
```

Southern Germany (S of 48 deg.- Karlsruhe and LED) (Fig. 22)

```
Instrumental:
1984 Mw=1.5   high station density
1975 Mw=1.8   lower station density
```

Germany (BGR) (Figs. 22 and 27)

```
Instrumental:
1975 Mw=2.5 estimated from catalog info.
```

```
Macroseismic:
1900 Mw=4.0 from Stepp-plot
pre-1900 unknown
```

3.3.2   Completeness assessment of macro zones

The seismicity parameters, which are to be used for hazard computation (a- and b-values, M_{max}) must be defined for each seismic source of the seismogenic zonation (Figs. 4 and 5). However, given the small size of these source zones and the consequent scarce amount of data in many of them, a separate evaluation of catalog completeness for each seismic source is impossible. It is also meaningless, because a given completeness is expected to hold for regions characterized by similar data collection, covering several source areas. For this reason, the completeness analysis was performed for larger regions, referred to as "macro zones" (Fig. 6) and obtained by simplifying the "seismotectonic zones" given in Figure 2. All the following analyses are based on histograms of seismicity rate (Figs. 31 – 36) and on Stepp-plots (Figs. 37 – 48). Even for some of the macro zones, the available data is not sufficient for a reliable assessment of completeness and the corresponding b-values are unreliable as well (section 3.5.1.1). In these cases, the final b-values will rely mainly on evalutions of the larger national catalog zones or on extrapolations from neighboring macro zones (see section 3.5.1.3). As in the previous section, below we list for each zone individual completeness periods, giving the beginning year and the minimum magnitude for each period.

Macro zone A: Apennines (330 events, Figs. 31 and 37)

Catalog seems complete back to the following calendar years:

1975	Mw = 3.2
1976	Mw = 4.2
1800	Mw = 4.8

Given the different de-clustering method and the different binning used in the Stepp-plots, these completeness periods agree reasonably well with the national catalog estimates.

Macro zone B: Po Plain (85 events, Figs. 31 and 38)

There are not enough data in this zone for an estimate of completeness. Because of this fact, the final b-value for this zone will rely heavily on results from the analysis of the whole Italian catalog (see section 3.5.1.3).

Macro zone C: Western Alps, including southern Valais (1183 events, Figs. 32 and 39)

The earthquakes in this zone are compiled from three different catalogs (Swiss, French and Italian). This leads to a space heterogeneity which manifests itself in the Stepp-plot as a reversal of the order of the curves for the various magnitude bins over time periods for which the curves are more or less horizontal. Note that the 1.65 bin is lower than the 2.05 bin, the 2.85 bin is lower than the 3.25 bin, the 3.65 bin is lower than the 4.05 bin, and finally, the 4.45 bin is at an approximately equal level to the 4.45 bin. Part of the inconsistency could also be due to magnitude errors. Based on the available data, it is not possible to assess the completeness. Consequently, the b-value for a zone with this geometry will have a large uncertainty.

Macro zone D1: Northern Alps, including Haute Savoie (2172 events, Figs. 32 and 40)

Catalog seems complete back to the following calendar years:

1980 Mw = 1.5
1975 Mw = 1.9
1965 Mw = 2.3
1880 Mw = 3.1
1700 Mw = 4.7

Despite the fact that the earthquakes in the Haute Savoie (zone D1b, see Fig. 5) are from the French catalog, while the rest is mainly from the Swiss catalog, the Stepp-plot looks reasonable. The completeness estimated from the Stepp-plot is more optimistic than that estimated by the compilers of ECOS.

Macro zone D2D3: Central and eastern Alps (1683 events, Figs. 33 and 41)

This zone comprises data from the Swiss catalog (Ticino and Graubünden) and from a combination of the Austrian, Italian and BGR catalogs. The very different cut-off magnitude inherent in these catalogs shows up again in the Stepp-plot in form of a higher seismicity level for the magnitude 3.25 bin, compared to the 2.85 bin. Therefore, a uniform assessment of completeness is not possible for this zone, based on the available data, and the corresponding b-value will have a large uncertainty.

Macro zone D4: Southern Alps (244 events, Figs. 33 and 42)

1860 Mw = 4.0

Most of this zone is covered by the Italian catalog, with some contributions of the Swiss catalog particularly for the instrumental period.

Macro zone E1: Massif Central (28 events, Figs. 34 and 43)

There are not enough data in this zone for an estimate of completeness. As for marcrozone B, the final b-value for this zone will have to rely on an extrapolation from neighboring zones.
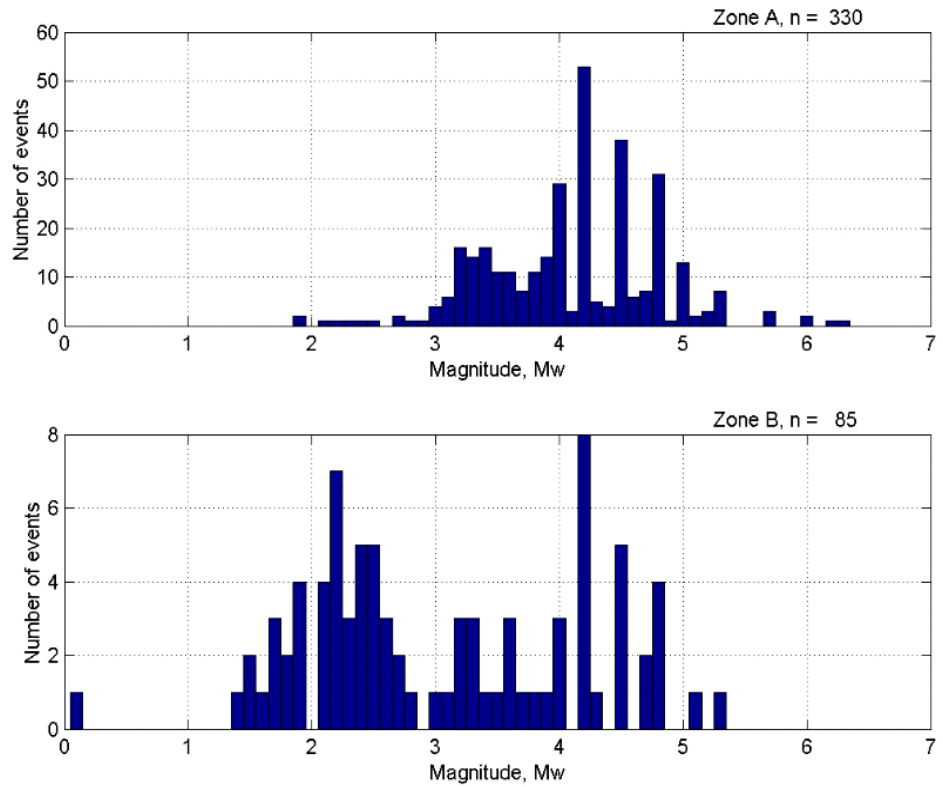
Fig. 31:   Analysis of the catalog contents for the macro zones
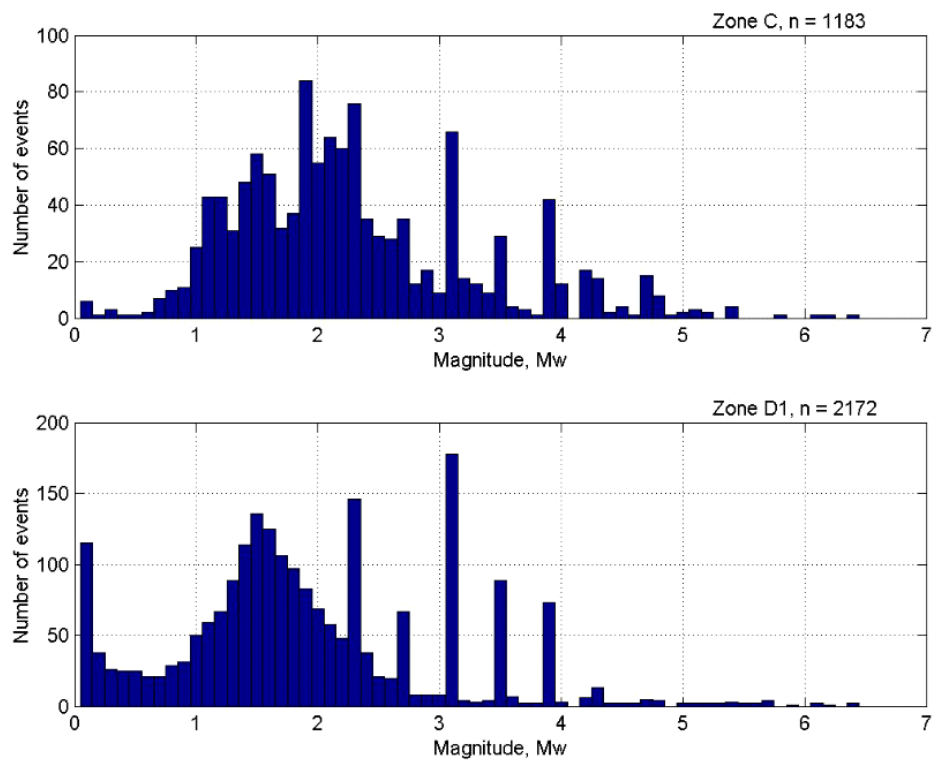
Fig. 32:   Analysis of the catalog contents for the macro zones
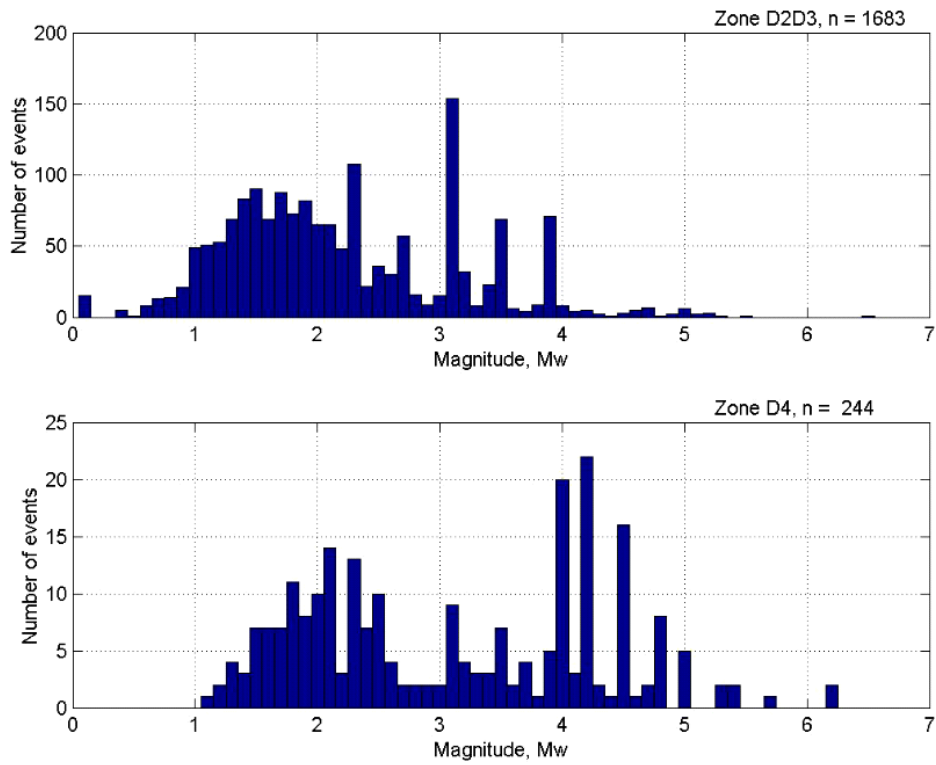
Fig. 33:   Analysis of the catalog contents for the macro zones
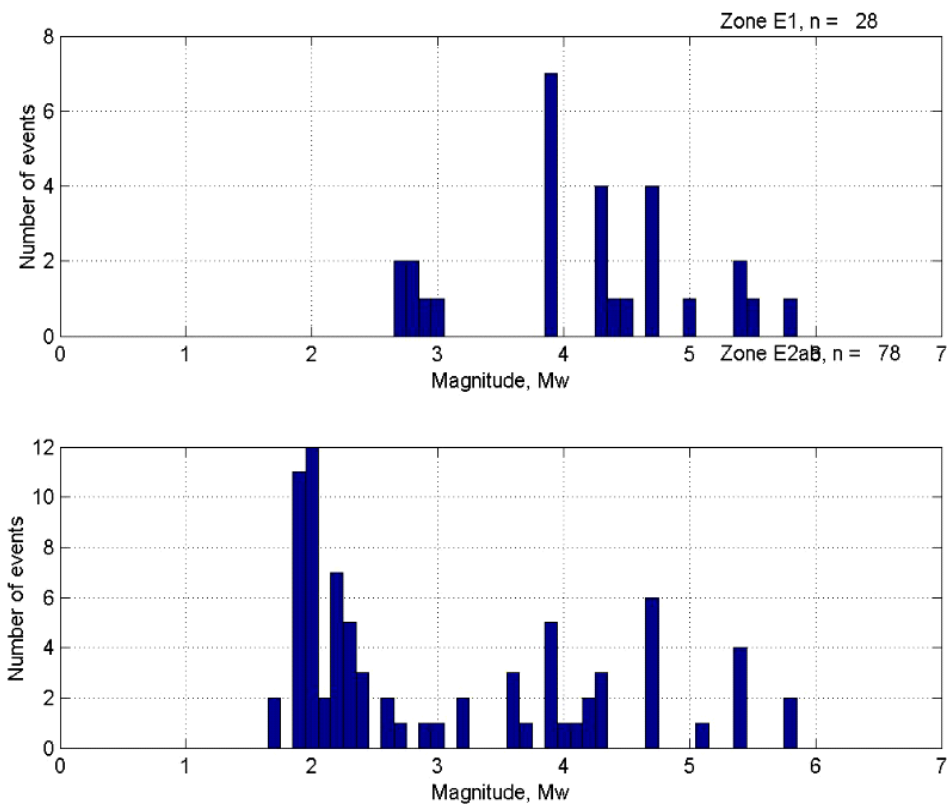
Fig. 34:   Analysis of the catalog contents for the macro zones
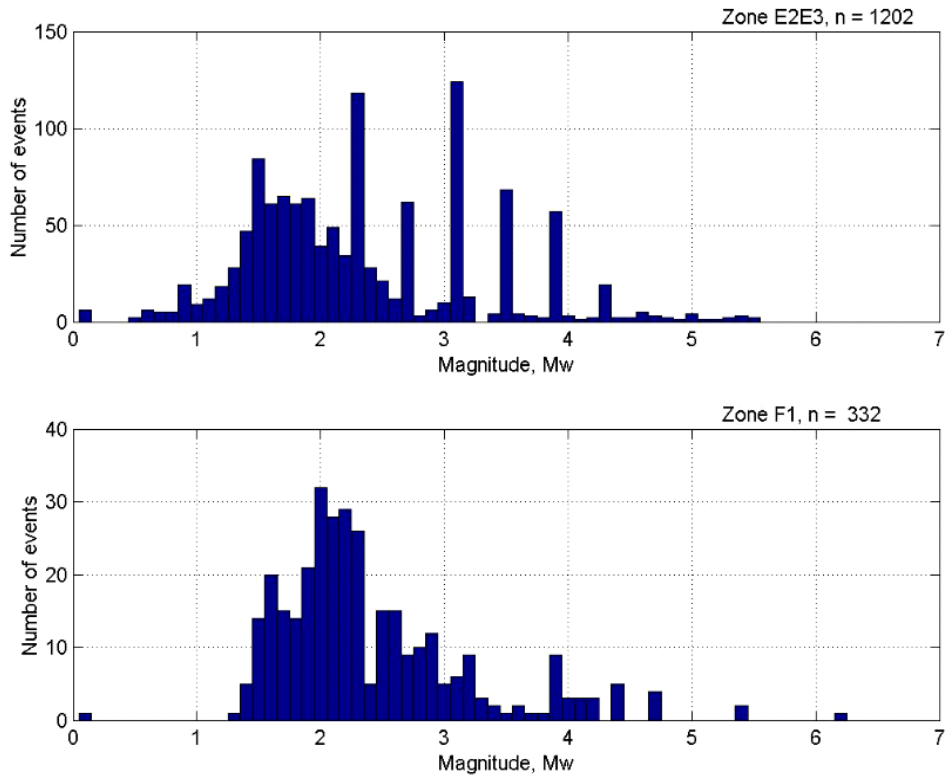
Fig. 35:   Analysis of the catalog contents for the macro zones
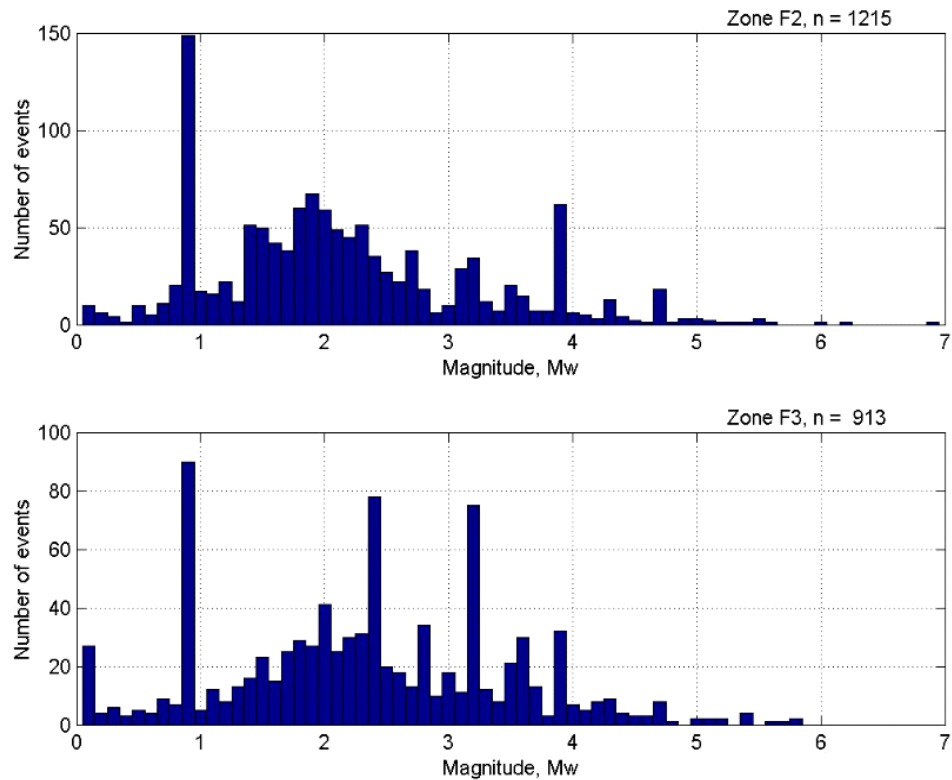
Fig. 36:   Analysis of the catalog contents for the macro zones
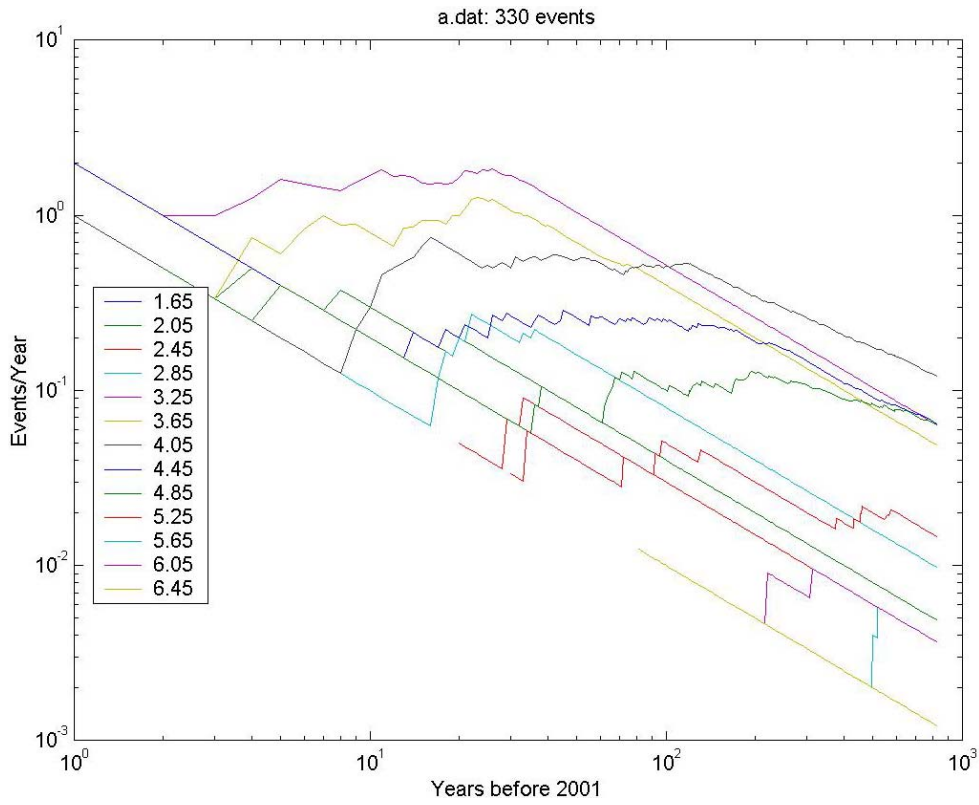
Fig. 37:   Stepp plot for macro zone A
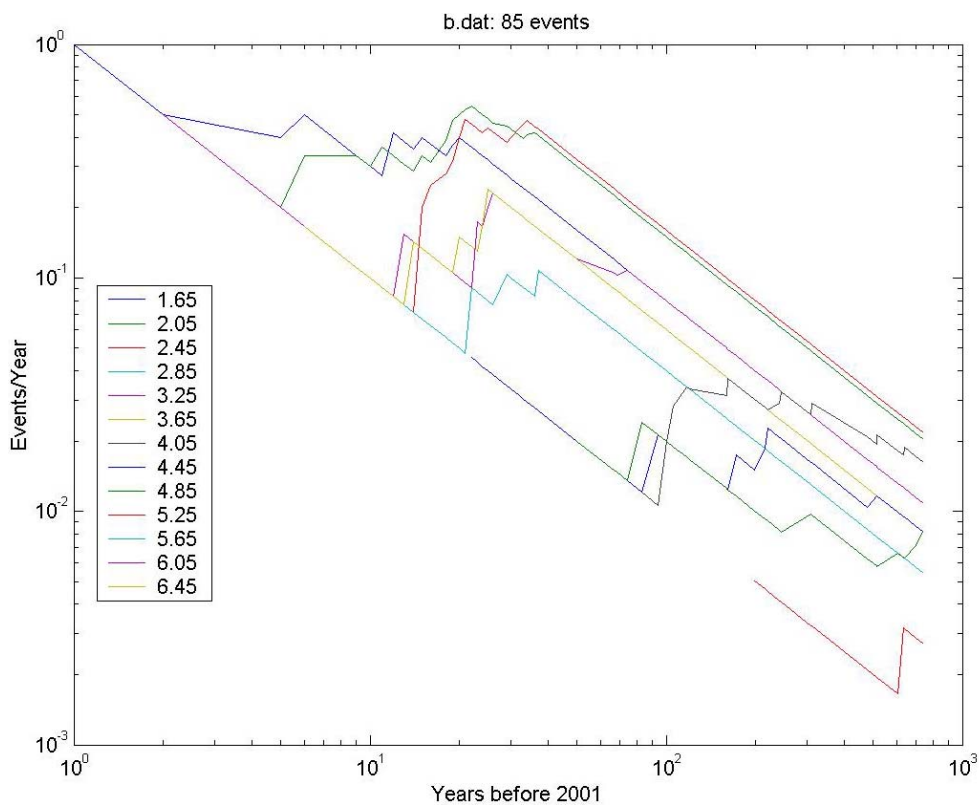
Fig. 38:   Stepp plot for macro zone B
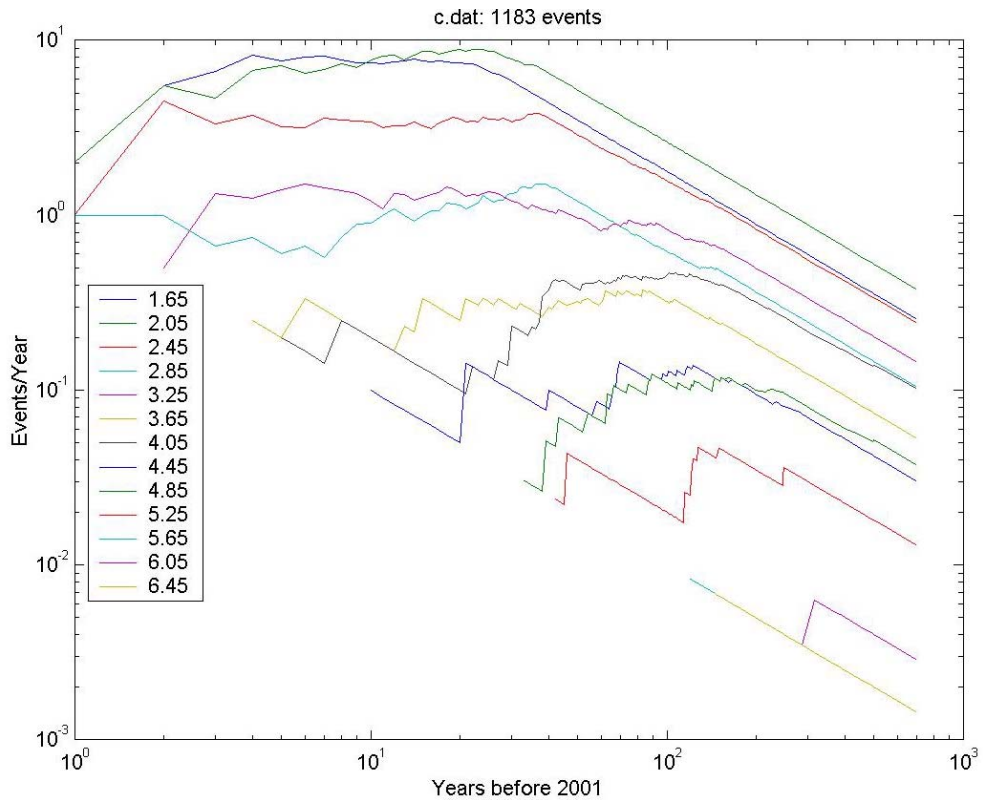
Fig. 39:   Stepp plot for macro zone C
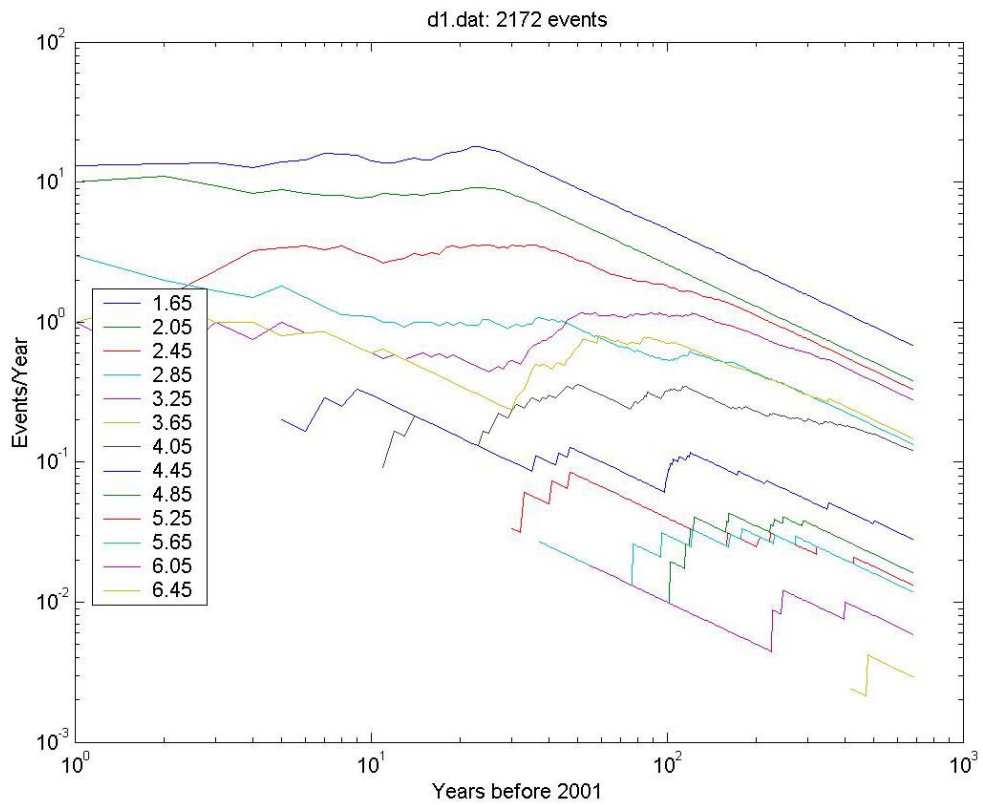
Fig. 40:   Stepp plot for macro zone D1
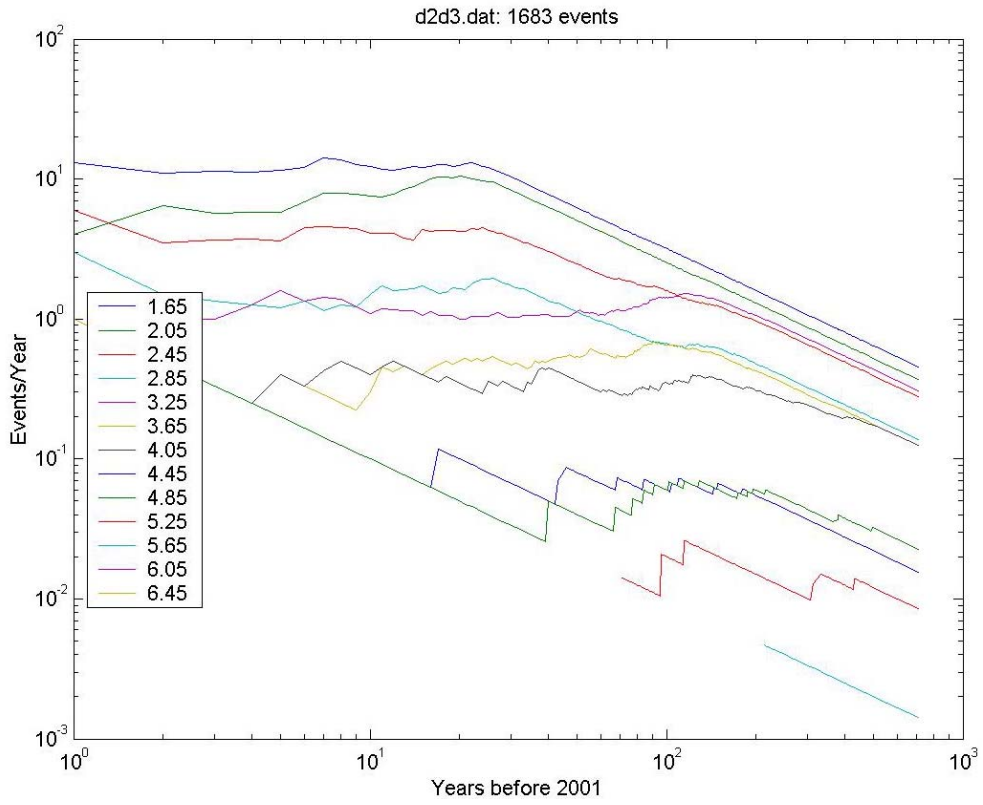
Fig. 41: Stepp plot for macro zone D2-3
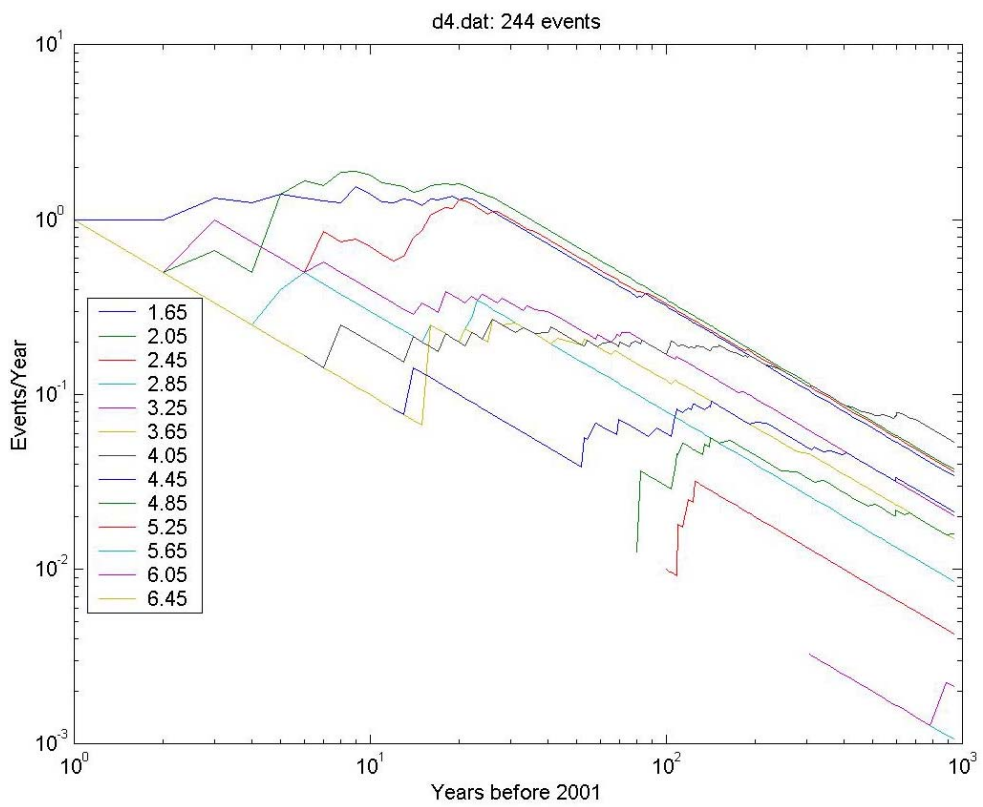
Fig. 42: Stepp plot for macro zone D4
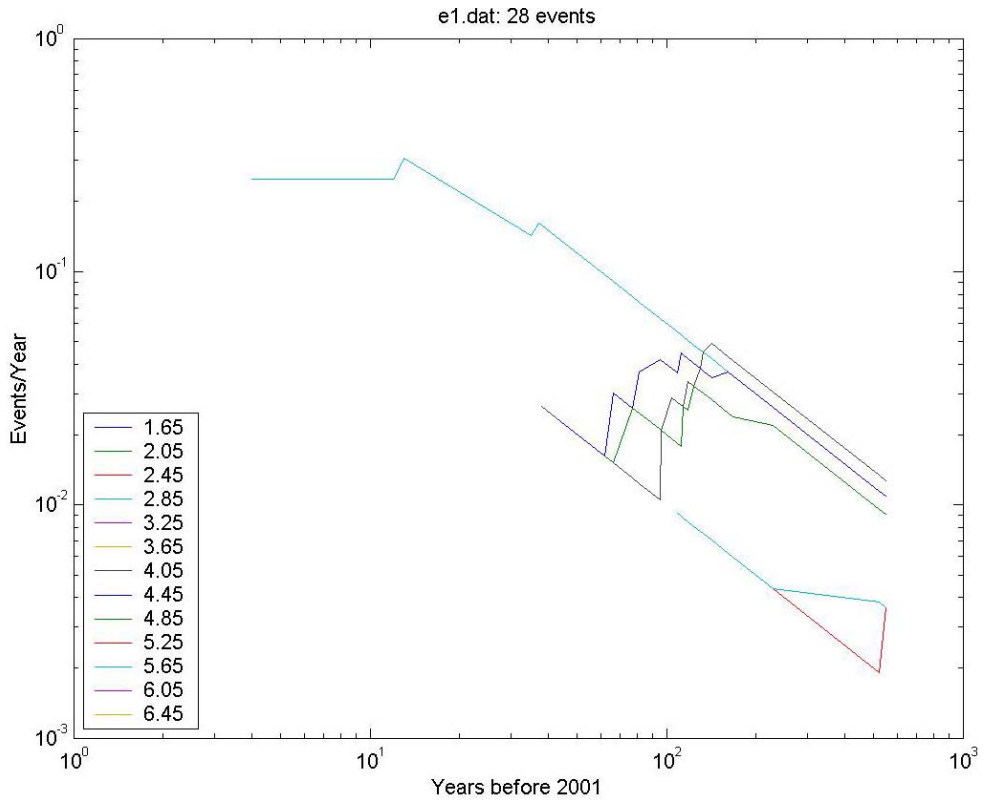
Fig. 43:   Stepp plot for macro zone E1
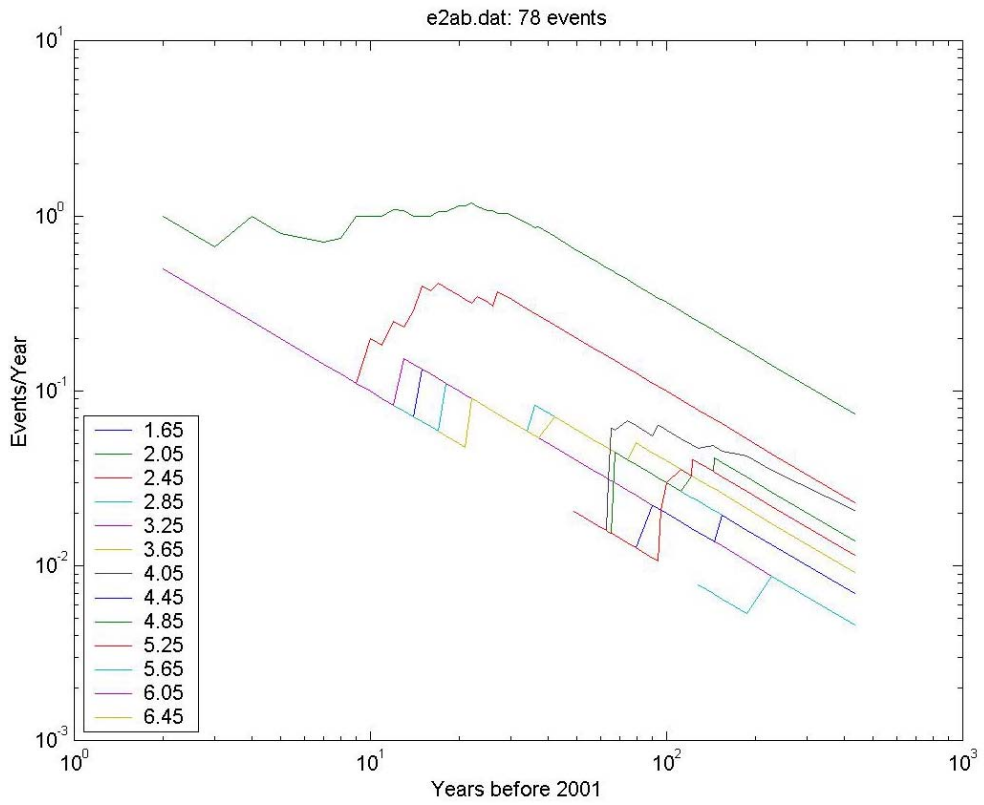
Fig. 44:   Stepp plot for macro zone E2ab
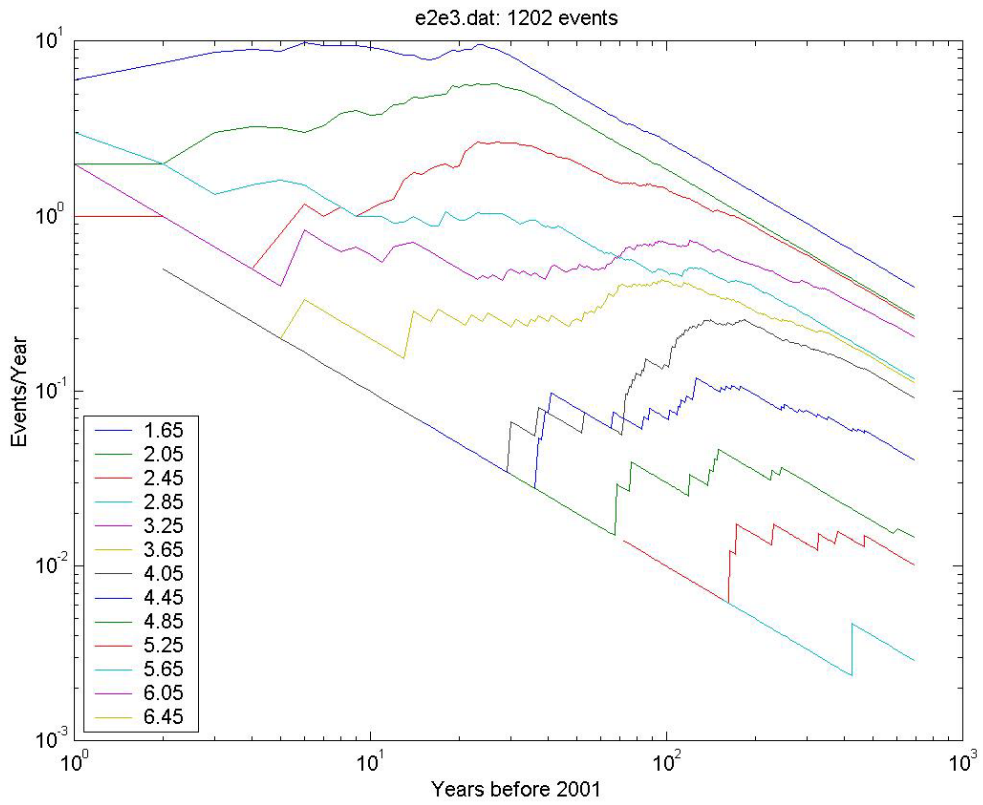
Fig. 45:   Stepp plot for macro zone E2-3
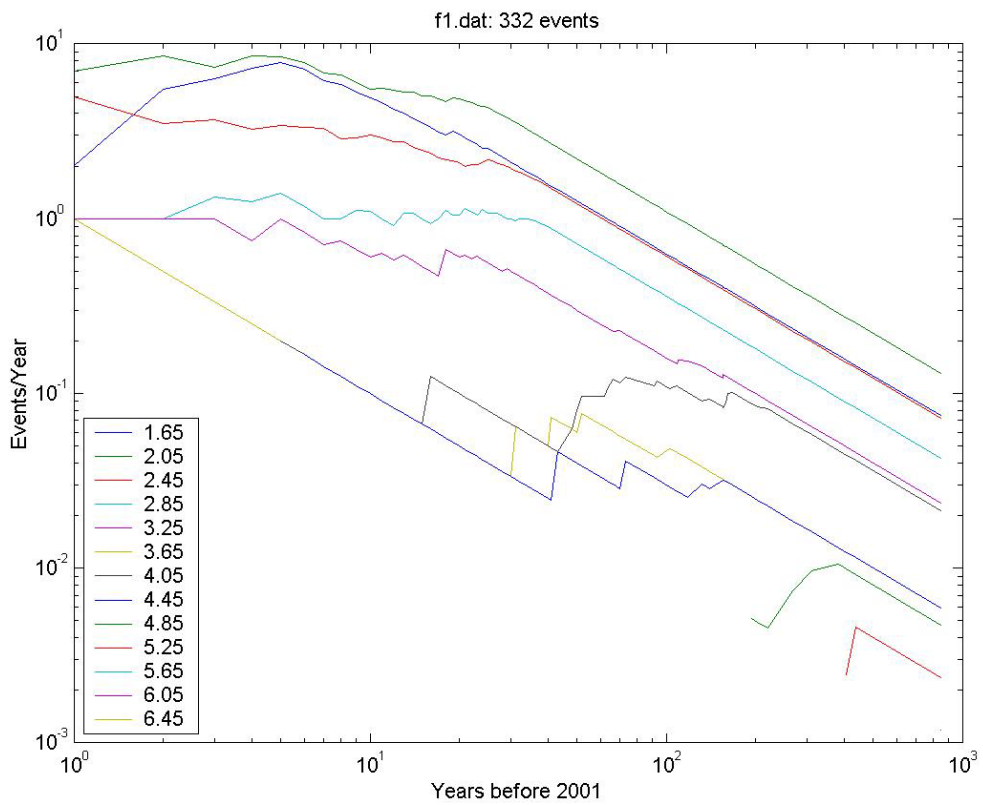
Fig. 46:   Stepp plot for macro zone F1
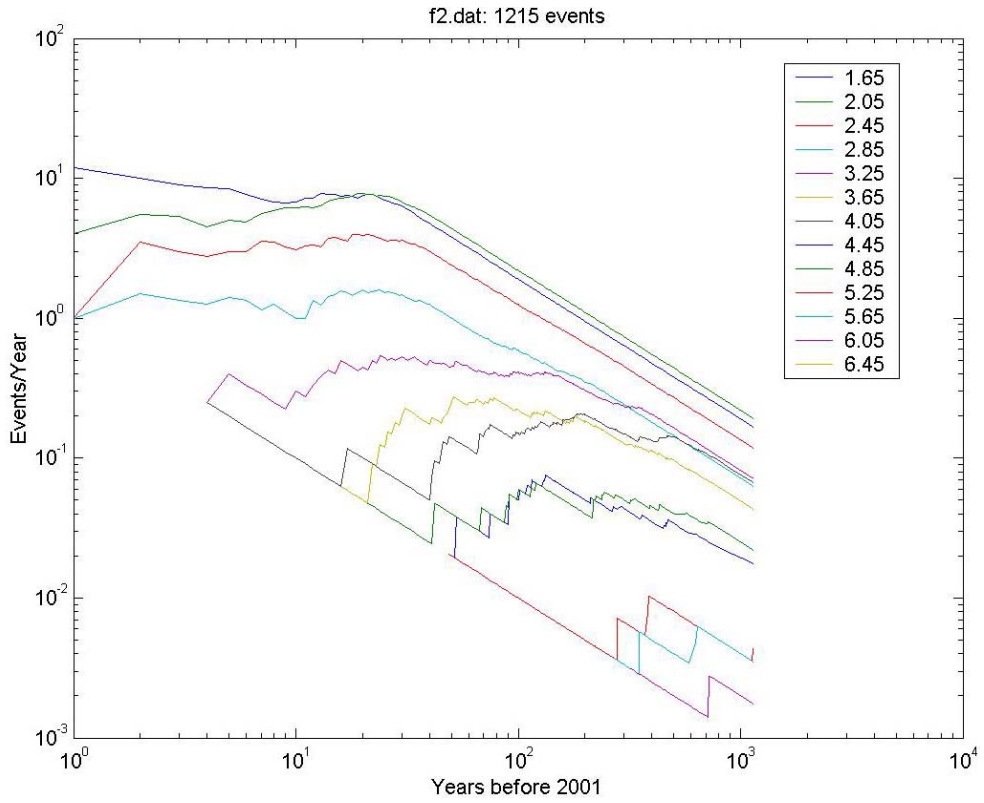
Fig. 47:   Stepp plot for macro zone F2
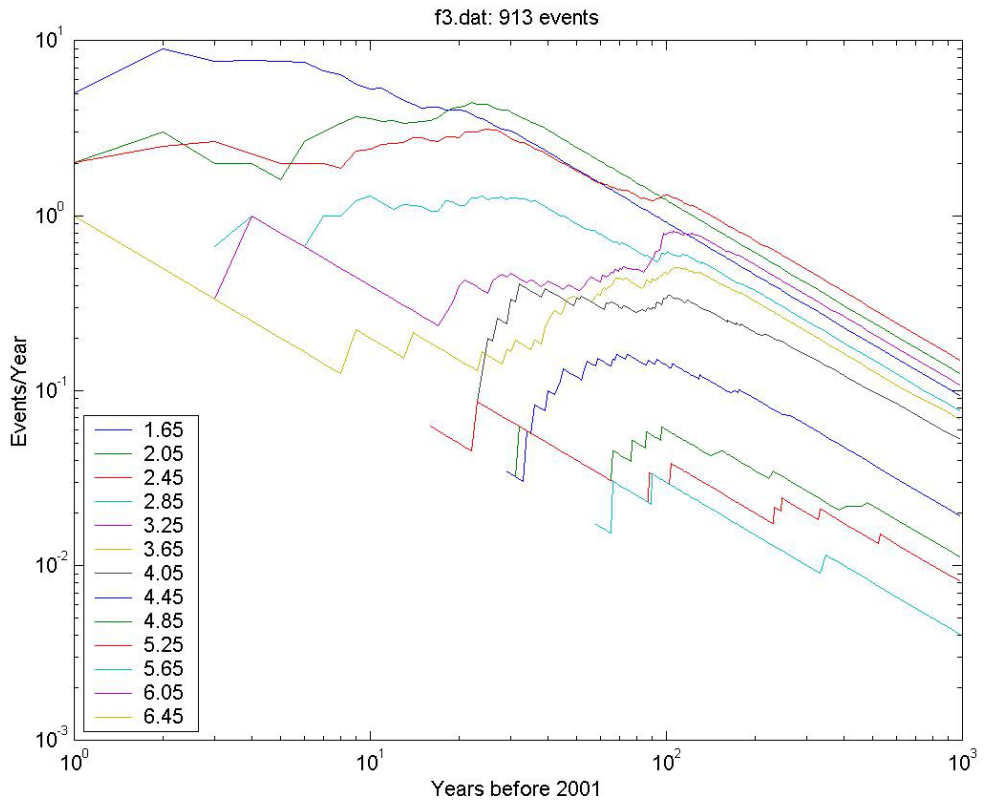
Fig. 48:   Stepp plot for macro zone F3

Macro zone E2-3: Northern Alpine foreland (1202 events, Figs. 35 and 45)

Catalog seems complete back to the following calendar years:

1978 Mw = 1.5
1975 Mw = 1.9
1970 Mw = 2.3
1880 Mw = 3.1 (Io = IV)
1820 Mw = 3.9 (Io = V)
1800 Mw = 4.7 (Io = VI)
1600 Mw = 5.1

For this analysis, the macro zone E2-3 did not include the Bresse Graben (zone E2ab, see below). The western part of this macro zone comprises area E2c which is covered mainly by the French catalog. The rest, i.e. the eastern part, is covered by the Swiss catalog. Since the French catalog has a cut-off at Ml(LDG) = 2.5, which corresponds to Mw = 1.9, this leads to some spatial heterogeneity for magnitudes Mw < 2. However, the Stepp-plot seems to behave reasonably well, hence this zone should give reliable b-value estimates. The completeness estimated from the Stepp-plot is more optimistic than that estimated by the compilers of PEGASOS.

Macro zone E2ab: Bresse (78 events, Figs. 34 and 44)

In a first step, this macro zone was regarded as a separate one. However, there are not enough data for an estimate of completeness. Subsequently for the assessment of the b-value, this zone was included into macro zone E2-3.

Macro zone F1: Paris Basin, Lower Rhinegraben (332 events, Figs. 35 and 46)

Catalog seems complete back to the following calendar years:

1970 Mw = 2.7
1850 Mw = 4.0

This zone is covered by the French (LDG) and the German (BGR) catalogs. Below Mw = 2.7 the Stepp-plot curves do not reach a plateau for any time period.

Macro zone F2: Rhinegraben and Basel (1215 events, Figs. 36 and 47)

Catalog seems complete back to the following calendar years:

1975 Mw = 2.3
1880 Mw = 3.1
1800 Mw = 3.9
1750 Mw = 4.7

This zone is covered by five different catalogs (SED, LDG, BGR, LED and Karlsruhe) and extends over a very large area. The completeness of zones F2a (in the SW) and F2c (to the N) is certainly not as good as that in the southern part of the Rhinegraben and around Basel. Therefore, the lower cut-off for completeness (Mw = 2.3) is relatively high. Again, the estimate of completeness for Mw = 3.1 and 3.9 is more optimistic than that of the compilers of PEGASOS.

Macro zone F3: Southwestern Germany (913 events, Figs. 36 and 48)

Catalog seems complete back to the following calendar years:

1975 Mw = 2.4
1960 Mw = 2.8
1890 Mw = 3.2

Given the instrumental coverage of the eastern flank of the Rhinegraben (zone F3a) after 1975, the completeness would be better in this part of macro zone F3. However for the whole macro zone, given the heterogeneity of the database (BGR, LED and Karlsruhe), the cut-off at Mw = 2.4 is more realistic.

3.4   Strain rate, fault slip rate and paleoseismic data

No data on strain rate and fault rate are available within the area of interest. Strain rates, as expected from the estimations of plate convergence rates based on geological reconstructions and plate tectonic constraints, are very low. As a consequence, no unequivocal GPS-data are available yet. Also, we do not know how displacements and/or strains are partitioned within the area of investigation.

A limited amount of data is available from paleoseismological investigations (Swiss Seismological Service 2002). Regarding the Basel area, a combination of investigations based on trench data, paleothems, lake deposits and rockfalls suggests that 6 events between magnitudes 6 and 7 have occurred within the last 12'000 years. The trench data provide the most complete set of events. The estimates of the magnitudes attributed to these events (see Swiss Seismological Service PALEOSEIS, their table 3) are questionable, however, because we have doubts that the Reinach fault is an active fault scarp. The evidence from the colluvial wedges, however, indicates a periodicity of "events", which are likely to have been induced by earthquakes, regardless of the interpretation of the features seen in the trench (gravitational slide induced by seismic event vs. active fault scarp). Three out of the six events can be correlated with the data obtained by other methods in the area.

In summary, it is likely that 3-6 "strong" events did occur within the last 12'000 years. These "strong" or "Basel-type" earthquakes are estimated to have a magnitude between 6 and 7.

Taking a time span of 12 000 years and 6 events (there might have been more which remained undetected!) a minimum recurrence rate of 2000 years is calculated for the magnitude 6-7 range. This estimate will be used in order to constrain the information gathered from the earthquake catalog, where only one event of similar size is reported (the first record in the catalog is dated 250 A.D.).

Paleoseismological data are also available from lake research in Central Switzerland (Swiss Seismological Service PALEOSEIS 2002). However, no estimates of magnitude are available for these data at this stage. Hence, these data cannot yet provide additional constraints in comparison to the magnitude-frequency relationships deduced from the earthquake catalog at this stage.

3.5   Magnitude – frequency relationships

Similar to the analysis on catalog completeness described in chapter 3.3, the assessment of the parameters of the magnitude vs. frequency (Gutenberg - Richter: GR) relation (a- and b-values) is also performed on the basis of larger areas, as compared to the seismic sources defined in Figures 4 and 5. Hence, the macro zones (Fig. 6), previously used for investigating catalog completeness, are now considered again for calculating a- and b-values. Generally, a smooth variation of seismicity in space is accepted, i. e. neighbouring areas with similar tectonic style are generally characterised by similar b-values and maximum magnitudes (M_{max}). As the source zones are rather small and, often, characterized by a small number of earthquakes, where any statistical analysis is, consequently, weak, we decided to determine the b-values for larger macro zones. These are assumed to have common seismotectonic characteristics. The a-values, however, will be computed separately for each individual source zone in order to account for its specific seismicity rate. The a- values derived from macro zones (see Table 7) will only be used for maximum magnitude calculations.

3.5.1   Evaluation of b-values

As mentioned earlier, we regard our seismic source areas to be too small for evaluation of b-values. Therefore we will evaluate b-values according to two alternative approaches for larger areas. In a first approach we will evaluate them for the macro zones whose boundaries follow a seismic source zone rationale. Then we evaluate b-values for national catalog zones, because we want to assess the effects of mixing different national catalogs. The b-values will then be compared and a set of b-values, that also includes information from analysing national catalog boundaries, will finally be proposed for all macro zones.

3.5.1.1   Evaluation of b-values for the macro zones

The PEGASOS catalog, modified according to the analysis documented in chapter 3.1, has been de-clustered according to the Gardner & Knopoff (1974) approach and using the parameters proposed by Grünthal for the European region. This new and modified catalog version, archived under the designation TP1-CAT-0009, is considered to be the most suitable product for hazard purposes by the SP1a team. Hence it is used for all the following computations (a- and b-values, M_{max}).

The methodology described in the previous chapter 3.2.1. was also applied to the 11 macro zones (MZs) that are defined in Figure 6. More precisely, sub-catalogs have been extracted for each MZ from the de-clustered PEGASOS catalog. Seismicity rates have been computed according to the Albarello & Mucciarelli (2002) approach. As pointed out previously, the Albarello & Mucciarelli (2002) approach evaluates the probability that each 5-year segment of the catalog is complete and weights this accordingly in the global seismicity rate assessment on a statistical basis. It is not, therefore, very sensitive on the completeness of the individual national catalogs contributing to the PEGASOS catalog. The b-values have been estimated with both the least-square (LS) and the maximum-likelihood (ML) approaches with the estimated seismicity rates. As the rates computed according to the Albarello & Mucciarelli (2002) approach are based on the whole catalog data, the time period covered by each sub-catalog has been considered as complete and it enters into the estimation of the b-value standard deviation. The differences in the initial dates of the sub-catalogs are limited and can be checked in Table 7. An exception to this rule has been applied only for the magnitude 6.9 class (Basel earthquake), where the paleoseismological information has been used, indicating one event every 2000 years (see chapter 3.4). The number of earthquakes treated in each MZ varies strongly from one MZ to another and conditions the quality of the results obtained. In particular, MZ E1 only collects 28 earthquakes and MZ B collects 85 events. For these MZs the quality of the results is questionable. All the other MZs have more than 240 earthquakes, and in 5 cases their number exceeds 1000.

An 0.3 interval in magnitude has been considered for the calculation of seismicity rates: they are associated to the average magnitude value of the interval. The most delicate part of the procedure was the choice of the minimum magnitude considered: it determines the number of seismicity rates used for the b-value estimation. A first trial was done by choosing all the data from the magnitude with the highest seismicity rate associated (this could be the minimum complete class). When a large difference was encountered between the b-values calculated by using the LS and ML approaches, respectively, a threshold magnitude was introduced by an evaluation of the seismicity rate graphs "by eye" (see Figs. 49 to 59). As can be seen from these figures the seismicity rates show a nice linear alignment only in the case of macro zones D1 and F1, for which no introduction of a magnitude threshold is needed, the resulting b-value being well constrained. In some other cases the difference is notable, but sometimes the choice of the magnitude threshold is questionable (see e.g.: MZ B in Fig. 50).

As pointed out in the previous chapters, there could be a bias in the magnitude values between historical and instrumental periods in the PEGASOS catalog. In order to account for this possibility, a separate analysis has been performed for the two periods for all the macro zones.

The results thus obtained are reported in Table 7. In the following we will discuss details concerning the individual macro zones:

Macro zone A. The fit obtained for this macro zone looks fair (Fig. 49a) when a threshold magnitude 3.8 is introduced (b-value = 0.99) and no differences are encountered when separating historical and instrumental periods (Fig. 49b). The b-value for these periods varies between 0.92 and 0.91. The LS fit is close enough to the ML fit in all cases (the maximum difference is 0.14). An average b-value of 0.96, obtained from the different estimates can be suggested as representative for this macro zone.

Macro zone B. No reasonable solution is found for this macro zone (Fig. 50a), even when a magnitude threshold of 3.2 is introduced. This is due to the low number of earthquakes in this macro zone. The instrumental seismicity shows a completely different behaviour when compared to historical seismicity (Fig. 50b). No bias in magnitude can be invoked in this case because the events in this MZ come from the Italian catalog. The explanation is that the Italian catalog predominantly lists events exceeding Ms magnitude 4. Hence, it is proposed to use the b-value computed from the historical period.

Tab. 7:   Seismicity parameters for the MZs

MZ	Start	Neqs	Mo	Mx	LSa	LSσa	LSb	LSσb	MLa	MLb	MLσb
A	1182	340	3.2	6.3	3.67	0.17	0.95	0.04	3.18	0.82	0.01
A			3.8	6.3	3.91	0.24	0.99	0.05	3.91	0.99	0.02
Ah			3.8	6.3	3.81	0.26	0.96	0.05	3.62	0.92	0.02
Ai			3.2	4.9	4.06	0.31	1.05	0.08	3.52	0.91	0.09
B	1268	85	2.0	5.3	1.44	0.18	0.70	0.05	1.00	0.56	0.02
B			3.2	5.3	2.33	0.26	0.90	0.06	1.86	0.78	0.05
Bh			4.1	5.3	3.30	0.53	1.09	0.11	3.00	1.02	0.15
Bi			1.7	4.6	1.34	0.16	0.62	0.05	1.07	0.52	0.06
C	1311	1181	2.0	6.4	2.75	0.09	0.79	0.02	2.47	0.70	0.01
C			3.2	6.4	3.06	0.13	0.85	0.03	2.79	0.78	0.02
Ch			3.5	6.4	3.40	0.19	0.90	0.04	3.08	0.82	0.02
Ci			1.4	4.6	2.82	0.14	0.89	0.04	2.44	0.72	0.02
D1	1322	2136	1.4	6.4	2.50	0.07	0.73	0.02	2.52	0.74	0.00
D1h			2.9	6.4	2.72	0.20	0.76	0.04	2.79	0.77	0.01
D1i			1.4	4.6	2.86	0.10	0.90	0.03	2.78	0.86	0.02
D2-3	1295	1683	1.4	6.5	3.01	0.18	0.92	0.04	2.29	0.65	0.00
D2-3			2.9	6.5	3.69	0.30	1.05	0.06	3.07	0.88	0.01
D2-3h			2.9	6.5	3.69	0.31	1.05	0.06	3.07	0.87	0.01
D2-3i			1.4	4.9	2.86	0.11	0.85	0.03	2.58	0.73	0.02
D4	1065	244	2.3	6.2	2.33	0.25	0.78	0.05	1.47	0.53	0.01
D4			4.1	6.2	3.89	0.48	1.07	0.09	3.58	1.01	0.05
D4h			4.1	6.2	4.07	0.52	1.10	0.10	3.57	0.99	0.05
D4i			2.0	4.6	1.97	0.22	0.68	0.07	1.70	0.59	0.05

MZ	Start	Neqs	Mo	Mx	LSa	LSσa	LSb	LSσb	MLa	MLb	MLσb
E1	1450	28	2.6	5.8	0.78	0.33	0.53	0.08	0.17	0.36	0.03
E1			3.8	5.8	2.38	0.53	0.85	0.11	1.62	0.68	0.08
E2-3	1313	1281	1.7	5.8	2.47	0.13	0.75	0.03	2.41	0.74	0.01
E2-3h			3.5	5.8	3.30	0.47	0.90	0.10	2.89	0.81	0.02
E2-3i			1.7	4.6	2.94	0.12	0.97	0.04	2.75	0.90	0.04
F1	1155	331	2.0	6.2	2.56	0.13	0.92	0.03	2.39	0.85	0.01
F1h			3.8	6.2	2.60	0.41	0.92	0.08	3.24	1.06	0.08
F1i			2.0	4.6	2.77	0.12	0.94	0.04	2.81	0.95	0.05
F2	858	1213	1.7	6.9	2.79	0.08	0.89	0.02	2.57	0.82	0.00
F2h			3.5	6.9	3.34	0.15	0.98	0.03	3.00	0.90	0.02
F2i			1.7	4.8	2.94	0.16	0.97	0.05	2.86	0.92	0.03
F3	1021	911	2.0	5.8	2.45	0.10	0.74	0.02	2.10	0.62	0.01
F3			3.2	5.8	2.96	0.09	0.84	0.02	2.75	0.79	0.02
F3h			3.2	5.8	3.33	0.18	0.91	0.04	3.03	0.83	0.01
F3i			1.7	5.2	2.34	0.14	0.77	0.04	2.45	0.80	0.03

MZ	macro zone,
Start	initial year of the sub-catalog,
Neqs	number of earthquakes in the sub-catalog,
Mo	minimum magnitude,
Mx	maximum observed magnitude,
LSa	a-value from LS,
Lσsa	error on a-value from LS,
LSb	b-value from LS,
LSσb	error on b-value from LS,
MLa	a-value from ML,
MLb	b-value from ML,
MLσb	error on b-value from ML.
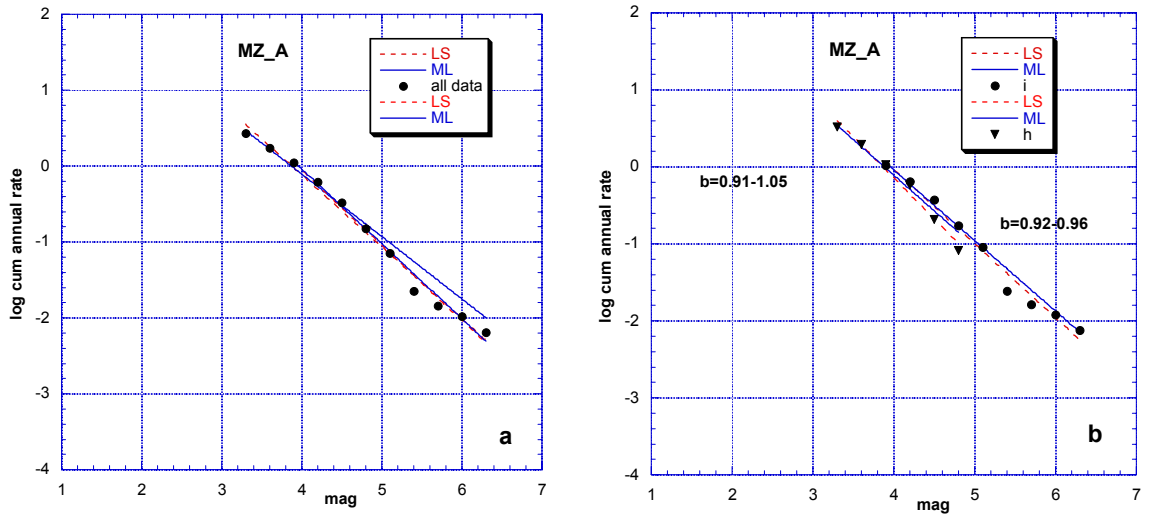
Fig. 49:   MZ A: a) all data; b) historical (h) and instrumental (i) periods
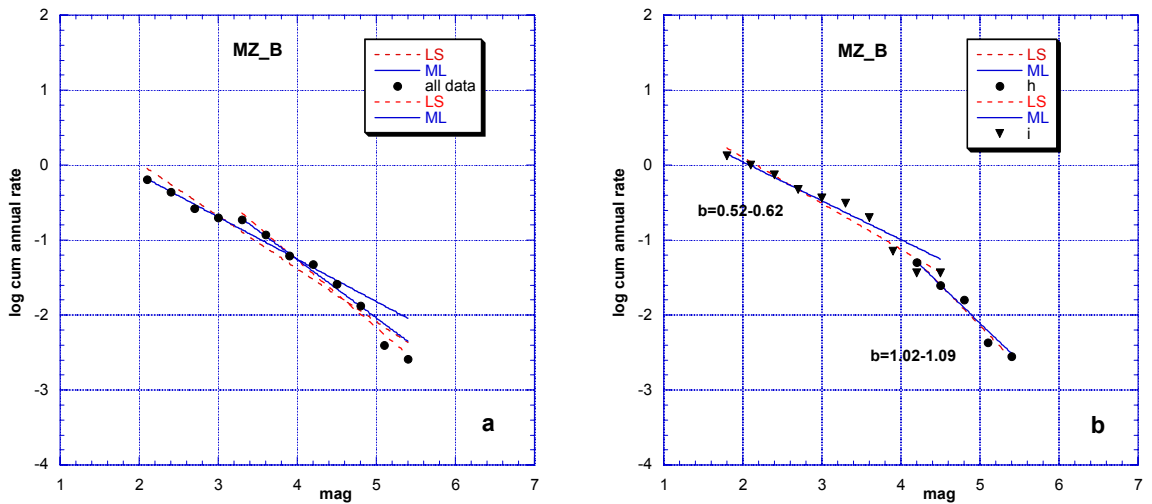
Fig. 50:   MZ B: a) all data; b) historical (h) and instrumental (i) periods
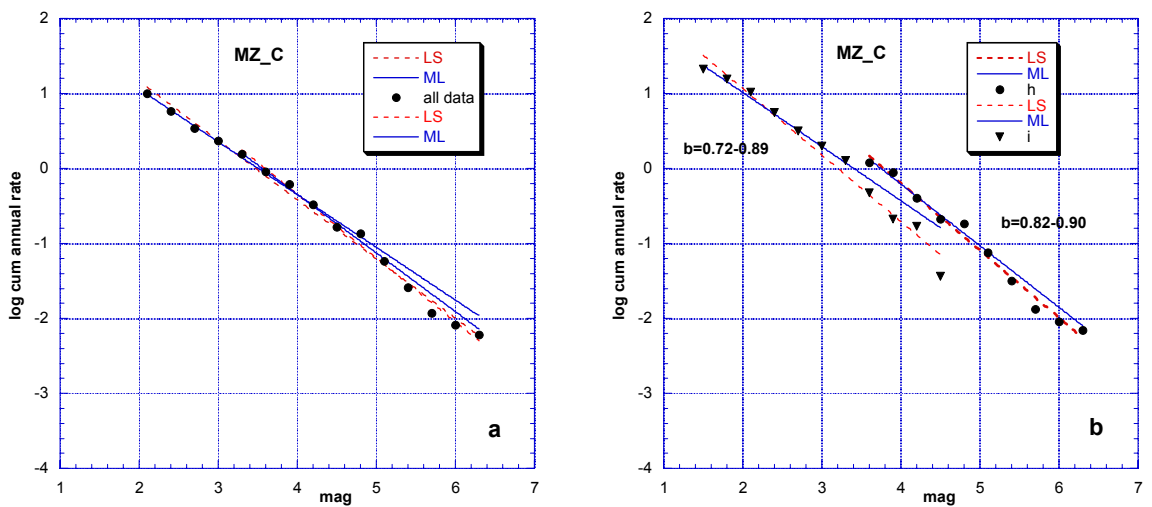
Fig. 51:   MZ C: a) all data; b) historical (h) and instrumental (i) periods
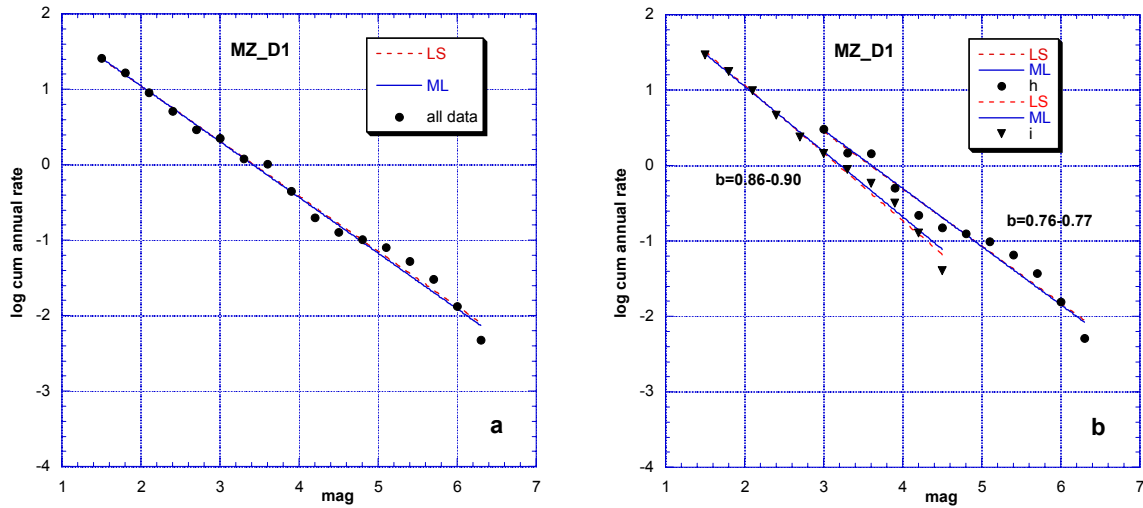
Fig. 52: MZ D1: a) all data; b) historical (h) and instrumental (i) periods
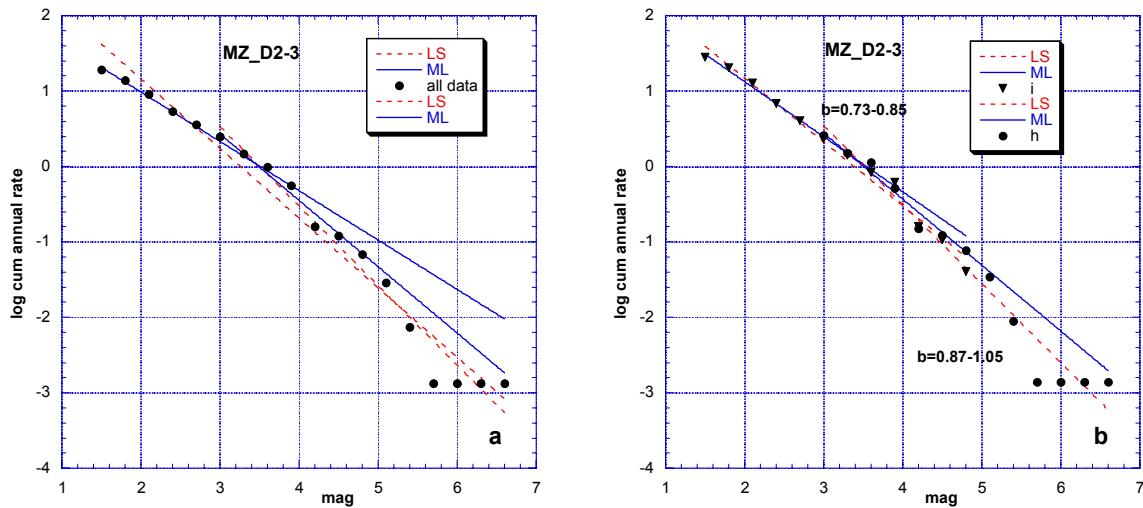
Fig. 53: MZ D2-3: a) all data; b) historical (h) and instrumental (i) periods
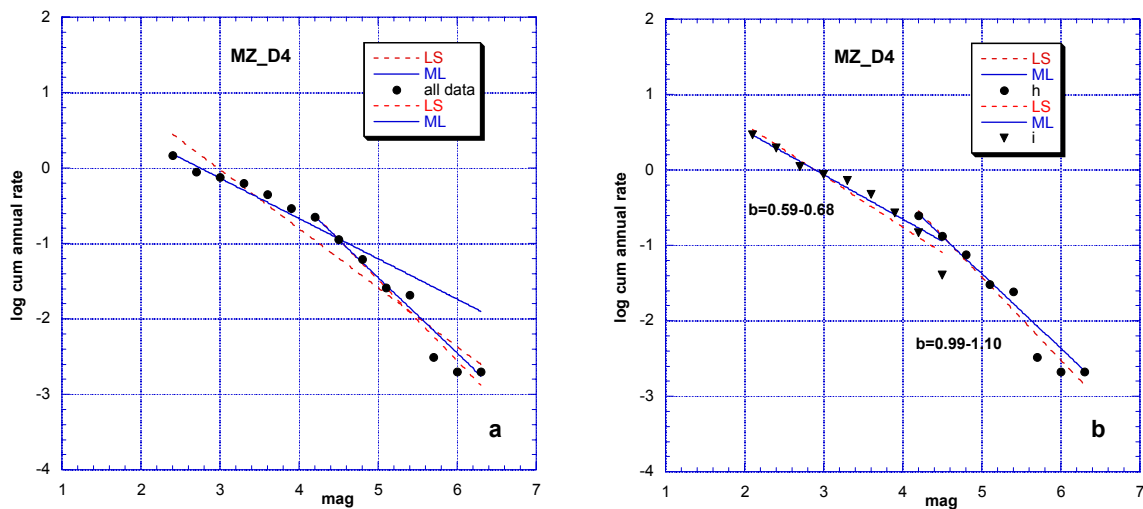
Fig. 54: MZ D4: a) all data; b) historical (h) and instrumental (i) periods
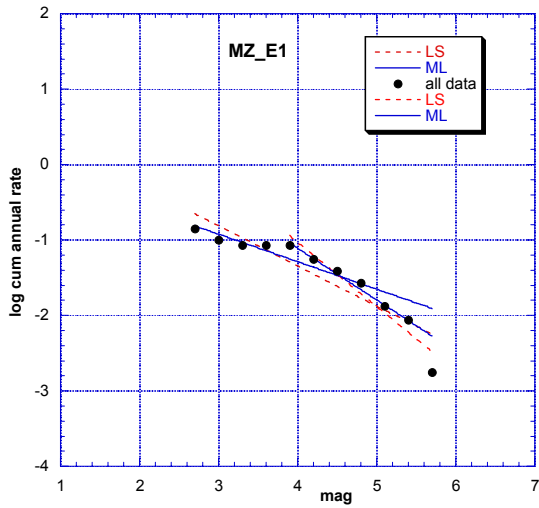
Fig. 55:   MZ E1
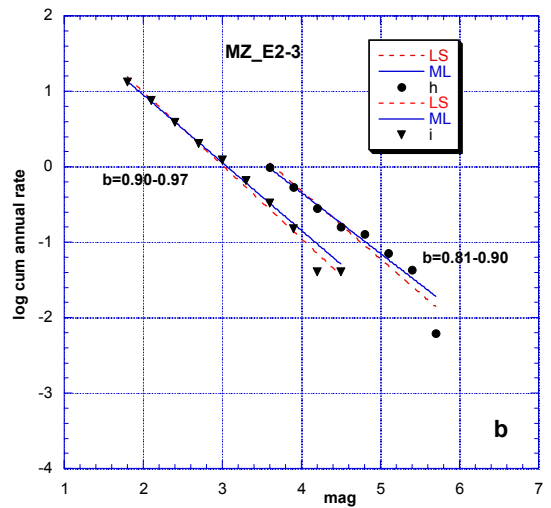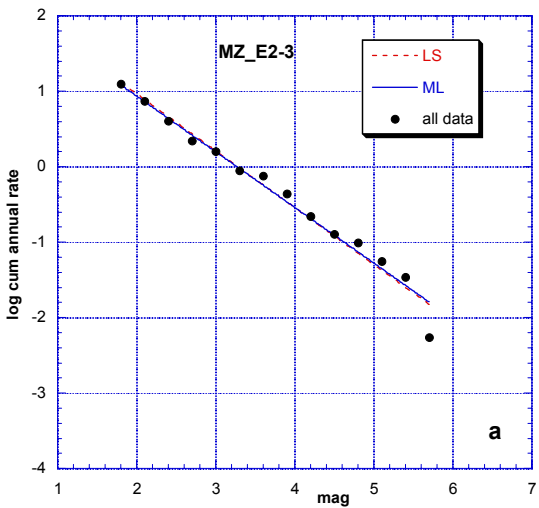
Fig. 56:   MZ E2-3: a) all data; b) historical (h) and instrumental (i) periods
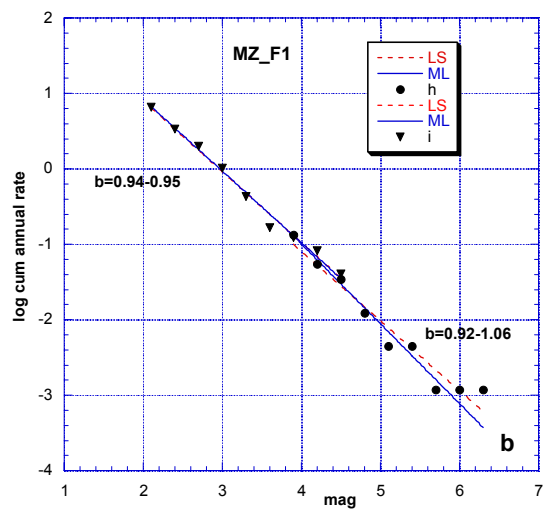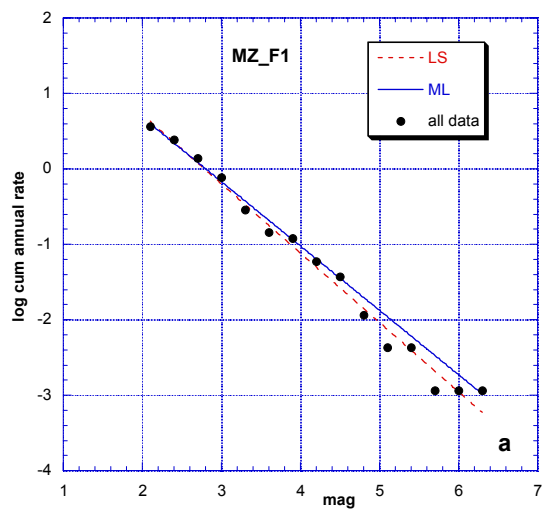
Fig. 57:   MZ F1: a) all data; b) historical (h) and instrumental (i) periods
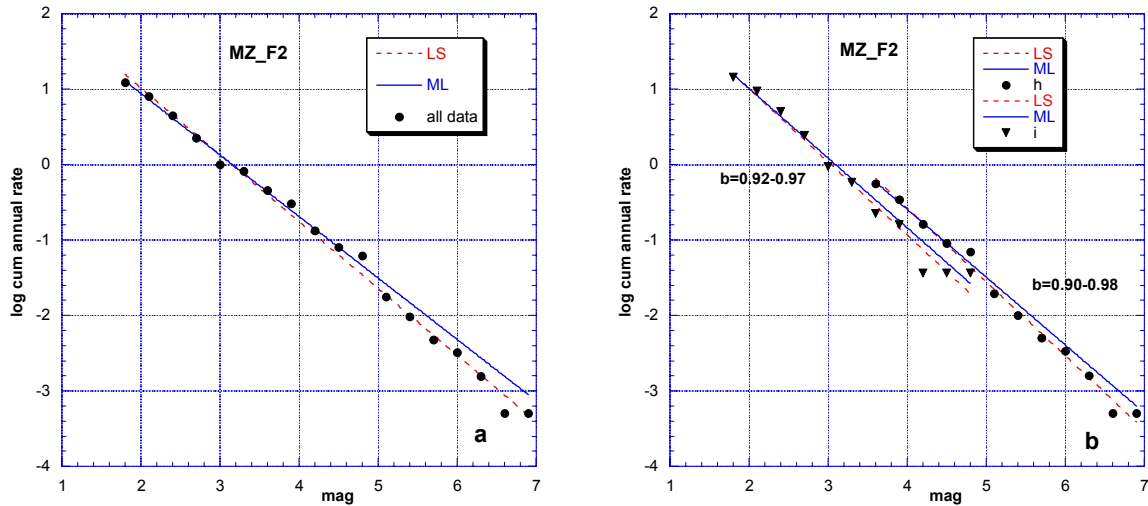
Fig. 58: MZ F2: a) all data; b) historical (h) and instrumental (i) periods
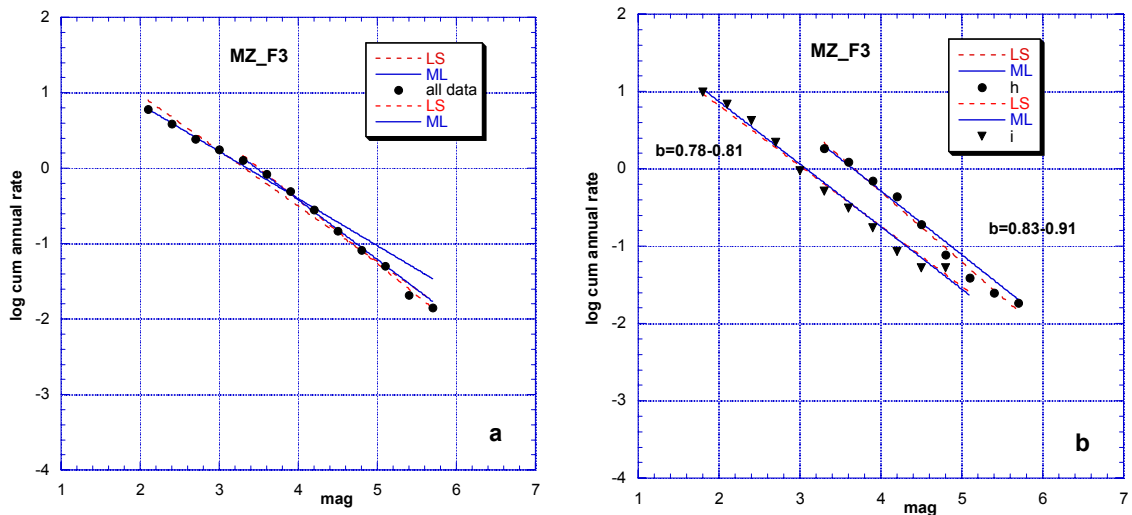
Fig. 59: MZ F3: a) all data; b) historical (h) and instrumental (i) periods

Macro zone C. The introduction of a magnitude threshold of 3.2 leads to a rather well constrained b-value (Fig. 51a). This value (0.78) is in agreement with the separate evaluations of the historical (0.82) and instrumental (0.72) periods and can be taken as representative. The relatively high magnitude threshold of 3.2 seems to mitigate the effects of the two different catalogs that this zone comprises (see section 3.3.2.).

Macro zone D1. A nice linear trend with a b-value of 0.74 characterises this macro zone. There is no need for a threshold magnitude (Fig. 52a). When investigating historical and instrumental periods separately, a clear shift between the two lines can be seen (Fig. 52b), with a difference of about 0.1 in their b-values (0.77 and 0.86, respectively). Nevertheless, the b-value can be considered as well established, with a value close to that of the instrumental period (note that the historical data show some fluctuations) with an uncertainty of 0.1.

Macro zone D2-3. The seismicity in this macro zone shows a problematic behaviour. Earthquakes in the 5.6 to 6.4 magnitude range are completely missing (the seismicity rates have the same value in Fig. 53a) and the number of instrumental events is low (Fig. 53b). Any b-value estimation is, consequently, doubtful between the low 0.73 b-value obtained by the ML

method for the instrumental seismicity (the LS estimate is 0.85) and the value 1.0, which is obtained by adjusting the ML fit of total events larger than 2.8 to the LS fit. No magnitude bias can be invoked and it seems that the most reasonable choice is a b-value of 0.88, obtained from the complete catalog.

Macro zone D4. The lack of low magnitude earthquakes is even more pronounced in this macro zone (Fig. 54a). The b-value is 0.99 for the historical period, but 0.59 for the instrumental period. Also for this macro zone a magnitude bias cannot be invoked. A b-value of 1.0, close to the value for the complete catalog, can be assigned.

Macro zone E1. E1 again contains only very few data in the recent period, but the historical period is badly represented as well. A total (historical and instrumental) number of only 28 earthquakes was registered (Fig. 55). Even when introducing the 3.8 threshold magnitude, the b-value estimate of 0.68 remains of poor quality.

Macro zone E2-3. The characteristics are similar to those of macro zone D1. A good linear fit with a b-value of 0.74 (Fig. 56a) masks a shift between historical and recent seismicity. The b-value is well established between 0.81 and 0.90 (Fig. 56b), and an average b-value of 0.85 is considered adequate.

Macro zone F1. There is good agreement between the total set of data in this macro zone (b = 0.85; Fig. 57a) and the values obtained separately for the historical and instrumental periods (b = 1.06, and, 0.95 respectively; Fig. 57b). The ML fit for the historical rates suffers from a lack of quakes in the 5.6 to 6.1 magnitude range, and the b-value can be easily corrected to 0.92 if a LS fit is considered. The b-value of 0.95 for the instrumental period is considered as representative.

Macro zone F2. This macro zone shows characteristics, which are similar to those of macro zones D1 and E2-3. More specifically, a quite nice fit (b-value = 0.82) was obtained for all the data (Fig. 58a), but a clear shift can be seen between historical (b-value = 0.90) and instrumental (b-value = 0.92) seismicity (Fig. 58b). The b-value is, nevertheless, well constrained at an average value of 0.91.

Macro zone F3. A shift between historical and instrumental seismicity is also seen in this macro zone and produces the uncertainty shown in Figure 59a. The problem can be solved by analysing separate fits, whereby a rather stable b-value around 0.81 can be found (Fig. 59b).

Conclusion: For 7 (A, C, D1, E2-3, F1, F2, F3) out 11 macro zones the b-value can be reasonably well established. For macro zone D2-3 we propose an average b-value value, that has a large uncertainty. For macro zones B and D4 the b-value calculated for the historical seismicity is considered as a best estimate. Macro zone E1 collects a too small number of events, hence a valid result cannot be obtained by the above method and will have to rely on estimates from the larger national catalog zones discussed in the next section.

3.5.1.2   Evaluation of b-values for national catalog zones (Figs. 7/8)

The definition of the eleven macro zones for computing b-values was a logical consequence of wanting to create zones sufficiently large to include enough earthquakes for reliable and representative b-values, but based entirely on amalgamations of subsets of the previously defined source zones (Figs. 4 and 5). As a result, the macro zones straddle different national earthquake catalogs, each with different magnitudes of completeness as a function of time. In order to assess the degree to which spatial heterogeneity of catalog completeness within a single macro zone might bias the resulting b-values, we chose to follow an additional alternative approach, based on a zonation which more closely follows the boundaries of the national catalogs. Subsequently (section 3.5.1.3), we compare the results obtained from the two approaches (macro zones vs. catalog zones) and define the b-values to be used for the hazard assessment for each of the original source zones as defined in Figures 4 and 5.

We again start from the premise that spatial variations of b-values occur smoothly and that they are only statistically resolvable on the basis of a large number of events from a very homogeneous catalog. Thus the bias in b-values derived for zones that follow catalog boundaries, which then can be assigned to seismotectonically defined source zones, is possibly smaller than the uncertainty associated with b-values derived directly for zones with problems of catalog completeness.

Assuming that the catalog is both more complete and more homogeneous for Switzerland and the immediate surroundings (the southernmost part of the Rhinegraben), we further subdivide this area into a few smaller zones ("Swiss zones", see Fig. 8), in order to check for possible spatial variations. Note that the zone referred to as "Swiss Alps" includes the Valais area, the area of Eastern Switzerland, as well as an intermediate more quiescent area (see Fig. 8). For the wider surroundings of Switzerland we stick more or less to national boundaries, with the exception of the area referred to as "Western Alps", which straddles Italian, French and Swiss catalogs, and is seismically more active than the other regions south and southwest of Switzerland (Fig. 7).

In calculating b-values for the Swiss and German regions, the apparent rate change during the second half of the 20th century is again taken into account. Whether this reflects a true fluctuation in seismic activity, or whether it is an artifact due to the transition from macroseismic data to instrumental magnitudes, is irrelevant for b-value calculations. In both cases it introduces a bias, that should be corrected for. In fact, the results (see below) show that ignoring this effect leads to poor fits of the regressions and to relatively low b-values. So for the German and Swiss data, we calculate separate b-values for the historic and instrumental periods.

All calculations were made with the "advanced mag-freq" tool in WizmapII, Version 1.7, which is an implementation of the maximum likelihood method that accounts for periods of variable catalog completeness (Weichert 1980). The basic parameters M_{max} = 7.0, b_prior = 0.85, weight_b_prior = 1 were kept fixed for all zones, except for M_{max}, which was set to 6.5 or 6.0 for some zones (see below). The results are much less sensitive to the choice of these parameters than to the assumptions about catalog completeness, in particular for the low magnitude range. In the following, the completeness periods for each zone are given as two lines in square brackets with the magnitude values and the corresponding years. In addition to the max-likelihood b-value, we also list the activity rate for the lowest magnitude (in brackets) for which we assume the catalog to be complete over some time period, e.g. "no(3.1)". Plots of the mag-freq data together with the max- likelihood fit (truncated exponential model) are shown in Figures 60-72. In these figures, activity rates, plotted as + or x, and cumulative rates, plotted as diamonds or squares, are binned over 0.3 magnitude values and adjusted according the assumed completeness periods for each magnitude interval. The number of events listed for each zone is the total number found in the catalog; due to the completeness limits, the number of events actually used for the regressions is considerably smaller.

The results of this analysis are:

Austria (321 events)

Completeness is based on Stepp-plots, and on the assessment made for the DACH hazard map (Grünthal et al. 1998) using the conversion from epicentral intensity to Mw for intermediate depth events, as given in Table 4.7 of the PEGASOS catalog report (EXT-TB-0043).

M_{max} = 6.0

```
[ 3.2  4.7  5.4  6.2  7.0]
[1900 1850 1670 1550 1200]
b = 0.981 +/- 0.120       no(3.2) = 0.87 +/- 0.32
```

This zone contains only a small number of events (Fig. 60). Therefore, although the cumulative freq-mag plot looks smooth, and the resulting b-value is reasonable, the result is not considered to be really well constrained.

Italy (614 events)

Completeness based on the assessment by Italian catalog compilers (Camassi & Stucchi 1996) and on Stepp-plots plus assessment by authors of the DACH hazard map (Grünthal et al. 1998).

```
I
  [ 3.0  4.0  4.4  4.8  5.4  6.2  7.0]
  [1975 1870 1830 1550 1250 1100 1000]
  b = 0.915 +/- 0.045     no(3.0) = 6.16 +/- 0.32
```
II
$M_{max} = 6.5$;
```
  [ 3.3  4.0  4.8  5.4  6.2  7.0]
  [1975 1900 1800 1400 1200 1000]
  b = 1.019 +/- 0.055     no(3.3) = 4.58 +/- 0.29
```

The freq-mag plots showed that assessment (I) is too optimistic. Figure 61 is based on assessment (II). The remaining magnitude range is 3 units. Despite the fact that this zone covers several very different tectonic units and the number of events is limited, the mag-freq plot is reasonably smooth.

Western Alps (835 events):

Completeness is based on two alternative interpretations of Stepp-plots.

```
I
  [ 3.1  3.9  4.7  5.5  7.0]
  [1975 1900 1820 1750 1000]
  b = 0.739 +/- .060       no(3.1) = 3.12 +/- 0.21
```
II
$M_{max} = 6.5$;
```
  [ 3.9  4.7  5.5  7.0]
  [1900 1820 1750 1000]
  b = 0.892 +/- .082       no(3.9) = 0.92;
```

Assessment I is too optimistic: the catalog for this zone is too heterogeneous. The remaining magnitude range is only 2 units (Fig. 62). The resulting b-value is not well-constrained.

France (640 events):

Completeness is based on Stepp-plots and on the extrapolation from other catalogs.

$M_{max} = 6.0$
```
  [ 3.1  3.9  7.0]
  [1975 1820 1000]
```

The Weichert algorithm in Wizmap gives b = 0.629 +/- 0.129 and no(3.1) = 0.93, but the result does not match the data points. The curve shown in Figure 63, obtained by trial-and-error, corresponds to

```
  b = 0.85       no(3.1) = 0.8
```

This matches the data much better. However, the events in this zone are few and are distributed very unevenly over the whole area. Hence, the resulting b-value is not well constrained.

Germany: (977 events)

Completeness is based on Stepp-plots (I) and the assessment made for the DACH hazard map (II) (Grünthal et al. 1998).

(I)
```
 [ 2.4  3.2  5.4  6.2  7.0]
 [1975 1875 1500 1250 1000]
  b = 0.788 +/- .041      no(2.4) = 7.54 +/- 0.35
```
(II)
$M_{max} = 6.5$;
```
 [ 3.9  4.7  5.4  6.2  7.0]
 [1825 1775 1500 1250 1000]
  b = 0.984 +/- .084      no(3.9) = 0.53
```

Completeness assessment (I) is overly optimistic, resulting in a relatively low b-value, when compared with the result from assessment (II). As can be seen in Figure 64, the lower magnitude range of the freq-mag plot does not lie on a straight line with the higher magnitude range ($M \geq 3.9$). Indeed, Figure 65 shows that for this zone the data can be separated into an instrumental and a macroseismic period.

For the instrumental period starting in 1975, the b-value is based on all events with $Mw \geq 2.3$ and the curve in Figure 65 was fitted to the data by trial-and-error:

```
b = 0.90        no(2.3) = 7.50
```

For the historic period until 1970, assuming $M_{max} = 6.5$ and completeness for

```
 [1825 1775 1500 1250]
 [ 3.9  4.7  5.4  6.2]
```

the Weichert algorithm gives

```
  b = 0.988 +/- .088     n(3.9) = 0.54.
```

The average of the two values is 0.94.

Switzerland (5898 events)

The assessment about completeness is partly based on Stepp-plots (particularly for the low magnitudes) and in part on the assessments made by the catalog compilers (ECOS Report, Table 4.3). The assumption that the catalog is complete from the year 1200 only for $Mw \geq 7.0$ implies that the Mw 6.5 Chur event of 1295 and the Mw 6.9 Basel event of 1356 are not included in this regression.

(I)
```
 [ 1.6  1.8  3.1  3.9  4.7  5.4  6.2  7.0]
 [1984 1975 1964 1879 1750 1680 1500 1200]
  b = 0.789 +/- .012
```
(II)
```
 [ 2.3  3.1  3.9  4.7  5.4  6.2  7.0]
 [1975 1900 1879 1750 1680 1500 1200]
  b = 0.736 +/- .020            no = 20.7
```

As shown in Figure 66, the relatively low b-value results from the max-likelihood algorithm fitting the lower magnitude range of the freq-mag data, while the match of the higher magnitudes is poor. Fitting the instrumental and macro seismic data separately gives better results (Fig. 67).

Instrumental data (3933 events, 1975-2000):

```
[1984 1975]
[ 1.8  2.3]
b = 1.014 +/- .040      no(1.8) = 48.45
```

Macroseismic data (1774 events, 1500-1970):

```
[1900 1879 1750 1680 1500]
[ 3.1  3.9  4.7  5.4  6.2]
b = 0.917 +/- .030      no(3.1) = 7.80
```

The average b-value for the two periods is 0.97

Subzones within Switzerland: "Swiss zones" (see Fig. 8)

In order to assess possible spatial variations of b-values within Switzerland, we also subdivided the country into the following subzones (Fig. 8):

```
completeness assumptions:        (I)            (II)

                  events   b     +/-      b     +/-
Basel               846   0.838 .041    0.906 .081
Northern foreland  1171   0.742 .025    0.737 .042
Eastern Switz.     1352   0.815 .012    0.766 .040
Wallis             1733   0.794 .024    0.691 .048
Swiss Alps         3881   0.798 .015    0.719 .024
```

Note: the Swiss Alps zone covers the zones "Wallis" and "Eastern Switzerland" plus the relatively aseismic region in between.

As for the whole country, the relatively low b-values are a consequence of the max-likelihood algorithm that fits the lower magnitude range, dominated by the apparently more quiescent instrumental period. Therefore we again calculated b-values for instrumental and macroseismic periods separately, based on the same completeness assumptions as for the separate periods of the whole country (Fig. 68 – 72). In the following, we list b-value, activity rate and number of events first for the instrumental and then for the macroseismic period, followed by the average of the two periods, for each subzone. The magnitude value for the activity rates is 1.8 for the former and 3.1 for the latter.

```
      b-value              N(m_o)      events
Basel:
     0.946 +/- .107        6.31         630
     0.817 +/- .115        0.38         161
     0.88

Northern Switzerland (Mmax = 6.0):
     0.892 +/- .083        9.83         581
     0.883 +/- .063        1.82         542
     0.89
```

```
Eastern Switzerland:

     1.038 +/- .076        14.69          936
     0.985 +/- .065         1.98          400
     1.01

Wallis:

     1.037 +/- .087        11.11         1292
     0.872 +/- .052         2.22          389
     0.96

Swiss Alps:

     1.070 +/- .050        32.31         2722
     0.928 +/- .035         5.56         1071
     1.00
```

The calculated standard deviations given for each b-value are not a realistic measure of the uncertainty of the results, since they cannot account for possible errors in the catalogs or for possible deviations of the data from the underlying model assumptions. An indication of this fact can be found from the examination of the differences between b-values obtained from instrumental and macro seismic data for each zone:

	Difference	Average
Germany:	0.088	0.94
Switzerland:	0.097	0.97
Basel:	0.129	0.88
Northern Switzerland:	0.009	0.89
Eastern Switzerland:	0.053	1.01
Wallis:	0.165	0.96
Swiss Alps:	0.142	1.00

The mean of these discrepancies is about 0.1, whereas most of the calculated standard deviations are between 0.03 and 0.08. Thus a standard error of the resulting b-values on the order of 0.1 is more realistic.

Nevertheless, the average values seem to suggest a small but systematic difference in b-value between Alps (1.0) and foreland (0.89). On the other hand, the difference between the Wallis (0.96) and eastern Switzerland (1.01) is probably not significant, in particular considering that the historic data from the Wallis deviate strongly from an ideal Gutenberg-Richter relationship (see Fig. 71).

Considering that the b-values calculated for the zones of Austria (0.98) and the Western Alps (0.89) are poorly constrained and that these zones are tectonically related to the zone of the Swiss Alps, it is in principle possible to assign the corresponding b- value (1.0) to the whole Alpine domain. The value of 1.02 obtained from the more conservative completeness assessment of the Italian zone is also not sufficiently well constrained, so that the value of 1.0 could apply to this zone as well. The b- value obtained for the zone of France (0.85) is based on an eye- ball fit to very little data, and there is no evident seismotectonical reason for eastern France to be significantly different from the rest of the more distant Alpine foreland. Therefore the same b-value for both the French and German zones (0.94) appears as a more plausible proposal.
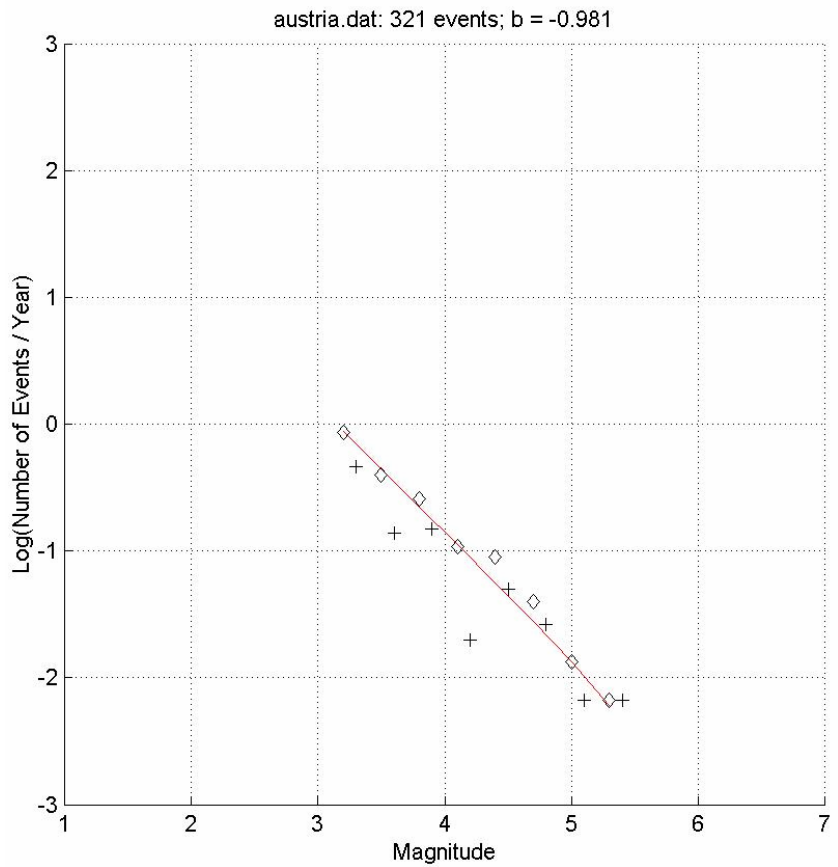
Fig. 60:   Austria
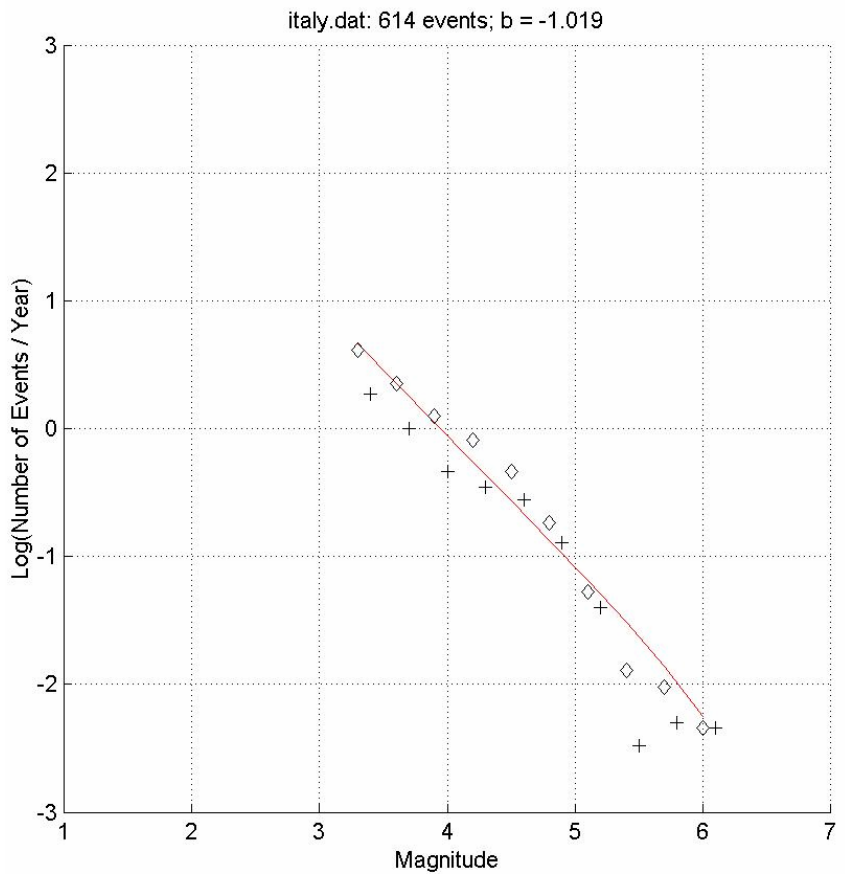
Fig. 61:   Italy
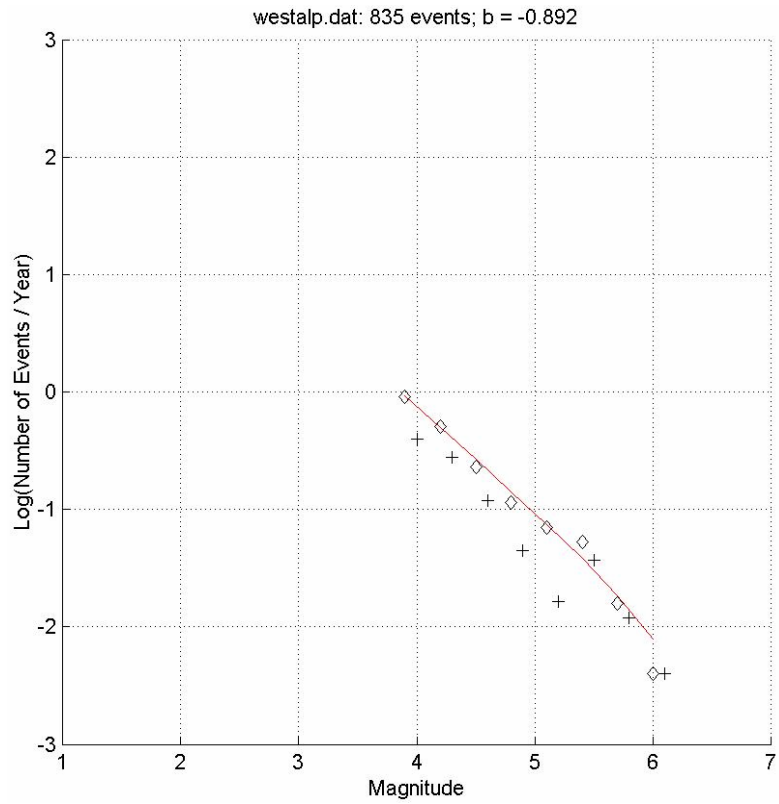
Fig. 62:   Western Alps
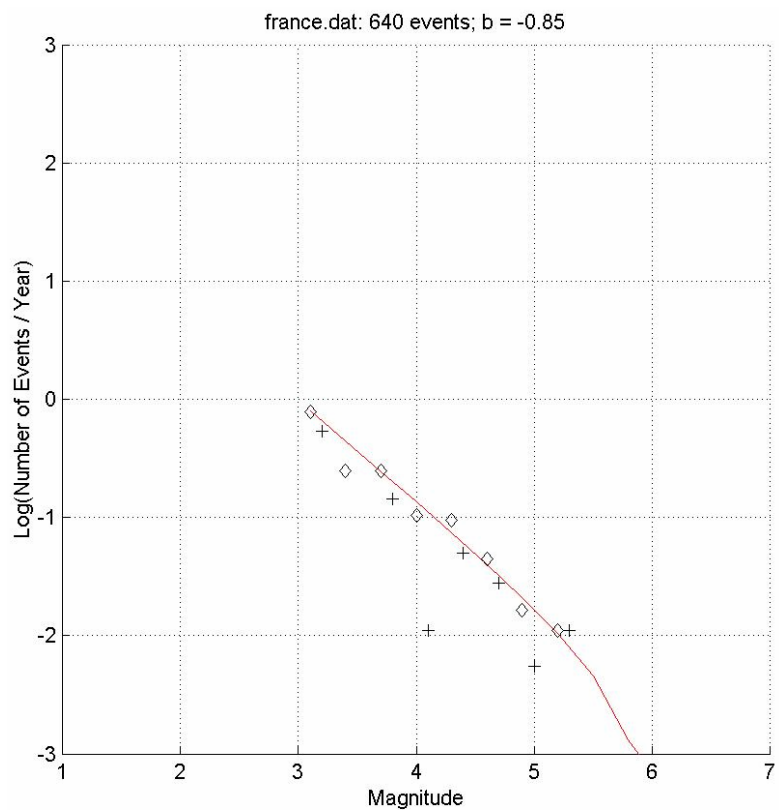
Fig. 63:   France
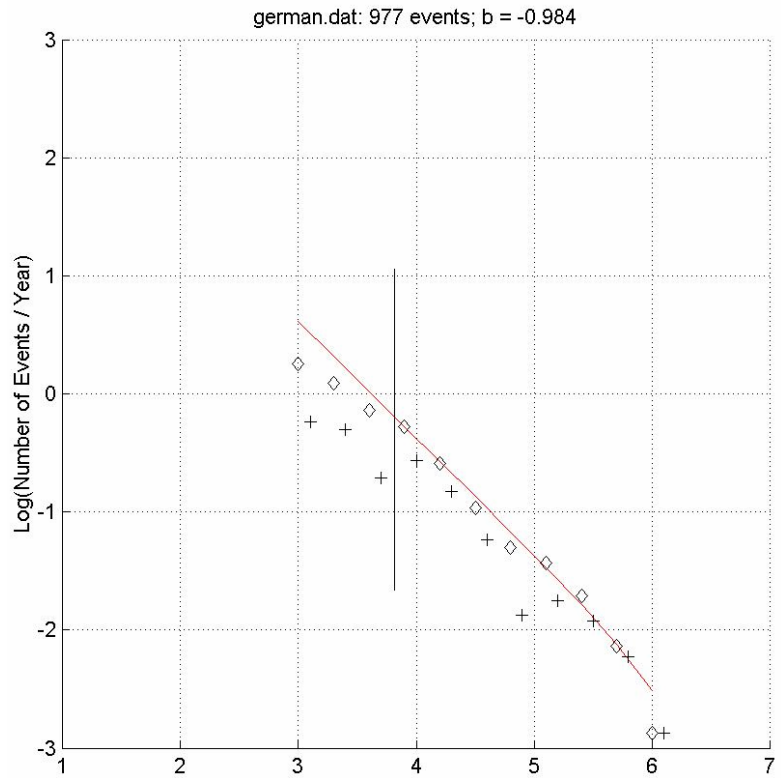
Fig. 64:   Germany; b-value for magnitudes ≥ 3.9
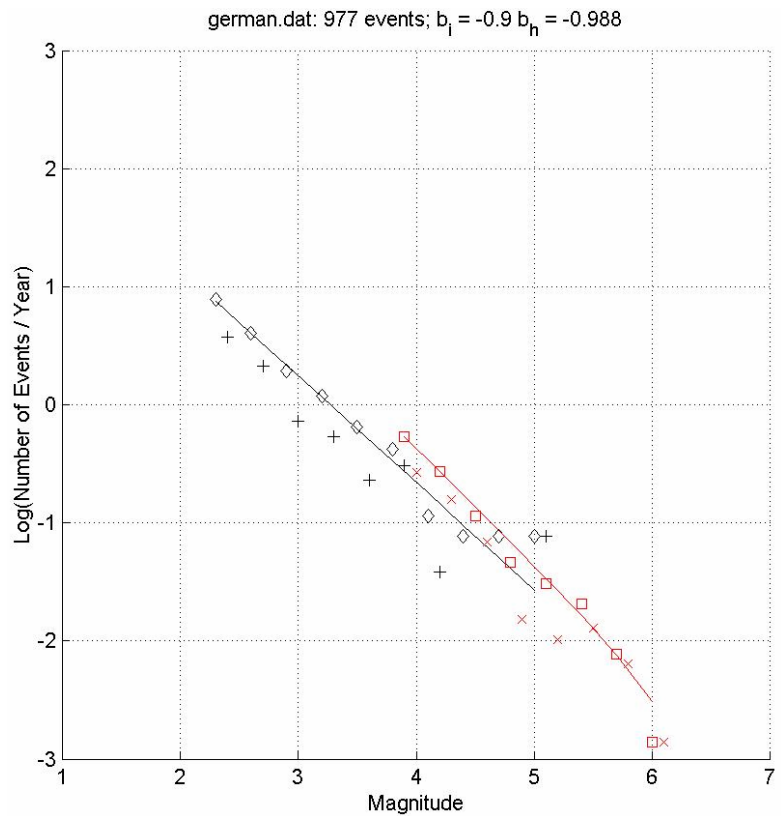
Fig. 65:   Germany; b-values for instrumental period (b_i, black) and historical period (b_h, red)
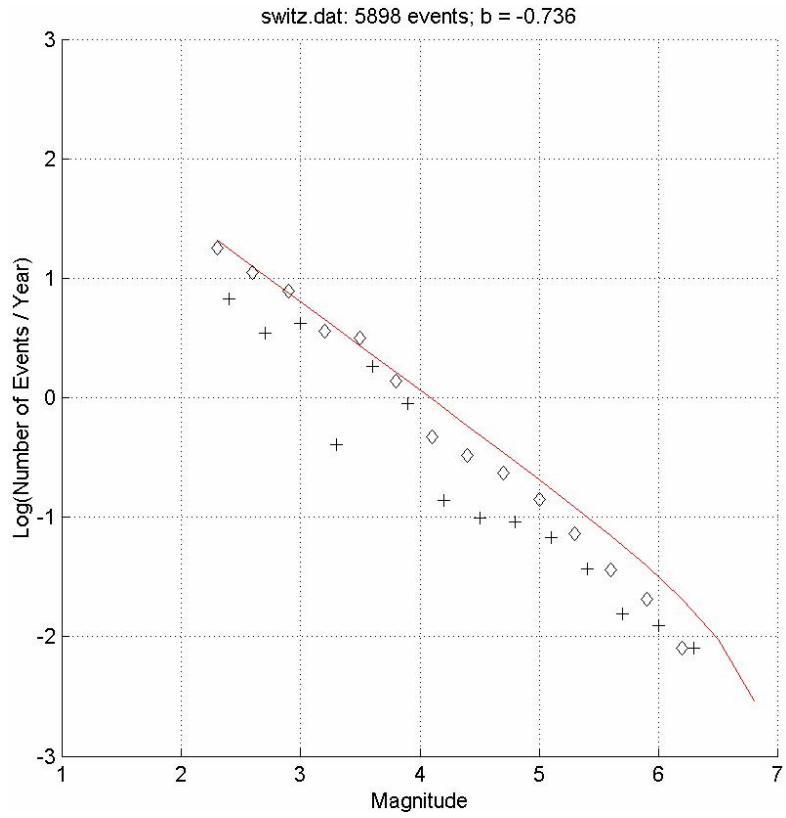
Fig. 66: Switzerland
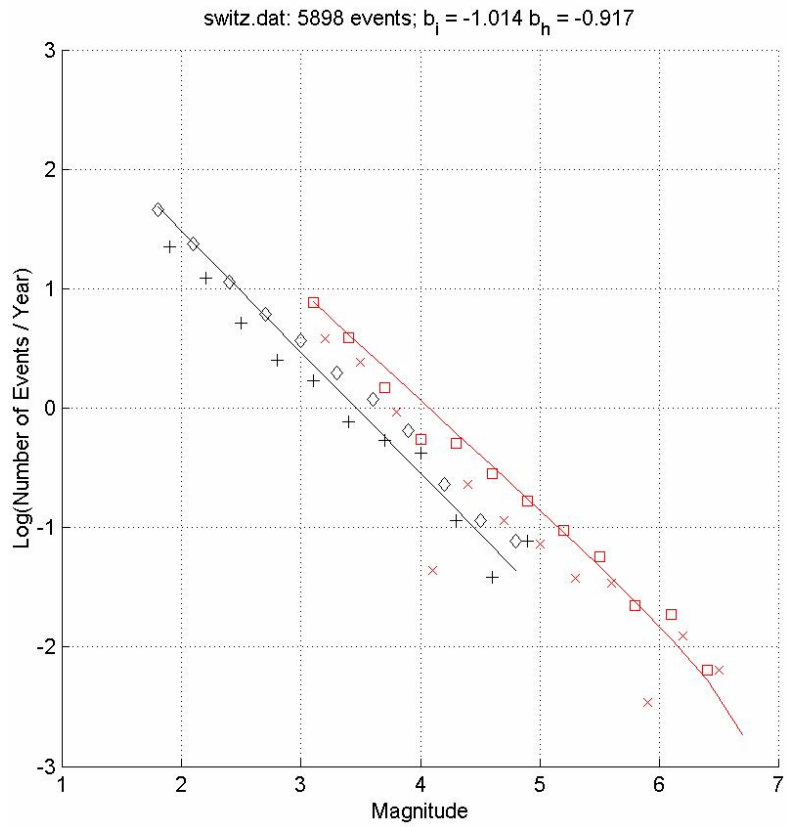
Fig. 67: Switzerland; b-values for instrumental period (b_i, black) and historical period (b_h, red)
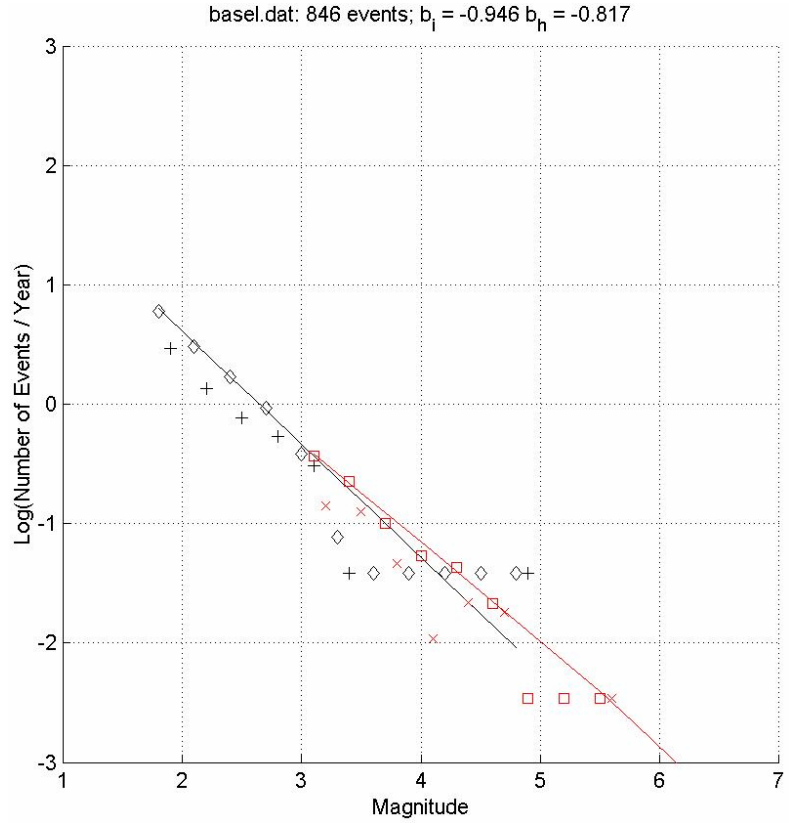
Fig. 68:   Basel; b-values for instrumental period (b_i, black) and historical period (b_h, red)
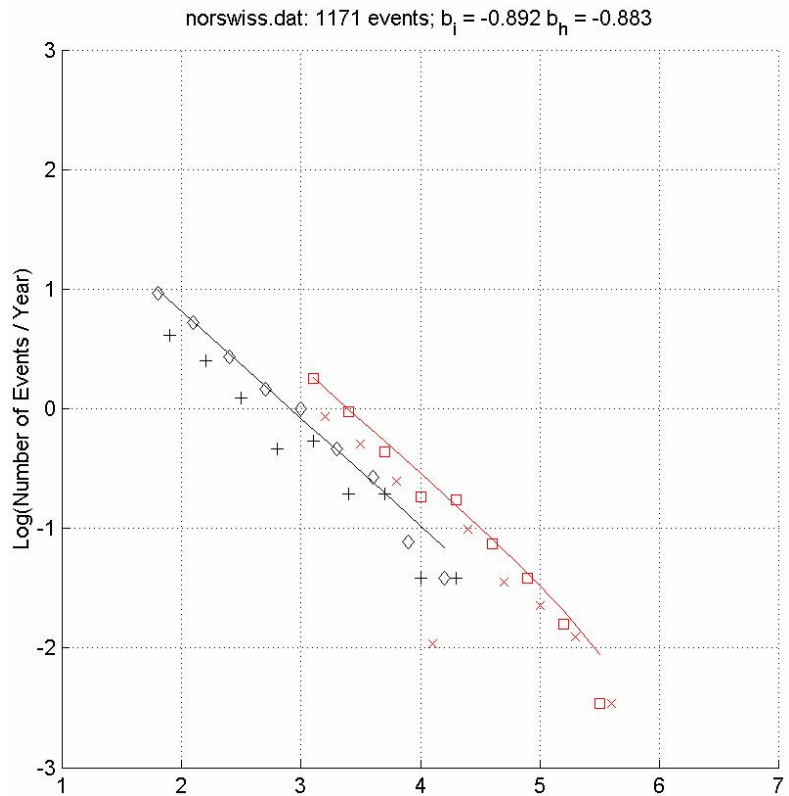
Fig. 69:   Northern Switzerland; b-values for instrumental period (b_i, black) and historical period (b_h, red)
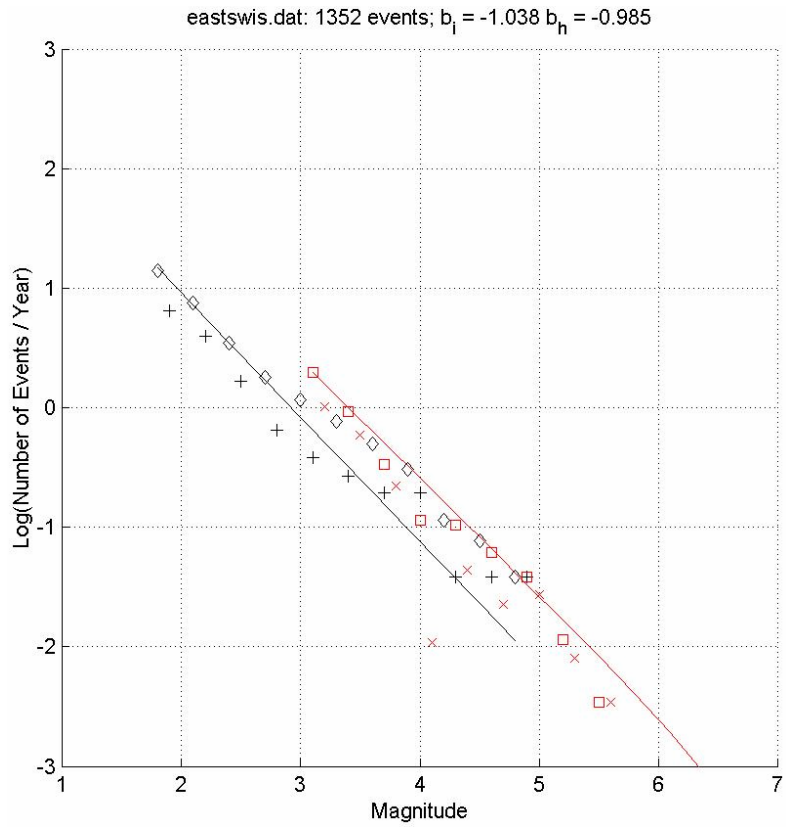
Fig. 70:   Eastern Switzerland; b-values for instrumental period (b_i, black) and historical period (b_h, red)
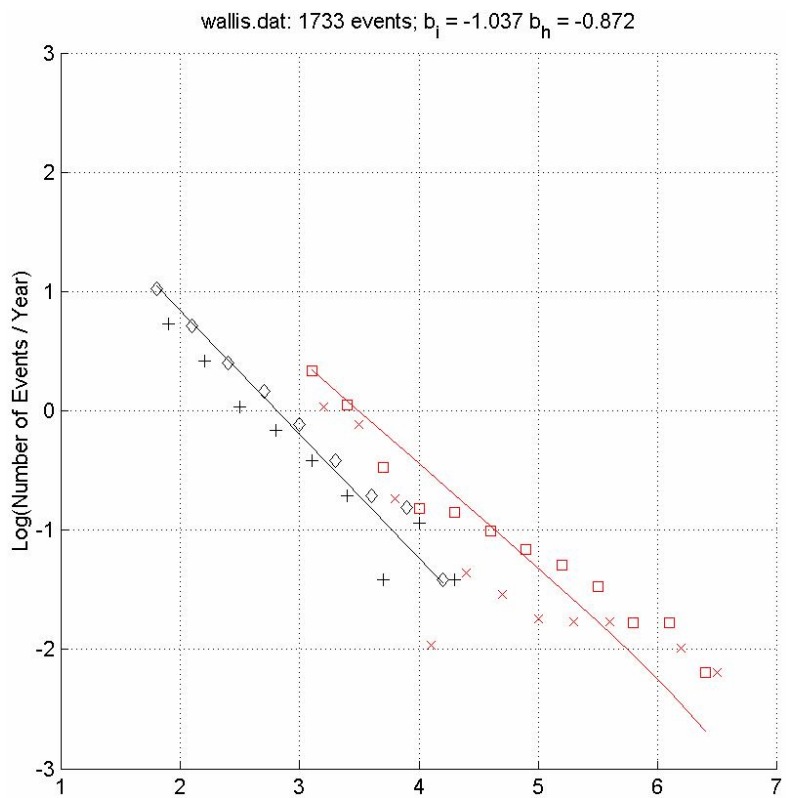
Fig. 71:   Wallis; b-values for instrumental period (b_i, black) and historical period (b_h, red)
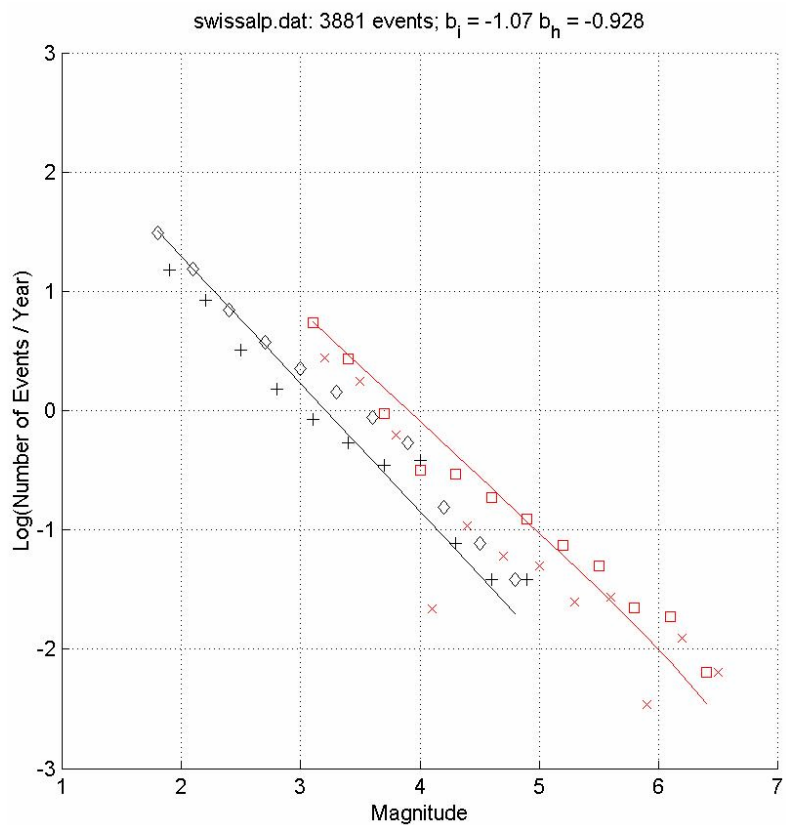
Fig. 72:   Swiss Alps; includes eastern Switzerland and Wallis

b-values for instrumental period (b_i, black) and historical period (b_h, red).

3.5.1.3   Conclusions regarding b-values for hazard calculations

In a first step, and in order to compare the b-values based on a zonation that follows national catalog boundaries (section 3.5.1.2 and Fig. 7) to the b-values obtained for the seismo-tectonically defined macro zones (section 3.5.1.1), we assign the b-values derived from the national catalogs to the individual macro zones, as defined in Figure 6:

Alps and south of the Alps
macro zones A, B, C, D1, D2-3, D4:   b = 1.0 +/- 0.1

Northern and western Alpine foreland
macro zone E2-3:   b = 0.89 +/- 0.1

Rhinegraben including Basel
macro zone F2:   b = 0.88-0.94 +/- 0.1

Distal Alpine foreland (Germany and France)
macro zones E1, F1, F3:   b = 0.94 +/- 0.1

The above cited b-values are also reported in Table 8 (column b-cat), together with their standard deviation (column σb-CAT). In this Table 8 they are compared with those calculated for the macro zones (see chapter 3.5.1.1). These latter identify a b-value range (column b-MZ range in Table 8) obtained by the analysis of the different results (ML and LS methods; whole, historical, and instrumental periods) inside which a preferred value is extracted (column b-MZ).

Tab. 8:   Comparison between the different b-values calculated and final b-values proposed

MZ	CAT	b-CAT	σb-CAT	b-MZ	b-MZ range	b	σb
A	I	1.0	0.1	0.96	0.92-1.00	0.96	0.1
B	I	1.0	0.1	1.00	0.78-1.00	1.00	0.1
C	F,I,CH	1.0	0.1	0.78	0.72-0.82	0.92	0.1
D1	CH,F	1.0	0.1	0.85	0.74-0.86	0.93	0.1
D2-3	CH,A	1.0	0.1	0.88	0.85-0.90	0.94	0.1
D4	I,CH	1.0	0.1	1.00	0.99-1.03	1.00	0.1
E1	F	0.94	0.1		0.68-0.90	0.95	0.1
E2-3	CH,F	0.89	0.1	0.85	0.80-0.90	0.89	0.1
F1	F	0.94	0.1	0.95	0.84-1.04	0.95	0.1
F2	D,CH,F	0.88-0.94	0.1	0.91	0.89-0.93	0.90	0.1
F3	D	0.94	0.1	0.81	0.79-0.85	0.88	0.1

MZ   macro zone;
CAT   dominating catalog(s) for the MZ;
b-CAT   b-values for CAT. A direct association of CAT to MZ is problematic but can drive the choice;
b-MZ   b-values for MZ;
b-MZ range   range of possible b-values for MZ;
b   final b-values proposed;
σb   b-value standard deviation.

Conclusion:

As can be seen from Table 8, the agreement between the two estimates, which are derived from completely different considerations, is not bad. Hence, we chose a final b-value (column b) by taking into account all the considerations previously described and, especially, the quality of the data available in each MZ. This final choice should be seen as a sort of "expert judgement weighted average" value. It is reported in Table 8 ("b", second last column), together with its standard deviation ("σb", last column in Table 8). The same value of 0.1, chosen as standard deviation (column σb) for all MZs, quantifies the uncertainty we associate with this final estimate from all the detailed considerations reported above.

3.5.2   Evaluation of a-values

The recurrence rates $N(m > m_0)$ were calculated by Geomatrix Consultants, using a modification of the maximum likelihood approach outlined in Weichert (1980). The modifications of this approach include (a) variable magnitude bin widths, (b) use of different complete periods for different regions, and (c) use of a fixed b-value. The rate calculations were performed for each of the source zones defined in Chapter 2 (Figures 4, 5 and 9) on the basis of the earthquake catalog, de-clustered according to the procedure already described in Chapter 3.2. and by using the fixed b-values listed in Table 8 (see "final b-values proposed") of Chapter 3.5.1.3. The completeness analysis reported in chapter 3.3 was taken into account. However, the 1356 Basel event was additionally included in the calculation, with a return period of 2000 years (Chapter 3.4), for all zones that contain this event.

The apparent change in activity rate during the time period 1970-1975, visible in the Swiss and German data, is likely to have an important influence on the resulting a-values. Either there is an error in the catalog, in which case we face an epistemic uncertainty that we cannot resolve at this time, or alternatively, it is an expression of a natural fluctuation of seismic activity. In the latter case we face an aleatory uncertainty regarding the predictability of future activity rates. In either case, it is necessary to perform the computations separately for the post-1975 instrumental period and the pre-1975 macroseismic period when estimating a-values for the seismic source zones covered by the Swiss and German catalogs.

In addition, preliminary calculations showed that for several source zones the data (in particular the historical data) significantly deviate from the ideal Gutenberg-Richter (G-R) relation. In those cases the Maximum-Likelihood fit tends to be anchored by the more numerous low-magnitude events and fails to match the higher magnitudes. The deviation from a good fit is somewhat systematic in the sense that when the fit is poor, the observed cumulative number of high-magnitude events is almost always higher than that predicted by the G-R relation. This could be due to two reasons. A first reason could be that the GR relation and the fixed b-values derived from the macro-zones are not a good model for the earthquake recurrence in Switzerland and surroundings, and the data is telling us that. The other reason could be that the (truncated) G-R relation does hold over the whole magnitude range, but that the data quality is not sufficiently good to reflect this. Because there are no well-developed faults in the area for which we would expect that they feature large characteristic earthquakes, that occur more frequently than predicted by the low magnitude events, the first explanation is considered unlikely.

This leaves the possibility of the existence of a systematic magnitude bias in the historical data between low- and high-magnitude events. Such a bias could have entered the catalog through the way in which the intensity information was converted into Mw: events that were listed in the old catalog (MECOS) with an intensity of at least VI were completely re-evaluated and Mw was determined from an analysis of the entire macroseismic field. The magnitudes of the weaker events, on the other hand, were calculated from a simple regression between observed intensity and magnitudes. Since in this case there is no objective way basis for deciding whether the magnitudes of the stronger events have been overestimated (alternative 1) or whether the magnitudes of the weaker ones have been underestimated (alternative 2), it is reasonable to treat this as another element of uncertainty and introduce two additional branches in the logic tree, that reflect this epistemic uncertainty.

Given that the unweighted maximum-likelihood regression tends to be anchored at the more numerous smaller events, this approach covers the first alternative. To account for the second alternative, we consider a maximum-likelihood regression that is restricted to larger magnitudes (nominally above minimum magnitude $m_0 = 4.3$). This cut-off is justified by the fact that in the general conversion formula used for the new earthquake catalog (ECOS), Io = VI corresponds approximately to Mw = 4.7; given that the revision of the old catalog certainly resulted in several events being reclassified to lower intensities and given the general uncertainty involved in all these earthquake size estimates, a threshold of Mw = 4.3 is appropriate. Thus for source zones in Switzerland and southern Germany we have three branches (pre-1975 with all events, pre-1975 with larger magnitudes (again nominally above $m_0 = 4.3$, and post 1975) each with a weight of one third, whereas for all other source zones we have only the first two branches each with a weight of one half.

Table 9 lists the individual source zones, the assumed *b*-values and the alternative a-value calculations. Figures 73 to 124 were prepared by Geomatrix Consultants and show the fitted maximum-likelihood recurrence curves for each source and for three specified *b*-values (1. median value; 2. median value minus one standard deviation, and, 3. median value plus one standard deviation) for each region.

Tab. 9:   Seismic source sets for recurrence parameters

Sources with correlated *b*-values	*b*-value	Seismicity Rate Alternatives	
A	0.96 ± 0.1	All data All data, larger mag	(wt 0.5) (wt 0.5)
B	1.00 ± 0.1	All data All data, larger mag	(wt 0.5) (wt 0.5)
C1, C2, C3	0.92 ± 0.1	All data All data, larger mag	(wt 0.5) (wt 0.5)
D1a, D1b, D1c, D1e, D1f, D1bcd, D1bcde, D1de	0.93 ± 0.1	Instrumental data Historical data Historical data, larger mag	(wt 0.333) (wt 0.334) (wt 0.333
D2, D3a, D3b	0.94 ± 0.1	Instrumental data Historical data Historical data, larger mag	(wt 0.333) (wt 0.334) (wt 0.333
D4a, D4b, D4c	1.00 ± 0.1	All data All data, larger mag	(wt 0.5) (wt 0.5)
E1	0.95 ± 0.1	All data All data, larger mag	(wt 0.5) (wt 0.5)
E2a, E2b, E2c, E2d, E2e, E2cde, FF, E2dF2f, E2eF2f, E2cdeF2f, E2n, E2s, E2f, E3a, E3aF2f, E3b	0.89 ± 0.1	For E2a, E2b: All data All data, larger mag For rest of sources: Instrumental data Historical data Historical data, larger mag	 (wt 0.5) (wt 0.5) (wt 0.333) (wt 0.334) (wt 0.333)
F1a, F1b, F2c	0.95 ± 0.1	All data All data, larger mag	(wt 0.5) (wt 0.5)
F2a, F2b, F2b_RF, RF, F2bpcy, F2bF2f, F2d, F2e, F2f	0.90 ± 0.1	Instrumental data Historical data Historical data, larger mag	(wt 0.333) (wt 0.334) (wt 0.333)
F3a, F3aF2f, F3b, F3c	0.88 ± 0.1	Instrumental data Historical data Historical data, larger mag	(wt 0.333) (wt 0.334) (wt 0.333)

The distribution for the rate of activity given a fixed b-value was developed as follows. Assuming a truncated exponential model for earthquake recurrence, the likelihood function for an observed catalog of data is given by (Weichert 1980):

$$L = \prod_i \frac{(\lambda_i t_i)^{n_i} e^{-\lambda_i t_i}}{n_i!}$$

$$\lambda_i = \text{rate for magnitude interval } m_i - m_{i-1} = N(m_0)\frac{e^{-\beta(m_i - m_0)} - e^{-\beta(m_{i-1} - m_0)}}{1 - e^{-\beta(m^u - m_0)}}$$

$$\beta = b \ln(10)$$

$$t_i = \text{completeness period for magnitude interval } m_i - m_{i-1}$$

$$n_i = \text{number of events in magnitude interval } m_i - m_{i-1}$$

With the *b*-value fixed, the likelihood, *L*, of obtaining the observed catalog was computed for a array of closely-spaced values of $N(m_0)$, the annual frequency of earthquakes larger than the minimum magnitude used for recurrence calculations, m_0. These likelihoods represent relative likelihoods for the parameter $N(m_0)$ given the *b*-value. The relative likelihoods were normalized into a discrete probability distribution for $N(m_0)$ and used to construct a cumulative distribution function. This cumulative distribution function was then represented by a discrete five-point approximation to a continuous distribution developed by Miller & Rice (1983). For each discrete value of $N(m_0)$, the frequency of earthquakes of magnitude 5 and larger is computed from the truncated exponential model:

$$N(5) = N(m_0)\frac{e^{-\beta(5-m_0)} - e^{-\beta(m^u - m_0)}}{1 - e^{-\beta(m^u - m_0)}}$$

3.5.3   Final earthquake recurrence parameters for hazard computation

The earthquake recurrence parameters for the sources were modeled by using the truncated exponential recurrence relation. The recurrence parameters were defined by first establishing the *b*-value for sets of seismic source zones ("macro zones"). This fixed *b*-value was then used to calculate the seismicity rate for each seismic source zone as defined in Figures 9 to 14. Thereby a regional *b*-value was assumed to be common to all source zones within a given set of regional zones (i.e. within a given macro zone) used to define the *b*-value. A three-point distribution representation of a normal distribution was used to model the uncertainty in the regional *b*-value, and, 7-point distributions are used to model the uncertainty in $N(m \geq 5)$ for each source, conditional on a given *b*-value. The results are summarized in Table 10 for each branch in the logic tree.

Fig. 73:   Seismicity rates and fitting curves (solid line = considering all data, dashed line = considering magnitudes larger than 4.2) for Zone A

The 3 b-values are: the estimated one − 1 σ, the estimated one, the estimated one + 1 σ.

Fig. 74:   Seismicity rates and fitting curves (solid line = considering all data, dashed line = considering magnitudes larger than 4.2) for Zone B

The 3 b-values are: the estimated one − 1 σ, the estimated one, the estimated one + 1 σ.

Fig. 75:   Seismicity rates and fitting curves (solid line = considering all data, dashed line = considering magnitudes larger than 4.2) for Zone C1

The 3 b-values are: the estimated one − 1 σ, the estimated one, the estimated one + 1 σ.

Fig. 76:   Seismicity rates and fitting curves (solid line = considering all data, dashed line = considering magnitudes larger than 4.2) for Zone C2

The 3 b-values are: the estimated one − 1 σ, the estimated one, the estimated one + 1 σ.

Fig. 77:   Seismicity rates and fitting curves (solid line = considering all data, dashed line = considering magnitudes larger than 4.2) for Zone C3

The 3 b-values are: the estimated one − 1 σ, the estimated one, the estimated one + 1 σ.

Fig. 78:   Seismicity rates and fitting curves (solid line = considering all data, dashed line = considering magnitudes larger than 4.2) for Zone D1a

The 3 b-values are: the estimated one − 1 σ, the estimated one, the estimated one + 1 σ.

Fig. 79:   Seismicity rates and fitting curves (solid line = considering all data after 1975, dashed line = considering all data before 1975, dotted-dashed line = considering magnitudes larger than 4.2 before 1975) for Zone D1b

The 3 b-values are: the estimated one − 1 σ, the estimated one, the estimated one + 1 σ.

Fig. 80:   Seismicity rates and fitting curves (solid line = considering all data after 1975, dashed line = considering all data before 1975, dotted-dashed line = considering magnitudes larger than 4.2 before 1975) for Zone D1bcd

The 3 b-values are: the estimated one − 1 σ, the estimated one, the estimated one + 1 σ.

Fig. 81:   Seismicity rates and fitting curves (solid line = considering all data after 1975, dashed line = considering all data before 1975, dotted-dashed line = considering magnitudes larger than 4.2 before 1975) for Zone D1bcde

The 3 b-values are: the estimated one − 1 σ, the estimated one, the estimated one + 1 σ.

Fig. 82:   Seismicity rates and fitting curves (solid line = considering all data after 1975, dashed line = considering all data before 1975, dotted-dashed line = considering magnitudes larger than 4.2 before 1975) for Zone D1c

The 3 b-values are: the estimated one − 1 σ, the estimated one, the estimated one + 1 σ.

Fig. 83: Seismicity rates and fitting curves (solid line = considering all data after 1975, dashed line = considering all data before 1975, dotted-dashed line = considering magnitudes larger than 4.2 before 1975) for Zone D1de

The 3 b-values are: the estimated one − 1 σ, the estimated one, the estimated one + 1 σ.

Fig. 84: Seismicity rates and fitting curves (solid line = considering all data after 1975, dashed line = considering all data before 1975, dotted-dashed line = considering magnitudes larger than 4.2 before 1975) for Zone D1e

The 3 b-values are: the estimated one − 1 σ, the estimated one, the estimated one + 1 σ.

Fig. 85: Seismicity rates and fitting curves (solid line = considering all data after 1975, dashed line = considering all data before 1975, dotted-dashed line = considering magnitudes larger than 3.0 before 1975) for Zone D1f

The 3 b-values are: the estimated one − 1 σ, the estimated one, the estimated one + 1 σ.

Fig. 86: Seismicity rates and fitting curves (solid line = considering all data after 1975, dashed line = considering all data before 1975, dotted-dashed line = considering magnitudes larger than 3.8 before 1975) for Zone D2

The 3 b-values are: the estimated one − 1 σ, the estimated one, the estimated one + 1 σ.

Fig. 87: Seismicity rates and fitting curves (solid line = considering all data after 1975, dashed line = considering all data before 1975, dotted-dashed line = considering magnitudes larger than 4.2 before 1975) for Zone D3a

The 3 b-values are: the estimated one – 1 σ, the estimated one, the estimated one + 1 σ.

Fig. 88: Seismicity rates and fitting curves (solid line = considering all data after 1975, dashed line = considering all data before 1975, dotted-dashed line = considering magnitudes larger than 4.2 before 1975) for Zone D3b

The 3 b-values are: the estimated one – 1 σ, the estimated one, the estimated one + 1 σ.
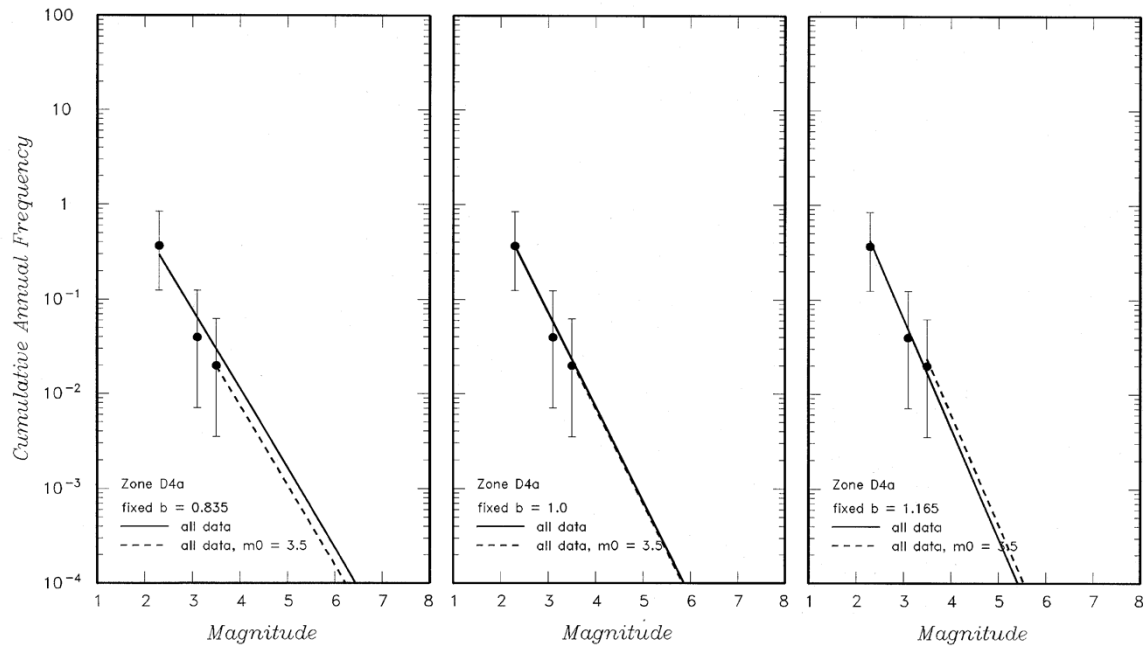
Fig. 89:   Seismicity rates and fitting curves (solid line = considering all data, dashed line = considering magnitudes larger than 3.4) for Zone D4a

The 3 b-values are: the estimated one − 1 σ, the estimated one, the estimated one + 1 σ.
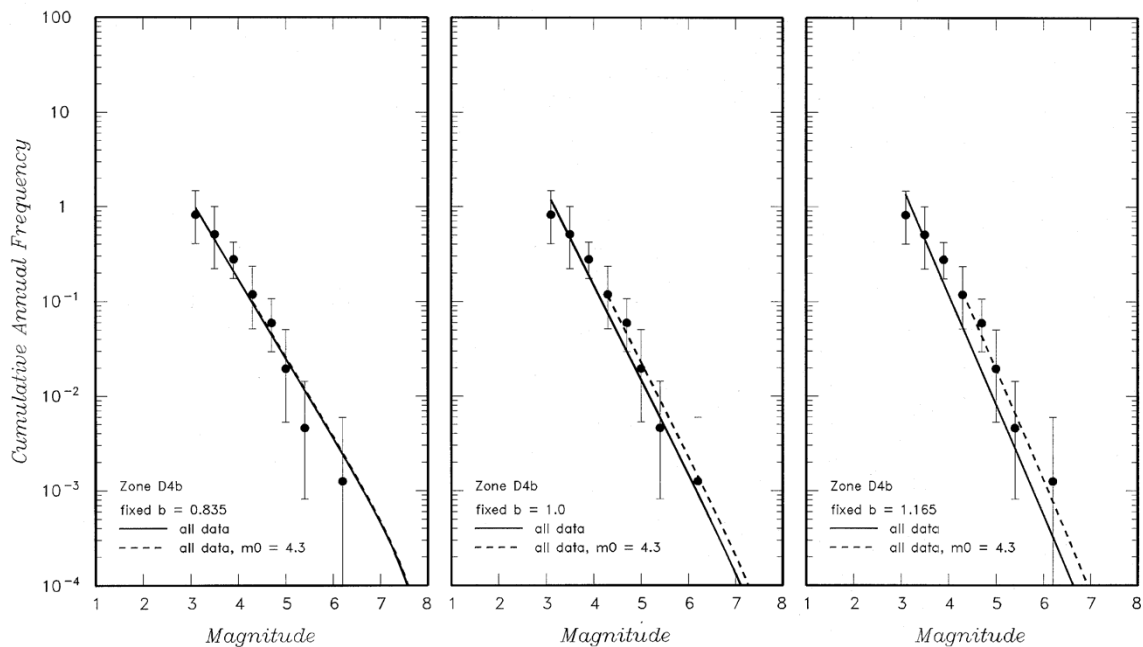
Fig. 90:   Seismicity rates and fitting curves (solid line = considering all data, dashed line = considering magnitudes larger than 4.2) for Zone D4b

The 3 b-values are: the estimated one − 1 σ, the estimated one, the estimated one + 1 σ.
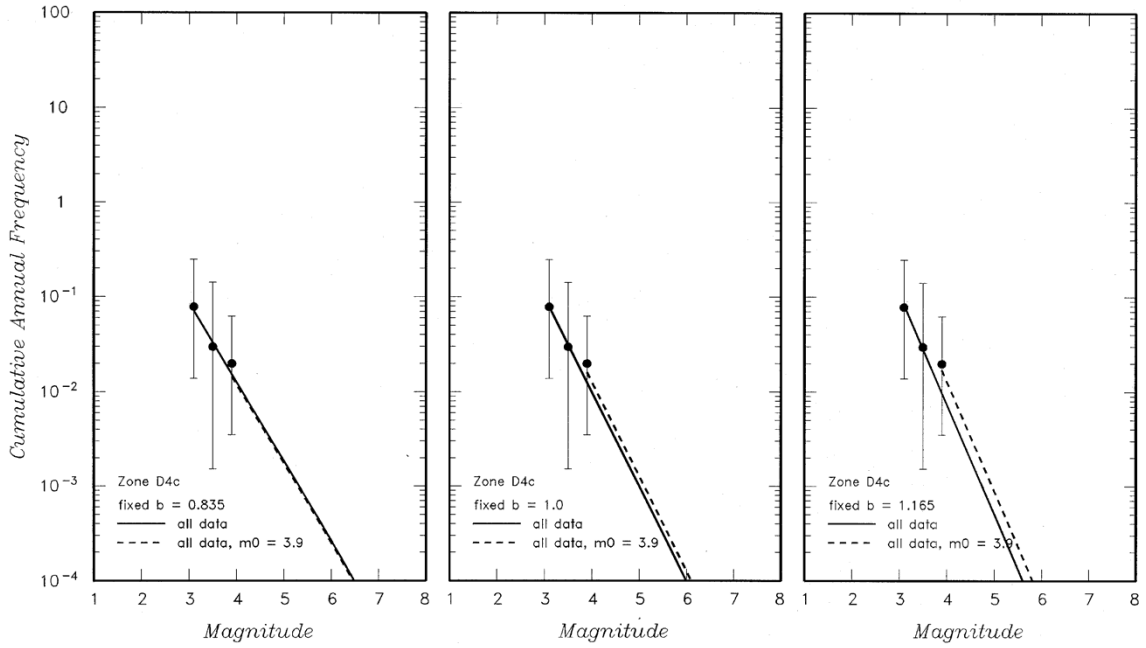
Fig. 91: Seismicity rates and fitting curves (solid line = considering all data, dashed line = considering magnitudes larger than 3.8) for Zone D4c

The 3 b-values are: the estimated one − 1 σ, the estimated one, the estimated one + 1 σ.
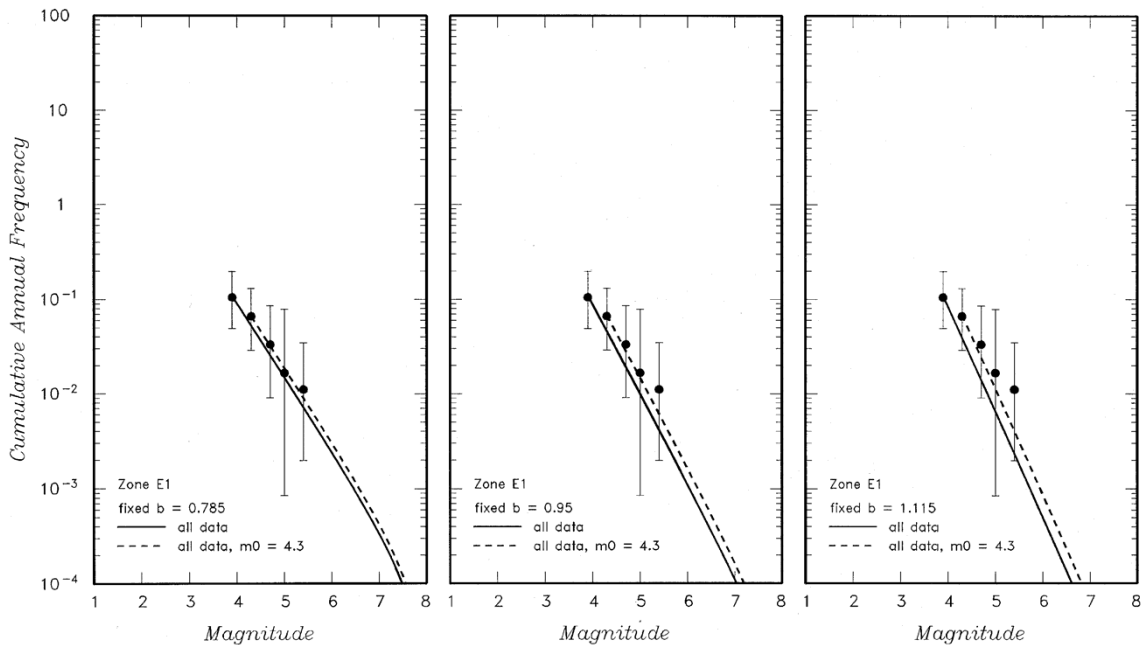
Fig. 92: Seismicity rates and fitting curves (solid line = considering all data, dashed line = considering magnitudes larger than 4.2) for Zone E1

The 3 b-values are: the estimated one − 1 σ the estimated one, the estimated one + 1 σ.
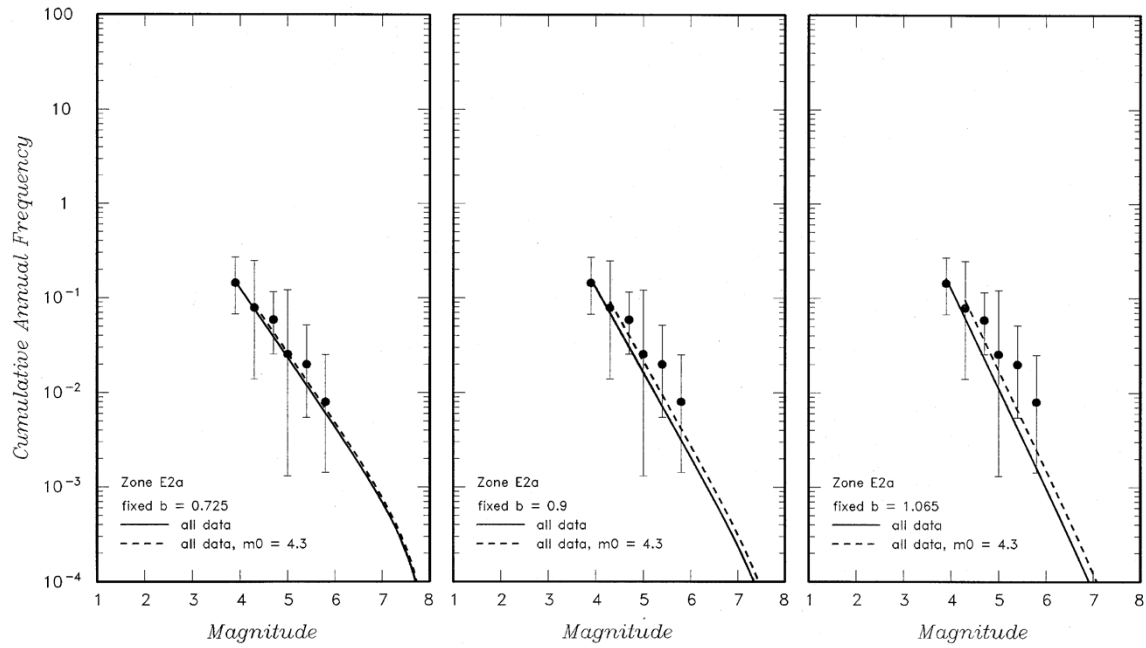
Fig. 93: Seismicity rates and fitting curves (solid line = considering all data, dashed line = considering magnitudes larger than 4.2) for Zone E2a

The 3 b-values are: the estimated one − 1 σ, the estimated one, the estimated one + 1 σ.
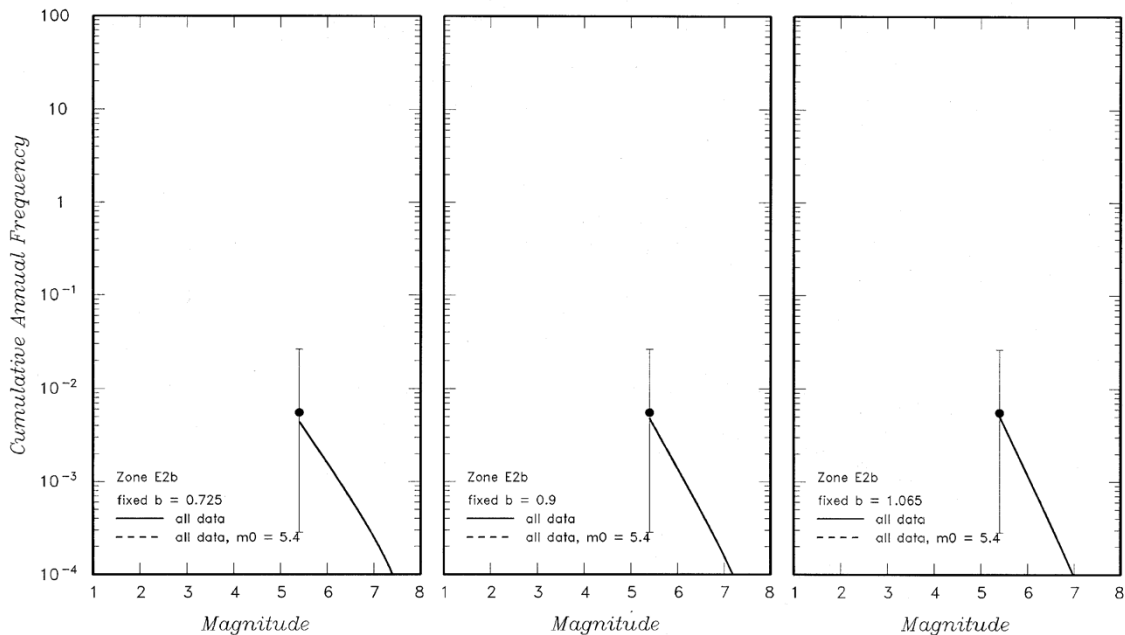
Fig. 94: Seismicity rates and fitting curves (solid line = considering all data, dashed line = considering magnitudes larger than 5.3) for Zone E2b

The 3 b-values are: the estimated one − 1 σ, the estimated one, the estimated one + 1 σ.
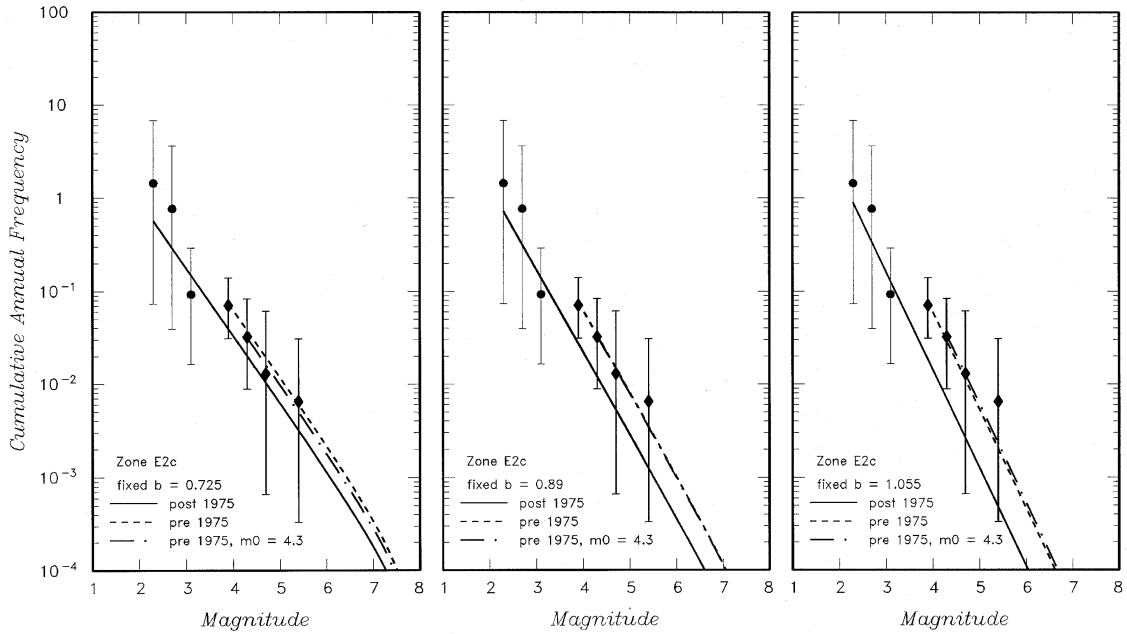
Fig. 95:   Seismicity rates and fitting curves (solid line = considering all data after 1975, dashed line = considering all data before 1975, dotted-dashed line = considering magnitudes larger than 4.2 before 1975) for Zone E2c

The 3 b-values are: the estimated one − 1 σ, the estimated one, the estimated one + 1 σ.
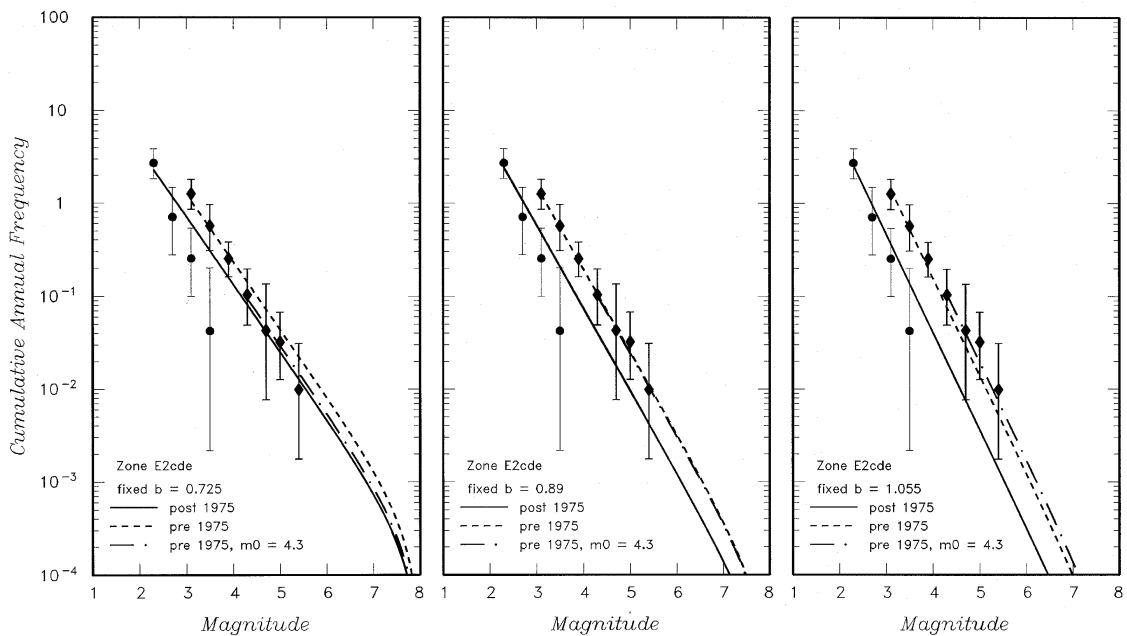
Fig. 96:   Seismicity rates and fitting curves (solid line = considering all data after 1975, dashed line = considering all data before 1975, dotted-dashed line = considering magnitudes larger than 4.2 before 1975) for Zone E2cde

The 3 b-values are: the estimated one − 1 σ, the estimated one, the estimated one + 1 σ.
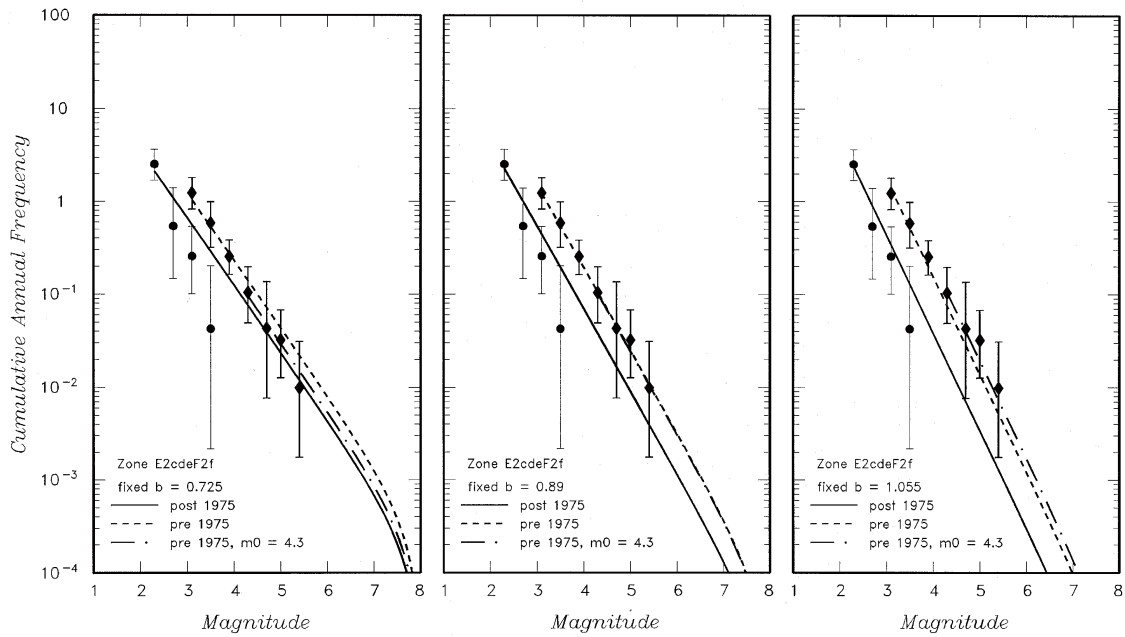
Fig. 97: Seismicity rates and fitting curves (solid line = considering all data after 1975, dashed line = considering all data before 1975, dotted-dashed line = considering magnitudes larger than 4.2 before 1975) for Zone E2cdeF2f

The 3 b-values are: the estimated one − 1 σ, the estimated one, the estimated one + 1 σ.
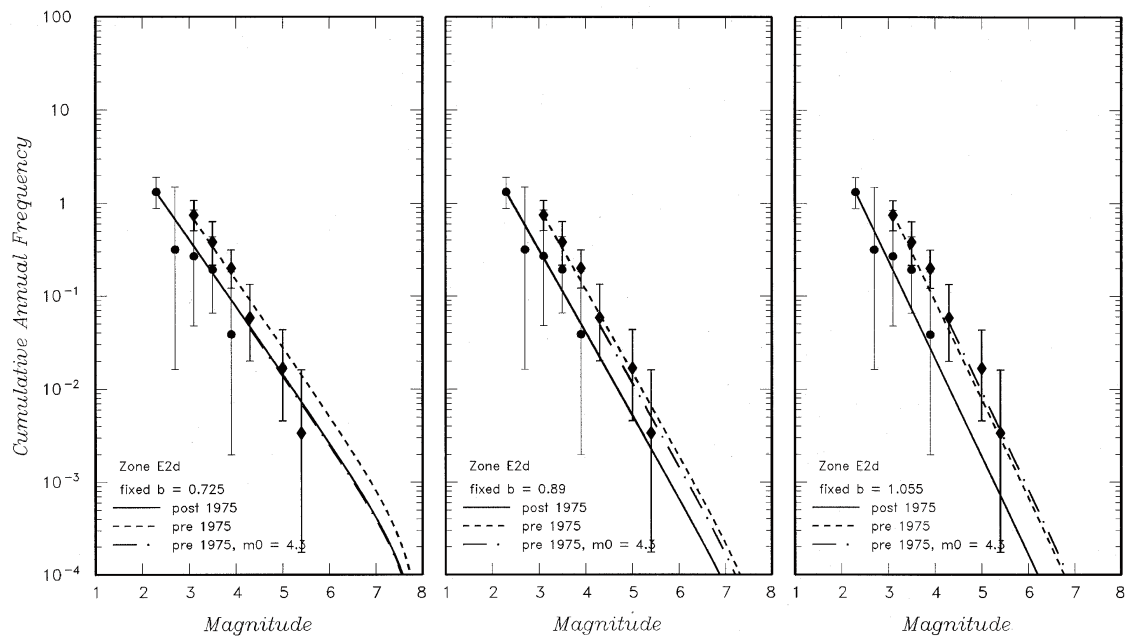
Fig. 98: Seismicity rates and fitting curves (solid line = considering all data after 1975, dashed line = considering all data before 1975, dotted-dashed line = considering magnitudes larger than 4.2 before 1975) for Zone E2d

The 3 b-values are: the estimated one − 1 σ, the estimated one, the estimated one + 1 σ.
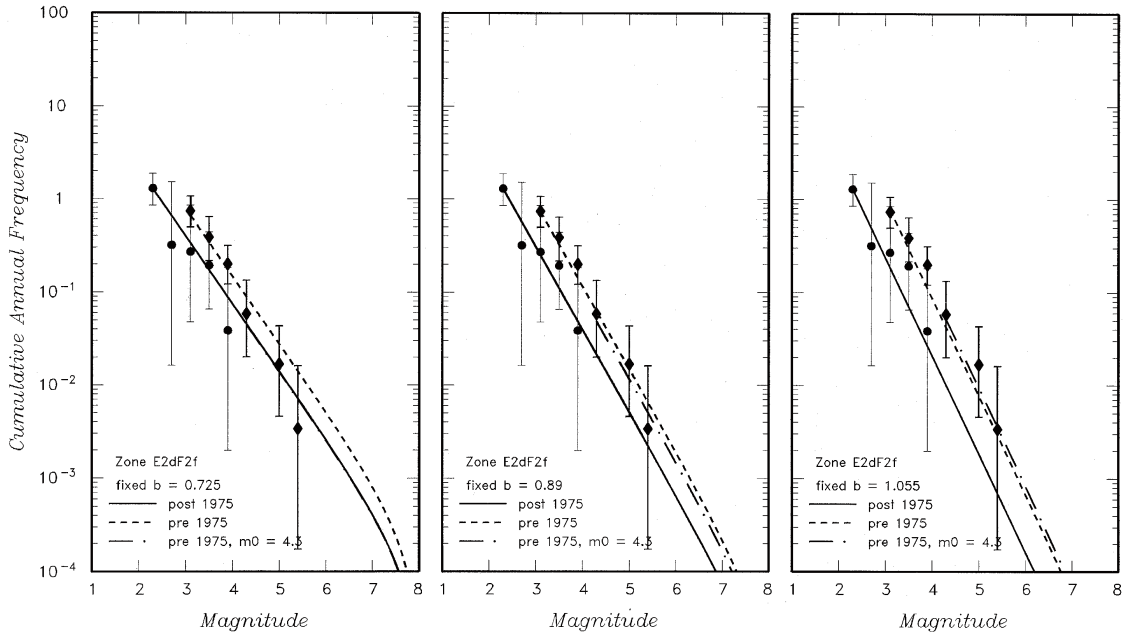
Fig. 99:   Seismicity rates and fitting curves (solid line = considering all data after 1975, dashed line = considering all data before 1975, dotted-dashed line = considering magnitudes larger than 4.2 before 1975) for Zone E2dF2f

The 3 b-values are: the estimated one − 1 σ, the estimated one, the estimated one + 1 σ.
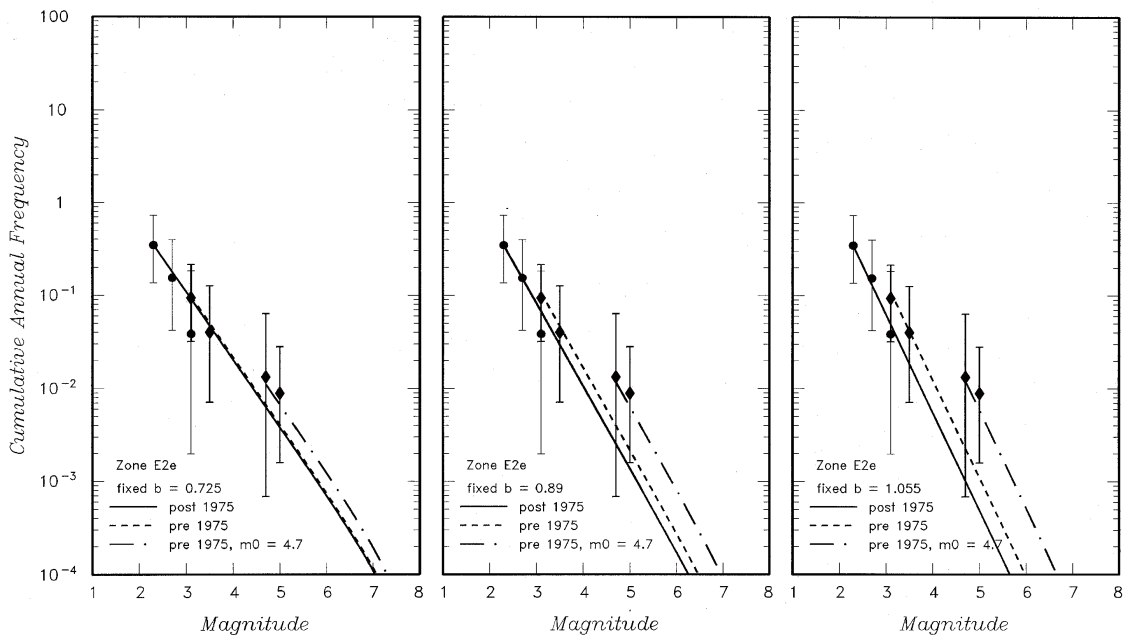
Fig. 100:   Seismicity rates and fitting curves (solid line = considering all data after 1975, dashed line = considering all data before 1975, dotted-dashed line = considering magnitudes larger than 4.6 before 1975) for Zone E2e

The 3 b-values are: the estimated one − 1 σ, the estimated one, the estimated one + 1 σ.
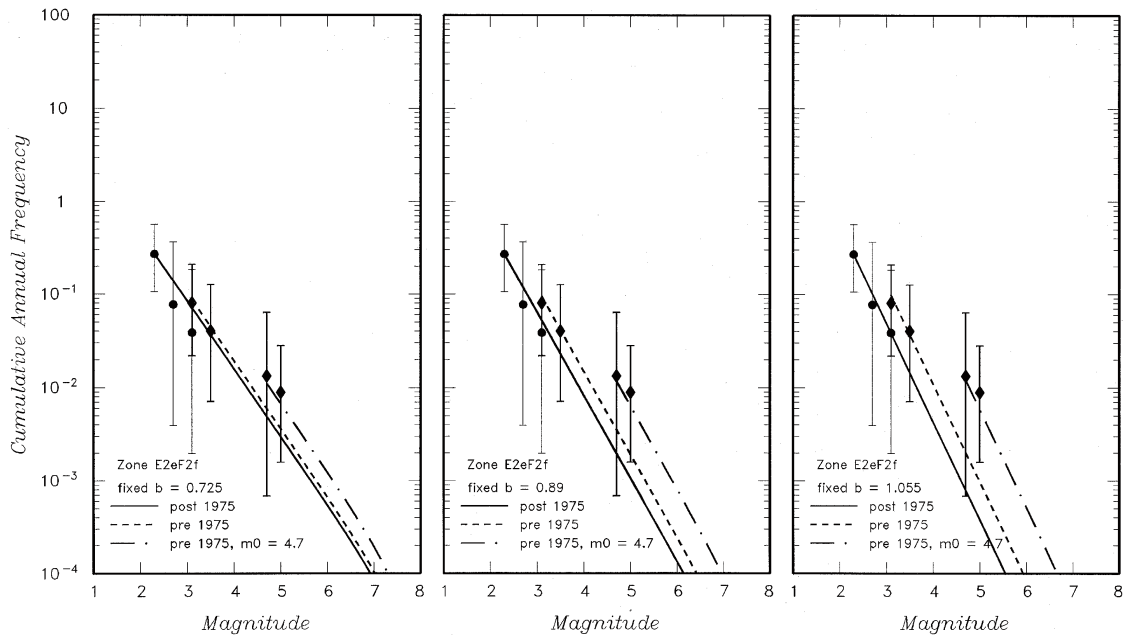
Fig. 101:   Seismicity rates and fitting curves (solid line = considering all data after 1975, dashed line = considering all data before 1975, dotted-dashed line = considering magnitudes larger than 4.6 before 1975) for Zone E2eF2f

The 3 b-values are: the estimated one − 1 σ, the estimated one, the estimated one + 1 σ.
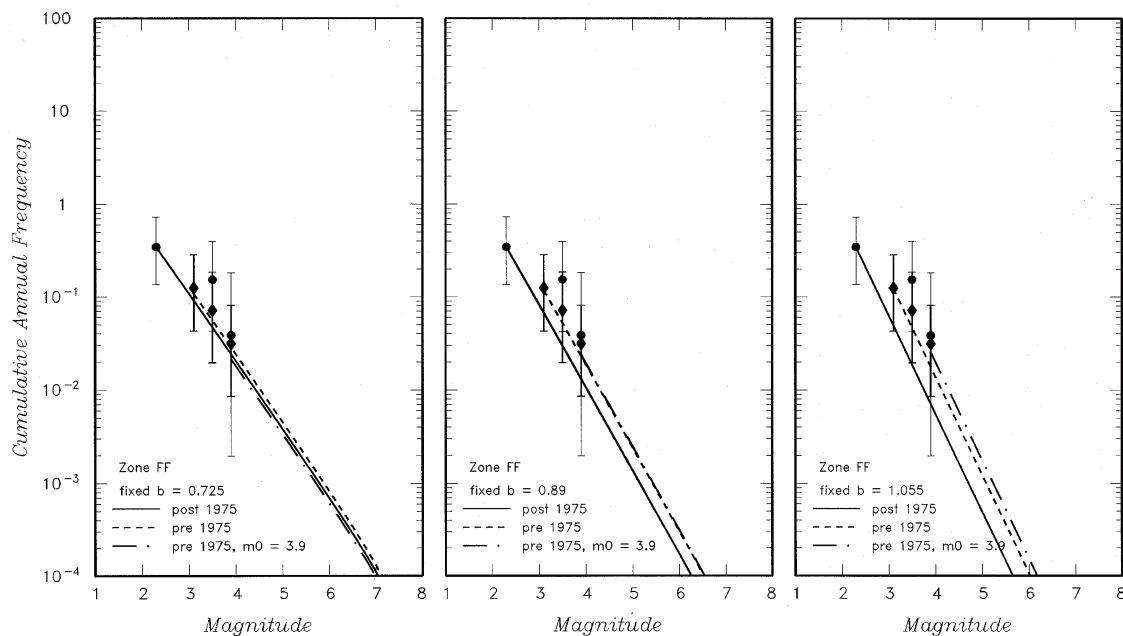
Fig. 102:   Seismicity rates and fitting curves (solid line = considering all data after 1975, dashed line = considering all data before 1975, dotted-dashed line = considering magnitudes larger than 3.8 before 1975) for Zone FF

The 3 b-values are: the estimated one − 1 σ, the estimated one, the estimated one + 1 σ.
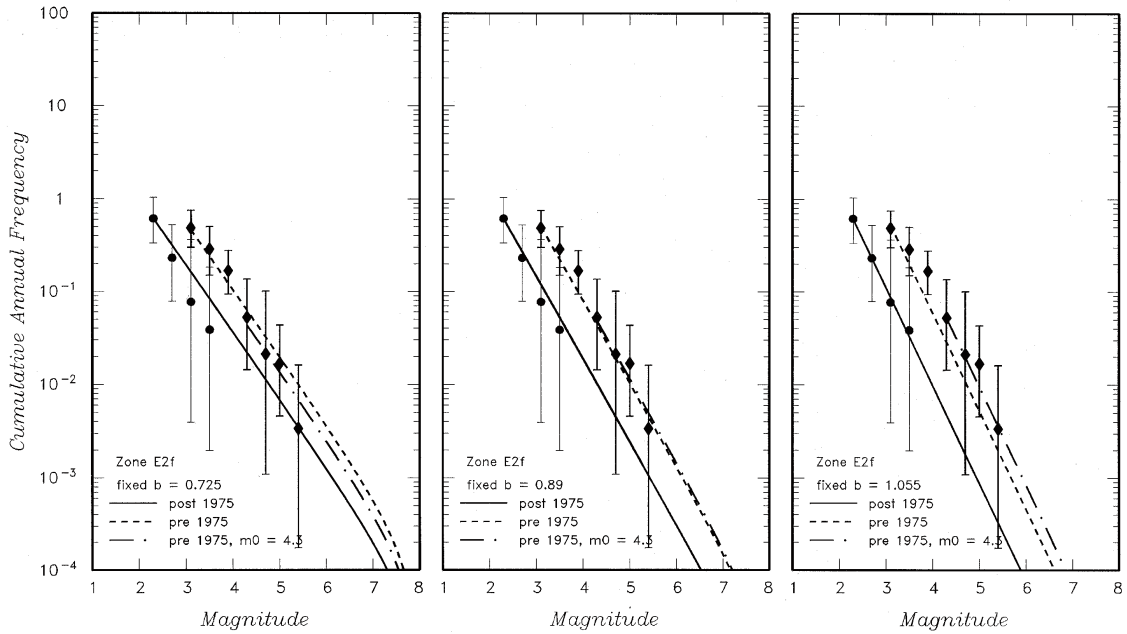
Fig. 103: Seismicity rates and fitting curves (solid line = considering all data after 1975, dashed line = considering all data before 1975, dotted-dashed line = considering magnitudes larger than 4.2 before 1975) for Zone E2f

The 3 b-values are: the estimated one − 1 σ, the estimated one, the estimated one + 1 σ.
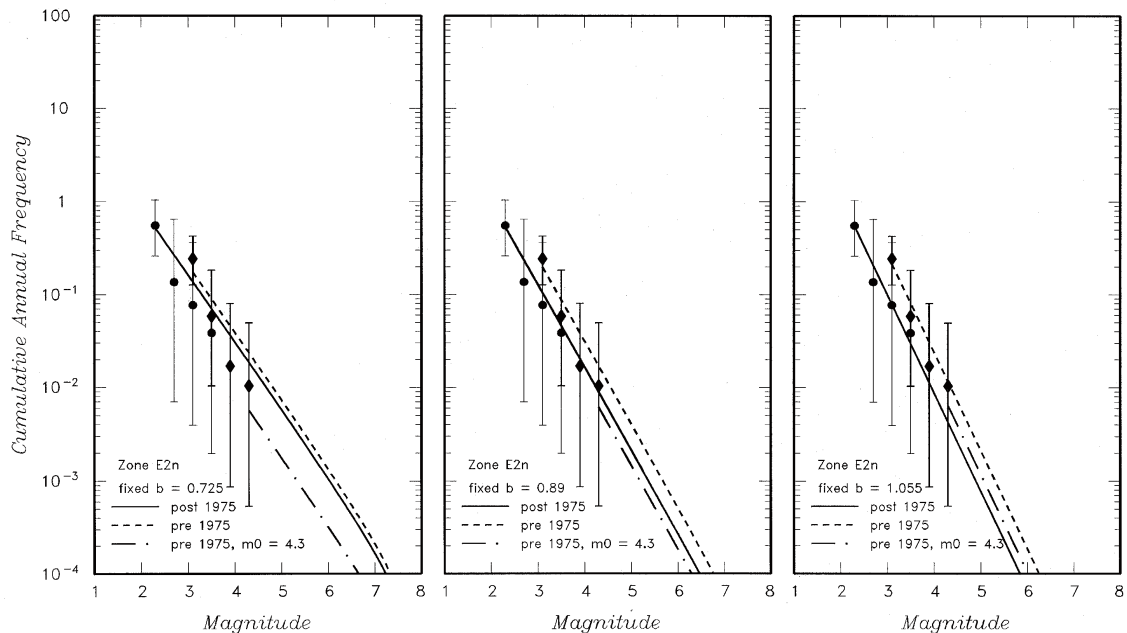
Fig. 104: Seismicity rates and fitting curves (solid line = considering all data after 1975, dashed line = considering all data before 1975, dotted-dashed line = considering magnitudes larger than 4.2 before 1975) for Zone E2n

The 3 b-values are: the estimated one − 1 σ, the estimated one, the estimated one + 1 σ.
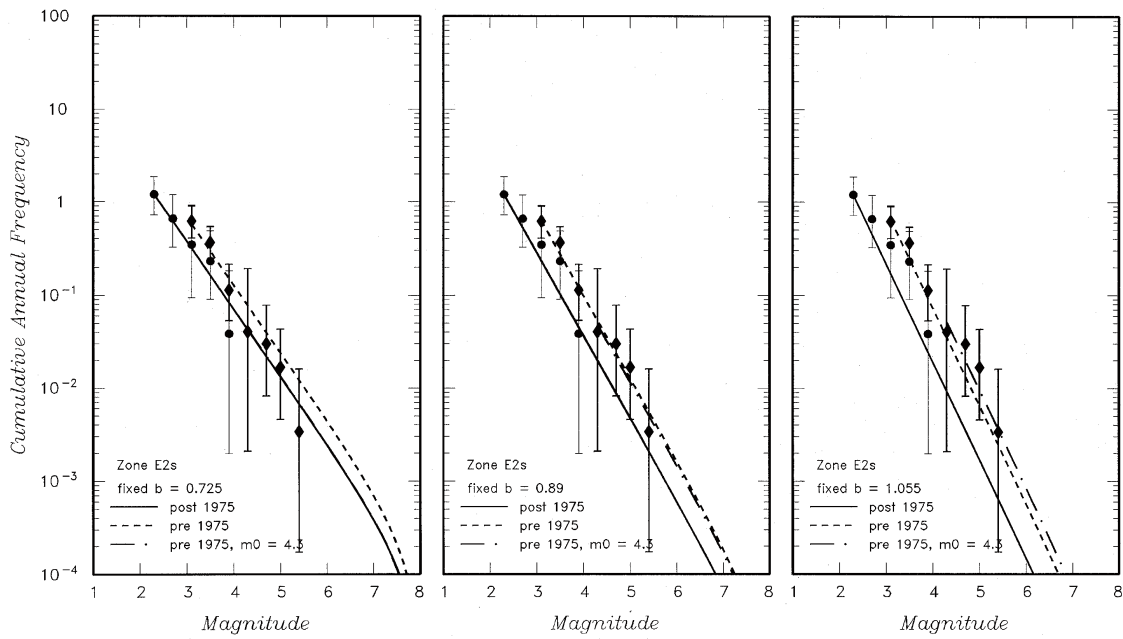
Fig. 105: Seismicity rates and fitting curves (solid line = considering all data after 1975, dashed line = considering all data before 1975, dotted-dashed line = considering magnitudes larger than 4.2 before 1975) for Zone E2s

The 3 b-values are: the estimated one − 1 σ, the estimated one, the estimated one + 1 σ.
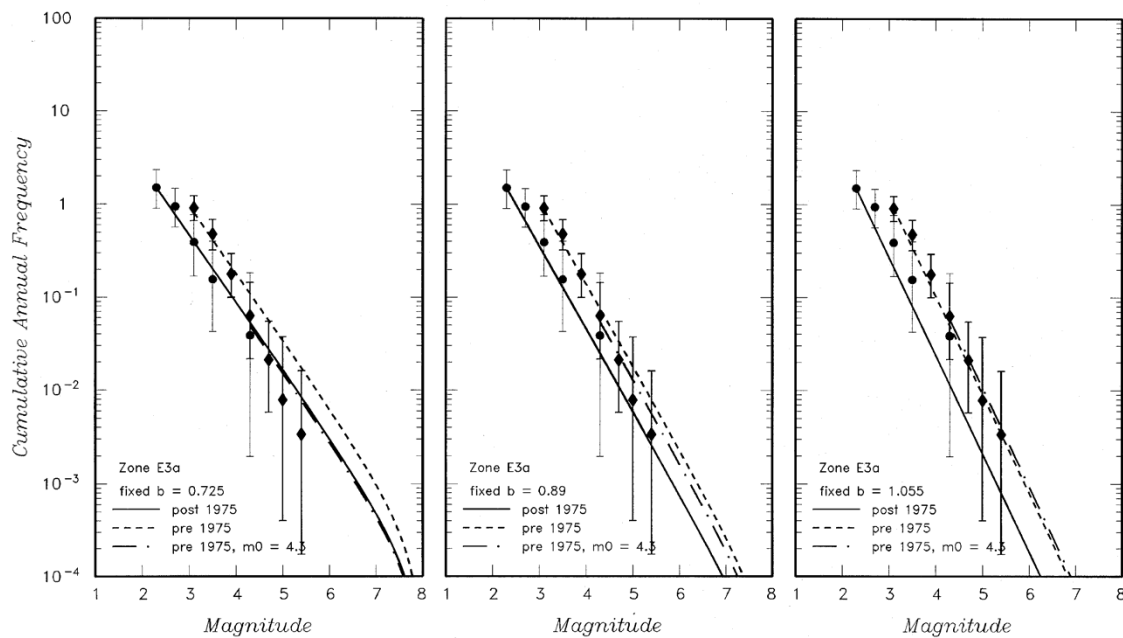
Fig. 106: Seismicity rates and fitting curves (solid line = considering all data after 1975, dashed line = considering all data before 1975, dotted-dashed line = considering magnitudes larger than 4.2 before 1975) for Zone E3a

The 3 b-values are: the estimated one − 1 σ the estimated one, the estimated one + 1 σ.
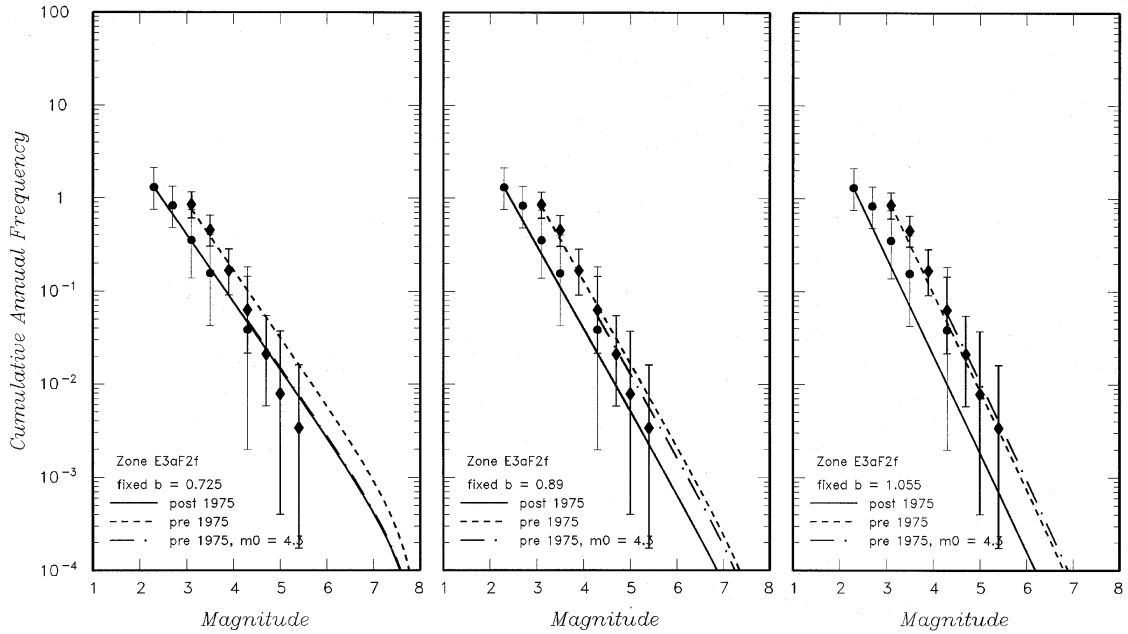
Fig. 107:   Seismicity rates and fitting curves (solid line = considering all data after 1975, dashed line = considering all data before 1975, dotted-dashed line = considering magnitudes larger than 4.2 before 1975) for Zone E3aF2f

The 3 b-values are: the estimated one − 1 σ, the estimated one, the estimated one + 1 σ.
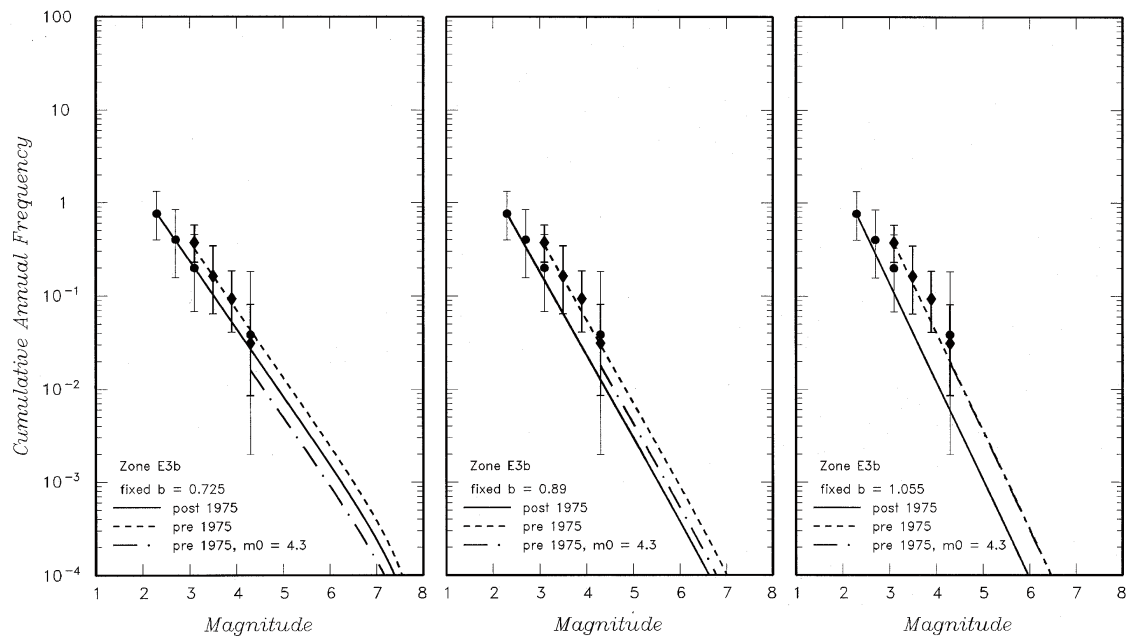
Fig. 108:   Seismicity rates and fitting curves (solid line = considering all data after 1975, dashed line = considering all data before 1975, dotted-dashed line = considering magnitudes larger than 4.2 before 1975) for Zone E3b

The 3 b-values are: the estimated one − 1 σ, the estimated one, the estimated one + 1 σ.
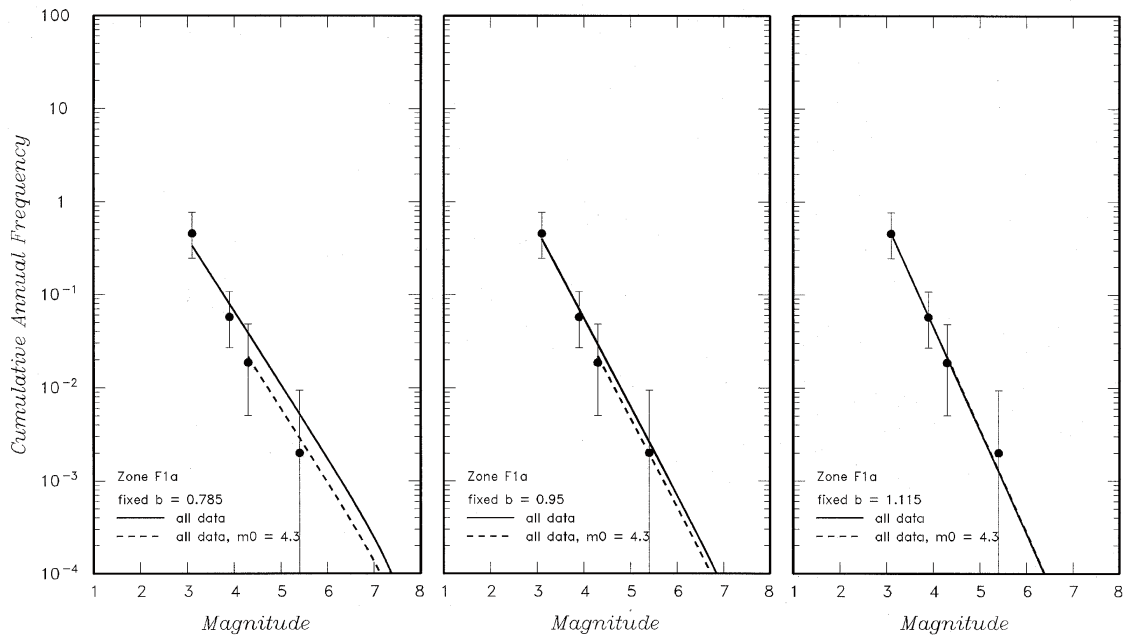
Fig. 109:　Seismicity rates and fitting curves (solid line = considering all data, dashed line = considering magnitudes larger than 4.2) for Zone F1a

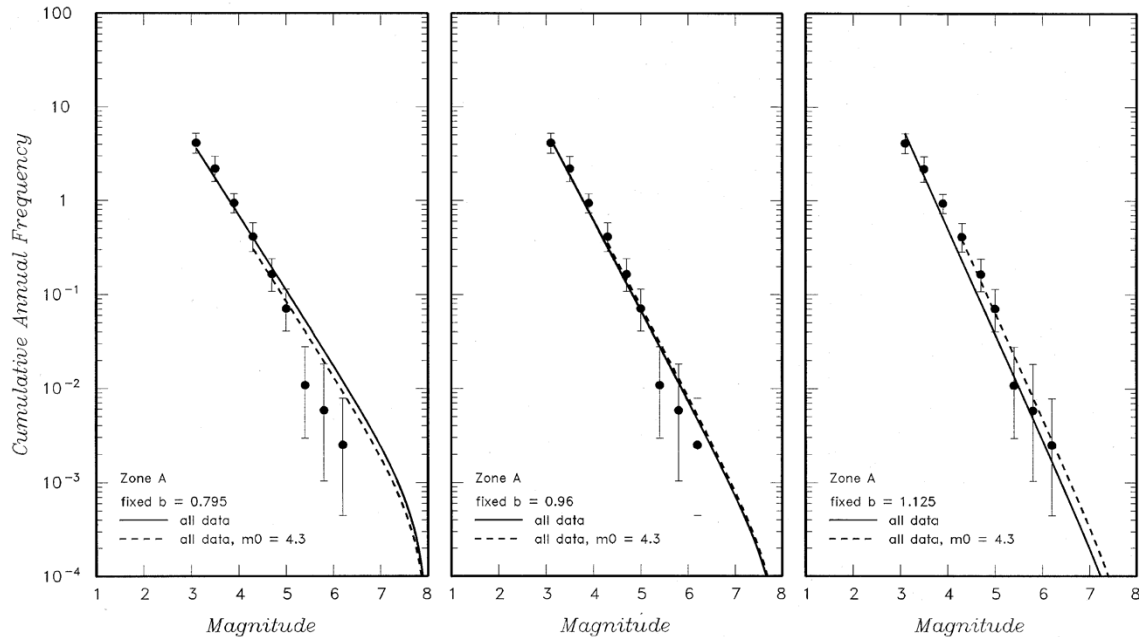The 3 b-values are: the estimated one − 1 σ, the estimated one, the estimated one + 1 σ.
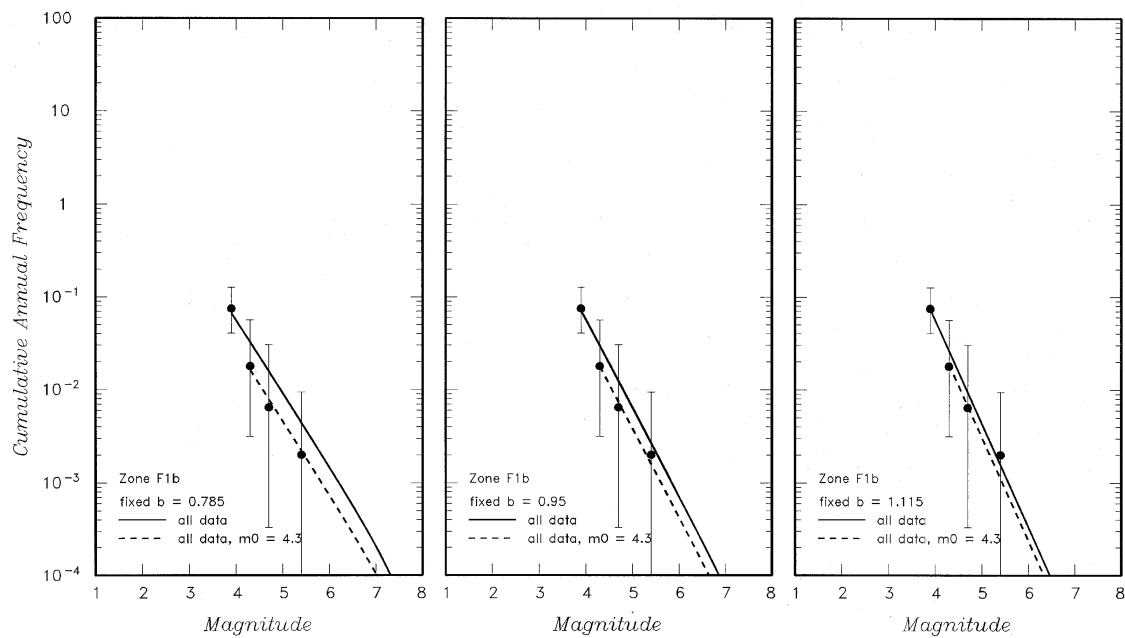
Fig. 110:　Seismicity rates and fitting curves (solid line = considering all data, dashed line = considering magnitudes larger than 4.2) for Zone F1b

The 3 b-values are: the estimated one − 1 σ, the estimated one, the estimated one + 1 σ.
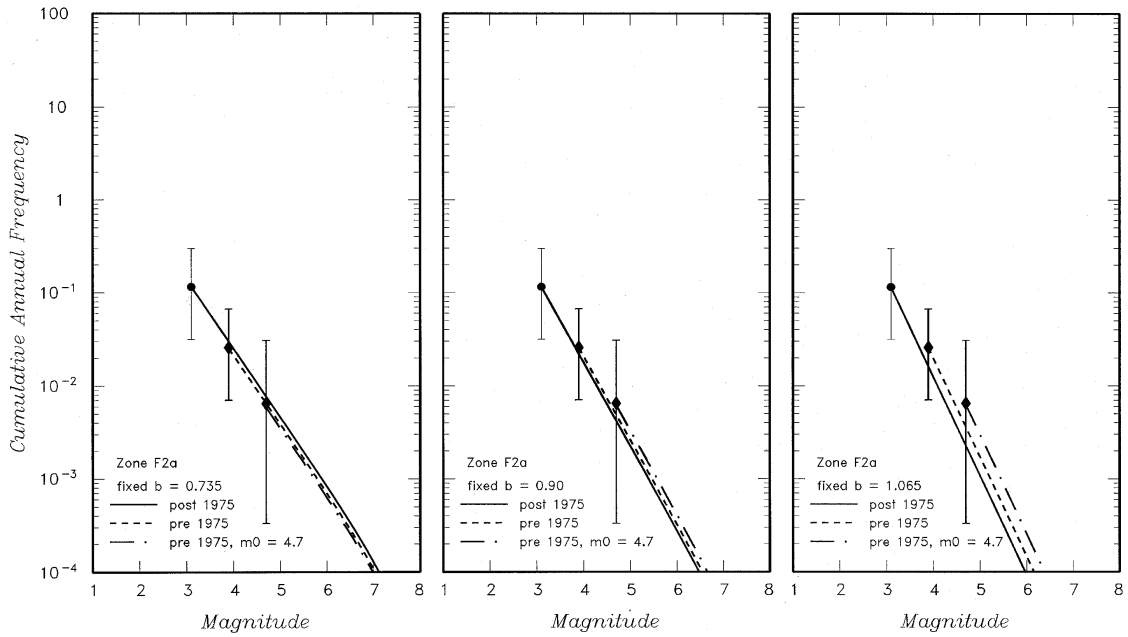
Fig. 111:   Seismicity rates and fitting curves (solid line = considering all data after 1975,
            dashed line = considering all data before 1975, dotted-dashed line = considering
            magnitudes larger than 4.6 before 1975) for Zone F2a

            The 3 b-values are: the estimated one − 1 σ, the estimated one, the estimated one
            + 1 σ.
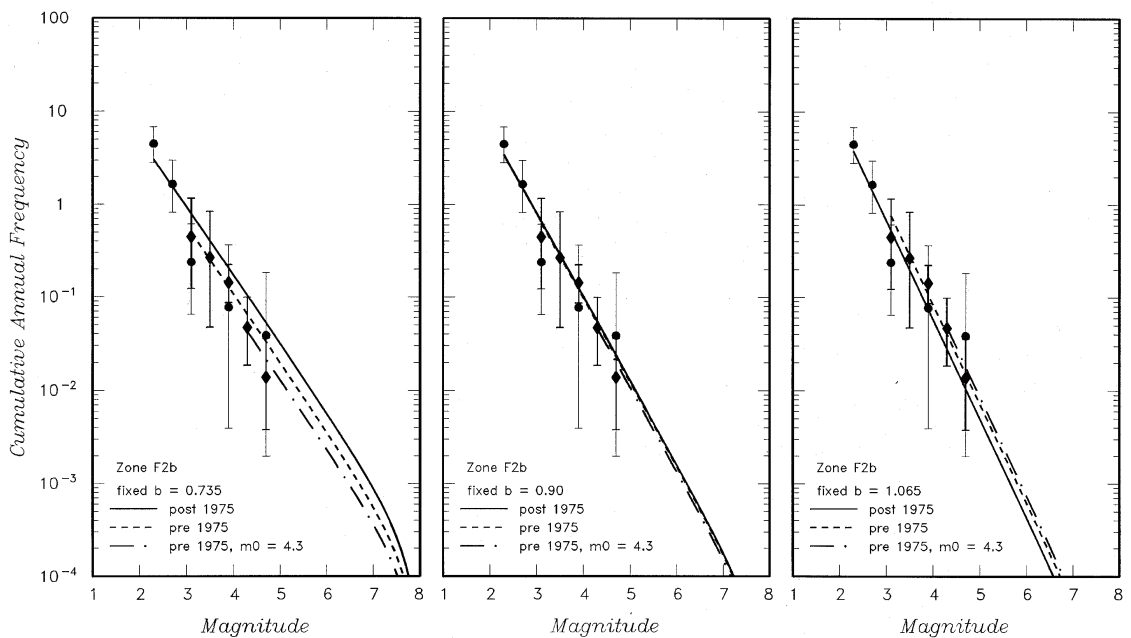
Fig. 112:   Seismicity rates and fitting curves (solid line = considering all data after 1975,
            dashed line = considering all data before 1975, dotted-dashed line = considering
            magnitudes larger than 4.2 before 1975) for Zone F2b

            The 3 b-values are: the estimated one − 1 σ, the estimated one, the estimated one
            + 1 σ.
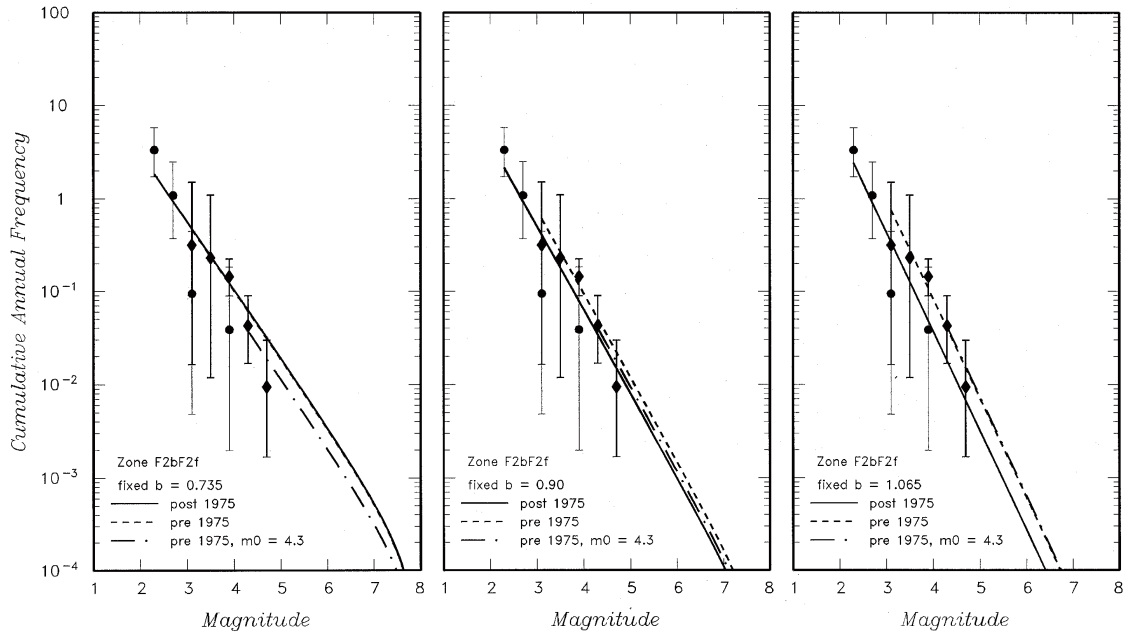
Fig. 113:   Seismicity rates and fitting curves (solid line = considering all data after 1975, dashed line = considering all data before 1975, dotted-dashed line = considering magnitudes larger than 4.2 before 1975) for Zone F2bF2f

The 3 b-values are: the estimated one − 1 σ, the estimated one, the estimated one + 1 σ.
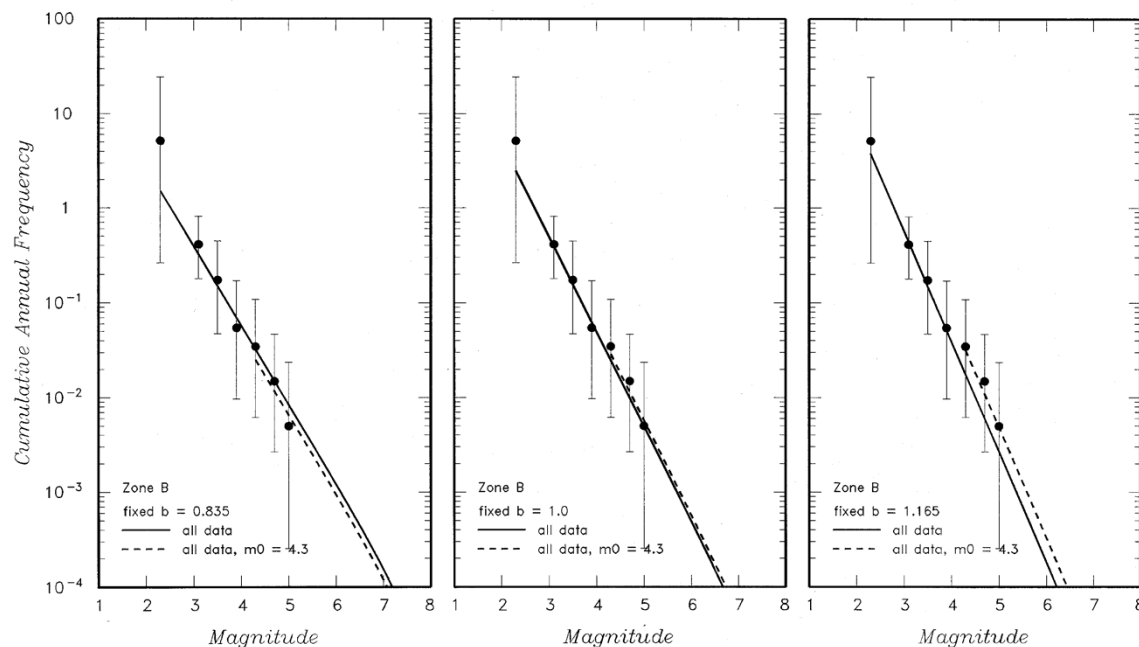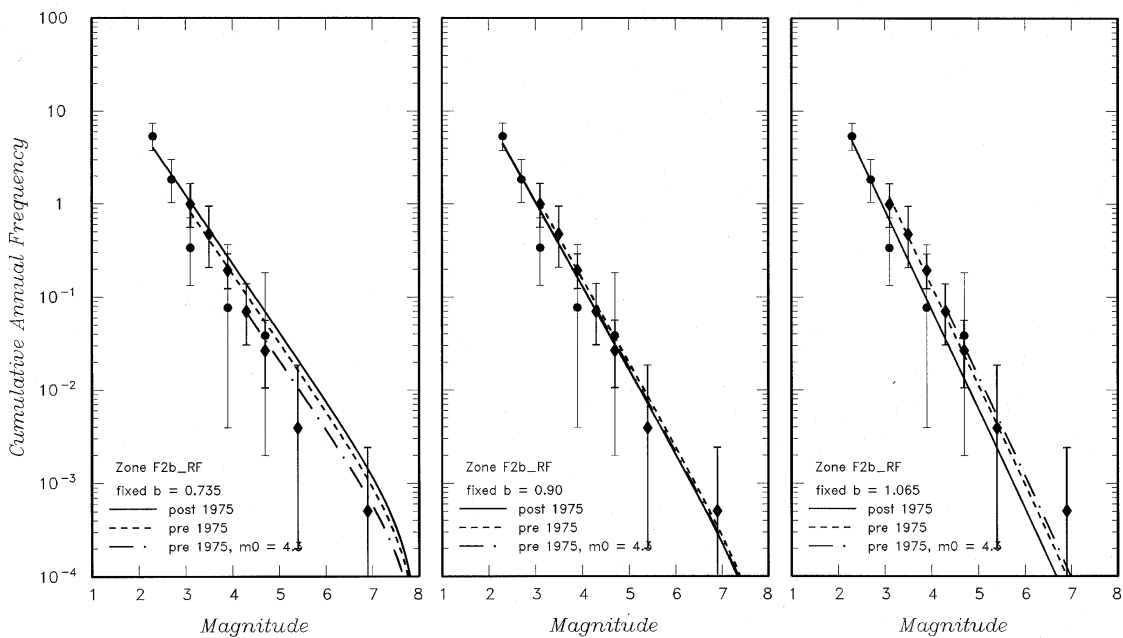

Fig. 114:   Seismicity rates and fitting curves (solid line = considering all data after 1975, dashed line = considering all data before 1975, dotted-dashed line = considering magnitudes larger than 4.2 before 1975) for Zone F2b_RF

The 3 b-values are: the estimated one − 1 σ, the estimated one, the estimated one + 1 σ.
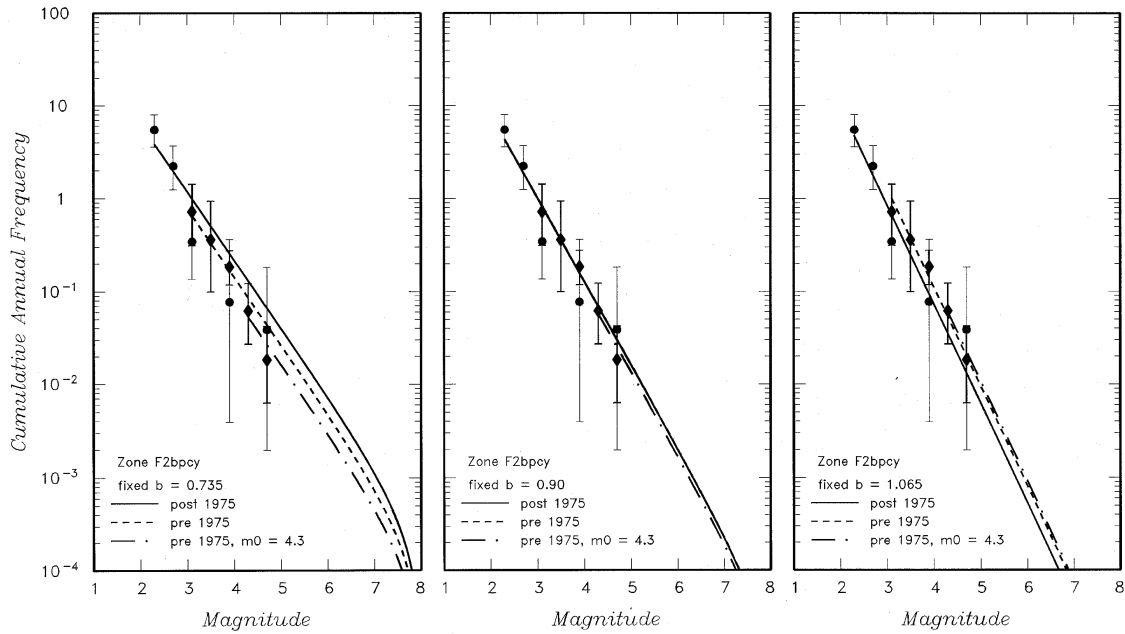
Fig. 115:   Seismicity rates and fitting curves (solid line = considering all data after 1975, dashed line = considering all data before 1975, dotted-dashed line = considering magnitudes larger than 4.2 before 1975) for Zone F2bpcy

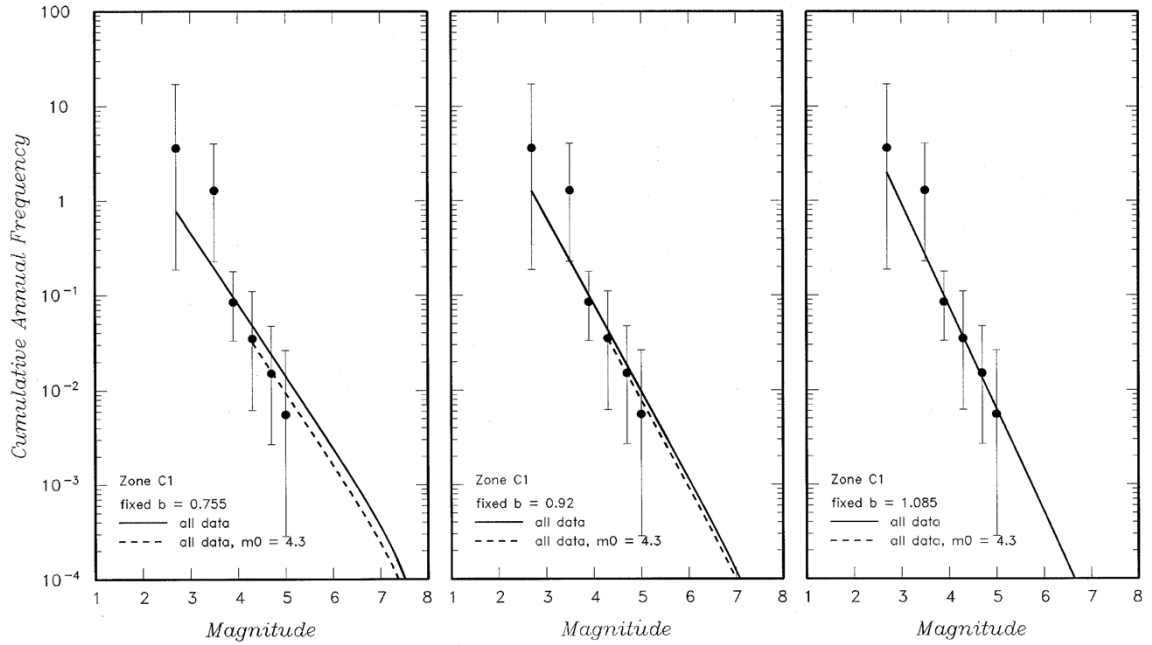The 3 b-values are: the estimated one − 1 σ, the estimated one, the estimated one + 1 σ.
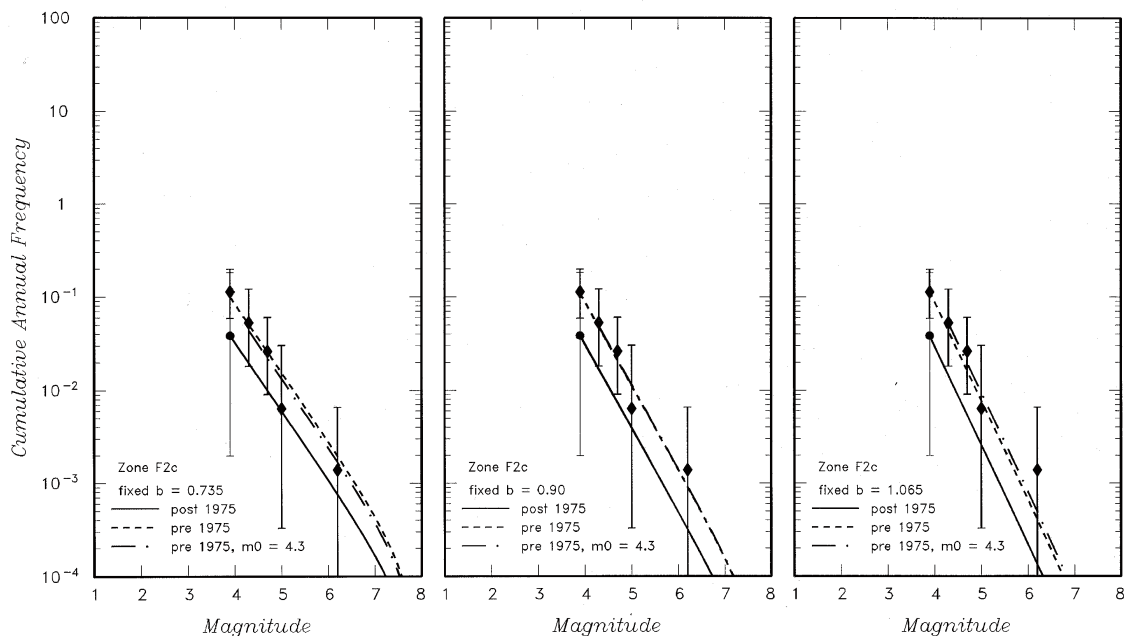
Fig. 116:   Seismicity rates and fitting curves (solid line = considering all data after 1975, dashed line = considering all data before 1975, dotted-dashed line = considering magnitudes larger than 4.2 before 1975) for Zone F2c

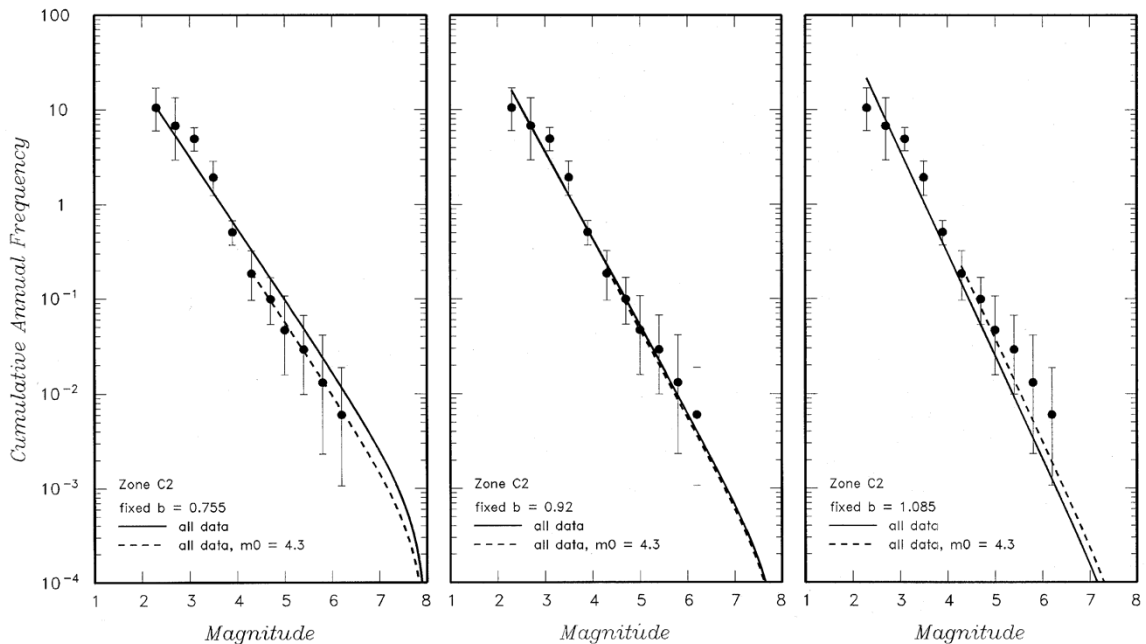The 3 b-values are: the estimated one − 1 σ, the estimated one, the estimated one + 1 σ.
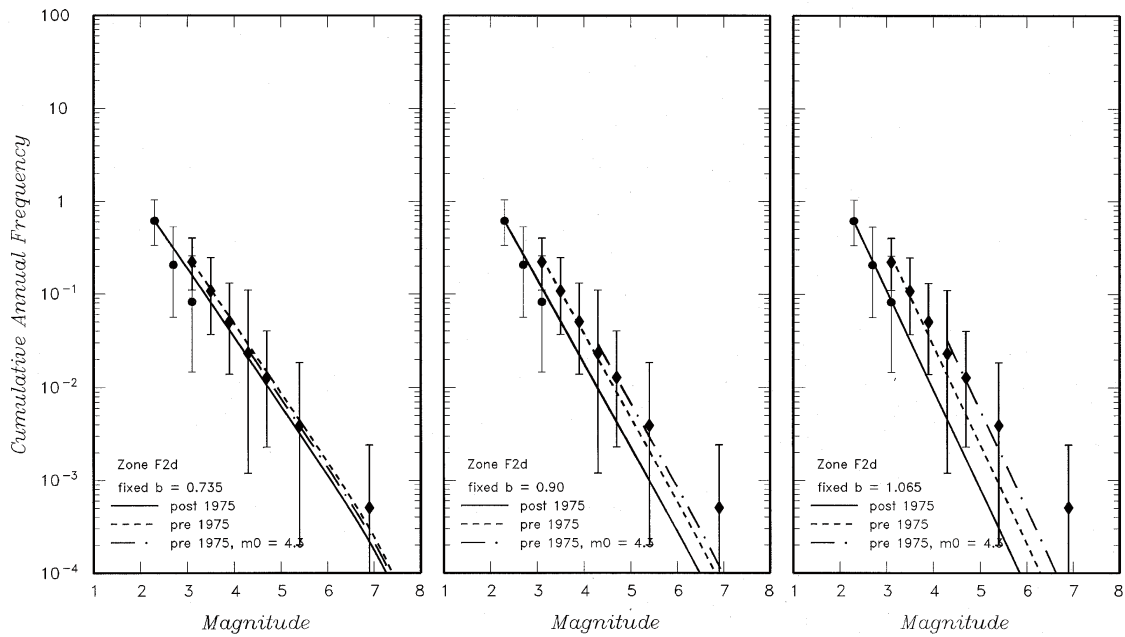
Fig. 117:   Seismicity rates and fitting curves (solid line = considering all data after 1975, dashed line = considering all data before 1975, dotted-dashed line = considering magnitudes larger than 4.2 before 1975) for Zone F2d

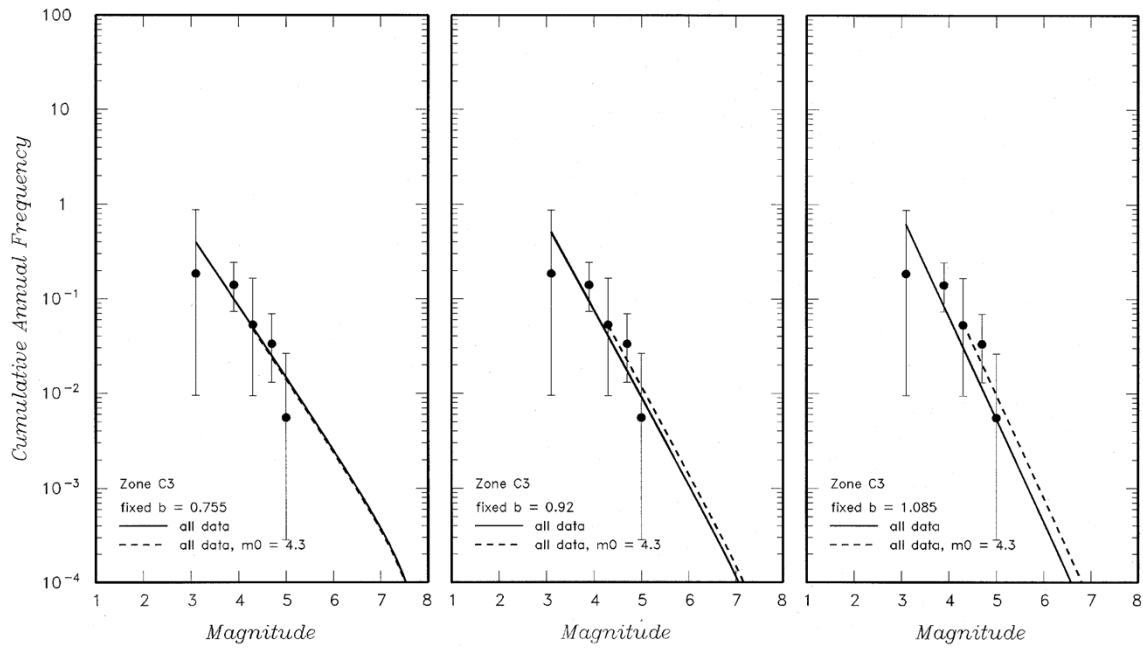The 3 b-values are: the estimated one − 1 σ, the estimated one, the estimated one + 1 σ.
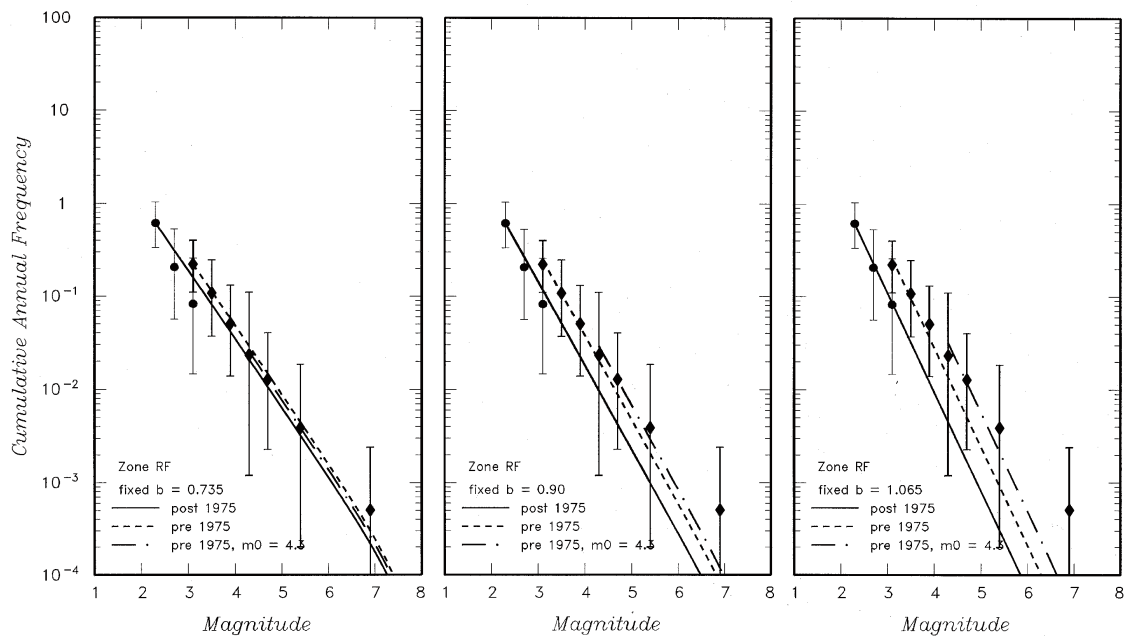
Fig. 118:   Seismicity rates and fitting curves (solid line = considering all data after 1975, dashed line = considering all data before 1975, dotted-dashed line = considering magnitudes larger than 4.2 before 1975) for Zone RF

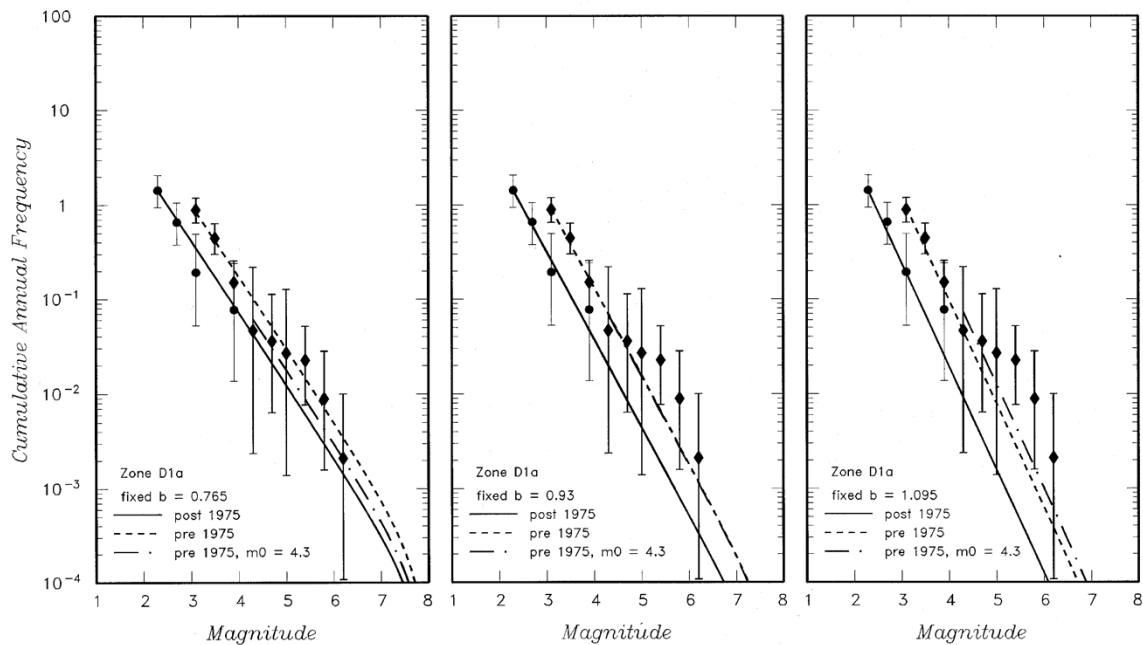The 3 b-values are: the estimated one − 1 σ, the estimated one, the estimated one + 1 σ.
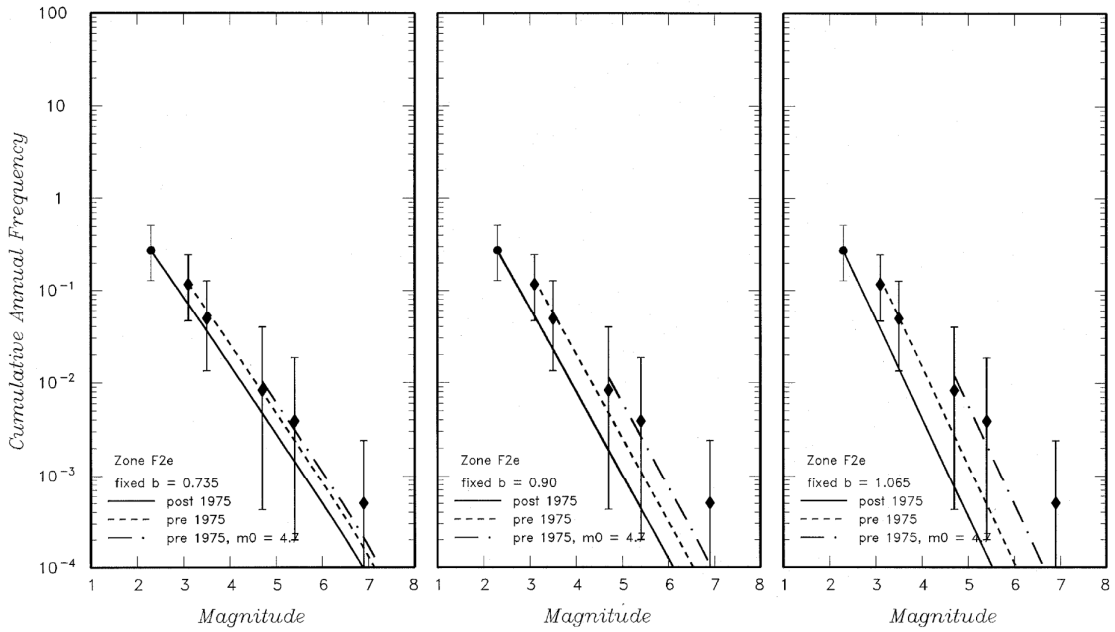
Fig. 119:   Seismicity rates and fitting curves (solid line = considering all data after 1975, dashed line = considering all data before 1975, dotted-dashed line = considering magnitudes larger than 4.2 before 1975) for Zone F2e

The 3 b-values are: the estimated one − 1 σ, the estimated one, the estimated one + 1 σ.
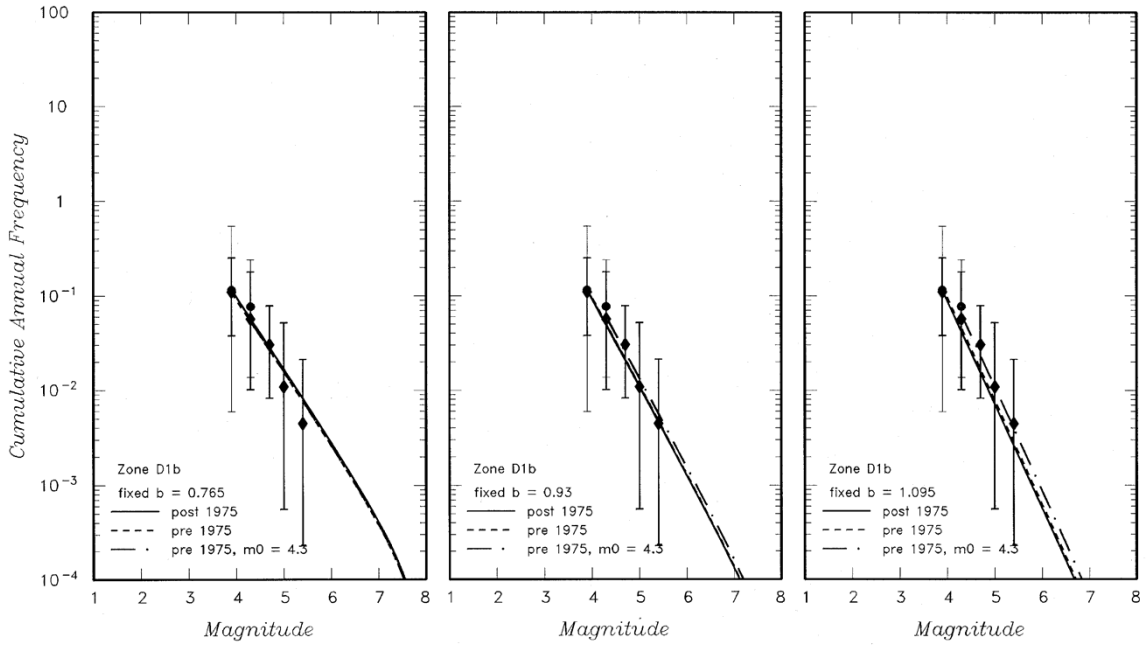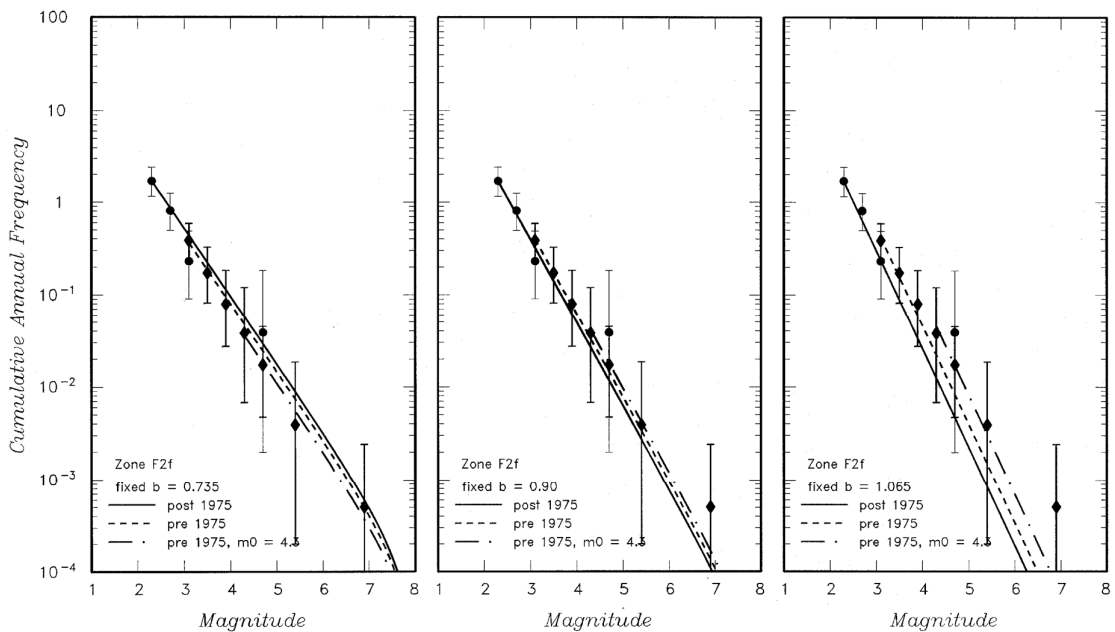

Fig. 120:   Seismicity rates and fitting curves (solid line = considering all data after 1975, dashed line = considering all data before 1975, dotted-dashed line = considering magnitudes larger than 4.2 before 1975) for Zone F2f

The 3 b-values are: the estimated one − 1 σ, the estimated one, the estimated one + 1 σ.
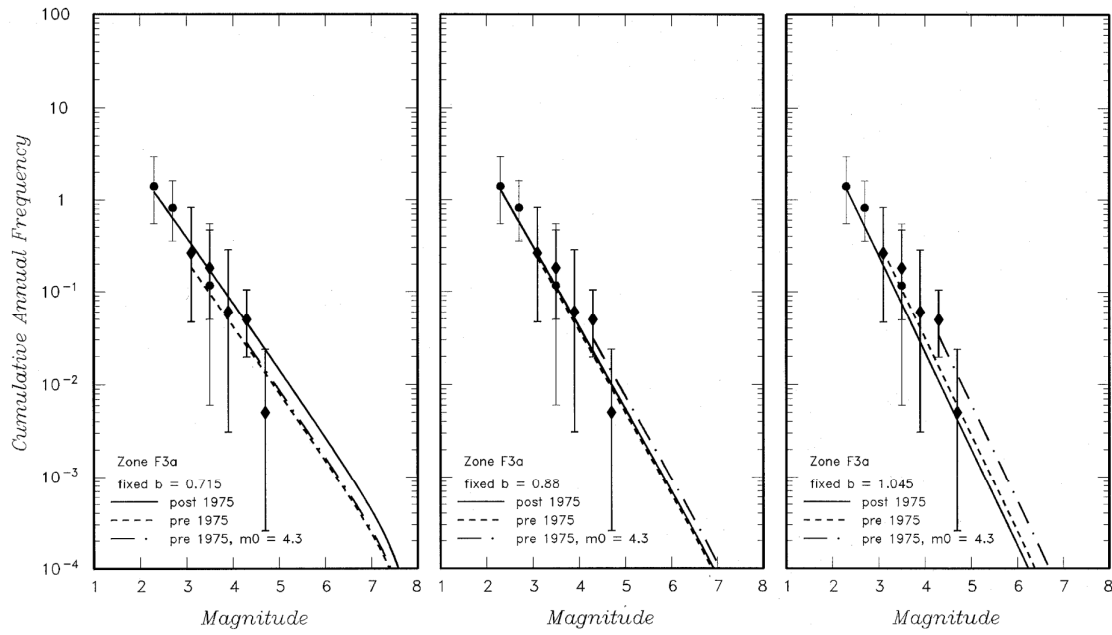
Fig. 121:   Seismicity rates and fitting curves (solid line = considering all data after 1975, dashed line = considering all data before 1975, dotted-dashed line = considering magnitudes larger than 4.2 before 1975) for Zone F3a

The 3 b-values are: the estimated one − 1 σ, the estimated one, the estimated one + 1 σ.
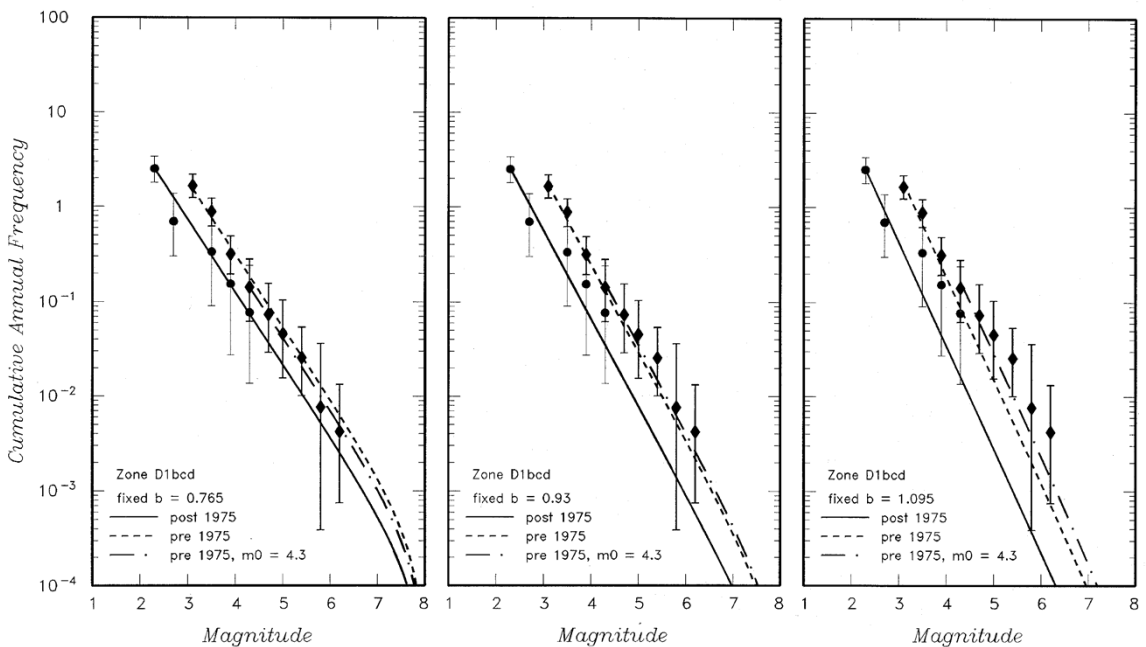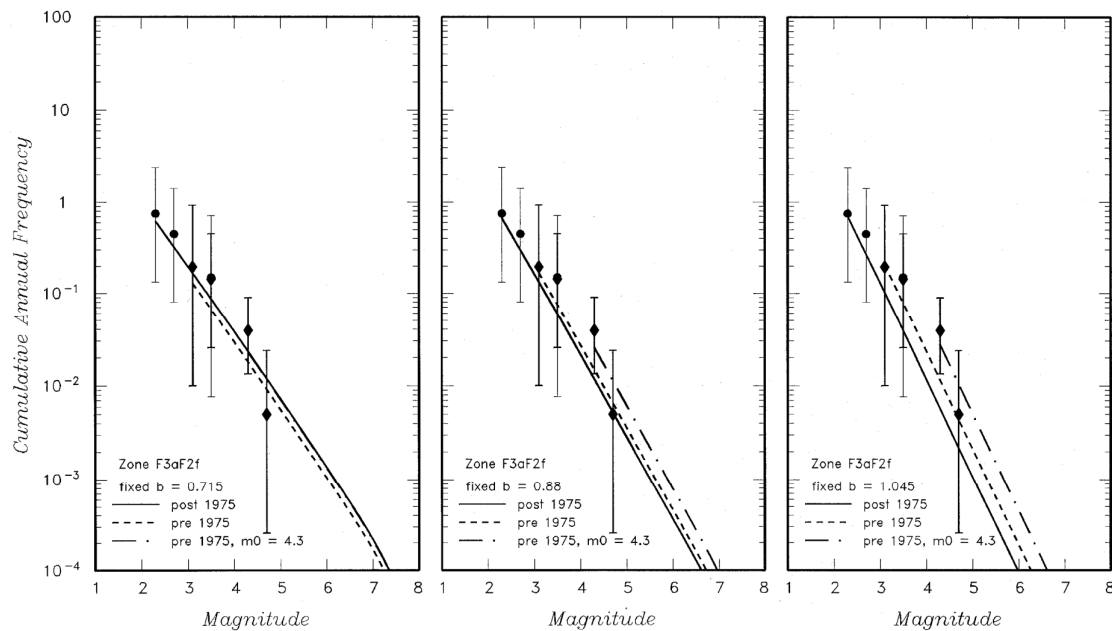

Fig. 122:   Seismicity rates and fitting curves (solid line = considering all data after 1975, dashed line = considering all data before 1975, dotted-dashed line = considering magnitudes larger than 4.2 before 1975) for Zone F3aF2f

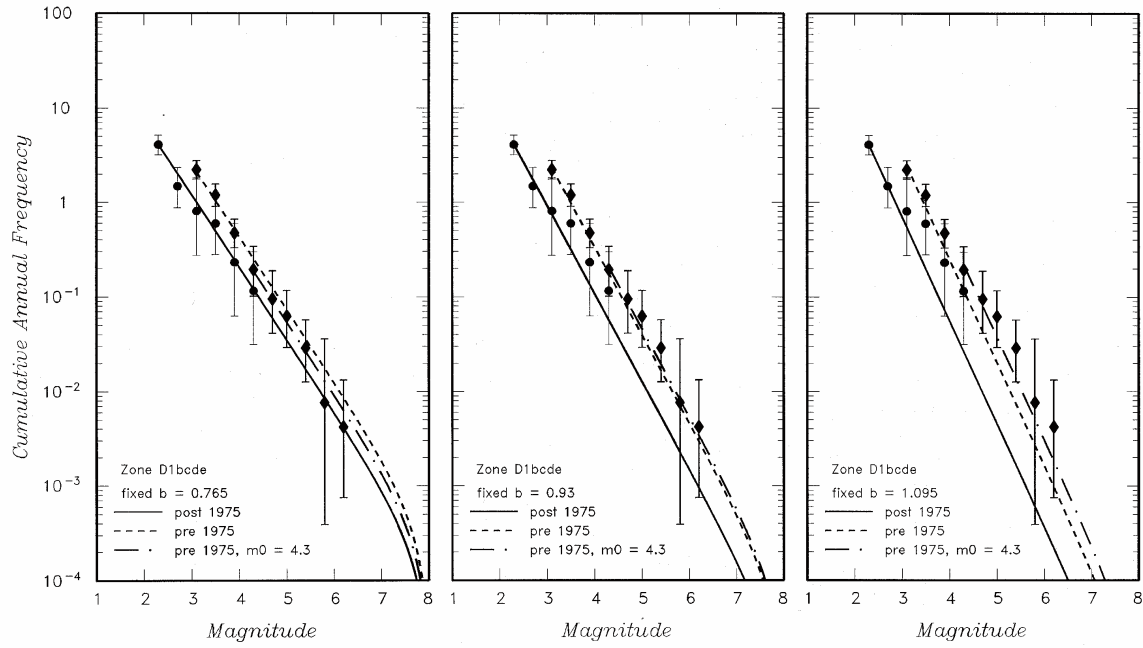The 3 b-values are: the estimated one − 1 σ, the estimated one, the estimated one + 1 σ.
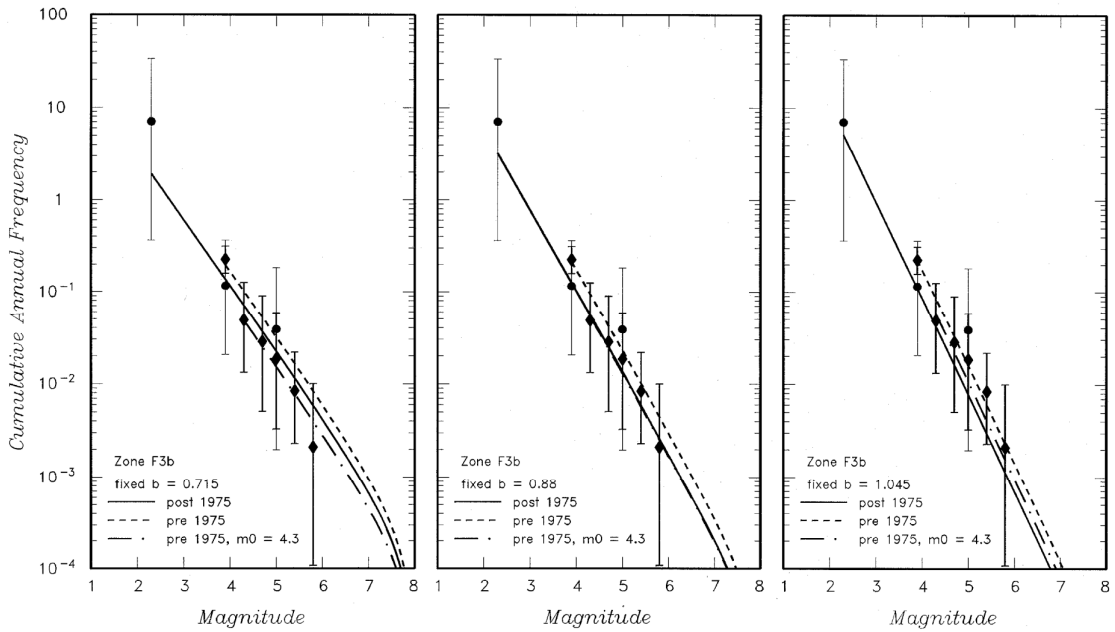
Fig. 123:   Seismicity rates and fitting curves (solid line = considering all data after 1975, dashed line = considering all data before 1975, dotted-dashed line = considering magnitudes larger than 4.2 before 1975) for Zone F3b

The 3 b-values are: the estimated one − 1 σ, the estimated one, the estimated one + 1 σ.
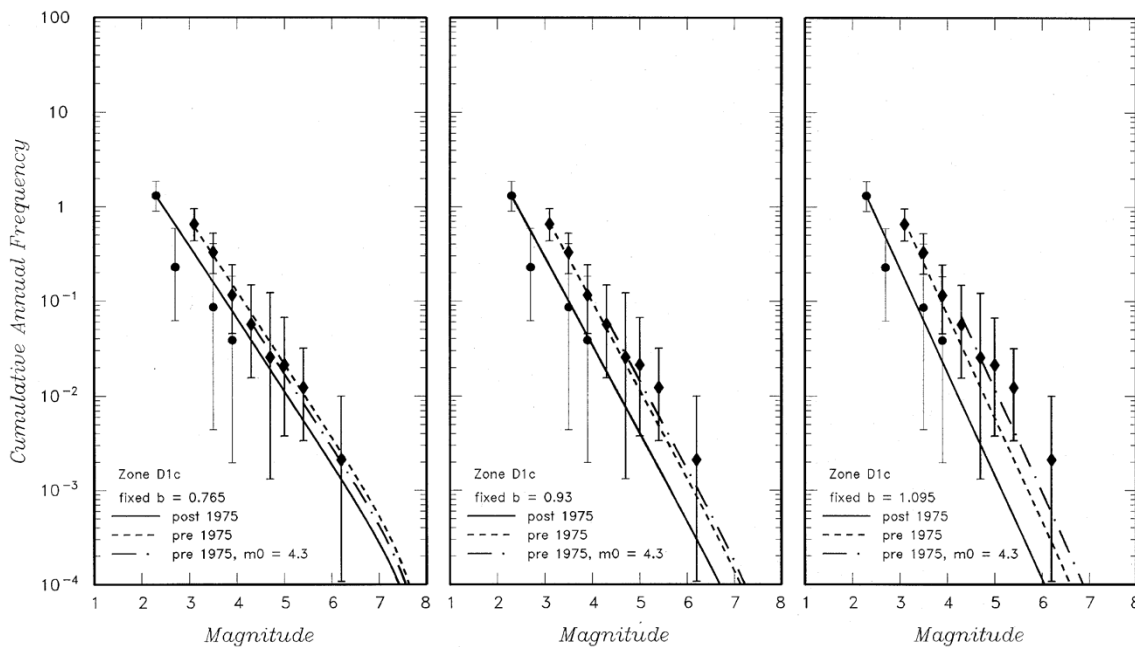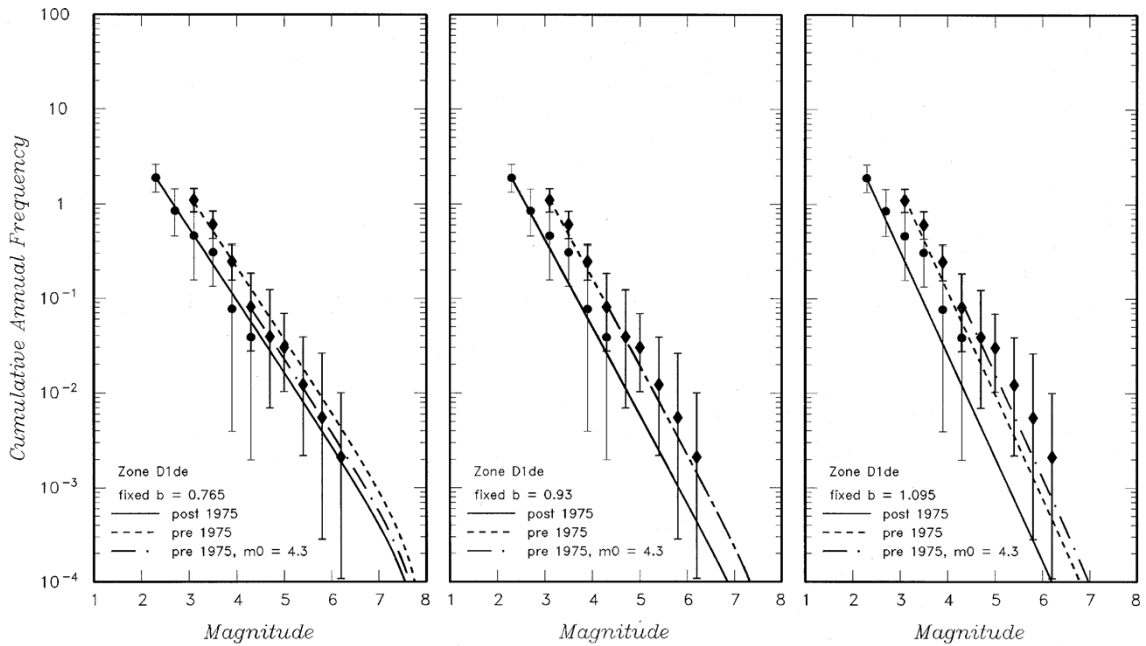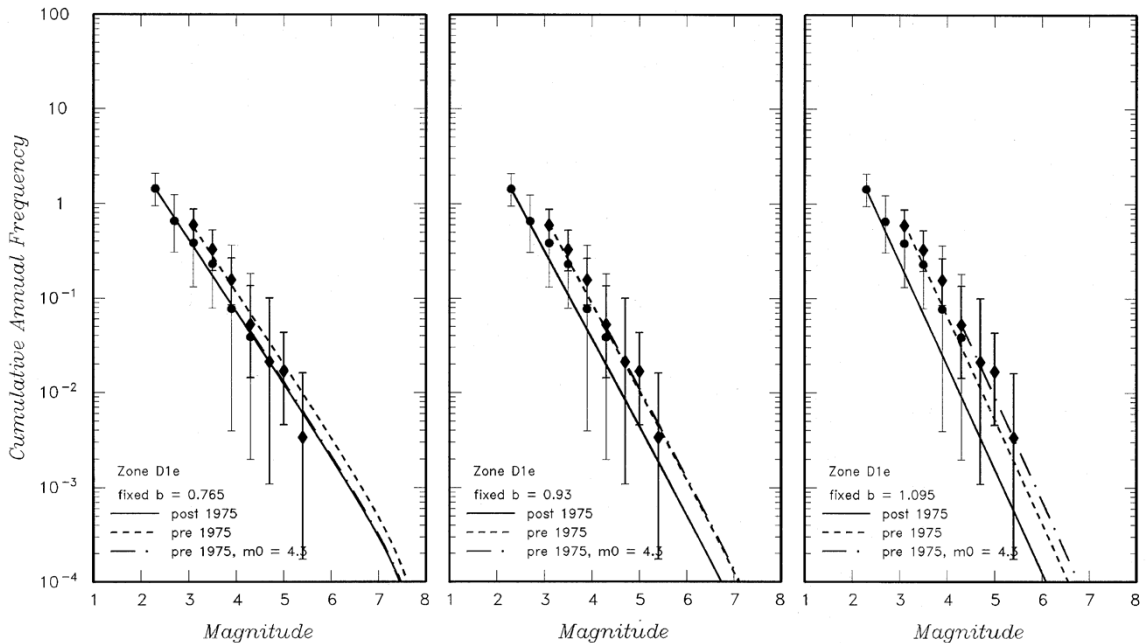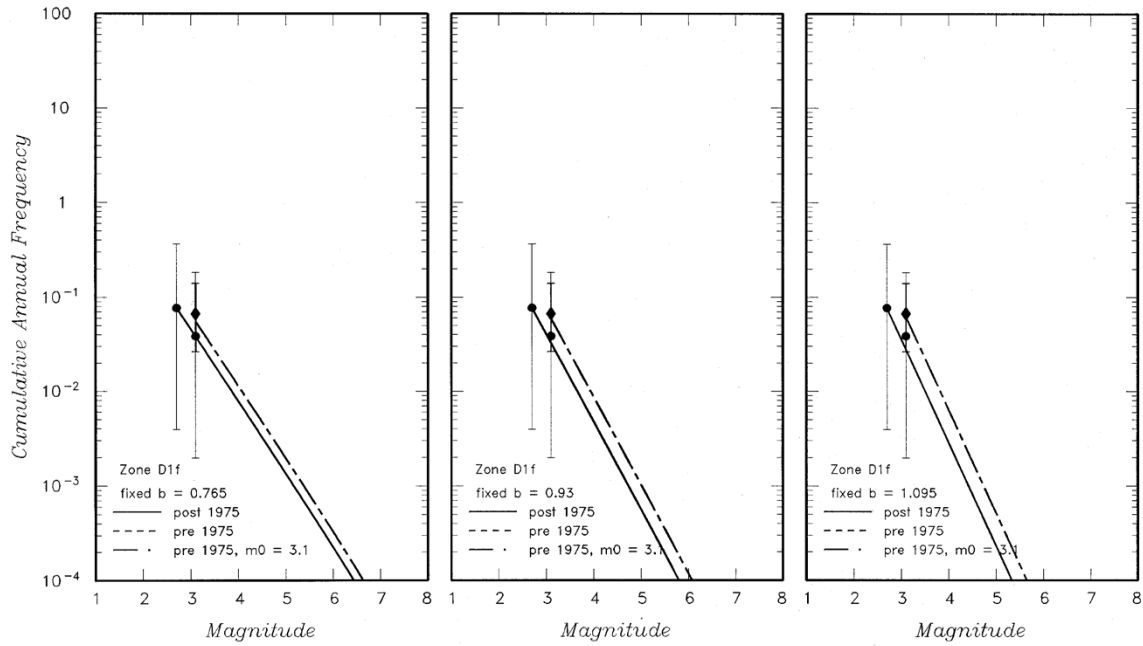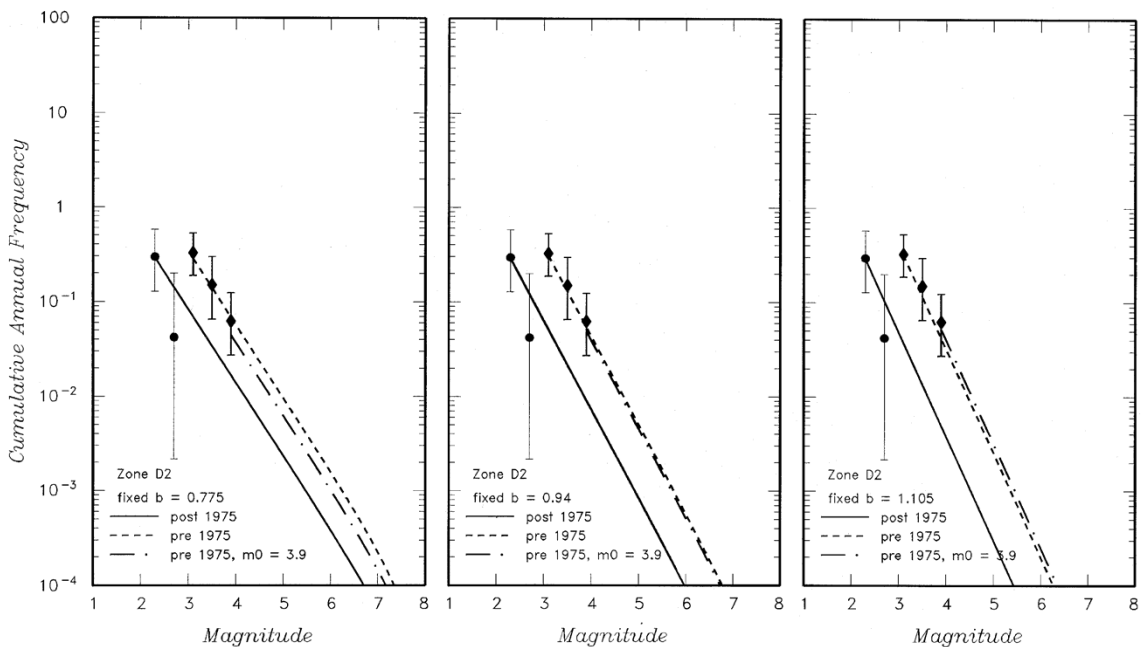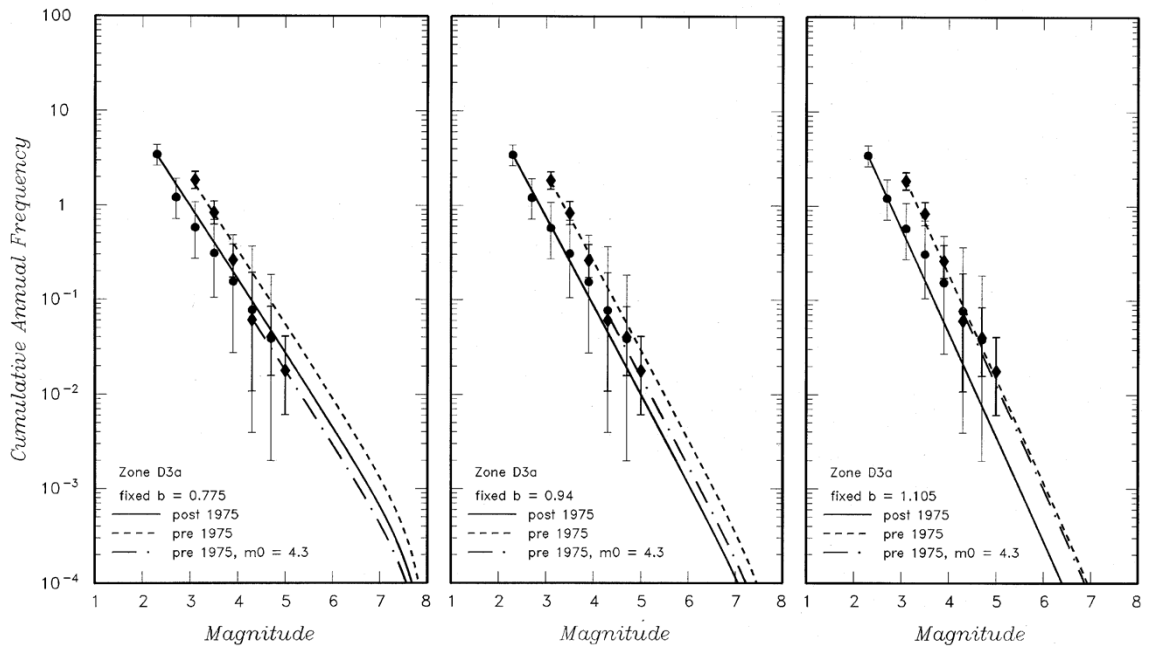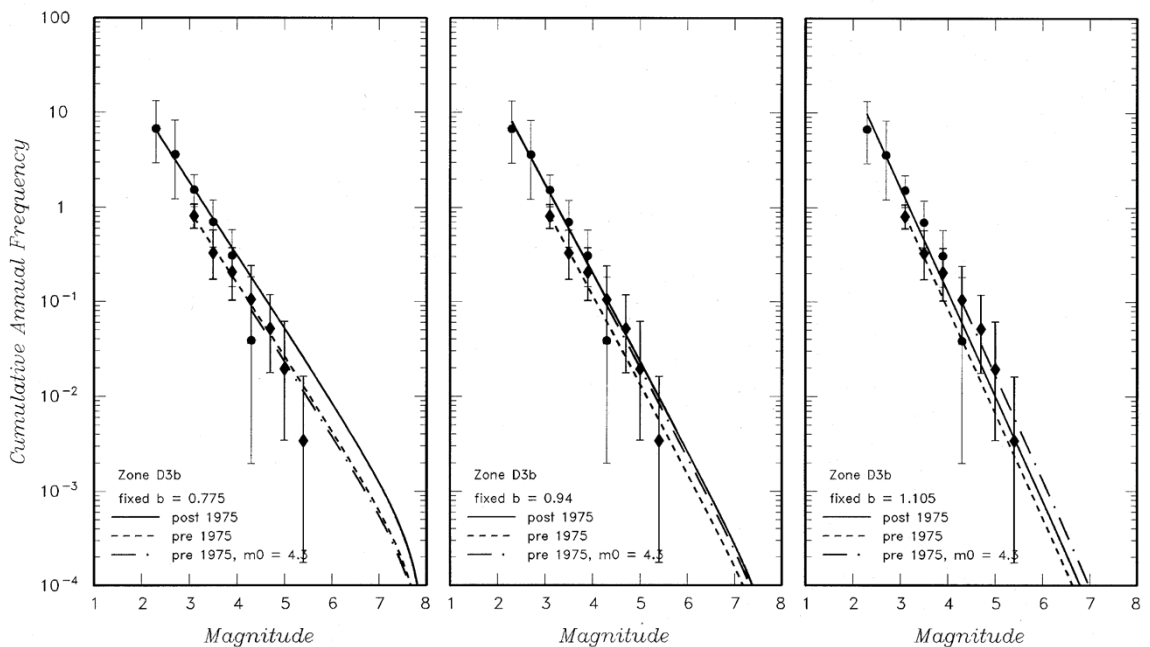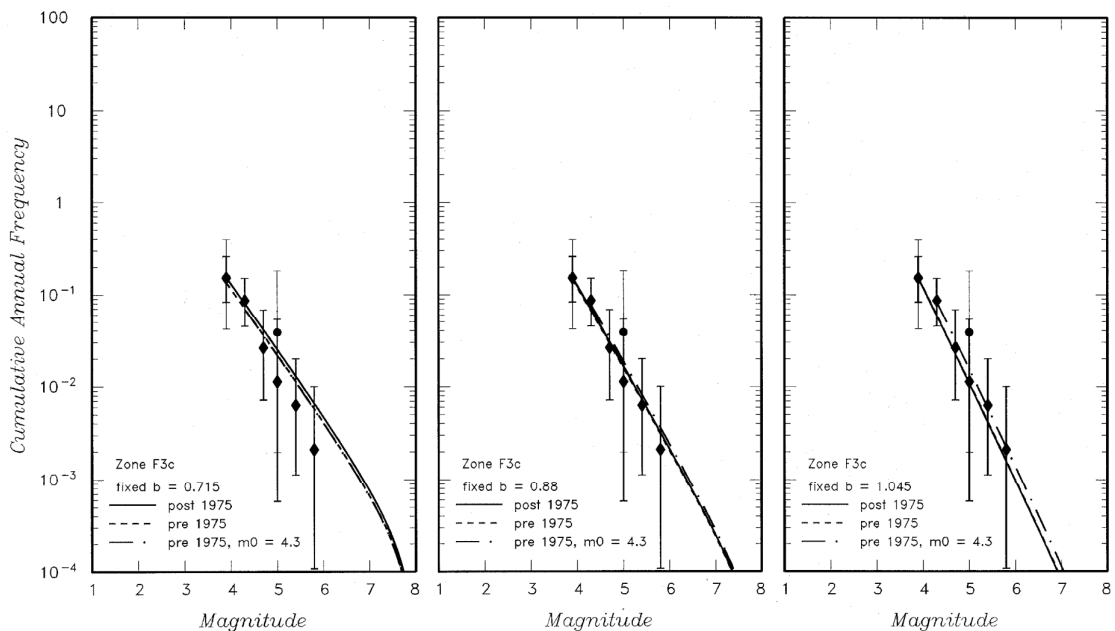

Fig. 124:   Seismicity rates and fitting curves (solid line = considering all data after 1975, dashed line = considering all data before 1975, dotted-dashed line = considering magnitudes larger than 4.2 before 1975) for Zone F3c

The 3 b-values are: the estimated one − 1 σ, the estimated one, the estimated one + 1 σ.

Tab. 10: Seismicity parameters calculated for all seismic sources

Source	case*	m_0	N(m > 5)	b	N(m > 5)	b	N(m > 5)	b
A	a	3.1	0.1106E+00	0.795	0.6736E-01	0.960	0.3829E-01	1.125
A	l	4.3	0.8436E-01	0.795	0.7480E-01	0.960	0.6419E-01	1.125
B	a	2.3	0.8351E-02	0.835	0.4913E-02	1.000	0.2702E-02	1.165
B	l	4.3	0.6503E-02	0.835	0.5718E-02	1.000	0.4875E-02	1.165
C1	a	2.7	0.1404E-01	0.755	0.9671E-02	0.920	0.6386E-02	1.085
C1	l	4.3	0.9359E-02	0.755	0.7819E-02	0.920	0.6374E-02	1.085
C2	a	2.3	0.9684E-01	0.755	0.5220E-01	0.920	0.2531E-01	1.085
C2	l	4.3	0.5605E-01	0.755	0.4689E-01	0.920	0.3828E-01	1.085
C3	a	3.1	0.1460E-01	0.755	0.9132E-02	0.920	0.5399E-02	1.085
C3	l	4.3	0.1395E-01	0.755	0.1178E-01	0.920	0.9683E-02	1.085
D1a	i	2.3	0.1222E-01	0.765	0.4397E-02	0.930	0.1578E-02	1.095
D1a	h	3.1	0.2955E-01	0.765	0.1552E-01	0.930	0.7875E-02	1.095
D1a	l	4.3	0.1771E-01	0.765	0.1512E-01	0.930	0.1258E-01	1.095
D1b	i	3.9	0.1655E-01	0.765	0.1093E-01	0.930	0.7201E-02	1.095
D1b	h	3.9	0.1545E-01	0.765	0.1119E-01	0.930	0.7845E-02	1.095
D1b	l	4.3	0.1566E-01	0.765	0.1328E-01	0.930	0.1096E-01	1.095
D1c	i	2.3	0.1114E-01	0.765	0.4031E-02	0.930	0.1451E-02	1.095
D1c	h	3.1	0.2147E-01	0.765	0.1145E-01	0.930	0.5881E-02	1.095
D1c	l	4.3	0.1696E-01	0.765	0.1447E-01	0.930	0.1202E-01	1.095
D1e	i	2.3	0.1223E-01	0.765	0.4403E-02	0.930	0.1581E-02	1.095
D1e	h	3.1	0.1979E-01	0.765	0.1039E-01	0.930	0.5269E-02	1.095
D1e	l	4.3	0.1289E-01	0.765	0.1101E-01	0.930	0.9157E-02	1.095
D1f	i	2.7	0.1332E-02	0.765	0.5576E-03	0.930	0.2330E-03	1.095
D1f	h	3.1	0.1939E-02	0.765	0.1018E-02	0.930	0.5164E-03	1.095
D1f	l	3.1	0.1939E-02	0.765	0.1018E-02	0.930	0.5164E-03	1.095
D1bcd	i	2.3	0.2138E-01	0.765	0.7808E-02	0.930	0.2825E-02	1.095
D1bcd	h	3.1	0.5348E-01	0.765	0.2915E-01	0.930	0.1522E-01	1.095
D1bcd	l	4.3	0.4115E-01	0.765	0.3507E-01	0.930	0.2911E-01	1.095
D1bcde	i	2.3	0.3489E-01	0.765	0.1267E-01	0.930	0.4572E-02	1.095
D1bcde	h	3.1	0.7308E-01	0.765	0.3931E-01	0.930	0.2031E-01	1.095
D1bcde	l	4.3	0.5381E-01	0.765	0.4588E-01	0.930	0.3811E-01	1.095

Source	case*	m_0	N(m > 5)	b	N(m > 5)	b	N(m > 5)	b
D1de	i	2.3	0.1617E-01	0.765	0.5819E-02	0.930	0.2089E-02	1.095
D1de	h	3.1	0.3646E-01	0.765	0.1914E-01	0.930	0.9710E-02	1.095
D1de	l	4.3	0.2254E-01	0.765	0.1925E-01	0.930	0.1601E-01	1.095
D2	i	2.3	0.2316E-02	0.775	0.8376E-03	0.940	0.3019E-03	1.105
D2	h	3.1	0.9491E-02	0.775	0.5021E-02	0.940	0.2561E-02	1.105
D2	l	3.9	0.6164E-02	0.775	0.4527E-02	0.940	0.3212E-02	1.105
D3a	i	2.3	0.2716E-01	0.775	0.9920E-02	0.940	0.3602E-02	1.105
D3a	h	3.1	0.5470E-01	0.775	0.2911E-01	0.940	0.1491E-01	1.105
D3a	l	4.3	0.1773E-01	0.775	0.1528E-01	0.940	0.1281E-01	1.105
D3b	i	2.3	0.5178E-01	0.775	0.2317E-01	0.940	0.1014E-01	1.105
D3b	h	3.1	0.2605E-01	0.775	0.1335E-01	0.940	0.6656E-02	1.105
D3b	l	4.3	0.2302E-01	0.775	0.1999E-01	0.940	0.1678E-01	1.105
D4a	a	2.3	0.1646E-02	0.835	0.7266E-03	1.000	0.3025E-03	1.165
D4a	l	3.5	0.1079E-02	0.835	0.6882E-03	1.000	0.4232E-03	1.165
D4b	a	3.1	0.2480E-01	0.835	0.1477E-01	1.000	0.8256E-02	1.165
D4b	l	4.3	0.2581E-01	0.835	0.2274E-01	1.000	0.1942E-01	1.165
D4c	a	3.1	0.1827E-02	0.835	0.9893E-03	1.000	0.5137E-03	1.165
D4c	l	3.9	0.1727E-02	0.835	0.1266E-02	1.000	0.8944E-03	1.165
E1	a	3.9	0.1476E-01	0.785	0.9891E-02	0.950	0.6564E-02	1.115
E1	l	4.3	0.1857E-01	0.785	0.1462E-01	0.950	0.1135E-01	1.115
E2a	a	3.9	0.2337E-01	0.725	0.1644E-01	0.890	0.1126E-01	1.055
E2a	l	4.3	0.2613E-01	0.725	0.2161E-01	0.890	0.1743E-01	1.055
E2b	a	5.4	0.8620E-02	0.725	0.1094E-01	0.890	0.1347E-01	1.055
E2b	l	5.4	0.8620E-02	0.725	0.1094E-01	0.890	0.1347E-01	1.055
E2c	i	2.3	0.6201E-02	0.725	0.2846E-02	0.890	0.1274E-02	1.055
E2c	h	3.9	0.1173E-01	0.725	0.8001E-02	0.890	0.5359E-02	1.055
E2c	l	4.3	0.9742E-02	0.725	0.7833E-02	0.890	0.6161E-02	1.055
E2d	i	2.3	0.1429E-01	0.725	0.5229E-02	0.890	0.1900E-02	1.055
E2d	h	3.1	0.2773E-01	0.725	0.1505E-01	0.890	0.7827E-02	1.055
E2d	l	4.3	0.1364E-01	0.725	0.1156E-01	0.890	0.9531E-02	1.055
E2e	i	2.3	0.3792E-02	0.725	0.1366E-02	0.890	0.4903E-03	1.055
E2e	h	3.1	0.4047E-02	0.725	0.2150E-02	0.890	0.1098E-02	1.055
E2e	l	4.7	0.6666E-02	0.725	0.6343E-02	0.890	0.5899E-02	1.055

Source	case*	m_0	N(m > 5)	b	N(m > 5)	b	N(m > 5)	b
E2cde	i	2.3	0.2493E-01	0.725	0.9600E-02	0.890	0.3629E-02	1.055
E2cde	h	3.1	0.4365E-01	0.725	0.2519E-01	0.890	0.1388E-01	1.055
E2cde	l	4.3	0.2915E-01	0.725	0.2410E-01	0.890	0.1941E-01	1.055
FF	i	2.3	0.3792E-02	0.725	0.1366E-02	0.890	0.4903E-03	1.055
FF	h	3.1	0.4496E-02	0.725	0.2389E-02	0.890	0.1220E-02	1.055
FF	l	3.9	0.3345E-02	0.725	0.2476E-02	0.890	0.1765E-02	1.055
E2dF2f	i	2.3	0.1391E-01	0.725	0.5093E-02	0.890	0.1852E-02	1.055
E2dF2f	h	3.1	0.2738E-01	0.725	0.1487E-01	0.890	0.7744E-02	1.055
E2dF2f	l	4.3	0.1366E-01	0.725	0.1157E-01	0.890	0.9529E-02	1.055
E2eF2f	i	2.3	0.2949E-02	0.725	0.1062E-02	0.890	0.3813E-03	1.055
E2eF2f	h	3.1	0.3597E-02	0.725	0.1911E-02	0.890	0.9760E-03	1.055
E2eF2f	l	4.7	0.6666E-02	0.725	0.6343E-02	0.890	0.5899E-02	1.055
E2cdeF2f	i	2.3	0.2324E-01	0.725	0.8988E-02	0.890	0.3409E-02	1.055
E2cdeF2f	h	3.1	0.4298E-01	0.725	0.2491E-01	0.890	0.1378E-01	1.055
E2cdeF2f	l	4.3	0.2924E-01	0.725	0.2414E-01	0.890	0.1942E-01	1.055
E2n	i	2.3	0.5701E-02	0.725	0.2123E-02	0.890	0.7820E-03	1.055
E2n	h	3.1	0.7258E-02	0.725	0.4023E-02	0.890	0.2134E-02	1.055
E2n	l	4.3	0.1741E-02	0.725	0.1457E-02	0.890	0.1187E-02	1.055
E2s	i	2.3	0.1313E-01	0.725	0.4732E-02	0.890	0.1699E-02	1.055
E2s	h	3.1	0.2385E-01	0.725	0.1267E-01	0.890	0.6468E-02	1.055
E2s	l	4.3	0.1333E-01	0.725	0.1147E-01	0.890	0.9595E-02	1.055
E2f	i	2.3	0.6741E-02	0.725	0.2428E-02	0.890	0.8716E-03	1.055
E2f	h	3.1	0.1933E-01	0.725	0.1027E-01	0.890	0.5246E-02	1.055
E2f	l	4.3	0.1330E-01	0.725	0.1145E-01	0.890	0.9575E-02	1.055
E3a	i	2.3	0.1636E-01	0.725	0.5896E-02	0.890	0.2118E-02	1.055
E3a	h	3.1	0.3356E-01	0.725	0.1787E-01	0.890	0.9142E-02	1.055
E3a	l	4.3	0.1493E-01	0.725	0.1285E-01	0.890	0.1075E-01	1.055
E3aF2f	i	2.3	0.1423E-01	0.725	0.5130E-02	0.890	0.1843E-02	1.055
E3aF2f	h	3.1	0.3131E-01	0.725	0.1668E-01	0.890	0.8532E-02	1.055
E3aF2f	l	4.3	0.1493E-01	0.725	0.1285E-01	0.890	0.1075E-01	1.055
E3b	i	2.3	0.8320E-02	0.725	0.3000E-02	0.890	0.1078E-02	1.055
E3b	h	3.1	0.1329E-01	0.725	0.7103E-02	0.890	0.3643E-02	1.055
E3b	l	4.3	0.4939E-02	0.725	0.4251E-02	0.890	0.3554E-02	1.055

Source	case*	m_0	N(m > 5)	b	N(m > 5)	b	N(m > 5)	b
F1a	a	3.1	0.1077E-01	0.785	0.6267E-02	0.950	0.3538E-02	1.115
F1a	l	4.3	0.5975E-02	0.785	0.4685E-02	0.950	0.3626E-02	1.115
F1b	a	3.9	0.9076E-02	0.785	0.6404E-02	0.950	0.4395E-02	1.115
F1b	l	4.3	0.4556E-02	0.785	0.3824E-02	0.950	0.3122E-02	1.115
F2a	i	3.1	0.4603E-02	0.735	0.2245E-02	0.900	0.1092E-02	1.065
F2a	h	3.9	0.3881E-02	0.735	0.2611E-02	0.900	0.1732E-02	1.065
F2a	l	4.7	0.3495E-02	0.735	0.3297E-02	0.900	0.3023E-02	1.065
F2b	i	2.3	0.3140E-01	0.735	0.1279E-01	0.900	0.5053E-02	1.065
F2b	h	3.1	0.1964E-01	0.735	0.1227E-01	0.900	0.7278E-02	1.065
F2b	l	4.3	0.1285E-01	0.735	0.1075E-01	0.900	0.8696E-02	1.065
F2b_RF	i	2.3	0.4166E-01	0.735	0.1653E-01	0.900	0.6387E-02	1.065
F2b_RF	h	3.1	0.3226E-01	0.735	0.1971E-01	0.900	0.1142E-01	1.065
F2b_RF	l	4.3	0.2079E-01	0.735	0.1748E-01	0.900	0.1420E-01	1.065
F2bpcy	i	2.3	0.3954E-01	0.735	0.1605E-01	0.900	0.6323E-02	1.065
F2bpcy	h	3.1	0.2601E-01	0.735	0.1621E-01	0.900	0.9590E-02	1.065
F2bpcy	l	4.3	0.1604E-01	0.735	0.1342E-01	0.900	0.1087E-01	1.065
F2bF2f	i	2.3	0.1892E-01	0.735	0.7972E-02	0.900	0.3248E-02	1.065
F2bF2f	h	3.1	0.1851E-01	0.735	0.1184E-01	0.900	0.7229E-02	1.065
F2bF2f	l	4.3	0.1127E-01	0.735	0.9374E-02	0.900	0.7559E-02	1.065
F2c	i	3.9	0.5946E-02	0.735	0.3928E-02	0.900	0.2590E-02	1.065
F2c	h	3.9	0.1542E-01	0.735	0.1114E-01	0.900	0.7754E-02	1.065
F2c	l	4.3	0.1325E-01	0.735	0.1138E-01	0.900	0.9453E-02	1.065
F2d	i	2.3	0.6314E-02	0.735	0.2278E-02	0.900	0.8186E-03	1.065
F2d	h	3.1	0.8782E-02	0.735	0.4753E-02	0.900	0.2448E-02	1.065
F2d	l	4.3	0.7645E-02	0.735	0.6788E-02	0.900	0.5757E-02	1.065
RF	i	2.3	0.6314E-02	0.735	0.2278E-02	0.900	0.8186E-03	1.065
RF	h	3.1	0.8782E-02	0.735	0.4753E-02	0.900	0.2448E-02	1.065
RF	l	4.3	0.7645E-02	0.735	0.6788E-02	0.900	0.5757E-02	1.065
F2e	i	2.3	0.2809E-02	0.735	0.1012E-02	0.900	0.3638E-03	1.065
F2e	h	3.1	0.4731E-02	0.735	0.2542E-02	0.900	0.1302E-02	1.065
F2e	l	4.7	0.6143E-02	0.735	0.6092E-02	0.900	0.5788E-02	1.065

Source	case*	m_0	N(m > 5)	b	N(m > 5)	b	N(m > 5)	b
F2f	i	2.3	0.1743E-01	0.735	0.6275E-02	0.900	0.2253E-02	1.065
F2f	h	3.1	0.1448E-01	0.735	0.7769E-02	0.900	0.3974E-02	1.065
F2f	l	4.3	0.1081E-01	0.735	0.9628E-02	0.900	0.8179E-02	1.065
F3a	i	2.3	0.1425E-01	0.715	0.5451E-02	0.880	0.2025E-02	1.045
F3a	h	3.1	0.7988E-02	0.715	0.4957E-02	0.880	0.2885E-02	1.045
F3a	l	4.3	0.8648E-02	0.715	0.7458E-02	0.880	0.6222E-02	1.045
F3aF2f	i	2.3	0.7239E-02	0.715	0.2830E-02	0.880	0.1065E-02	1.045
F3aF2f	h	3.1	0.5585E-02	0.715	0.3561E-02	0.880	0.2130E-02	1.045
F3aF2f	l	4.3	0.7098E-02	0.715	0.6122E-02	0.880	0.5105E-02	1.045
F3b	i	2.3	0.2207E-01	0.715	0.1347E-01	0.880	0.7860E-02	1.045
F3b	h	3.9	0.3152E-01	0.715	0.2289E-01	0.880	0.1600E-01	1.045
F3b	l	4.3	0.1499E-01	0.715	0.1293E-01	0.880	0.1077E-01	1.045
F3c	i	3.9	0.2500E-01	0.715	0.1653E-01	0.880	0.1090E-01	1.045
F3c	h	3.9	0.2190E-01	0.715	0.1590E-01	0.880	0.1111E-01	1.045
F3c	l	4.3	0.2158E-01	0.715	0.1861E-01	0.880	0.1550E-01	1.045

*rates based on: a – all data; i – post 1975 data; h – pre 1976 data; l – m_0 = 4.3 using either all data or pre 1976 data, depending on alternative for source

4   MAXIMUM EARTHQUAKE MAGNITUDE

Two global approaches have been used for the maximum magnitude (M_{max}) assessment: the Kijko and the EPRI methodologies. Both approaches have been applied to all the seismic sources and produce, then, two alternative branches in the logic tree. As we are not able to judge which approach is more suitable for the study area, equal weight is given to the two approaches. The maximum magnitude distributions were developed for the larger macro zones and then applied to the seismic sources within each macro zone. The reason why M_{max} was computed for the macro zones, instead of the individual seismic sources, is given by the fact that M_{max} is often a characteristic of the wide geological environment rather than of the individual faults. Moreover, M_{max} can be better assessed on the basis of a rich earthquake catalog than on few events recorded in a limited portion of crust.

4.1   Maximum earthquake magnitude for the macro zones

The maximum magnitude has been computed for the macro zones previously described (Fig. 6) according to the Kijko & Graham (1998) and the EPRI approaches. In Table 11 these two alternative maximum magnitudes are indicated as "MK" and "ME", respectively. The exact formulation proposed by Cisternas (personal communication) was used in order to calculate the values in the "MC" column. This modification replaces the original approximation used by Kijko & Graham (1998).

The Kijko & Graham (1998) approach needs the maximum observed magnitude within a given macro zone, the minimum magnitude which is considered to be complete in the catalog of a given macro zone and the seismicity parameters a and b. The chosen b-values and their errors are the results of the calculations reported in chapter 3.5.1 (final values in Table 7). The a-values have been computed with the maximum likelihood approach based on the seismicity rates of the macro zones, taking the b-value as fixed within a given macro zone. In the case of the Kijko & Graham (1998) approach, the total length of the catalog for each macro zone is taken as complete over the period of the catalog within which the seismicity parameters have been assessed, because the Albarello & Mucciarelli (2002) approach weights the different time segments according to the automatically computed completeness. This complete time interval is reported in column "T" of Table 11.

The results obtained are reported in Table 11. As can be seen from this table, the values of the maximum magnitude calculated ("MC" and "MK") are notably larger (+0.3) compared to the value of the maximum observed magnitude ("Mx") only in a few cases. This is because the observation period considered to be at about 1000 years is very long. By considering shorter completeness periods the difference would increase progressively.

The EPRI approach for the maximum magnitude assessment was applied as well. We considered the chosen b-values and the completeness periods for the different magnitude classes as defined in chapter 3.5.1.3. for the different catalogues constituting PEGASOS. More precisely, the catalog completeness has been associated with the macro zones in the following way.

Tab. 11:   Statistical maximum magnitude for the MZs

MZ	Mo	Mx	a	b	σb	rate	T	MC	σ MC	MK	σ MK	ME	σ ME	note
A	3.8	6.3	3.80	0.96	0.10	1.42	900	6.3	0.2	6.3	0.2	6.3	0.1	
B	3.2	5.3	2.90	1.00	0.10	0.50	800	5.3	0.2	5.4	0.2	6.2	0.6	1
C	3.2	6.4	2.97	0.92	0.10	1.06	700	6.5	0.2	6.6	0.3	6.5	0.2	
D1	2.9	6.4	2.90	0.93	0.10	1.60	700	6.6	0.3	6.6	0.3	6.4	0.2	
D2,3	2.9	6.5	3.27	0.94	0.10	3.50	800	6.6	0.2	6.6	0.2	5.5	0.1	2
D4	4.1	6.2	3.56	1.00	0.10	0.29	1000	6.2	0.2	6.3	0.2	6.3	0.4	
E1	3.8	5.8	2.76	0.95	0.10	0.14	600	6.1	0.3	6.0	0.3	6.2	0.4	3
E2,3	2.3	5.8	2.73	0.89	0.10	0.41	700	5.8	0.2	5.9	0.2	5.8	0.1	
F1	3.8	6.2	2.78	0.95	0.10	0.15	900	6.5	0.3	6.5	0.3	6.2	0.4	4
F2	3.5	6.9	3.01	0.90	0.10	0.72	1200	7.1	0.3	7.1	0.3	6.1	0.5	5
F3	3.2	5.8	3.22	0.88	0.10	2.54	1000	5.8	0.2	5.8	0.2	5.9	0.2	

MZ	macro zone
Mo	minimum magnitude
Mx	maximum observed magnitude
a	a-value
b	b-value
σb	error on b-value
rate	annual number of eqs with mag ge Mo
T	completeness period
MC	Cisternas maximum magnitude
σMC	error on Cisternas maximum magnitude
MK	Kijko maximum magnitude
σMK	error on Kijko maximum magnitude
ME	EPRI maximum magnitude
σME	error on EPRI maximum magnitude

Notes: 1 = the catalog is poor of eqs, especially before 1900;
            2 = the 1295 eq is not taken by the CH completeness, taking the catalog complete for 6.5 from 1000 instead of 7.0, ME = 6.6 and σME = 0.2;
            3 = the catalog has a few eqs before 1800; the completeness periods are only 3;
            4 = the 6.2 eq occurred in 1155 and is neither taken by the F completeness nor by the CH one, taking the catalogue complete for 6.2 from 1000 ME = 6.3 and σME = 0.3;
            5 = considering the catalog complete from 1000 for 6.9 instead of 7.0, the 1356 eq is taken and ME = 7.0 and σME = 0.2.

Completeness is taken from:

        (a) the Italian catalog for macro zones A, B, C, and D4,
        (b) the Swiss catalog for D1, D2-3, E2-3, and F2,
        (c) the French catalog for E1 and F1,
        (d) the German catalog for F3.

The distribution of maximum magnitude in extended crust (mean value = 6.4 and error = 0.84) was chosen as the "prior" distribution for all macro zones with the exception of E1, F1, and F3, for which a non-extended crust (mean value = 6.3 and error = 0.5) was considered. The latter seismotectonic regions (E1, F1 and F3, see Fig. 2) have not been affected by Mesozoic or Cenozoic rifting and are hence regarded as non-extended. The rest of the seismotectonic regions have been affected by intensive rifting, before some of these regions were involved in Alpine orogeny. To identify the peak of the distribution, a small magnitude bin size (0.1) has been used to pinpoint the maximum magnitude between 5.0 and 7.5. This upper limit for M_{max} is taken from the assessment of the maximum possible magnitude according to the geological evidence (see the following chapter). It is possible to take into account in the M_{max} computation the possible error in the magnitude estimates reported in the catalogue (Tinti & Mulargia 1985). Some tests which have been performed have shown that the effect of this option consists, generally, in a lowering of the M_{max} estimate, sometimes to questionable values. It was decided, then, not to take into account the event magnitude error in our computation.

The results obtained, in terms of the maximum magnitude value with the highest probability, are also reported in Table 11. The estimates are rather sensitive to the completeness periods chosen and to the number of earthquakes in a given macro zone. For this reason, the completeness periods have been modified in 3 cases in order to take into account the maximum observed earthquake, that would otherwise have been excluded. The maximum magnitude exceeds the maximum observed magnitude by a large amount only in two cases. In macro zone B the difference between the two values is 0.9, while in macro zone E1, poorly documented by the catalog data, the difference is 0.4.

The estimates obtained with the Kijko & Graham (1998) approach seem more robust but they depend very strongly on the maximum observed magnitude. In general both approaches give results that are not very different from the maximum observed magnitude. In the EPRI approach the prior magnitude significantly shapes the final probability distribution. The number and size of the events that occurred in the past play a limited role in both approaches. Consequently, the associated probability distributions are not very robust. Hence an additional geological (or tectonic) constraint is proposed and discussed below.

4.2   Geological evidence for M_{max}

M_{max}, as derived by the Kijko and EPRI approaches were combined with "geological" approaches for estimating M_{max}. These geological estimates provide an upper bound (or cut-off value) for the distribution of M_{max} calculated by the two catalog-based approaches. For this purpose we estimated maximum fault surface length based on geological arguments (L_{max}) in a first step. In a second step L_{max} was converted into the surface rupture length, which can be reactivated during an earthquake (SRL), corresponding to between 30 and 50% of L_{max}. In some of the source areas L_{max} cannot really be estimated on "geological" grounds due to the lack of data. Approximate estimates are possible in other areas. For areas without data we set L_{max} to 100 km. This is a conservative value and therefore on the safe side, because amongst the geologically well-constrained areas $L_{max} > 100$ km can only be postulated for the Rhine Graben area (see list below). The case of the Rhine graben area (area F2) is unique, in that the presence of through-going single fault segments with a length of up to 200 km cannot be completely excluded in this region (but in all the other regions). Below is a list of all the "macro zones" for which "geological M_{max}" was evaluated:

Macro zone A: No "geological" arguments available. Take L_{max} = 100 km.

Macro zone B: No "geological" arguments available. Take L_{max} = 100 km.

Macro zone C: No "geological" arguments available. Take L_{max} = 100 km.

Macro zone D1:   Source area D1a: L_{max} = 100 km (Rhone strike slip fault). Other source areas in macro zone D1: no "geological" arguments available.
Take L_{max} = 100 km.

Macro zone D2-3:   Source areas D3a and D3b: L_{max} = 100 km (Engadine and Inntal lines); source area D2: no "geological" arguments available. Take L_{max} = 100 km.

Macro zone D4: L_{max} = 100 km in entire macro zone (Giudicarie and Tonale, Pustertal lines).
Take L_{max} = 100 km.

Macro zone E1:   No "geological" arguments available. Take L_{max} = 100 km.

Macro zone E2-3:   Source areas E2a & E2b: L_{max} = 100 km (Bresse graben);
Source area E2c: L_{max} = 100 km (Pontarlier fault);
Source area E2d: L_{max} = 100 km (Fribourg fault);
Source area E2e: L_{max} = 20 km (subsurface Molasse data);
Source area E2n: L_{max} = 50 km (Rheingraben-type faults);
Source area E2f: L_{max} = 100 km (PC-trough);
Source area E2s: L_{max} = 100 km (PC-trough and subsurface Molasse data);
Source area E3a: L_{max} = 50 km (subsurface Molasse data);
Source area E3b: L_{max} = 100 km (PC-trough).
Take L_{max} = 100 km.

Macro zone F1:   No "geological" arguments available. Take L_{max} = 100 km.

Macro zone F2: L_{max} = 200 km in entire macro zone (Rhinegraben). Take L_{max} = 200 km.

Macro zone F3: L_{max} = 50 km in entire macro zone (pre-existing faults E of Rhinegraben).
Take L_{max} = 50 km.

The Wells & Coppersmith (1994) relation between SRL (for all types of faults) and M_{max} is the following:

$$M_{max} = 5.08 \ (+/-0.10) + 1.16 \ (+/-0.07) \log (SRL)$$

with a standard deviation of 0.28. If we apply this relationship to all our cases, we find the results reported in Table 12. The " M_{max}" reported in this table will be used as upper bounds (i.e. cut-off values) for the probability distribution of M_{max}.

Tab. 12:   Upper bounds of M_{max} for different L_{max}

L_{max} [km]	SRL [km]	logSRL	M_{max}
200	80 ± 20	1.9 ± 0.1	7.3 ± 0.3
100	40 ± 10	1.6 ± 0.1	6.9 ± 0.3
50	20 ± 5	1.3 ± 0.1	6.6 ± 0.3
20	8 ± 2	0.9 ± 0.1	6.1 ± 0.3

4.3 M_{max} for hazard computation

The calculations of the discrete maximum magnitude distributions for the seismic sources to be used as input for the hazard calculations were done by Geomatrix Consultants. Two sets of maximum magnitude calculations were performed: one set obtained by the Kijko & Graham (1998) approach, with the Cisternas implementation, the other one calculated with the EPRI approach.

For the Kijko & Graham (1998) method we used the values listed in Table 13. Actually, the values reported in Table 13 summarize those in Table 11 with a few differences. These differences refer to the pathological situations that are mentioned in the notes of Table 11. The remarks made in these notes have been incorporated into the final estimates. The listed values of maximum observed (MX), maximum magnitude (MC), and maximum magnitude standard deviation (σMC) were used to construct an exponential distribution for M_{max}. This distribution was discretized in 0.5 magnitude unit bins to develop weights on alternative values of M_{max}. The resulting distributions are shown on the upper part of Figures 125 to 128.

The second approach, based on the EPRI methodology, used a code designed by Geomatrix Consultants that allows the use of multiple zones to collect the seismicity sample. The calculations were performed for all MZs. The *b*-value and catalog completeness periods for each macro zone was taken in agreement with the previous considerations (see chapter 3.5.1.3.). The extended crust prior mean M_{max} of 6.4 and a σ of 0.84 was used for all macro zones, with the exception of E1, F1, and F3, where a non-extended crust prior mean M_{max} of 6.3 and a σ of 0.5 was used. The option of the EPRI approach to consider the magnitude uncertainty was not included into the calculation because some tests done gave M_{max} estimates considered too low in some cases. The posterior distributions were discretized in 0.5 magnitude unit bins to develop weights on alternative values of M_{max}. The resulting distributions are shown in the lower part of Figures 123 to 126.

For both approaches, the tail of the M_{max} distributions at very high magnitudes is cut off according to the geological estimates given in Table 12. This cut-off ensures that physically impossible high magnitude events are excluded from the subsequent hazard calculations. This is based on the premise that nature provides a set of pre-existing faults that may rupture over a given percentage of their total length during one single event.
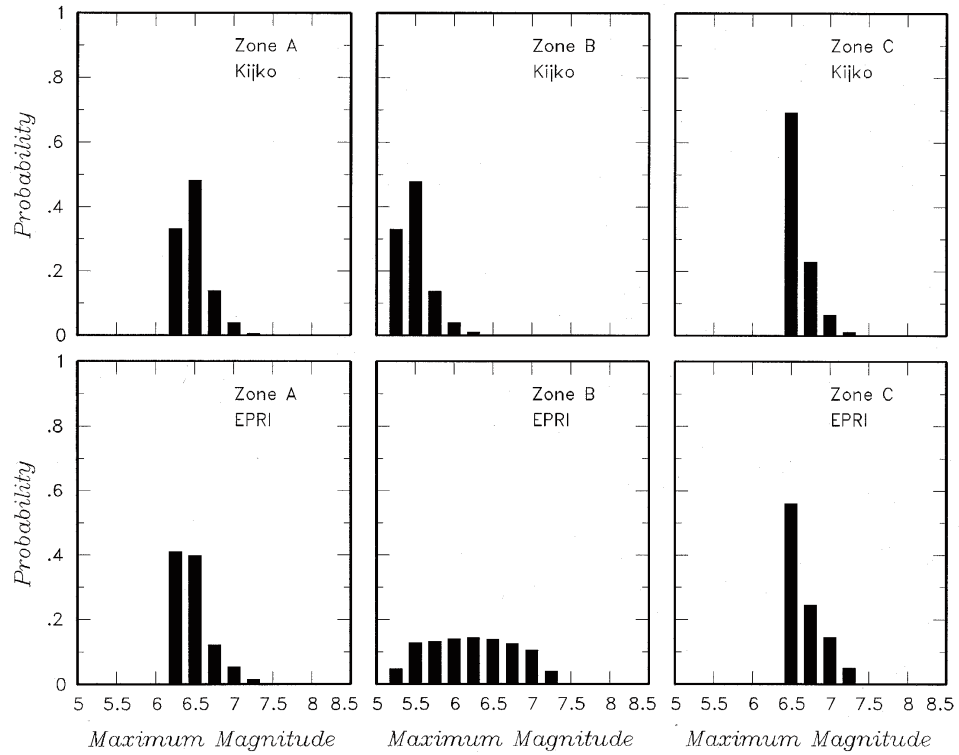
Fig. 125: Probability distributions (Kijko and EPRI approaches) for maximum magnitude in the macro zones A, B, and C
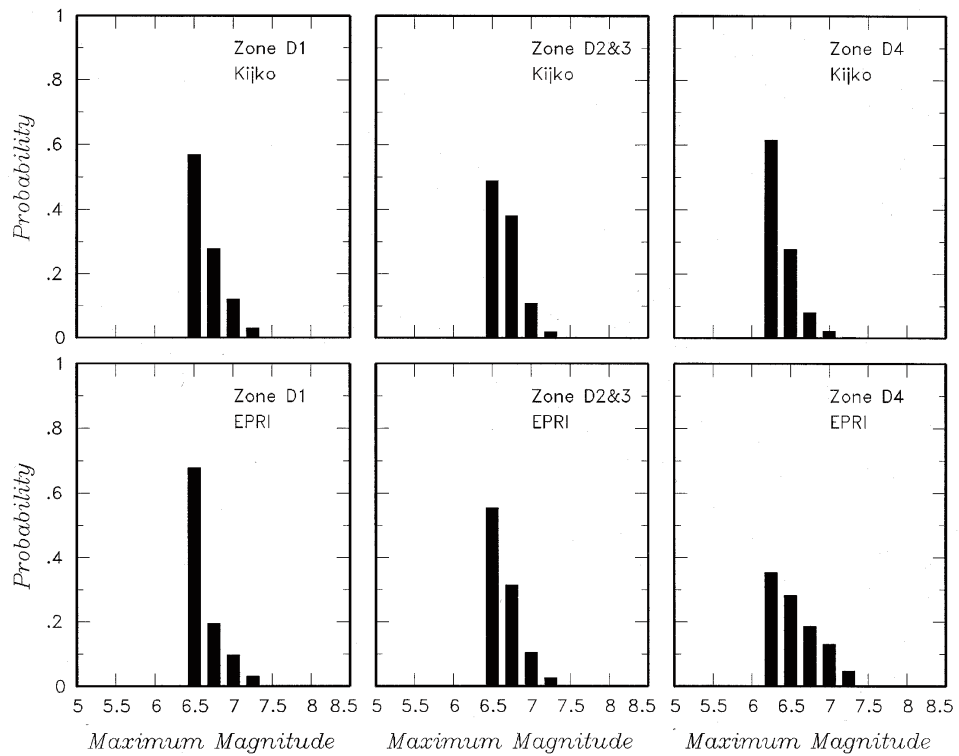
Fig. 126: Probability distributions (Kijko and EPRI approaches) for maximum magnitude in the macro zones D1, D2-3, and D4
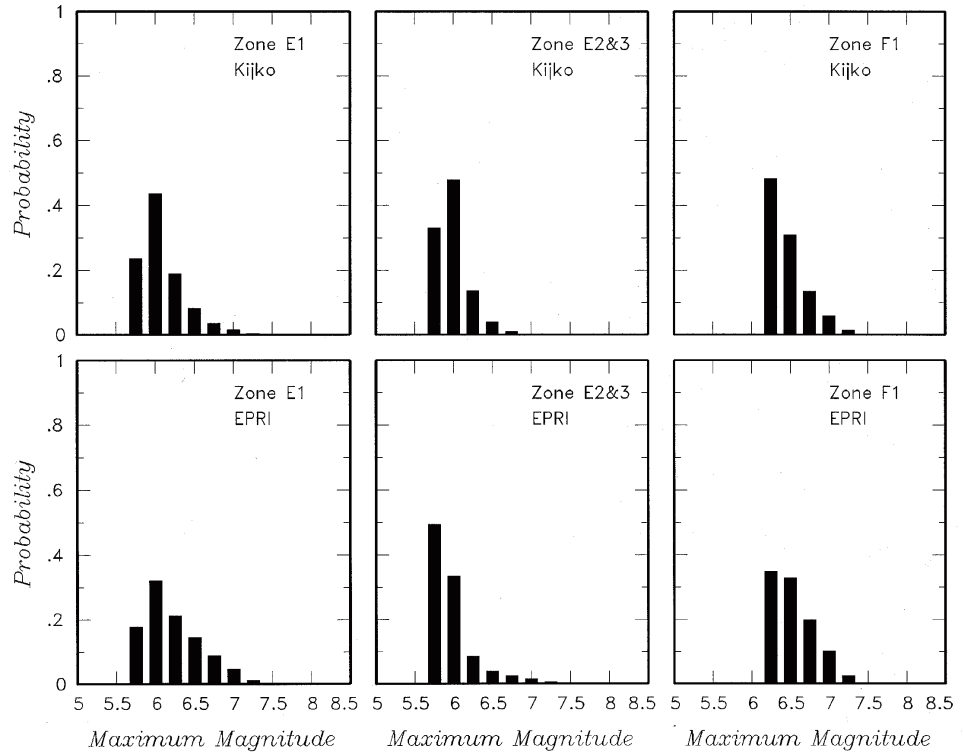
Fig. 127: Probability distributions (Kijko and EPRI approaches) for maximum magnitude in the macro zones E1, E2-3, and F1
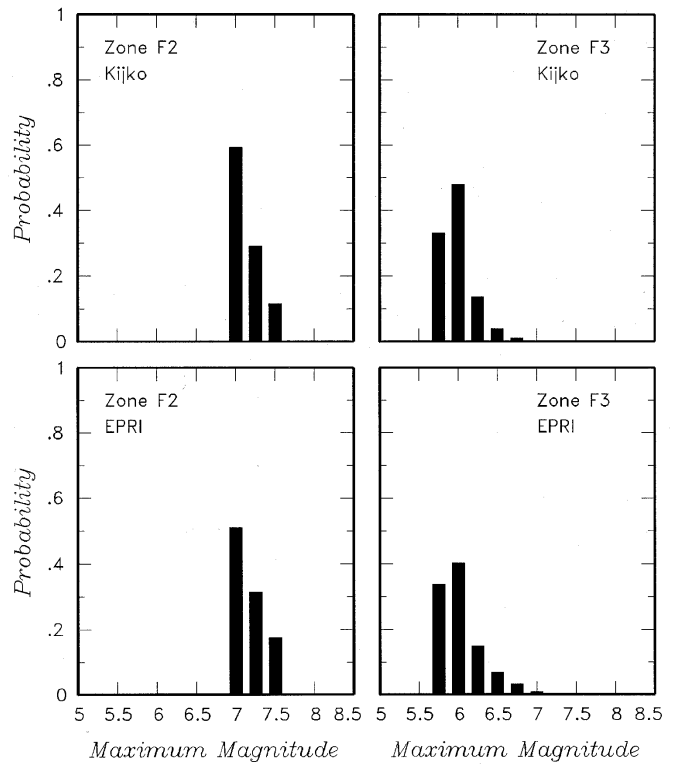
Fig. 128: Probability distributions (Kijko and EPRI approaches) for maximum magnitude in the macro zones F2 and F3

Tab. 13:   Maximum magnitude for the MZs

MZ	Mx	MC	σMC	ME	σME	MG	σMG
A	6.3	6.3	0.2	6.3	0.1	6.9	0.3
B	5.3	5.3	0.2	6.2	0.6	6.9	0.3
C	6.4	6.5	0.2	6.5	0.2	6.9	0.3
D1	6.4	6.6	0.3	6.4	0.2	6.9	0.3
D2-3	6.5	6.6	0.2	6.6	0.2	6.9	0.3
D4	6.2	6.2	0.2	6.3	0.4	6.9	0.3
E1	5.8	6.1	0.3	6.2	0.4	6.9	0.3
E2-3	5.8	5.8	0.2	5.8	0.1	6.9	0.3
F1	6.2	6.5	0.3	6.3	0.3	6.9	0.3
F2	6.9	7.1	0.3	7.0	0.2	7.3	0.3
F3	5.8	5.8	0.2	5.9	0.2	6.6	0.3

MZ	macro zone
Mx	maximum observed magnitude
MC	Cisternas maximum magnitude
σMC	error on Cisternas maximum magnitude
ME	EPRI maximum magnitude
σME	error on EPRI maximum magnitude
MG	geological maximum magnitude
σMG	error on geological maximum magnitude

4.4   Conclusions regarding M_{max}

Two statistical approaches and a geological one have been considered for the assessment of M_{max}. The geological estimates are larger because they represent extreme values in the sense that a possible reactivation of an entire pre-existing fault length is considered, regardless of the past record in the catalogues. Only in the case of macro zone B do the two statistical approaches differ significantly (Fig. 125). While M_{max} computed with the Kijko & Graham (1998) approach is near to the maximum observed magnitude, the EPRI approach is very much conditioned by the prior distributions used, especially were the catalogue data are scarce. The geological approach is independent from the catalogue data and leads to a larger value as it forecasts the maximum event that the known tectonic structures would give, assuming that all existing faults are subject to reactivation in the present stress field and that recurrence time may approach infinite. In a few cases the estimates based on the geological approach are much larger when compared to the other two estimates. Macro zone E2-3 (Fig. 127) is a good example. There the statistical maxima are around 5.8 while 100 km-long faults do exist and, hence, magnitude around 6.9 cannot be excluded. This shows that catalogue length is possibly not long enough to catch large earthquakes.

In conclusion, we use both Kijko & Graham (1998) and EPRI approaches with equal weight in a logic tree. These alternative branches are calculated for all macro zones. The resulting distributions are cut off at the "geological M_{max}". Subsequently, these M_{max} distributions are exported into the source zones, which are contained within in a given macro zone. Hence, the maximum magnitude distributions were developed for larger macro zones and then imported into the individual and often much smaller source zones.

5 REFERENCES

Albarello, D. & Mucciarelli, M. 2002: Seismic hazard estimates using ill-defined macroseismic data at site. Pure Appl.Geophys. 159, 1289-1304.

Birkhäuser, Ph., Roth, Ph., Meier, B. & Naef, H. 2000: 3D-Seismik: Räumliche Erkundung der mesozoischen Sedimentschichten im Zürcher Weinland. Nagra Tech. Ber. NTB 00-03. Nagra, Wettingen, Switzerland.

Burkhard, M. 1990: Aspects of the large-scale Miocene deformation in the most external part of the Swiss Alps (Subalpine Molasse to Jura fold belt). Eclogae geol. Helv. 83, 559-583.

Burkhard, M. & Sommaruga, A. 1998: Evolution of the western Swiss Molasse basin: Structural relations with the Alps and the Jura belt, in Cenozoic Foreland Basins of Western Europe (edited by C. Mascle et al). Geol. Soc. Spec. Publ. 134, 279-298.

Camassi, R. & Stucchi, M. 1996: NT4.1, un catalogo parametrico di terremoti di area italiana al di sopra della soglia del danno. C.N.R. GNDT, Milano, 86 pp.

Ceriani, S., Fügenschuh, B. & Schmid, S.M. 2001: Late-stage thrusting at the "Penninic Front" in the Western Alps between Mont Blanc and Pelvoux massifs. Int. J. Earth Sciences 90, 685-702.

Deichmann, N., Ballarin Dolfin, D. & Kastrup, U. 2000: Seismizität der Nord- und Zentral-schweiz. Nagra Tech. Ber. NTB 00-05. Nagra, Wettingen, Switzerland.

Deichmann, N. 2002: Seismotectonic constraints on possible ground motions in Switzerland. PEGASOS SP-2 Workshop, 17.4.2002.

Eva, E., Solarino, C., Eva, C. & Neri, G. 1997: Stress tensor orientation derived from fault plane solution in the southwestern Alps. J. Geophys. Res. 102, 8171-8185.

Fügenschuh, B. & Schmid, S.M. (in press): Late stages of deformation and exhumation of an orogen constrained by a large set of fission track data: a case study in the Western Alps. Geol. Soc. America Bull.

Gardner, J.K. & Knopoff, L. 1974: Is the sequence of earthquakes in southern California, with aftershocks removed, Poissonian? Bull. Seism. Soc. Am. 64, 1363-1367.

Giamboni, M., Ustaszewski, K., Schmid, S.M., Schumacher, M. & Wetzel, A. (submitted): Plio-Pleistocene deformation in the Rhine-Bresse transform zone: geological and geomorphological evidence for ongoing transpressional reactivation of Paleozoic and Paleogene structures. Int. J. Earth Sciences.

Grellet, B., Combes, P., Granier, T. & Philip, H. 1993: Seimotectonique de la France Métropolitaine. Mém. Soc. Géol. France, 164/1-2, 76 pp.

Grünthal, G. 1985: The up-dated earthquake catalogue for the German Democratic Republic and adjacent areas − Statistical data characteristics and conclusions for hazard assessment. *In:* Proceedings 3rd International Symposium on the Analysis of Seismicity and Seismic Risk, Czech.Ac.Sc., Prague, 19-25.

Grünthal, G., Mayer-Rosa, D. & Lenhardt, W.A. 1998: Abschätzung der Erdbebengefährdung für die D-A-CH-Staaten − Deutschland, Österreich, Schweiz. Bautechnik 10, 19-33.

Kastrup, U. 2002: Seismotectonics and stress field variations in Switzerland. PhD thesis ETH Zürich No. 14527, 153pp.

Kastrup, U., Zoback, M.L., Deichmann, N., Evans, K.F., Giardini, D. & Michael, A.J. 2004: Stress field variations in the Swiss Alps and the northern Alpine foreland derived from inversion of fault plane solutions. J. Geophys. Res. 109, B1, doi:10.1029/2003JB002550B01402.

Kijko, A. & Graham, G. 1998: Parametric-historic procedure for probabilistic seismic hazard analysis. Part I: estimation of maximum regional magnitude m_{max}. Pure Appl. Geophys. 152, 413-442.

Laubscher, H.P. 1992: Jura kinematics and the Molasse basin. Eclogae geol. Helv. 85, 653-675.

Lopez Cardoso, G. (pers. comm.): Presentation at the third EUCOR-URGENT workshop in Tiengen-Waldshut, October 2002.

Maurer, H.R., Burkhard, M., Deichmann, N. & Green, A.G. 1997: Active tectonism in the central Alps: Contrasting stress regimes north and south of the Rhone valley. Terra Nova 9, 91-94.

Meghraoui, M., Delouis, B., Ferry, M., Giardini, D., Huggenberger, P., Spottke, I. & Granet, M. 2001: Active Normal Faulting in the Upper Rhine Graben and Paleoseismic Identification of the 1356 Basel Earthquake. Science 293, 2070-2073.

Meier, B.P. 1994a: Untere Süsswassermolasse des zentralen und östlichen Mittellandes: Regionale Interpretation bestehender Seismik und petrophysikalische Interpretation von Fremd- und Eigenbohrungen. Unpubl. Nagra Interner Bericht 94-27. Nagra, Wettingen, Switzerland.

Meier, B.P. 1994b: Untere Süsswassermolasse des westlichen Mittellandes: Regionale Interpretation bestehender Seismik und petrophysikalische Interpretation von Fremdbohrungen. Unpubl. Nagra Interner Bericht 94-28. Nagra, Wettingen, Switzerland.

Meletti, C., Patacca, E. & Scandone, P. 2000: Construction of a seismootectonic model: the case of Italy. Pure appl. geophys. 157, 11-35.

Miller, A.C. & Rice, T.H. 1983: Discrete approximations of probability distributions. Management Science 29, 352-362.

Müller, W.H., Blümling, P. & Becker, A. 1987: Die Entkoppelung des tektonischen Spannungsfeldes an der Jura-Überschiebung. Eclogae geol. Helv. 80, 473-489.

Müller, W.H., Naef, H. & Graf, H.R. 2001: Geologische Entwicklung der Nordschweiz, Neotektonik und Langzeitszenarien Zürcher Weinland. Nagra Techn. Ber. NTB 99-08, first draft dating from December 2001, 226pp. Nagra, Wettingen, Switzerland.

Pavoni, N. 1961: Faltung durch Horizontalverschiebung. Eclogae Geol. Helv. 54, 515-534.

Plenefisch, T. & Bonjer, K.-P. 1997: The stress filed in the Rhine Graben area infered from earthquake focal mechanisms and estimation of frictional parameters. Tectonophysics 275, 71-97.

Reasenberg, P.A. 1985: Second-order moment of central California seismicity. J. Geophys. Res. 90, 5479-5495.

Schmid, S.M. (http://www.unibas.ch/earth/tecto/index.html): Regional tectonics: from the Rhine graben to the Po plain, a summary of the tectonic evolution of the Alps and their forelands.

Schmid, S.M. 2002: Trenching active fault-scarps in the Basle region (e.g. the Reinach fault). Workshop Summary WS-2/SP 1, p.28.

Schmid, S.M. & Kissling, E. 2000: The arc of the Western Alps in the light of geophysical data on deep crustal structure. Tectonics 19, 62-85.

Schumacher, M. 2002: Upper Rhine Graben: Role of preexisting structures during rift evolution. Tectonics 21/1, 6-1 – 6-17.

Stepp, J.C. 1972: Analysis of completeness of the earthquake sample in the Puget Sound area and its effect on statistical estimates of earthquake hazard. *In:* Proceedings of the International Conference on Microzonation, v. 2, pp. 897-910.

Sue, Ch., Thouvenot, F. & Fréchet, J. 1999: Widespread extension in the core of the Western Alps revealed by earthquake analysis. J. Geophys. Res. 104/B11, 25611-25622.

Swiss Seismological Service 2002: PALEOSEIS, Reconstructing the paleoseismological record in northern Switzerland. Final report to HSK and NAGRA, 30.06.2002, 28 pp.

Tinti, S. & Mulargia, F. 1985: Effects of magnitude uncertainties on estimating the parameters in the Gutenberg – Richter frequency – magnitude law. Bull. Seism. Soc. Am. 75, 1681-1697.

Toro, G. 2003: Technical note on the treatment of hypocentral depths and rupture-length effects for area sources in the FRISK88MP software. PEGASOS Technical Note TP1-TN-0373.

Uhrhammer, R. 1986: Characteristics of northern and southern California seismicity. Earthquake Notes 57, 21.

Weichert, D.H. 1980: Estimation of the earthquake recurrence parameters for unequal observation periods for different magnitudes. Bull. Seismol. Soc. Am. 70, 1337-1346.

Wells, D.L. & Coppersmith, K.J. 1994: New empirical relationship among magnitude, rupture length, rupture width, rupture area, and surface displacement. Bull. Seismol. Soc. Am. 84, 974-1002.

Wiemer, S. 2002: De-clustering the PEGASOS earthquake catalog. PEGASOS Report EXT_TN_0208, 10 pp.

Youngs, B. 2002: Assessment of catalog completeness using Stepp plots. PEGASOS EXT-RF-0402.

Youngs, B. 2002: Assessment of earthquake recurrence for seismic sources. PEGASOS EXT-RF-0401.

APPENDIX 1:   EG1-HID-0032   HAZARD INPUT DOCUMENT FINAL MODEL, EXPERT TEAM EG1a

This document describes the final seismic source model developed by Expert Team EG1a. The data files associated with this seismic source model are located in the zip file EG1-HID-0032_EG1a_data.zip.

A 1.1   Seismic Source Zonation

The master logic tree that defines the alternative seismic source zonations is shown on Fig. A1-1. The first node addresses whether or not the Permo-Carboniferous troughs are an active source. Fig. A1-2 shows the seismic source zonation of the Alpine foreland for the case when the Permo-Carboniferous troughs are an active source ("PC YES" case). If the Permo-Carboniferous troughs are not active ("PC NO" case), a number of alternatives for Basel and the Alpine foreland are included.

The second node address whether or not the Reinach fault is modeled as active fault-specific source localizing seismicity and the third node addresses the source . For the PC YES case, the fault is not considered to be a localizer of seismicity, and the Basel source is an east-west trending zone F2e (Fig. A1-2). For the PC NO case, Fig. A1-3 shows the alternative seismic sources. If the Reinach fault (RF) is considered a line source, then it lies within a larger zone, source F2b_RF. If not, then the Basel region is modeled as a narrow, north-south trending zone (F2d), or as a large zone representing the intersection of north-south and east-west structures (F2f). In the case that source F2f is use, the surrounding source zones have modified boundaries (e.g. zone F3a is changed to zone F3aF2f).

The next node of the logic tree addresses the source zonation in the Alpine foreland and the Fribourg area. The alternative source models are shown on Fig. A1-4 for the PC NO case. If the Fribourg fault (FF) is considered to be an active fault localizing seismicity, it is modeled as a line source within a large Alpine foreland source E2cde (lower left plot of Fig. A1-4). If not, then the Alpine foreland is modeled by the three zones E2c, E2d, and E2e (upper left plot of Fig. A1-4). The right-hand plots on Fig. A1-4 show the modifications to the Alpine foreland zones in the case that the Basel source is represented by zone F2f.

The final node of the logic tree (Fig. A1-1) shows the source zonation for the Alps (regional zone D1). Three alternatives are considered, as shown on Fig. A1-5.

The remaining portion of the study region is modeled by a number of source zones whose geometry does not change with the alternative zonations described above. Fig. A1-6 shows these source zones.

The right-hand column in Fig. A1-1 indicates the various source sets produced by the logic tree. The source zones comprising these source sets are listed in Tab. A1-1 (Source Sets for EG1a).

PC Active	Reinach Fault Source	Basel Source Geometry	Fribourg Fault Source	Alps Zone D1	Source Set

Yes (0.3) — No (1.0) — F2e (1.0) — No (1.0) —
- 1 subzone (0.2) — Set 1
- 2 subzones (0.4) — Set 2
- 3 subzones (0.4) — Set 3

No (0.7) — Yes (0.1) — RF (1.0)
- Yes (0.5)
  - 1 subzone (0.2) — Set 4
  - 2 subzones (0.4) — Set 5
  - 3 subzones (0.4) — Set 6
- No (0.5)
  - 1 subzone (0.2) — Set 7
  - 2 subzones (0.4) — Set 8
  - 3 subzones (0.4) — Set 9

No (0.9) — F2d (0.7)
- Yes (0.5)
  - 1 subzone (0.2) — Set 10
  - 2 subzones (0.4) — Set 11
  - 3 subzones (0.4) — Set 12
- No (0.5)
  - 1 subzone (0.2) — Set 13
  - 2 subzones (0.4) — Set 14
  - 3 subzones (0.4) — Set 15

F2f (0.3)
- Yes (0.5)
  - 1 subzone (0.2) — Set 16
  - 2 subzones (0.4) — Set 17
  - 3 subzones (0.4) — Set 18
- No (0.5)
  - 1 subzone (0.2) — Set 19
  - 2 subzones (0.4) — Set 20
  - 3 subzones (0.4) — Set 21

Fig. A1-1:   Logic tree for EG1a seismic source zonation

Fig. A1-2:   The Alpine foreland zones for the "PC YES" case (Permo-Carboniferous troughs are an active source)
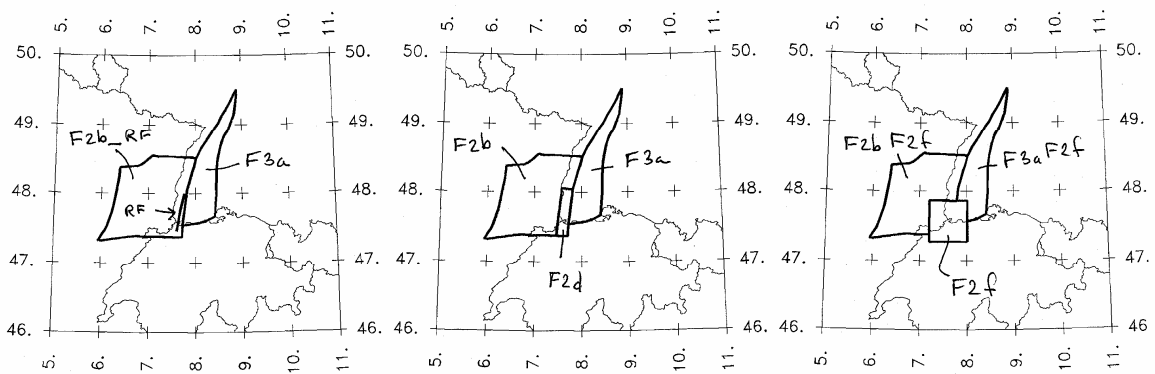
Fig. A1-3:   Alternative source zonations for Basel area for the "PC NO" case (Permo-Carboniferous troughs not an active source)
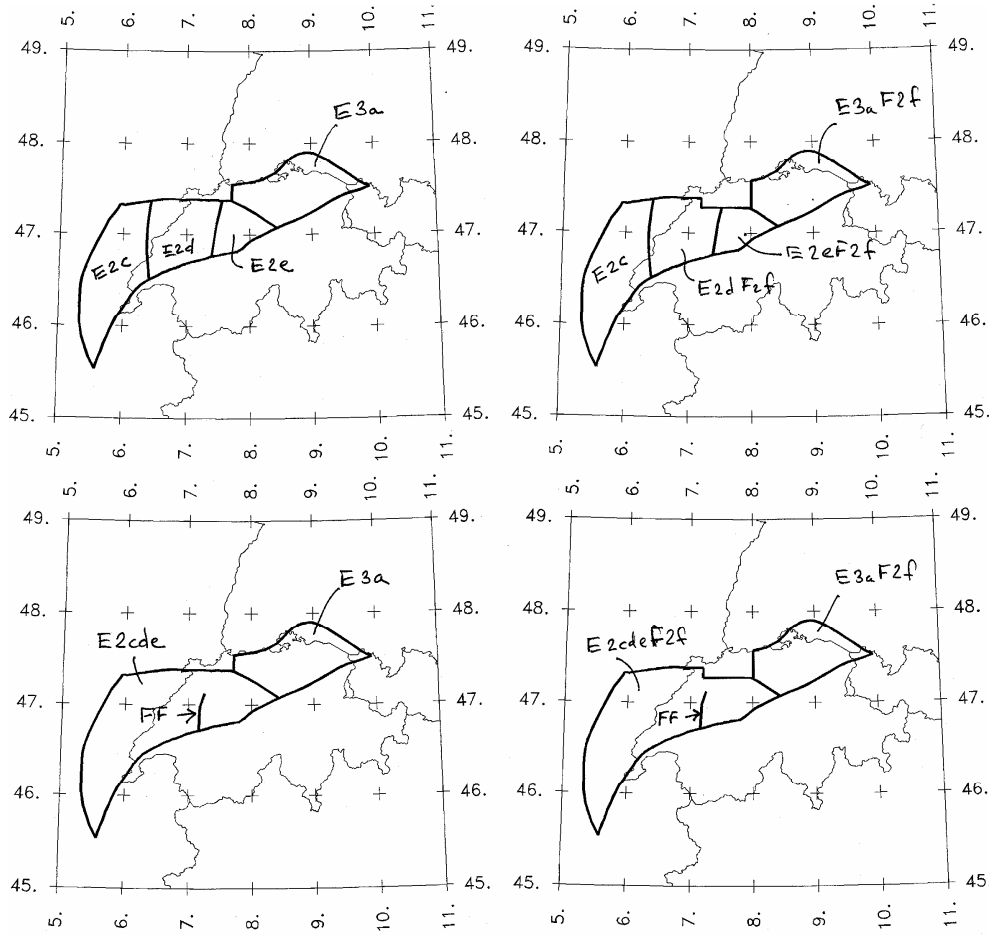
Fig. A1-4:   Alternative source zonations for Alpine foreland for the "PC NO" case (Permo-Carboniferous troughs are not an active source)
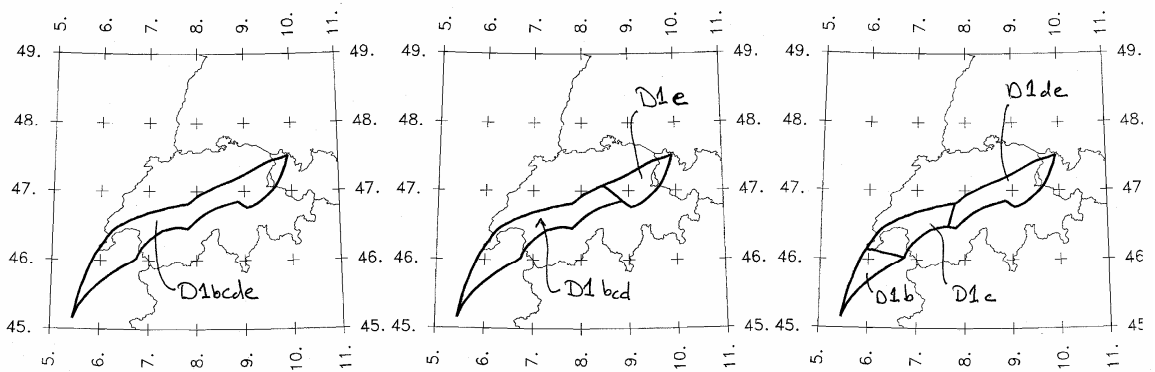
Fig. A1-5:   Alternative source zonations for the Alps
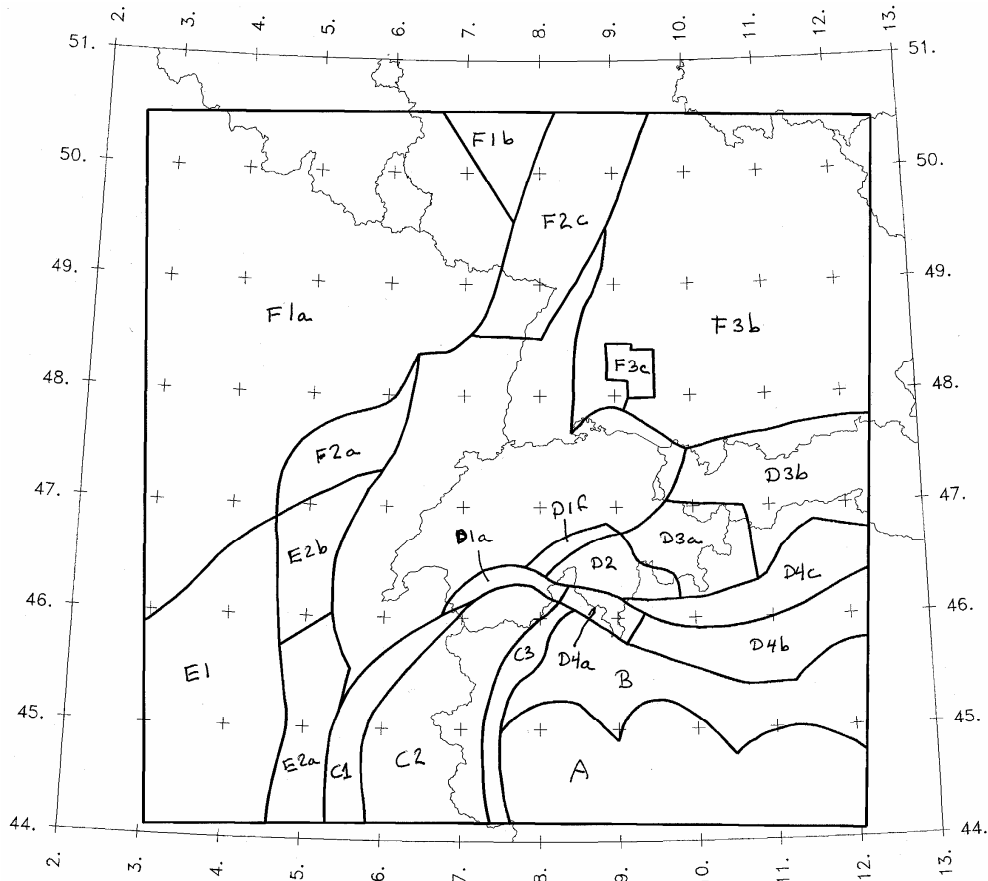
Fig. A1-6: Source zones whose boundaries do not change as a function of alternative zona-
tions

The zone boundary files are located in directory ./ZONES with the extension *.zon. The FF and
RF fault traces are located in the same directory with the extension *.flt. Note that the RF source
dips to the east.

Tab. A1-1: Source sets for EG1a

Source Set	Sources
Set 1	F2bpcy, F2e, F3a, E2c, E2n, E2f, E2s, E3b, D1bcde + UC*
Set 2	F2bpcy, F2e, F3a, E2c, E2n, E2f, E2s, E3b, D1bcd, D1e + UC
Set 3	F2bpcy, F2e, F3a, E2c, E2n, E2f, E2s, E3b, D1b, D1c, D1de + UC
Set 4	F2b_RF, RF, F3a, E2cde, FF, E3a, D1bcde + UC
Set 5	F2b_RF, RF, F3a, E2cde, FF, E3a, D1bcd, D1e + UC
Set 6	F2b_RF, RF, F3a, E2cde, FF, E3a, D1b, D1c, D1de + UC
Set 7	F2b_RF, RF, F3a, E2c, E2d, E2e, E3a, D1bcde + UC
Set 8	F2b_RF, RF, F3a, E2c, E2d, E2e, E3a, D1bcd, D1e + UC
Set 9	F2b_RF, RF, F3a, E2c, E2d, E2e, E3a, D1b, D1c, D1de + UC

Source Set	Sources
Set 10	F2b, F2d, F3a, E2cde, FF, E3a, D1bcde + UC
Set 11	F2b, F2d, F3a, E2cde, FF, E3a, D1bcd, D1e + UC
Set 12	F2b, F2d, F3a, E2cde, FF, E3a, D1b, D1c, D1de + UC
Set 13	F2b, F2d, F3a, E2c, E2d, E2e, E3a, D1bcde + UC
Set 14	F2b, F2d, F3a, E2c, E2d, E2e, E3a, D1bcd, D1e + UC
Set 15	F2b, F2d, F3a, E2c, E2d, E2e, E3a, D1b, D1c, D1de + UC
Set 16	F2bF2f, F2f, F3aF2f, E2cdeF2f, FF, E3aF2f, D1bcde + UC
Set 17	F2bF2f, F2f, F3aF2f, E2cdeF2f, FF, E3aF2f, D1bcd, D1e + UC
Set 18	F2bF2f, F2f, F3aF2f, E2cdeF2f, FF, E3aF2f, D1b, D1c, D1de + UC
Set 19	F2bF2f, F2f, F3aF2f, E2c, E2dF2f, E2eF2f, E3aF2f, D1bcde + UC
Set 20	F2bF2f, F2f, F3aF2f, E2c, E2dF2f, E2eF2f, E3aF2f, D1bcd, D1e + UC
Set 21	F2bF2f, F2f, F3aF2f, E2c, E2dF2f, E2eF2f, E3aF2f, D1b, D1c, D1de + UC
*Set UC	A, B, C1, C2, C3, D1a, D1f, D2, D3a, D3b, D4a, D4b, D4c, E1, E2a, E2b, F1a, F1b, F2a, F2c, F3b, F3c

A 1.2   Earthquake Rupture Geometry

The size of earthquake ruptures is defined by the relationship:

$$\text{Mean } \log_{10}(\text{rupture area}) = \mathbf{M}\text{-}4$$
$$\sigma_{\log10\,(\text{rupture area})} = 0.24$$

Using the relationship for the expectation of a lognormal distribution, the mean (expected) rupture area is given by the relationship:

$$\text{mean rupture area} = 10^{(\mathbf{M} - 3.934)}$$

The relationship for the mean rupture area will be used in the hazard computations. The rupture length and width have an aspect ratio of 1:1 until the maximum rupture width for a source is reached. The maximum rupture width is determined on the basis of the maximum depth and fault dip, as define below. For larger ruptures, the width is held constant at the maximum width and the length is obtained by dividing the rupture area by this width.

Earthquake epicenters are uniformly distributed within the source. Earthquake ruptures are located symmetrically on the epicenters (the epicenter is at the midpoint of the rupture). For those epicenters located closer than ½ rupture length to the source zone boundary, the ruptures are allows to extend beyond the source boundary.

Table A1-2 defines the relative frequency of the style of faulting and rupture orientations for the individual sources. Three specific styles of faulting are considered, normal, strike-slip and reverse. For each style of faulting, there is a preferred fault dip that should be used to model ruptures.

Tab. A1-2:   Style of faulting and rupture orientation for EG1a sources

Sources	Rel. Freq. for Style of faulting			Orientation of Ruptures		
	SS*	NF*	TF*	SS*	NF*	TF*
A, B, D1f, D2, D4a, D4c, E1, E2e, E2eF2f, F3c	0.33	0.33	0.33	Random	Random	Random
C1, C3	0.75		0.25	N20E		N20E
C2		1.0			N20E	
D1a	1.0			N90E		
D1b, D1d, D1e, D1bcde, D1bcd, D1de,	0.75		0.25	Random		Random
D1c	0.8	0.1	0.1	Random	Random	Random
D3a	0.25	0.75		Random	Random	
D3b	1.0			N70E		
D4b, E2f			1.0			N70E
E2a, E2b, E2c, E2d, E2dF2f, E2n, E2cde, E2cdeF2f, F2c	1.0			N15E		
E3a, E3aF2f, F1b	0.5.	0.5		N45W	N45W	
F2a	0.75	0.25		N15E	N15E	
F2b, F2bpcy, F2b_RF, F2bF2f	0.5	0.5		N15E	N15E	
F1a	0.5	0.5		Random	Random	
E2s	0.7	0.2	0.1	Random	Random	Random
E3b			1.0			N80E
F2d	0.3	0.7		N15E	N15E	
F2e	0.3		0.7	N90E		N90E
F2f	0.4	0.4	0.2	Random	Random	Random
F3a, F3aF2f	0.25	0.75		N15E & N45W	N15E & N45W	
F3b		1.0			N45E	
RF	0.3	0.7				
FF	1					

* SS – strike slip, dip 80°, NF normal slip, dip 60°, TF thrust, dip 30°

The depth distribution of hypocenters for small magnitude earthquakes within the sources is defined by the following three distributions. For the northern Alpine foreland sources (FF, E2d, E2dF2f, E2e, E2eF2f, E2cde, E2cdeF2f, E2n, E2f, E2s, E3a, E3aF2f, E3b) the distribution is triangular over the depth range of 1 to 30 km, with the mode at a depth of 10 km (Fig. A1-7). For the southern Alpine foreland and southern Germany sources (C3, D4a, D4b, D4c, F3a, F3aF2f, F3b, F3c) the depth distribution is triangular over the depth range of 1 to 25 km, with the mode at a depth of 10 km (Fig. A1-8). For the remaining zones and RF, the distribution is trapezoidal over the depth range of 1 to 20 km, with the upper uniform region extending over the depth range of 1 to 10 km (Fig. A1-9). For larger earthquakes, a magnitude-dependent depth distribution is to be developed using the weighted approach outlined in Toro (2003, PEGASOS TP1-TN-0373) with T = 0.5 (hypocenter in lower half of rupture).
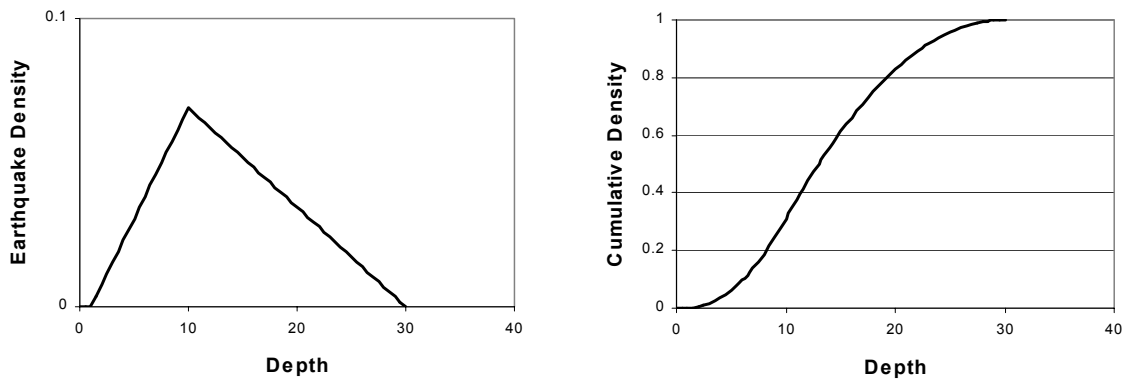
Fig. A1-7:   Earthquake depth distribution for sources FF, E2d, E2dF2f, E2e, E2eF2f, E2cde,
             E2cdeF2f, E2n, E2f, E2s, E3a, E3aF2f, and E3b
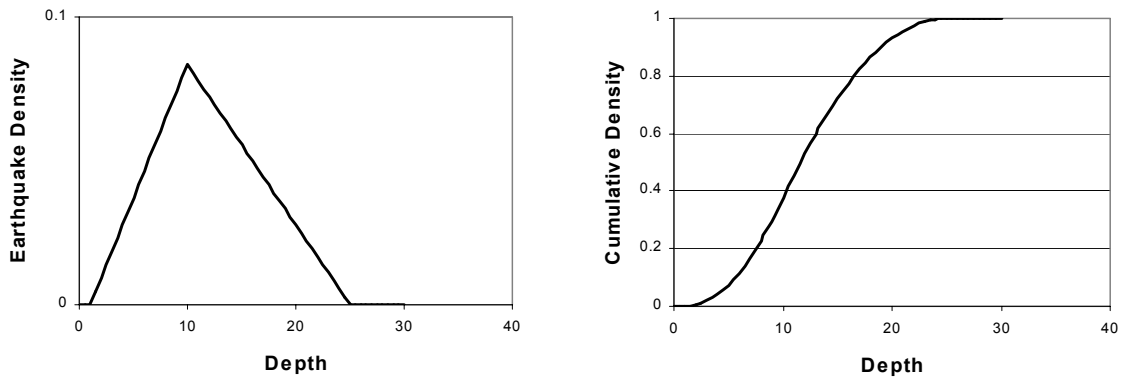
Fig. A1-8:   Earthquake depth distribution for sources C3, D4a, D4b, D4c, F3a, F3aF2f, F3b,
             and F3c
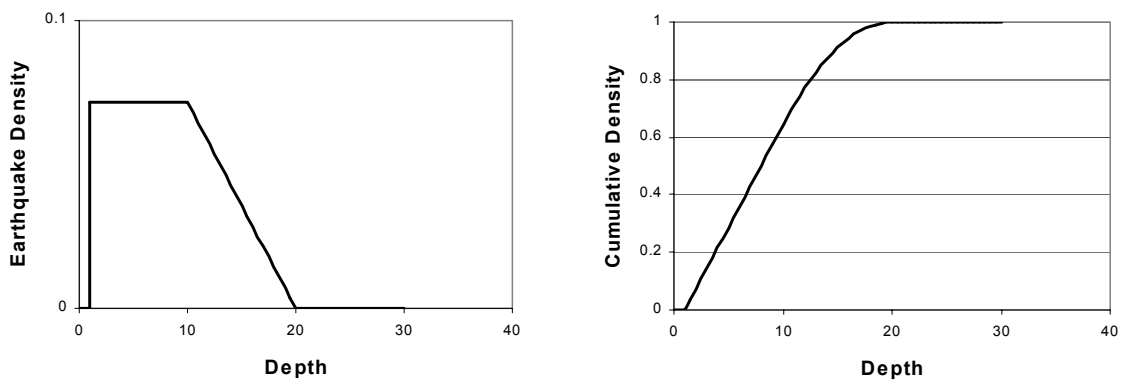
Fig. A1-9:   Earthquake depth distribution for all other sources except those listed for Figures 7
             and 8

A 1.3   Earthquake Recurrence Parameters

Maximum Magnitude:

Two global options are used for the maximum magnitude assessment. The first is the Kijko approach and the second is the EPRI approach. These alternative branches are dependent across all sources. Equal weight is given to the two approaches. These two alternatives are correlated over all sources. The maximum magnitude distributions were developed for larger regional zones and then applied to the source zones within each regional source zone. The files are located in directory .\MMAX. Files with the extension *.KMX contain the results for the Kijko approach and files with the extension *.EMX contain the results for the EPRI approach.

Seismicity Rates:

The earthquake recurrence parameters for the sources are modeled by the truncated exponential recurrence relationship. The recurrence parameters were defined by first establishing the *b*-value for a "macrozone" and then using this fixed *b*-value to calculate the seismicity rate for each source within the macrozone. The *b*-value is assumed to be correlated among all sources that make up the macrozone . A three-point representation of a normal distribution is used to model the uncertainty in the regional *b*-value and 5-point distributions are used to model the uncertainty in $N(m \geq 5)$ for each source, conditional on a given *b*-value. The zones that make up each marcozone with correlated *b*-values are listed in Table 3.

In addition, there are two or three alternatives for defining the seismicity rate that apply to all zones that make up a macrozone. These occur in one of two cases, as indicated in Table 3.

Case 1: Two alternatives, one based on all data and one based on larger magnitude data (nominally above minimum magnitude $m_0 = 4.3$). These two alternatives have equal weight of ½ each.

Case 2: Three alternatives, one based on the instrumental (post-1975) data, one based on the historical (pre-1975) data, and one based on the historical (pre-1975) data for larger magnitudes (again nominally above minimum magnitude $m_0 = 4.3$). These three alternatives have equal weight of 1/3 each.

The data files are contained within directory .\REC. The file extension indicates the particular branch. The results for the three *b*-values are indicated by *.?b0 for the median *b*-value value with weight 0.63, *.?bm for the 5th percentile *b*-value, and *.?bp for the 95th percentile *b*-value. The first character of the extension is "a" for the rates based on all data; "i"" for the rates based on instrumental data; "h" for the rates based on historical data; and "l" for the rates based on larger magnitude data, either all large magnitude data for Case 1 or large magnitude data pre 1975 for Case 2.

Tab. A1-3:   Seismic source sets for recurrence parameters

Sources with correlated *b*-values	Seismicity Rate Alternatives		
A	All data All data, larger mag	(wt 0.5) (wt 0.5)	*.ab? *.lb?
B	All data All data, larger mag	(wt 0.5) (wt 0.5)	*.ab? *.lb?
C1, C2, C3	All data All data, larger mag	(wt 0.5) (wt 0.5)	*.ab? *.lb?
D1a, D1b, D1c, D1e, D1f, D1bcd, D1bcde, D1de	Instrumental data Historical data Historical data, larger mag	(wt 0.333) (wt 0.334) (wt 0.333	*.ib? *.hb? *.lb?
D2, D3a, D3b	Instrumental data Historical data Historical data, larger mag	(wt 0.333) (wt 0.334) (wt 0.333	*.ib? *.hb? *.lb?
D4a, D4b, D4c	All data All data, larger mag	(wt 0.5) (wt 0.5)	*.ab? *.lb?
E1	All data All data, larger mag	(wt 0.5) (wt 0.5)	*.ab? *.lb?
E2a, E2b, E2c, E2d, E2e, E2cde, FF, E2dF2f, E2eF2f, E2cdeF2f, E2n, E2s, E2f, E3a, E3aF2f, E3b	For E2a, E2b: All data All data, larger mag For rest of sources: Instrumental data Historical data Historical data, larger mag	 (wt 0.5) (wt 0.5) (wt 0.333) (wt 0.334) (wt 0.333)	 *.ab? *.lb? *.ib? *.hb? *.lb?
F1a, F1b, F2c	All data All data, larger mag	(wt 0.5) (wt 0.5)	*.ab? *.lb?
F2a, F2b, F2b_RF, RF, F2bpcy, F2bF2f, F2d, F2e, F2f	Instrumental data Historical data Historical data, larger mag	(wt 0.333) (wt 0.334) (wt 0.333)	*.ib? *.hb? *.lb?
F3a, F3aF2f, F3b, F3c	Instrumental data Historical data Historical data, larger mag	(wt 0.333) (wt 0.334) (wt 0.333)	*.ib? *.hb? *.lb?

APPENDIX 2: QA-CERTIFICATE FOR EG1-HID-0032

QA Certificate for Hazard Input Documents

QA Certificate	**PEGASOS PROJECT**

Hazard Input Document (HID)

Expert group:	EG1a	HID designation:	EG1-HID-0032
Expert:		Expert Model (EXM)	EG1-EXM-0030

HID parameterisation of Expert Model:

TFI:	K. Coppersmith	Hazard Input Specialist of TFI-team:	B. Youngs
HID based on Elicitation Documents:	☒	EG1-ES-0044		
HID based on Expert Assessments:	☐			

Remarks on the HID model parameterisation in terms of hazard computation input:

The undersigned Hazard Input Specialist confirms that this HID includes all required (subproject specific) input information for hazard computations. No further interpretations of this input will be required and no simplifications except Algorithmic Pinching according to paragraph 2.9 of the QA-Guidelines will be applied to convert this HID into hazard software Input Files.

Signature:

HID acceptance by the Expert / Expert Group:

Date of HID review by the Expert / Expert group:

	HID accepted: ☐	HID not accepted: ☐

Reasons for non-acceptance of HID / Recommendations:

The undersigned Expert(s) accept(s) the parameterisation proposed in this HID as a faithful and adequate representation of his/their Expert Model. He/they confirm(s) that this HID is free of errors and agree(s) to its use as hazard computation input.

Signature Expert 1 / Expert:

Signature Expert 2:

Signature Expert 3:

QA-TN-0287 HID acceptanc form rev 02.doc

Part II:

SP1 Seismic Source Characterisation, Elicitation Summary

Expert Team EG1b

Prof. Dr. Martin Burkhard

Institut de Géologie
Université de Neuchâtel
Neuchâtel – Switzerland

Dr. Armando Cisternas

Institute Physique du Globe
Université Louis Pasteur
Strasbourg – France

Dr. Gottfried Grünthal

GeoForschungsZentrum Potsdam – Germany

Probabilistische Erdbeben-Gefährdungs-Analyse für die KKW-StandOrte in der Schweiz
(PEGASOS)

SP1 Seismic Source Characterisation

Elicitation Summary

Expert Team EG1b

Martin Burkhard

Institute of Geology / University of Neuchâtel
Neuchâtel – Switzerland

Armando Cisternas

Institute Physique du Globe / Université Louis Pasteur
Strasbourg – France

Gottfried Grünthal

GeoForschungsZentrum Potsdam – Germany

nagra

PEGASOS

TABLE OF CONTENTS

LIST OF TABLES

LIST OF FIGURES

1 SEISMOTECTONIC FRAMEWORK

1.1 Large scale Tectonics – Architecture

The tectonic situation of Switzerland and surrounding areas is influenced by the following events, all of which left their imprint in the 'rocks' and their present day architecture:

Paleozoic:	Variscan-Hercynian orogeny
Carboniferous – Permian:	Extension-Transtension: graben formation E-W
Permian – Early Trias:	Peneplenation
Triassic – Cretaceous:	Passive margin, 'epicontinental sea'
Tertiary:	Foreland basin (in front of the Alps)
	Extension: Rhine – Bresse Graben formation N-S
	Alpine collision, including
	Jura folding and thrusting

There is a large body of literature dealing with all of these themes. A general summary about the 'Geology of Switzerland' is provided by Trümpy (1980); a modern compilation of data relevant to 'The deep structure of the Alps' and Switzerland is found in the NFP20 Atlas (Pfiffner et al. 1997b). The most important map documents used directly for the delimitation of our source zones are:

- 'Modello Strutturale' Italy (tectonic map, compilation of various national sources)

- Compiled tectonic map (PEGASOS base map)

- Various structure contour maps (top basement, Permo-carboniferous grabens)

- Geophysical maps (Moho-depth, Gravimetry)

- Satellite images

- Digital elevation models (Gtopo30, Atlas_CH in Figure 1-2)

The present day architecture of the north-western Alpine Foreland is largely the result of two geologically recent (last 50 Million years), but contrasting events:

1. Alpine Subduction – Collision
2. Oligocene Extension and Graben Formation in the Northern Foreland

Interferences between the two events (collision and extension) are obvious both in time and space. The most complex interference zone runs through northern Switzerland, i.e. through the central part of the study area.

The Alpine subduction – collision event is responsible for the large scale architecture of the Alps, best visualized in general NW-SE cross sections (Figure 1-1). The northern European plate is going down below the southern, Apulia plate. This collision event lead to the complex internal structure of the Alps, dominated by stacks of both sedimentary and basement nappes, intense folding, the Molasse- and Po-plain foredeeps, the Jura fold- & thrust-belt and the presence of a suspected but ill defined lithospheric forebulge some 150 km in front of the topographic crest line of the Alps.

The Oligocene extension event lead to the formation of the Rhine – Bresse graben system within the European plate, immediately adjacent to the alpine collision zone. The structures resulting from this event are best seen in map view. The large scale doming of the Black Forest-, Vosges- and Massif-Central-basement highs are interpreted as remaining thermal domes / rift shoulders associated with this Extension event rather than being a direct result of alpine collision. The Rhine and Bresse Grabens are well defined by depressions in the present day topography.

A sinistral 'transform' has to exist between the northern end of the Bresse Graben and the southern end of the Rhine Graben. Fgure 3 (modified from Illies 1981) illustrates this problem. There is not a single major 'transform' fault, but rather a diffuse transfer zone in which both rhenish (NNE-SSW) and conjugate (E-W) striking faults are present.

This transfer zone is overprinted by the Late Miocene event of Jura folding & thrusting. The timing of the main extension event is well documented as Oligocene from subsidence curves established from drill hole data of the Rhine Graben filling. NNE-SSW striking extensional faults of the southern Rhine Graben were demonstrably re-activated in sinistral strike-slip, most probably in Late Miocene in association with Jura folding (Bergerat 1987). In the Jura Fold Thrust belt, paleo-stress-measurements provide evidence for several successive deformation phases, including the Oligocene extension event and the Miocene folding / thrusting event (Homberg et al. 1999).
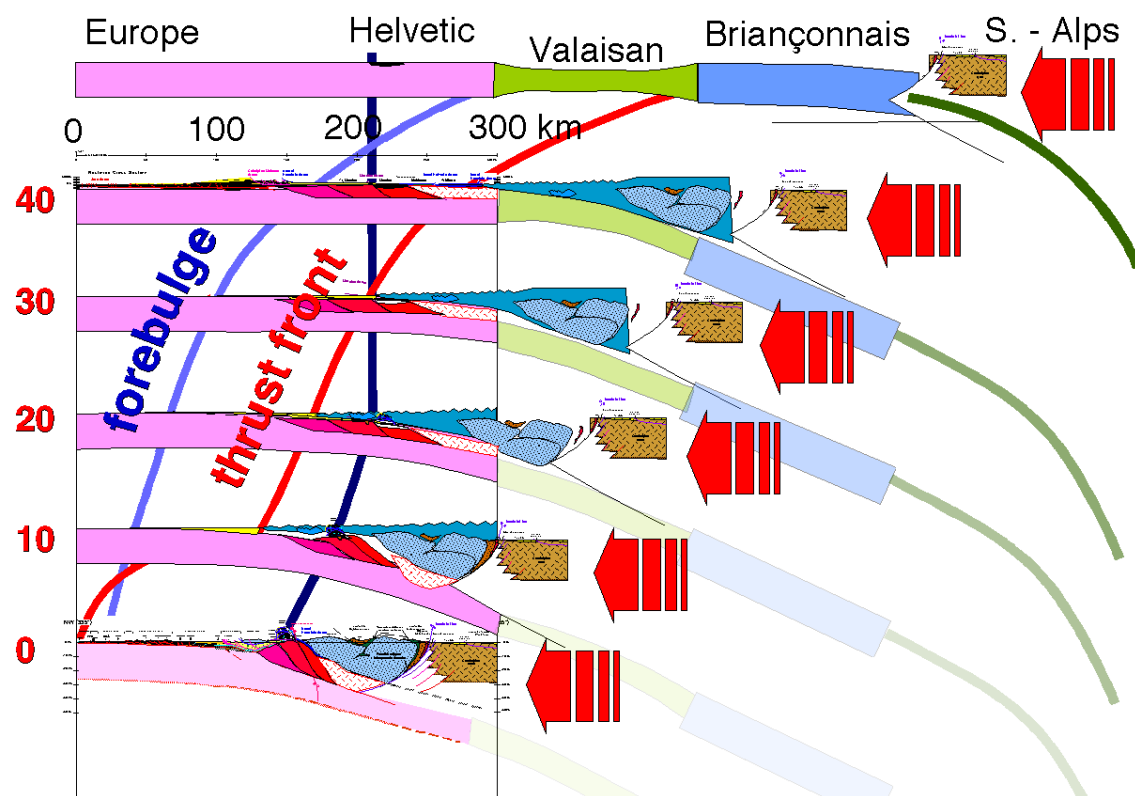
Fig. 1-1:   Tectonic evolution of the Alps during the last 40 Million years

Cartoon to illustrate the gross horizontal NW-SE shortening as based on balancing estimates derived from thin skinned cover series on the NW side of the Alps (Jura, Subalpine Molasse, Helvetic nappes), modified from Burkhard & Sommaruga (1998).
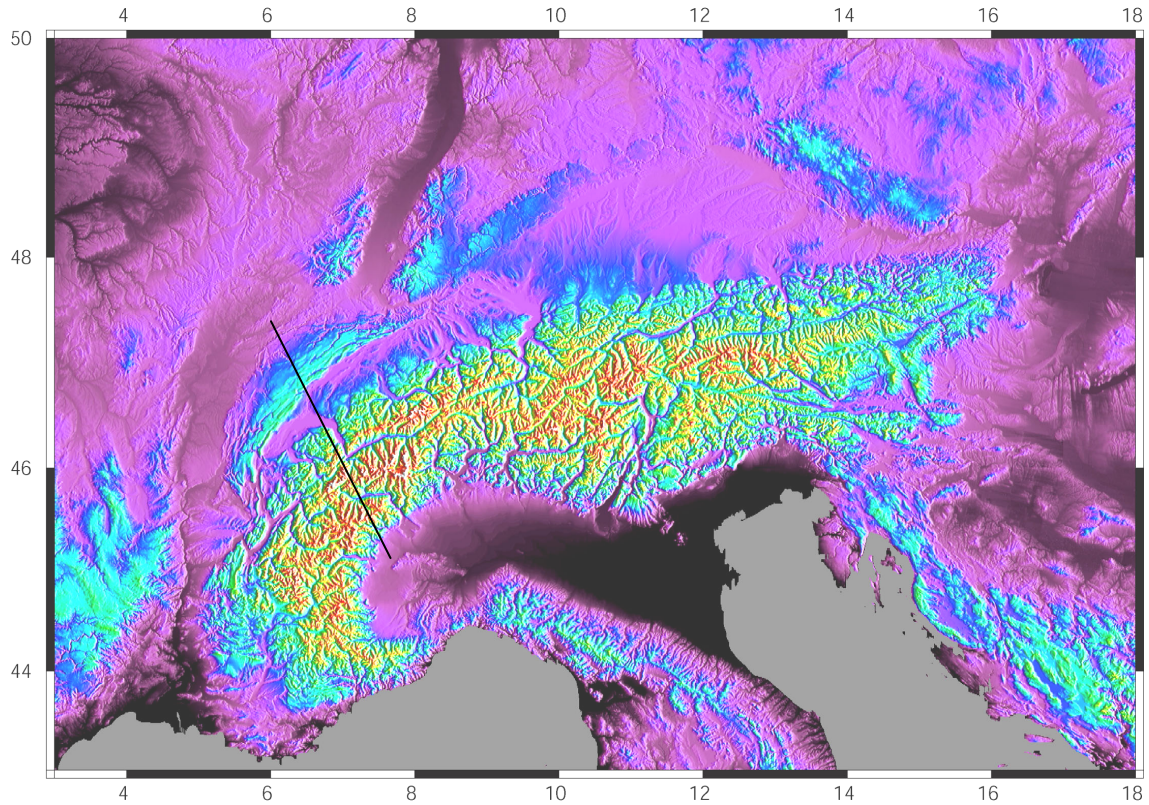
Fig. 1-2: Digital Elevation Model of the Alps and surroundings

Location of cross section of Figure 1-1 is shown by thin black line. Data are from Gtopo 30; image processing, courtesy of B. Delacou, Neuchâtel University.
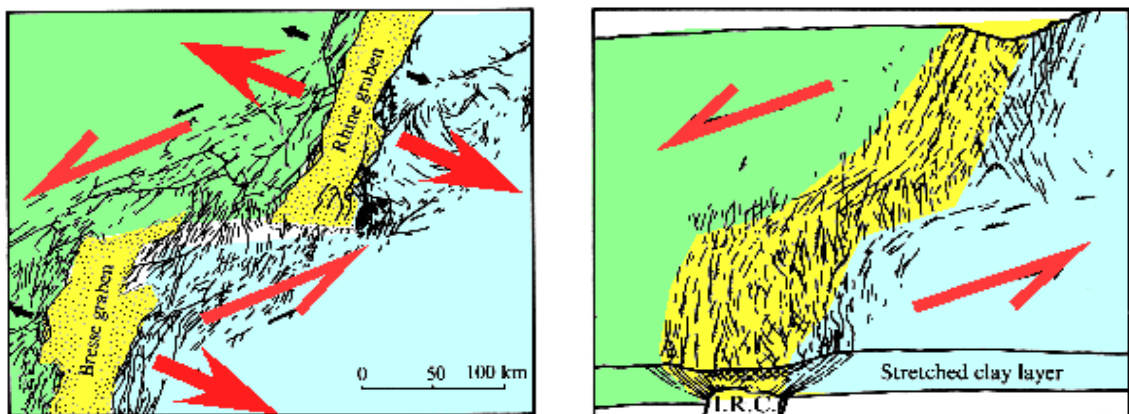
Fig. 1-3: The Oligocene Rhine and Bresse- Grabens are offset in a right lateral step, which requires a sinistral, left-lateral transform zone

The area in-between the two Grabens is highly fractured indeed, Rhenish, NNE-SSW striking faults seem to predominate, however, whereas ideally oriented E-W striking faults are the exception. From (Price & Cosgrove 1990).

1.2   Alpine collision

1.2.1   Thrust systems considerations

The exact geometry of the Alpine thrust system still is a matter of debate. Despite excellent out-crop conditions and more than hundred years of mapping in this mountain chain, large inaccessible volumes below the Jura, the Molasse basin and in front of the External Crystalline Massifs leave some freedom in the linking together various parts of the Alpine thrust system. Seismic reflection data partly fill this gap, but the most important constraints are provided by balancing and thrust system considerations. A schematic large-scale profile through the frontal Alps is shown in Figure 1-4.

Absolute age ranges for thrusting activity along the various systems are constrained by the youngest foreland basin sediments found below thrusts and radiometric, mostly cooling-ages (Burkhard 1999):

Penninic thrust system > 45 to 25 Ma   red

Helvetic thrust system	35 to 15 Ma	dark purple
Subalpine Molasse system	20 to 10 Ma	light purple
Jura – ECM thrust system	12 – 5 (to 0?)Ma	blue
thick skinned, inversion	(5 ?) to 0 Ma	green

The latest, thick skinned thrust system, indicated in green, is not universally accepted to exist. Overlapping ages are not only due to uncertainties in age determinations, but also to simultane-ous activity along higher and lower thrust systems. The Helvetic nappes can be considered as a large scale duplex structure, with a basal Helvetic floor thrust at the bottom and a simultaneous-ly active (basal) Penninic roof thrust at the top (Burkhard 1988, Pfiffner 1986).

In summary, our preferred interpretation of the alpine thrust system at the NW border of the Alps is characterized by the following elements, which provide the structural framework within the study area:

- Thin skinned Jura fold & thrust belt

- Basal decollement in Triassic evaporites

- No (compressional) basement involvement (below Jura and Molasse basin)

- Piggy Back involvement of Molasse basin and older, higher thrust systems

- Rooting of Jura thrust below the External Crystalline Basement Massifs (ECM)

- ECM interpreted as a stack of crustal thrust slices

- At least 30 km of total NW-SE convergence during the last 12 Ma, measured between the crest line of the ECM and the stable European foreland;

- This convergence is consumed by folding and thrusting in the Jura and/or most external Subalpine Molasse.

This view of the Alpine frontal thrust system, initially proposed by Boyer & Elliott (1982), is now adopted by many authors, including Laubscher (1992), and, at least partly: Guellec et al. (1990), Philippe et al. (1996), Schmid et al. (1997) and many non-alpine structural geologists. Alternative views exist in explicit form (Pavoni 1961, Pfiffner et al. 1997a, Ziegler 1982) or implicitly expressed in cross sections (Schmid et al. 1997). It is important to note that a large majority of alpine sections drawn prior to about 1985 include 'Autochthonous External

Crystalline Massifs' (ECM) and no explicit link between the basal Jura décollement and any Alpine thrusts. An exception is Laubscher, who discussed this question in detail in many of his papers since 1961 (Laubscher 1961). It is not before 1992, however, that Laubscher adopted a basal rooting of the Jura décollement below the External Crystalline Massifs. In earlier papers, he favoured 'higher', 'more internal positions' such as a connection with the basal Helvetic thrust (Morcles – Doldenhorn nappe) or a gravitational gliding / spreading interpretation (Laubscher 1988).

Alternative interpretations of the latest alpine thrust system include:

− Thick skinned Jura folding and thrusting

− Compressional involvement of basement below the Jura and Molasse basin

− 'Autochthonous' External Crystalline Massifs

− Jura folding interpreted as wrenching above basement rooted strike slip faults

There is little solid geometric evidence for any of these alternative models, neither from surface and subsurface data nor in terms of internal consistency regarding balancing and thrust system considerations. They will nevertheless be considered as alternatives in our seismic hazard evaluation.

In map view, the Jura Arc poses some additional geometric problems, notably in laterally linking together time equivalent frontal thrusts of the Alps (Figure 1-5). This problem is most obvious at the eastern termination of the Jura Arc, where the most frontal emergent thrusts and deformation features of the Alps seem to disappear eastward.

In eastern Switzerland the front of the Alps is located in a much more internal position, at the southern edge of the Molasse basin. In-between the two alpine fronts, there needs to exist a diffuse dextral transfer zone crossing the apparently undeformed, flat lying Plateau Molasse (Burkhard 1990). Some evidence for a change in structural style across this diffuse zone is provided by reflection seismic data of the petroleum industry, summarily published in (Bachmann & Müller 1992). More detailed confirmation of very subtle post-Late-Miocene wrenching deformations within this diffuse zone is provided by a recent 3-D seismic survey of the Nagra in the Zürich Weinland (Birkhäuser et al. 2001).

1.2.2 Older, pre-Jura-folding alpine thrust systems (40 to 12 Ma)

Exhumation and erosion allows deep insight into the alpine nappe pile and there is better agreement about the geometry and kinematics of these older thrust systems, namely the Helvetic and Penninic thrusts and nappe piles. With respect to the Tectonics of the study area, these thrust systems are not as relevant as the Jura / ECM – link and the associated thin vs. thick skin question. Accordingly, we will not go into any details of the complex tectonic history of the Central Alps here. There is general agreement, that none of the older (Helvetic and Penninic) thrusts is active today (in as ongoing thrusting), nor is there much evidence for inner alpine thrusting younger than ca. 15 Ma. Some reference will nevertheless be made to the classical tectonic subdivision of the Alps since many of the older structures have been reactivated in extension and/or strike slip. Some of these structures seem to be seismically active today. The classic subdivision of the Alps includes the following tectonic elements (compare with Figures 1-1 and 1-2):

− External Crystalline Massifs (ECM)

− Helvetic nappes, including 'infrahelvetic' basement cored, 'Morcles-style' nappes

− Northern steep 'root' zone, (Helvetic 'roots', Frontal Pennine Thrust)

- Penninic nappe pile, subdivided into lower (Ticino) and upper units (Briançonnais)

- Southern steep 'root' zone; Penninic 'roots', Insubric line, Insubric Backfold

- Southern Alps

- Ivrea body

All of these structures have complex 3-D geometries at depth, which makes their use as 'zone boundaries' problematic. As a typical example, the classic 'front of the Alps', as seen on tectonic maps corresponds to the most frontal position of either Helvetic or Penninic (Prealps) nappes riding above subalpine Molasse units. Helvetic and Penninic nappes are present as Klippen only, whereas their basal décollements are 'rooted' behind, i.e. south east of the External Crystalline Massif culminations. This geometry is particularly important for the delimitation of source zones: Helvetic and Penninic Klippen nappes have less than 3 km vertical thickness and they mask the more relevant geometry within the basement below them.
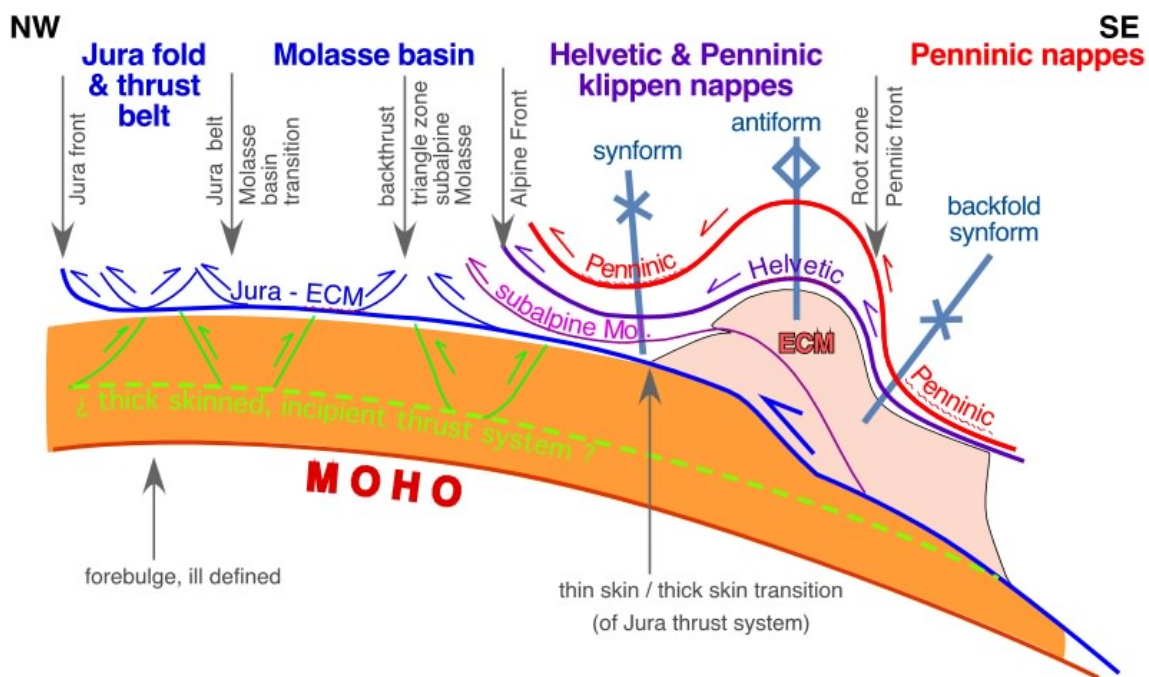
Fig. 1-4:   Generic cross section through the NW alpine front

Thrust systems are color-coded according to their relative age from red, oldest, to blue, youngest (Burkhard 1999).
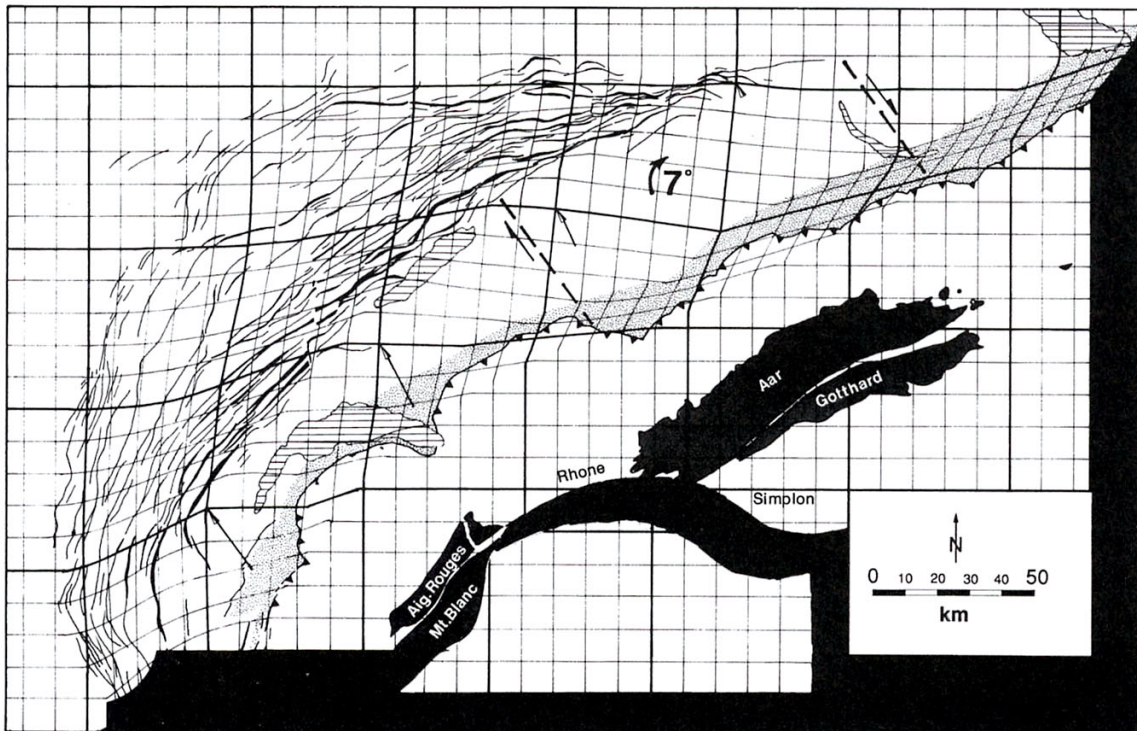
Fig. 1-5:   Schematic illustration of the Jura – Subalpine Molasse transfer problem in map
             view

             An originally square grid with 25 km spacing is shown in its present day, deformed
             state, taking into account known and estimated shortening estimates from the Jura
             fold thrust belt and the Subalpine Molasse belt. A transfer zone with an overall
             dextral shear sense has to exist between the eastern tip of the Jura Arc and the
             Mountain front in eastern Switzerland (Burkhard 1990).

1.3   Neotectonics

1.3.1   Triangulation, Trilateration, GPS

On the scale of the North-western Alps and their surroundings, relative movements between
plates and 'tectonic blocks' are too slow to be accurately established with classical, ground-
based methods of triangulation and trilateration. Up to 100 years of observations failed to pick
up any significant signals of horizontal length changes (Kahle et al. 1997). The same is true for
the more recent GPS measurements with up to 10 years of observation (op. cit). According to
some french authors, however, there seem to be some significant block-movements within the
Western Alps (Calais et al. 2001, Vigny et al. 2002), indicating extension in a NW-SE direction
in the internal (french) Alps. These movements remain to be confirmed, their origin is a matter
of debate. Geodesists agree, however, that there is no measurable movement between northern
Italy and 'stable Europe', across the Alps on a profile through western Switzerland documented
by GPS measurements of the last 5 years.

This situation leaves some freedom in the interpretation of the present day 'tectonic regime' of
the Alps and their forelands. Two extreme views are as follows:

- Alps are 'dead': convergence has come to a complete halt (some 5 Ma ago?)

- Alps are 'alive': convergence continues at a rate of < 5 mm/a (Apulia – Europe).

Both interpretations have their advocates and followers in the geologic literature. The arguments are mostly indirect. The more important points will be discussed below.

1.3.2　The latest dated faults

One of the main problems is the lack of 'young', i.e. Late Miocene and Pliocene sediments north of the Alps. The youngest Molasse sediments are now well dated as Serravallian and lowermost Tortonian, ca. 12 to 10 Ma (Berger 1996); note that many geologic maps indicate these very same sediments as 'Mio-Pliocene', often leading to some confusion about the age of Jura folding and thrusting. Such sediments are found below the frontal Jura thrust in the Bresse Graben as well as folded into synclines in a few places of the Swiss Jura, e.g. the Le Locle syncline and the Delemont basin (see Berger 1996 for an exhaustive review). This clearly indicates that main Jura folding has to be younger than 12 Ma. A reorganization of the Alpine thrust system at this date is hold responsible for the end of sedimentation within the Molasse basin, which is riding in piggy back fashion above the basal Jura-ECM thrust, leading to a general uplift and therefore bypassing of this foredeep (Burkhard & Sommaruga 1998). The end of this thrust movement is not documented by any dated sealing sediments. Some rare Pliocene sediments are present outside of the Alpine thrust system, notably within the Rhine and Bresse Grabens and in the Po-plain. (Laubscher 1987) inferred a pre-Messinian (> 5 Ma) age for Jura folding based on the subsurface observation of sealed folds and thrusts at the northern edge of the Apennines, below the Po-plain. His postulate is based on the hypothesis that the two thrust systems, frontal Apennine and Jura were time equivalent! This hypothesis is obviously questionable and an ongoing Jura folding and thrusting cannot so easily be ruled out. If we consider the latest Alpine thrust system north of the Alps and if we assume a continuous and ongoing activity for the last 10 Million years, a total convergence rate of 30 km/10 Ma yields an average rate of 3 mm/a horizontal convergence to be consumed somewhere north of the crest line of the ECM, i.e. within the Jura fold thrust belt and/or within the Molasse basin. Such a rate is small enough to be invisible in the currently available geodetic data sets! Some indication for post-Pliocene folding and thrusting has been described in the most external Jura south of the Rhine Graben (Meyer et al. 1994; compare also with Schmid et al. PEGASOS WS-2 reports).

The question of neo-tectonic movements has been addressed by Nagra, concerned by the long term stability of northern Switzerland, the very same area under scrutiny in the PEGASOS project. An exhaustive summary of over 300 citations (up to 1984) regarding Neotectonics in Switzerland is published in an Nagra Report (Isler 1985).

1.3.3　Levelling data: Alps – dead or alive ?

In the absence of clear evidence for or against ongoing thrust faulting and folding, geologists and geophysicists have tried to use alternative data sets in order to evaluate the present day state of the latest alpine thrust system. One of the data sets often quoted in favour of ongoing shortening are vertical motions determined from levelling data (Gubler et al. 1984), see Figure 1-6.

The general idea has been most clearly expressed by Molnar (1987), who inverted the Swiss vertical motion data in order to determine horizontal shortening rates. The underlying assumptions in this paper are subject to discussion, however. On the crustal scale considered, Molnar's 'inversion' method implicitly assumes that the entire thickening induced by horizontal convergence is pushing the land surface upward. Two additional factors have to be considered, however, both of them have been neglected in Molnar's 'inversion' approach. First, for reasons of isostatic equilibrium, thickening in the absence of erosion should lead to a depression of the Moho, a factor several times larger than the upward growth of topography. Second, in the

absence of thickening, erosion should be just about compensated by vertical uplift as long as there remains an overthickend crust and topography.

1.3.4   Erosion- / Exhumation- / Cooling- rates of the Alps

Erosion rates are available for short time periods of the last one hundred years for many alpine rivers (Jaeckli 1958), they vary from 0.1 to 0.6 mm/a, calculated from the accumulation of sediments in peri-alpine lakes. Long-term rates for the last 15'000 years (post-Würm glaciation) yield values on the same order of magnitude (Hinderer 2001, Schlunegger & Hinderer 2001). For the last several Million years, exhumation rates of the Alps are well established from a large and coherent data set of apatite fission track data (Figure 1-7), see (Hunziker et al. 1997) for references. Fission Track ages are unanimously considered as cooling ages, documenting the time at which a rock is cooled below a critical 'blocking temperature'. In the case of apatite this $T_{crit,}$ is $100 \pm 20°$ C. Cooling may have many causes, but in the Alps, there is general agreement that the last increment of cooling from 150° C down to zero is dominated by erosion. Cooling assumed to be equal to erosion rates of 0.4 to 1.2 mm/a vertical movement have been determined from '3-D best-fitting' of FT-age data sets (Burkhard 1999, Rahn et al. 1997).

Interestingly, however, maximum geodetic present day vertical uplift rates of 1.6 mm/a exceed all available estimates of erosion rates. This discrepancy could find an explanation in short term isostatic disequilibrium, induced by ice-loading / unloading during the last cycle of glaciation / deglaciation. The effects of isostatic rebound after the removal of an important alpine ice-load has been evaluated by Gudmundsson (1994), as shown in Figure 1-8. According to this model, such an effect could easily explain a large part of up to 1.2 mm/a or more of the present day uplift rate. These values are obtained for 'reasonable' values of ice cap size and thickness, time of ice removal, elastic thickness of the lithosphere and viscosity of the underlying astenosphere.

In summary, the geodetic vertical motion and GPS data for the Swiss Alps do not provide any evidence in favour or against ongoing convergence and thrusting in the Alpine collision system.

1.3.5   Present day stress regime

The orientation of the present day stresses and the prevailing stress regime (Figure 1-9) is fairly well established for most of the study area, based on a large data set of focal plane mechanisms (included in the PEGASOS data base and available as backdrop in Wizmap) (Deichmann 1992a, Kastrup 2002, Pavoni 1987, Pavoni et al. 1997). The type of faulting is predominantly strike slip. There are a few areas with dominant extensional mechanisms and locally some thrusting is also observed.

Along the Arc of the Western Alps, a nice correlation seems to exist between topography and type of faulting. Normal faulting is found along the centre line of the Alps while thrusting is found on either side of the Western Alps at the transition between high and low topography. Note that in Figure 1-9, alpine topography has been smoothed with a filter of 50 km diameter in order to remove small-scale features.

This correlation suggests a causal relationship between topographic load and seismicity; the relationships observed are reminiscent of 'gravitational collapse' (Avouac & Burov 1996). Some evidence for this phenomenon has been found in all major orogens of the world (Dewey 1988). But again, just as in the case of geodetic observations, this does not provide any evidence for, nor against ongoing convergence between Europe and Italy across the Alps.

APPLICATION TO THE ALPS
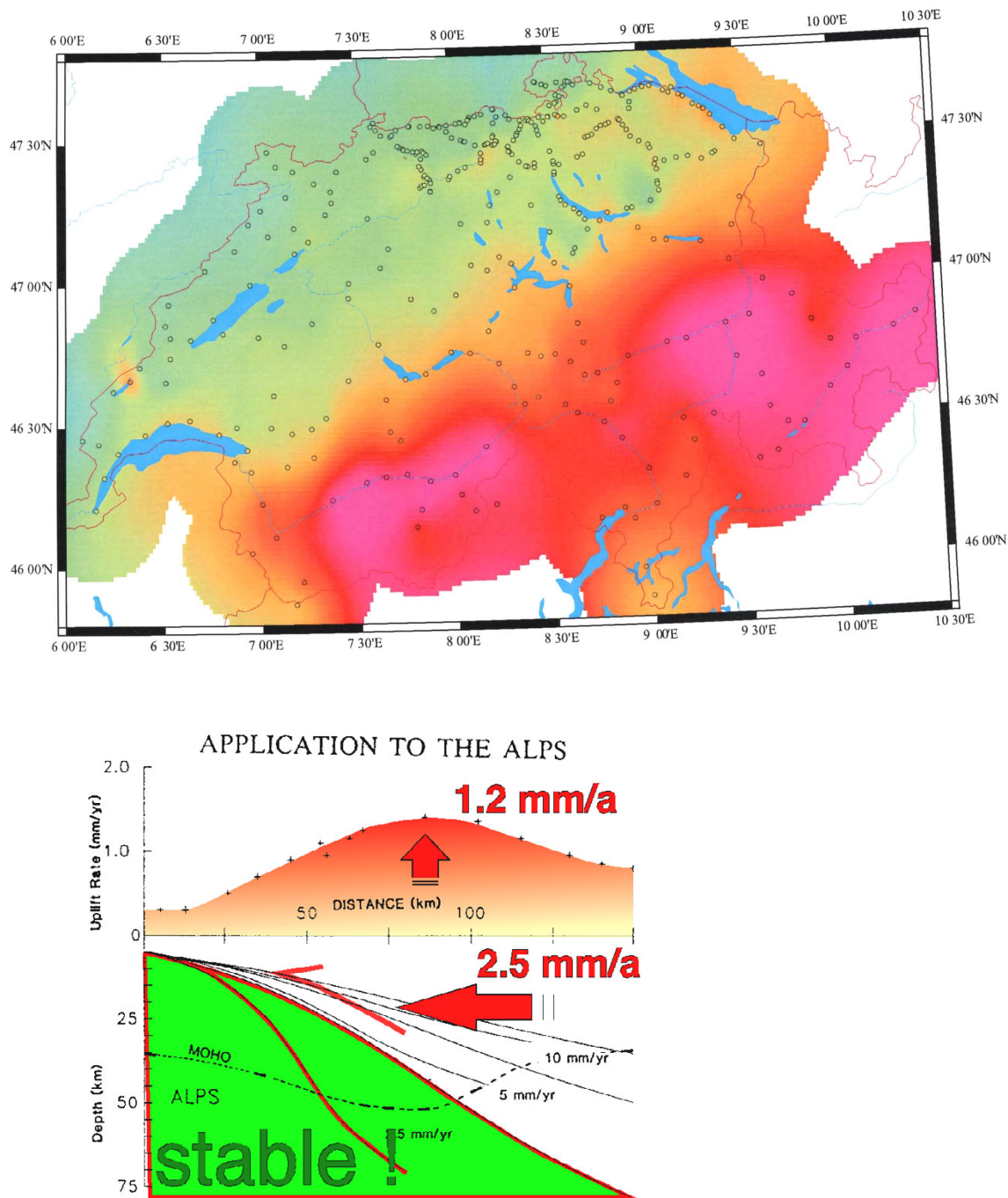
Fig. 1-6:   Leveling data and one of their interpretations.

Above: Vertical uplift rates in Switzerland; data include the Swiss Leveling Data (Gubler in Kahle et al. 1997) as well as non-corrected data (with a slightly different zero point) of a Nagra survey in Zürich – Bodensee region (data provided by Philippe Roth on request). Maximum uplift rates are 1.6 mm/a (purple); minimum is light blue (-0.3 mm/a). Arbitrary zero point is at Aarberg (greenish). Contouring and smoothing was produced with GMT software. Below: Molnar's (1987, Fig. 3) interpretation of vertical uplift in the Swiss Alps as evidence for ongoing horizontal shortening along a crustal scale thrust ramp (colours, arrows and large letters are added).

Gotthard. âges FT apatite
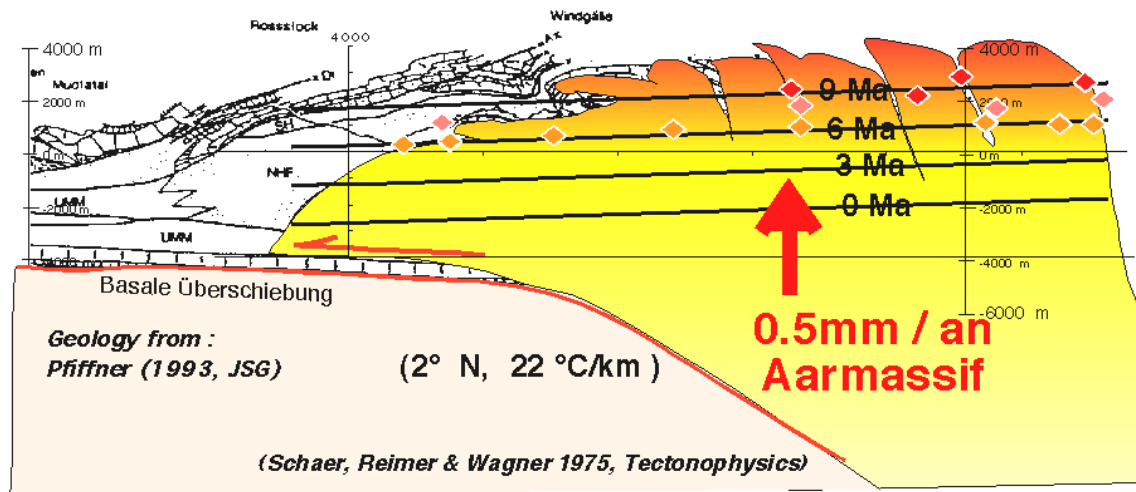
Fig. 1-7:   Fission Track data record the time of cooling below an estimated 100° C isotherm

FT data sampled from high summits, valleys and tunnels show a clear altitude dependency. Projected data points are indicated with rhombi. Their ages have been used to calculate a family of paleo-100°C isotherms by 'linear regression'. In the Gotthard cross section, FT ages indicate a 0.5mm/a rate of vertical cooling, interpreted as due to erosion. A slight northward tilt of 2° of these paleo-isotherms is thought to be due to differential uplift and/or ramping along a basal thrust below the Aarmassif. Data and inspiration from Schaer et al. (1975).

1.3.6   In situ stress measurements

Additional, but in places contradictory stress data are provided by in situ stress determination methods such as borehole slotter (Jura Mountains), borehole break outs, hydrofracs etc.; this data set is included in the PEGASOS data base (Becker 1989, 2000) and is shown in Figure 1-10.

Overall, maximum horizontal stresses are oriented NNW-SSE, at a high angle to the Alpine crest-line in front of the Eastern and Central Alps. Further to the west, a radiating pattern in front of the Alps seems to interfere with a N-S oriented west European stress field. In the Jura Arc, where a particularly dense data set is available from borehole slotter experiments, the stress pattern deviates significantly from the expected arcuate fold & thrust pattern (Becker 2000).

This lack of coincidence between paleo- and in-situ-stress orientations has been used as an argument in favour of a 'dead' Jura fold & thrust system at least as far as thin skinned thrusting and folding is concerned. High absolute stress values in the Central and Western Jura, have been used as an argument in favour of ongoing shortening in thick skinned fashion (Becker 2000, Mosar 1999), however.
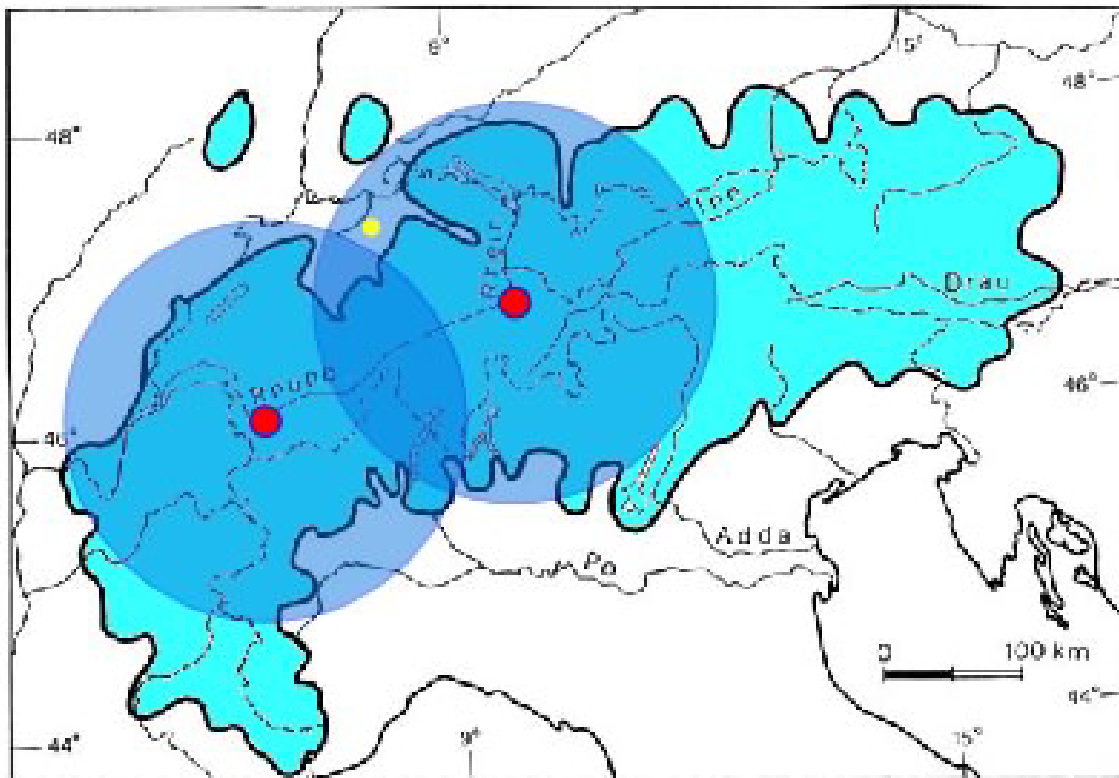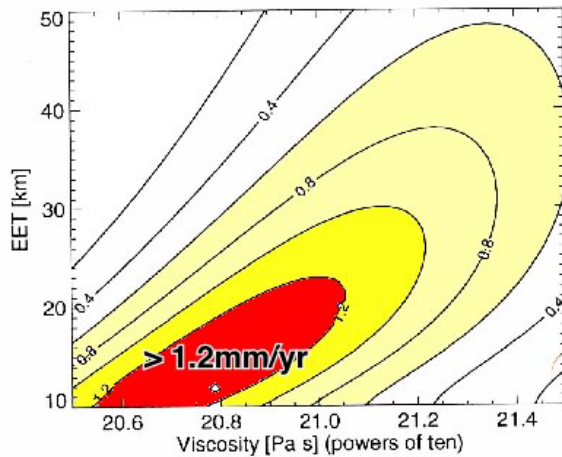
Fig. 1-8:   Isostatic rebound model of Gudmundsson (1994, Figs. 4 and 1, modified), (above) vertical uplift rates, (below) schematic representation of the Alps with the maximum extent of ice-cover during the last glacial maximum (ca. 18 ka before present)

Vertical uplift rates, expressed in mm/a, are calculated as function of Effective Elastic Thickness (EET) of the Lithosphere and Viscosity of the underlying Astenosphere. The elastic rebound model assumes a circular ice cap with 150 km radius, an ice thickness of 250 m and a duration of 10 ka for the loading. It is further assumed that this ice cap disappeared instantaneously 13 ka ago. Superimposed are two circles to illustrate the size of Gudmundsson's model ice-sheet, centered onto Chur and Martigny respectively, indicated by red dots. The yellow dot in northern Switzerland indicates the approximate position of Aarberg, the relative zero for Swiss leveling studies. Gudmundsson's rates are calculated with respect to a reference point 200 km away from the centre of the ice load.
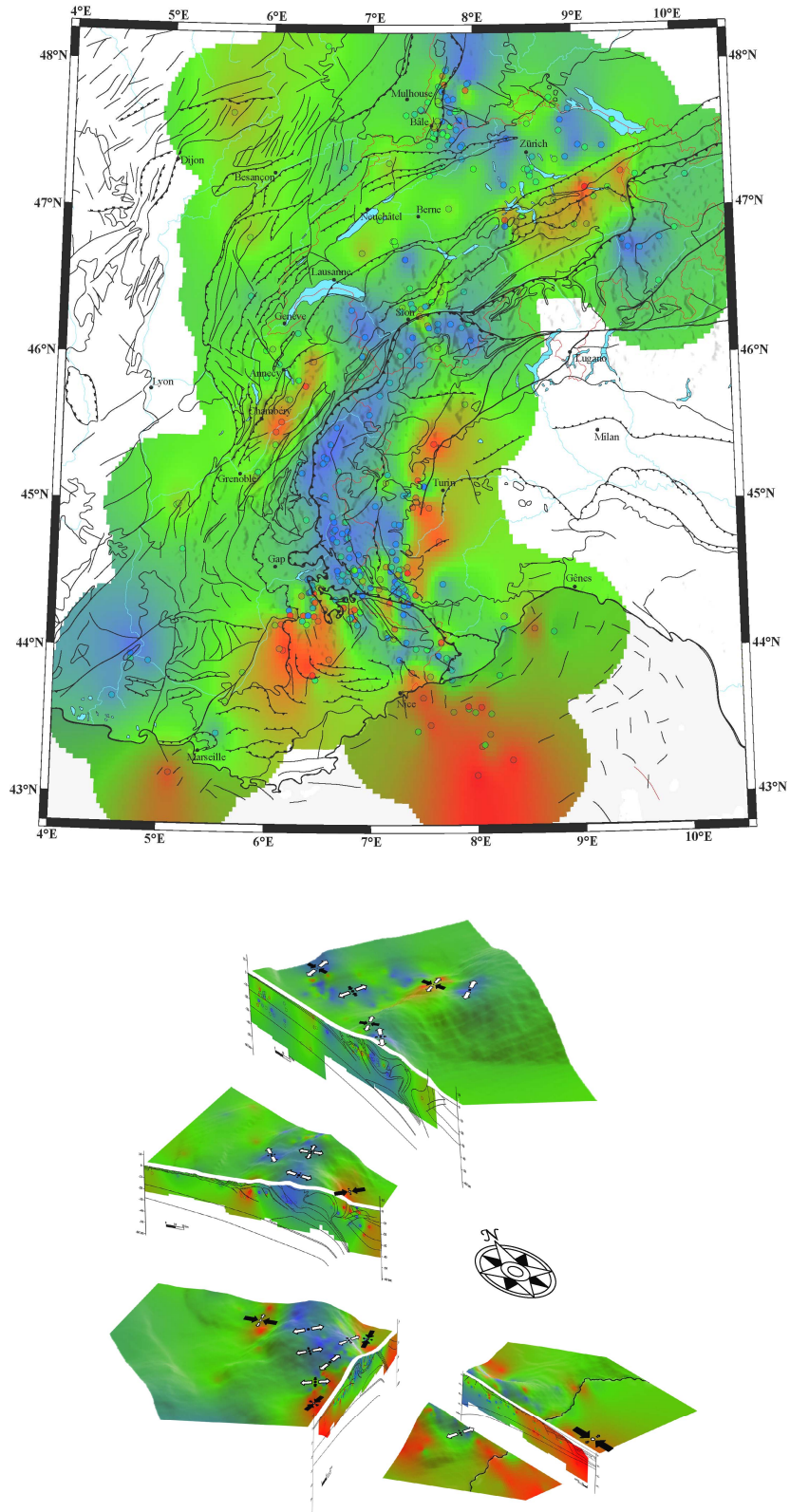
Fig. 1-9: Stress regime of the Western Alps and surrounding areas

Green is for strike slip, red = thrusting, blue = normal faulting. All available (published) earthquake focal plane solutions have been used for this interpolation between observations (small dots with appropriate colour). Courtesy of B. Delacou (2002, PhD thesis at Neuchâtel, *in prep.*).
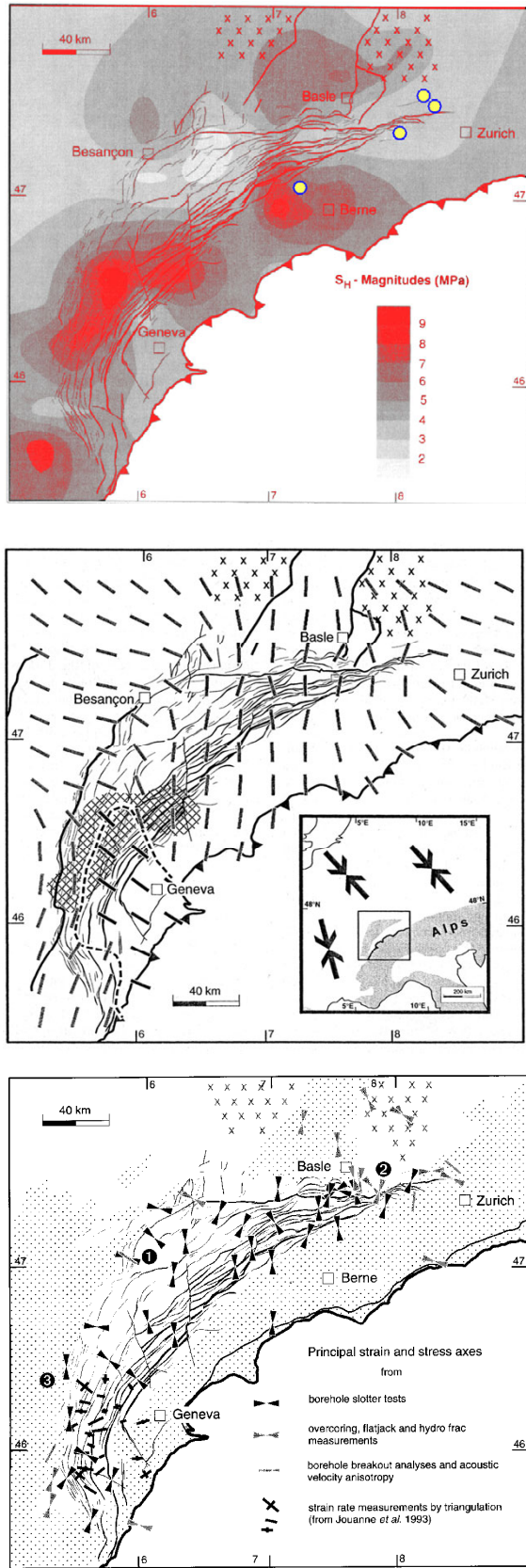
Fig. 1-10:   In situ stress measurements in the Jura Arc (Becker 2000, Figs. 6, 7 and 13)

1.4   Thick skinned, active Jura ?

The idea of basement involvement below the Jura fold thrust belt is not a new one (Aubert 1945) but it has become increasingly fashionable again in recent years. Extreme views are presented by Ziegler (1982) and Pfiffner et al. (1997a) where most of the cover shortening seen in the Jura fold belt is explained by thick skinned thrusting along a 'basal décollement' at several kilometers depth within the pre-Triassic basement. This idea is not substantiated by any tangible data.

Similar, but more subtle views have been presented recently in a series of publications (Guellec et al. 1989, Mosar 1999, Philippe et al. 1996). These authors all accept a thin skinned interpretation with a major Triassic décollement to explain the gross shortening by folding and thrusting seen in the cover rocks of the Jura fold thrust belt. But they all propose that skinned thrusting should have been replaced recently by a thick skinned compressional regime, leading to inverse faulting along pre-existing normal faults, mostly boundary faults of Permo-Carboniferous Grabens, which are proposed to be slightly inverted or just about to be inverted. The entire scenario remains speculative, however, there is no hard (reflection seismic) evidence in favour of inversion. The only place, where such an inversion has been 'seen' is the ECORS profile across the south-western Jura (Figure 1-11). A recent re-evaluation of this profile conducted at the Institut Français du Pétrole (IFP) reveals that the previously interpreted 'basement high' below the 'Haute Chaîne du Jura' is simply a velocity pull-up, which disappears entirely upon depth-conversion of this seismic line (Coletta et al. 2002).

In summary:

−   A basement high is postulated below the 'Haute Chaîne du Jura' in the official interpretation of the french ECORS seismic line (Guellec et al. 1990)

−   Pfiffner et al. (1997a) proposes a basement high below the Chasseral anticline (northwest of Biel), based on balancing arguments of a surface geology cross section

−   Incipient thrusting deep within the crust, below the Molasse basin and Jura is proposed by Mosar (1999) based on 'critical taper' considerations and patterns of present day vertical uplift as well as in situ stresses (Becker 2000).

−   An E-W striking culmination of the basal unconformity below the Vosges gravels has been identified SW of Basel by Schmid and co-workers. They interpret this structure as a young (post 3 Ma) anticline, formed above a deep seated basement thrust fault (Schmid in WS-2 Summary SP1, PEGASOS PMT-TN-0135)

Despite weak and circumstantial evidence for all of these basement thrusts and their present day activity, they will be given some consideration in our source zone models.
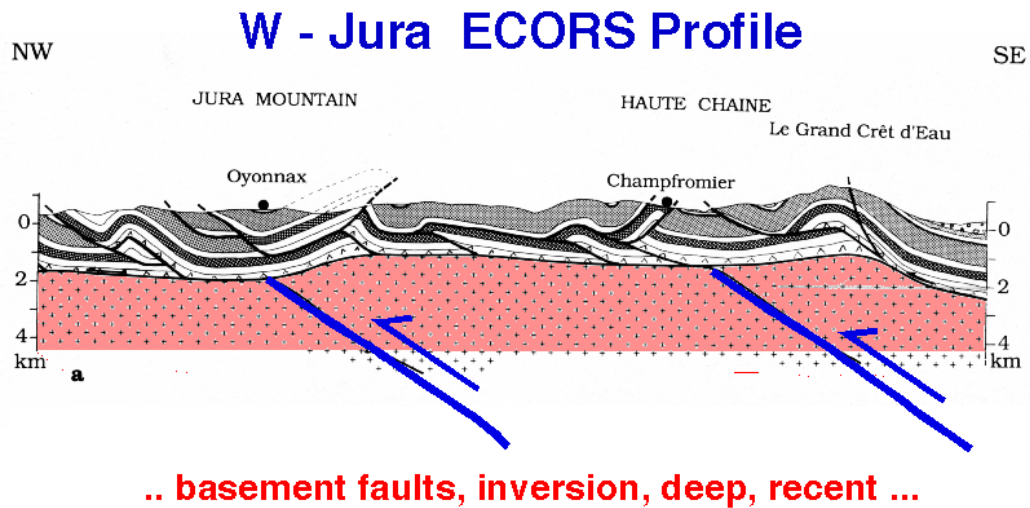
Fig. 1-11: Two stage evolution of the Western Jura fold thrust belt according to Guellec et al. (1989, part of Fig. 10, modified and coloured)

A first (post 12 Ma thin skinned thrusting is followed by a second stage of recent ? even 'ongoing' ? thick skinned basement inversion, underlined in blue. This proposal helps to explain the relative height of the Jura 'haute chaîne'.

2   SEISMIC SOURCE DEFINITION

2.1   Large scale zonation

A first large scale subdivision of the study area is based on structural, 'architectural' considerations with little input from the present day seismicity. Our guiding philosophy was to distinguish larger areas (shown in Figure 2-1 below), which share common characteristics on a lithospheric and/or crustal scale – as seen on a Moho-map.

Limits between these large zones were drawn on a tectonic basemap, mostly following obvious, 'classic' tectonic boundaries. Most of our lines are <u>not</u> identical with these boundaries, however. First, we opted for a considerable smoothing in order to obtain simple zones boundaries. In general, we extended the 'more active' zones some 5 to 10 km outward on the expense of the neighbouring 'less active' zones. Despite the complex 3-D structure of the Alps with many shallow dipping fault zones and nappe boundaries, all zone boundaries are kept vertical at depth for simplicity, however. Our rationale for the delimitation of the large-scale source zones will be given below.
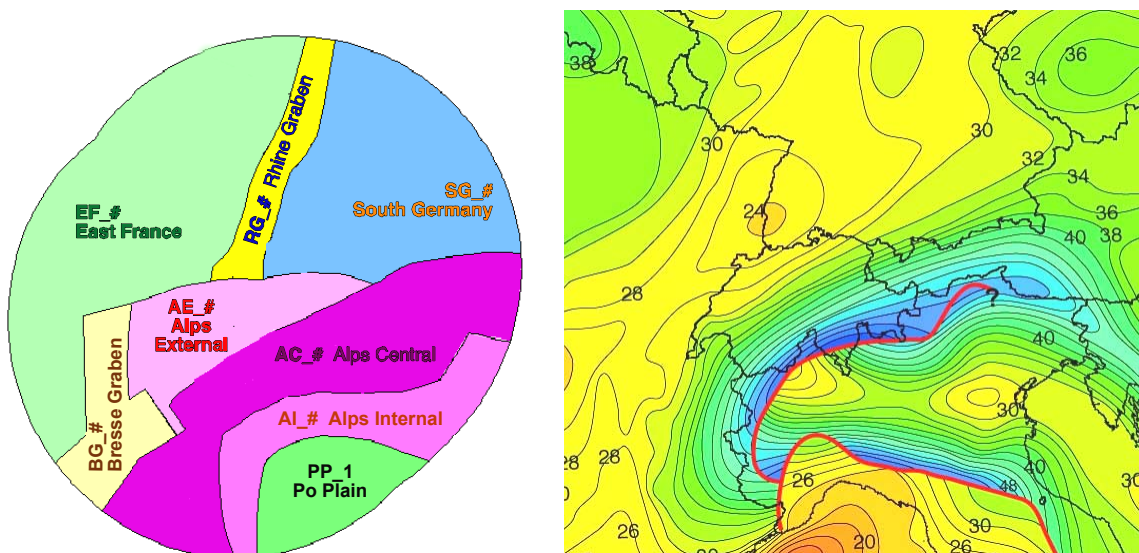
Fig. 2-1:   Large-scale zonation (left) compared to Moho map (right)

The Moho map is a compilation by Dèze & Ziegler (2002) which is available on http://comp1.geol.unibas.ch/index.php.

2.1.1   East France (EF) and South Germany (SG)

Both of these two zones are considered as 'stable European foreland' to the Alps. They are characterized by a normal crustal thickness on the order of 30 to 35 km see also http://comp1.geol.unibas.ch/index.php for a new compilation of the European Moho-map.

Despite some large scale 'undulations', interpreted by some (Lefort & Agarwal 2002) as buckling under the influence of Alpine tectonics, this foreland lithosphere lacks obvious signs of alpine thrusting, folding and inversion. The most important large-scale tectonic elements are

the Vosges and Black Forest basement culminations, various small localized graben zones (with the exclusion of the major Rhine and Bresse Grabens) and fault zones along inherited 'lineaments' of known or suspected older, pre-Triassic structures. Re-activations are predominantly in strike slip mode. In Bavaria, the lithosphere of the South Germany zone has been bent downward below the Alps leading to the formation of the Tertiary Molasse foredeep. Despite this involvement in 'alpine tectonics', we opted to group this part of the Molasse basin with 'stable foreland crust'. From petroleum exploration work in the Bavarian Molasse basin, it is known that this part of the crust has been slightly extended in a NNW-SSE direction in Oligocene times, most likely as an effect of lithospheric flexure. These extensional structures are still present as such and have not been inverted (Bachmann & Müller 1992); this is in contrast to the Swiss Molasse basin, where at least the sedimentary cover has been involved in alpine compression.

Crustal thickness: Normal, about 30 km
Key words: Stable continent
Age of (reactivated) faults: Hercynian, Permo-Carboniferous, (Oligocene)
Style of present day faulting: Strike slip

2.1.2   Rhine Graben (RG) and Bresse Graben (BG)

The Rhine and Bresse Graben zones are characterized by well-marked surface depressions, vast Quaternary alluvial plains, Tertiary graben fills and complex faulted border areas with Mesozoic and basement outcrops. Both graben zones have a reduced crustal thickness (Moho depth around 25 km), a weak positive Bouguer anomaly and a large thermal anomaly, most pronounced in the case of the southern Rhine Graben.

Lateral eastern and western boundaries of the Rhine Graben zone are systematically chosen a few kilometres outside of the mapped boundary faults and fault zones. This choice is deliberate in order to include earthquakes from this bordering area, not to miss ill-located earthquakes and also because there might be non-mapped faults, or blind faults in the boundary zone between the graben border and the Vosges and Black forest rift shoulders.

The limits of the Bresse Graben zone are quite obvious in the northern part of this graben structure. Further south, however, we opted to include parts of the south-western Jura fold thrust belt as well as a small area of stable crust within a generalized and simplified southern Bresse graben zone. This choice is artificial and not motivated by any tectonic considerations.

Crustal thickness: Attenuated, ca. 25 km
Key words: Oligocene Extension $\Rightarrow$ graben formation
Age of (reactivated) faults: Oligocene, (Permo-Carboniferous, Hercynian)
Style of present day faulting: Strike slip

2.1.3   Alps External (AE)

This zone comprises areas, which have visibly undergone some alpine shortening in the form of folds and thrusts. Alpine deformation within this zone is mostly if not exclusively in thin skinned mode, limited to the sedimentary cover of some 2 km (NW) to 5 km (SE) thickness. Décollement is located within a weak basal layer of Triassic evaporites and/or within higher stratigraphic levels (e.g. Aalénian shales or Lower Marine Molasse). The crustal scale architecture of this zone is dominated by a SE-ward bending down of the European crust, best documented on structure contour maps of Moho-depth (and top basement). This downward flexure is a direct result of alpine subduction in a SE ward direction. Basement thickness is

constant at ca. 28 km, the SE-ward bending down of the european lithosphere documented by an increasing depth of the Moho is compensated by an increasing thickness of Tertiary Molasse sediments.

The Alps External zone comprises the Jura Fold & Thrust belt and large parts of the Swiss Molasse basin. In contrast to the Bavarian Molasse basin which is characterized by the preservation of Oligocene normal faults (known from sub-surface petroleum exploration data (Bachmann & Müller 1992) the Swiss Molasse basin is characterized by compressional structures with Mesozoic and Tertiary sediments.

The northern and north-western limit of the Alps External zone has been chosen so as to generously include the most external folds and thrusts of the Jura Arc, including controversial areas such as the massif de la Serre basement high and surroundings, which may be an Oligocene horst (according to 'Carte Géologique de la France' 1:50'000 sheet Pesmes, and Modello strutturale Italia) rather than a Late Miocene thrust inversion structure (as given on the french geologic map 1:500'000, reproduced in the PEGASOS – Wizmap – geologic basemap). The limit to the SW is chosen somewhat artificially, slightly to the SW of the Vuache fault. This choice is purely topologic and has nothing to do with the alpine thrust system architecture in this area; we feel comfortable with this simplification (excluding a small part of the southwestern, thin skinned Jura Arc) since we are far from the center of our study area. The limit to the NE, i.e. east of the eastern-most obvious Jura structures (Lägern-fold and Mandach-fault) is ill defined. We have chosen a straight line to connect the tip of the north-eastern Jura Arc with the subalpine Molasse triangle zone of eastern Switzerland near lake Konstanz.
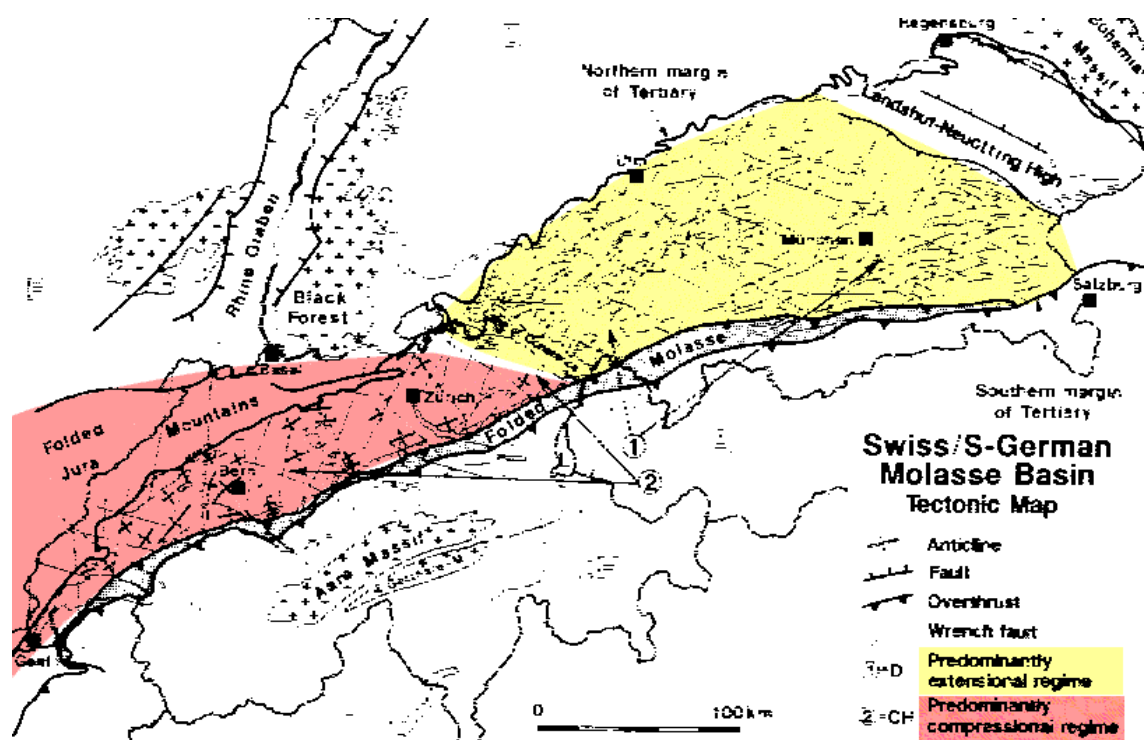
Fig. 2-2:   Tectonic style observed within the Molasse foredeep

Compilation of observations, made on thousands of kilometres of seismic reflection lines (not publicly available) by Brink et al. (1992). Red: compressional structures. Yellow: extensional structures.

There is some evidence for subtle compressional wrenching deformation south of this limit (Birkhäuser et al. 2001). Further east, there is better agreement on the locus of the most external alpine deformation front: it runs a few kilometres north of a prominent triangle zone or back-thrust, marking the transition between flat lying, undeformed Plateau Molasse and progressively NW ward tilted 'subalpine Molasse' or 'folded Molasse' (Bachmann et al. 1987).

The SE limit of the Alps External zone is chosen as a smooth line close to but <u>not</u> identical with the classical Alpine Front, either defined as the frontal emergence of the basal Helvetic thrust on a tectonic map or as the northern limit of Alpine relief as seen on a digital elevation model. Any choice of a 'northern limit to the Alps' is problematic, however, since no surface feature does have any significance at deeper crustal levels of interest. A more relevant choice would probably be the thin skin / thick skin transition, i.e. the locus where the Late Miocene alpine basal 'Jura' thrust cuts down into the basement. The position of this line is unknown, however. Most probably it runs some 5 to 10 km south of the actually chosen 'Alpine Front'. Our choice is a conservative one since it reduces the lateral extent of the area of the Alps External zone, where tectonics are thin skinned, from the Alps Central zone, characterized by thick skinned tectonics.

Crustal thickness:	Normal, 28 km plus sediments
Key words:	Thin skinned Alpine deformation
	Folding & Thrusting
	Foreland-basin, lithospheric flexure
Age of (reactivated) faults:	Miocene, Oligocene, (Permo-Carboniferous)
Style of present day faulting:	Strike slip

2.1.4   Alps Central (AC) and Alps Internal (AI)

The Alps Central and Alps Internal zones represent the main body of the Alps as defined by its topographic expression. This topography is a direct result of the collision process which lead to an overthickened crust. The crustal thickness of the Central and Internal Alps is increasing from about 35 km at the outer borders to more than 60 km along a line running from Chur to Martigny and further SW-ward, approximately along a median line of the Western Alps. This Alpine crust is made of an intricate stack of basement nappes, separated from each other by thin slivers of Mesozoic sedimentary rocks. Nappe stacking, strong internal deformation and meta-morphism are geologically young events (40 to 15 Ma). Evidence for young thrusting (15 Ma and younger) is limited to the bordering areas, such as the subalpine Molasse and southern Alps, however. Within the main body of the Alps, well documented young, i.e. Late Miocene tectonic activity is mostly in the form of normal and strike slip faulting. Uplift (up to 1.6 mm/a) and erosion (up to 0.5 mm/a) are still taking place at high rates today. The external limit of the Alps Central zone is chosen as a smooth line, loosely following the 'alpine front'.

Crustal thickness:	Thickened, 35 to 60 km
Key words:	Oligo-Miocene Alpine Collision
Age of (reactivated) faults:	Mostly Alpine structures (< 50 Ma)
	Liassic, Permo-Carboniferous (Hercynian)
Style of present day faulting:	Strike slip, normal faulting, locally thrusting

2.1.5   Alps Internal (AI)

The limit between the Central and Internal Alps is chosen along the Insubric and Giudicarie Lines respectively. Both of these limits are major, long-lived faults separating the Central from the Southern Alps. Further to the southwest, in the Western Alps, such a distinction is less

obvious and our subdivision becomes somewhat artificial. The main difference between the Alps Central and Alps Internal zones is the vergence of the latest thrusting: NW-ward in Alps Central, SE-ward in Alps Internal. The southern (and eastern) limit of the Alps Internal zone is chosen deliberately south of the obvious surface expression of the Alpine front of the Southern Alps in order to include some known and suspected south-vergent thrust faults hidden below the sedimentary cover of the Po-plain (Scandone 1990, Schoenborn 1992).

2.1.6   Po-Plain (PP)

The Po-plain zone represents the Southern Foreland Basin to the Alps and the Northern Foreland to the Appennines, covering the vast, Quaternary alluvial lowlands of the Po-plain. This zone also comprises frontal parts of the Appennines, both emergent and hidden below Latest Miocene, Pliocene and Quaternary sediments of the Po-plain, compare with 'Modello Strutturale, Italian map' (Scandone 1990). Despite this internal heterogeneity, we did not want to subdivide this Po-plain zone any further, since it is located very far from the center of our study area. The northern and western border of this zone has been chosen to follow the surface morphologic expression of the Alpine front.

Crustal thickness:	Normal, 30 km
Key words:	Foreland basin, thin skinned thrusting,
	Lithospheric flexure (two ways! Alps, Appennines)
Age of (reactivated) faults:	Miocene, Oligocene, (Pre-Triassic?)

2.2   Fault parameters (orientation, style, depth, rupture geometry)

The large scale zones outlined above are characterized by their geologic history, crustal structure and their relative location with respect to the Alps. We used the available information (most of it is available in the PEGASOS data base, some is even directly accessible as backdrop in Wizmap) in order to determine:

−   the representative orientation for maximum horizontal stress σ_1

−   the predominant style of faulting

−   the most likely depth distribution for large earthquakes.

2.2.1   Fault orientation and Style of faulting

The 'representative' orientation for the maximum horizontal stress σ_1-axis has been determined by visually inspecting maps of compiled stress information (Figure 2-3) including focal plane solutions and in situ stress determinations (outputs of PEGASOS maps on the scale 1:800'000). For each style of faulting, the most likely fault orientation has been determined based on a very simple set of rules, following Anderson's fault types (Anderson 1951), see Figure 2.4:

−   normal faults have their strike at 90° to the σ_3-axis, 60° dip

−   thrust faults have their strike at 90° to the σ_1-axis, 30° dip

−   strike slip faults have their strike at + or − 45° from the σ_1-axis, 90°dip

−   however, and most important: preexisting, faults are reactivated if their orientation (pole) is no more than 30° different from the optimum orientation of a new 'Andersonian fault'.

In a very large majority of cases, the present day seismic activity is taking place along pre-existing faults and fractures. They are numerous indeed. Superregional trends of structures are widely accepted as Alpine, Rhenish, Eggisch, Permo-Carboniferous, Variscan (Wetzel & Frantzke 2001). Major lineaments seen on an ESR Radarmosaic of southern Germany are shown in Figure 2-5; we used this figure of Wetzel & Frantzke for inspiration in:

1. choosing the most likely orientation of reactivate-able faults and

2. as an additional argument in the choice of zone boundaries.
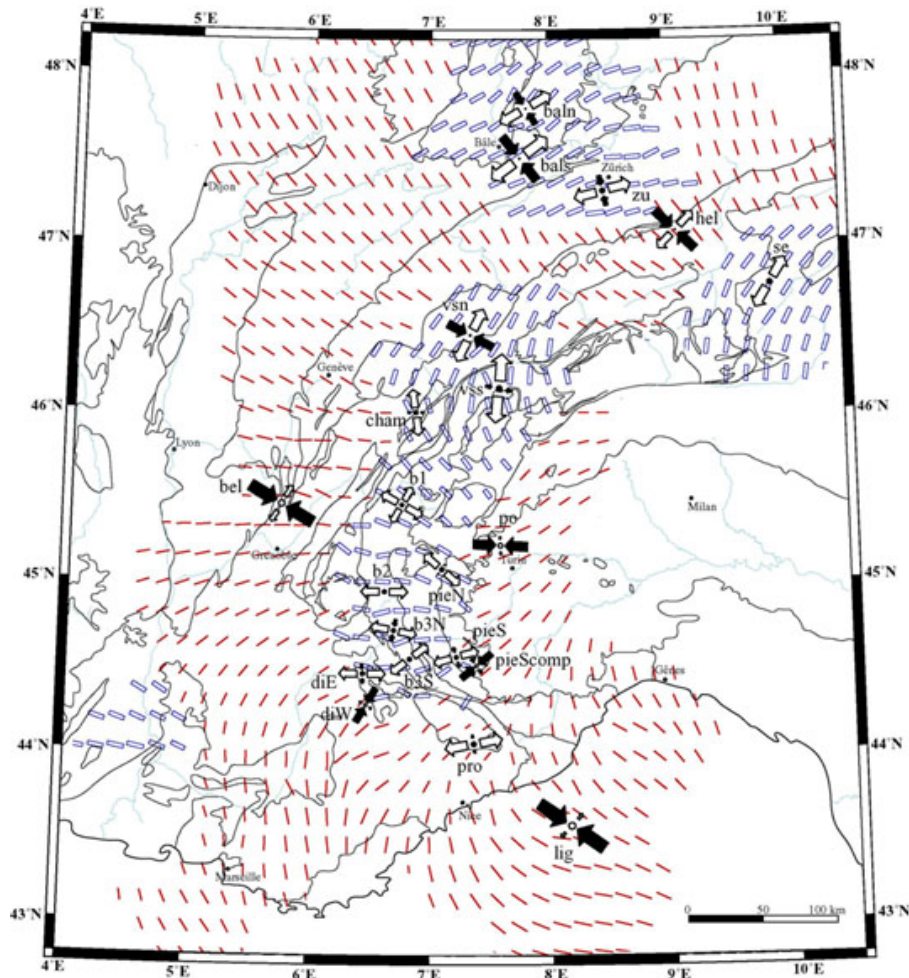
Fig. 2-3:   Synthetic map of the alpine strain / stress state

A large data set of Fault Plane solutions (including the data available in the PEGASOS data base, e.g. Kastrup (2002) has been used to interpolate regional stress fields. Black arrows are for horizontal σ_1, open arrows stand for horizontal σ_3. Thin red lines are interpolated P-axes (mainly transcurrent to transpressive tectonic mode). Thick blue lines are interpolated horizontal T-axes in areas in extension or extensional strike slip mode. Courtesy of B. Delacou (2002, PhD work at Neuchâtel University, submitted for publication in JGI).

For each large zone, we estimated the relative percentage of earthquakes in normal faulting, strike slip and thrusting mode based on focal plane solutions and our understanding of the regional tectonics (see Figure 2.6).
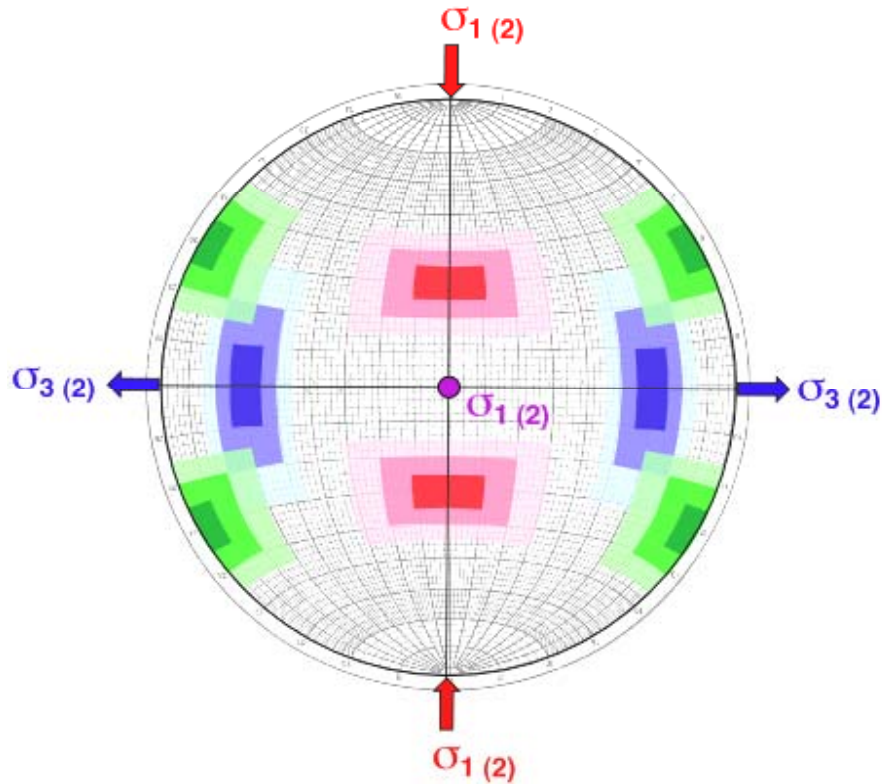
Fig. 2-4:   Anderson's fault orientations, illustrated on a stereogram

Anderson assumes that two principle stresses are horizontal, parallel to the earth surface. Most likely fault orientations (poles) can be predicted from a knowledge of the orientation of principle stresses. If sigma 1 is N-S oriented, thrust faults should have their poles falling within the fields coloured in red (if σ_3 is vertical). If σ_2 is vertical instead, the most likely faults to be activated would be strike slip faults, with their poles falling within the fields indicated in green. In an extensional regime, with σ_1 vertical, and σ_3 horizontal (E-W), normal faults should have their normals falling within the blue fields. Any pre-existing fault with its pole falling outside of the coloured fields is very unlikely to be re-activated under the given stress field, even allowing for stress permutations ($\sigma_1 <-> \sigma_2$) or ($\sigma_2 <-> \sigma_3$). This type of stereogram will be used later on in order to rapidly examine the likelihood of pre-existing faults being reactivated in the present-day stress field.

Fig. 2-5:   Fracture lineaments of Southern Germany, from Wetzel & Frantzke (2001)

thrusting   strike slip   normal faulting
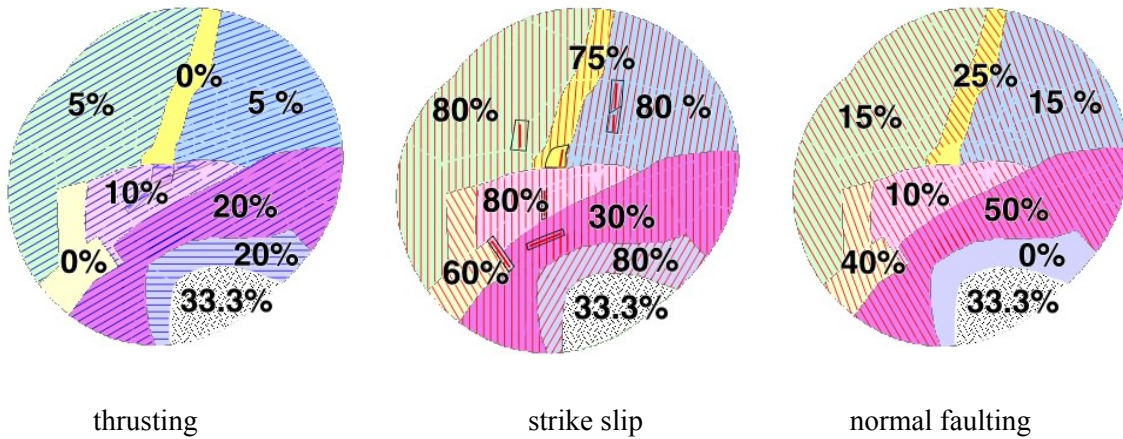
Fig. 2-6:   General expected fault orientations are indicated by a hatching overlain onto our
             large zones

             The strike orientation of the most likely fault orientation is given separately for
             each faulting mode. Numbers (in %) indicate the estimated percentage of large
             earthquakes to occur in 'thrusting, strike slip and normal faulting mode'
             respectively.

2.2.2   Depth distribution of earthquakes

In order to estimate a characteristic depth for large earthquakes, we used the PEGASOS
Earthquake Catalogue in Wizmap (PEGASOS EXT-TB-0043 2002). We only considered events
of Magnitude 3.5 and larger that have occured since 1972 (i.e. the instrumental catalogue of
Switzerland). For each zone, an optimally oriented cross section has been chosen in order to
collect all earthquakes lying within and excluding earthquakes outside of this zone. Visual
inspection of this cross section was then used to determine an average depth with its 1σ standard
deviation as well as a lower bound (Figure 2-7).

Length of section = 175 km; width of section = 58 km
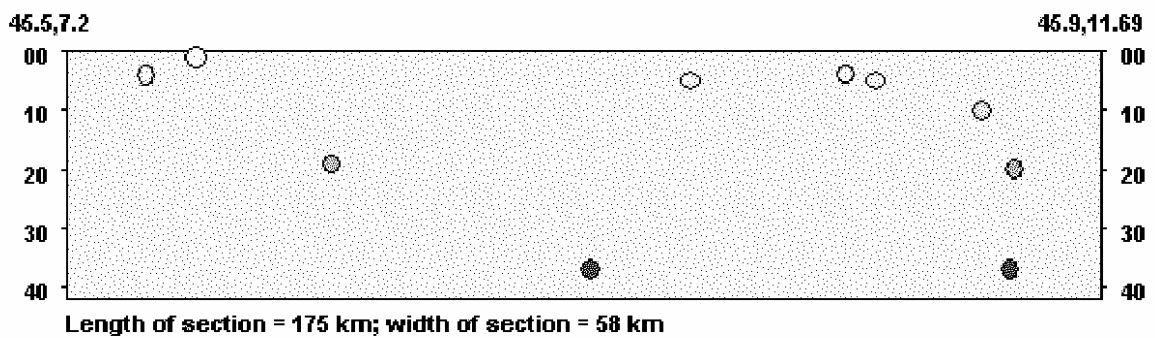
Fig. 2-7:   Example of most likely depth distribution of large earthquakes

             From this cross section with earthquakes collected along the AI, Alps Internal
             zone, we have chosen a most likely depth of 18 ± 10 km and a maximum depth of
             37 km.

Earthquake depth distributions obtained in this way are ill defined, however. First, there are only very few large events in the catalogue for each zone. Secondly, the catalogue contains ill-constrained depths. For the Central Alps, where Deichmann et al. (2000) document a maximum depth of seismicity at 18 km, the PEGASOS catalogue features earthquakes at more than 30 km depth. This is why we have not chosen any rigourous approach. We assume a normal 'Gaussian' frequency vs. depth distribution of earthquakes and we estimate three (four) parameters to describe this distribution to the best of our knowledge:

1. an average depth

2. a 1σ value (standard deviation) for a normal distribution

3. a maximum depths (lower truncation value)

4. the earth surface represents a natural 'upper truncation'.

Earthquake depth distributions have been a focus of research in the central study area of Northern Switzerland and the Central Swiss Alps (Deichmann 1992a and 1992b, Deichmann et al. 2000, Deichmann & Garcia Fernandez 1992, Deichmann & Rybach 1989). An important finding of these studies is the definition of a thick seismogenic layer which encompasses most if not all of the continental crust in the Northern Alpine Foreland (our zone Alps External zone) (Figure 2-9). Here earthquakes are well known to occur down to depths of about 30 km – but not a single event is documented from below the Moho. Within the Central Alps (our Alps Central zone), the seismogenic layer is significantly thinner; a large majority of earthquakes occur between 0 and 12 km depth, the deepest events reach 18 km below sea level (Deichmann et al. 2000, Fig. 8). Similarly detailed studies of the depth distribution of earthquakes for the rest of the PEGASOS project area remain scarce, however.

Reasonably good information about the depth distribution of small earthquakes outside of the Alps External and Alps Central zones is available locally in the Suabian Alb area (our small zone SG_1) of South Germany (Reinecker & Schneider 2002), for the Remiremont area (our small zone EF_1) of East France (Audin et al. 2002) and for the western part of the Internal Alps zone (our small zone AI_1 Dora Maira), where seismicity is documented down to depths of 20 km (Sue 1998). We have taken this additional information into account in our estimation of the depth distributions shown in Figure 2-8, for the different large zones, hosting these local 'hot spots'.

The reason for the difference between Northern Foreland and inner alpine earthquake depth distributions remains a matter of debate. The most obvious explanation for the lack of deep earthquakes below the Alps is temperature. The base of the seismogenic layer could be interpreted as an isotherm of say 350° C or so. Above this temperature, at depth below about 15 km, quartz-rich rocks such as granites start to deform in a plastic manner, thereby prohibiting the buildup of high differential stressses and the generation of earthquakes. Using this very same argument in the Northern Alpine Foreland poses a problem, however, since we would have to postulate quite a low temperature of less than about 350° C at Moho depth of 30 km. Such a temperature is difficult to reconcile with measurements of heatflow and geothermal gradients. (Both are measured within the topmost 3 km of the crust, and extrapolations down to Moho depths are not straightforward, however). Alternative explanations for the seismicity within the lower crust of northern Switzerland are the presence of fluids at high, i.e. near lithostatic pressure, and this is the favoured explanation of Deichmann and co-workers. Another possibility is the postulate of a quartz-poor lower crust – in a quartz-poor, feldspar dominated rock the brittle plastic transition could be as high as 500° C. Still, this very same crust must be present within the European lithosphere extending SE-ward down below the Alps, where it stops to be seismic – most likely because of an increased temperature within this young orogen and/or because it is bent downward to greater depth and into a higher temperature field. This situation is schematically drawn in Figure 2-9.
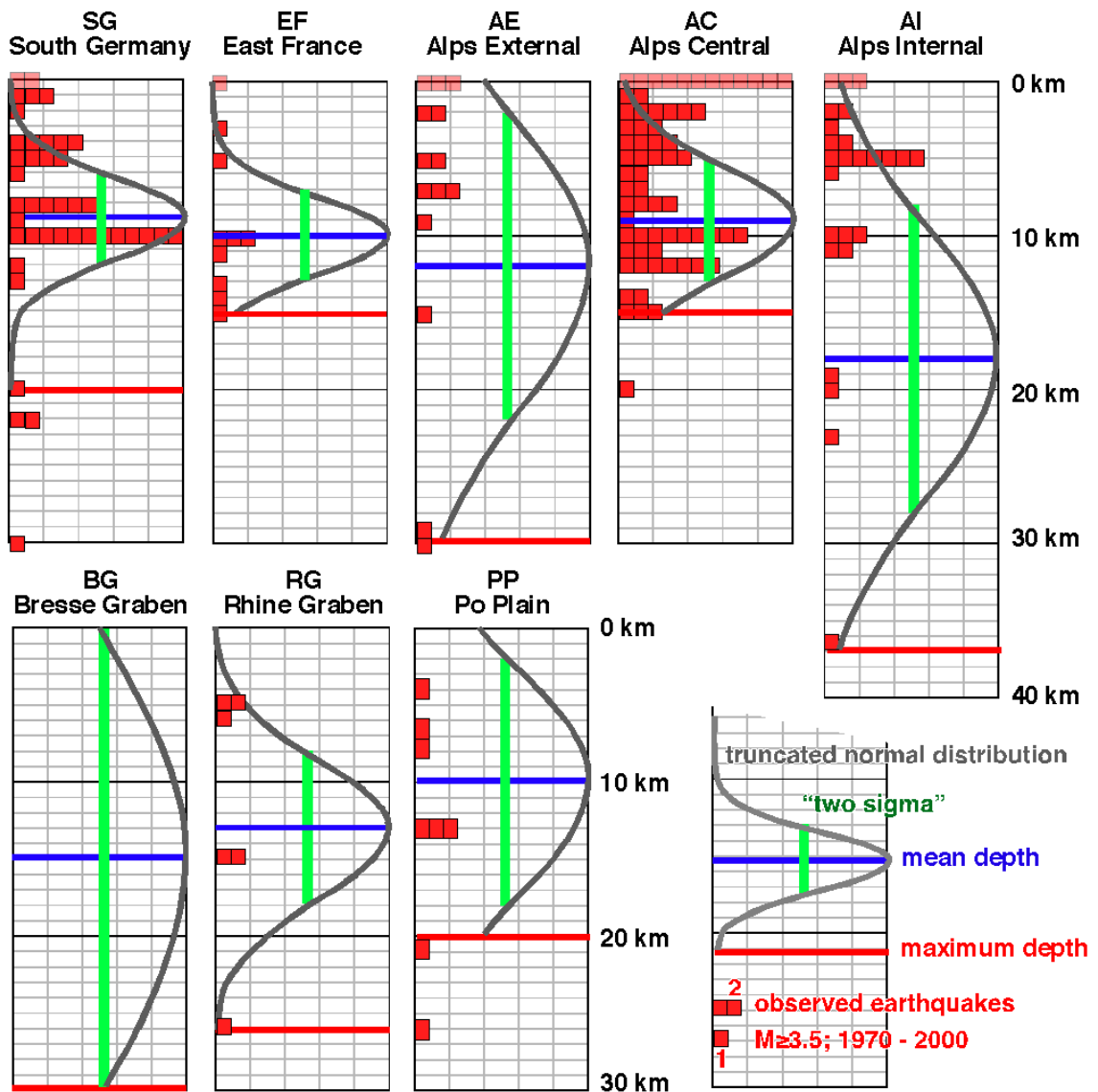
Fig. 2-8:   Depth distributions proposed for the different large zones

Histograms (red) illustrate the depths of observed earthquakes of Magnitude ≥ 3.5 between 1972 and 2000 as listed in the PEGASOS earthquake catalogue; data have been sampled on the screen in Wizmap → the diagrams are not rigorously correct because of overlap between earthquakes and involuntary omissions; zero depth earthquakes have definitely ill-defined depths and they have been shaded in lighter red. Estimated mean depths (horizontal blue line), 2σ standard deviations (vertical green bar) and a normal distribution (grey Bell curve) are schematically indicated for each zone. Truncations are applied at an estimated maximum depth (horizontal red line) as well as at the earth's surface.
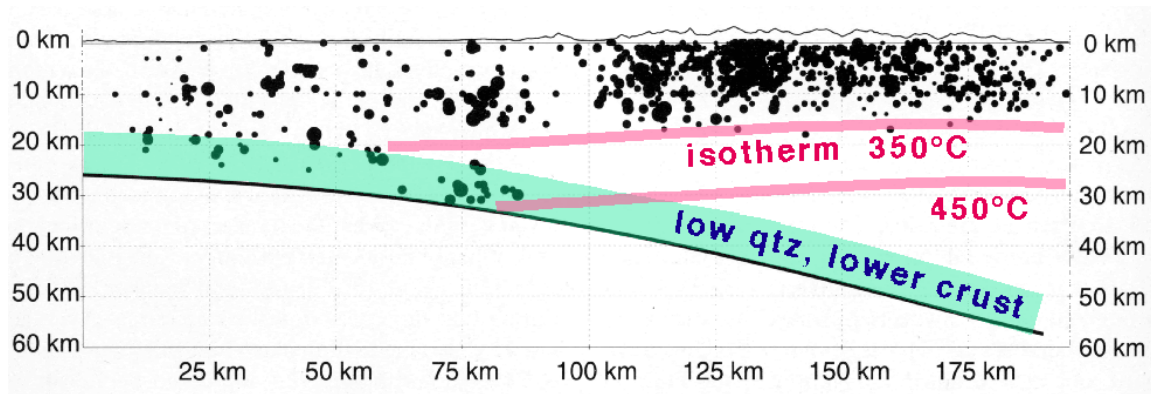
Fig. 2-9:   Depth distribution of well constrained small earthquakes of Switzerland, projected onto a N-S profile across the Alps (Deichmann et al. 2002)

We superimposed (colour) a tentative interpretation in terms of temperature and lithology. The 350° C isotherm is proposed as the base of the seismogenic layer for quartz-rich (granitic) upper crustal rocks, while a 450° C isotherm might correspond to the brittle ductile transition in quartz-poor (dioritic) rocks of the lower crust.

2.2.3   Rupture geometry

In a second stage (during implementation of our source parameters into the actual hazard calculation) additonal constraints about the rupture geometry and depth distribution of large earthquakes had to be provided for all source zones (Toro 2003, PEGASOS TP4-TN-0360).

Again, there are no direct observational constraints about these parameters and our choices are therefore necessarily intuitive. For fault dimension we adopt the relationship:

$$M = 4.07 + 0.98 * \log(RA),$$

where RA is rupture area in square kilometres (Wells & Coppersmith 1994). The associated standard deviation in $\log(RA)$ is 0.24. Small earthquakes are assumed to have equidimensional - square (same horizontal length and downdip width) rupture surfaces. In the case of large earthquakes, which require rupture areas larger than available for a square patch within the 'seismogenic crust' as defined in the preceeding chapter, additional rupture area is obtained by an increase of the fault's horizontal length. No fault is allowed to rupture outside of the zone boundary, however. Earthquakes are allowed to rupture to the earth's surface whenever the rupture area and hypocentral depth allows it to do so geometrically. Despite the fact that there is still not a single unambiguously identified earthquake surface rupture known anywhere in Switzerland (with the possible exception of the Reinach fault near Basel), we do not see any physical obstacle that could prevent a large earthquake from rupturing all the way to the earth's surface.

In terms of a magnitude dependent depth distribution of earthquakes our choice is a weighted approach with T = 0.5; in other words, we expect large earthquakes to have their hypocenters within the lower half of the rupture plane.

This choice too is based on theoretical considerations, rather than actual observations made within the study area. (Note that the entire PEGASOS catalogue contains only four earthquakes with a magnitude larger than 5 that have been recorded since 1972 and we have little confidence in depth determinations for older events). Our choice is inspired by the 'christmas trees' of

differential stress vs. depth curves for the lithosphere. Maximum strengths of the continental lithosphere are generally expected at depths between 10 and 20 km, depending on age and temperature as well as the assumed lithologic layering within the lithosphere (Jackson 2002, Lamb 2002). Our admittedly simple-minded interpretation of such strenght / depth curves leads us to expect large earthquakes to originate at greater depth, where large differential stresses are supported within the lithosphere, rather than within the uppermost portions of the continental crust; this is the main reason for our choice of T = 0.5, the lower 50 % of the rupture plane. Our model is in line with Scholz's synoptic crustal scale shear zone model (Scholz 1988) in Figure 2-10 and following an earlier analyses (Das & Scholz 1983). We are well aware of the fact that our reasoning is flawed; indeed even a very large earthquake could potentially be triggered by a near surface rupture which would subsequently propagate downward and side-ward through the entire seismogenic crust. A sensitivity analyses (Toro 2003, PEGASOS TP1-TN-0373) showed that the difference between a weighted and unweighted approach to the earthquake depth distribution is very small indeed.
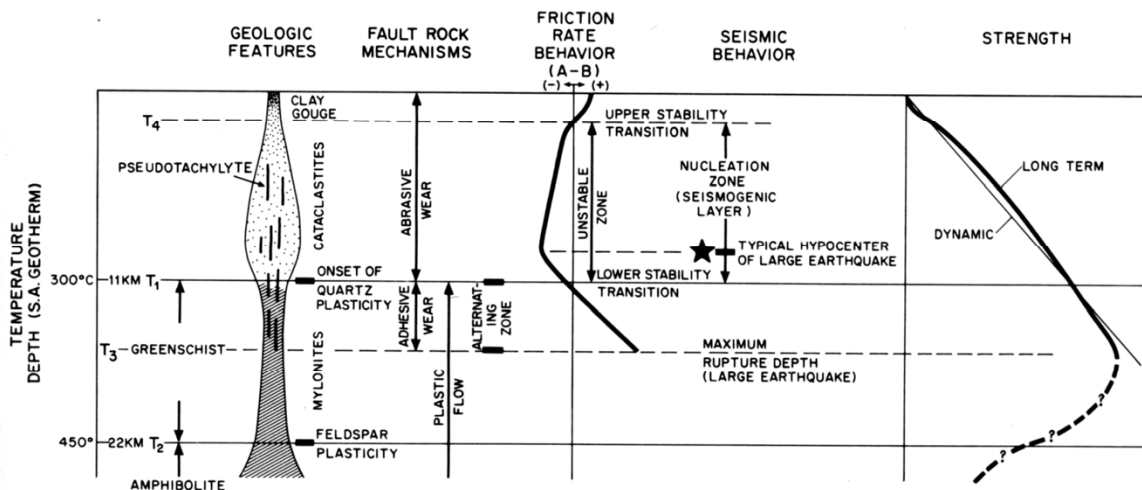
Fig. 2-10:   Scholz's (1988) crustal scale shear zone model

Note the expected 'typical hypocenter depth of large earthquake' is located at a temperature of slightly less than 300°C; just below the supposed onset of 'quartz plasticity'.

2.2.4   Summary

From all these considerations we designed 'default' fault orientations for the three possible types of faulting, likelihood of each faulting type and characteristic earthquake depth distributions for the large zones. Such default values will be modified or 'overridden' later on in the case of some small source zones, where additional information is available, particularly in zones with faults (this will be discussed in the appropriate chapters in more detail).

All this information has been summarized in a data table (PEGASOS EG1-HID-0033_EG1b, Table A-1 in Appendix 1) and we want this information to be applied as source-related input in the hazard calculation.

2.3 Small scale zonation ⇒ seismic source zones

A further subdivision of the larger zones is based mostly on information provided by the seismicity patterns. The main document used for the delimitation of small source-zones was the PEGASOS Earthquake catalogue (printout of all events, lain over the geologic base-map on a scale 1:800'000, PEGASOS EXT-TB-0043). Additional informations were our knowledge of the local geology, the suspected / known presence / absence of faults, more detailed information about the local seismicity and geology. The guiding philosophy in the delimitation of these source zones was to capture the maximum information provided by localized sources of seismicity on the one hand, to 'build fences around the wild dogs' on the other hand, wherever our limited knowledge of the local seismicity allows us to make some informed guess about the size of the 'dog-house'.

2.3.1 Labeling scheme

The large zones carry names such as Rhine Graben and their abbreviation in two capital letters (RG). For the small zones, we simply add a number to this large scale lettering.

We started numbering with one of the most prominent seismic sources within each larger zone and then continued numbering in a general clockwise sense (see Figure 2-11). In addition to this short label such as RG_01, we also named each small zone according to some geographic refer-ence, e.g. Basel. In the following, we provide an exhaustive list of all small source zones. Detailed descriptions and justification for our choices will be given in the case of the more seis-mically active or potentially active zones near the center of the study area. Many of the remote zones with little activity will receive very little coverage, however. Quantitative data for each source zone are provided as a data table (PEGASOS EG1-HID-0033_EG1b, see Table A-1).
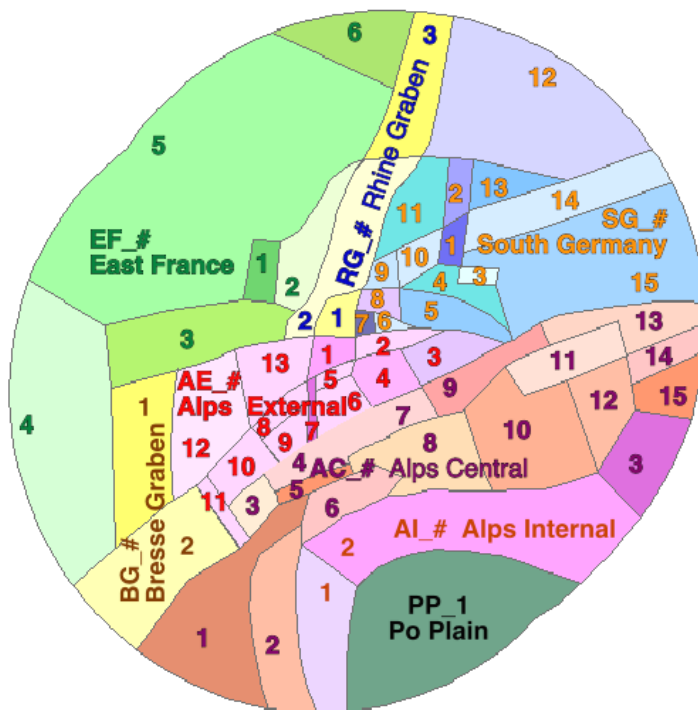
Fig. 2-11: Configuration of small source zones of EG1b

Labeling is according to large scale tectonic province (EF for East France, SG for South Germany, RG for Rhine Graben, etc.) complemented with a number.

2.3.2   Rhine Graben: RG_01 through RG_03

2.3.2.1   RG_01 Basel: with NNE-SSE strike-slip fault

The Basel zone lies in the south-eastern corner of the Rhine Graben, an area characterized by high seismic activity, both historical and instrumental (Figure 2-12). This zone hosts an epi-center of one of the large historical Basel events of 18.10.1356, M 6.2. The big Basel 1356 earthquake, however, is not located in this zone, but in AE_1 to the south, according to iso-seismals as determined from historical documents (Mayer-Rosa & Cadiot 1979).

Within this south-eastern part of the Rhine Graben, the total thickness of Tertiary sediments is not very important, it varies between 0 and 500 m (according to a compilation by Scandone (1990). An abrupt increase to more than 1500 m of Tertiary graben fill occurs along normal faults in the Mulhouse area. The trend of these buried normal faults has been chosen as rough limits of RG_01 to the north and to the west. The eastern and southern boundaries of SG_1 are 'natural' tectonic boundaries too. To the east, the Rhine Graben is limited against the Black Forest high, to the south, the Rhine Graben is interfering with the folded Jura. There is quite some uncertainty in the choice of the lateral limits of this zone to the east (SG_8, SG_7) and to the south (AE_1), however, where high seismic activity straddles our boundaries.

These uncertainties will be taken into account in the form of a probability tree, in which we sequentially remove some of these boundaries (between small zones) in order to regroup small adjacent zones into larger ones.

The RG_01 zone contains the northern part of the Reinach fault (highlighted yellow or black in Figures 2-12 and 2-13), a NNE-SSW striking geomorphic feature that has been proposed as the surface rupture of the 1356 Basel earthquake by Meghraoui et al. (2001). Their Fig. 2 (our Figure 2-13) shows isoseismals on top of a digital elevation model of the Basel area. In trenches dug across this fault scarp, Meghraoui et al. identified three slip events, constrained by C^{14} age dating. The total amount of slip accumulated over the last 8500 years is 1.8 m vertical displace-ment. Based on such paleo-seismic data, combined with the historical record of seismicity, they estimate a recurrence time of 1500 to 2500 years for a 1356-type earthquake (op. cit., p. 2073). They further use these data to extrapolate and constrain the occurence rate of earthquakes in the Basel region for the last 10'000 years.

There are a series of open questions, however, most of them have been adressed by S. Schmid (WS-3 Summary SP1, PEGASOS PMT-TN-0237, june 2002 talk):

−   the strike of this fault is not well oriented for a normal fault in the present day stress regime

−   tilted bedding in the hangingwall of the fault indicates a very shallow listric geometry at depth

−   other geomorphic features in the area have been proposed as candidates for the big Basel earthquake (Meyer et al. 1994).

The problem of fault orientation is illustrated in Figure 2-14. If we accept the paleo-stress orientations determined from earthquakes in northern Switzerland, such as presented by Kastrup (2002), the Reinach fault is ill oriented for any type of faulting, even if we allow for substantial uncertainty in the orientations of the principal stresses and/or permutations of principal stress axes orientations. In the prevailing field of strike slip / normal faulting, with a NE-SW oriented extension direction, the Reinach fault is very unlikely to act as a normal fault, but even reactiva-tion in sinistral strike slip seems almost impossible.

Given this orientation problem, one could argue that the paleo-stresses determined from 20 years of earthquake data are not representative for the regional stresses. Alternative in situ stress

orientations are available for the larger Basel area (Becker 2000). Near Basel, however, in situ stress measurements show quite some scatter in the orientation of the measured 'maxium horizontal stress σ_1', with three sites of quality B (no quality A data are available), indicating N-S, NNW-SSE and WNW-ESE orientation respectively (op. cit., Fig. 6). This rather ill-defined orientation of maximum horizontal compression could be taken as an indication for a pure extensional regime with vertical σ_1 and an ill defined extension direction, i.e. similar magnitudes for σ_3 and σ_2.

Additional problems arise from the new Magnitude of 6.9 attributed to the 1356 event (and an older 250 a earthquake 'Augusta Raurica') in the PEGASOS catalogue, while both Meghraoui et al. (2001) and Becker et al. (2002) used a Magnitude of 6 to 6.5. Taken at face value, the paleo-seismic data of Meghraoui et al. (2001, Fig. 5) or Becker et al. (2002, Fig. 3) plot below the actually observed historical activity plot for the Basel region such as given by the PEGASOS catalogue (Figure 2-15).

Faced with this dilemma – in estimating a and b as well as Rmax for the RG_1, Basel zone, we conclude that the trenched Reinach fault does not provide any useful additional constraints for these parameters.

The alternative view, presented by Meghraoui et al. (2001) was to extrapolate a downward trend of the activity curve, fitting the observed paleo-seismic data. Even if the observed fault was along the surface rupture of the 1356 Basel earthquake this approach is questionable, however since it assumes that:

1. the fault was trenched in its central portion

2. the observed slip is close to to the maximum co-seismic slip

3. this is the only active fault in the Basel area

4. the trenches provide a complete earthquake record for Basel for the last 8500 years.

Given these doubts, the paleo-seismic record of the Reinach fault provides at best a lower, but hardly an upper limit to the Basel activity curve as shown in Figure 2-13.

New paleoseismic data presented by Becker et al. (2002) are based on disturbed lake sediments collected in two small lakes near Basel as well as landslides and other geomorphic features (compare Paleoseis report to HSK and Nagra of 31.12.2001). Becker et al. (2002) conclude that " *... earthquakes with size comparable to the AD 1365 Basle earthquake have occured several times within the last 12'000 yr and that the recurrence time for such strong earthquakes are in the range of 1500-3000 yr.*" They do not provide any additional data or opinion about the still open question of the active fault responsible for these earthquakes.

Alternative views (to the Reinach fault as responsible for the Basel earthquake) have been published by Meyer et al. (1994) and Niviere & Winter (2000). Both argue in favour of a thrust mechanism, in relation with ongoing Jura or rather Alpine shortening in a (N)NW-(S)SE direction, possibly by reactivation of older, Permo-Carboniferous and or Oligocene faults within the basement. These interpretations will be discussed in more detail in section 2.3.5.
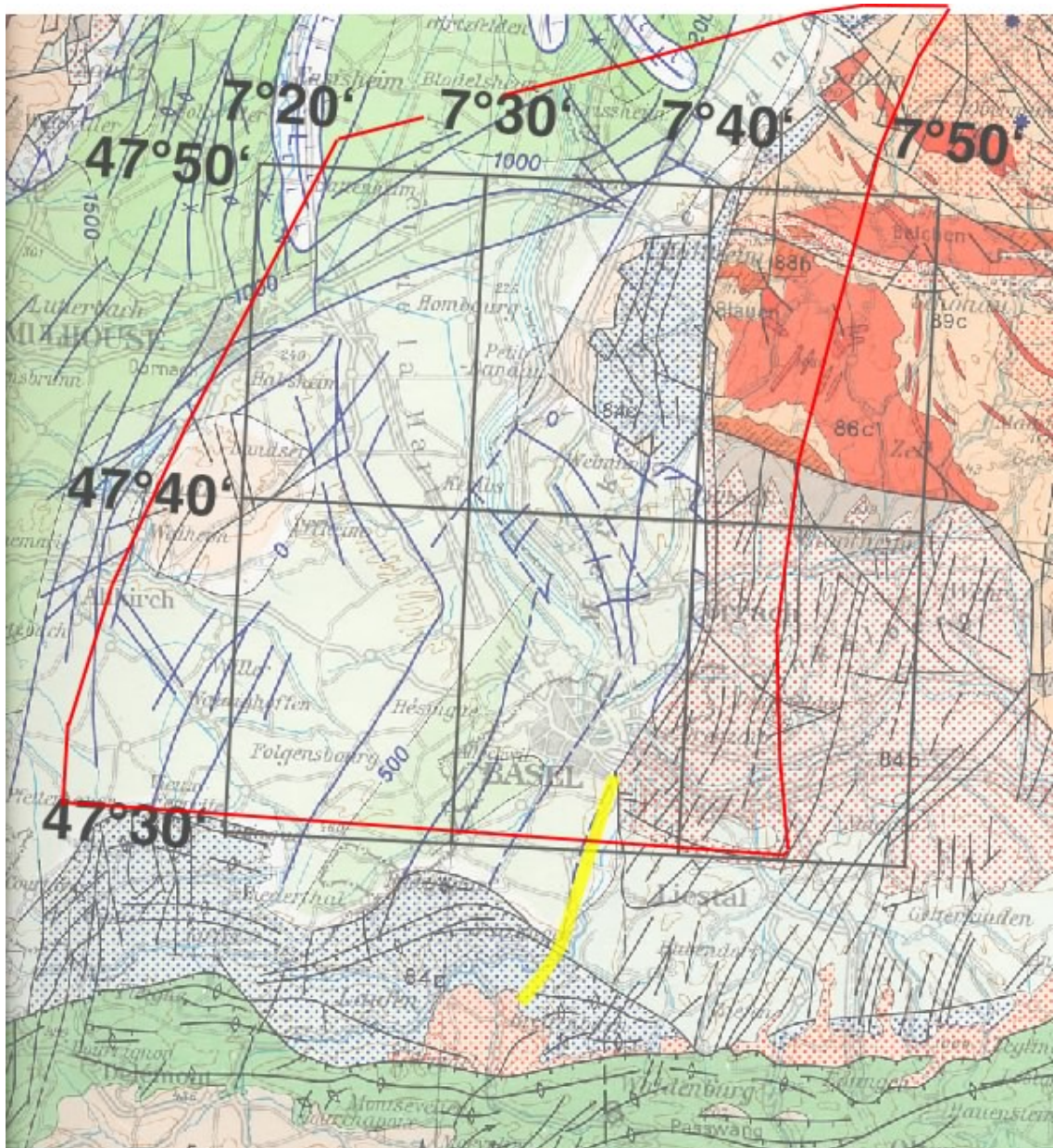
Fig. 2-12:   Zone boundaries of the Basel source zone RG_01 are superimposed onto a tectonic
              map (Structural Model of Italy (Scandone 1990)

              Shades of green within the Rhine Graben reflect the total thickness of the Tertiary
              graben fill. Known, mapped faults are indicated in blue. The Reinach fault is high-
              lighted in yellow.
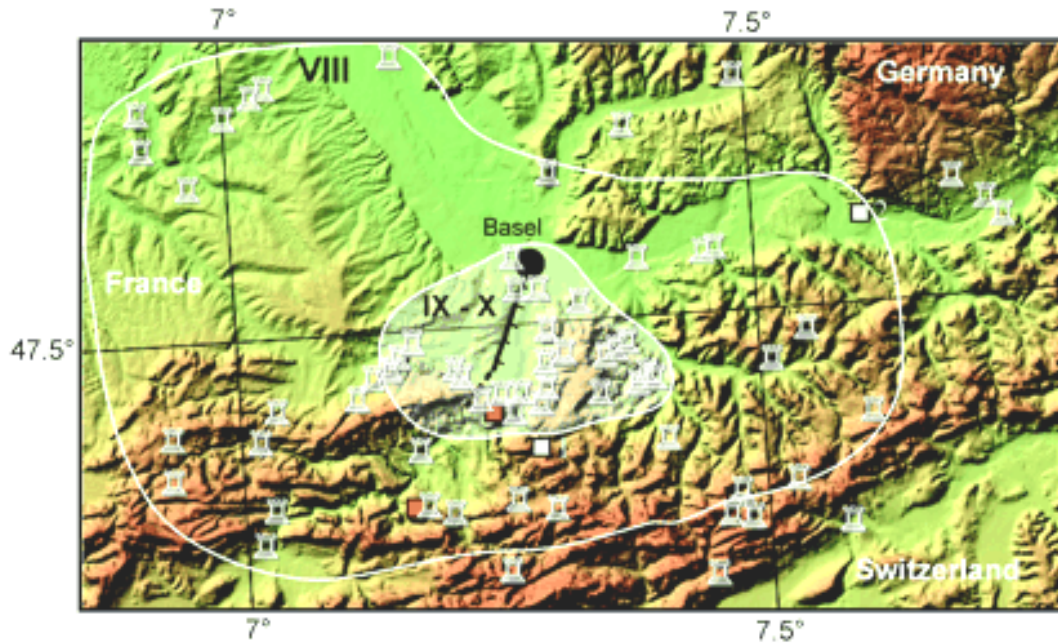
Fig. 2-13:   Isoseistes of the Basel 1356 Earthquake, superimposed onto a Digital Elevation Model of the larger Basel area

The surface expression of the Reinach fault is indicated with black line south of Basel. Non-modified from Meghraoui et al. (2001, Fig. 2).
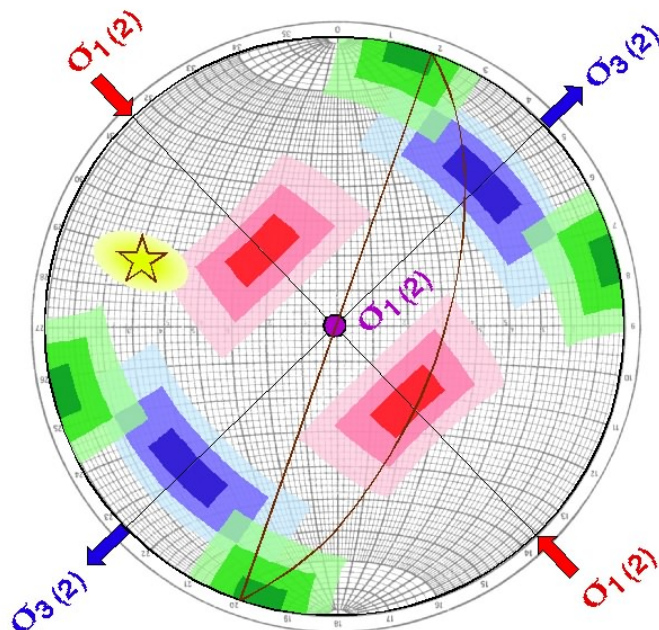
Fig. 2-14:   'Back of the envelope' evaluation of the relationships between present day stress orientation (σ_1 orientation from Kastrup 2002, her stress tensor F3 for northern Switzerland) and pre-existing faults in the Basel area.

The Reinach fault (in brown, great circle trace and its pole, star highlighted in yellow) is not in an orientation for reactivation in any type of faulting!
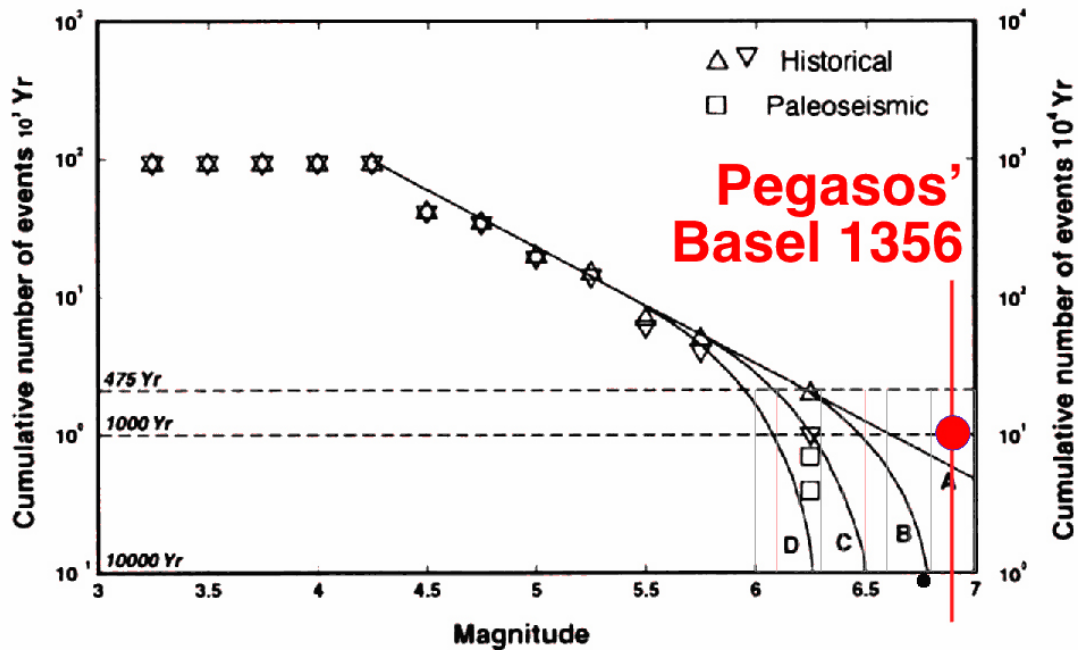
Fig. 2-15:   Activity plots of for the Basel Area

We superimposed the Basel 1356 earthquake, with a magnitude of M = 6.9 according to the PEGASOS catalogue onto the analysis of Becker et al. (2002, in black, Fig. 3). The exact position on the vertical axis of the Basel earthquake, determined from the PEGASOS catalogue, is dependant on the 'filters' (completeness and declustering, etc.) applied to this catalogue, which, in its raw form features two events of M 6.9 near Basel at A.D. 250 and 1356.

2.3.2.2   RG_02 South Rhine Graben vs. RG_03 North Rhine Graben

We have chosen to cut the Rhine Graben into a southern and a northern part (Brun et al. 1991, Wenzel et al. 1991). Such a subdivision is justified on geologic and seismologic grounds. Geologically, the southern and northern parts of the Rhine Graben have markedly different geo-histories (Brun et al. 1992), or subsidence curves. Subsidence in the northern half of the Rhine Graben follows a straight regular trend since more than 40 Ma, the maximum thickness of Tertiary graben fill is over 3 km thick. In the southern Rhine Graben, subsidence is irregular in space and time, maximum thickness of Tertiary is less than 2 km. The southern Rhine Graben hosts the young, i.e. Late Miocene Kaiserstuhl Volcano and is bordered by two important base-ment highs, 'rift shoulders' in the form of the Vosges and Black forest massifs. Seismically, the southern part of the Rhine Graben seems to be more active than the northern one.

The present day stress regime in the Rhine Graben is documented by Plenefisch & Bonjer (1997), who analyzed a total of some 97 earthquake focal plane mechanisms. At least the upper part of the crust seems to be deforming in strike slip mode with a tendency for extension. The most stable stress orientation is found to be σ_3, oriented in a WSW-ENE to SW-NE direction. A slight, counterclockwise rotation in this orientation is observed from south to north.

2.3.3   South Germany: SG_01 through SG_15

We tried to delineate our zonation for south Germany independently from earlier ones, e.g. those by Grünthal et al. (1998a) for the D-A-CH study. But the well established obvious seismo-tectonic constraints lead consequently to a seismic source zone model which resembles the earlier proposed ones. These first order seismotectonic elements are e.g. the Upper Rhine

Graben, the Swabian (Schwäbische) Alb or the Altmühl Valley seismicity cluster. The source zone model uses the seismotectonic schemes by Schneider (c.f. presentation by Grünthal at the WS 2/SP1), the ERS-1 mosaic of radar data sets (Wetzel & Frantzke 2001) in combination with seismicity plots and fault plane solutions as well as general geologic maps (as in the PEGASOS database).

2.3.3.1   SG_01 Schwäbische Alb: single N-S fault within zone

The Schwäbische Alb zone is a well confined small area with considerable seismic activity (Haessler et al. 1980, Reinecker & Schneider 2002, Schneider 1973, Schneider 1979, Turnovsky & Schneider 1982). It contains one large historical event of M = 5.8 (29.03.1655). Limits to this zone were chosen in order to capture this seismic activity. According to Reinecker & Schneider (2002), this seismic activity is mostly along a N-S striking fault or fault zone within within the Hercynian basement. For simplicity, we assume the seismic activity of zone SG_01 as stemming from a single N-S oriented strike slip fault, running in the middle of the zone. Such faults are numerous within southern Germany and the question arises if any or all of these faults have the same chance of being seismically active – albeit at different times. Although we give this view some thought (large zonation, spatial smoothing of seismicity), we prefer an alternative view, in which seismicity is locally constrained, e.g. at the intersection of different fault lines, notably the intersection of SG_01 and SG_14, a 'conjugate' ENE-WSW running lineament which seems to host some increased seismic activity as well.

2.3.3.2   SG_02 Stuttgart: single N-S fault within zone

We consider this zone as a northern extension of the SG_01, alinged along a set of N-S striking basement fractures. Historically, seismic activity seems to have jumped southward, being confined to SG_01 at present. Just as its neighbour to the south, seismicity within this zone is considered to stem from one single fault running in its middle.

2.3.3.3   SG_03 Saulgau

Another small 'hot spot' of seismic activity is found in the Saulgau, apparently disconnected from the former two zones SG_1 and SG_2. We surrounded this zone with 'fences' which have similar strike as SG_1, assuming the same two fault orientations are present in this area. EW oriented structural elements constrain the elongation of this zone.

2.3.3.4   SG_04 Linzgau

This is a small 'left-over' zone with very little seismicity. In terms of crustal structure it is comparable to the larger zone SG_15 (Bavaria) to the east – see below for some description. Southward, the Linzgau zone SG_04 is limited against the more active Singen-Bodensee zone along a gently curved WNW-ESE line, running just north of Lake Konstanz (Bodensee). This line follows a well know structural trend know from the Schwarzwald, Swabian Alb and Lake Konstanz itself is probably (glacially) excavated along such a 'zone of weakness'.

2.3.3.5   SG_05 Singen – Bodensee

Tectonically, this zone lies clearly outside of the Alpine front but it shows an increased seismic activity with respect to its northern neighbours (SG_4 and SG_15). Seismicity plots including historical events indicate a WNW-ESE striking trend apparently along Lake Konstanz. Some geologists have suspected the presence of faults below this lake but no major feature has been mapped so far. Lake Konstance (Bodensee) and the Singen – Bodensee zone have the orientation of a familiy of faults which is well known also from subsurface seismic data of the Bavarian Molasse basin, however (Brink et al. 1992), see Figure 2-16. It seems likely that the

Rhine river and Rhine glacier followed such a fault line or family of faults to erode and overdeepen the Lake Konstanz basin. In the present day stress field, such faults are reactivated in dextral strike slip as confirmed by fault plane solutions (Kastrup 2002).
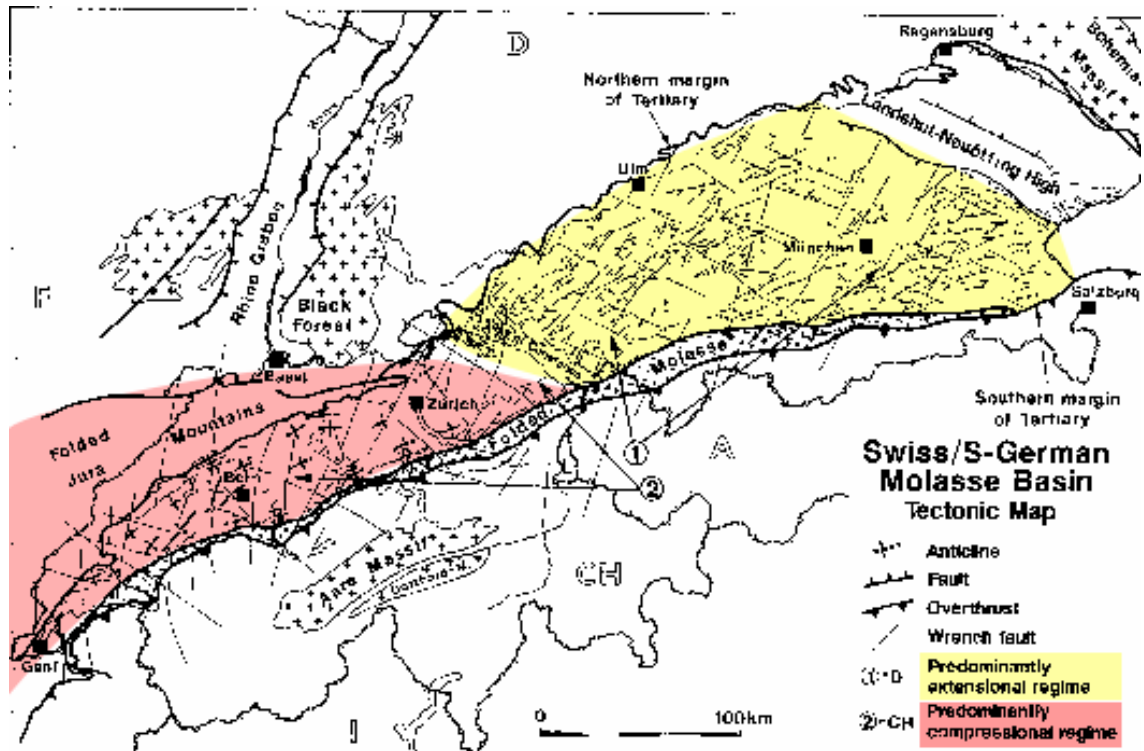
Fig. 2-16:   Contrasting structural styles in the Northern Alpine Foreland basin – Molasse trough

Subsurface information, gained from petroleum industry seismic reflection profiles are compiled into a tectonic overview map, indication major faults and folds (according to Brink et al. 1992).

2.3.3.6   SG_06 Leibstadt

A small zone representing a somewhat smaller seismicity than the surroundings. This zone is the resulting 'rest' due to the definition of the surrounding source zones.

It will be removed, however in some branches of our logic tree dealing with the 'Tucan beak'.

2.3.3.7   SG_07 Dinkelberg

This is the eastern neighbour of our Basel RG_1 zone. The limits between the two are motivated by a geologic argument: the Dinkelberg-'Scholle' represents a block which is intermediate in height between the Rhine Graben to the west and the Black Forest 'horst' to the north and to the east. Southward, the Dinkelberg dips gently below the Tabular Jura and Molasse basin but it remains clearly outside of any visible trace of alpine compression. The seismicity of this area is discussed by Faber et al. (1994).

2.3.3.8   SG_08 S Schwarzwald

2.3.3.9   SG_09 W Schwarzwald

2.3.3.10   SG_10 Rottweil

2.3.3.11   SG_11 N Schwarzwald

The four zones SG_08 through SG_11 are located within the basement high of the Black forest 'massif' – Schwarzwald in german. This area is well known by the geologists because it allows access to the Late Variscan basement – wich is a complex assemblage of terranes with different metamorphic histories, and with granitic intrusions during in Carboniferous / Permian times. The present day elevated position is due to Late Oligocene – Miocene extension, which lead to the formation of the Rhine Graben and associated Rift shoulders in the form of the Vosges and Black Forest massifs. Our internal subdivision of the larger Black forest area into four indivi-dual small zones is based on a visual inspection of seimicity patterns. Zones SG_08 and SG_09 have apparently higher activity than the adjacent SG_10 and SG_11. Limits between these zones have then been drawn along well known structural trends (compare Figure 2-5, Wetzel & Frantzke 2001).

2.3.3.12   SG_12 Würzburg

This is a large 'background' zone in the northeastern corner of our larger South Germany zone which is characterized by a very low seismic activity. The limit to the west is naturally defined by the Rhine Graben. Towards the SSE, the limit is defined by an apparent increase in seismicity.

2.3.3.13   SG_13 'Dreieck'

This small zone located between Stuttgart to the west and Aalen to the east, has been called 'Dreieck' (= triangle) for lack of an obvious geographic feature. The characterization in terms of geology or seismicity is defined by its neighbours – it can be regarded as a 'left-over' zone. There seems to be more seismic activity within this triangular zone SG_13 than within its northeastern neighbour SG_12. However, we did not want to incorporate this seismicity with the south-eastern zone SG_14 either, because the latter seems to be associated with a vague tectonic lineament. To the west the triangle is limited in a more straightforward manner against the N-S oriented fault-bound zone SG_2.

2.3.3.14   SG_14 Fränkische Alb

The Frankian Alb zone SG_14 is chosen along a geologic trend, roughly followed by the Danube river and the limit between the gently SSE dipping Mesozoic limestones to the north and the flatlying Molasse series to the south. This geologic trend is confirmed by a series of ENE-WSW structural elements after Franzke & Wetzel (2001) and was repeatedly described as a zone of 'bookshelf tectonics' (Schneider 1968, 1972, 1973 and 1993). A vast zone of (slightly) increased seismicity seems to run in a WSW-ENE direction all along from the northern end of the Bresse Graben across the southern end of the Rhine Graben, then towards the ENE crossing the southern tip of the central Schwarzwald block and the Swabian Alb seismic zone. The eastern part of this lineament in the Frankian Jura represents our zone SG_14. SG_14 has some seismic activity which is apparently higher than the almost aseismic SG_15 München zone to the south and the fairly aseismic SG_12 Würzburg zone to the north. Westward, the Frankian Alb zone is limited against the earthquake cluster of the much more active fault zone SG_1; the location of the latter at the intersection of a vague WSE-ENE and a better defined N-S lineament may not be fortuitous (Schneider 1993).

2.3.3.15   SG_15 München

A large portion of the Bavarian Molasse basin seems to be seismically quite quiet. This is in contrasts with the the Swiss Molasse basin which seems to have a higher seismic activity. The transition between the two areas within the same tectonic unit, the Alpine foredeep, better known as the 'Molasse basin', may be due to the above mentioned position of the most external alpine thrust front. The Bavarian Molasse basin has been involved in downwarping of the European lithosphere below the Alps, it has seen some extension in the Oligocene. Normal faults from this period are well known from Petroleum exploration since they form structural traps (Bachmann et al. 1982, Bachmann & Müller 1992, Bachmann et al. 1987). They have not been inverted to any seizable degree, a strong argument in favour of this region to ly outside of the Alpine thrust regime (be it thin- or thick-skinned).

2.3.4   East France: EF_01 through EF_06

East France hosts two seismic 'hotspots' near Remiremont and in the Lorraine. Only the former (RG_01) is considered as an individual source zone, however, since the latter is mostly induced by mining activity. The remaining subdivisions are roughly following geologic provinces, such as the Massif Central or the Dijon – Saône area, representing the Northern Foreland to the Folded Jura. An overview of the seismicity of France is found in Grellet et al. (1993).

2.3.4.1   EF_1 Remiremont with a N-S trending Fault (?)

The Remiremont area in the Vosges is well known for its seismicity, which shows up clearly on seismicity maps. The shape of the chosen Remiremont zone EF_1 reflects a North-South alignment of seismicity as revealed by instrumental as well as historical earthquakes (Audin et al. 2002). This zone hosts the significant historical Remiremont earthquake of 12 mai 1682, with an MSK intensity of VIII, translated to a M = 6.0 in the PEGASOS catalogue. At present, there seem to be two distinct areas of increased seismic activity, located in the northern and southern half of the zone, near Epinal and Remirement respectively. The alingnment of seismicity suggests the presence of a fault or fault zones at depth. There is no clear correspondence with any mapped surface faults, however. The NNE-SSW trend of seismicity (in the southern part of the zone) would suggest a Rhenish trend. Surface faults as seen on a geologic map (BRGM 1989) on the other hand strike either NE-SW or NW-SE.

On 22nd februrary 2003, 20:41, a significant earthquake of Magnitude ML/Ms = 5.8 took place at Lat. / Lon. 48.350 / 6.800 (EMS) in the Vosges area; (according to SED, Zürich ETH). This earthquake plots onto the northern border of our Remirement zone, outside of the map shown in Figure 2-17. What should we conclude from this localisation? First of all, this most recent earthquake happened close to a well known 'hotspot' of seismic activity, the Remirement area. However, this earthquake did not occur along any recognized fault line, be it a geomorphically or micro-seismically defined lineament. Future studies may probably reveal the culprit fault(s), but what is important here and now: we (geologists and seismologists) did not exactly anticipate an earthquake to take place where it did! Our zone boundary around the Remiremont seismicity was choosen just about large enough to still include this latest earthquake. Statistically speaking, however, we anticipated this event in the middle of the zone, along the 'Remirement lineament', leaving a very small probability to a 'Remiremont' type earthquake to happen on the very zone boundary.
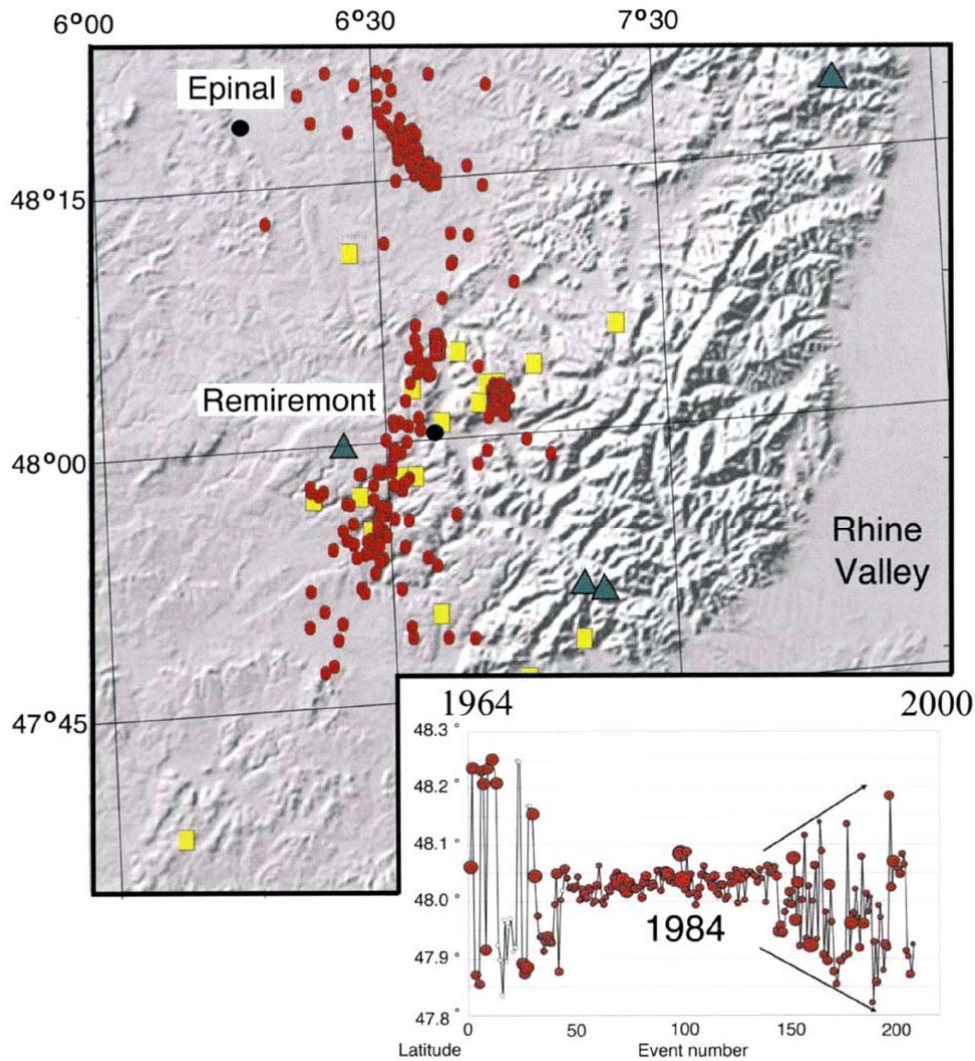
Fig. 2-17:   Seismic activity in the Remiremont area, southwestern Vosges

Historical events are shown in yellow whereas red dots represent selected instrumental events since 1964 which have been used by Audin et al. (2002, GRL 29/6, 15th of March, cover) for relocalisation and a study of the spatial and chronological evolution of seismicity.

2.3.4.2   EF_2 Vosges

The Vosges zone EF_2 is defined geologically, as the western shoulder of the southern Rhine Graben. This zone includes faulted blocks along the eastern border of the Rhine Graben as well as the highest basement culmination of the Vosges massif. Seismicity within this zone is somewhat heterogeneous; from a visual inspection of the PEGASOS data, seismicity seems to be concentrated within the southern part of this zone, we nevertheless included a northern 'tip' of block faulted terrains based on the argument of a very similar stucture and estimated likelihood of re-activation.

2.3.4.3   EF_3 Dijon – Saône

The Dijon – Saône zone EF_3 in the Northern Foreland, immediately adjacent to the Jura Fold and Thrust Belt, is separated from its neighbours for two reasons:

1. This E-W corridor corresponds to the 'left lateral transform' necessary to accomodate strains between the Rhine and Bresse Graben (Bergerat 1987).

2. Seismicity within this zone seems to be more important than in the adjacent Lorraine to the NW, the Massif Central to the West or the Bresse graben to the South.

Seismicity is clearly less important and less confined than in the Remiremont zone to the NE. The southern limit, toward the Jura Fold Thrust belt is motivated by a geologic argument, Dijon-Saône lies clearly outside of the alpine thin skinned thrust belt. The entire zone is strongly faulted, however. At least two sets of 'Oligocene' faults are present, a dominant rhenish trend with NNE-SSW strike as well as an 'Alpine' or 'Jura' trend of roughly ENE-WSW strike. Both fault families are 'thick skinned', basement rooted strike slip faults. In the present day stress field these two fault families do not define a conjugate set, however! The Rhenish faults are likely to be reactivated in sinistral strike slip, whereas the Jura trend faults could potentially be re-activated in thrusting mode.

2.3.4.4   EF_4 Massif Central

The Massif Central can be regarded as the Western shoulder of the Oligocene Bresse graben. It is characterized by some topographic relief, recent Volcanism and some seismic activity.

2.3.4.5   EF_5 Lorraine

The Lorraine EF_5 zone represents a large zone, far from the centre of the study area and can be regarded more as a left over 'back ground' zone rather than as a seismic source zone with particular seismic activity. The Lorraine zone hosts an apparent hot spot of seismic activity which is induced by mining activity. We chose not to consider this seismicity as an individual source zone but rather to have this activity diluted over the entire Lorraine zone.

2.3.4.6   EF_6 Rheingau

Some increased seismic activity is observed near the Northwestern border region to the Rhine Graben. We consider this activity as related to complex tectonic situation in this area, where the Rhine Graben abuts the 'Rheinische Schiefergebirge'. Similar to the situation at the southern termination of the Rhine Graben – Bresse Graben transform zone, some accomodation zone, right lateral in this case, had or has to exist between the northern Rhine Graben and the Rhenisch Bight in Holland. Paleomagetic measurements document some block movement post-dating the Late Oligocene (Schreiber & Rotsch 1998).

2.3.5   Bresse Graben: BG_01 through BG_06

In contrast to the age equivalent Rhine Graben structure further to the northeast, the Bresse Graben is seismically rather quiet. The Graben structure is defined mostly morphologically as lowland surrounded by the Jura Montains to the East, by the Burgundy platform (carbonates) to the North and the Massif Central to the West. From drill holes, industry seismic lines and an ECORS line, the depth and internal structure of the Tertiary graben fill is quite well known, it reaches up to 3 km (Bergerat et al. 1990).

The orientation of the present day 'european' stress field is orientated nearly orthogonal with respect to the N-S orientation of the graben structure. Fault plane solutions are scarce, however, and there is no indication for ongoing normal faulting despite the accumulation of quite young (Pleistocene) sediments within this graben.

2.3.5.1   BG_1 Bresse Graben

This zone is choosen roughly along the trend of the northern Bresse graben structure. It is caracterized through the absence of seismicity! Towards the East, we have not included 'boundary faults'. The graben bounding normal faults are hidden below the overriding Jura fold and thrust belt. The seismicity observed within the most external Jura has been included in the western Jura zone, treated as belonging to the Alpine realm. We recognize the possibility that some of this seismic activity along the western boundary of AE_12 Western Jura zone could be due to normal faults bounding the Bresse Graben, rather than being connected with the alpine thrust system. Given the large distance to the central study area, the weak seismicity and the scarcity of fault plane solutions, we regard this simplification as justified.

2.3.5.2   BG_2 S Bresse Graben

This zone straddles three geologic domains, namely the External Jura, the Bresse Graben and the Massif Central. The limits have not been chosen by any geologic arguments but purely for 'topologic reasons'. The southern Bresse Graben cleary has a higher seismic activity than its northern neighbour $\Rightarrow$ this is how we chose to cut the Northern Bresse Graben into two parts. West of the Vuache fault, some seismic activity is present within the Southwesternmost Jura. Following our tectonic reasoning, this part of the Jura should belong to the Alps external zone. However, given the far distance with respect to the center of the study zone, we feel authorized to neglect such subtleties and regroup two small areas, namely the southern Bresse Graben and the southwesternmost folded Jura into one single zone which an apparently homogeneous seismic activity.

2.3.6   Alps External: AE_01 through AE_13

2.3.6.1   AE_1 Basel Jura: with E-W thrust faults

This zone hosts the historical main Basel 1356 event of M 6.9. The larger Basel area is charcterized by a hot spot of seismic activity. This seismicity straddles the limit between the Rhine Graben to the north and the Jura fold-thrust-belt to the south. Focal plane solutions indicate mostly strike slip faulting with a tendency for extensional deformation with a SW-NE oriented minimum horizontal stress σ_3 (Kastrup 2002). With regard to the Basel 1356 event, at least two alternative interpretations have been proposed, however. Meghraoui et al. (2001) 'identified' the Reinach Fault as an 'active normal fault' responsible for the Basel 1356 earthquake. Meyer et al. (1994) on the other hand, propose this major historical earthquake to be related to thrusting along a basement fault with an E-W orientation, mainly based on the elliptical shape of isoseismals. These authors furthermore identified several geomorphic features in the northernmost folded Jura apparently indicating recent inversion of talwegs, interpreted again, as due to active folding and thrusting along deep-seated N-vergent E-W-striking thrust faults (see Figure 2-18). Although the site itself does not lie in our AE_1 zone but in its western neighbour AE_13, we prefer to mention it here, since it has a direct relationship to the Basel earthquake – which is unlikely to have occured in AE_13 if we believe in isoseismals constructed from historically documented damage reports (Mayer-Rosa & Cadiot 1979).

Similar findings of recent thrusting and folding have been presented by S. Schmid at the PEGASOS WS-2 (PEGASOS PMT-TN-0135) for post 3 Ma old Sundgau gravels, apparently folded into a series of anticlines in the northernmost Basel Jura and southernmost Rhine Graben.

Both cases (dry valleys and folded Sundgau substratum) are questionable, however, since neither structure involves unequivocally the folding of a dated / datable marker horizon. In the case of the dry valleys, the folded talwegs find an easy non-tectonic explanation as karst features: an alignment of enlarged sink holes and other closed depressions along a former talweg, with a underground drainage through caves – the real 'Talweg' being located underground in a karst-system. The Sundgau Schotter itself, might still be perfectly flatlying, but onlapping onto a pre-existing fold-morphology which was not completely levelled prior to the deposition of these gravels. The Sundgau gravel case has at least the potential of being verified in the future, using high-resolution reflection seismics and/or geo-radar to prove or disprove the postulated folding of internal bedding of these young strata.

Additional evidence for a recent, i.e. younger than ca. 3 Ma, northward propagation of thrusting deformation up to Mulhouse! (in thin skinned mode) has also been presented by Niviere & Winter (2000) based mostly on a geomorphic analysis of river terraces and additional constraints from seismic reflection profiles. They propose a complex Istein – Allschwil – Rhine Valley fault system (inverse, thick skinned, but essentially a blind thrust) as culprit for the 1356 Basel earthquake.

In summary, the source of the 1356 Basel earthquake remains wide open to discussion!

−   From the present day stress regime and fault plane solutions, one would expect it to be along a Rhenish, NNE-SSW oriented steep fault or faults reactivated in sinistral strike slip.

−   From paleo-seismic evidence dug out near Reinach, it could be a Rhenish, NNE-SSE oriented normal fault with the east side dropping down.

−   From geomorphologic studies it might be an E-W oriented steep reverse fault, possibly reactivating a former Permo-Carboniferous graben boundary fault.

We address all of these three possibilities in two ways:

−   On the one hand we assign default values for fault orientations and the estimated percentage of earthquakes taking place in thrust, normal and strike slip mode. (Numbers are given in our data table PEGASOS EG1-HID-0033_EG1b, see Table A-1). Such values have been estimated for each zone.

−   On the other hand, various regroupings of small zones around Basel are treated as separate branches in a logic tree, (see below, at the end of this chapter). Merging zones AE_1 and RG_1 for instance provides a larger N-S extension for a potential Reinach fault, whith earthquake data collected from the same merged zones. Alternatively, merging AE_1, AE_2 and AE_15 – in various combinations – allows to host a considerable potential thrust fault with a E-W extension of well over 100 km length. Various such alternative conceptual models are considered in the form of a logic tree, where the relative credibility of these models is expressed as the weights on the different branches.

Note that as a proponent of thin skinned Jura tectonics one of the team members (M. Burkhard) would give the thrusting – thick skinned scenario a zero weight. As a representative of the larger structural geologist's community, however, he estimates that the current thinking at this time is rather in favour of an ongoing compressional thick skinned thrusting tectonic interpretation of the Jura in general and the Basel region in particular. Taking a vote in the Swiss community would probably give something like a 50 : 50 result (thin vs. thick skin). Our compromise in this situation: the thrusting scenario is given an intermediate weight of up to 0.3 (compare Table 2-1). This weight seems outrageously high to the thin skinned proponents, but much too small to adepts of the thick skinned school.
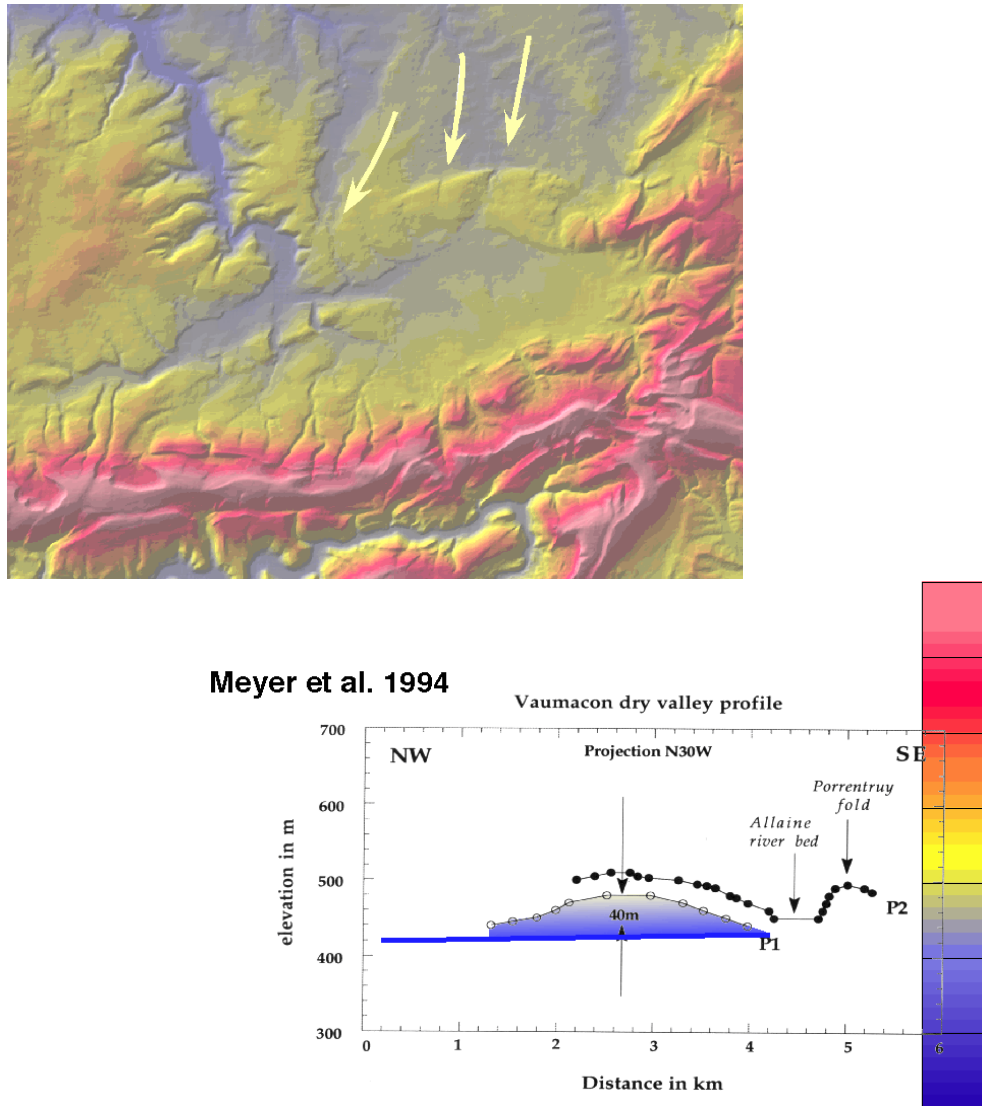
Fig. 2-18:   Digital Elevation Model of the northernmost Jura Anticlines northeast of Porrentruy

Dry river valleys indicate 'reverse' slopes, interpreted as due to active folding and blind thrusting underneath. Note that this site is not located within our Basel Jura zone AE-1, but in its western neighbour AE_13. Digital elevation model above has been produced with Atlas CH CD-Rom, altitudes are colour-coded according to legend given below. An anomalous 'hump' in a Talweg has been interpreted as a recent fold by Meyer et al. (1994) and is used as evidence for thick skinned ongoing thrusting along the northern border of the Jura.

2.3.6.2   AE_2 East Jura: with E-W thrust faults

The northern and southern limits of the Eastern Jura zone AE_2 are motivated by geologic arguments. The northern limit is chosen to include the northernmost occurrence of alpine compressional structures, notably the Mandach fault.

The southern limit is chosen so as to include all of the large, clearly visible folds (and blind thrusts) of the Jura fold thrust belt, but to exclude the more subtle compressional structures present within and below the Molasse basin. Seismic surveys in this area as well as a series of

drill holes by Nagra have allowed to map a deep, narrow, SSE-NNW trending graben structure within the basement below the Jura detachment (Diebold et al. 1991, Müller et al. 2002) – see Figures 2-19 and 2-20.

More than 2 km thickness of Permo-Carboniferous strata are not affected by alpine deformation to any mappable degree. Despite clear seismic evidence for a thin skinned detachment of the Jura fold and thrust belt above this graben structure, many authors have speculated about a causal relationship between the two structures, Jura folds and Permo-Carboniferous Graben, however.

The most likely and plausible relationship has been formulated by Laubscher (1985) who speculated about the role of a disrupted basal Triassic décollement level as a 'nucleation line' to trigger the ramping up of the basal Jura thrust, thus leading to the formation of ramp anticlines within the 'thin skinned' cover (Figure 2-20).

According to this theory, the internal limit of the Jura, i.e. the transition between Molasse basin and Jura fold thrust belt, might be located above such pre-existing basement structures. This idea has been followed by others, notably Philippe (1995), see Figure 2-21.

While the boundary faults of the graben structures are passive in this scenario, other authors have proposed a more active role for them. Pfiffner et al. (1997a), for instance, argue in favour of an inversion of such structures in the Central Jura (near Hermringen, in our zone AE_5 Biel). Similar inversion has also been proposed in the french Jura (Guellec et al. 1990), see Figure 2-22 and for the Western Central Jura (Mosar 1999).

From the fault orientation with respect to the present day stresses, a reactivation of any of these graben bounding faults in thrusting mode seems unlikely, however. Even if we disregard the type stress regime, which is in strike slip to normal faulting rather than thrusting mode at present (according to stress inversion calculations of Kastrup 2002, Fig. 3.8), the present day orientation of the maximum horizontal stress axis σ_1 makes an angle of 50° to 60° even with the most ideally oriented basement faults and boundary faults to the Permo-Carboniferous grabens. Note that, according to simple, Anderson's rules 'of thumb', a 30° dip-angle is considered ideal, 45° is possible still, but angles above are considered very unlikely for reactivation. A summary sketch of this situation is presented in a 'back of the envelope' stereographic analysis (Figure 2-23). Two representative fault orientations have been obtained from Nagra maps for strike (Diebold et al. 1991, NTB 90-04, Beilagen 37 and 40) and profiles for dips (45 to 55°, Müller et al. 1984, NTB 84-25, Beilage 3). The present day orientation of maximum horizontal stress σ_1-axis orientation is taken from Kastrup (2002, Fig. 3.8, i.e. her F3 stress tensor).

In summary, we consider the reactivation of Permo-Carboniferous graben bounding faults and other old basement faults by way of estimating the relative percentage of earthquakes in thrusting, normal and or strike slip mode. Permo-Carboniferous grabens are documented to exist in our zones AE_1, AE_2, AE_5 and AE_8, we further suspect a continuation of such grabens westward into AE_13 and AE_12.

An extract of our data table (PEGASOS EG1-HID-0033_EG1b, Table A-1) is given in Table 2-1.

Default values for faulting style within the larger Alps External zone are 0.1, 0.8 and 0.1 for normal, strike slip and thrust faulting respectively. In other words, we expect a large majority of 80 % of earthquakes to be in strike slip mode, but we do not rule out the occasional normal or thrust fault to occur – we estimate their relative percentage to one in ten events each. Locally, however, within certain small zones of the Alpine Foreland, structural arguments lead us to override these default values.

Such modifications are indicated through colors in Table 2-1. Blue colors indicate lowered numbers, red colors are increased numbers. Note that we give the thick skinned Permo-Carboniferous graben inversion, i.e. the thrust faulting scenario up to 30 % weight in the region of the Basel- and Eastern Jura. This is against the better knowledge of the seismologists, who do not see such fault plane solutions in their earthquake database (Kastrup 2002), but this honors a community of structural geologists who find evidence for geologically recent inversion in the southernmost Rhine Graben (RG_1) and adjacent folded Basel Jura (AE_1) (Meyer et al. 1994, Niviere & Winter 2000) and work in progress at Basel (Stefan Schmid, EUCOR-Urgent project).
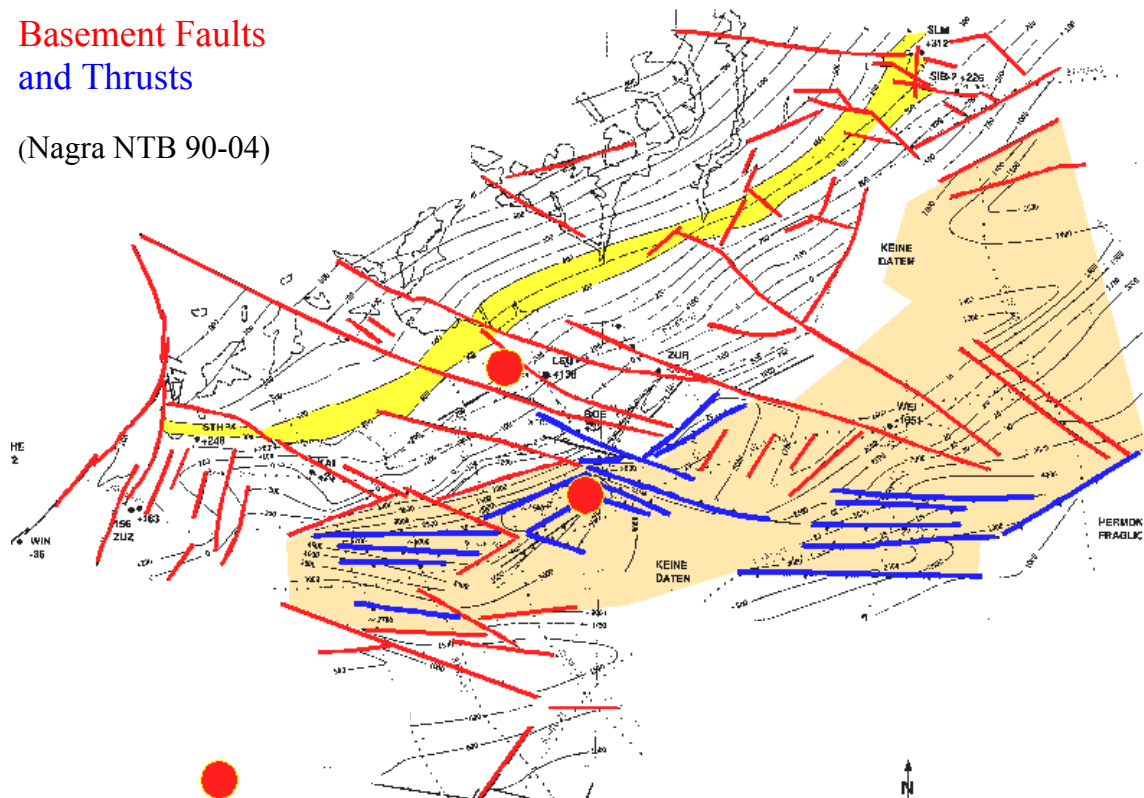
Fig. 2-19: Structure contour map of top pre-Triassic basement according Diebold et al. (1991)

A Permo-Carboniferous graben structure, the so called 'Weiach Graben' is highlighted in brown. Mapped basement faults include WNW-ESE strike slip faults, highlighted in red, E-W oriented faults with some indication of thrust movement are highlighted in blue. Red dots represent the approximate location of KKL, KKB and KKG.
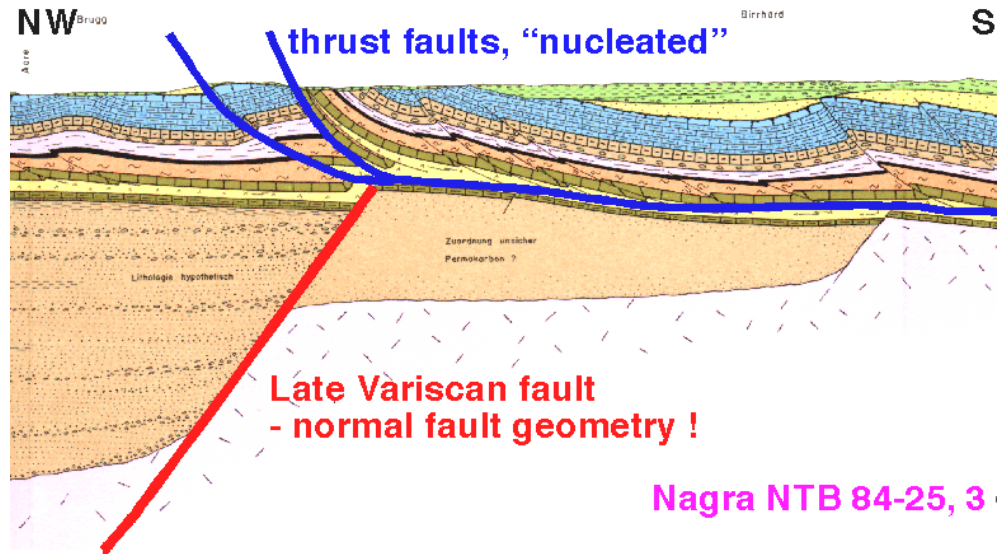
Fig. 2-20:   Geometric relationship between old basement faults and young thrust faults as proposed by Laubscher (1985)

Irregularities at the basal décollement level, caused by the presence of underlying boundary faults to the Permo-Carboniferous graben structure, reactivated in Oligocene times (?) in extension are thought to trigger the cutting up-section of thrust ramps during Late Miocene Jura thrusting. Illustration, copied from Müller et al. (1984). Note the 45° dip to the NW of the southeastern boundary fault to the Weiach Graben structure! The dipping angle of such boundary fault to the Permo-Carboniferous graben is critical to the question if such pre-existing faults could be re-activated in thrusting in the present day stress field. The general rule: the shallower it dips, the easier it is to reactivate!
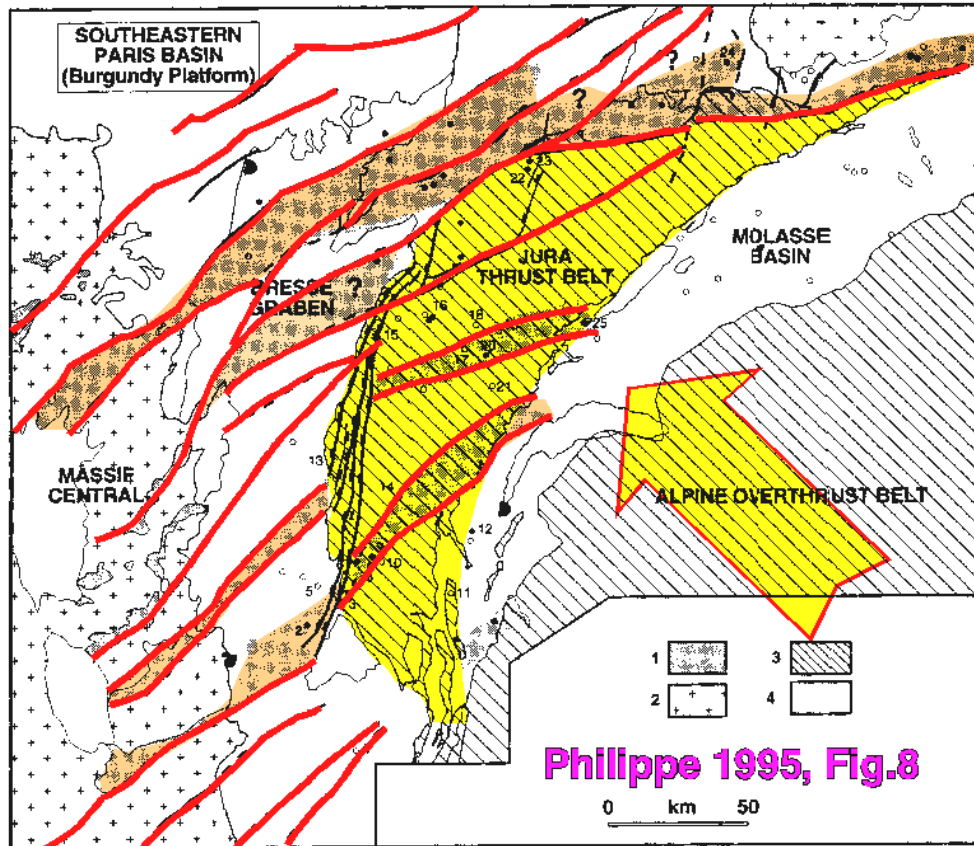
Fig. 2-21: Large scale tectonic sketch map of the Jura fold thrust belt (in yellow), late hercynian fault lineaments (red), and Permo-Carboniferous graben structures (brown) are well known in the outcropping Massif Central, Vosges and Black Forest areas

Below The Bresse Graben, the Molasse basin and the Jura fold belt, information is scarce, however. There exists a striking parallelism between the internal border of the folded Jura (in the eastern half of the Arc at least) and Late Variscan graben structures. Philippe (1995) and Laubscher (1985) propose a causal relationship, such as illustrated in the previous Figure 2-20.
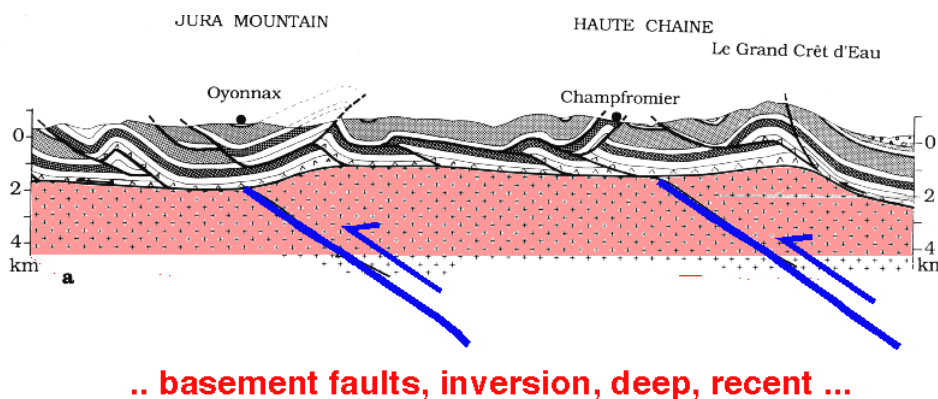
Fig. 2-22: Cross section through the Western Jura along the french ECORS line

Thick skinned thrust faulting, 'inversion' is proposed to have occurred in a late stage of Jura folding by Guellec et al. (1990) after a main thin skinned décollement along Triassic evaporites.
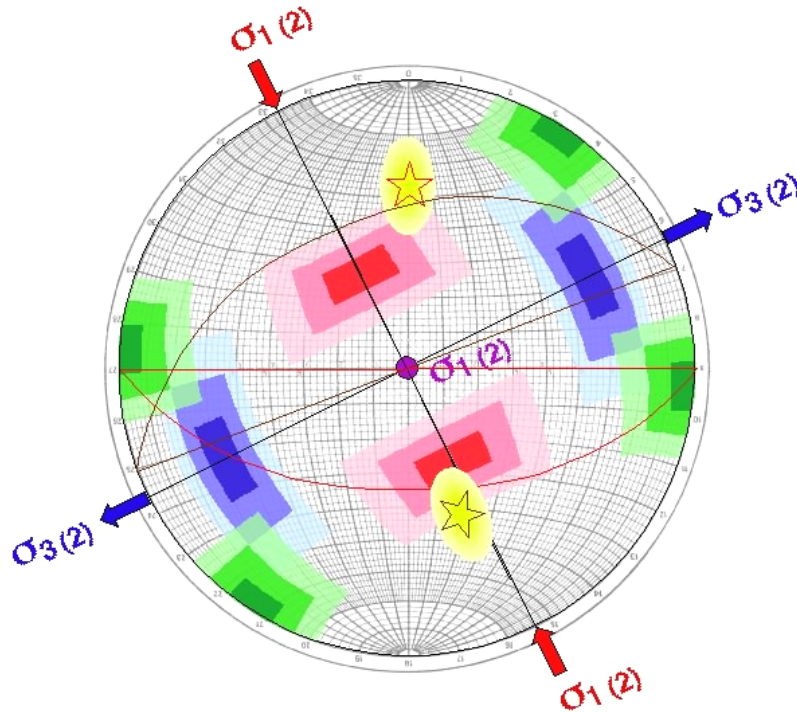
Fig. 2-23:   Rapid estimation of the geometric relationships between pre-existing basement faults and the present-day stress orientation in central northern Switzerland

Equal Area Stereogram, lower hemisphere. Red and brown great circles and poles (stars highlighted in yellow) represent two pre-existing basement fault trends according to Nagra surveys. Maximum horizontal stress orientation σ_1 is from Kastrup (2002, Fig. 3.8, population F3 stress tensor). Optimum fault orientations (poles) for reactivation should fall into the coloured areas, red for thrust, green for strike slip and blue for normal faulting. The pre-existing faults are quite different from these ideal orientations. The only marginally possible thrust-reactivation is for the brown fault, i.e. the south-eastern boundary fault of the Permo-Carboniferous Weiach Graben (as depicted in the previous Figure 2-19). Considering the fact that σ_3 is horizontal, rather than vertical, makes a reactivation in thrusting mode unlikely, however. None of the graben bounding faults is in a likely orientation for strike slip reactivation either.

Tab. 2-1: Estimated percentage of earthquakes to occur in normal, strike slip and thrusting mode within the Alps External small zones

Overall, we estimate that 80 % of earthquakes are in strike slip mode with only 1 out of 10 earthquakes in either in thrusting or normal mode. Local corrections to this overall 'default values' are indicated using a colour code. Blue colours indicate a lower percentage, red numbers are increased percentages.

Faulting style		Normal	StrikeSlip	Thrust
AE	Alps external large zone	0.1	0.8	0.1
Small zones:				
AE_1	Basel Jura	0.1	0.6	0.3
AE_2	E_Jura	0.1	0.7	0.2
AE_3	Zürich – Thurgau	0.2	0.7	0.1
AE_4	Aarau – Luzern	0.1	0.8	0.1
AE_5	Biel	0	0.8	0.2
AE_6	Napf	0.1	0.8	0.1
AE_7	Fribourg single fault	0.05	0.9	0.05
AE_8	Neuchâtel Lake	0	0.8	0.2
AE_9	Vaud	0.1	0.8	0.1
AE_10	Geneva	0.1	0.8	0.1
AE_11	Vuache single fault	0.05	0.8	0.15
AE_12	Jura West	0.1	0.8	0.1
AE_13	Jura Center	0.1	0.8	0.1
Basel area: 'Rhinozeros' – regroupings:				
RG_1 + AE_1		0.15	0.6	0.25
AE_1+2		0.1	0.6	0.3
AE_1+2+13		0.1	0.65	0.25
AE_1+13		0.1	0.7	0.2

2.3.6.3 AE_3 Zürich – Thurgau

The northern limit of this zone is chosen along the Molasse basin – Jura Fold Thrust Belt boundary. The southern limit corresponds to the classic Alpine thrust front. The limit to the west is somewhat arbitrary, we believe to see a change in seismic activity within the Molasse basin along strike (from east to west). Our subdivisions honor such changes, and the zonations within the Molasse basin have been choosen along somewhat arbitrary NW-SE lines in order to make more or less equilateral zones within the Molasse basin. Seismically, the Zürich-Thurgau area is rather quiet. A very nice new geologic map of the canton Thurgau and explanations thereof have been published recently (Schlaefli 1999).

2.3.6.4   AE_4 Aarau-Luzern

Same comments as the previous zone.

2.3.6.5   AE_5 Biel: with a potential ENE-WSW thrust fault

As discussed above (see AE_2), the internal border of the folded Jura might be located above some hidden basement faults, identified in eastern Switzerland as boundary faults to the Permo-Carboniferous Weiach Graben. There is some non-published seismic evidence for the existence of such grabens in the area of Biel too (Meier 1994), as shown in Figure 2-24. The petroleum exploration drill hole of Hermrigen, located on a broad anticline south of Lake Biel, was stopped within Triassic strata, however, and did not even reach the basal Jura décollement. This situation leaves some freedom in the interpretation of the corresponding seismic line(s).

Two alternative solutions have been put forward by Pfiffner & Heitzmann (1997) and Erard (1999) respectively. Pfiffner argues in favour of a recent (last 10 Million years) inversion of a (non-confirmed) Permo-Carboniferous Graben. Erard (1999) re-treated this seismic line(s) and interprets the critical anticline drilled by the Hermrigen well in a thin skinned fashion, as due to a Triassic evaporite accumulation above a perfectly flat basal Jura décollement and a non-affected basement below. This latter interpretation is in line with the work by Meier (1994). In this report the Hermrigen drill hole is given as above crystalline basement (suspected) rather than above a Permo-Carboniferous graben fill. The presence of widespread Permo-Carboniferous is nevertheless suspected, notably along the transition between the Jura fold belt and the Molasse basin, i.e. with a general NE-SW strike (Figure 2-25).

In our AE_5 Biel zone (as well as in the zone AE_8 Lake Neuchâtel) we allow for the presence of such strike parallel, deep seated faults but we give them only a small chance of being reactivated in thrusting mode (compare Table 2-1).
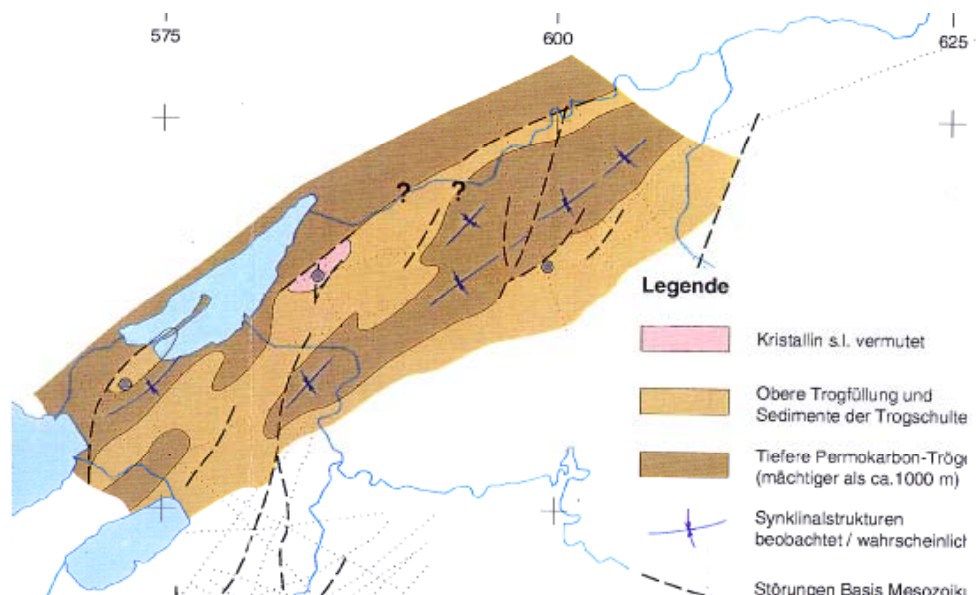
Fig. 2-24:   Subsurface geologic map of the Biel region according to Meier (1994)

Dark and light brown are used to indicate the suspected extent of thick and thin Permo-Carboniferous sediments respectively. The Hermrigen drill hole is located within the pink area, above a suspected non-carboniferous crystalline basement. This drill hole was stopped within Triassic evaporites and did not even reach any sub-Jura décollement rocks.
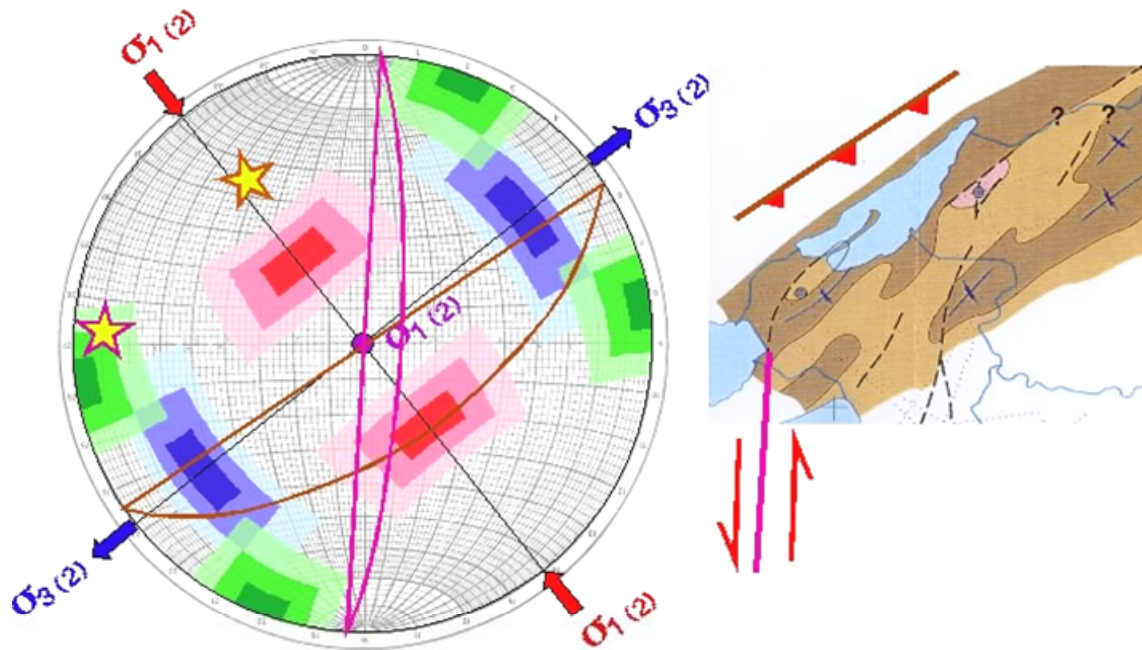
Fig. 2-25:   Rapid estimation of the geometric relationship between pre-existing basement faults and the present-day stress orientation in the central internal Jura, especially in the area of Lake Biel and Lake Neuchâtel

Equal area stereogram, lower hemisphere. The brown great circle represents the fault orientation for a suspected Permo-Carboniferous graben boundary fault, with a 60° dip to the SE. Maximum horizontal stress orientation σ_1 is from Kastrup (2002, Fig. 3.8, population F3 stress tensor). The pre-existing fault has an almost ideal strike for reactivation in thrusting mode, but its dip is too steep by 30° degrees. A reactivation of such faults in strike slip mode is clearly impossible under the present day stress regime. A suspected steep N-S trending Fribourg fault is shown in purple. This fault has an almost ideal orientation for re-activation in sinistral strike slip.

2.3.6.6   AE_6 Napf

Within the larger Swiss Molasse basin, the Napf zone AE_6 is rather undistinct and it could be considered as a 'background', surrounded by zones which have been delimited for their own, more distinct characteristics, higher seismic activity and/or the presence of documented or suspected faults.

2.3.6.7   AE_7 Fribourg: with a N-S strike slip fault

The Fribourg zone AE_7 is characterized by a N-S alignment of seismic activity, strongly suggesting the presence of an active fault at depth. Detailed studies of some seismic swarm activity in this area have indeed provided convincing evidence for the presence of such a fault or fault zone (Kastrup 2002). Precisely relocated earthquakes out of two swarm activties clearly define N-S oriented strike slip faults in good agreement with fault plane solutions from the larger area. The most likely depth for these earthquakes is around 7 km (Kastrup 2002, p. 13), clearly within the crystalline basement.

Petroleum seismic data, reinterpreted by Nagra (Meier 1994, confidential) reveal the presence of a series of complex faults and wrench folds with a general NNE-SSW orientation. Quite surprisingly, however, detailed geologic maps of the area and digital elevation models do not show any such faults nor any subtle geomorphic features with the same orientation. Opinions, diverge on this latter topic, however, and Berger (1994) has presented an entire tectonic / petroleum prospectivity analysis of this area in his book on 'remote sensing' (Figure 2-26).

The 'Fribourg syncline' has indeed long been identified as a 'weird' structure which deviates strongly from the regional strike of Alpine folds and thrusts such as seen further North in the Jura or further to the South in the Alps. The most likely interpretation of these structures is compressional wrenching above pre-existing basement faults. Their N-S orientation makes them most likely candidates for a 'Rhenish' trend, i.e. Oligocene age. There is little evidence for any significant graben structures of this orientation below the Molasse basin, however. The re-interpretation of Meyer et al. (1994) reveals little if any graben-like topography in E-W lines across this structure.
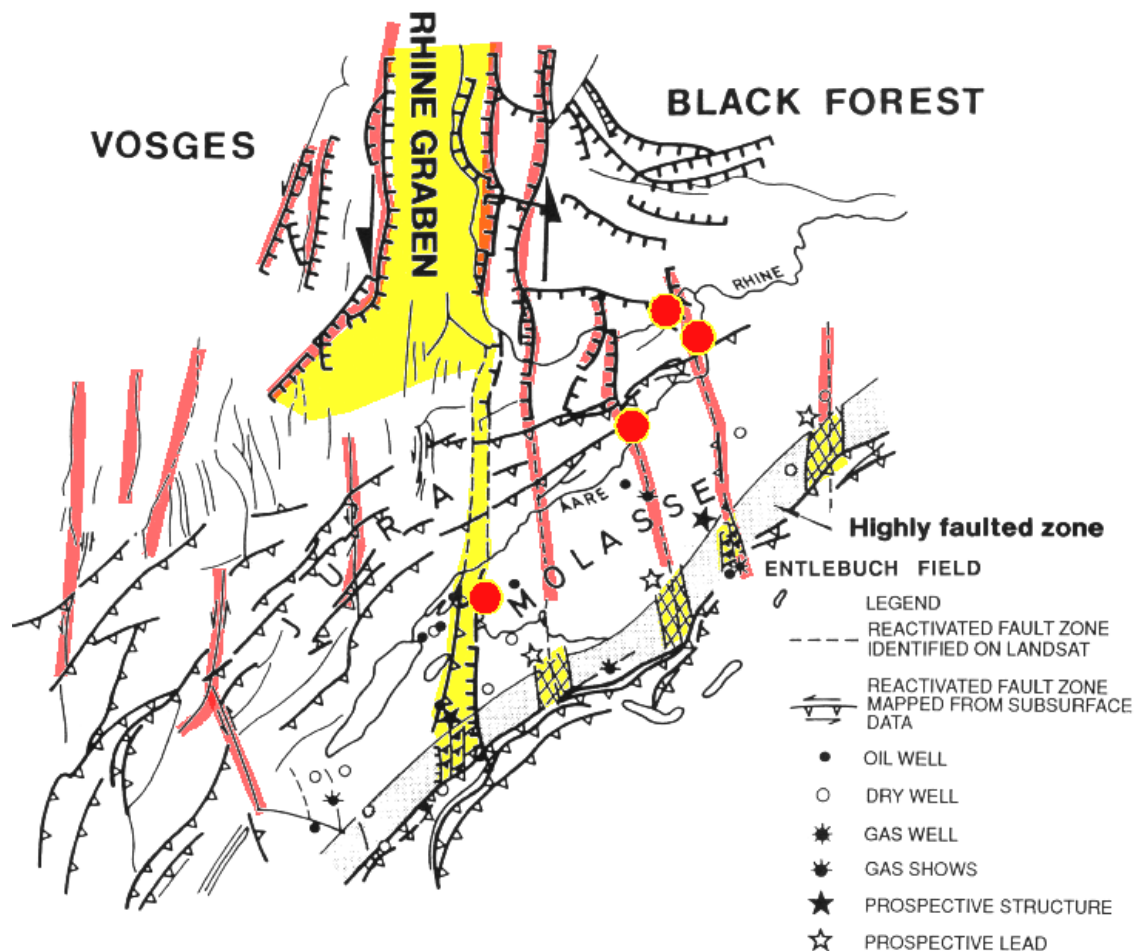
Fig. 2-26:   Tectonic analysis of the Swiss Molasse basin, 'based on satellite imagery' (and in-accessible petroleum seismic data ?) according to Berger (1994, Fig. 7.12)

Colours are superimposed onto the original figure in order to highlight the suspected / suggested presence of a N-S trending appendix of the Rhine Graben, extending southward up to the Alpine front. Red dots represent the approximate position of KKL, KKG, KKB, and KKM.

Whatever their origin, NNE-SSW oriented faults are present in the Fribourg area and they have an almost ideal 'Anderson's' geometry for reactivation in sinsistral strike slip mode (see Figure 2-27).

In our source model, this Fribourg seismic activity is considered to stem from a single N-S oriented strike slip fault located in the crystalline basement (Figure 2-28). The location of this fault is determined from the seismicity pattern, running in the middle of the cloud of earthqukes. Given some uncertainty in this location however, we model the eastern boundary of our source zone as a 'soft boundary'. We model this softness by moving the eastern boundary of the Fribourg zone AE_7 by 2.5 (inward, to the west) and by 5 km outward, to the east respectively. The central position of the boundary is given a weight of 0.5, while the alternative locations are given a weight of 0.25 each. We are content with having this 'softness' applied only to the source zone as provider of earthquake-energy, but not for the collection of characteristic data within the zone, such as a- and b-values, M_{max} and so forth.
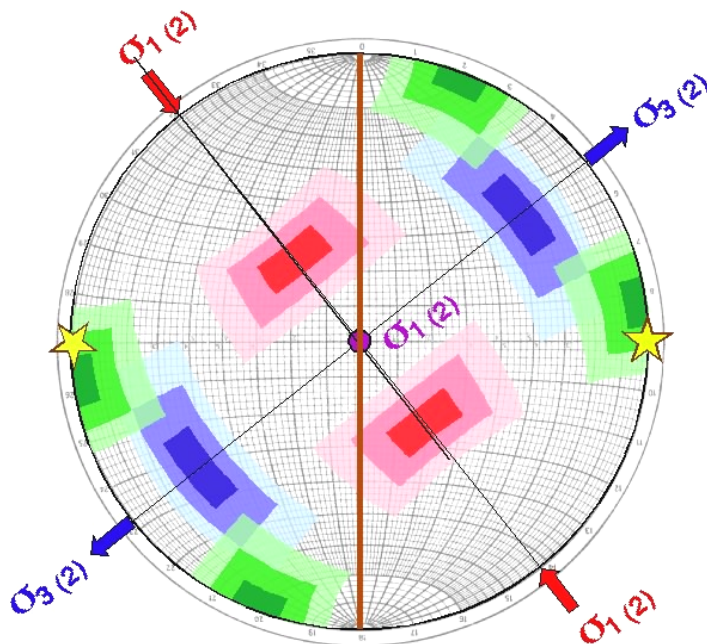
Fig. 2-27:   The Fribourg fault, supposedly a vertical N-S oriented (brown trace) and yellow poles) is almost ideally oriented reactivation in sinistral strike slip

The maximum horizontal present day stress orientation σ_1 is taken from Kastrup (2002, Fig. 3.4, Tensor F2).
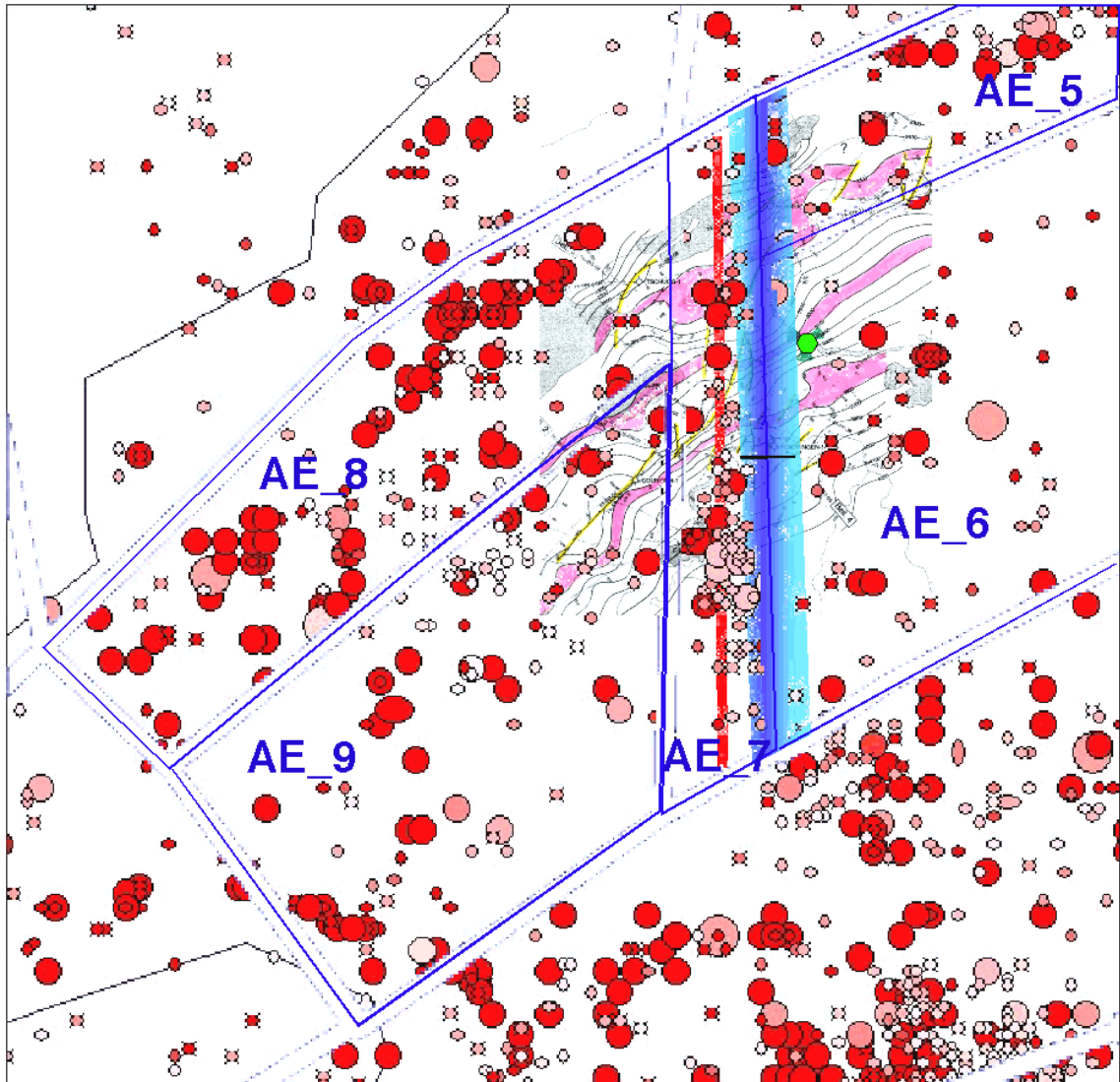
Fig. 2-28:   Source zone model in the Fribourg area

Seismic activity along a N-S earthquake cluster within AE_7 Fribourg zone is interpreted as stemming from a single N-S oriented sinistral strike slip fault within the basement. Seismicity is copied / pasted out of Wizmap (entire PEGASOS catalogue). Structure contours are copied from Meyer et al. (1994, Beilage 13): they represent the interpreted 'base Mesozoic'. Pink is used to highlight a series of these wiggly contours which are not significantly displaced across the Fribourg fault. Minor faults identified at the base Mesozoic are highlighted in yellow. Note that non of these faults is identical with the N-S orientation of the seismicity cluster. Note also that no subsurface data is available for the southern part of this cluster, where most of the recent seismic activity has taken place (see analysis of Kastrup 2002). The eastern boundary of zone AE_7 is modelled as a soft boundary, allowed to move westward by 2.5 km and eastward by 5 km (illustrated using different shades of blue). Light green dot is KKM.

2.3.6.8   AE_8 Neuchâtel Lake: with ENE-WSW thrust fault

Little subsurface information is availbable for this area, which has been spared from petroleum seismic exploration because of the presence of Lake Neuchâtel. The very presence of this lake however, might be used as a geomorphic argument in favour of some pre-existing fault zone. The transition between weakly deformed Molasse basin to the SE and highly deformed Jura fold & thrust belt to the NW is very sharp in this part of the Central Jura and may well reflect the presence of some hidden basement structure below. Over 300 km of seismic data, acquired in 1988 by BP in the canton of Neuchâtel (entirely located within the folded Jura and not crossing the critical transition toward the flatlying Molasse basin) provide a unique database for the analysis of the internal structure of this central part of the Jura fold belt (Sommaruga 1997, 1999). One of the outstanding results of this thesis is the documentation of a major, NW vergent thrust fault with a throw of more than 3 km below the most internal, high Jura Anticline border-ing Lake Neuchâtel immediately to the north (see Figure 2-29). Seismic lines do not extend sufficiently far southward (below Lake Neuchâtel) for the mapping of any basement offsets which might be responsible for triggering the location of this thrust (in a way discussed in section 2.3.6.2).

See discussion of AE_5 Biel zone for more information about the suspected presence of ENE-WSW trending thrust faults at the Jura-Molasse basin transition. In analogy with the adjacent zone Biel AE_5, we postulate the presence of such a hidden basement structure, but again, the chance of re-activation in thrusting mode in the present day stress field is low for graben bound-ing normal faults with an expected 60° dip.
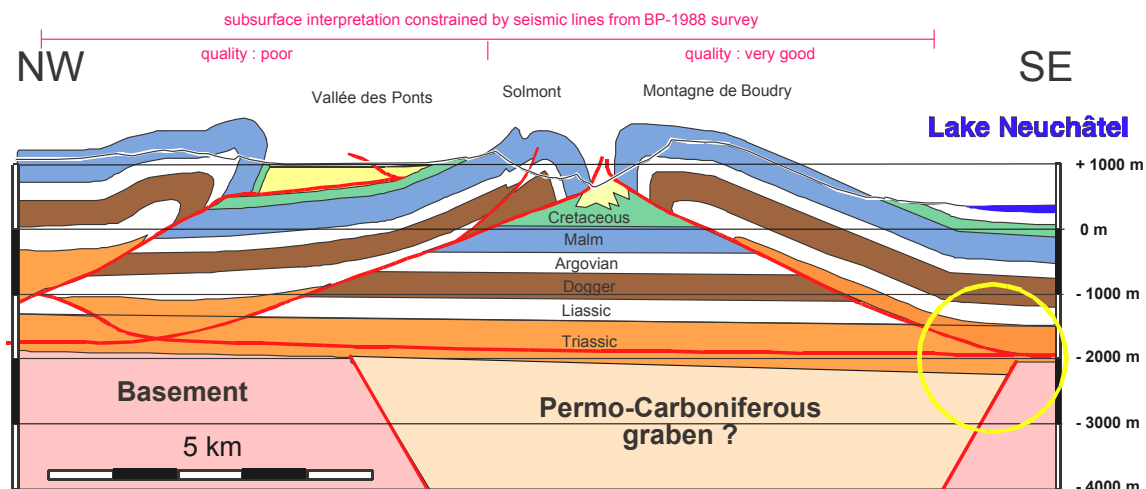
Fig. 2-29:   Geologic profile across the Neuchâtel Jura immediately north of Lake Neuchâtel

The Montagne de Boudry anticline is well documented as riding above a major, NW-vergent thrust rooting in the Triassic décollement level. The flat lying Mesozoic series in the footwall of this thrust are well imaged in seismic lines of a BP survey conducted in 1988. Seismic data does not leave any room for a basement high or inversion structure below this anticline, however, they do not exclude the presence of a Permo-Carboniferous graben nor the possibility of a subtle normal offset or other 'step' within the basal décollement level which might be responsible for localising the branching up of the most internal Jura thrust (compare Figure 2-19). Modified from Burkhard et al. (1998) and Sommaruga (1997).

2.3.6.9   AE_9 Vaud

This is a 'left over' back ground zone limited to the East by the 'Fribourg fault' AE_7, to the North by the Neuchâtel lake zone AE_8, to the South by the Alpine front and to the West by Geneva Lake AE_10. Based on tectonic maps, digital elevation models and geomorphologic features in general, this zone seems to be much more faulted than the active Fribourg zone to the east (see Figure 2-30) and it remains an enigma to the structural geologist why some areas with no visible surface faults (Fribourg) are presently active in strike slip faulting mode while other areas, with clear geomorphic and structural evidence for such faulting do not display any localized seismicity along the expected fault zones (the southward continuation of the Pontarlier fault in this case).

Despite the absence of any clear signs of seismic activity along the Pontarlier fault we will give the re-activation of N-S trending faults some consideration in the form of a high estimated likelihood for earthquakes to be in strike slip mode, rather than in thrusting.
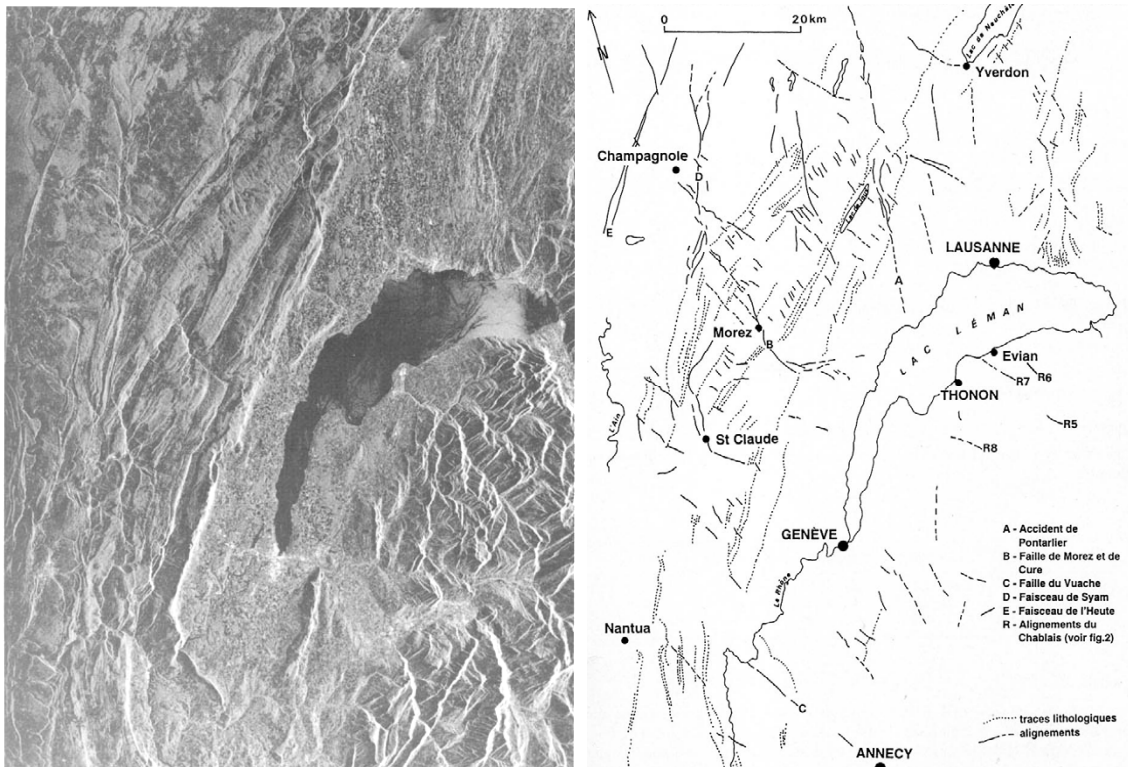
Fig. 2-30:   Fault lineaments around Lake Geneva ('Le Léman' in french), from Raymond et al. (1996)

Left hand side: a Radar satellite image nicely reveals the geomorphic scarps, fault lines with the Jura fold & thrust belt (W and NW), the Molasse basin (centre – NE) and the Penninic Chablais Préalps (SE). Right hand side: line drawing of major lineaments, known and labelled with their classic names such as 'Pontarlier fault' and newly discovered scarps within the SE corner. According to the authors, the latter are 'documented' to be of Latest Quaternary, post-glacial age!

2.3.6.10 AE_10 Geneva

The Geneva zone AE_10 has similar characteristics as AE_5 Biel and AE_8 Neuchâtel. It encompasses the most internal, highest Jura anticline, which is certainly riding above a major NW vergent thrust. As in all the other zones along the Jura fold belt – Molasse basin transition, the question remains open if this limit is located above some hidden, pre-existing basement faults, if any such step in the basal Jura décollement was responsible for the localisation / triggering of this thrust fault, and if such basement faults have a chance of being reactivated in thrusting mode. There is at least one published occurence of a pure thrusting fault plane mechanism, for an earthquake which occured in the french Jura some 30 km northwest of Geneva on 5.2.1968 (Sambeth & Pavoni 1988). A general shift from strike slip – normal faulting in the eastern Jura to strike slip – thrust faulting in the western Jura is noted by Kastrup (2002, e.g. Fig. 3.8).

Given the narrow NW-SE width of the Molasse basin below Lake Geneva we generously included this entire area into one single zone – in contrast to the Molasse basin further east, where a distinction between Jura fold belt and flatlying Molasse basin has been made.

2.3.6.11 AE_11 Vuache: with NNW-SSE strike slip fault

The Vuache fault is part of an entire family of sinistral strike slip faults which have an intimate relationship with the formation of the Jura fold & thrust belt (Figure 2-31). Two competing theories have been proposed with regard to these strike slip faults. Pavoni (1961) interprets them as deep seated, crustal scale strike slip faults and proposes them as the motor for the entire Jura folding by wrenching. In the alternative, more largely accepted thin skinned view of 'Jura Fernschub' (e.g. promoted by Heim 1921, in his 'Geologie der Schweiz', p. 548ff.), the strike slip faults are interpreted as a secondary feature, subordinate to folds and thrusts and essentially limited to the Mesozoic cover series where they are necessary as 'tear faults' in order to accomodate some strike parallel stretching within the Jura arc. This view is confirmed in more recent studies (Hindle & Burkhard 1999, Sommaruga 1999) and the wrenching theory as motor for Jura folding & thrusting has not stood the test of time.

The relevant question is one of strain partitioning, of strain rates and here, of course also for the present day tectonic activity.

The seismologist's argument in favor of a deep seated motor for Jura folding was based on two key observations:

1. earthquakes occur within the basement below the Jura, almost down to Moho depth as we know today and

2. focal plane mechanisms are mostly strike slip, and in cases a N-S sinistral sense of shear could be documented (Pavoni et al. 1997, Sambeth & Pavoni 1988).

Among all the well known strike slip faults of the Jura arc, the Vuache fault is the only one which is clearly seismically active today (Blondel et al. 1988). A recent earthquake of Magnitude M_L 5.3 took place near Annecy on 15th of July in 1996 (Thouvenot et al. 1998). Note that the Magnitude of his earthquake is 4.6 in the PEGASOS catalogue (PEGASOS EXT-TB-0043 2002).

The Vuache fault is well known as a major geomorphic and tectonic feature (Figure 2-32). Cumulative offsets derived from independent restoration of folds on either side of the fault are on the order of 10 km in the middle of this fault, but decrease progressively to the NW and the SE along the fault (Meyer 2000), see Figure 2-33. This observation alone provides a strong argument in favor of a thin skinned, tear fault interpretation because it is rather difficult to imagine, how a displacement on the order of 10 km could decrease laterally over such short distances if this was a deep seated, basement rooted strike slip fault!

According to Thouvenot et al. (1998, abstract), the 1996 earthquake- " ... *hypocenter was located in Mesozoic limestones at shallow depths (1 to 3 km)*". This observation provides an additional argument in favor of a thin skinned interpretation for this (tear) fault (Figure 2-34). On a larger scale (in time and space) it is clear, however, that earthquakes with similar focal plane mechanisms, and problably similarly oriented fault planes occur at deeper levels, within the basement.

For the sake of completeness, it has to be mentioned that an extreme, thick skinned thrusting model of fast ongoing NW-SE shortening in this part of the Jura has been proposed by Jouanne et al. (1995). Their main argument was based on an inversion of levelling data and they arrived at a very improbable rate of over 4 mm/a present day horizontal shortening to take place across the Western Jura fold belt. In the meantime, this conclusion is already invalidated by more recent studies of repeated GPS triangulation which failed to measure any shortening above the error bars (estimated at ca. 1 mm/a) in this part of the Alpine Foreland (Vigny et al. 2002).
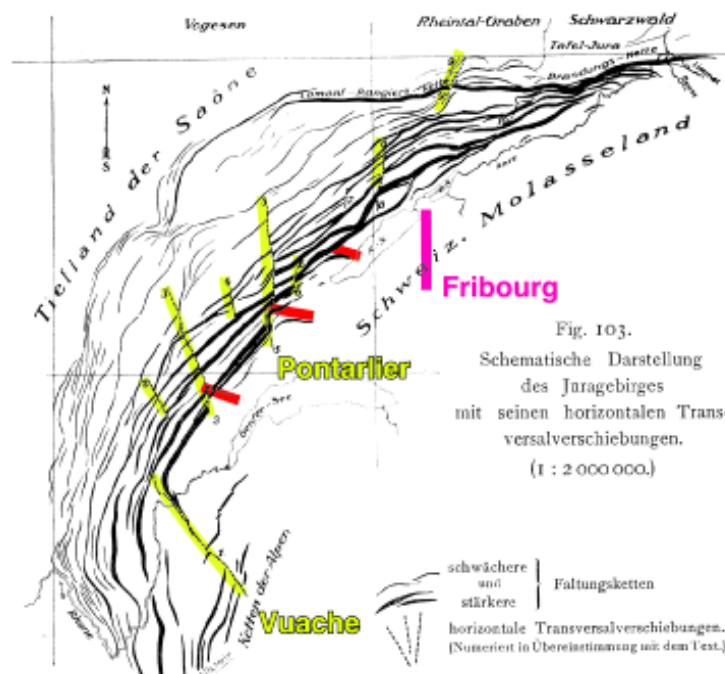
Fig. 2-31:   Geometric relationship between Jura Arc fold and thrust belt and a family of associated sinistral strike slip faults.

For Heim (1921) and most modern structural geologists, the tear faults, highlighted in yellow, are a direct consequence of thin skinned arc formation. These tear faults accommodate some arc parallel stretching. Dextral conjugate sets of faults, highlighted in red, do exist, but they are less frequent and not as through-going as the sinistral set (Heim 1915, 1921). The new Fribourg fault is added in pink.

In summary, the Vuache fault or fault zone is probably the best defined active fault structure of the entire study area. Historical and instrumental seismicity cluster along a well known and mapped major tear fault with a cumulative offset of over 10 km. A signifcant earthquake with Magnitude M_L = 5.3 (M = 4.6 in the PEGASOS catalogue) took place on this fault in 1996. Thouvenot et al. (1998, abstract) identified a seismic gap of some 12 km length to the north of the 1996 earthquake where they postulate that a series of M 5 events or alternatively a single Magnitude 6 event might take place in the near future.
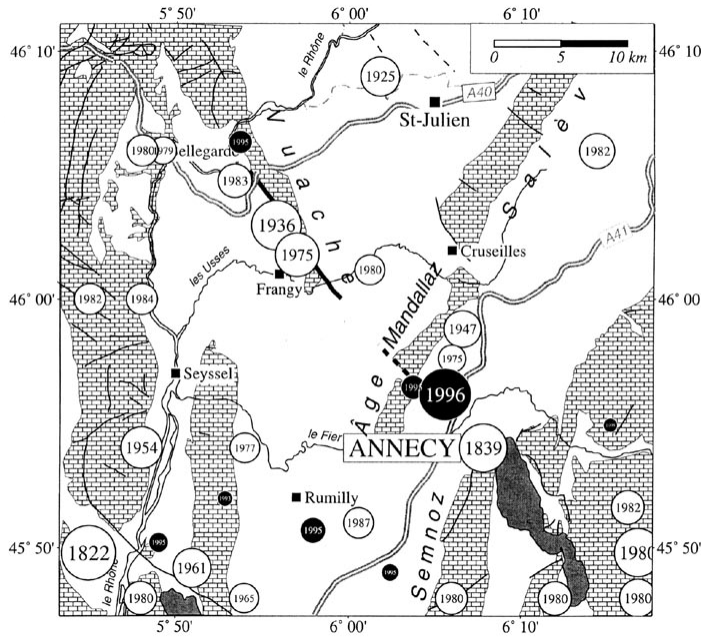
Fig. 2-32: Tectonic map of the Vuache fault and associated folds near Annecy; from Thouvenot et al. 1998, Fig. 3)
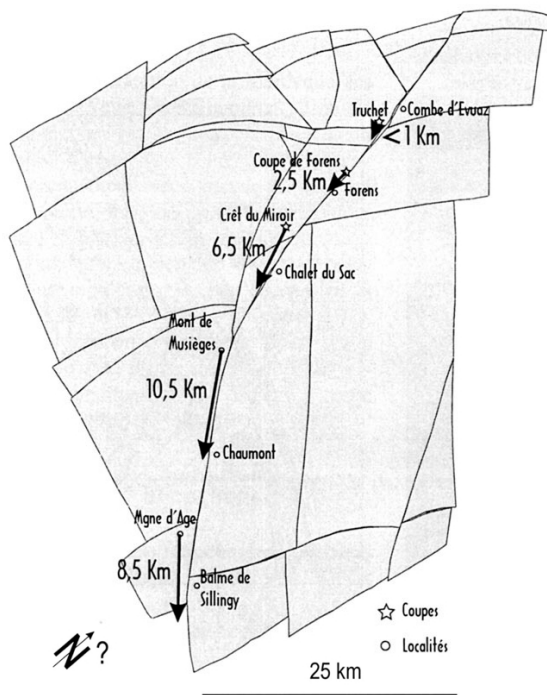
Fig. 2-33: Total cumulated displacements along the Vuache fault have been determined from a restoration of folds on either side of the Vuache tear fault in a block mosaic

This restoration exercise documents a rapid northward decrease in total fault displacement along the Vuache fault (Meyer 2000, PhD thesis Geneva, Fig. 18).
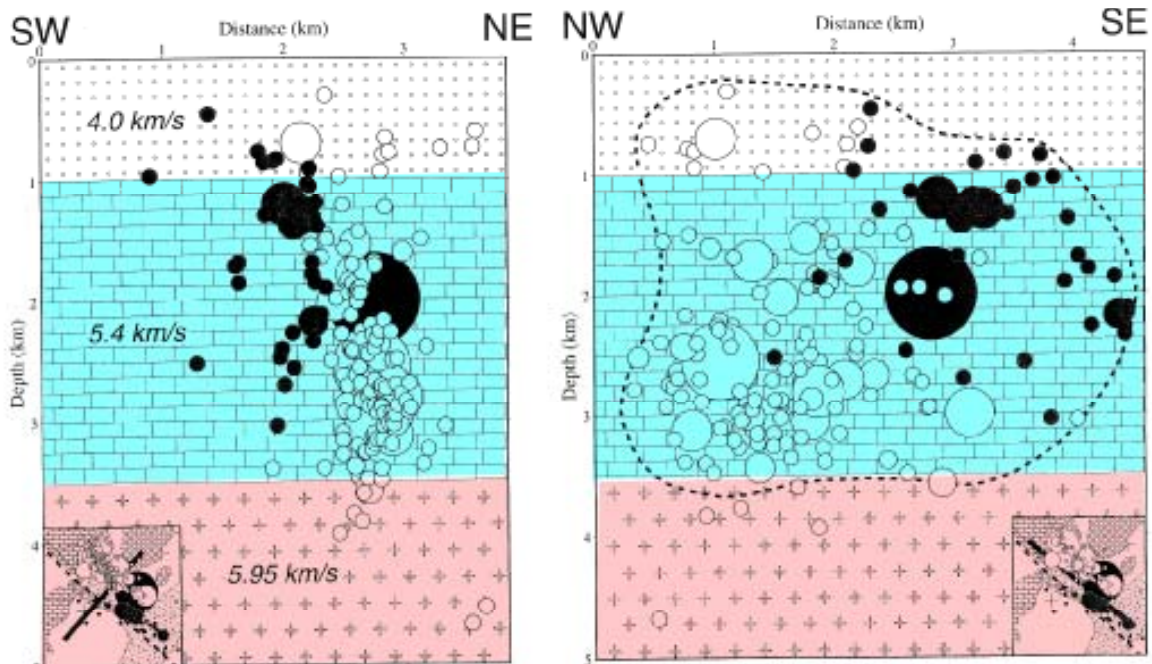
Fig. 2-34:   Mainshock and aftershocks of the Annecy 1996 earthquake define a planar cluster
which corresponds nicely with the known Vuache fault zone in strike, but seems to
be slightly offset to the NE, probably due to a steep NE-ward dip of the fault

Earthquakes are clearly located within the cover series, highlighted in light blue
(Thouvenot et al. 1998, Fig. 8; colours added) and barely extend downward into the
crystalline basement (light red).

Our zone AE_11 is chosen so as to include the entire mapped length of the Vuache fault. The
width is chosen in order to collect only seismic events stemming from this fault or fault zone.
Given the far distance from the centre of the study area, no uncertainty in the fault location
and/or the softness of the zone boundaries will be considered. Southward, the Vuache zone
extends into the realm of truly Alpine tectonics of the Chablais Prealps. Although the geometry
of our zone boundaries may seem somewhat artificial in this respect, such a 'bridge' between the
External Alps and the Jura fold thrust belt quite nicely reflects the fact that the Molasse basin
separating the two provinces (Jura and Alps) further East dies out towards the SW, abutting the
Vuache tear fault.

2.3.6.12   AE 12 Jura West

This generously large zone includes an important portion of the Western Jura fold and thrust
belt, an area bordering the Bresse Graben to the West along a major thin skinned thrust fault
(Guellec et al. 1990). To the North, the transition between Alpine thrust belt and stable Euro-
pean foreland has been extended somewhat northward beyond the thin skinned front of the Jura
fold belt, in order to include the 'Massif de la Serre', a small basement high which is regarded by
some authors as due to thick skinned alpine inversion (e.g. french geologic map 1:500'000,
included in the compiled PEGASOS basemap), compare also Mosar (1999).

The AE_12 zone contains many mapped strike slip faults similar to the Vuache fault, but none
of them is documented to be seismically active. Seismicity seems to be distributed rather evenly
over the entire area. Pre-existing faults of different ages could be reactivated in the present day
stress field. NNW-SSE striking tear faults of the Vuache type are expected to be reactivated in
sinistral strike slip. N-S trending, boundary faults of the Bresse graben, hidden below the most

frontal Jura folds and thrusts, might equally be reactivated in sinistral strike slip. WSW-ENE trending Hercynian, Oligocene and/or Miocene faults are potentially reactivated in thrusting (Sambeth & Pavoni 1988).

2.3.6.13   AE 13 Jura Center

The Central Jura zone AE_13 is limited to the west along another major sinistral tear fault, the Pontarlier fault zone, which has been included in AE_13. To the north, this zone is limited generously so as to include any thin or thick skinned alpine compression features. To the south, we delimited the central Jura zone towards a seemingly more active boundary zone AE_8 Neuchâtel Lake, transitional towards the Molasse basin. The boundary with its eastern neighbour AE_1, Basel Jura is again chosen along another N-S striking fault zone which itself, has been included in AE_1.

The Jura Center zone is structurally dominated by Jura folds and thrusts in a general E-W to NE-SW direction, potentially reactivateable in thrusting mode as well as widespread N-S trending, 'rhenish' tear faults, ideally oriented for reactivation in sinistral strike slip. None of these faults is documented to be seismically active, however.

2.3.7   Alps Central: AC_01 through AC_15

2.3.7.1   AC_1 Grenoble

The Grenoble zone AC_1 includes large parts of the thin skinned 'Chaînes subalpines', as well as thick skinned, hinterland portions such as the Mt. Blanc massif. If it were located closer to the center of the study area, we certainly would have subdivided this zone further in order to take such major structural and tectonic differences into account (we do so further eastward). This simplification seems justified by the rather erratic pattern of seismicity within the larger Grenoble area. An interesting observation about the present day activity and stress state of the Alpine chain has been made in this zone, however. This is indeed one of the few places where thrusting fault plane solutions have been observed. The location of thrusting fits nicely with the proposed frontal / basal ramp of the youngest alpine floor thrust at the transition where the External Crystalline massifs (Belledonne massif in this case) are thrust upon the non-affected European foreland basement (Sue et al. 1999).

2.3.7.2   AC 2 Briançon

The Briançon zone belongs to the core part of the Central Alps (in the geological literature often referred to as 'internal' in contrast to 'external'). It is clearly separated from the External Crystalline Massifs to the west by the frontal or rather basal penninic thrust zone. Long recognized as one of the more important 'sutures' (some questionable ophiolites of the Valais ocean are present indeed) within the Alps, this thrust zone has now also been identified as being re-activated in normal faulting mode in late alpine times (from Miocene onward).

A normal faulting regime is also well documented through focal plane solutions (Sue et al. 1999). On the scale of the Western Alps, the Briançon zone is defined by an elongate N-S oriented area with some elevated seismicity, 'the Briançon arc' of french authors, following closely the surface trace of the penninic front, or rather some kilometers to the east of it (Figure 2-35). The eastward dip of this zone is well documented through seismic reflection profiles of ECORS (Tardy et al. 1990) and NFP20 (Escher et al. 1997) and extends downwards to mid-crustal depths of some 15 km. Seismicity seems to be confined to the nappe pile above this package of reflectors, i.e. to the Penninic nappe pile, while the underlying 'European basement' appears to be devoid of seismicity (in this internal position), see Figure 2-36. The Briançon zone is limited to the east along a rough N-S line in order to distinguish it from another seismic arc

along the Alps / Po-plain transition, the 'Piemontais Arc' (Sue et al. 1999), called AI_1 Dora Maira in our zonation.
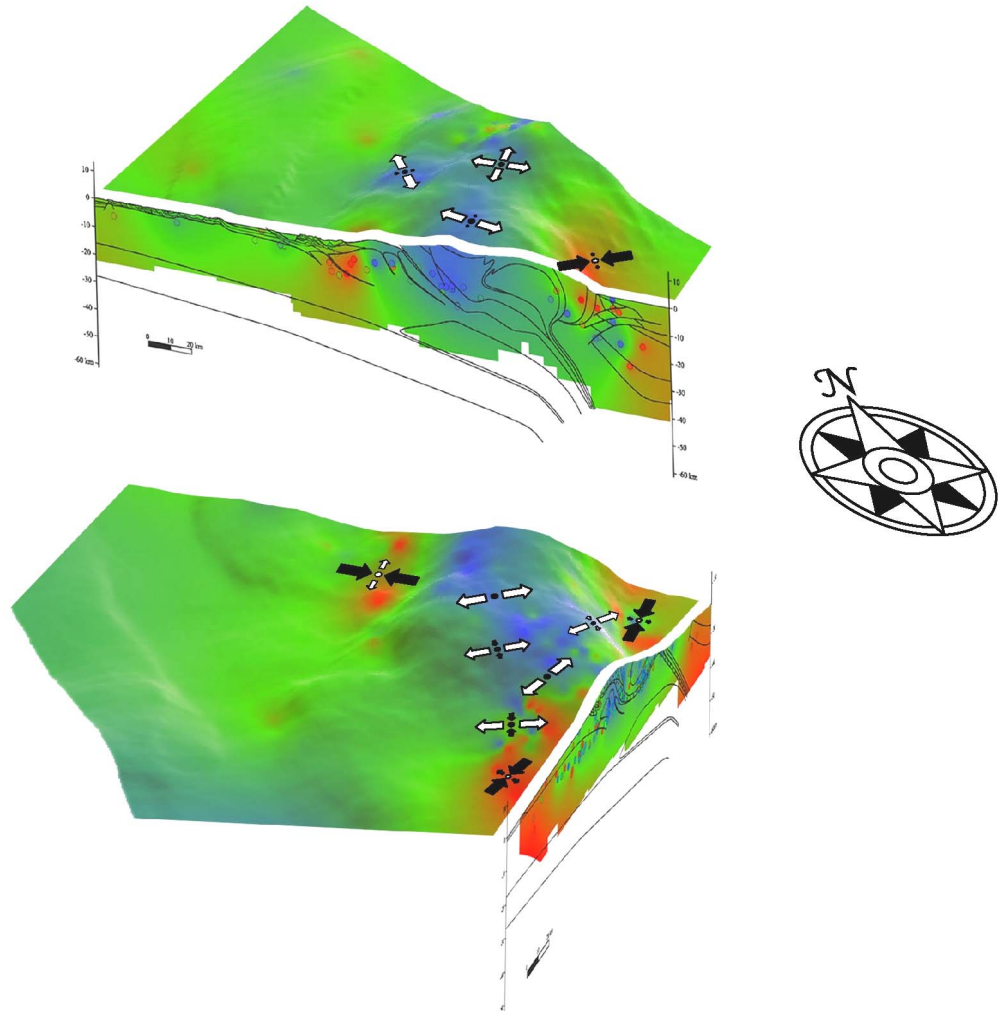
Fig. 2-35:   Schematic block diagram of the Western Alps color-coded for stress regime

Red is thrusting, green is strike slip, blue is extension. Arrows are obtained from stress inversion of a series of fault plane mechanisms. Dots (on the faces) are projected positions of earthquake epicenters. Topography of the Alps is smoothed with a 50 km diameter filter. NW-SE cross section is from ECORS. Courtesy of B. Delacou 2002, PhD thesis (in progress) at Neuchâtel University.

(a)　　　　　　　　　　　　　　　　　(b)
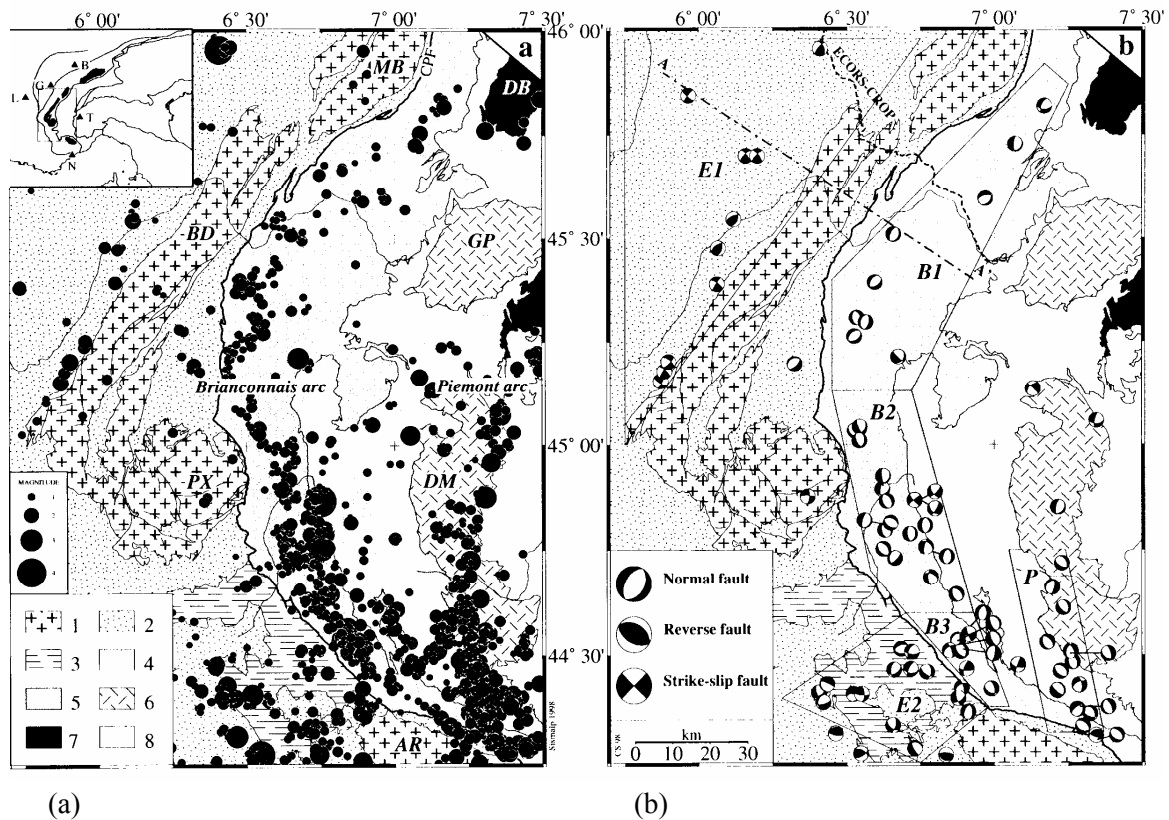
Fig. 2-36:　Seismicity and seismotectonic maps of the western Alps, from Sue et al. (1999, Fig. 2)

(a) Earthquakes recorded by the Sismalp and IGG seismic networks between 1989 and 1997. Only events with $M_L > 1$, root-mean-square residual smaller than 1 σ and azimuthal gap smaller than 180° are plotted. The Briançonnais seismic arc is located beneath the Briançonnais Zone, just east of the Frontal Penninic Thrust (bold line); the Piemont seismic arc is located between the Dora Maira (DM) and Argentera (AR) massifs.

(b) Seismotectonic map showing reliable focal mechanisms computed with the same database. Six seismic domains have been defined using structural considerations: E1 and E2 in the external zone; B1, B2, and B3 along the Briançonnais seismic arc; and P along the Piemont seismic arc. All domains except E1 undergo extension, whereas E1 undergoes transpression.

2.3.7.3　　AC_3 Arve

To the Alpine geologists, this area is very similar to the zone AC_4 (Préalps) further east. Both areas are characterized by the presence of a thin (in terms of crustal structure) thrust sheet of far travelled, thin skinned Briançonnais cover units. The internal structure of the topmost 2 kilometers or so is highly complex, with generally NE-SW trending folds and thrust faults. N-S and E-W trending tear-faults are equally present, but their age is ill-constrained. Many of the these major tear-fault certainly owe their origin to the emplacement history, starting in the late Eocene. Final emplacement in their present day position on the northern border of the Alps is younger than Early Miocene, since some Molasse deposits are found below and in front. The deeper structure of this part of the Alps is ill constrained. Most probably, the top of the European foreland crust is gently bending downward to reach a depth of around 6 km. There is no evidence for thick skinned tectonics below the Arve zone.

In terms of seismicity, the Arve zone seems to be somewhat less active than the neighbouring Préalps. This was the main reason for introducing a subdivision between AC_3 and AC_4.

2.3.7.4   AC 4 Préalpes

To the alpine geologist, the Prealps represent a far travelled, thin skinned package of thrust sheets which have been intensely folded, thrust upon each other and wrenched sideways during more than 100 km of total travelling distance. The starting point was located at a latitude somewhere near the present day Apennines south of Torino! In other words, we have the difficulty of distinguishing inherited structures due to this long travel from structures which might have a more recent origin. Experts of Prealpine tectonics have long claimed the omnipresent N-S oriented sinistral strike slip or tear faults being imparted to the Prealps klippen nappes after arrival in their final present day position. A similar orientation and attitude of such N-S lineaments and tear faults is indeed present within the Molasse basin (Fribourg fault zone) and within the Jura fold belt to the North (Plancherel 1979). This cross cutting relationship 'of rhenish' oriented late faults, makes a late reactivation origin likely. New geomorphic evidence for a recent, post-glacial age of faulting activity along such lineaments has been provided by Raymond et al. (1996). The orientation of the geomorphic fault lines fits very well with the present day stress orientation as obtained from fault plane solutions (Kastrup 2002) – extrapolated from neighbouring areas, since no such fault plane solutions are available for the Prealps proper!

Seismicity within the Prealpes zone AC_4, is rather diffuse and does not align along any of the geologically identified fault zones. This zone is limited to the north roughly along the classic Alpine front – note that the latter is a thin skinned feature, which does not have any profound meaning at depth. To the south, the Prealps zone is limited against the well defined Wildhorn fault zone AC_5.

2.3.7.5   AC 5 Wildhorn: with WSW-ENE strike slip fault

The Wildhorn zone AC_5 is part of the larger Valais area of high seismic activity. North of the Rhone valley, instrumentally recorded earthquakes are alinged along a rough WSW – ENE trend (visible in the PEGASOS catalogue), suggesting the presence of an active fault at depth. This trend is much more pronounced in a detailed study of microseismicity in this area which has provided strong evidence for such a fault zone, located within the basement at a depths of 5 to 10 km (Maurer et al. 1997). The microseismicity in this area is clustered within a 3-D vertical 'wall' of WSW-ENE orientation (Figure 2-37).

Further confirmation of this fault alignment is provided by the seismicity of the year 2000, as reported by Baer et al. (2001), as shown in Figure 2-38.

Some additional evidence for a single fault in this area came in 2001, when an increased activity near Martigny was recorded by the deployment of a temporary seismometer network. The 2001 activity took place exactly vertically below the well known Carboniferous graben of Salvan Dorenaz (Deichmann et al. 2002). The strike of the active fault matches perfectly the strike of this graben (NE-SW). This poses a new problem, however, since this strike is some 5 to 10° more to the N than the overall strike of the regional seismic lineament of the Wildhorn zone. Could it be that the Salvan Dorenaz graben changes its strike below the Helvetic nappes to a more WSW-ENE trend ? Such a trend would make sense in comparison with the known Carboniferous – Permian structures of the Northern Foreland, but it is at odds with the SSW-NNE trend of the Salvan – Dorenaz Graben of the Aiguille Rouge Massif.

On the regional scale, on either side of the Rhone valley, there are very numerous late brittle faults cross-cutting the Helvetic and Penninic nappes. Above the seismic lineament, none of the mapped faults matches the trend, size and precise location of the earthquake cluster at depth, however. A series of suspiciously fresh fault scarps are present in the Rawil- and Sanetsch-area,

but definite proof for a post-glacial faulting activity has not been found (yet), despite intense search for such structures (notably two diploma theses at Neuchâtel University, by Th. Affolter and V. Kohler in 1998). Fault plane solutions and paleo-stress axes determined from the latest alpine faults correspond very nicely, however, both indicate a dextral strike slip regime with a component of SW-NE oriented, orogen parallel extension (Franck et al. 1984).

The Wildhorn zone hosts some of the most important earthquakes of the entire 20th century recorded in Switzerland. The 1946 events near Sierre are listed in the PEGASOS catalogue as follows:

25.1.	1946	M = 6.1
26.1.	1946	M = 5.2
04.2.	1946	M = 5.1
19.5.	1946	M = 5.4
30.5.	1946	M = 6.0

No surface ruptures have been recorded which would allow to tie this activity with the Wildhorn lineament. The location of the main event (25 january) could not be determined from seismo-meter readings in northern Switzerland, because most of them were temporarily damaged by the strong motion induced, making readings of the s-arrivals impossible. Isoseismals drawn after the event indicate an epicenter near Sierre (intensity VIII), but this may be biased by the high population density in the Rhone valley – and the obvious absence of damage reports from the un-inhabited high mountains north of the Rhone valley (Weidmann 2002). In the PEGASOS catalogue, the epicenter is now located north of the Wildhorn lineament, quite far from the town of Sierre.

The Wildhorn zone AE_5 is designed as a fault zone and we model the seismic activity as stemming from a single dextral strike slip fault running in the middle. Earthquake activity is collected from a small couloir along this fault only – despite the fact that considerable seismic activity is recorded on either side of this fault zone too. At least towards the south, a separation from the Valais zone AE_6 is justified by a change in spatial distribution of hypocenters as well as focal plane solutions (Maurer et al. 1997).

Maurer et al. 1997 (Terra Nova)

Affolter, (1998, diplôme NE)
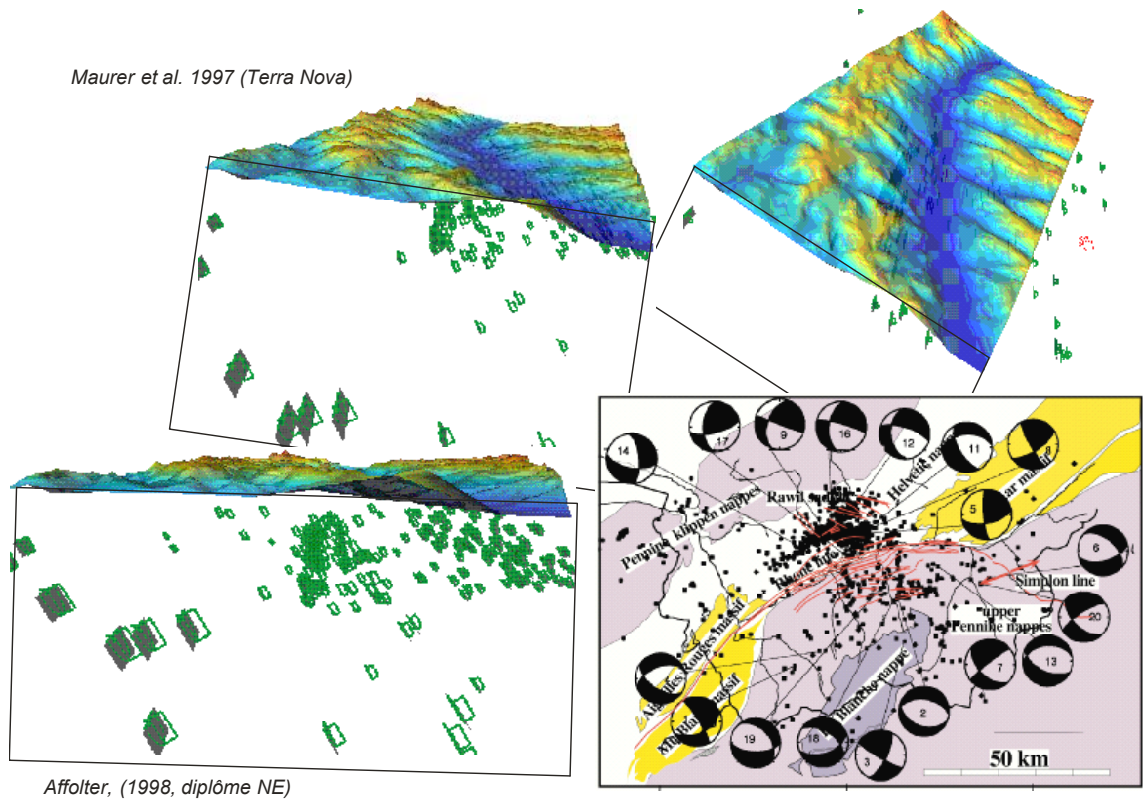
Fig. 2-37: Microseismicity in the larger Valais area according to Maurer et al. (1997)

Block diagrams with a half transparent upper (rough) topographic surface are viewed under three different angles in order to visualise the 3-D alignment of earthquakes below the mountains on the northern side of the Rhone valley – the Wildhorn zone. (Earthquake epicenters are shown as green dihedral symbols, their size varies as a function of distance from the observer). Earthquakes south of the Wildhorn alignment are distributed rather evenly within the topmost 10 km or so. Fault plane solutions and map from Maurer et al. (1997, Fig. 2, colours added). Block diagrams from Affolter (1998, unpublished diploma thesis Neuchâtel University).
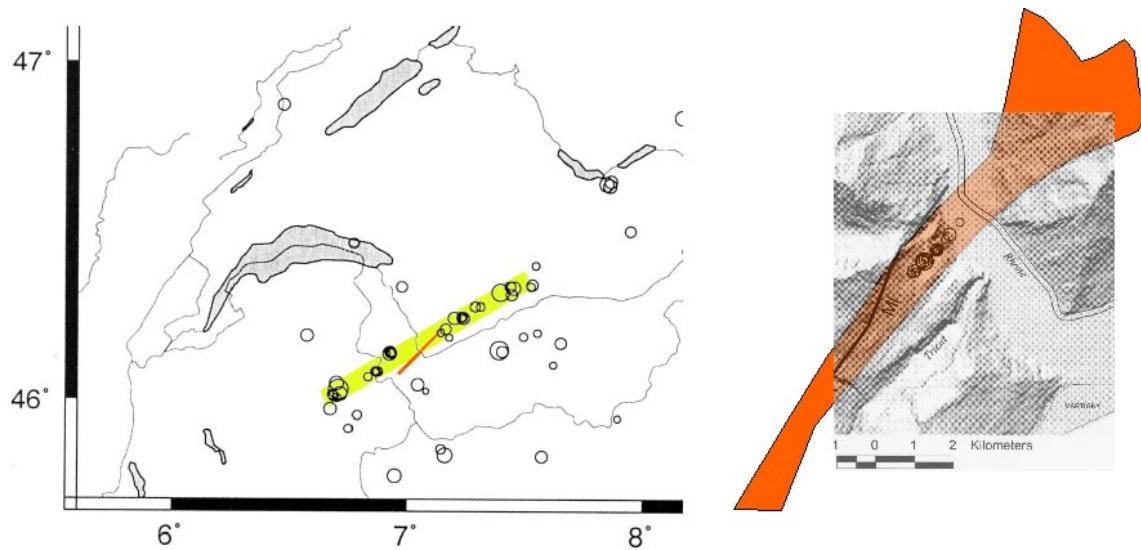
Fig. 2-38:   Epicenters of earthquakes recorded by the Swiss Seismological Survey during the year 2000

Left hand side from Baer et al. (2001; zoom out of Fig. 3). Right hand side: In 2001, a series of earthquakes were recorded again in the lower Rhone valley (zoom, Deichmann, pers. communication, in press at Eclogae Geologicae Helvetiae, annual report of seismic activity in Switzerland). The alignment of the 2001 activity took place right below the middle of the Carboniferous Salvan Dorenaz Graben (highlighted in orange). The strike of this small cluster is not identical with the overall strike of the larger Wildhorn seismic lineament (yellow), however.

2.3.7.6   AC 6 Valais

In contrast to the 3-D alignment of earthquakes along a hidden basement fault, north of the Rhone Valley, seismicity of the larger Valais area to the south of the Rhone river seems to occur in a much more random fashion, widely distributed throughout the entire volume of some 15 km of upper crust (Maurer 1993, Maurer et al. 1997). Fault plane solutions indicate a different stress regime on either side of the Rhone fault zone. South of this major fault line, running along the Rhone valley, and above the basal penninic thrust which follows the very same valley, the present day stress regime is in extension, with roughly N-S oriented σ_3 (Figure 2-39). The southern Valais represents the northernmost tip of a larger region with similar earthquake characteristics prevailing all along the crest-line of the Arc of the Western Alps (Sue et al. 2000, Sue et al. 1999). We subdivided this larger area into three zones AC_1, AC_2 and AC_6 Valais.

Some remarkable historical earthquakes of the Valais are hosted within the AC_6 Valais zone, notably a Magnitude 6.4 event near Visp in 1855 (Figure 2-40) as well as a M 6.1 event in 1755 in the Lötschental. Neither of these earthquakes can be tied to any mapped major surface fault and several possibilities exist. Wagner et al. (2000) suppose a direct connection of the 1855 Visp earthquake with the Simplon fault.

Given the fault plane solutions recorded by Maurer et al. (1997), such a connection seems some-what unlikely, however, since the Simplon normal fault is ideally oriented for an extension σ_3 in a SW-NE direction. Such focal plane mechanisms have not been recorded by Maurer et al. (1997) in this area, and the known Simplon fault is not in a likely orientation to be re-activated in the well defined stress field representative for the Penninic Nappes of the Valais zone (Kastrup 2002).

Limits of the Valais zone were defined as follows:

− the northern limit does not follow any mapped surface feature but is defined by the trend of the seismicity lineament of the adjacent Wildhorn zone,

− to the east, the Valais zone generously includes the area around Brig and the Simplon pass, a major normal fault with some suspected potential of being reactivated

− to the south, the Valais zone is limited on a structural/geological argument, following a line separating north vergent alpine structures of the Central Alps from southeast vergent (late) structures of the Southern Alps

− to the southwest, the limit is chosen against the N-S boundary of the Mt. Blanc massif, including the steeply eastward dipping basal penninic front.
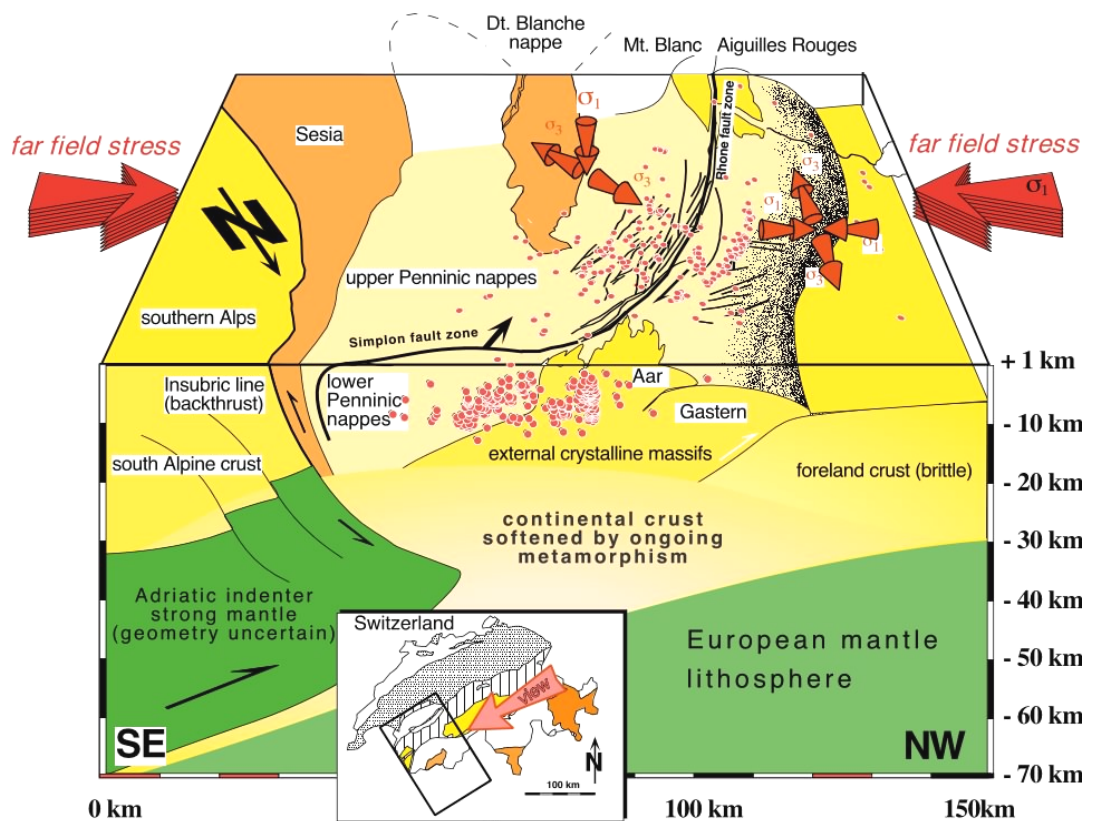
Fig. 2-39: Block diagram of the larger Valais area illustrating the observed seismicity in the context of major Late Alpine structures such as the External Crystalline massifs and Insubric backthrust, Penninic nappes have been removed

Epicenters of earthquakes are projected vertically onto the upper surface of the block for their localisation in x, y and onto the front side of the block diagram along the regional strike. Modified (coloured version) from Maurer et al. (1997).
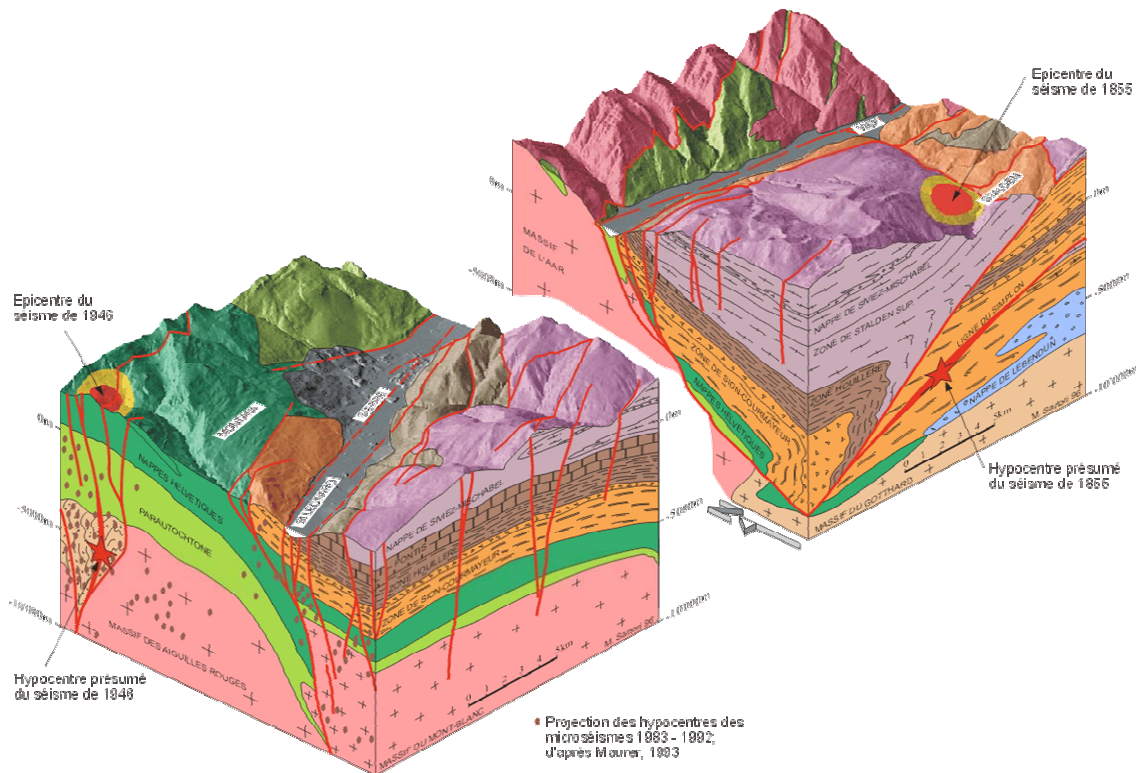
Fig. 2-40:   Block diagrams illustrating the assumed connection of two major Valais earth-
             quakes with well known faults at the earth surface, drawing by Mario Sartori
             (http://www.crealp.ch/fr/contenu/seismes_blocs_x.asp)

             The Sierre 1946 earthquake (left hand side) is depicted as a dextral strike slip fault
             along a steep WSW-ENE running fault of the Wildhorn zone. The Visp 1855 earth-
             quake (right hand side) is shown in relation to the major late alpine Simplon fault,
             dipping gently SW-ward below the Zermatt Valley.

2.3.7.7   AC 7 Sarnen

The Sarnen zone AC_7 is well known for its historical event of 1601 listed with a Magnitude of
6.2 in the PEGASOS catalogue as well as some more recent activity, e.g. a M 5.7 earthquake
recorded in 1964 near Sarnen. Note that former catalogues listed this last event with a Magni-
tude of 4.8 only (e.g Schindler et al. 1996) and maximum intensities observed in the entire
Central Swiss area are listed as VII to VIII both for the Sarnen and the 1601 earthquake.

We extend the Sarnen zone eastward in order to include another M 5.9 (Intensity VIII) event
which took place in 1774 in the canton of Uri.

Recent paleoseismological investigations in Lake Luzern by the ETH-Zürich group, using high
resolution seismic profiling covering large parts of Lake Luzern in a systematic survey, have
allowed to identify at least five laterally correlated slumping events within the last 15'000 years
(Schnellmann et al. 2002). These slump events are interpreted as triggered by large earthquakes
such as the 1601 event which has induced a series of well dated slumps within the Lake as well
(Figure 2-41) as a major seiche wave observed and recorded in the archives of the town of
Luzern.
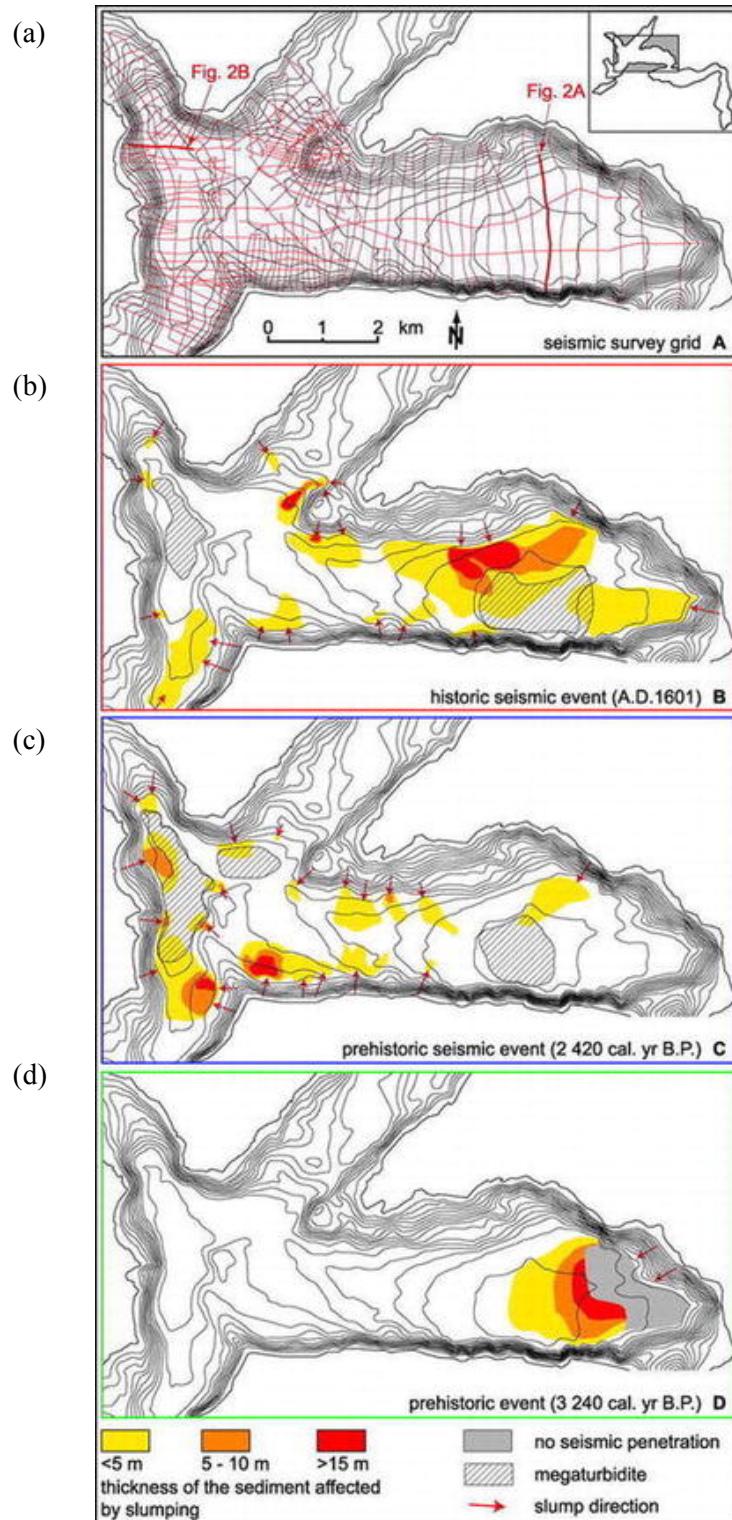
Fig. 2-41: A series of slumps have been indentified and dated within Lake Luzern (Schnell-mann et al. 2002, Fig. 3)

(a) Seismic grid. (b) Slumps correlated with a major historical earthquake in 1601. (c), (d) Laterally correlated historical slump events, radiocarbon dated as 2420 and 3240 before present. Bathymetric contour intervals are 10 m.

Geologists are at a lack of arguments to explain the Sarnen earthquakes and the question arises if this type of activity could take place just anywhere within the northern part of the Alps. The three zones AC_4 Préalpes, AC_7 Sarnen and AC_9 share very similar geology, tectonic history, structure and so forth and their lateral subdivision is essentially based on the apparently higher seismic activity observed historically as well as instrumentally within the central area around Lake Luzern – now also highlighted through paleo-seismic studies. According to the PEGASOS catalogue, seismic activity within this zone is limited to the top-most 10 km of crust. This means that seismicity is taking place mostly within sedimentary cover series, or to be more precise, above the latest alpine basal floor thrust – and not within the european crust bent downward, southeastward below the Alpine pile of thrust sheets. The main Sarnen earthquake with an estimated depth of 5 km (Schindler et al. 1996, p. 41) could well have been a thrusting event, located on the basal (blind) floor thrust of the Alps. Some indication for ongoing shortening in thrusting mode is at least provided by (admittedly rare) focal plane solutions along a narrow zone at the NW front of the Central Alps (Sarnen – Walensee) according to Kastrup (2002, Fig. A1.1).

2.3.7.8 AC 8 Ticino

The larger 'Ticino' zone AC_8 is characterized by a complete lack of seismic activity. There is not a single earthquake of Magnitude larger than 4 included in the PEGASOS catalogue falling into this zone and this is how we chose to delineate the boundaries of this 'background' zone to the west, north and east. Southward, the Ticino zone is limited by a major tectonic boundary, the Insubric Line. There is no easy geological explanation for the seismic quietness in this core part of the Central Alps. Similar tectonic areas to the west (Valais AC_6) and to the east (Grisons AC_10) show substantially increased seismic activity and belong to the more active zones of the entire Alpine belt. Paradoxically, this central alpine zone contains some of the most spectacular evidence for post-glacial (i.e. younger than 18'000 years) tectonic activity in the form of fault scarps with displaced scree slopes, including moraine material. Fault scarps are well visible in the field, in aerial photography, in numerical altitude models and even as lineaments in satellite imagery. The interpretation of these scarps has long been and still remains a riddle (Eckart 1957, 1974, Eckart et al. 1983). The most obvious scarps are found along and on either side of the Urseren valley where they form long linear features crossing several side-streams of the main E-W striking valley (Figure 2-42). Overall, the scarps seem to follow the steeply dipping tectonic foliation of the Aar and Gotthard massifs. Locally, however, the associated faults are seen to be late brittle features, cross-cutting the gneissic foliation (Frei & Löw 2001). Scarps are systematically facing the 'mountain side', an observation that lead earlier authors to the conclusion that the relative uplift of the valley floor could have been induced somehow by post-glacial unloading (Eckart 1957), an interpretation which seems very unlikely, at least the isostatic interpretation given by this author. An isostatic response on the scale of a small valley would indeed require ridiculously small elastic thickness values for the crust. Alternative explanations include elastic response and 'squeezing out' of weak fractured rocks between the stiff granitic massifs on either side. Whatever the mechanism, the strong pre-existing anisotropy of the gneissic rocks and the presence of a vertical zone of metasediments within the central part of the valley may also play some role in the localization of theses scarps.

THE BIG open question remains, however: are these fault scarps indicators for paleo-seismic activity within the central Alps? And if yes, could the relative quietness within zone AC_8 Ticino be regarded as a 'seismic gap' between the presently much more active zones Grisons and Valais to the east and west respectively? This question is particularly relevant in the assessment of the maximum magnitude of earthquakes. If we consider the entire length of the Rhine – Rhone lineament (>180 km), between Chur and Brig (or the Wildhorn zone), we easily have the potential fault for an M_{max} on the order of 7.5. More about this topic will be discussed later in chapter 4 about Maximum Magnitudes.
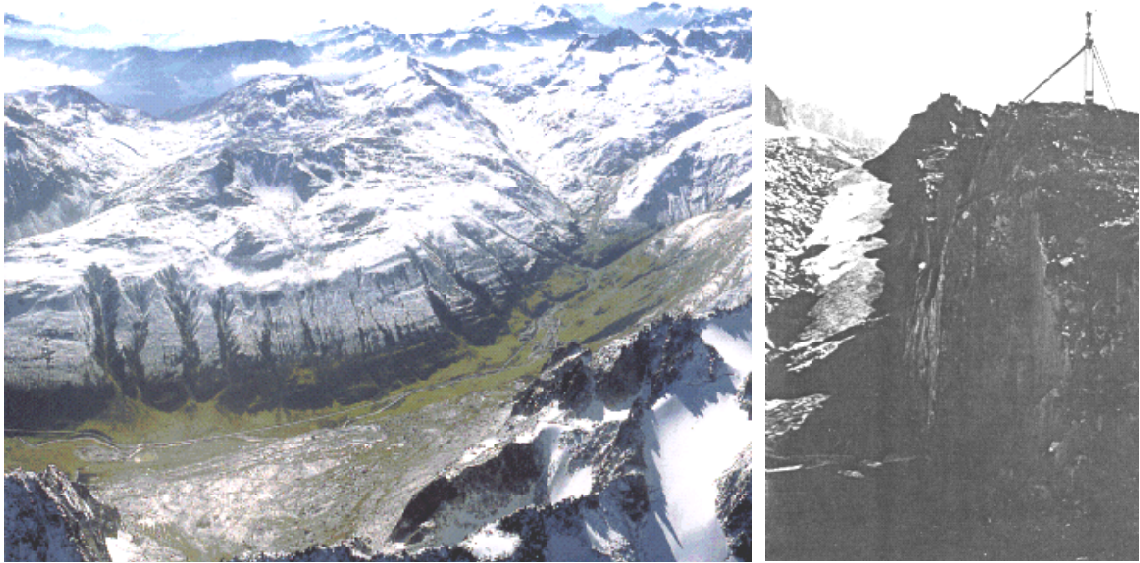
Fig. 2-42: Post-glacial fault scarps are omnipresent in a large area along, i.e. on either side of the Urseren valley

Left hand side: oblique air photograph of the Urseren Valley, looking to the SSW (calendar image, Swissair photography). Note the valley-parallel ridges in the snow covered slope facing the observer. Right hand side: close up view of a 'recent', post-glacial fault scarp with more than 5 m total vertical displacement (Funk & Gubler 1980). This scarp is from the northern flank of the Urseren Valley near Oberalp pass, looking eastward. Overall, the valley floor has risen upward with respect to the flanking mountains on either side !

2.3.7.9 AC 9 Walensee

The Walensee zone AC_9 shares similar geology and tectonics with its western neighbours Sarnen and Prealps. The motivation for a subdivision into three zones, rather than a single strike parallel long 'Alpine front zone' is motivated by the apparently higher seismic activity around Lake Luzern.

2.3.7.10 AC 10 Graubünden

The Graubünden zone AC_10 has a seismicity which resembles the Valais zone AC_6 in many respects. It hosts a large historical earthquake of intensity VIII at Chur on 4th of september 1295, listed with a Magnitude 6.5 in the PEGASOS catalogue as well as a whole series of significant earthquakes with magnitudes greater or equal to 5. Only one of these M 5 events is 'instrumental', however, on 9.8.1961 in the lower Engadine.

A seismotectonic study of Roth et al. (1992) is one of the earlier records documenting the limited thickness of the seismogenic zone, within the Alps, given as 13 km. A correlation of seismic activity with runoff (rain fall and snow melt!) has been discovered by Roth et al. (1992) for earthquakes within the topmost 5 km. Focal plane mechanisms in the central portion of Graubünden are of true extension type, with a NE-SW oriented σ_3 direction (op. cit., Fig. 6). Transitions to extensional strike slip are observed north of Chur and along the Engadine line, data quantity is very limited, however.

The seismcity within the Graubünden zone seems to be more or less distributed over a large area extending between the Rheintal north of Chur and the Engadine to the SE. From a visual inspection of the seismicity patterns, there might be some clustering of seismic activity along the Rhine valley north of Chur, as well as along the Inn Valley or 'Engadine line'. The latter is well known as a major late alpine fault cross-cutting the Austroalpine and Penninic nappe piles in sinistral strike slip with the SE block being downfaulted (Schmid & Froitzheim 1993). The Engadine line belongs to a familiy of faults which are recoginzed as responsible for some substantial stretching parallel to the strike of the alpine chain, a mechanism also referred to as 'lateral extrusion' (Ratschbacher et al. 1989, Ratschbacher et al. 1991a and 1991b). According to Schmid & Froitzheim (1993), the Engadine line would belong to an older, Oligocene generation of such extrusion-accomodating faults. To our knowlegde, reactivation of this fault in recent times has not been documented neither by geologic / geomorphologic arguments nor through any detailed seismicity study.

In a recent neotectonic study conducted in this part of the Alps by Persaud (2002) at the University of Bern (http://www.earthsci.unibe.ch/people/persaud/pages/homemira.html) a multitude of post-glacial fault scarps have been identified throughout the Bündnerland (Grisons) area. No major fault or fault zone appears from this spatial pattern, however, and any link with seismic activity is speculative at best.

2.3.7.11   AC 11 Vorarlberg

Two ENE-WSW striking large 'strike slip fault couloirs' are distinguished within the eastern Alps of the study area: the Vorarlberg zone AC_11 and the Inntal zone AC_14 (Figure 2-43). Both zones are characterized by some clustered seismic activity roughly alinged along these 'couloirs'. During the last two decades or so, many such strike slip fault lines have been identified throughout the (eastern) Alps (Ratschbacher et al. 1989).
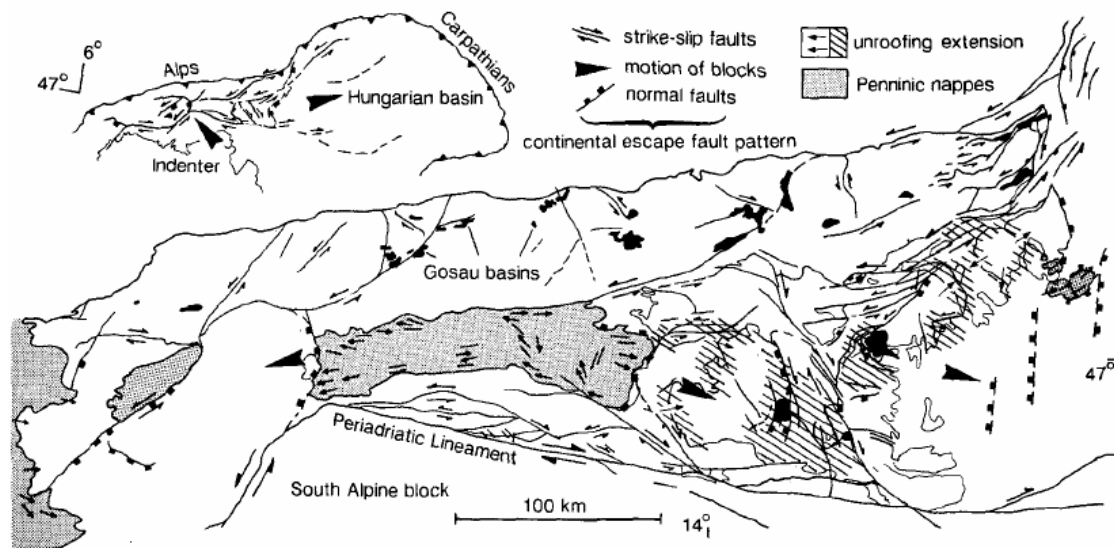
Fig. 2-43:   Escape tectonics in the Eastern Alps as proposed by Ratschbacher et al. (1989, Fig. 4) as responsible for many late alpine major fault lines such as the Engadine line, the Inntal- and Vorarlberg zones, the Brenner normal fault, Giudicarie line and Periadriatic Lineament (to mention just those mentioned in the context of our source zones)

Their significance as faults accomodating lateral, eastward extrusion of the Central Alps is now widely accepted in the tectonic community and an abundant body of literature documents the 'paleo-stress orientations' responsible for late brittle deformation in such a strike slip – lateral extrusion regime. To our knowledge, a direct, '1:1' correlation between earthquake activity and the latest mapped faults is still missing at this stage, however (Eisbacher & Brandner 1996, Eisbacher et al. 1990).

2.3.7.12   AC 12 Glorenza

This is a 'background zone', distinguished from neighbouring areas with higher seismic activity. The northern, eastern and southeastern boundaries are all motivated geologically – tectonically against WSW-ENE trending strike slip fault zones in the North and against the Giudicarie line to the SE. The limit to the west against the Grisons zone AC_10 is chosen more artificially, based entirely on the observed seismicity patterns : a straight line separating the high activity of the Bündnerland zone against the low activity of the AC_12 Glorenza zone.

2.3.7.13   AC 13 Allgäu

In contrast to the Swiss Alps, the morphologic and tectonic Alpine front in the Allgäu seems to be very quiet in terms of seismicity. Zone AC_13 is characterized through its low level of activity delimited to the south against the two strike slip fault zones Vorarlberg AC_11 and Inntal AC_14. To the north, the delimitation against the zone München SG_15 is entirely motivated by the presence of a major tectonic boundary: the Alpine front. In the seismicity pattern, this limit does not show up at all, however.

2.3.7.14   AC 14 Inntal

See section 2.3.11 for some more comments (Eisbacher & Brandner 1996, Eisbacher et al. 1990).

2.3.7.15   AC 15 Tauern

The Tauern window area has attracted a lot of attention by geologists worldwide. It is considered as a type example of 'metamorphic core complex', where highly metamorphic rocks (of amphibolite grade) have been exhumed rapidly through a combination of normal faulting, vertical extrusion and erosion (Axen et al. 1998). In this respect, the Tauern / Glorenza / Inntal area of the Eastern Alps and the Simplon fault / Valais / Wildhorn area of the Western Alps (Mancktelow 1985, 1992) share a very similar structural and tectonic history. In terms of their present day seismicity too, both 'core complexes', the Ticino – Lepontine dome of the Western Alps and the Tauern window of the Eastern Alps are very quiet themselves, but apparently surrounded by zones of higher activity. In both cases, present day activity seems to be concentrated along strike slip faults accomodating lateral extrusion (Inntal- and Wildhorn zones) but evidence for ongoing true extensional detachment faulting in the style of the former Simplon- or Brenner faults is lacking.

2.3.8   Alps Internal: AI_01 through AI_03

2.3.8.1   AI_1 Dora Maira

The transition between the Alps and the Po-plain coincides with a N-S alignment of seismicity, the so-called Piemontais seismic arc of french authors (Sue et al. 1999). On a tectonic map, such as the Structural Model of Italy (Scandone 1990), the zone of increased seismicity corresponds roughly to the eastern limit of the Dora Maira internal crystalline massif. In 3-D, however, a correlation between seismicity and the presence of the mostly hidden Ivrea body seems to make

more sense. Seismicity seems to be more or less localized along the western steep border of the Ivrea mantle indenter as identified from the gravimetric anomaly (Figure 2-44).

(Sue et al. 2002) compared the seismic activity of the Dora Maira zone, of the 'Piemontais arc' in their terminology, with the 'Briançonnais arc' and document a marked difference in b-values. They interpreted this behaviour as due to differences in earthquake depth (deeper in Dora Maira than in Briançonnais), in host rock composition (mantle vs. crustal rocks) and in fracture patterns.
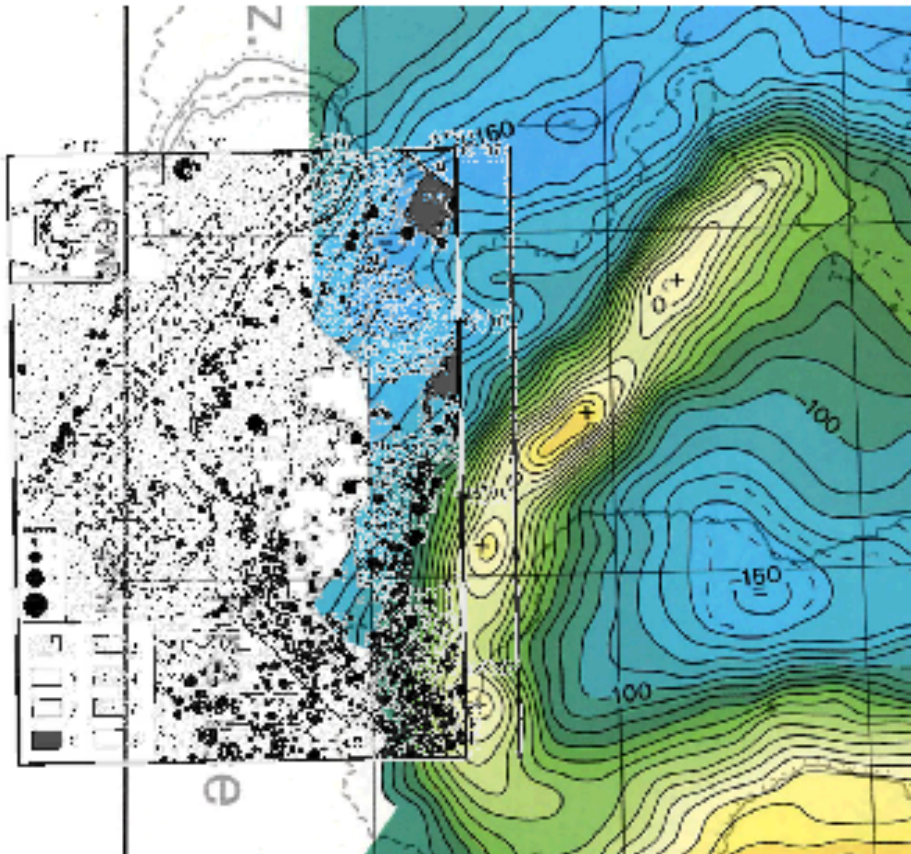
Fig. 2-44: The Ivrea body 'mantle indenter' seen as a strong positive anomaly on the Bouguer anomaly map of the European Geotraverse (Klingele et al. 1991)

Superimposed is a 'half transparent' figure of Sue et al. (1999) showing the instrumental seismicity pattern of the Western Alps with selected, well located events recorded between 1989 and 1997 and $M_L > 1$. Note the nice correspondence of this microseismicity along the western boundary of the 'Ivrea mantle wedge'.

2.3.8.2 AI_2 Alpi Sud

The Southern Alps zone AI_2 is geologically quite different from the adjacent Dora Maira zone to the SW. First of all, there is a very marked change in strike from N-S to E-W. This sharp bend at the inner arc of the Alps probably has its origin in the presence of a major hidden indenter in the form of the Ivrea body, known to be present only behind the Western Alps. The Southern Alps 'Foreland Fold and Thrust Belt' on the other hand terminates westward against the eastern flanc of the Ivrea – Strona Ceneri zone and does not have any 'cylindrical' equivalent further southwest (Schumacher 1997). Southward thrusting within the Southern Alps in general

is as young as 5 Ma, since thrust faults are at least partly sealed by Messinian sediments below the Po-plain (Figure 2-45). Locally, however (albeit quite some distance further to the east) ongoing south-ward thrusting has been documented by displaced terraces near Montebelluna as well as by a correlation between earthquake activity and hidden 'blind' thrust faults in the case of the 1976 Friuli earthquake (Aoudia et al. 2000, Poli et al. 2002).

Our zone AS_2 is limited to the north against the Insubric line, an obvious choice despite the fact that it does not seem to affect seismicity patterns at all. To the south, we choose deliberately to incorporate parts of the morphologically distinct Po-plain, in order to include potentially hidden south-vergent 'blind' thrust faults. The 'Structural model of Italy' tectonic map (Scandone 1990) also clearly indicates the polarity of the Po-plain foredeep, which is deepest adjacent to the Appennine but fairly shallow towards the Alps.
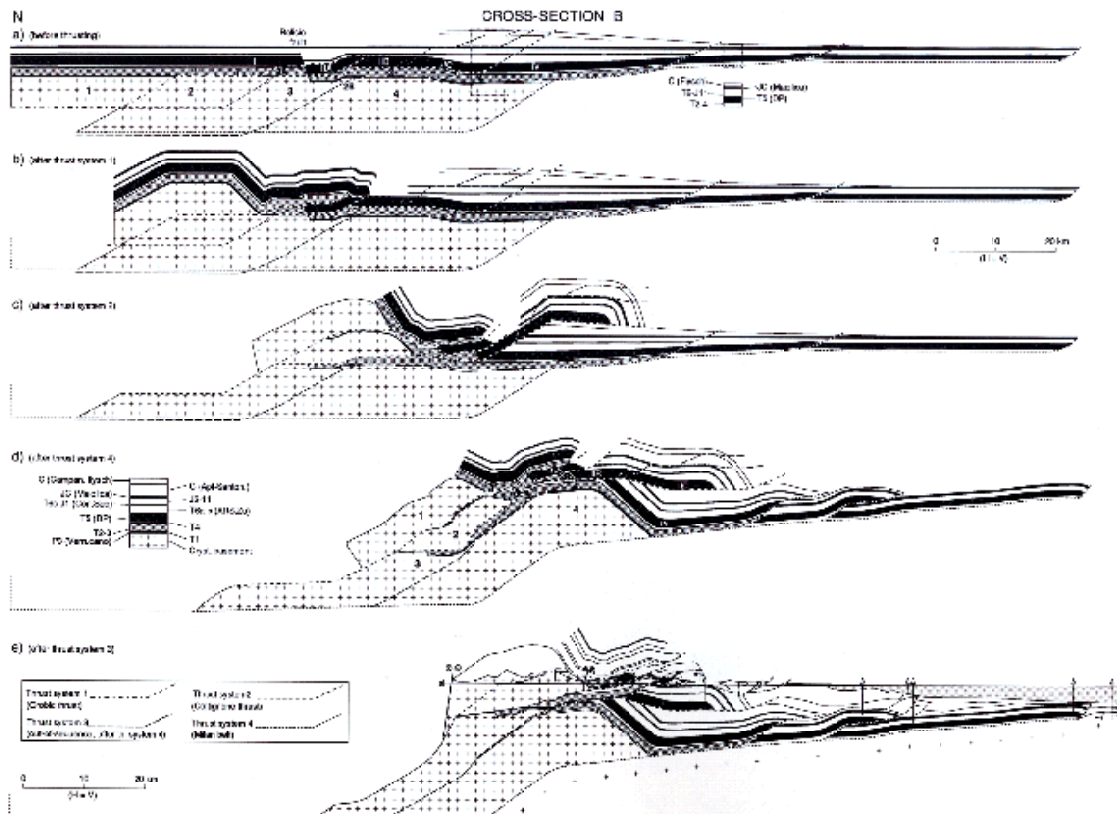
Fig. 2-45:   Kinematic evolution of the Southern Alps between the Insubric line IL and the Po-plain from Oligocene (top) to recent (bottom)

The latest, hidden shortening took place beneath the Late Miocene cover of the Po-plain where it is sealed by Messinian sediments as revealed by seismic reflection and drill hole data, from Schoenborn (1992).

2.3.8.3   AI_3 Bolzano

The most important tectonic feature of the Bolzano zone AI_3 is the Giudicarie line, limiting this zone to the NW. The Giudicarie Line is part of the Periadriatic lineament system, causing a major step (off-set) within the otherwise E-W trending Insubric line (Schmid et al. 1989). The Giudicarie line will certainly become a new focus of interest because it seems to be the surface expression of a flip in the subduction polarity as revealed by recent mantle tomographic studies (Lippitsch 2002), as shown in Figure 2-46.

This flip in subduction zone polarity comes as a big surprise! In the well established view, subduction of the European plate was southward below the Adriatic micro-plate. The flip in polarity below the eastern Alps must be a relatively recent one, it might be active since Late Oligocene / Earliest Miocene. For the same time period, southward thrusting at the southalpine front is well documented and quantified (Schoenborn 1999). In the new view, this youngest southward thrusting would now have to be considered as foreward, whereas the classical alpine front of the Eastern Alps toward the North (Bavarian Molasse basin) would become the 'back-thrust'.

This new polarity in the Alpine thrust system obviously offers a whole series of new constraints which might ultimately help explain the overall seismicity patterns in terms of ongoing plate tectonic processes. At this time however, no big 'aha' has emerged yet and we are still struggling to see the intimate relationship between crustal structure, tectonic history and present day earth-quake activity.

Given the low seismic activity within the Bolzano zone and around the Giudicarie line there is no indication for any recent re-activation of this fault system.

2.3.9   PP_1 Po-Plain

The Po-plain zone PP_1 is a composite of different tectonic areas and regimes. It encompasses parts of the Po-plain, i.e. the foredeep of the Appennines as well as frontal, north-vergent, thin skinned portions of this latter fold and thrust belt. To make things more complicated, the frontal Appennines are not a straight belt in this area, but consist in two major curvatures with a recess inbetween. The two arcs are located east of Torino 'Montferrato' and centered on Piacenza respectively. A deep recess is located south of Voghera (compare Structural Model of Italy, tectonic map, Scandone 1990).

Given this complex map scale structure one should not expect a homogeneous seismicity within this zone, where thin skin thrusting and tear faulting as well as reactivation of older, complex basement structures are to be considered. Despite all this, we did not see the need for any further subdivision of this zone, however, first of all because it is located far from the center of the study area and second because seismicity as reported in the PEGASOS catalogue for this area is rather weak and distributed. No suspect lineaments or active faults are identified within this large zone, in our zonation scheme, it can be regarded as 'back-ground'.
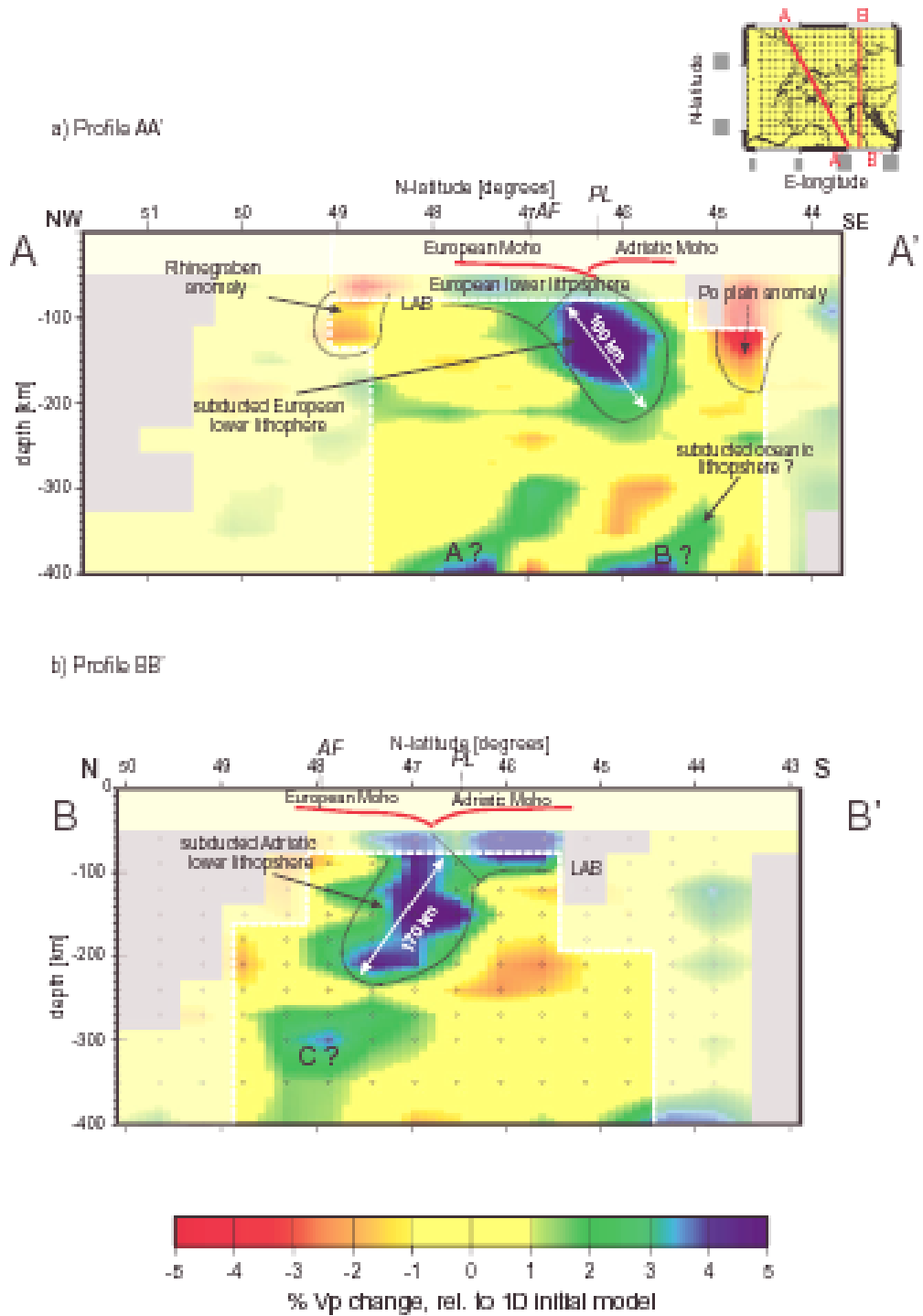
Fig. 2-46:   Two cross-sections through the upper mantle model crossing a) the central and b) the eastern Alps

Velocity variations are plotted relative to the 1D initial reference model. Areas with no resolution (no hits) are left grey, areas of critical resolution are displayed in faded colours. The crustal layers are set to zero (yellow), with Moho topography (red) extracted from 3D crustal model superimposed. Red line in inset map indicates location of profiles. From Lippitsch (2002).

2.4 Logic Trees – Alternative Source Zone Configurations

2.4.1 Large vs. small zones

As explained in detail above, we distinguish large and small zones. As a reminder, large zones have been defined on the basis of what we believe to be distinct tectonic provinces, such as the European foreland zones Eastern France and Southern Germany, separated by the Oligocene Rhine Graben. We do not understand why seismicity does not really respect this most obvious, tectonic zonation. Present day seismicity rather occurs in localized 'hot spots', in some places along known or unknown faults, but more often in ill defined regional clusters. We tried to honour these seismicity patterns through the delineation of small seismic source zones, which are defined primarily on the basis of a seismicity map, using additional regional geologic arguments, for instance in order to choose the strike direction of zone boundaries.

In our first logic branch (Figure 2-47), we consider the 'large zone only' approach as less important (0.2) than our small scale zonation, to which we give a much larger weight (0.8).

The basic issue addressed with these two alternative zonation approaches is stationarity of seismicity. In the case of large zones, the observed seismicity is smoothed with a Gaussian operator, using three different diameters for the counting circles: 5, 7.5 and 10 km respectively. The 7.5 km smoothing is our preferred model (shown in Figure 2-48) with a weight of (0.6) in comparison to smaller and larger circles (0.2 each). With this smoothing we try to anticipate variations in the expected future spatial distribution of seismicity within our large zones.

Despite the fact that this approach remains very close to the actually observed seismicity of the last 500 to 1000 years and the expectation that 'the past is a good key to the present', we prefer an alternative small zone approach in which we have more geologic reasoning built into the anticipated future seismicity. We believe to have a sufficiently good understanding of the geological past, the structural elements and the present day geo-dynamic situation of the study are to build a seismotectonic framework, expressed in our case in the form of small zones, each with its very own characteristics.
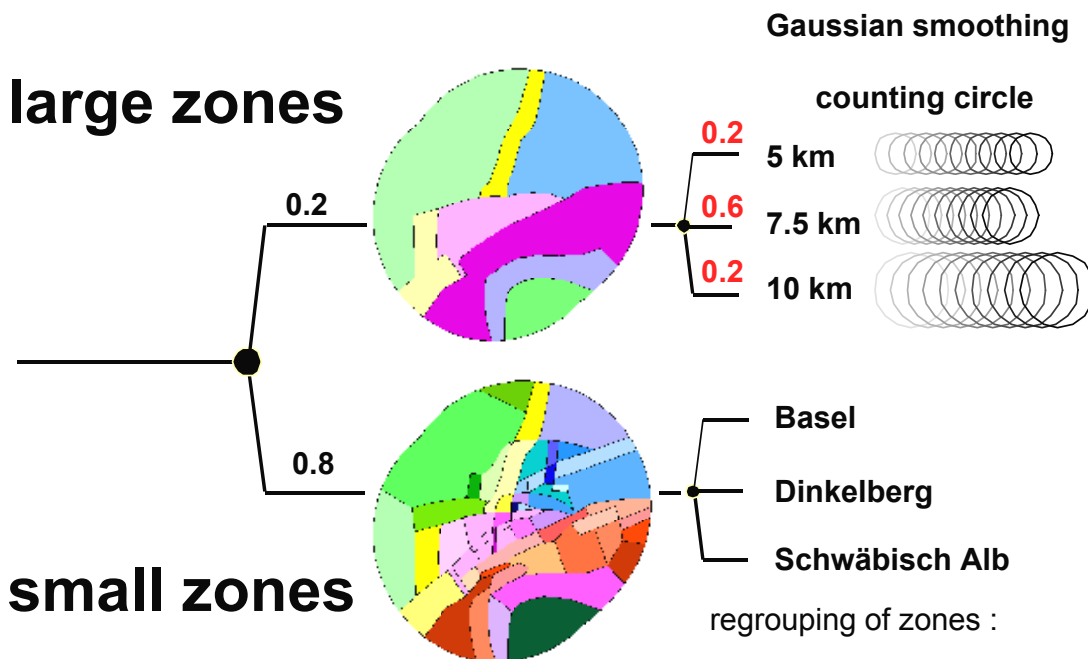
Fig. 2-47:   Master tree of EG1b
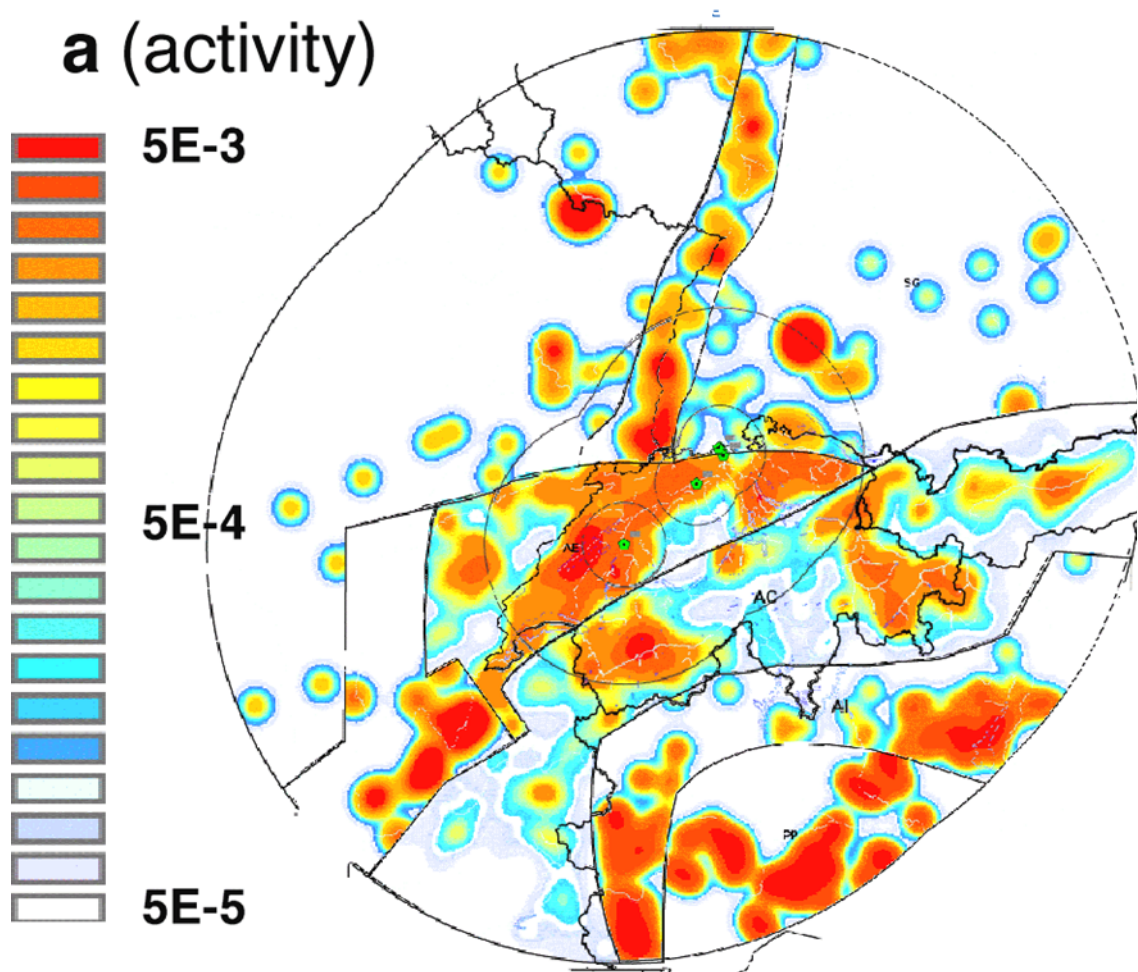
Fig. 2-48: Smoothing of the observed seismicity is conducted within each large zone independently

This example shows the smoothing with a 7.5 km Gaussian kernel (from PEGASOS TP1-SUP-0046 2002).

2.4.2 Small zone regroupings

Many of our small source zones have been defined on the basis of subtle differences in seismicity and/or geology. We take these uncertainties into account in three particular areas in which we consider several alternatives of regroupings of small zones – sequentially removing certain zone boundaries.

2.4.2.1 The Basel area: 'Rhinoceros'

Located in the middle of the study area and hosting the most important seismicity of the entire PEGASOS catalogue, the larger Basel area merits some special attention. Our considerations concern four small zones RG_1, AE_1, AE_2 and AE_13 (Figure 2-49). This regrouping straddles two tectonic provinces, the Rhine Graben (RG) to the north and the Alps External (AE) to the south. Seismicity patterns seem to disregard this subdivision despite the fact that it seems quite straightforward on a tectonic map.

In order to take this uncertainty into account, we regroup RG_1 and AE_2 into one zone and give this N-S oriented, larger Basel zone a weight of 0.25. This merged zone contains all of the

large Basel events of the PEGASOS catalogue, as well as all of the geomorphic features which have been proposed as faults responsible for the Basel 1356 earthquake. In particular, the Reinach fault straddles our zones RG_1 and AE_1. The combined RG_1 and AE_2 zone allows to host a large NNE-SSW striking Reinach type fault, cutting across both Rhine Graben filling in the north and frontal Jura folds in the south.

The largest weight (0.75 * 0.7 = 0.525) remains with a subdivision into four individual small zones. This is our preferred model for this area.

Three additional subdivisions within the Jura Fold belt are proposed, regrouping the Basel Jura (RG_1) with either the Eastern Jura (AE_2) or the Central Jura (AE_13) to the west. The most extreme case considered is the one in which the three Jura zones AE_1, AE_2 and AE_13 are grouped together in one single zone, with a very long E-W extension. Each of these regroupings receives a low weight of 0.75*0.1 = 0.075. They are all motivated by the small but extant possibility of E-W striking normal faults which could be reactivated as thrusts in a thick skinned mode or lead to the triggering of thin skinned thrusting. The subsurface geology is fairly well constrained in the eastern zone AE_2, where the presence of an E-W striking Permo-Carboniferous graben structure has been documented through reflection seismic studies of Nagra (Müller et al. 2002). The continuation of these structures futher west is not documented, but highly probable.
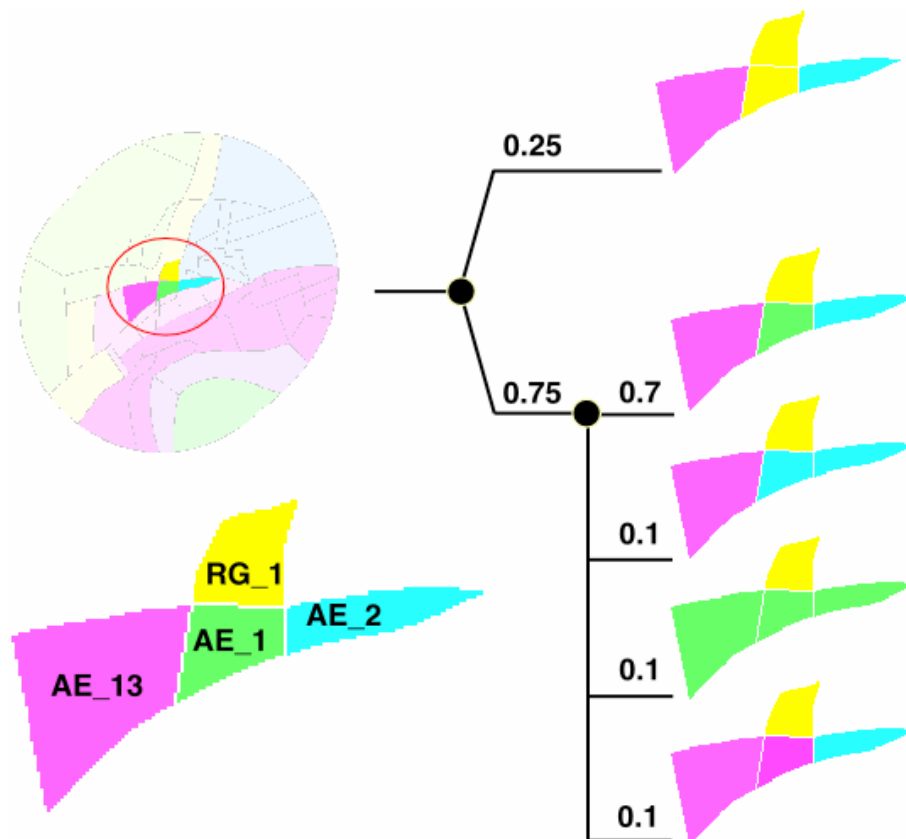
Fig. 2-49: Seismic zonation in the larger Basel area: 'the Rhinoceros'

Regroupings of two or more small zones are considered according to the tree given at the right hand side.

'Impermeable' strict boundaries

We consider all of our boundaries be it large or small zones as strict or 'impermeable' to faults. By 'impermeable' we mean that faults are not allowed to rupture across zone boundaries. Any earthquake is allowed to initiate at the very zone boundary, but will then have to propagate asymmetrically to the inside of the zone only, and it is not allowed to rupture across the boundary on the opposite side either. This may sound as a somewhat artificial condition, but we have given it consideration in choosing the location of zone boundaries. Wherever known or suspected faults are present in any one zone, the size of this zone has been carefully evaluated so as to:

a) collect all seismicity potentially stemming from this fault zone, and

b) be large enough in order to accomodate the maximum size of fault which seems geologically reasonable in this area. Uncertainties are implicitly treated by way of alternative regroupings of small zones into larger ones such as treated in the Basel Rhinoceros or the Tucan beak.

Soft boundaries for AE_2 in all cases

In all of the regroupings shown above, as well as in all models with small zones, the boundaries of zone AE_2 East Jura are to be considered as somewhat 'soft'. With this softness, we express the uncertainty in the location of zone boundaries. This is quite critical here, since AE_2 is close to three of the four power plants. Our demand is motivated by the fact that none of our boundaries is truly fixed in space by a well defined major tectonic feature. In order to express this uncertainty, we are moving the northern and southern boundaries of AE_2 in and outward by ± 5 km. We are content with having this 'softness' applied only to the source zone as provider of earthquake energy, but not for the collection of characteristic data within the zone, such as a- and b-values and M_{max}.

2.4.2.2 The Dinkelberg – Bodensee area: 'Tucan beak'

There are many small zones in the center of the study area, which all belong to the larger teconic zone of South Germany : SG_5, SG_6, SG_7 and SG_8.

The smallest zone in this family is SG_6 Leibstadt which contains KKL. Most of the choosen boundaries within this 'Tucan beak' are subject to discussion and we consider these uncertainties by removing them sequentially according to a scheme illustrated in Figure 2-50. Our regroupings can be subdivided into two categories.

In the first category, the one shown in the upper branch, the Dinkelberg zone (SG_7) remains separated from the rest of the 'beak'. This is by far our preferred solution with a weight of 0.8. The Dinkelberg area does indeed have a seismicity and structure of its own (Faber et al. 1994). The remaining boundaries, however, are rather ill defined, and in further subdivisions we give some considerations to the isolation or not of the Leibstadt zone SG_6. This small zone SG_6 Leibstadt remains isolated in two cases, each is given a weight of 0.8 * 0.2 = 0.16.

A second branch, in which the Dinkelberg is not isolated is given a lesser weight of 0.2. Three different regroupings are proposed, with a clear preference of merging Dinkelberg SG_7 with Leibstadt SG_6, while the separation between SG_8 and SG_5 is considered of lesser importance. In theory, there are more possible recombinations of zones within this group, but we do not want to explore them all! From a visual inspection of the red areas, it becomes obvious that we consider the boundary between SG_8 southern Schwarzwald and SG_5 Singen-Bodensee zone as a fairly weak boundary. Weak here is meant in the sense that we do not have any strong geologic or seismologic argument in favor of its existence. Accordingly, most of our regroupings disregard it entirely. This boundary remains in place only in two models, together they weight only (0.8 * 0.2 + 0.2 * 0.25) = 0.21.
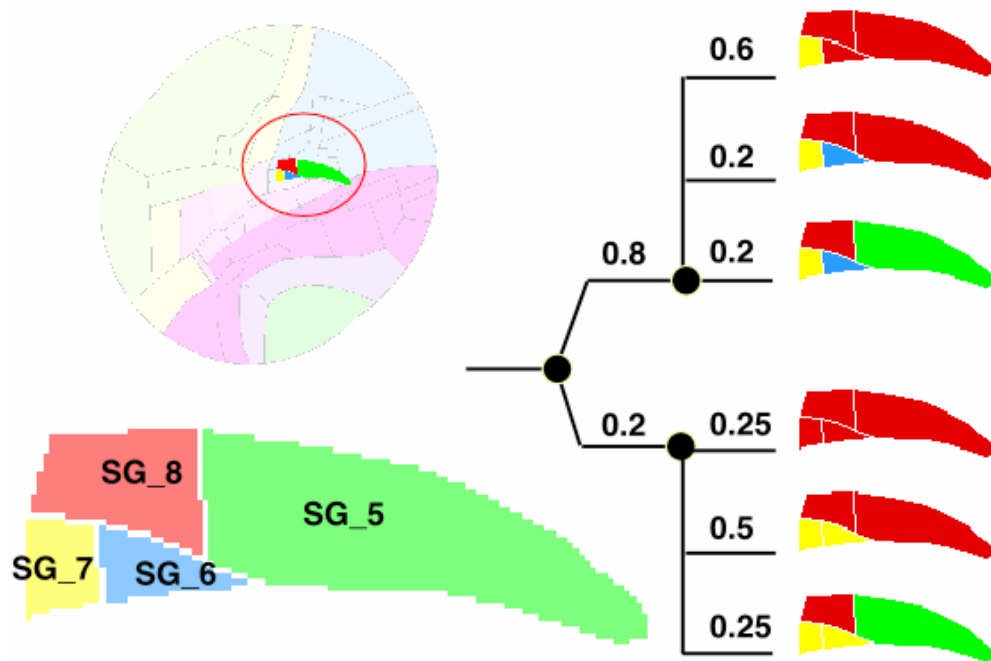
Fig. 2-50:   Seismic zonation in the Dinkelberg – Bodensee area: 'the Tucan beak'
                Regroupings small zones are considered according to the tree given at the right
                hand side.

2.4.2.3   Schwäbische Alb

The zones SG_1 and SG_2 are re-combined in to one larger N-S zone. This recombination is motivated by the historically observed high activity which has occured in SG_2, adjacent and immediately north of SG_1. This recombination allows to host a longer N-S trending strike slip fault. Such a regrouping is notably motivated by our 'impermeable' boundaries rule. In the case considered here, seismic activity is currently confined to SG_1 (Reinecker & Schneider 2002) where it seems to be localized along a N-S trending fault within the basement. The likelihood of a larger fault extending along the entire length of the recombined SG_1 and SG_2 zone is considered as small but definitely existant.

3 MAXIMUM EARTHQUAKE MAGNITUDES

Given the general nature of seismicity in all of the study area, with very few and very small seismically active faults and very low (if any) deformation rates, the discussion of maximum earthquake magnitude is very much reduced to statistical rather than geological, tectonic or geodetical argumentation. There is only very limited geologic evidence for the size of individual faults and fault zones, for fault segmentation, for maximum fault displacements and other geologically useful information that might have provided constraints on maximum earthquake Magnitudes. For a discussion of the geology of individual areal seismic sources, hypothetical faults and their size, their likelihood of being seismic at all and so on, we refer to chapters 1 and 2.

In the following, we provide an overview of the 'statistical' approaches we used in order to determine maximum earthquake magnitude distributions as well as various arguments used to apply truncations (upper limits). Initially, two alternative approaches have been considered for M_{max} distributions, the EPRI (Johnston et al. 1994) and the Kijko (Kijko & Graham 1998) approaches respectively.

In the course of our evaluations, the Kijko results have been discarded, however. The main reason was the small number of earthquakes in most of the small zones, which lead in many instances to unrealistic M_{max} values based on the Kijko method. We also clearly preferred the 'asymmetrical' EPRI-M_{max} distributions, which provide geologically acceptable M_{max} 'mode' values and long upper tails with very low probabilities towards higher M_{max} values. The Kijko approach, in comparison provides a single mean value albeit with a 1σ standard deviation – for a log-normal distribution. At some stage in our discussions, we hesitated between using Kijko values either as an alternative to the EPRI distribution or as an alternative way to determine truncation values to the EPRI-M_{max} distributions. Indeed, in many instances, the mean value of the Kijko approach turned out to lie even above an uppermost 'acceptable' M_{max} value that we determined independently based on geologic reasoning.

In order to prevent unrealistically high upper tails in the EPRI M_{max} distributions, reaching magnitudes of 8 and above, we apply truncations. We use both geological (size of individual faults and seismic source zones) and statistical arguments in order to assign ultimate upper limits to the EPRI M_{max} distributions.

3.1 EPRI approach to M_{max} distributions

In order to compensate the limited time of observation (and small size of study area) covered by the PEGASOS earthquake catalog, a comparison is made with worldwide observations of seismicity in 'stable continental' regions (Johnston et al. 1994). In this 'EPRI' approach, the observed seismicity of a limited study area is used in order to determine an adapted M_{max} distribution, based on the 'a priori' world wide distribution, corrected 'a posteriori' for the observed seismicity especially the observed maximum magnitude within each seismic source zone.

3.1.1 EPRI approach applied to 'large zones'

As a reminder, our group EG1b considers large and small seismic source zones. The large zones have been choosen based on large scale tectonic arguments such as crustal structure, tectonic history, and most important, their role in Neogene alpine tectonics.

In comparison with criteria used in the EPRI study (Johnston et al. 1994), it appears that only two of our large source zones fit the definition of non-extended, 'stable continental' crust, namely East France (EF) and South Germany (SG). All the other large zones have suffered some complex, recent tectonics, including Oligocene extension in the Rhine Graben (RG) and Bresse Graben (BG) and/or alpine collision from the Eocene onward in all of the Alpine zones

(AE, AC, AI) and the Po-plain (PP). All of these more tectonized zones are therefore compared with 'extended continental crust' of the EPRI study (Figure 3-1).

A preliminary set of posterior M_{max} distributions has been calculated by Proseis AG (PEGASOS TP1-SUP-0049 EPRI Mu Distributions for Large Zones, 18.12.2002). Input data for these calculations were provided by G. Grünthal in the form of data tables with a and b values – which will be discussed in the following chapter 4. In the final PEGASOS EG1-HID-0033_EG1b in Appendix 1 a revised set of a and b values led to slightly different M_{max} distributions too.
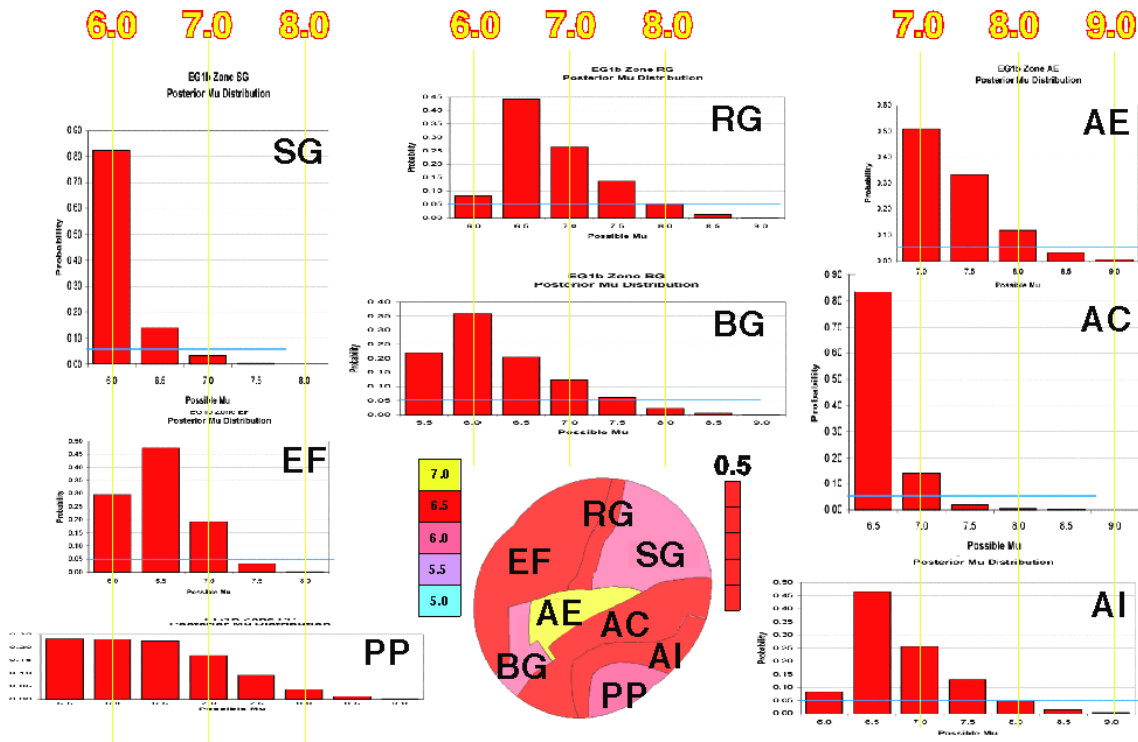
Fig. 3-1:   Posterior Mu distributions calculated using the EPRI approach for the eight large seismic source zones, their configuration is shown in the center bottom, color coded for M_{max} mode of the posterior EPRI distribution, legend to the left

Horizontal scale of histograms is earthquake magnitude. For comparison between the different zones, vertical yellow lines have been added. Vertical scale is probability, scale is given as a red bar at the right hand side of large scale zonation scheme. Thin blue lines are drawn horizontally at p = 0.05. (Attention: this figure does not show the latest Mu distributions, it has been drawn using a preliminary set of values – available in January 2003; the final PEGASOS EG1-HID-0033_EG1b (Appendix 1) has slightly different values!, but there is no major change in tendencies).

The posterior M_{max} distributions for all of our large zones are shown in Figure 3-1. For a comparison between different zones, the histograms produced by Prosesis have been aligned along Magnitudes 6, 7, 8, (9) as well as vertically squeezed to variable degrees, in order to have a common vertical scale for probability. Peripheral zones SG, EF and PP are shown at the left hand side of the figure, the Rhine- and Bresse Graben zones are in the middle, while the Alpine zones are shown at the right hand side. From this comparison, it appears clearly, that the External Alps zone AE has the highest M_{max} mode at 7.0 with a probability of 0.5 and an upper tail reaching magnitude 8.0. This is easily explained by the fact that the largest earthquake of the catalog, the Basel 1356 event, lies in this Alps External zone.

3.1.2   EPRI approach applied to 'small zones'

Posterior Mu distributions according to the EPRI approach have also been calculated for each individual small zone as well as for regroupings of zones used in alternative source zone configurations such as the 'Rhinoceros', the 'Tucan beak' and the 'Schwäbische Alb – Stuttgart' combinations. Many of these small zones have very low seismicity. Input data (b - values) were therefore collected from larger areas, including two or more small source zones with similar characteristics, but always from within the same parent 'large zone' (SG, EF, AE, AC, AI, PP, RG, BG). Note that these regroupings were used only for the purpose of calculating common b-values, a-values were always determined for each small zone individually. This issue will be discussed in more detail in chapter 4. Posterior Mu distributions have been calculated by Proseis AG (PEGASOS TP1-SUP-0049 EPRI Mu Distributions for small zones, 13.012.003), based on input data provided by G. Grünthal in the form of a data table, which will be discussed in the next chapter 4.

The highest probability ('mode') of posterior Mu distributions obtained for each small zone is shown graphically in Figure 3-2. From this figure it appears that the EPRI approach yields M_{max} values in the range 6.0 to 6.5 for most small zones. Notable exceptions are the Basel area AE_1 with an M_{max} value of 7.0 (because it contains the 1356 M = 6.9 earthquake).
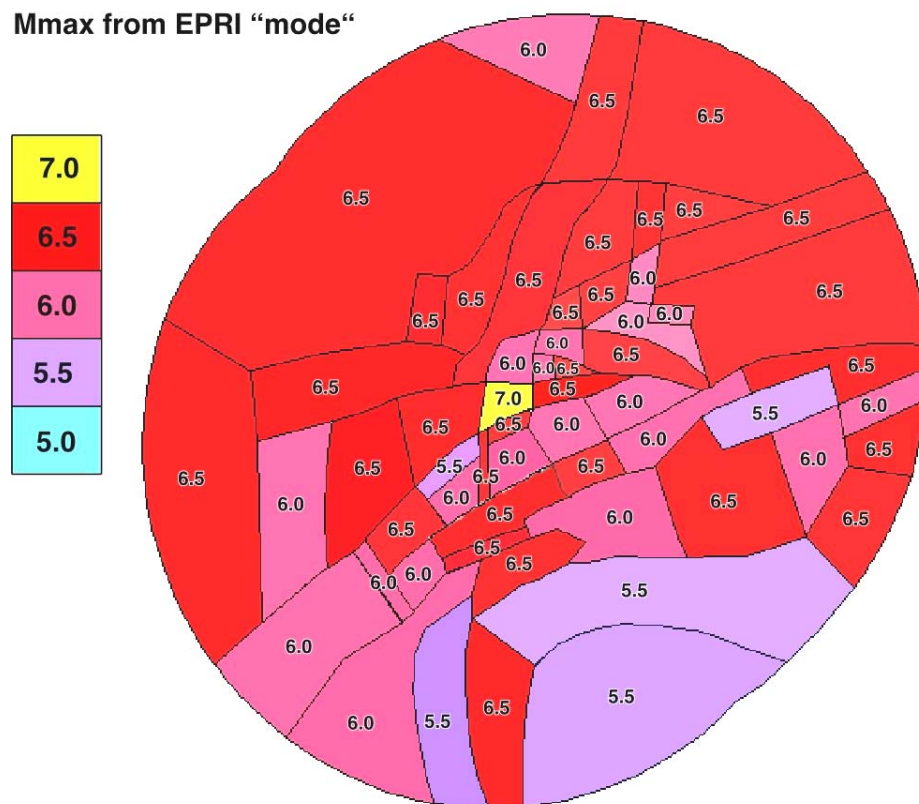
Fig. 3-2: M_{max} according to EPRI approach within small zones

Colour coded according to bar given at left hand side. The values shown here correspond to the highest probability (mode) of the EPRI posterior Mu probability distributions. Note the outstandingly high value of M_{max} = 7 observed in AE_1, Basel (yellow) which contains the Basel earthquake (M_{max} observed = 6.9).

 Full probability distribution of EPRI approach posterior Mu distributions for all the small zones are tablulated below in Table 3-1.

Tab. 3-1:   Seismic source maximum magnitude distributions

Source	Discrete Maximum Magnitude Distribution											
	Mu	Weight	Mu	Weight	Mu	Weight	Mu	Weight	Mu	Weight	Mu	Weight
Large Zones												
AC	6.5	0.880	7.0	0.120								
AE	7.0	0.535	7.5	0.303	7.8	0.162						
AI	6.0	0.088	6.5	0.490	7.0	0.270	7.5	0.126	7.9	0.026		
BG	5.5	0.232	6.0	0.377	6.5	0.215	7.0	0.130	7.5	0.045		
EF	6.0	0.311	6.5	0.422	6.8	0.215	7.2	0.052				
PP	5.5	0.144	6.0	0.274	6.5	0.265	7.0	0.167	7.3	0.087	7.6	0.062
RG	6.0	0.087	6.5	0.466	7.0	0.234	7.3	0.131	7.7	0.082		
SG	6.0	0.796	6.3	0.165	6.7	0.039						
Small Zones												
AC01	6.0	0.442	6.5	0.293	7.0	0.166	7.4	0.098				
AC02	5.5	0.626	6.0	0.289	6.5	0.072	6.8	0.013				
AC03	5.5	0.196	6.0	0.298	6.5	0.202	6.8	0.304				
AC04	6.5	0.340	6.8	0.310	7.2	0.350						
AC05	6.0	0.279	6.5	0.341	6.8	0.161	7.1	0.219				
AC06	6.5	0.506	6.8	0.254	7.1	0.240						
AC07	6.0	0.100	6.5	0.448	6.8	0.452						
AC08	5.5	0.125	6.0	0.275	6.5	0.223	6.8	0.145	7.1	0.232		
AC09	5.5	0.330	6.0	0.331	6.5	0.192	7.0	0.097	7.3	0.049		
AC10	6.5	0.314	6.8	0.379	7.2	0.306						
AC11	5.5	0.408	6.0	0.323	6.5	0.138	6.8	0.079	7.2	0.052		
AC12	5.5	0.139	6.0	0.286	6.5	0.220	6.8	0.159	7.2	0.195		
AC13	5.5	0.107	6.0	0.263	6.5	0.228	6.8	0.152	7.1	0.251		
AC14	5.5	0.167	6.0	0.296	6.5	0.211	6.8	0.130	7.1	0.195		
AC15	5.5	0.112	6.0	0.267	6.5	0.280	7.0	0.341				
AE01	6.8	0.128	7.1	0.872								
AE02	5.5	0.119	6.0	0.273	6.5	0.277	7.0	0.175	7.3	0.156		
AE03	5.5	0.216	6.0	0.316	6.5	0.239	7.0	0.133	7.3	0.096		
AE04	5.5	0.134	6.0	0.278	6.5	0.221	6.8	0.142	7.1	0.225		
AE05	5.5	0.118	6.0	0.272	6.5	0.225	6.8	0.147	7.1	0.237		
AE06	5.5	0.125	6.0	0.275	6.5	0.224	6.8	0.166	7.2	0.210		
AE07	5.5	0.116	6.0	0.271	6.5	0.278	7.0	0.177	7.3	0.158		
AE08	5.5	0.387	6.0	0.341	6.5	0.170	7.0	0.078	7.3	0.024		
AE09	5.5	0.141	6.0	0.286	6.5	0.219	6.8	0.139	7.1	0.215		
AE10	5.5	0.118	6.0	0.272	6.5	0.278	7.0	0.176	7.3	0.157		
AE11	5.5	0.125	6.0	0.275	6.5	0.275	7.0	0.173	7.3	0.153		
AE12	5.5	0.116	6.0	0.264	6.5	0.277	7.0	0.214	7.5	0.130		
AE13	5.5	0.102	6.0	0.259	6.5	0.283	7.0	0.184	7.3	0.172		
AI01	6.0	0.136	6.5	0.584	7.0	0.182	7.3	0.072	7.6	0.026		
AI02	5.5	0.734	6.0	0.206	6.3	0.049	6.6	0.011				
AI03	5.5	0.094	6.0	0.364	6.5	0.330	6.8	0.159	7.1	0.053		

Source	Discrete Maximum Magnitude Distribution											
	Mu	Weight	Mu	Weight	Mu	Weight	Mu	Weight	Mu	Weight	Mu	Weight
BG01	5.5	0.135	6.0	0.279	6.5	0.271	7.0	0.168	7.3	0.087	7.6	0.060
BG02	5.5	0.184	6.0	0.325	6.5	0.243	7.0	0.167	7.5	0.081		
EF01	6.0	0.319	6.5	0.498	7.0	0.183						
EF02	5.5	0.099	6.0	0.367	6.5	0.326	6.8	0.157	7.1	0.052		
EF03	5.5	0.098	6.0	0.366	6.5	0.360	6.9	0.177				
EF04	5.5	0.102	6.0	0.367	6.5	0.324	6.8	0.156	7.1	0.051		
EF05	5.5	0.098	6.0	0.365	6.5	0.327	6.8	0.158	7.1	0.052		
EF06	5.5	0.115	6.0	0.377	6.5	0.375	7.0	0.133				
PP01	5.5	0.154	6.0	0.278	6.5	0.261	7.0	0.163	7.3	0.085	7.6	0.058
RG01	5.5	0.158	6.0	0.306	6.5	0.252	7.0	0.284				
RG02	6.0	0.094	6.5	0.480	7.0	0.270	7.5	0.156				
RG03	5.5	0.115	6.0	0.267	6.5	0.278	7.0	0.178	7.3	0.093	7.6	0.069
SG01	6.0	0.751	6.5	0.205	6.8	0.044						
SG02	5.5	0.095	6.0	0.364	6.5	0.330	6.8	0.159	7.1	0.053		
SG03	5.5	0.059	6.0	0.459	6.5	0.309	6.8	0.173				
SG04	5.5	0.121	6.0	0.295	6.3	0.292	6.7	0.293				
SG05	5.5	0.106	6.0	0.371	6.5	0.322	6.8	0.201				
SG06	5.5	0.094	6.0	0.362	6.5	0.330	6.8	0.214				
SG07	5.5	0.096	6.0	0.278	6.3	0.261	6.6	0.365				
SG08	5.5	0.096	6.0	0.278	6.3	0.261	6.6	0.365				
SG09	5.5	0.094	6.0	0.363	6.5	0.329	6.8	0.214				
SG10	5.5	0.094	6.0	0.363	6.5	0.363	6.9	0.179				
SG11	5.5	0.103	6.0	0.368	6.5	0.323	6.8	0.155	7.1	0.051		
SG12	5.5	0.094	6.0	0.362	6.5	0.330	6.8	0.160	7.1	0.055		
SG13	5.5	0.094	6.0	0.363	6.5	0.362	6.9	0.181				
SG14	5.5	0.094	6.0	0.363	6.5	0.362	6.9	0.181				
SG15	5.5	0.096	6.0	0.364	6.5	0.328	6.8	0.158	7.1	0.052		
Regrouping of Small Zones												
SG5_6_7_8	5.5	0.112	6.0	0.374	6.5	0.317	6.8	0.150	7.1	0.047		
SG5_6_8	5.5	0.113	6.0	0.374	6.5	0.317	6.8	0.149	7.1	0.047		
SG5_8	5.5	0.113	6.0	0.374	6.5	0.317	6.8	0.149	7.1	0.047		
SG6_7	5.5	0.097	6.0	0.365	6.5	0.361	6.9	0.177				
RG1_AE1	7.0	0.381	7.3	0.619								
AE1_13	7.0	0.547	7.5	0.453								
AE1_2	7.0	0.441	7.3	0.294	7.6	0.265						
AE1_2_13	7.0	0.548	7.5	0.299	7.8	0.153						
SG1_2	6.0	0.747	6.5	0.206	6.8	0.046						

Out of the three areas with alternative source zone recombinations ('Tucan beak', 'Rhinoceros', Schwäbische Alb), we have chosen to illustrate here the all important Basel area ('Rhinoceros'), where the consequences of alternative source zone combinations on the M_{max} EPRI-distributions is quite dramatic as shown in Figure 3-3 below.

As expected, the posterior EPRI M_{max} probability distributions are heavily influenced by the largest observed M_{max} within each source zone. Any combination of small source zones which contains the AE_1, Basel zone, with the observed M = 6.9 1356 earthquake, has a mode of

M = 7 and invariably an important upper tail. Note that probabilities for magnitude M = 8 are greater than 0.05 in all cases!

Thin blue lines have been added in Figure 3-3, in order to visualize truncations, as will be discussed in the next chapter. Horizontal blue lines are drawn at p = 0.05. Vertical blue lines are drawn at variable magnitude values, determined to the tenth of a Magnitude step, as determined from the maximum size of fault which could possibly be hosted within any zone combination.
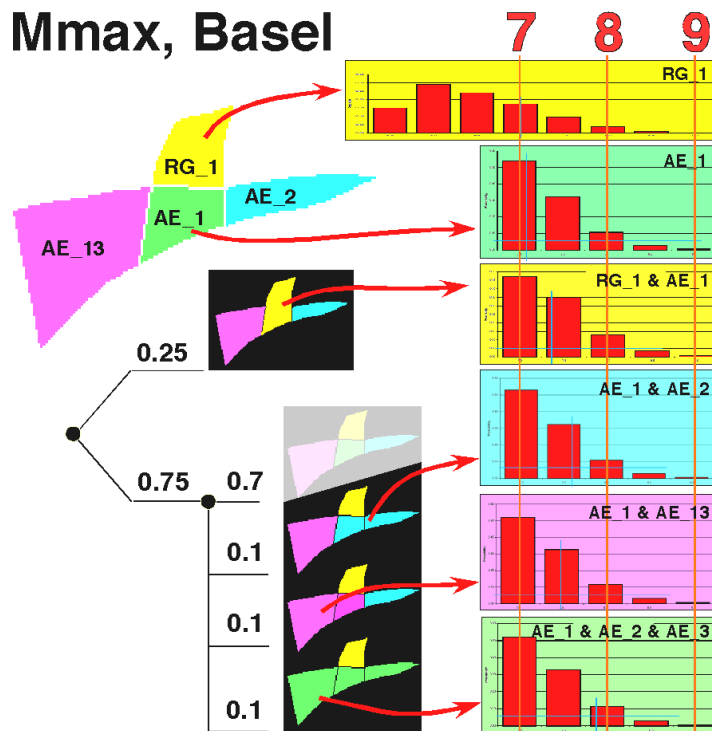
Fig. 3-3:   EPRI M_{max} distributions in small zones and groups of small zones in the Basel area

Note that colours are used solely for the purpose of identification of zones and groups of zones, they have no significance in terms of Magnitude). Original histograms (from PEGASOS TP1-SUP-0049) have been re-scaled in order to align Magnitude (x-axis) and probabilities (y-axis). Note that AE_1 is the zone that contains the Basel 1356, M = 6.9 earthquake.

3.2   Kijko's Approach to M_{max} (by A. Cisternas)

3.2.1   Introduction

The probabilistic evaluation of M_{max} in a region has been studied by Kijko & Graham (1998), by comparing two methods applied to a synthetic sequence of seismic events: the method of Tate and Pisarenko (Tate 1959, Pisarenko et al. 1996) and that of Kijko and Sellevoll (Kijko & Sellevoll 1989). Their test shows that the Kijko-Sellevoll method is more reliable. This method is designed to combine the positive aspects of two popular techniques of seismic hazard evaluation: The 'deductive' and the 'historical' ones. The Kijko-Graham paper calls it 'Procedure II' or 'advanced method'. This procedure is based on a comparison of the largest observed magnitude, and the maximum expected magnitude within a time interval. Since the authors

claim that the integral expressions for M_{max} cannot be obtained analytically, the formulae given in the paper are the result of two approximations:

1. Cramer's approximation (Cramer 1948) and
2. an approximation to the Exponential Integral.

We show below that the given approximation to the exponential integral is incomplete, and that this fact is crucial in our case, leading to wrong estimations of M_{max}. On the other hand we show that we can obtain exact analytical expressions for M_{max}, and that, in our case, Cramer's approximation (Cramer 1948) gives very good results in comparison.

3.2.2   Application to PEGASOS

The PEGASOS application of Kijko's method to the evaluation of maximum magnitude in a region is based on the 'a priori' knowledge of an observed maximum magnitude M_{max}^{obs} in that region during a time interval T, containing n earthquakes of magnitudes larger than M_{min}.

The estimation of M_{max} is obtained in equation (33) of Kijko & Graham (1998):

a) $$M_{max} = M_{max}^{obs} + \int_{Mmin}^{Mmax} [F_M(m/M_{max})]^n\, dm = M_{max}^{obs} + A \qquad (33)$$

Here, Kijko & Graham (1998) indicate that this integral can only be evaluated numerically, and they propose an analytical approximation, which they call Cramer's approximation (Cramer 1948). Indeed, Cramer's approximation corresponds to the well known one of the exponential function:

$$[1 - x/n]^n \sim \exp(-x); \qquad \text{for } |x| << n.$$

Namely, that if

$$\alpha = \beta\,(m - M_{min}),$$

and

$$\alpha_m = \beta\,(M_{max} - M_{min}),$$

we have:

$$[F_M(m/M_{max})]^n = [\{1 - \exp(-\alpha)\}/\{1 - \exp(-\alpha_m)\}]^n \sim$$
$$\sim \exp\{-n(1 - e^{-\alpha})/(1 - e^{-\alpha m})\}$$

which is the form in which they use Cramer's approximation (Cramer 1948).

But we can use directly the left side of these expressions within the integral of equation (33) of Kijko & Graham (1998) to obtain exact expressions after integration:

$$A = \gamma^n\,[-\log(1 - 1/\gamma) - \{1/\gamma + 1/(2\gamma^2) + \ldots + 1/(n\gamma^n)\}]/\beta$$

where

$$\gamma = 1 / \{1 - \exp(-\alpha_m)\},$$

and

$$M_{max} = M_{max}{}^{obs} + A$$

It is convenient to recall that the power series for the natural logarithm is slowly convergent when $1/\gamma$ is not small, so that there is a significant difference between the log and the sum.

b) The results obtained below are the approximate ones, and they are mainly based on equations (45) and (46) of Kijko & Graham (1998), which are obtained after Cramer's approximation by using an additional approximation to the exponential integral:

$$M_{max} = M_{max}{}^{obs} + [Ei(Tz2) - Ei(Tz1)]/beta/\exp(-Tz2) + M_{min}*\exp(-n) \qquad (45)$$

$$= M_{max}{}^{obs} + A$$

$$Var(M_{max}) = sigma^2 + A^2 \qquad (46)$$

Here $Ei(x)$ is the exponential integral, $beta = b*\log(10)$, Tz1 is related to M_{min} and Tz2 to $M_{max}{}^{obs}$:

$$Tz1 = n/[1 - \exp(-\beta*\Delta M)];$$

$$Tz2 = n/[\exp(\beta*\Delta M) - 1];$$

$$\Delta M = M_{max}{}^{obs} - M_{min}$$

The variance $Var(M_{max})$, is the square of sigma1, and increases with increasing A, namely, with the difference between M_{max} and $M_{max}{}^{obs}$.

a) Kijko proposes the following approximation to the $Ei(x)$ function which is valid only for $x \geq 1$:

$$Ei(x) \sim \exp(-x) * [(x^2 + a1*x + a2)/(x^2 + b1*x + b2)]/x$$

where

$$a1 = 2.334733;$$

$$a2 = 0.250621;$$

$$b1 = 3.330657;$$

$$b2 = 1.681534.$$

b) Since we have in some cases very small values of x, we need to have an approximation to $Ei(x)$ that is good to six decimal places for $0 < x < 1$. We have used the following one:

$$Ei(x) \sim -0.577218 - \log(x) +$$

$$+ x * (1 - x*(1/4 - x*(1/18 - x*(1/96 - x*(1/600 - x*(1/4320 - x/35280))))))$$

3.2.3   Kijko applied to large zones

First we show the evaluation for the larger zones. The values of M_{max} are calculated for two cases: $M_{min} = 4.0$ and $M_{min} = 3.5$ (Table 3-2). In this way we try to see the effect of M_{min} on the evaluation, and secondly we try to see the stability of the results. The results show that the values of M_{max}, and their variances, are in general a little larger for $M_{min} = 3.5$, than for $M_{min} = 4.0$, independently of the b-value. In particular, there is an increase of M_{max} (from 6.857 to 7.172) for zone EF. This continues to be true, even if we have corrected the approximation to $Ei(x)$ proposed by Kijko & Graham (1998), which is not a good one for very small values of x. We have now two zones ($x \geq 1$ and $0 < x < 1$) for $Ei(x)$ with approximations that are good to the sixth decimal place. The comparison between Cramer's approximation and the exact values gives very little differences in M_{max}, of the order of 0.012 in the worst case (see Figure 3-4).
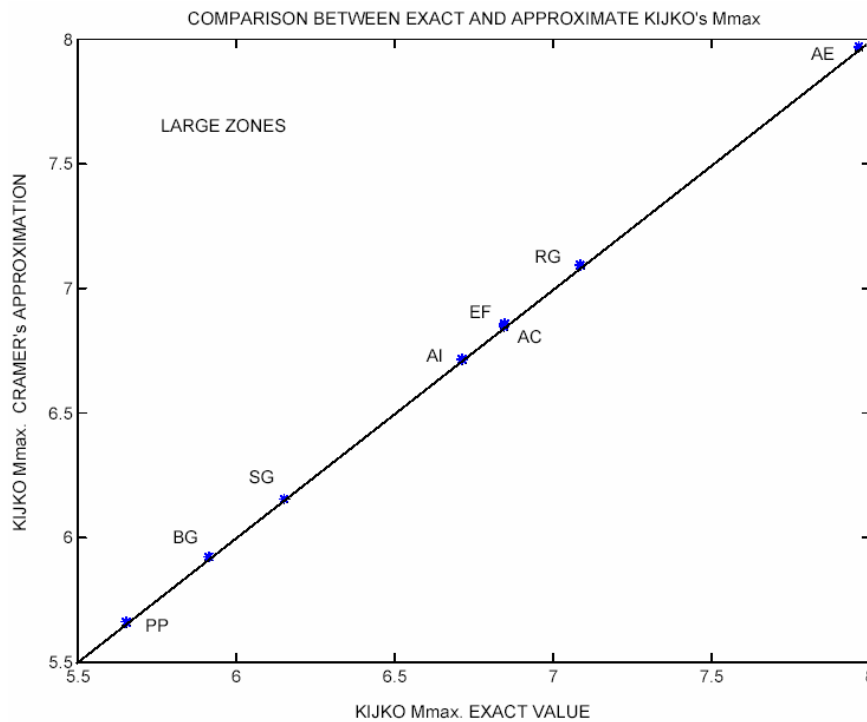
Fig. 3-4: M_{max} values determined for the large zones using two different methods

3.2.4   Comparison with EPRI approach

The Kijko results for M_{max} ($M_{min} = 4.0$), as shown in Figure 3-7, can be compared with the most likely ones produced by the EPRI method for the large zones (PEGASOS TP1-SUP-0049). We have to underline that the EPRI values are discretized at steps of magnitude of 0.25, what roughens the comparison. The values of M_{max} are not too different, except for those corresponding to the largest values (Figure 3-5). Nevertheless, we should remark that the Kijko values for M_{max} are all below magnitude 8 now. This is an effect of the correct approximation to M_{max}, because we have corrected the approximations to $Ei(x)$ (Kijko & Graham 1998, page 20, formula 41) and Cramer's approximation is close to the exact values of M_{max}. Indeed, the values for PP, BG, SG, EG, AC and EF are very similar. It is somewhat different for RG, and very different for AE (the Kijko values being larger).

Tab. 3-2:   Kijko analysis of PEGASOS seismicity applied to large zones

Exact values of Maximum Magnitude using M_{min} = 4.0 top and M_{min} = 3.5, bottom.

Zone	$M_{max}{}^{obs}$	M_{min}	n	sigma	b	M_{max}	Sigma1	Sigma2
M_{min} = 4.0								
AC	6.5	4.0	117.	0.25	0.867	6.844598	0.425732	0.344598
AE	6.9	4.0	39.	0.25	0.956	7.965095	1.094042	1.065095
AI	6.2	4.0	60.	0.25	1.057	6.712982	0.570658	0.512982
BG	5.6	4.0	16.	0.25	0.737	5.912125	0.399902	0.312125
EF	6.0	4.0	15.	0.25	1.164	6.845493	0.881680	0.845493
RG	6.2	4.0	23.	0.25	1.165	7.085052	0.919684	0.885053
PP	5.3	4.0	15.	0.25	1.184	5.652421	0.432089	0.352421
SG	5.8	4.0	42.	0.25	1.037	6.150852	0.430810	0.350852
M_{min} = 3.5								
AC	6.5	3.5	391.	0.25	0.867	6.801948	0.392011	0.301948
AE	6.9	3.5	112.	0.25	0.956	7.986622	1.115010	1.086622
AI	6.2	3.5	74.	0.25	1.057	7.013209	0.850770	0.813210
BG	5.6	3.5	16.	0.25	0.737	6.152649	0.606565	0.552649
EF	6.0	3.5	22.	0.25	1.164	7.164074	1.190617	1.164074
RG	6.2	3.5	55.	0.25	1.165	7.242312	1.071875	1.042313
PP	5.3	3.5	20.	0.25	1.184	5.917947	0.666602	0.617946
SG	5.8	3.5	114.	0.25	1.037	6.198474	0.470405	0.398474

Another way to compare Kijko's and EPRI's results is to use the average value of M_{max} produced by EPRI, instead of the most likely one. The results are seen in Figure 3-6. The largest changes are seen for the extreme cases, namely the PP and AE regions. The AE average EPRI M_{max} increases to 7.4 (the most likely one is 7.0), and moves closer to the diagonal. The PP average EPRI M_{max} is now 6.4, while the most likely one was 5.7.
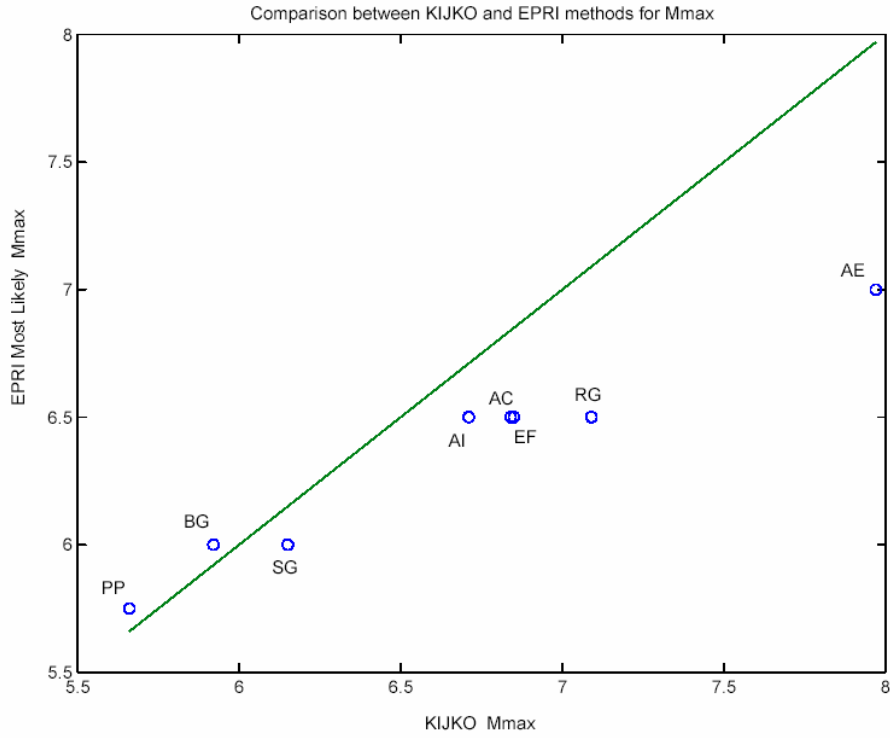
Fig. 3-5:   EPRI vs. Kijko for large zones, comparison of the Kijko M_{max} value with most likely 'mode' M_{max} value obtained obtained with EPRI approach
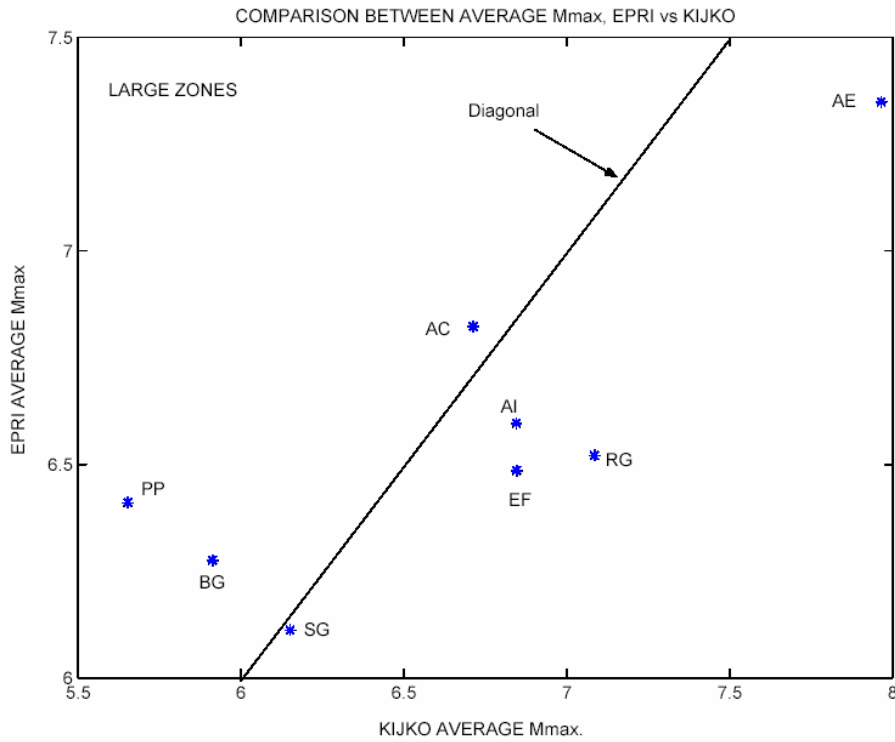
Fig. 3-6:   EPRI vs. Kijko for large zones, comparison of the average Kijko M_{max} value with average M_{max} value obtained obtained with the EPRI approach
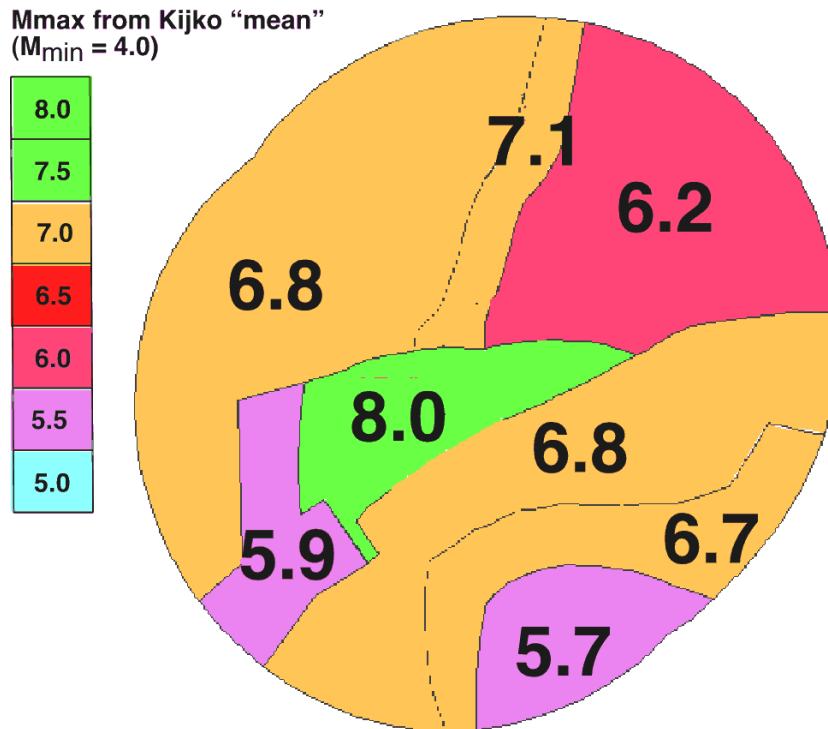
Fig. 3-7: M_{max} values for large zones using the Kijko method (mean values, $M_{min} = 4$)

3.2.5 Effect of the 'b-value' and of 'n'

We also tried to examine the effect of the variations in the b-value, and of n, the number of earthquakes, on the estimations of M_{max}. Indeed, the b-values for large zones are between 0.737 and 1.184, and the values of 'n' for large zones vary between 15 and 117 when $M_{min} = 4.0$. For the case in which $M_{min} = 3.5$ the value of 'n' varies between 16 and 391. For small zones $11 < n < 42$.

In order to have a feeling for the dependency of M_{max} on the external parameters, we varied the b-values and n, in two extreme zones: AE (large M_{max}) and PP (small M_{max}). The reason for this is that the b-values have been taken to be those of the larger zones, without errors, and the value of n is determined by the selection of the geometry of the zones. But the important point is to see how Kijko's method affects the estimation of M_{max} for different values of 'b' and 'n'.

The effect of the number of earthquakes, n, is given in Figures 3-8 and 3-9. The variation of M_{max} is very large for small values of n, and diminishes as n increases. This explains the uncertainty of M_{max} for n small. It is also clear that the value of $M_{max} = 7.97$ for the AE zone (Figure 3-8) is strongly dependent on the relatively large number of events in that zone (n = 39). A similar behaviour is seen in Figure 3-9 for zone PP, but the variation is smaller, only 0.3 of a unit of magnitude. In short, small values of n give high values of M_{max} and strongly varying. Large values of n give rather stable smaller values of M_{max}

The effect of the b-value is given in Figures 3-10 and 3-11. We can see that M_{max} grows almost linearly with the b-value within the chosen interval. In the case of the large zone AE (the one with the largest M_{max}) M_{max} may vary by half a magnitude unit. In the case of the large zone PP, which has only moderate seismicity, the variation may be 0.2 of a unit of magnitude.
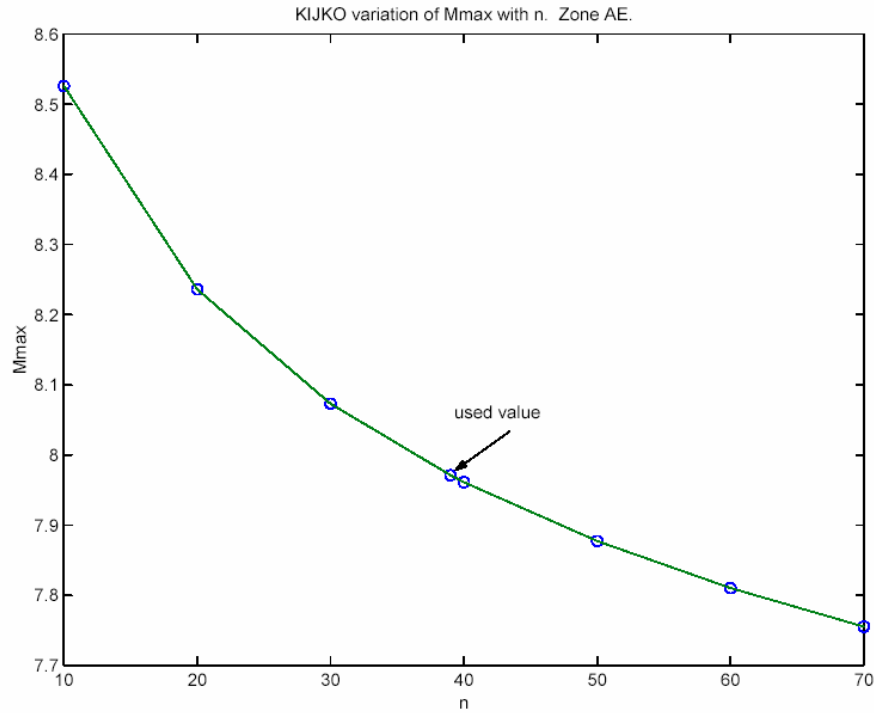
Fig. 3-8:   The effect of number of earthquakes on M_{max} using Kijko's method, the example of large zone AE (Alps External)
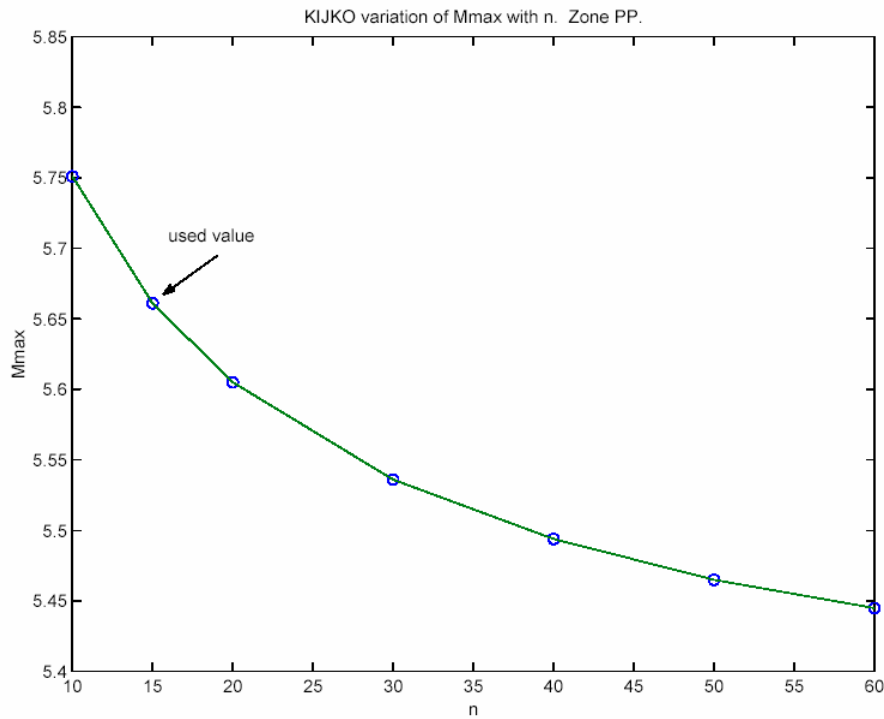
Fig. 3-9:   The effect of number of earthquakes on M_{max} using Kijko's method, the example of large zone PP (Po-plain)
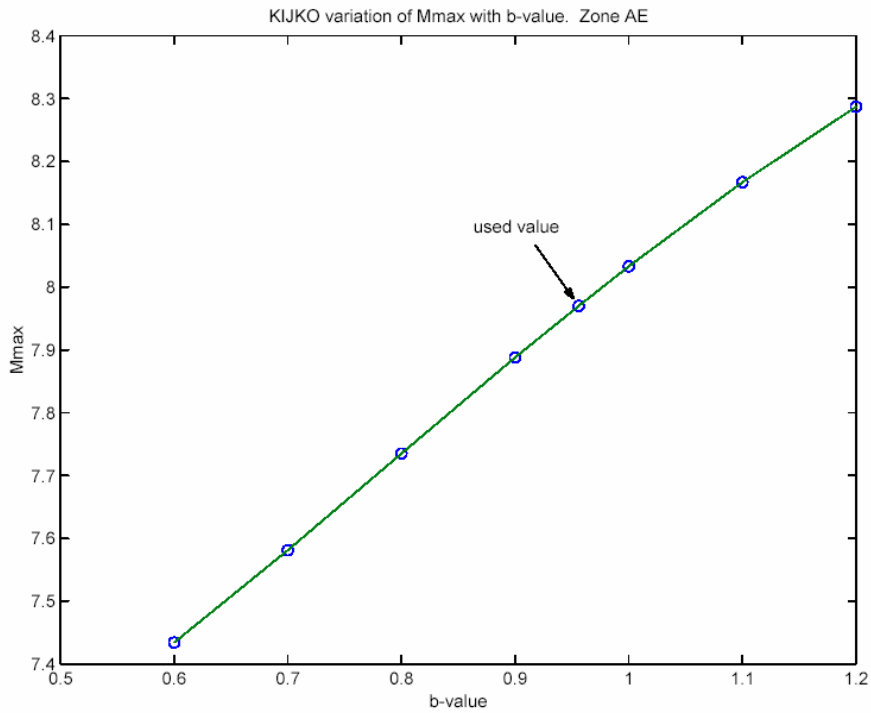
Fig. 3-10:   The effect of variations in the b-value on M_{max} (Kijko's method), illustrated for Zone AE
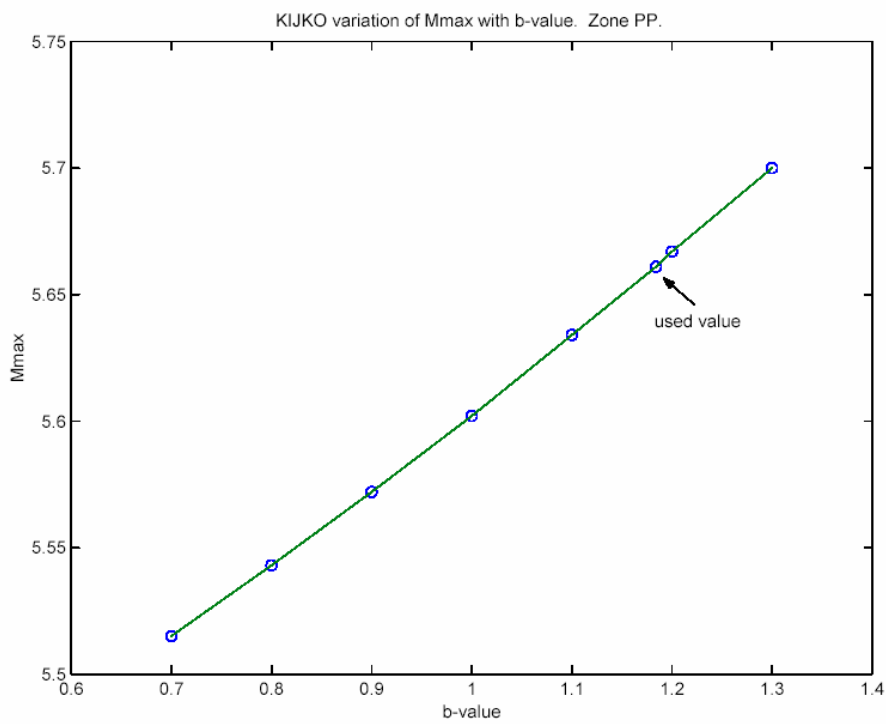
Fig. 3-11:   The effect of variations in the b-value on M_{max} (Kijko's method), illustrated for Zone PP

3.2.6 Kijko applied to small zones

Next, we try to have a more detailed evaluation for the smaller zones (Figure 3-12, Table 3-3). The b-value of the Gutenberg-Richter law (Gutenberg & Richter 1944) for a small zone is the same as the corresponding one for the larger EG1b zoning. It is also assumed that the magnitudes of the catalogue are determined with an uncertainty given by sigma (a reasonable value of 0.25 has been chosen in this case). The output of the estimation is given with its standard deviation sigma1 that includes both uncertainties, that of the method and that of the catalogue. We also include the value of the standard deviation sigma2, which assumes that the catalogue's magnitudes are exact. The calculation has been performed over the same choices made by the EPRI method (PEGASOS, TP1-SUP-0049). The EG1b zoning contains small zones, and the data of the catalogue was not enough to have reasonable estimations in some cases. Therefore, some of the small zones were considered together for the estimation of M_{max}. Even then, there was one case, AE_1_2_3_11_12_13, in which the estimation of M_{max} was 7.97, evidently large, due to the separation between the maximum event and the smaller ones. Therefore, we made new calculations with the choice of a small grouping AE_3_11, which has a better distribution of events and a value of M_{max} = 5.75.
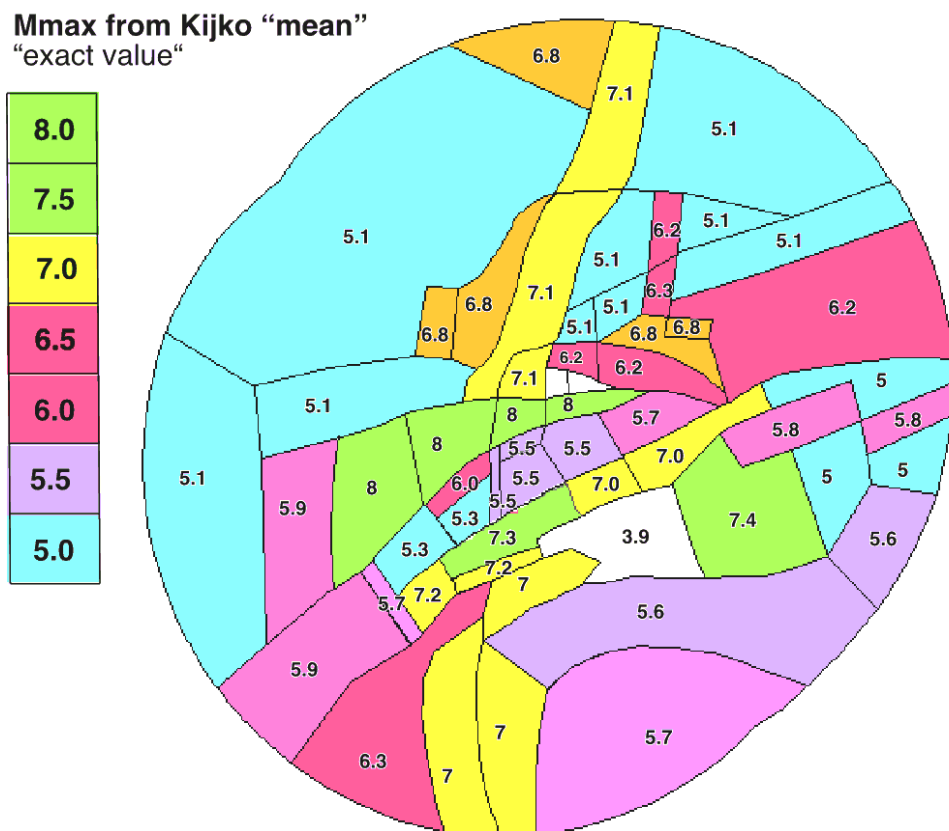
Fig. 3-12: M_{max} values (mean) of Kijko's method obtained for small zones

Tab. 3-3: Kijko analysis of PEGASOS seismicity applied to small zones, exact values of maximum magnitude

EG1b Zone (or zone regrouping)	M_{max}^{obs}	M_{min}	n	sigma	b	M_{max}	Sigma1	Sigma2
AC_10	6.5	4.0	17.0	0.25	0.867	7.435938	0.968752	0.935938
AC_8	3.9	3.5	15.0	0.25	0.867	3.935399	0.252494	0.035398
AC_4	6.4	3.0	59.0	0.25	0.767	7.370810	1.002482	0.970809
AC_1	5.8	4.0	14.0	0.25	0.867	6.314335	0.571875	0.514335
AC_11_14	5.5	4.0	16.0	0.25	0.867	5.824936	0.409980	0.324936
AC_12_13_15	4.7	3.5	11.0	0.25	0.867	4.966732	0.365577	0.266732
AC_2_6	6.4	4.0	32.0	0.25	0.867	7.042439	0.689368	0.642439
AC_3_5	6.4	4.0	19.0	0.25	0.867	7.219015	0.856321	0.819015
AC_7_9	6.2	4.0	13.0	0.25	0.867	7.005043	0.842967	0.805043
AE_4_5_6_7	5.2	3.0	40.0	0.25	0.712	5.533135	0.416508	0.333135
AE_8	5.5	3.0	36.0	0.25	0.712	5.995343	0.554855	0.495343
AE_9_10	5.0	3.0	36.0	0.25	0.712	5.281734	0.376662	0.281734
AE_1_2_3_11_12_13	6.9	4.0	39.0	0.25	0.956	7.965095	1.094042	1.065095
AE_3_11	5.5	4.0	29.0	0.25	0.956	5.748062	0.352186	0.248062
AI_1	6.2	4.0	24.0	0.25	1.057	6.977503	0.816708	0.777504
AI_2_3	5.4	4.0	36.0	0.25	1.057	5.608839	0.325751	0.208839
BG_1_2	5.6	4.0	16.0	0.25	0.737	5.912125	0.399902	0.312125
EF_1_2_6	6.0	4.0	15.0	0.25	1.164	6.845493	0.881680	0.845493
EF_3_4_5	4.7	3.0	29.0	0.25	1.135	5.129306	0.496794	0.429306
PP_1	5.3	4.0	15.0	0.25	1.184	5.652421	0.432089	0.352421
RG_1_2_3	6.2	4.0	23.0	0.25	1.165	7.085052	0.919684	0.885053
SG_1_3	5.8	4.0	26.0	0.25	1.037	6.259786	0.523357	0.459786
SG_3_4	5.7	3.0	16.0	0.25	0.853	6.803170	1.131143	1.103170
SG_2_5_8_15	5.8	4.0	42.0	0.25	1.037	6.150852	0.430810	0.350852
SG_9_10_11_12_13_14	4.7	3.0	28.0	0.25	1.048	5.090621	0.463772	0.390621

3.2.7 Conclusions – Kijko approach

The main problem with the application of Kijko's method has been the small amount of information in the small zones. We have been obliged to gather some of the zones into larger groupings, such as was done in the case of the EPRI – approach, but we had to do it in more cases. This is the main reason for the very high M_{max} values obtained in most of the Alps External (AE) small zones as seen in Figure 3-12 above, where the high observed Basel earthquake (M = 6.9) in AE_1 has a strong influence on the neighboring zones with which it has been regrouped.

Initially, we were considering to use Kijko M_{max} values as an alternative to EPRI-M_{max} distributions. Two reasons lead us to abandon this idea in the course of our evaluations. First, mean M_{max} values obtained with the Kijko method for many of the small zones are higher than what

we can accept using geologic arguments such as the possible maximum size of faults (see discussion below). Indeed, we would have been obliged to truncate Kijko M_{max} distributions at values lower than the mean M_{max}! A second argument in favour of EPRI and against the Kijko approach is based on the 'asymmetry' (EPRI) and 'symmetry' (Kijko) of the probability distributions. The asymmetry of the EPRI distributions with a mode at reasonably low M_{max} values and long tails with low probability in the upper (Magnitude 8 and above) regiona is intuitively quite appealing indeed. The log-normal distribution of the Kijko M_{max} values which is defined by a mean and a single 1 σ standard deviation is intuitively much less apealing as a probability function of M_{max}.

At one stage, we also considered the use of Kijko's values not as an alternative to the M_{max} distributions, but as a alternative method to obtain truncation values. However, even as such, the Kijko values appeared as too high in many cases of the small zones (Magnitude 8 seem unreasonable as will be discussed below). In a few cases (such as the AC_08 Ticino zone with a M_{max} of 3.9) the M_{max} seems too low.

In conclusion, we decided not to make any use of the Kijko values in our Hazard calculation.

3.3   Truncation of M_{max} distributions

EPRI M_{max} posterior distributions lead in many instances to unreasonably high M_{max} values up to and above 8 (not as mode, but as a long upper tail in the probability distribution). Based on 'common sense' and geological arguments, it is very difficult to accept the possibility, however small, of an earthquake this large to occur within the study area. The minimum length of a fault necessary to produce a Magnitude 8 earthquake is in excess of 200 km (Wells & Coppersmith 1994).There are very few if any such structures available within the study area.

In order to avoid such unrealistically large upper tails in the posterior Mu distributions (EPRI approach), we introduced some 'safeguards' in the form of truncations. Three different approaches to truncation are considered and applied. They are not mutually exclusive, but rather alternatives, in the sense: 'the method yielding the lowest truncation value will be the one that is applied'.

3.3.1   Probability cutoff (≥ 0.05)

In the case of the EPRI approach, it seems reasonable and straightforeward to use a certain threshold value of probability in order to cut the long upper tails of posterior Mu probability distributions. We propose the use of such a threshold value at $p \geq 0.05$. Maximum magnitudes below a probability of 0.05 are simply to cut out of the posterior EPRI Mu distributions. There are only a few small zones, where this criterion has to be applied. In most other cases, the size of the small zones provides a stronger criterion, i.e. a cut at even lower earthquake magnitude. It is not surprising that only the largest of our small zones are in need of a probability truncation, as listed in Table 3-4 (at the end of this section).

Posterior EPRI-M_{max} distributions for many large zones, shown in Figure 3-1, are characterized by long upper tails extending to high values of 8 and above. Again, truncation of the long upper tails at $p \leq 0.05$ has been applied to some of these zones (EF, SG and AC) – see Table 3-4.

While probablility truncations lead to acceptable M_{max} values in the case of small zones (with largest M_{max} at 7.25), largest M_{max} for many large zones remain very high, reaching values of $M > 8$ in the case of the Rhine Graben, and $M > 7.5$ for Bresse Graben, the Alps and Po-plain. The only large zones with acceptable M_{max} truncation values are South Germany, with an ultimate M_{max} of 6.75 and East France with ultimate M_{max} of 7.25.

3.3.2 Largest size of faults – within small zones

Geological arguments about the maximum possible size of faults provide an alternative and/or complementary way of estimating the maximum possible Magnitude of an earthquake. There are no large (i.e. longer than 200 km) faults or fault zones known in the entire study area. None of the known faults or fault zones is documented to be active. Clustered seismicity does occur at depth, on patches of faults. This activity is never documented over more than a few (tens of) kilometers, be it from instrumental seismicity observations (e.g. Wildhorn-, Fribourg-, Vuache-zones) or from paleo-seismic studies (e.g. Basel area). Given this lack of detailed knowledge about any large faults, we are again left with general and probabilistic considerations, rather than straightforward estimations based on fault size, maximum fault offsets or deformation rates.

For reasons of internal consistency, the size of the small seismic source zones does provide an upper limit for the size of faults that can possibly be fitted into any of these zones. Based on empirical relationships between Rupture Length and Earthquake Magnitude (Wells & Coppersmith 1994), we can estimate an M_{max} for each small source zone. In order to do so, we estimated the maximum Rupture Area using the following formula of Wells & Coppersmith (1994, Fig. 16a):

$$M = 4.07 + 0.98 \log (RA), \text{ where RA is Rupture Area in km}^2$$

Maximum possible Rupture Areas were determined for each individual small source zone, and regrouping of small zones, in the following way. First, we considered the orientations and most likely style of faulting (thrusting, strike slip, normal). This fault orientation was then intersected with the map view shape of the source zone $\Rightarrow$ this provides the longest possible fault which can be fitted into the source zone. This procedure has been done visually 'by hand' on a poster printout of the basemap with source zone boundaries, and fault lengths were rounded to the nearest 10 km.

Despite the fact that many of our source zones have a strong 'preferred orientation', we only consider one single 'ultimate' M_{max} value for each zone. The longest fault corresponds to the most likely fault orientation and faulting style. Examples are the Wildhorn AC_5, the Fribourg AE_7 and the Vuache AE_11 zones, the shape of which mimic the presence of a fault. In theory, however, it would have been possible to define three different M_{max} values based on the longest possible expected thrust, normal and strike slip faults that can be hosted within each indivdual small source zone. Given the large uncertainties in all other parameters, we did not want to go into this much detail, however. In our view, the maximum earthquake in each small source zone, is necessarily in the class of fault styles with the highest likelihood.

Some of our 'small' source zones are fairly large still and we therefore introduced an additional, admittedly arbitrary, but generous cut-off at 200 km ultimate fault length $\rightarrow$ no fault is allowed to be longer than 200 km, even if it would fit into the zone (eg. N-S strike slip faults in EF_4, EF_5 or E-W oriented thrust faults in AI_2). Some more geological arguments about the choice of this '200 km' value, will be given in the next section 3.3.3 below.

The second, downdip dimension of this maximum size fault was determined from the estimated maximum depth of the seismogenic zone.

$$RA = L*h$$

where L is fault length, h is the maximum seismogenic depth.

For simplicity, we assumed all faults to be vertical, even in the case of normal and thrust faults, for which the rupture area could be slightly increased due to inclined fault planes. Given the very arbitrary estimation of 200 km maximum fault length and all the other uncertainties in our estimations of fault dimension, we feel entitled to neglect this subtlety.

Based on all these premises, the largest possible fault (rupture area RA) has been determined for each zone. This information is provided in form of a data table (PEGASOS EG1-HID-0033_EG1b, see Table A-1 in Appendix 1) together with other fault information for each zone as well as groups of zones. The outcome of this M_{max} from the 'maximim size of faults' criterion is illustrated in Figure 3-13 below. The largest M_{max} truncation value of 7.7 is obtained for the AI_1 Dora Maira zone. This value results from a potential 200 km long N-S thrust fault, within a 37 km thick seismogenic crust.

The entire 'M_{max} from size of small source zones' argument is admittedly somewhat circular. By chosing small zones, we have implicitly limited the size of the largest faults that can possibly be active within any such small zone. We are well aware of this problem and we have considered it seriously. The choice of our small source zones, including their dimension, is based on geological and seismological information. In a few cases of known faults, such as the Fribourg and Wildhorn zones, or suspected ones (Neuchâtel lake, Biel) the shape and size of our source zones explicitly reflect the estimated maximum length of these faults. In other cases, such as the larger Basel region, the uncertainty about the fault(s) responsible for the big Basel 1356 earthquake is reflected in our alternative zone regroupings within the 'Rhinoceros'.
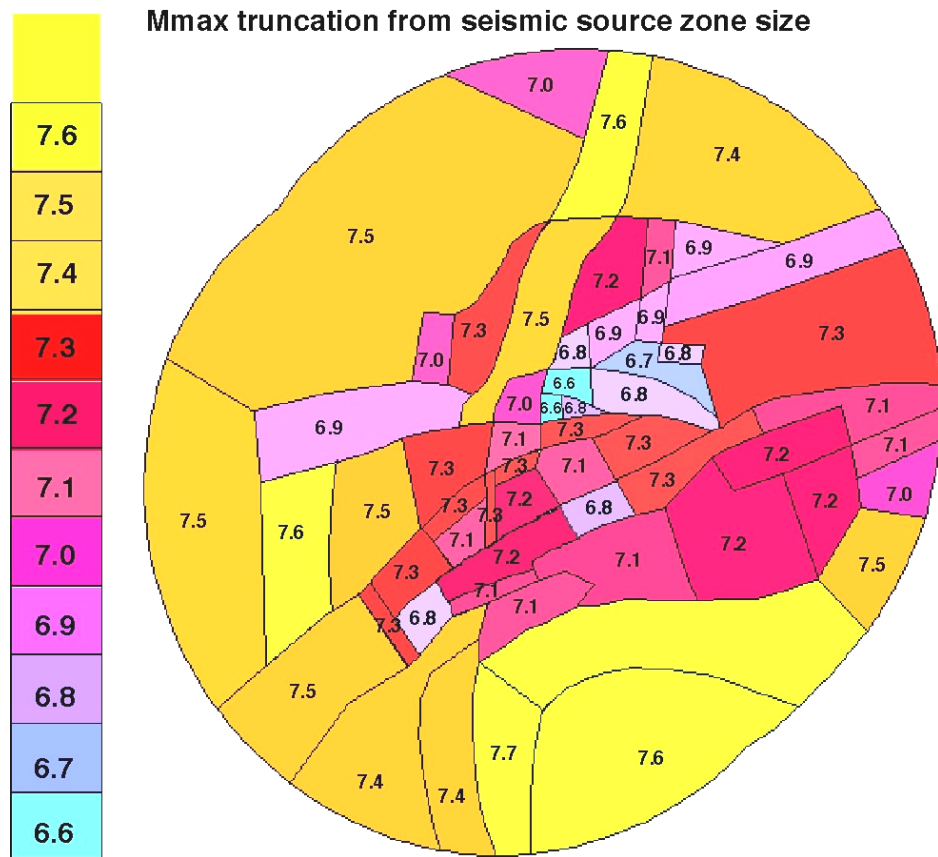
Fig. 3-13: M_{max} truncation values as determined from the size of small seismic source zones

The largest possible fault within each zone has been used to estimate M_{max} from maximum possible Rupture Area. An additional arbitrary truncation for maximum fault length at 200 km has been introduced in the case of the 'large' small zones near the periphery, yielding M_{max} values of 7.4 to 7.7, depending on the depth of the seismogenic zone.

As a side-effect of this very same reasoning truncation values for M_{max} distributions grow larger towards the periphery of the study area. This is due to the fact that we have not given as much attention to the local geological and seismological conditions in these areas. In other words, large small zones near the periphery of the study area should be regarded as somewhat similar to large background zones and in this sense, they start to resemble more their overall large parent zone.

3.3.3   Largest size of faults – within large zones

First of all, let's recall the fact that our group EG1b considers a scenario of large seismic source zones, the boundaries of which are based on geologic / tectonic arguments. This large zone approach is given a weight of 0.2 in comparison to 0.8 for the small scale zonation. In other words, we clearly prefer a detailed model, where the zone boundaries were choosen as best we could based on geological arguments and using all available information from historical and instrumental seismicity. We are well aware that none of these local arguments are absolute, and any of our small zone boundaries may be ignored by the next large earthquake. Nevertheless, we consider all boundaries of our small zones as strictly impermeable to fault ruptures. This strict impermeability condition is compensated by the 'large zone approach' (with a weight of 0.2), where the size of source zones does not provide any constraints about the M_{max} anymore. As we have seen before, the EPRI approach to large zones yields acceptable M_{max} values for the mode, but apparently still unreasonably high values within the long upper tails of the probability distributions; values of $M > 8.0$ remain even after a cutoff at $p < 0.05$. This is the main reason for introducing an additional cutoff based on a geological argument: what is the absolute maximum size of any fault which exists within the study area?

Large faults and lineaments do exist throughout the study area. Examples include blind, hidden boundary faults of identified and suspected E-W running Permo-Carboniferous graben structures in northern Switzerland and below the folded Jura. A seismic lineament in the western Helvetic Alps, the Wildhorn zone (AC_5) seems to be localized, at least partly along such an old Carboniferous graben within the External Crystalline Aiguilles Rouges massif, this fault zone is seismically active along a linear stretch of some 80 km in an SSW-NNE direction. N-S oriented, Rhenish faults of Oligocene age may be present in large parts of central and western Switzerland where they have a clear geomorphic expression as tear faults in the folded Jura. Seismic activity is known for such a structure below the Molasse basin in the Fribourg area (AE_7). The seismically active Vuache fault zone (AE_11) of the westernmost Jura belongs to this tear fault family, too. Both the Fribourg and Vuache faults have lenghts on the order of 50 to 60 km.

All of these fault zones extend over at least 50 km and many of them could easily be more than 100 km long. The Permo-Carboniferous graben structures of northern Switzerland are now well known and mapped to extend from the Bodensee to Kaisten over about 100 km (Müller et al. 2002). The westward extension of this graben structure is wide open to speculation. It could well extend another 100 km further to the west into the region of Besançon. Fault segmentation does exist, of course, but where known and mapped, as in the case of the Weiach trough, it does not seem to be too severe to preclude rupturing across bridges between individual fault strands (Rubin 1996).

Large, up to 200 km long, geomorphically expressed fault lineaments exist also within the Central Alps. The most striking example is the Rhine – Rhone lineament, a feature which has been recognized a long time ago and which is at least partly (within the Aarmassif) reported on the classical tectonic map of Switzerland (Spicher 1980). Quite surprisingly, in more recent tectonic maps of Switzerland, such as the basemap used in the PEGASOS project, none of these long lineaments are shown anymore. They still exist, however, and in places, there is even clear geomorphic evidence for considerable post-Würm ice age vertical displacements (Eckart et al. 1983) along faults with the same general orientation. In an extreme interpretation, the seismic

quiescence of the area with the most spectacular fault scarps in the Gotthard region (our Ticino AC_8 source zone), could possibly be interpreted as a 'seismic gap' inbetween the two seismic 'hot spots' of the Valais (AC_5 and AC_6) and the Grisons (AC_10) areas, located at either end of this large fault lineament.

The Central Alps lineaments are shown in digital elevation models (DEM) in Figures 3-14 and 3-15. A comparison with the Alaskan Denali fault is proposed in Figure 3-14. This figure is meant as to illustrate the following points:

−   the small size of the Alps (compared to Alaska)

−   the possibility/difficulty of placing a 200 km long fault within the Alps

−   the relative geomorphic expression of the Denali fault vs. Alpine lineaments.

In summary, we conclude that 200 km is an uppermost limit to the length of any fault within the entire study area. This limit is arbitrary, and our choice is deliberately on the large side. The present day seismicity and the historical record of the last 1000 years speak against seismic activity of faults this large, even if we allow for the fact that our wet climate is not favorable to the preservation of the paleoseismic record (Kaneda 2003). The present day plate tectonic situation of the Alps, with little if any ongoing plate convergence is another argument against active large faults.

Despite these arguments (which are reflected in the recurrence parameters of the different seismic source zones), we are reluctant to set the uppermost M_{max} values too close to the observed M_{max}. There are indeed hints to isostatic unloading phenomena within the Alps and their surroundings. The present day vertical uplift (of up to 1.5 mm/a (Gubler et al. 1984)) may still be influenced by post-glacial rebound (Gudmundsson 1994). Many of the seismic hot spots in the Alpine Foreland (Basel, Remiremont, Schwäbische Alb) bear some ressemblance to intra-plate, intracontinental earthquakes observed elsewhere (Meers fault, Ungava (Adams et al. 1991), New Castle, and to be extreme, why not New Madrid!? (Hough 2002). Such extreme events are included in the EPRI appraoach where they lead to the long upper tails in probability distributions. Here we opted to take an intermediate route, EPRI distributions, truncated at M_{max} of around 7.5.
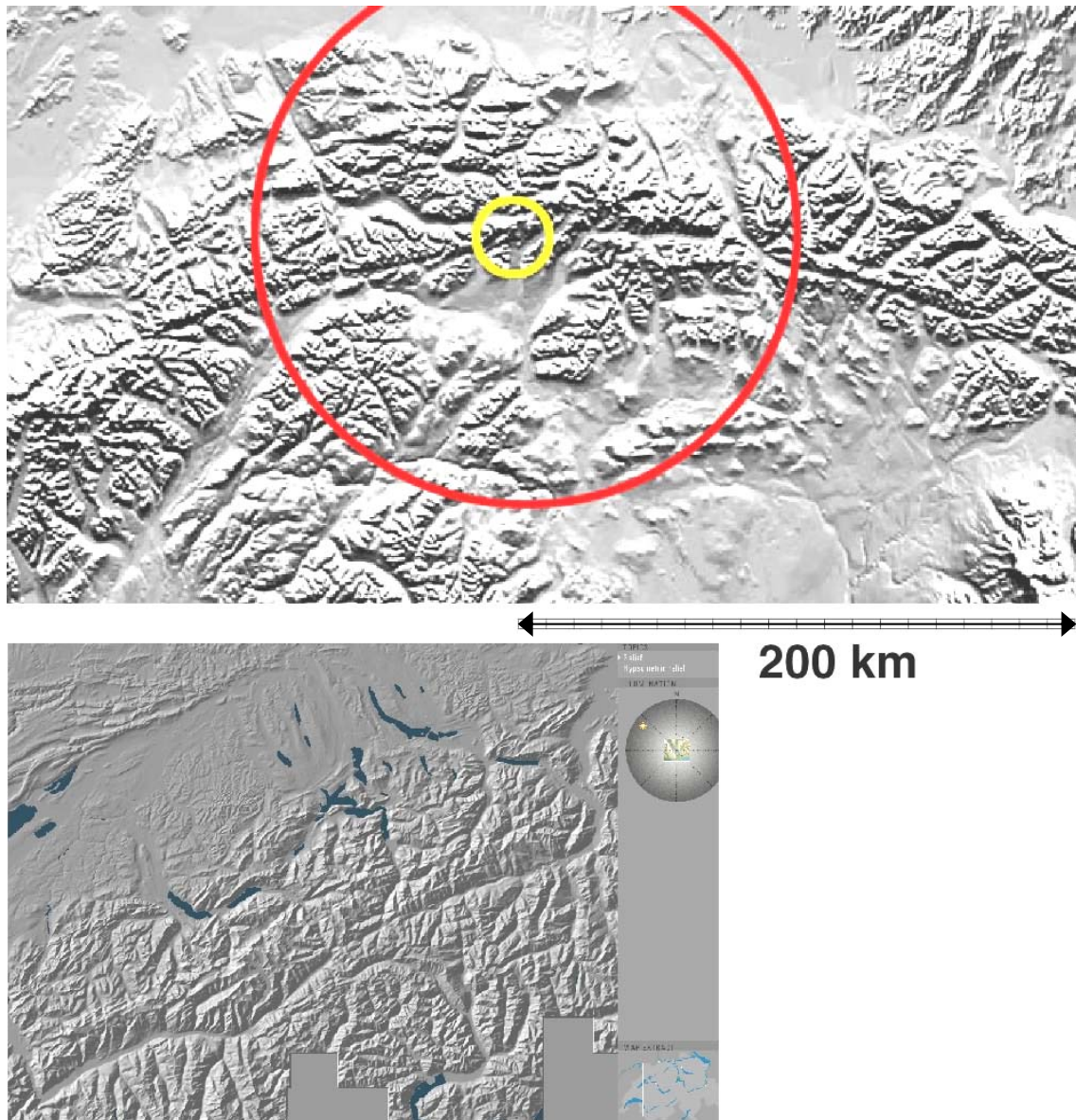
Fig. 3-14:   Geomorphic expression of large fault lineaments. A DEM of the Denali fault of Alaska, which hosted the M 7.9 earthquake of octobre 2002 is compared with a DEM of the Central Alps

Long ENE-WSW running 'lineaments' connect the Rhine valley with the Central Rhone valley, cutting across the western Aarmassif, oblique to main tectonic boundaries.
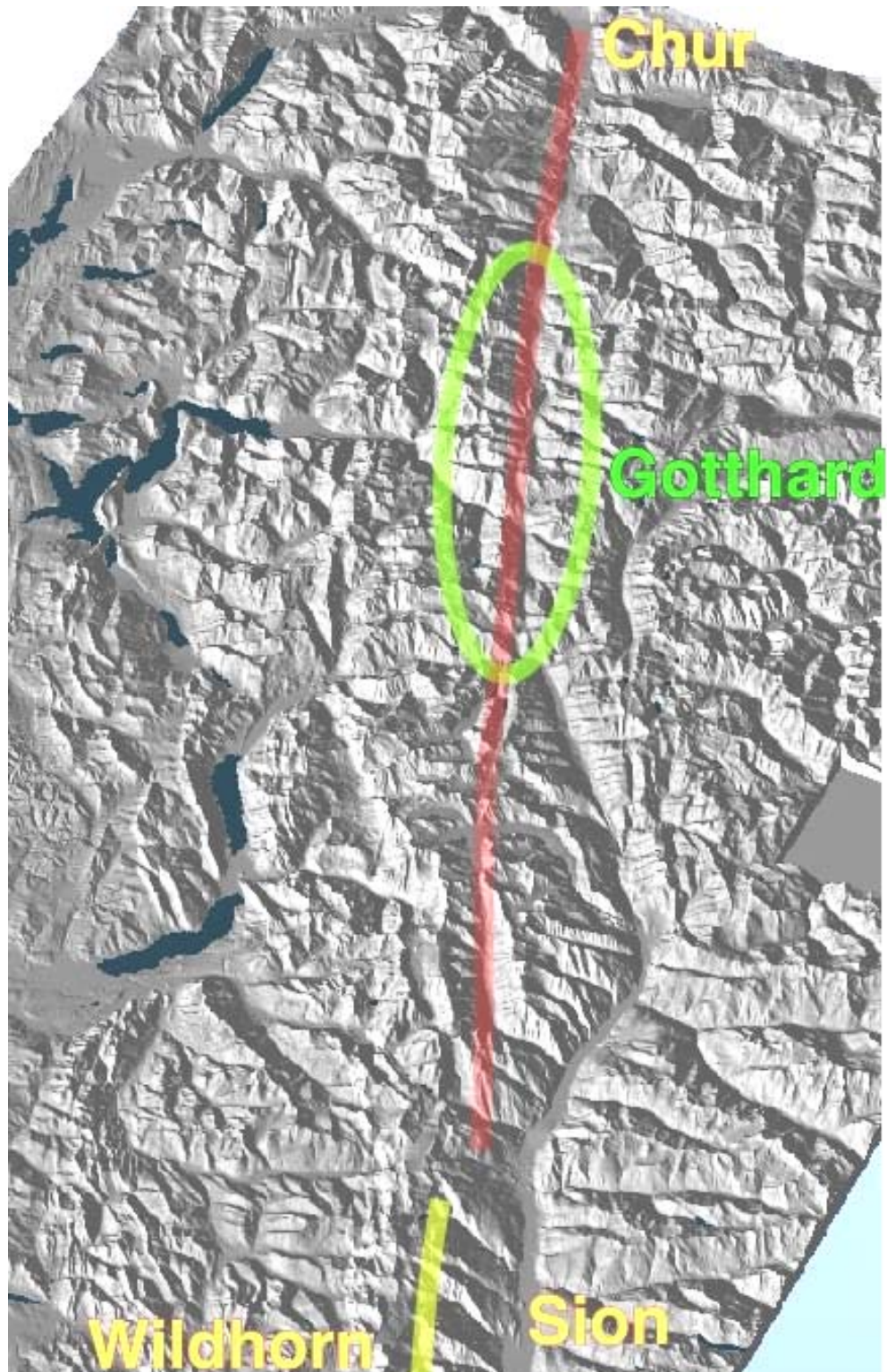
Fig. 3-15: MNT of the Central Alps, North is to the left. The Rhine − Rhone lineament lies inbetween two seismically active areas near Sion (Valais zone AC_6, Wildhorn lineament AC_5) and Chur (Grisons zone AC_10)

The Gotthard region inbetween the two, i.e. the northern part of the Ticino zone AC_8, is seismically quiet today, but known for post-Würm ice age fault scarps.

3.3.4   Summary – truncation of M_{max} distributions

Upper tails of the the EPRI – Mu posterior distributions are truncated in many cases of small seismic source zones and in all large scale source zones. Single upper truncation values have been obtained using three different approaches, yielding three different values for an ultimate M_{max}, the lowest value is the one that has been retained – data are provided in form of a data table (PEGASOS EG1-HID-0033_EG1b, see Table A-1 in Appendix 1).

− A probability cutoff at ($p \geq 0.05$) applies in a few cases of 'large' small source zones, mostly those located near the periphery of the study area.

− The size of small seismic source zones is used to constrain the maximum size of faults which can be fitted into any zone; this criterion yields an upper boundary for M_{max} for most of the small seismic source zones located near the center of the study area.

− No fault is allowed to be longer than 200 km; we had to introduce such an additional threshold in order to truncate unreasonably long upper tails in posterior EPRI Mu distributions for all of the large zones as well as isolated cases of 'large' small zones and alternative groups of small zones.

The 200 km threshold for longest faults is admittedly arbitray. It leads to variable M_{max} truncation values in the range of 7.4 to 7.9, depending on the variable depths of the seismogenic zone within different source zones. Alternatively, we could just as well have chosen a fixed uppermost M_{max} value, at say Magnitude 7.5 to 7.6.

3.3.5   Time evolution and M_{max} (by A. Cisternas)   (not applied to HID)

Another way of testing the values of maximum magnitude is provided by the use of Hurst's method to the time distribution of earthquakes within a region. The advantage of this procedure is threefold:

a) The use of time permits to follow the accumulation of seismic energy within the region and have an image of the history of the process. In particular, we can see the actual state, with respect to the historical evolution, and have a criteria to see if the cumulated seismicity is near the lower bound or close to the upper one.

b) The range of the cumulative distribution of seismicity (maximum minus minimum values) gives an estimation of the maximum earthquake.

c) The range of the cumulative function behaves like a power law with respect to window size (Hurst exponent). Thus we have a way to estimate the role of memory in the process, namely to see the degree of predictability. Short memory means high frequency oscillation of the cumulative function, and low predictability. Long memory means smoother behavior, and high degree of predictability.

In the case of the whole large region, the catalogue allows the construction of the cumulative seismic moment given in Figure 3-16. There we may see that the range corresponds to a seismic moment of 3.13×10^{26} dyne-cm, namely to magnitude M_{max} of 6.93. The actual state does not differ much from the value of M_{max} given by the range, since it lacks the equivalent of an earthquake of magnitude 6.87 if the existing strain energy were released as a whole. On the other hand, the Hurst exponent is 0.79, closer to 1 rather than to 0.5, meaning that the system has memory, and that it is expected that the behaviour will not change much (low frequency, cumulative curve). These values are the average values of the range, but if we allow an uncertainty of 0.25 to each magnitude, the range may increase by 0.5 units of manitude, namely to a value of 7.43, which is not too far from the $M_{max} = 7.9$ given by Kijko's method.

Tab. 3-4:   Truncation values applied to large and small zones, geologic truncations are based on the size of the largest fault within each zone, the 95 % cumulative truncation is applied to the EPRI probability distributions

The applied value ('whichever is smaller') is highlighted in grey for each zone – or regrouping of small zones.

Large Zone	Geologic Truncation	95 % Cumulative Truncation	Small Zone	Geologic Truncation	95 % Cumulative Truncation
EF	7.5	7.2	AE01	7.1	8.1
RG	7.7	7.9	AE02	7.3	7.8
SG	7.6	6.7	AE03	7.3	7.7
BG	7.8	7.5	AE04	7.1	7.8
AE	7.8	8.2	AE05	7.1	7.8
AC	7.5	7.0	AE06	7.2	7.8
AI	7.9	7.9	AE07	7.3	7.8
PP	7.6	7.8	AE08	7.3	7.3
			AE09	7.1	7.8
Small Zone			AE10	7.3	7.8
EF01	7.0	7.2	AE11	7.3	7.8
EF02	7.3	7.1	AE12	7.5	7.8
EF03	6.9	7.1	AE13	7.3	7.8
EF04	7.5	7.1			
EF05	7.5	7.1	AC01	7.4	7.7
EF06	7.0	7.1	AC02	7.4	6.8
			AC03	6.8	7.7
RG01	7.0	7.8	AC04	7.2	7.9
RG02	7.5	7.9	AC05	7.1	7.8
RG03	7.6	7.8	AC06	7.1	7.7
			AC07	6.8	7.8
SG01	6.9	6.8	AC08	7.1	7.8
SG02	7.1	7.1	AC09	7.3	7.5
SG03	6.8	7.1	AC10	7.2	7.8
SG04	6.7	7.1	AC11	7.2	7.4
SG05	6.8	7.1	AC12	7.2	7.8
SG06	6.8	7.1	AC13	7.1	7.8
SG07	6.6	7.1	AC14	7.1	7.7
SG08	6.6	7.1	AC15	7.0	7.8
SG09	6.8	7.1			
SG10	6.9	7.1	AI01	7.7	7.6
SG11	7.2	7.1	AI02	7.9	6.6
SG12	7.4	7.1	AI03	7.5	7.1
SG13	6.9	7.1			
SG14	6.9	7.1	PP01	7.6	7.8

Large Zone	Geologic Truncation	95 % Cumulative Truncation	Small Zone	Geologic Truncation	95 % Cumulative Truncation
SG15	7.3	7.1			
BG01	7.6	7.8			
BG02	7.5	7.7			
Zone regroupings					
SG1_2	7.3	6.8	RG1_AE1	7.3	8.2
SG5678	7.3	7.1			
SG5_6_8	7.3	7.1	AE1_2	7.6	8.1
SG5_8	7.3	7.1	AE1_2_13	7.8	8.2
SG6_7	6.9	7.1	AE1_13	7.5	8.2
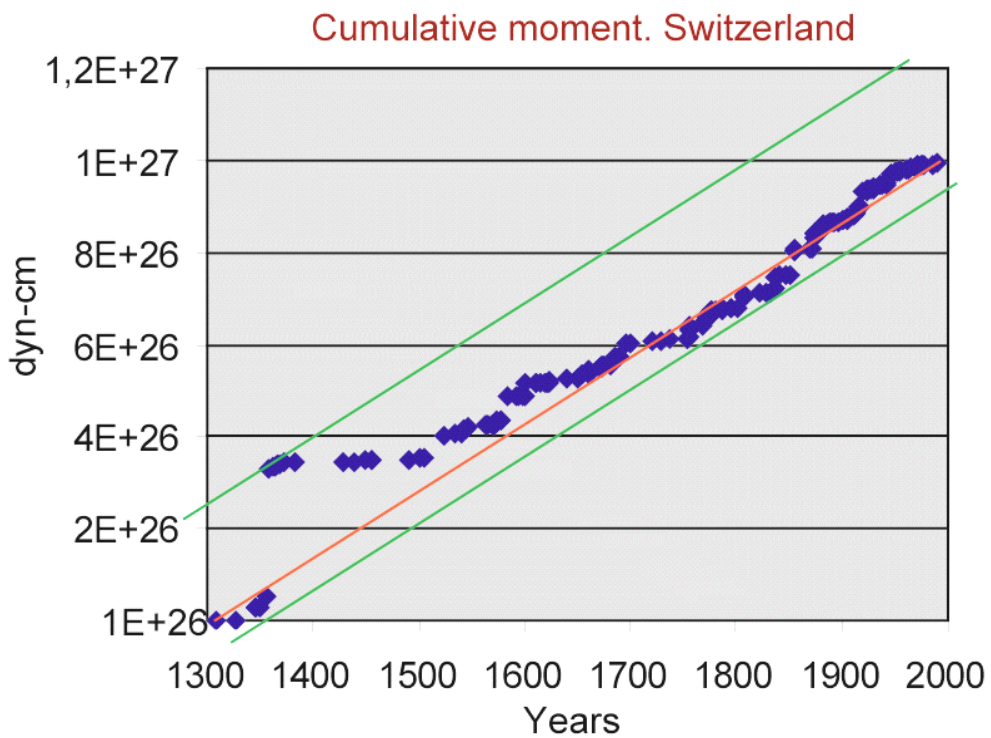
Fig. 3-16:   Cumulative Moment, determined from the entire PEGASOS catalogue

4 EARTHQUAKE RECURRENCE PARAMETERS

4.1 Introduction

The recurrence relationships describing the frequency of occurrence of earthquakes of various magnitudes within each seismic source is an essential element in probabilistic seismic hazard assessments (PSHA). The general philosophy of the source zone definition of EG1b was to develop:

1. a large scale model of source zones following the large scale tectonics,

2. a small scale model of detailed source zones reflecting the details of characteristics in seismicity and seismotectonics, and

3. different combinations or groupings of small zones in areas of special concern.

This philosophy of source zone characteristics was consequently continued for the determination of the recurrence parameters of earthquakes; i.e. to reflect areal variations of these parameters both as detailed as possible but also according to the large scale architecture of tectonics.

The used earthquake data are from the PEGASOS Earthquake Catalogue of Switzerland, (PEGASOS EXT-TB-0043 2002) provided for this project. The only used earthquake strength parameters are the moment magnitude values M_W given in the PEGASOS catalogue. No special analysis of these initial data has been made with one exception. This concerned the separation of several suspected mining induced events in the Saar mining district. However, this is of very minor importance for the PSHA within PEGASOS.

The next step of the data analysis concerned the declustering of the catalog, i.e. the identification and separation of foreshocks and aftershocks in order to create a Poissonian data file. This has been performed for the whole study area; i.e. the area covered by the EG1b source zones.

Furthermore, the completeness of catalogued data has been studied. This was carried out for the areas roughly covered by the different national data bases, i.e. for Switzerland, France, Germany, Austria, and Italy.

Finally, the parameters of the Gutenberg-Richter relations (Gutenberg & Richter 1944) were derived for each source zone as mentioned above.

For all these steps a magnitude classification with a width of 0.5 magnitude units is used for each class.

4.2 Declustering of the catalogue data

The declustering aims at the identification and separation of foreshocks and aftershocks in a seismicity file to generate the time-independent, Poissonian part needed for the further analysis.

Special studies have been performed within PEGASOS (Wiemer 2002, Deichmann 2002) to test the characteristics of different techniques commonly used in the seismological practice. These are approaches by Gardner & Knopoff (1974), Grünthal (1985, modified), Reasenberg (1985), Uhrhammer (1986) and Youngs et al. (1987, modified). In general, all these approaches apply space-time windows. Gardner & Knopoff (1974), Reasenberg (1985) and Uhrhammer (1986) derived their window parameters for the Californian catalogue, Youngs et al. (1987) for a study of the Wasatch Front seismicity, Utah. Grünthal (1985) derived his parameters for characteristics of the foreshock and aftershock activity according to the Central European earthquake

catalogue data with all their location uncertainties, e.g., of early 20th century earthquakes. As a result of a comparative study of the effectiveness of the above mentioned techniques, Deichmann (2002) concludes: "*the Grünthal scheme does the most rigorous job of declustering.*" Deichmann (2002) studied how the mentioned approaches identify, what manually would be chosen as the main shock for four cases of foreshock, mainshock and aftershock combinations from 1946 to 2000 in PEGASOS. Solely the Grünthal (1985) technique repeated the expert decision for all cases. So, the EG1b team decided, to apply this approach. The window parameters after Grünthal (1985, modified) are:

The foreshock time window:

$$dT_f(M_w) = \begin{vmatrix} \exp\left(-4.77 + \sqrt{0.62 + 17.32 \cdot M_w}\right) & \text{if } M_w < 7.8 \\ \exp(6.44 + 0.055\, M_w) & \text{otherwise} \end{vmatrix}$$

The aftershock time window:

$$dT_a(M_w) = \begin{vmatrix} \exp\left(-3.95 + \sqrt{0.62 + 17.32 \cdot M_w}\right) & \text{if } M_w < 6.6 \\ \exp(6.44 + 0.055\, M_w) & \text{otherwise} \end{vmatrix}$$

The distance window:

$$dR(M_w) = exp\left(1.77 + \sqrt{0.037 + 1.02 \cdot M_w}\right)$$

The graphical representation of these three windows is shown in Figure 4-1. The effect of declustering, as it is applied by EG1b, is shown in Figure 4-2.

According to Wiemer (2002) the application of this technique results in a reduction of the totally released seismic moment of 1.99 %. As Wiemer (2002) additionally has shown, the resulting catalogues of independent events can be considered consistent with a Poisson process in time.
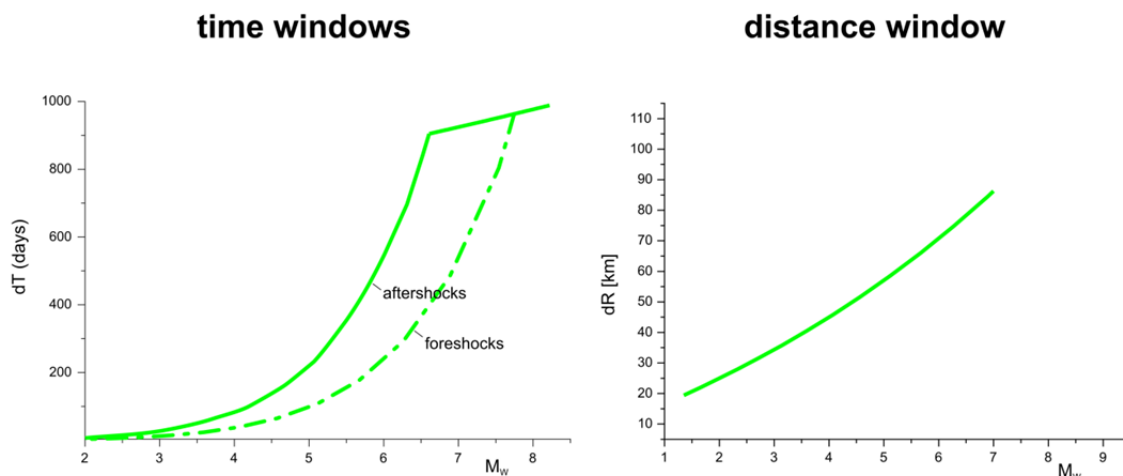
Fig. 4-1:   Definition of the time windows for foreshocks and aftershocks as well as the distance window for catalogue declustering according to the modified technique after Grünthal (1985)
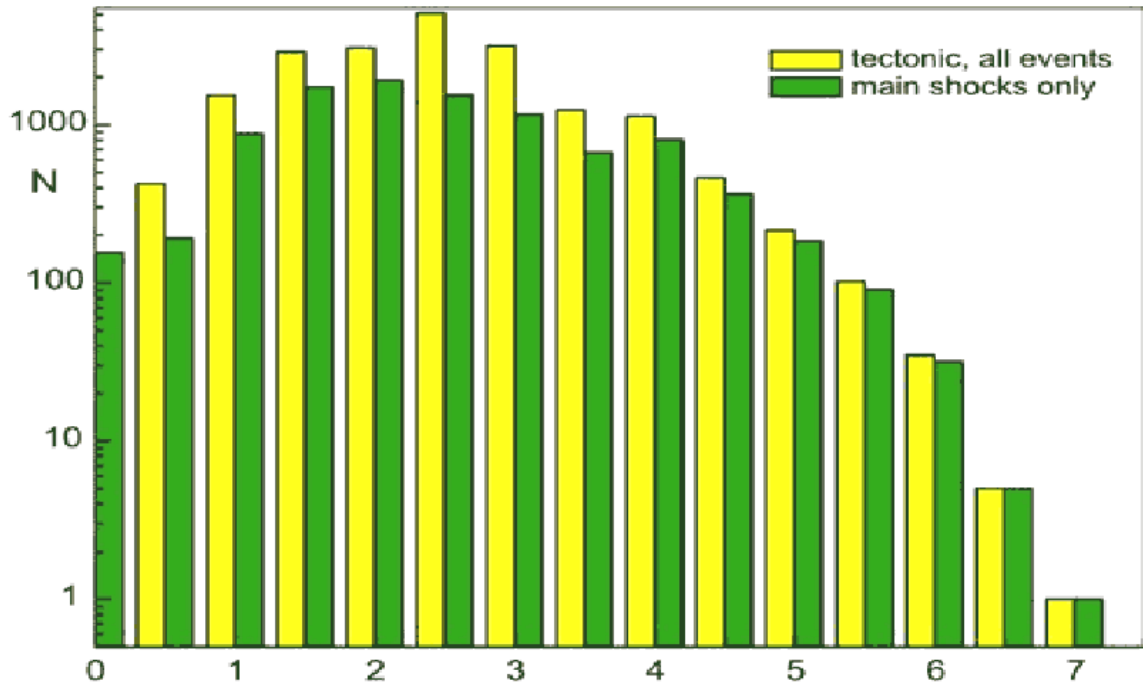
Fig. 4-2:   Effect of catalogue declustering

4.3   Catalogue completeness with time

The analysis of the catalogued data completeness with time is an essential element in the data pre-processing for the determination of the earthquake recurrence parameters. For this subtask EG1b applied a simple but powerful procedure successfully used since more than 20 years by one of the team members (G. Grünthal).

First, seismic gross zones have to be defined which should comprise larger areas of homogeneous cultural-historical conditions in the cataloguing of earthquakes. They should consist of larger areas specified by homogeneity of cultural-historical conditions as basis for the earthquake cataloging. For this project, the gross zones approximately agree with the areas covered by the national catalogs; i.e., as shown in Figure 4-3 in form of the polygons CH (Switzerland), D-SW (SW-Germany), A-W (western Austria), I-N (northern Italy, F-E (eastern France). The typical swarm quake area in the NE of the catalogued area is omitted since the temporal earthquake characteristics are somewhat different there.

For each of the gross zones the cumulative number of catalog entries for each magnitude class is plotted. The ordinate, displaying the numbers, is given in units so the step-like curve for each class is clearly visualized. This procedure has been applied in many studies in the last 20 years, e.g. for Switzerland by Grünthal & Mayer-Rosa (1998) and Grünthal et al. (1998b).

The plots for the gross zones CH, D-SW, I-N and F-E are shown in Figure 4-4 (a-d). The single step-like curves are interpreted in a retrospective way; i.e., time points are identified where the ascent of the step-like curve is significantly changing. It can be assumed that the times mark the beginning of periods of completeness. The periods of completeness derived in this way are summarized in Table 4-1.

Each of the different seismic source zones were associated with one of these completeness models. Due to the scarcity of data in the gross zone A-W (western Austria) its completeness assessments are less reliable and the completeness model derived for CH (Switzerland) was applied.
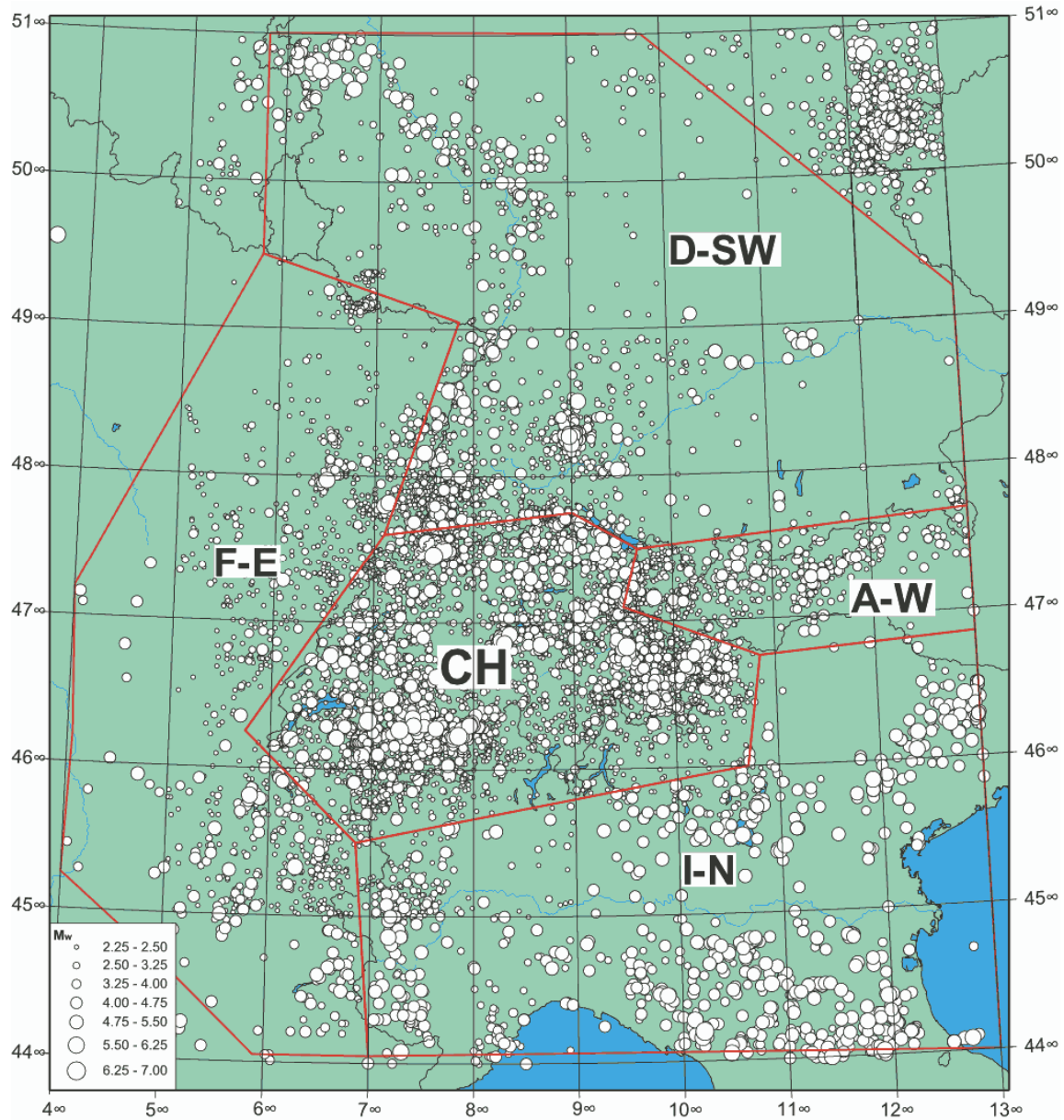
Fig. 4-3:   Polygons defining the gross zones for studying the catalogue completeness with time
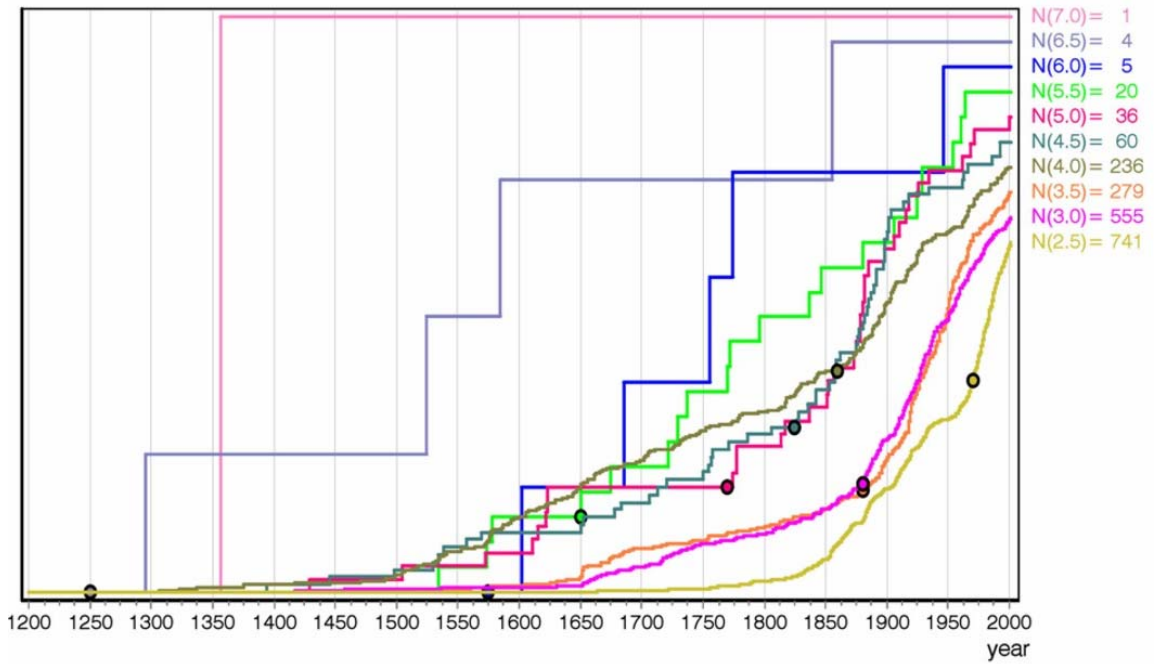
Fig. 4-4a: Cumulative plot of catalog entries for the gross zone Switzerland for each magnitude class

The bold dots determine the times from which on a sufficient completeness is assumed.
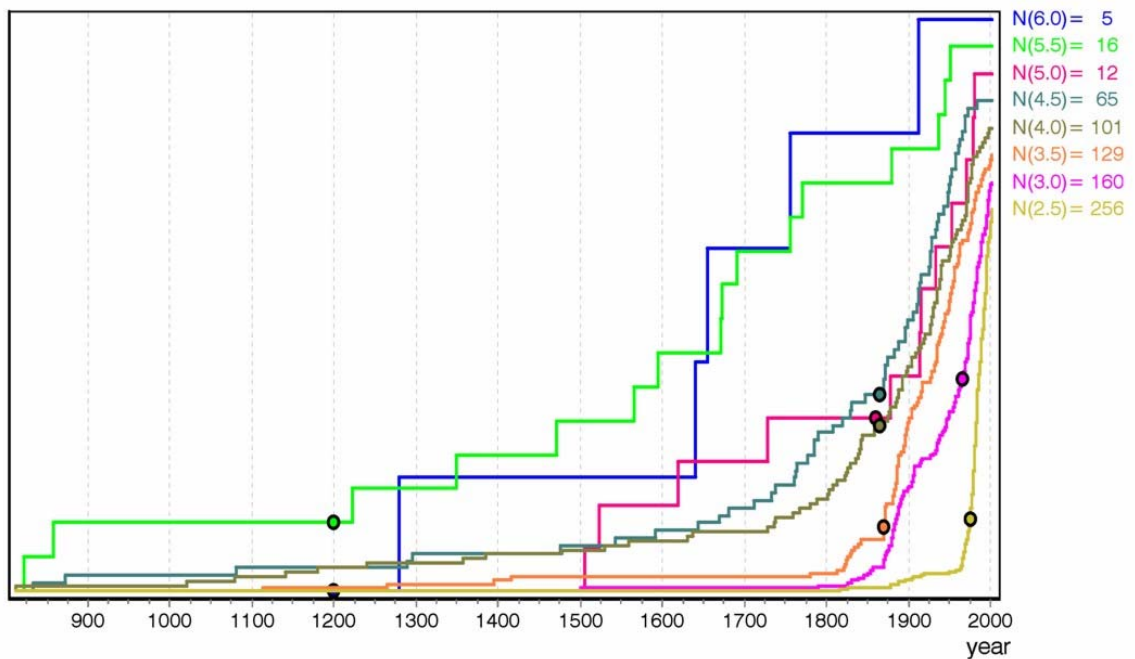
Fig. 4-4b: Cumulative plot of catalog entries for the gross zone SW Germany for each magnitude class

The bold dots determine the times from which on a sufficient completeness is assumed.
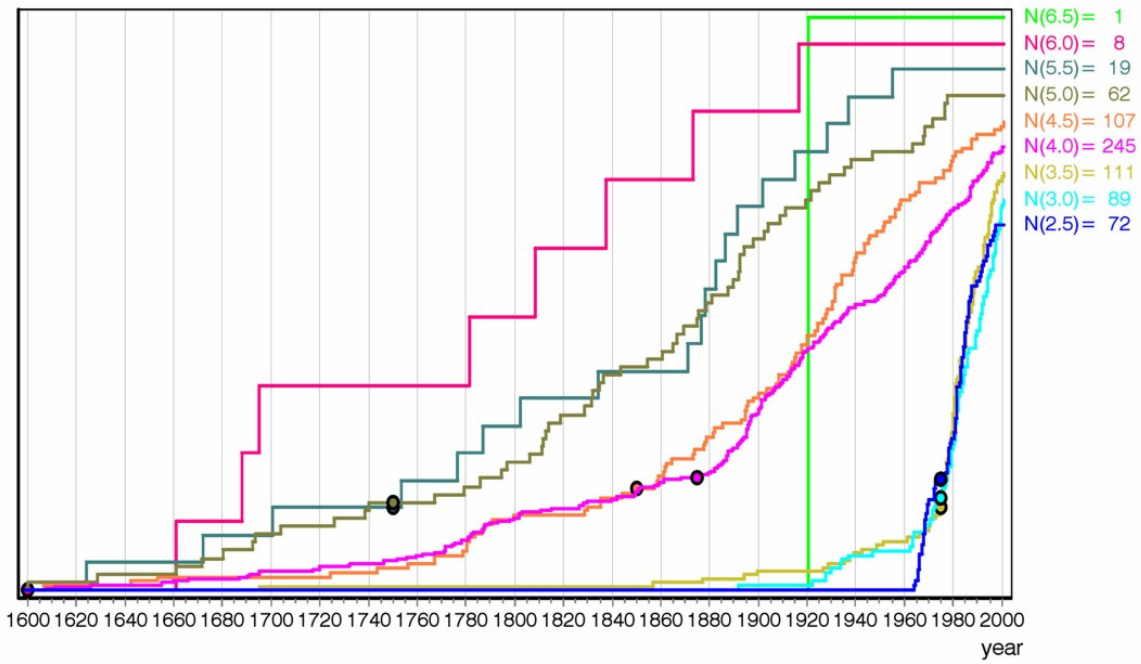
Fig. 4-4c: Cumulative plot of catalog entries for the gross zone northern Italy for each magnitude class

The bold dots determine the times from which on a sufficient completeness is assumed.
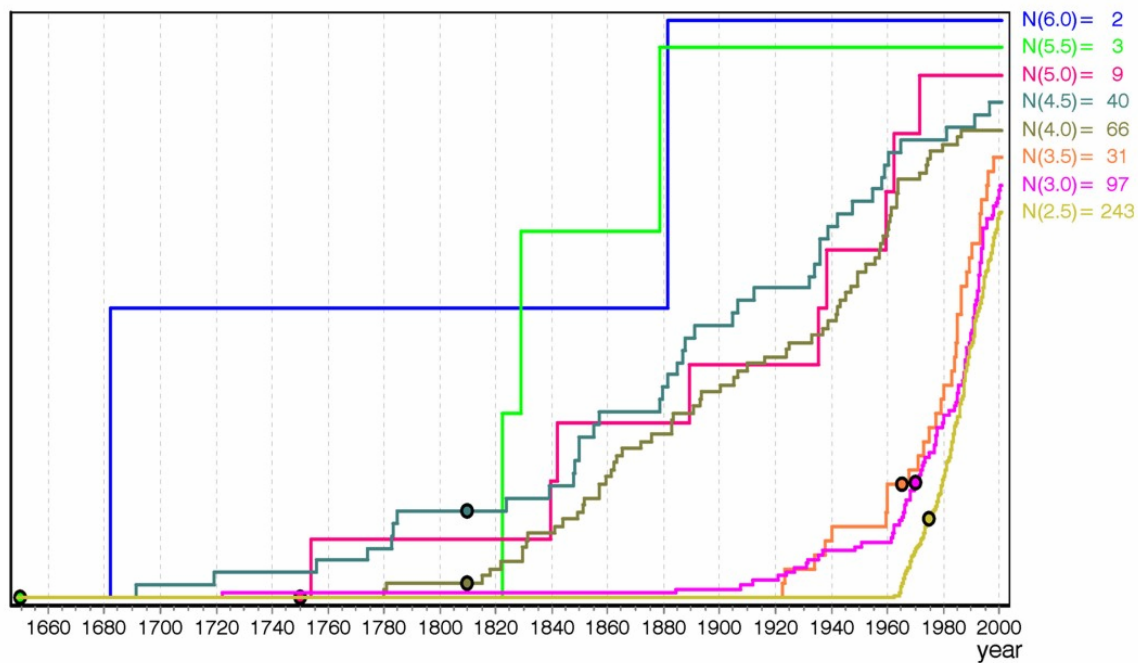
Fig. 4-4d: Cumulative plot of catalog entries for the gross zone eastern France for each magnitude class

The bold dots determine the times from which on a sufficient completeness is assumed.

Tab. 4-1:   Times of assigned PEGASOS data completeness in the gross zones

M_W / Gross zones	3.0	3.5	4.0	4.5	5.0	5.5	6.0	6.5	7.0
Switzerland CH	1880	1880	1860	1825	1770	1650	1575	1250	1250
Germany SW D - SW	1965	1870	1865	1865	1860	1200	1200		
France east F - E	1970	1965	1810	1810	1750	1650	1650		
Italy north I - N	1975	1975	1875	1850	1750	1750	1600	1600	
Austria west A - W	1975	1900	1875	1875	1550	1550			

4.4   Recurrence parameters

The crustal volumes derived within EG1b as seismic source zones comprise the combined effects from multiple independent processes of individual faults. This supports the assumption of a Poisson process in each source zone as well as the validity of the truncated exponential model for the earthquake recurrence. The truncated exponential model is derived from the Gutenberg-Richter recurrence relationship log N(m) = a – bm by truncating the rate density of earthquakes at the maximum magnitude, m_x. This truncated exponential model is given by the expression:

$$N(m) = N(m_o) \; \frac{e^{-\beta(m - m_o)} - e^{-\beta(m_x - m_o)}}{1 - e^{-\beta(m_x - m_o)}}$$

$N(m_o)$ is the annual frequency of earthquakes larger than the lower bound magnitude m_o, and $\beta = b\,ln(10)$, where b is the Gutenberg-Richter parameter.

The recurrence parameters of the truncated exponential relationship were estimated within EG1b with the maximum likelihood technique developed by Weichert (1980) which properly addresses the uncertainty of the parameters. We could make use of the computer code PLABD by B. Youngs (2002, PEGASOS TP1-ASW-0021). This code computes the maximum likelihood estimates of $N(m_o)$ = ν and b-values for variable magnitude increments (including the standard derivation σ) and outputs a distribution of relative likelihood for ν and β. The parameter m_x was set, as required, at m = 8. Output of the computer code PLFBAD is primarily the input for the PSHA code FRISK88M in form of tables of triplets of β, ν and their probabilities P for each source zone. σ of β is used to create a distribution of five values for β which is the basis to calculate corresponding ν and P. For the same set of the β-distribution σν is considered in a similar manner. This gives 25 triplets of P, ν and β where the sum of all P equals 1. Two examples of these 25 triplets for each source zone are given in Table 4-2. ν and b, as well as their uncertainties σν and σb, are extracted and summarized in Table 4-3. The parameters of the eight large zones, of the small zones as well as for the source zone combinations were calculated. Table 4-3 indicates the completeness model which was used for the respective source zone. The values for N (m > m_{min}) = ν reflect the level of seismic activity in the zones. The b-values in these zones are in the range of $0.68 - 1.18$, with corresponding σb in the range of $0.02 - 0.20$, when the extremes are excluded. Figure 4-5 shows the observed earthquake occurrence in each of the large zones with the corresponding maximum likelihood fit.

The recurrence parameters for the small zones, including their combinations (Tucan beak, Rhinoceros), have been calculated where a sufficient number of events is available. The small source zones with low seismicity were grouped according to the described seismotectonic constraints. A common b-value was then calculated for each group of source zones. Then this common b-value is set for each of the small zones of the groups to determine the corresponding v-value. In this way, the detailedness of the areal variation of the recurrence parameters could be kept. For these cases the computer code PLFBAD by B. Youngs (2003, PEGASOS TP1-ASW-0022) is used. The two different types of source zone combinations are depicted in Figure 4-6. Figure 4-6a shows the combination of certain seismic source zones with one or two others, while Figure 4-6b represents the three areas where source zones are combined to derive a common b-value. The common b-values are indicated with an asterisk in Table 4-3.

Tab. 4-2:   Examples of the input files for FRISK88M for two source zones

AE	Alp External		AC	Alps Central	
P	$n\psi$ (m ≥ 5.0)	beta	P	$n\psi$ (m ≥ 5.0)	beta
0.0057190	4.896e_02	1.609	0.0061318	1.511e_01	1.689
0.0171844	3.901e_02	1.693	0.0172795	1.339e_01	1.734
0.0114914	3.108e_02	1.778	0.0112839	1.187e_01	1.779
0.0019635	2.474e_02	1.863	0.0018216	1.052e_01	1.824
0.0000957	1.970e_02	1.948	0.0000758	9.323e_02	1.869
0.0159785	5.295e_02	1.609	0.0173350	1.573e_01	1.689
0.0892056	4.219e_02	1.693	0.0892480	1.395e_01	1.734
0.1061791	3.361e_02	1.778	0.1041840	1.236e_01	1.779
0.0315945	2.676e_02	1.863	0.0299759	1.095e_01	1.824
0.0026339	2.130e_02	1.948	0.0022269	9.707e_02	1.869
0.0096142	5.694e_02	1.609	0.0108660	1.635e_01	1.689
0.1006482	4.537e_02	1.693	0.1026088	1.450e_01	1.734
0.2123812	3.614e_02	1.778	0.2122816	1.285e_01	1.779
0.1089788	2.878e_02	1.863	0.1070211	1.139e_01	1.824
0.0154053	2.291e_02	1.948	0.0139418	1.009e_01	1.869
0.0011819	6.139e_02	1.609	0.0014585	1.701e_01	1.689
0.0248758	4.892e_02	1.693	0.0264161	1.508e_01	1.734
0.0975812	3.897e_02	1.778	0.0996405	1.337e_01	1.779
0.0890132	3.103e_02	1.863	0.0891544	1.185e_01	1.824
0.0217972	2.470e_02	1.948	0.0204311	1.050e_01	1.869
0.0000305	6.584e_02	1.609	0.0000414	1.767e_01	1.689
0.0013693	5.247e_02	1.693	0.0015059	1.567e_01	1.734
0.0104059	4.179e_02	1.778	0.0107100	1.389e_01	1.779
0.0172667	3.328e_02	1.863	0.0173279	1.231e_01	1.824
0.0074049	2.649e_02	1.948	0.0070321	1.091e_01	1.869

Tab. 4-3:   Recurrence parameters for all source zones and their combinations

Seismic Source Zones		Magnitude Frequency (maximum likelihood)					compl. model
		$\nu\,(m_{min})$	b	$\sigma\nu\,(m_{min})$	σ b	m_{min}	
label	name						
Large Zones							
EF	Eastern France	7.0190	1.0470	0.5012	0.0460	2.3	F-E
RG	Rhine Graben	2.8950	0.8580	0.3127	0.0570	2.3	D-SW01
SG	South Germany	5.1890	0.7750	0.4160	0.0370	2.3	D-SW01
BG	Bresse Graben	0.8781	0.6730	0.1788	0.0860	2.3	F-E
AE	Alps External	4.4160	0.7720	0.2858	0.0370	2.3	CH
AC	Alps Central	15.7200	0.7720	0.5392	0.0200	2.3	CH
AI	Alps Internal	1.3520	0.9170	0.1851	0.0930	3.3	I-N
PP	Po_Plain	0.4511	1.0750	0.1132	0.1990	3.3	I-N
all large zones		34.2400	0.7760	0.7970	0.0130	2.3	CH
Detailed Zones							
AC_01	Grenoble	1.0660	0.7690	0.1402	0.0740	2.3	CH
AC_02	Briancon	1.1100	0.7310	0.1408	0.0670	2.3	CH
AC_03	Arve	0.3494	0.7790	0.0806	0.1330	2.3	CH
AC_04	Prealpes	1.0130	0.7410	0.1351	0.0720	2.3	CH
AC_05	Wildhorn	1.4640	0.7560	0.1634	0.0620	2.3	CH
AC_06	Valais	1.3600	0.7280	0.1557	0.0600	2.3	CH
AC_07	Sarnen	0.6494	0.6810	0.1055	0.0790	2.3	CH
AC_08	Ticino	0.8332	0.9600	0.1336	0.1200	2.3	CH
AC_09	Walensee	1.2200	0.7330	0.1477	0.0640	2.3	CH
AC_10	Grisons	3.7480	0.8120	0.2675	0.0430	2.3	CH
AC_11	Vorarlberg	1.0280	0.7150	0.1346	0.0680	2.3	CH
AC_12	Glorenza	0.3638	0.8280	0.0728	0.1290	2.3	CH
AC_13	Allgaeu	0.2117	0.7910	0.0547	0.0510	2.3	CH
AC_14	Inntal	1.2620	0.8850	0.1599	0.0860	2.3	CH
AC_15	Tauern	0.0873	0.8280	0.0356	0.1290	2.3	CH
AE_01	BaselJura	0.1932	0.5840	0.0553	0.1160	2.3	CH
AE_02	E_Jura	0.2642	0.7180	0.0591	0.0610	2.3	CH
AE_03	Zuerich-Thurgau	0.8679	0.7290	0.1076	0.0410	2.3	CH
AE_04	Aarau-Luzern	0.1602	0.7290	0.0463	0.0410	2.3	CH
AE_05	Biel	0.2403	0.7290	0.0567	0.0410	2.3	CH

Tab. 4-3:   Continuation

Seismic Source Zones		Magnitude Frequency (maximum likelihood)					compl. model
		$\nu\,(m_{min})$	b	$\sigma\nu\,(m_{min})$	σ b	m_{min}	
Label	name						
Large Zones							
AE_06	Napf	0.1869	0.7290	0.0500	0.0410	2.3	CH
AE_07	Fribourg	0.2136	0.7290	0.0534	0.0410	2.3	CH
AE_08	Neuchatel lake	0.5341	0.7290	0.0844	0.0410	2.3	CH
AE_09	Vaud	0.3204	0.7290	0.0654	0.0410	2.3	CH
AE_10	Geneva	0.2670	0.7290	0.0597	0.0410	2.3	CH
AE_11	Vuache	0.1335	0.7290	0.0422	0.0410	2.3	CH
AE_12	West_Jura	0.7503	1.1830	0.1172	0.1400	2.3	CH
AE_13	Central_Jura	0.3843	1.1830	0.0839	0.1400	2.3	CH
AI_01	Dora Maira	2.3050	0.7000	0.2906	0.0520	2.3	I-N
AI_02	Alpi Sud	2.3900	0.7110	0.2956	0.0520	2.3	I-N
AI_03	Bolzano	0.0116	0.7110	0.0116	0.0510	3.3	I-N
BG_01	Bresse Graben	0.0642	0.6730	0.0371	0.0860	2.3	F-E
BG_02	Bresse_Sud	0.8306	0.6870	0.1735	0.0900	2.3	F-E
EF_01	Remiremont	0.7382	0.9220	0.1619	0.1210	2.3	F-E
EF_02	Vosges	0.5408	0.8660	0.1385	0.1330	2.3	F-E
EF_03	Dijon-Saone	0.7051	1.0320	0.1588	0.1420	2.3	F-E
EF_04	Massif Central	0.0406	1.1530	0.0143	0.0640	3.8	F-E
EF_05	Lorraine	4.0490	1.3330	0.3850	0.0880	2.3	F-E
EF_06	Mainz	0.9257	0.9070	0.1812	0.1070	2.3	F-E
PP_01	Po_Plain	0.4511	1.0750	0.1132	0.1990	3.3	I-N
RG_01	Basel	0.7386	0.8940	0.1544	0.1140	2.3	D-SW01
RG_02	South Rhine Graben	1.3280	0.8100	0.2046	0.0740	2.3	D-SW01
RG_03	North Rhine Graben	0.8876	0.8560	0.1683	0.0980	2.3	D-SW01
SG_01	Schwaebische Alb	2.0320	0.7580	0.2516	0.0550	2.3	D-SW01
SG_02	Stuttgart	0.0542	0.9050	0.0271	0.0680	2.8	D-SW01
SG_03	Saulgau	0.1973	0.7580	0.0624	0.0530	2.3	D-SW01
SG_04	Linzgau	0.4899	0.9050	0.1069	0.0680	2.3	D-SW01
SG_05	SingenBodensee	0.6185	0.8200	0.1149	0.0860	2.3	D-SW01
SG_06	Leibstadt	0.0594	0.8200	0.0423	0.0860	2.0	D-SW01
SG_07	Dinkelberg	0.1919	0.8200	0.0640	0.0860	2.3	D-SW01
SG_08	Sued Schwarzwald	0.2133	0.8200	0.0674	0.0860	2.3	D-SW01
SG_09	W_Schwarzwald	0.2100	0.9050	0.0700	0.0680	2.3	D-SW01

Tab. 4-3: Continuation

Seismic Source Zones	Magnitude Frequency (maximum likelihood)					compl. model
	$\nu\,(m_{min})$	b	$\sigma\nu\,(m_{min})$	$\sigma\,b$	m_{min}	
label name						
Large Zones						
SG_10 Rottweil	0.1633	0.9050	0.0617	0.0680	2.3	D-SW01
SG_11 N_Schwarzwald	0.2799	0.9050	0.0808	0.0680	2.3	D-SW01
SG_12 Wuerzburg	0.1633	0.9050	0.0617	0.0680	2.3	D-SW01
SG_13 Dreieck	0.2333	0.9050	0.0738	0.0680	2.3	D-SW01
SG_14 Fraenkische Alb	0.4899	0.9050	0.1069	0.0680	2.3	D-SW01
SG_15 Muenchen	0.3033	0.9050	0.0841	0.0680	2.3	D-SW01
Regrouping of small zones						
Dinkelberg Area: 'Tucan beak'						
SG_5_6_7_8	1.0240	0.8200	0.1799	0.0860	2.3	D-SW01
SG_5_6_8	0.8131	0.8010	0.1599	0.0940	2.3	D-SW01
SG_5_8	0.8131	0.8010	0.1599	0.0940	2.3	D-SW01
SG_6_7	0.2129	0.9200	0.0832	0.2210	2.3	D-SW01
Basel area: 'Rhinoceros'						
RG_1 AE_1	0.8386	0.7500	0.1615	0.0850	2.3	D-SW01
AE_1_13	0.5344	0.7870	0.1000	0.1090	2.3	CH
AE_1_2	0.4626	0.6640	0.0884	0.0900	2.3	CH
AE_1_2_13	0.8084	0.7760	0.1225	0.0870	2.3	CH
Schwaebische Alb						
SG_1_2	2.1150	0.7590	0.2567	0.0540	2.3	D-SW01

*: b and $\sigma\,b$ are taken from the respective common b area; $\sigma\nu(m_{min})$ is calculated from the respective source zone data using the common b (mean only)

Tab. 4-3:   Continuation

common b areas							applied to
	$\nu\,(m_{min})$	b	$\sigma\nu\,(m_{min})$	σ b	m_{min}	compl.	
AC_11_13_14	2.4850	0.7910	0.2161	0.0510	2.3	CH	AC_13
AC_12_15	0.4511	0.8280	0.0934	0.1290	2.3	CH	all
AE_02_03_04	1.2820	0.7180	0.1505	0.0610	2.3	CH	AE_02
AE_03_04_05_06_07_08_09_10_11	2.9240	0.7290	0.2283	0.0410	2.3	CH	all
AE_12_13	1.1350	1.1830	0.1671	0.1400	2.3	CH	all
AI_02_03	2.4160	0.7110	0.2972	0.0510	2.3	I-N	AI_03
BG_01_02	0.8781	0.6730	0.1788	0.0860	2.3	F-E	BG_01
EF_03_04_05	4.8230	1.1530	0.4173	0.0640	2.3	F-E	EF_04
SG_01_03	2.2290	0.7580	0.2635	0.0530	2.3	D-SW01	SG_03
SG_02_04_09_10_11_12_13_14_15	2.1240	0.9050	0.2623	0.0680	2.3	D-SW01	all
SG_05_06_07_08	1.0240	0.8200	0.1799	0.0860	2.3	D-SW01	all

Input from Deichmann 2002, Deichmann et al. 2002, Gardner & Knopoff 1974, Grünthal 1985, Grünthal et al. 1998a and 1998b, Grünthal & Mayer-Rosa 1998, Reasenberg 1985, Uhrhammer 1986, Weichert 1980
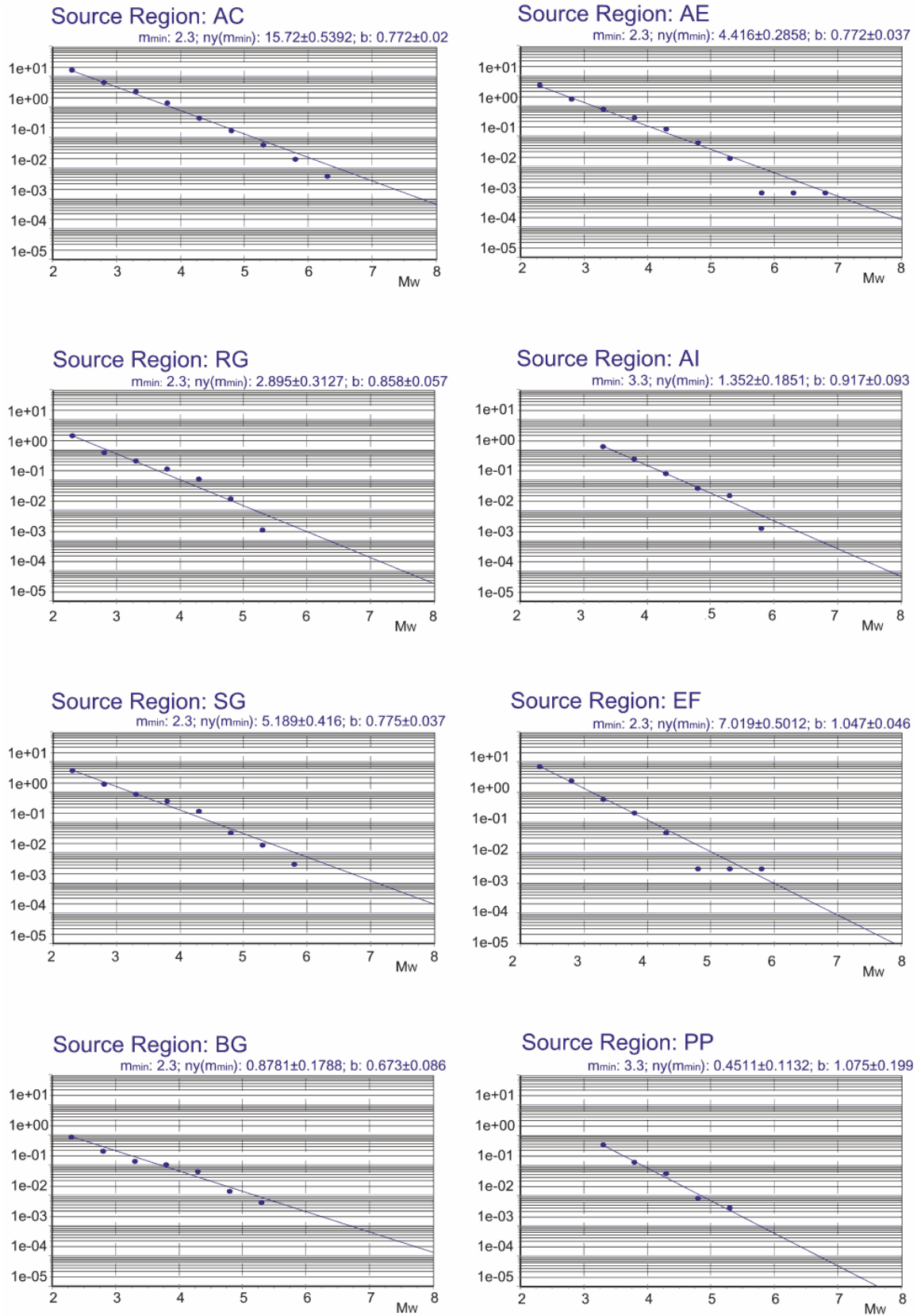
Fig. 4-5:   Observed earthquake occurrence in the eight large source zones with the corresponding maximum likelihood fit
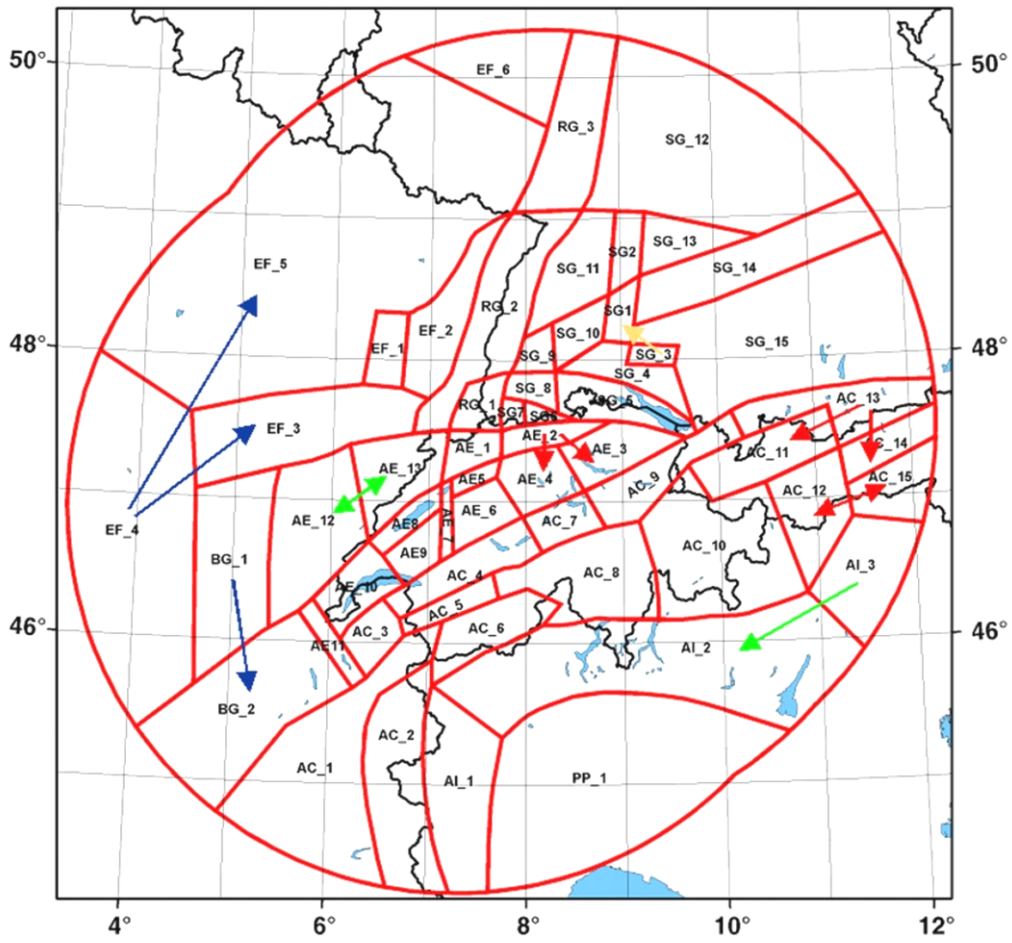
Fig. 4-6a: Combination of certain seismic source zones with one or two others to derive a common b-value

E.g. the zones BG-1 and BG-2 were joint to calculate the b-value for BG-1.
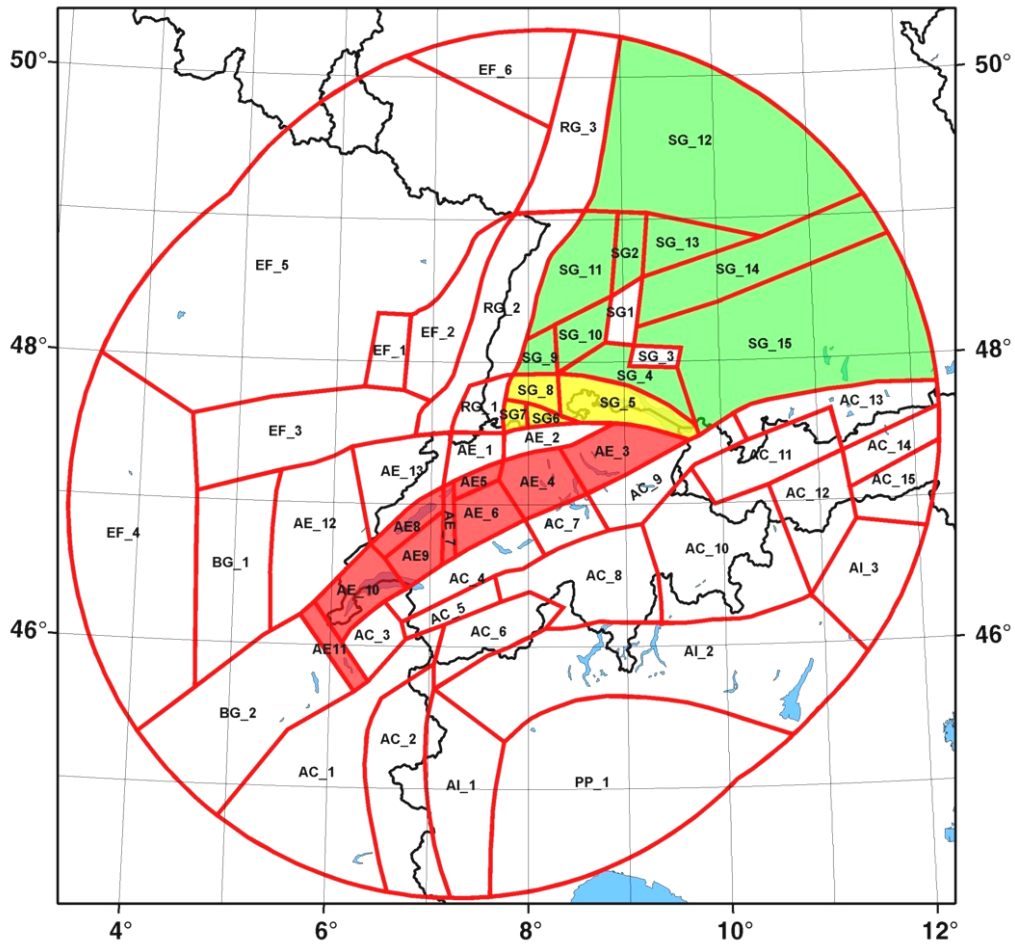
Fig. 4-6b: Combinations of seismic source zones to derive a common b-value in the three
              coloured areas

              These b-values are then applied to all sources.

5   REFERENCES

Adams, J., Wetmiller, R.J., Hasegawa, H.S. & Drysdale, J. 1991: The first surface faulting from a historical intraplate earthquake in North America. Nature 352.

Affolter, T. 1998: Néotectonique dans les Alpes suisses occidentales: la zone sismique du Wildhorn dans le cadre des déformations alpines tardives. Unpubl. Diploma thesis, University of Neuchâtel.

Anderson, E.M. 1951: Dynamics of faulting and dyke formation. Oliver and Boyd, Edinburgh.

Aoudia, A., Sarao, A., Bukchin, B. & Suhadolc, P. 2000: The 1976 Friuli (NE Italy) thrust faulting earthquake: A reappraisal 23 years later. Geophysical Research Letters 27/4, 573-576.

Aubert, D. 1945: Le Jura et la tectonique d'écoulement. Mémoire de la société vaudoise des sciences naturelles 8, 217-236.

Audin, L., Avouac, J.P. & Flouzat, M. 2002: Fluid-driven seismicity in a stable tectonic context; the Remiremont fault zone, Vosges, France. Geophysical Research Letters 29/6, 10.1029.

Avouac, J.P. & Burov, E.B. 1996: Erosion as a driving mechanism of intracontinental mountain growth. Journal of Geophysical Research 101/B8, 17747-17769.

Axen, G.J., Selverstone, J., Byrne, T. & Fletcher, J.M. 1998: If the strong crust leads, will the weak crust follow? GSA Today 8/12, 1-8.

Bachmann, G.H. & Müller, M. 1992: Sedimentary and structural evolution of the German Molasse Basin. Eclogae Geol. Helv. 85/3, 519-530.

Bachmann, G.H., Dohr, G. & Müller, M. 1982: Exploration in a classic thrust belt and its foreland: Bavarian Alps, Germany. American Association of Petroleum Geologists Bulletin 66, 2529-2542.

Bachmann, G.H., Müller, M. & Weggen, K. 1987: Evolution of the Molasse Basin (Germany, Switzerland). Tectonophysics 137, 77-92.

Baer, M., Deichmann, N., Braunmiller, J., Dolfin, D.B., Bay, F., Bernardi, F., Delouis, B., Fäh, D., Gerstenberger, M., Giardini, D., Huber, S., Kastrup, U., Kind, F., Kradolfer, U., Maraini, S., Mattle, B., Schler, T., Salichon, J., Sellami, S., Steimen, S. & Weimer, S. 2001: Earthquakes in Switzerland and surrounding regions during 2000. Eclogae Geol. Helv. 94/2, 253-264.

Becker, A. 1989: Detached neotectonic stress field in the northern Jura Mountains, Switzerland. Geologische Rundschau 78/2, 459-475.

Becker, A. 2000: The Jura Mountains − An active foreland fold-and-thrust belt? Tectonophysics 321/4, 381-406.

Becker, A., Davenport, C.A. & Giardini, D. 2002: Palaeoseismicity studies on end-Pleistocene and Holocene lake deposits around Basle, Switzerland. Geophysical Journal International 149/3, 659-678.

Berger, J.-P. 1996: Cartes plaéogéographiques-palinspastiques du bassin molassique suisse (Oligocène inférieur – Miocène moyen). Neues Jahrbuch für Geologie und Paläontologie, Abhandlungen 202/1, 1-44.

Berger, Z. 1994: Satellite hydrocarbon exploration: interpretation and integration techniques. Springer.

Bergerat, F. 1987: Paléo-champs de contrainte tertiaires dans la plate-forme européenne au front de l'orogène alpin. Bulletin de la Société géologique de France 8(3), 611-620.

Bergerat, F., Mugnier, J.L., Guellec, S., Truffert, C., Cazes, M., Damotte, B. & Roure, F. 1990. Extensional tecctonics and subsidence of the Bresse basin: an interpretation form ECORS data. *In*: Deep Structure of the Alps (edited by Roure, F., Heitzmann, P. & Polino, R.). Mémoire 1, 145-156.

Birkhäuser, P., Roth, P., Meier, B. & Naef, H. 2001: 3-D Seismik: Räumliche Erkundung der mesozoischen Sedimentschichten im Zürcher Weinland. Nagra Technischer Bericht NTB 00-03. Nagra, Wettingen, Switzerland.

Blondel, T., Charollais, J., Sambeth, U. & Pavoni, N. 1988: La faille du Vuache (Jura meridional); un exemple de faille a caractère polyphase. Bulletin de la Société Vaudoise des Sciences Naturelles 79/2, 65-91.

Boyer, S.E. & Elliott, D. 1982: Thrust systems. American Association of Petroleum Geologists Bulletin 66/9, 1196-1230.

BRGM 1989: Dijon – Carte géologique de la France 1:250'000, feuille No. 19. Service de la Carte géologique de la France.

Brink, H.J., Burri, P., Lunde, A. & Winhard, H. 1992: Hydrocarbon habitat and potential of Swiss and German Molasse Basin: A comparison. Eclogae Geol. Helv. 85/3, 715-732.

Brun, J.P., Gutscher, M.A., Blum, R., Bois, C., Burg, J.P., Colletta, B., Duerbaum, H., Damotte, B., Durst, H., Fuchs, K., Grohmann, N., Huebner, M., Karcher, T., Kessler, G., Kloeckner, M., Lucazeau, F., Lueschen, E., Marthelot, J.M., Meier, L., Ravat, M., Reichert, C., Vernassa, S., Villemin, T., Wenzel, F. & Wittlinger, G. 1992: Deep crustal structure of the Rhine Graben from DEKORP-ECORS seismic reflection data; a summary. *In*: Geodynamics of rifting; Volume I, Case history studies on rifts; Europe and Asia. (edited by Ziegler, P.A.). Tectonophysics 208, 1-3. Elsevier, Amsterdam, Netherlands, 139-147.

Brun, J.P., Wenzel, F., Blum, R., Bois, C., Burg, J.P., Colletta, B., Damotte, B., Durbaum, H., Durst, H., Fuchs, K., Grohmann, N., Gutscher, M.A., Huebner, M., Karcher, T., Kessler, G., Kloeckner, M., Lucazeau, F., Lueschen, E., Marthelot, J.M., Meier, L., Ravat, M., Reichert, C., Vernessa, S., Villemin, T. & Wittlinger, G. 1991: Crustal-scale structure of the southern Rhinegraben from ECORS-DEKORP seismic reflection data. Geology (Boulder) 19/7, 758-762.

Burkhard, M. 1988: L'Helvétique de la bordure occidentale du massif de l'Aar (évolution tectonique et métamorphique. Eclogae Geol. Helv. 81/1, 63-114.

Burkhard, M. 1990: Aspects of the large-scale Miocene deformation in the most external part of the Swiss Alps (Subalpine Molasse to Jura fold belt). Eclogae Geol. Helv. 83/3, 559-583.

Burkhard, M. 1999: Strukturgeologie und Tektonik im Bereich AlpTransit. *In*: Vorerkundung und Prognose der Basistunnels am Gotthard und am Lötschberg (edited by Löw, S., Wyss, R., Briegel, U., Oddson, B. & Schlickenrieder, L.). Balkema, Rotterdam, 45-56.

Burkhard, M. & Sommaruga, A. 1998: Evolution of the western Swiss Molasse basin: structural relations with the Alps and the Jura belt. *In*: Cenozoic Foreland Basins of Western Europe (edited by Mascle, A., Puigdefàbregas, C., Luterbacher, H.P. & Fernàndez, M.) 134. Geological Society Special Publications, London, 279-298.

Burkhard, M., Atteia, O., Sommaruga, A., Gogniat, S. & Evard, D. 1998: Tectonique et hydro-géologie dans le Jura neuchâtelois. Eclogae Geol. Helv. 91/1, 177-183.

Calais, E., Bayer, R., Chery, J., Cotton, F., Doerflinger, E., Flouzat, M., Jouanne, F., Kasser, M., Laplanche, M., Maillard, D., Martinod, J., Mathieu, F., Nicolon, P., Nocquet, J.M., Scotti, O., Serrurier, L., Tardy, M. & Vigny, C. 2001. REGAL: a permanent GPS network in the western Alps. Configuration and first results. Bulletin de la Société Géologique de France 172/2, 141-158.

Coletta, B., Cacas, R., Vially, R. & Lecompte, J.C. 2002: Southern Jura Petroleum Systems. Institut Français du Pétrole (IFP), Rueil-Malmaison (Paris).

Cramer, H. 1948: Mathematical methods of statistics. Princeton University Press. Princeton.

Das, S. & Scholz, C.H. 1983: Why large earthquakes do not nucleate at shallow depths. Nature 305/5935, 621-623.

Deichmann, N. 1992a: Recent seismicity of the northern Alpine foreland of Switzerland. Eclogae Geol. Helv. 85/3, 701-705.

Deichmann, N. 1992b: Structural and rheological implications of lower-crustal earthquakes below northern Switzerland. Physics of the Earth and Planetary Interiors 69/3-4, 270-280.

Deichmann, N. 2002: Performance of declustering methods. PEGASOS Technical Note EG1-TN-0305.

Deichmann, N. & Garcia Fernandez, M. 1992: Rupture geometry from high-precision relative hypocentre locations of microearthquake clusters. Geophysical Journal International 110/3, 501-517.

Deichmann, N. & Rybach, L. 1989: Earthquakes and temperatures in the lower crust below the northern Alpine Foreland of Switzerland. Geophysical Monograph 51, 197-213.

Deichmann, N., Baer, M., Braunmiller, J., Dolfin, D.B., Bay, F., Delouis, B., Fäh, D., Giardini, D., Kastrup, U., Kind, F., Kradolfer, U., Kunzle, W., Rothlisberger, S., Schler, T., Salichon, J., Sellami, S., Spuhler, E. & Wiemer, S. 2000: Earthquakes in Switzerland and surrounding regions during 1999. Eclogae Geol. Helv. 93/3, 395-406.

Deichmann, N., Baer, M., Braunmiller, J., Ballarin, D., Bay, F., Bernardi, F., Delouis, B., Fäh, D., Gerstenberger, M., Giardini, D., Huber, S., Kradolfer, U., Maraini, S., Oprsal, I., Schibler, R., Schler, T., Sellami, S., Steimen, S., Wiemer, S., Wössner, J. & Wyss, A. 2002: Earthquakes in Switzerland and surrounding regions during 2002. Eclogae Geol. Helv. 95/3, 249-261.

Dewey, J.F. 1988: Extensional collapse of orogens. Tectonics 7/6, 1123-1139.

Dèze P. & Ziegler, P. 2002: European Moho Map. Internet resource. EUCORE-URGENT project, University of Basel. http://comp1.geol.unibas.ch/modules.php?name=Downloads&d_op=viewdownload&cid=1 (last accessed in January 2004).

Diebold, P., Naef, H. & Ammann, M. 1991: Zur Tektonik der Zentralen Nordschweiz. Nagra Technischer Bericht NTB 90-04. Nagra, Wettingen, Switzerland.

Eckart, P. 1957: Zur Talgeschichte des Tavetsch, seine Bruchsysteme und jungquartären Verwerfungen, Zürich.

Eckart, P. 1974: Untersuchungen von rezenten Krustenbewegungen an der Rhein-Rhone-Linie. Eclogae Geol. Helv. 67/1, 233-235.

Eckart, P., Funk, H. & Labhart, T. 1983: Postglaziale Krustenbewegungen an der Rhein-Rhone-Linie. Vermessung, Photogrammetrie und Kulturtechnik 83/2, 43-56.

Eisbacher, G. & Brandner, R. 1996: Superposed fold-thrust structures and high-angle faults, northwestern Calcareous Alps, Austria. Eclogae Geol. Helv. 89/1, 553-576.

Eisbacher, G., Linzer, H., Meier, L. & Polinski, R. 1990: A depth-extrapolated structural transect across the northern calcareous Alps of western Tirol. Eclogae Geol. Helv. 83/3, 711-726.

Erard, P.F. 1999: Traitement et interprétation de cinq lignes sismiques réflexion à travers le Plateau molassique et les Préalpes suisses, de Bienne à Lenk. Unpubl. Doctorat thesis, Lausanne.

Escher, A., Hunziker J.C., Marthaler, M., Masson, H., Sartori, M. & Steck, A. 1997: Geologic framework and structural evolution of the Western Swiss-Italian Alps. *In*: Results of NRP 20 deep structure of the Swiss Alps (edited by Pfiffner, O.A., Lehner, P., Heitzmann, P., Mueller, S. & Steck, A.). Birkhäuser Verlag, Basel, 205-221.

Faber, S., Bonjer, K.P., Brüstle, W. & Deichmann, N. 1994: Seismicity and structural complexity of the Dinkelberg Block, Southern Rhine Graben. Geophysical Journal International 116/2, 393-408.

Franck, P., Wagner, J.J., Escher, A. & Pavoni, N. 1984: Evolution des contraintes tectoniques et sismicité dans la région du Col Sanetsch, Alpes valaisannes helvétiques. Eclogae Geol. Helv. 77/2, 383-393.

Frei, B. & Löw, S. 2001: Structure and hydraulics of fault zones in the Southern Aar Massiv near Sedrun. Eclogae Geol. Helv. 94/1, 13-28.

Funk, H. & Gubler, E. 1980: Höhenänderungen der Fixpunkte im Gotthard-Bahntunnel zwischen 1917 und 1977 und ihre Beziehung zur Geologie. Eclogae Geol. Helv. 73/2, 583-592.

Gardner, J.K. & Knopoff, L. 1974: Is the sequence of earthquakes in Southern California, with aftershocks removed, Poissonian? Bull. Seism. Soc. Am. 64, 1363-1367.

Grellet, B., Combes, P., Granier, T. & Philip, H. 1993: Sismotectonique de la France Métropolitaine. Mémoire Société Géologique France n.s. 164/1/2, 76 p. & 24 plates.

Grünthal, G. 1985: The up-dated earthquake catalogue – statistical data characteristics and conclusions for hazard assessment. *In*: Internat. Symp. Analysis of Seismicity and Seismic Risk, Liblice, Prague, 19-25.

Grünthal, G., Mayer-Rosa, D. & Lenhardt, W.A. 1998a: Abschätzung der Erdbebengefährdung für die D-A-CH-Staaten Deutschland, Österreich, Schweiz. Bautechnik 75/10, 19-33.

Grünthal, G., Mayer-Rosa, D. & Lenhardt, W.A. 1998b: Abschätzung der Erdbebengefährdung für die D-A-CH Staaten Deutschland, Österreich, Schweiz. Bautechnik, Verlag Ernst & Sohn, Berlin 75/10, 753-767.

Grünthal, G. & Mayer-Rosa, D. 1998: Einheitliche Erdbebengefährdungskarte für Deutschland, Österreich und die Schweiz (D_A_CH), Carte de l'aléa sismique unifiée pour l'Allemagne, l'Autriche et la Suisse (D_A_CH). Schweizerischer Pool für Erdbebendeckung, Geschäftsbericht, Bern, 11-24.

Gubler, E., Schneider, D. & Kellerhals, P. 1984: Bestimmung von rezenten Bewegungen der Erdkruste mit geodätischen Methoden. Nagra Technischer Bericht NTB 84-17. Nagra, Wettingen, Switzerland.

Gudmundsson, G.H. 1994: An order of magnitude estimate of the current uplift-rates in Switzerland caused by the Würm alpine deglaciation. Eclogae Geol. Helv. 87/2, 545-557.

Guellec, S., Mugnier, J.L., Tardy, M. & Roure, F. 1990: Neogene evolution of the western Alpine foreland in the light of ECORS data and balanced cross sections. *In*: Deep structure of the Alps (edited by Roure, F., Heitzmann, P. & Polino, R.). 1. Mém. Soc. géol. suisse, Zürich, 165-184.

Guellec, S., Tardy, M., Roure, F. & Mugnier, J.L. 1989: Une interprétation tectonique nouvelle du massif subalpin des Bornes (Alpes occidentales): apports des données de la géologie et de la géophysique profondes. Comptes Rendus de l'Académie des Sciences de Paris 309/II, 913-920.

Gutenberg, B. & Richter. R.F. 1944: Frequency of earthquakes in California Bull. Seism. Soc. Am. 34, 185-188.

Haessler, H., Hoangtrong, P., Schick, R., Schneider, G. & Strobach, K. 1980: The September 3, 1978, Swabian Jura Earthquake. Tectonophysics 68/1-2, 1-14.

Heim, A. 1915: Die horizontalen Transversalverschiebungen im Juragebirge. Geol. Nachlese Nr.22. Verhandlungen Naturforschende Gesellschaft Zürich 60/3-4, 597-610.

Heim, A. 1921: Geologie der Schweiz. Band I: Molasseland und Juragebirge. Tauchniz, Leipzig.

Hinderer, M. 2001: Late Quaternary denudation of the Alps, valley and lake fillings and modern river loads. Geodinamica Acta 14/4, 231-263.

Hindle, D. & Burkhard, M. 1999: Strain, displacement and rotation associated with the formation of curvature in fold belts; the example of the Jura arc. Journal of Structural Geology 21, 1089-1101.

Homberg, C., Lacombe, O., Angelier, J. & Bergerat, F. 1999: New constraints for indentation mechanisms in arcuate belts from the Jura Mountains, France. Geology (Boulder) 27/9, 827-830.

Hough, S.E. 2002: Earthshaking Science – What we know (and don't know) about earthquakes. Princeton University Press, Princeton and Oxford.

Hunziker, J.C., Hurfond, A.J. & Calmbach, L. 1997: Alpine cooling and uplift. *In*: Results of NRP 20 deep structure of the Swiss Alps (edited by Pfiffner, O.A., Lehner, P., Heitzmann, P., Mueller, S. & Steck, A.). Birkhäuser Verlag, Basel, 260-263.

Illies, J.H. 1981: Mechanism of graben transformation. Tectonophysics 73, 249-266.

Isler, A. 1985: Literaturzusammenstellung zur Neotektonik. Nagra Technischer Bericht NTB 84-29. Nagra, Wettingen, Switzerland.

Jackson, J. 2002: Strength of the continental lithosphere: time to abandon the jelly sandwich? GSA Today 9 (September 2002), 4-9.

Jaeckli, H. 1958: Der rezente Abtrag der Alpen im Spiegel der Vorlandsedimentation. Eclogae Geol. Helv. 51/2, 354-365.

Johnston, A.C., Coppersmith, K.J., Kanter, L.R. & Cornell, C.A. 1994: The earthquakes of stable continental regions – Assessment of large earthquake potential. Electric Power Research Institute (EPRI).

Jouanne, F., Ménard, G. & Darmendrail, X. 1995: Present day vertical displacements in the north-western Alps and southern Jura Mountains: Data from leveling comparisons. Tectonics 14/3, 606-616.

Kahle, H.G., Geiger, A., Buerki, B., Gubler, E., Marti, U., Wirth, B., Rothacher, M., Gurtner, W., Beutler, G., Bauersima, I. & Pfiffner, O.A. 1997: Recent crustal movements, geoid and density distribution, contribution from integrated satellite and terrestrial measurements. *In*: Results of NRP 20 deep structure of the Swiss Alps (edited by Pfiffner, O.A., Lehner, P., Heitzmann, P., Mueller, S. & Steck, A.). Birkhäuser Verlag, Basel, 251-259.

Kaneda, H. 2003: Threshold of geomorphic detectability estimated from geologic observations of active low slip-rate strike-slip faults. Geophysical Research Letters 30(5), doi:10.1029/2002GL016280.

Kastrup, U. 2002: Seismotectonics and stress field variations in Switzerland. Unpubl. PhD thesis, ETH-Zürich.

Kijko, A. & Graham, G. 1998: Parametric-historic procedure for probabilistic seismic hazard analysis. Part I: estimation of maximum regional magnitude m_{max}. Pure Appl. Geophys. 152, 413-442.

Kijko, A. & Sellevoll, M.A. 1989: Estimation of earthquake hazard parameters from incomplete data files. Part 1: Utilization of extreme and complete catalogues with different threshold magnitudes. Bull. Seism. Soc. Am. 79/3, 645-654.

Klingele, E., Lahmeyer, B. & Freeman, R. 1991: The EGT Bouguer gravity compilation. Tectonophysics 195, 437-441.

Kohler, V. 1999: Néotectonique dans l'ensellement du Rawil. Unpubl. Diploma thesis University of Neuchâtel.

Lamb, S. 2002: Earth science – Is it all in the crust? Nature 420/6912, 130-131.

Laubscher, H. 1992: The Alps – a transpressive pile of peels. *In*: Thrust tectonics 1990 (edited by McClay, K.R.), Egham, United Kingdom, 277-285.

Laubscher, H.P. 1961: Die Fernschubhypothese der Jurafaltung. Eclogae Geol. Helv. 54, 221-280.

Laubscher, H.P. 1985: The eastern Jura: relations between thin-skinned and basement tectonics, local and regional. Nagra Technischer Bericht NTB 85-53. Nagra, Wettingen, Switzerland.

Laubscher, H.P. 1987: Die tektonische Entwicklung der Nordschweiz. Eclogae Geol. Helv. 80/2, 287-303.

Laubscher, H.P. 1988: Material balance in alpine orogeny. Geological Society of America, Bulletin 100/9, 1313-1328.

Lefort, J.P. & Agarwal, B.N.P. 2002: Topography of the Moho undulations in France from gravity data: their age and origin. Tectonophysics 350, 193-213.

Lippitsch, R. 2002: Lithosphere and upper mantle p-wave velocity structure beneath the Alps by High-Resolution Teleseismic Tomography. Unpubl. PhD thesis, ETH.

Mancktelow, N. 1985: The Simplon Line: a major displacement zone in the western Lepontine Alps. Eclogae Geol. Helv. 78/1, 73-96.

Mancktelow, N. 1992: Neogene lateral extension during convergence in the Central Alps: evidence from interrelated faulting and backfolding around the Simplonpass (Switzerland). Tectonophysics 215, 295-317.

Maurer, H. 1993: Seismotectonics and upper crustal structure in the Western Swiss Alps. Unpublished PhD thesis, ETH-Zürich.

Maurer, H., Burkhard, M., Deichmann, N. & Green, A.G. 1997: Active tectonism in the central Alps: contrasting stress regimes north and south of the Rhone Valley. Terra Nova 9/2, 91-94.

Mayer-Rosa, D. & Cadiot, B. 1979: Review of the 1356 Basel Earthquake – Basic Data. Tectonophysics 53/3-4, 325-333.

Meghraoui, M., Delouis, B., Ferry, M., Giardini, D., Huggenberger, P., Spottke, I. & Granet, M. 2001: Active normal faulting in the Upper Rhine Graben and paleoseismic identification of the 1356 Basel earthquake. Science 293/5537, 2070-2073.

Meier, B.P. 1994: Untere Süsswassermolasse des westlichen Mittellandes – Regionale Interpretation bestehender Seismik und petrophysikalische Interpretation von Fremdbohrungen. Unpubl. Nagra Internal Report NIB 94-28. Nagra, Wettingen, Switzerland.

Meyer, B., Lacassin, R., Brulhet, J. & Mouroux, B. 1994: The Basel 1356 Earthquake – Which fault produced it? Terra Nova 6/1, 54-63.

Meyer, M. 2000: Le complexe récifal kimméridgien-thitonien du Jura méridional interne (France), évolution multifactorielle, stratigraphie, tectonique. Terre & Environnement 24, 179.

Molnar, P. 1987: Inversion of profiles of uplift rates for the geometry of dip-slip faults at depth, with examples from the Alps and the Himalaya. Annales Geophysicae 5B/06, 663-670.

Mosar, J. 1999: Present-day and future tectonic underplating in the western Swiss Alps: reconciliation of basement/wrench-faulting and decollement folding of the Jura and Molasse basin in the Alpine foreland. Earth and Planetary Science Letters 173/3, 143-155.

Müller, W.H., Naef, H. & Graf, H.R. 2002: Geologische Entwicklung der Nordschweiz, Neotektonik und Langzeitszenarien Zürcher Weinland. Nagra Technischer Bericht NTB 99-08. Nagra, Wettingen, Switzerland.

Müller, W.H., Huber, M., Isler, A. & Kleboth, P. 1984: Erläuterungen zur "Geologischen Karte der zentralen Nordschweiz 1:100'000". Nagra Technischer Bericht NTB 84-25. Nagra, Wettingen, Switzerland.

Niviere, B. & Winter, T. 2000: Pleistocene northwards fold propagation of the Jura within the southern Upper Rhine Graben: seismotectonic implications. Global and Planetary Change 27/1-4, 263-288.

Pavoni, N. 1961: Faltung durch Horizontalverschiebung. Eclogae Geol. Helv. 54/2, 515-534.

Pavoni, N. 1987: Zur Seismotektonik der Nordschweiz. Eclogae Geol. Helv. 80/2, 461-471.

Pavoni, N., Maurer,H.R., Roth, P. & Deichmann, N. 1997: Seismicity and seismotectonics of the Swiss Alps. *In*: Results of NRP 20 deep structure of the Swiss Alps (edited by Pfiffner, O.A., Lehner, P., Heitzmann, P., Mueller, S. & Steck, A.). Birkhäuser Verlag, Basel, 241-250.

PEGASOS EXT-TB-0043 2002: ECOS: Earthquake Catalogue of Switzerland. Final version, 16.04.02. SED-ETHZ.

Persaud, M. 2002: Active tectonics in the Eastern Swiss Alps. Unpubl. Doctorat thesis, Universität Bern.

Pfiffner, O.A. 1986: Evolution of the north Alpine foreland basin in the Central Alps. Special Publication of the international Association of sedimentologists 8, 219-228.

Pfiffner, O.A. & Heitzmann, P. 1997: Geological interpretation of the seismic profiles of the central traverse (lines C1, C2 and C3-north). *In*: Results of NRP 20 deep structure of the Swiss Alps (edited by Pfiffner, O.A., Lehner, P., Heitzmann, P., Mueller, S. & Steck, A.). Birkhäuser Verlag, Basel, 115-122.

Pfiffner, O.A., Erard, P.F. & Staeuble, M. 1997a: Two cross sections through the Swiss Molasse Basin (lines E4-E6, W1, W7-W10). *In*: Results of NRP 20 deep structure of the Swiss Alps (edited by Pfiffner, O.A., Lehner, P., Heitzmann, P., Mueller, S. & Steck, A.). Birkhäuser Verlag, Basel, 64-72.

Pfiffner, O.A., Lehner, P., Heitzmann, P., Mueller, S. & Steck, A. 1997b: Deep Structure of the Swiss Alps, results of NRP 20. Birkhäuser Verlag, Basel.

Philippe, Y. 1995: Rampes latérales et zones de transfert dans les chaînes plissées: géométrie, conditions de formation et pièges structuraux associés. Unpubl. PhD thesis, Chambéry (Savoie, France).

Philippe, Y., Coletta, B., Deville, E. & Mascle, A. 1996: The Jura fold-and-thrust belt: a kinematic model based on map-balancing. *In*: Peri-Tethys Memoir 2: Structure and Prospects of Alpine Basins and Forelands (edited by Ziegler, P.A. & Horvath, F.). Mém. Mus. natn. Hist. nat. 170, 235-261.

Pisarenko, V.F., Lyubushin, A.A., Lysenko, V.B. & Golubieva, T.V. 1996: Statistical evaluation of seismic hazard parameters: maximum possible magnitude and related parameters. Bull. Seism. Soc. Am. 86, 691-700.

Plancherel, R. 1979: Aspect de la déformation en grand dans les Préalpes médianes plastiques entre Rhône et Aar. Eclogae Geol. Helv. 72/1, 145-214.

Plenefisch, T. & Bonjer, K.P. 1997: The stress field in the Rhine Graben area inferred from earthquake focal mechanisms and estimation of frictional parameters. Tectonophysics 275/1-3, 71-97.

Poli, M.E., Peruzza, L., Rebez, A., Renner, G., Sleijko, D. & Zanferrari, A. 2002: New seismotectonic evidence from the analysis of the 1976-1977 and 1977-1999 seismicity in Friuli (NE Italy). Bolletino Geofisica Teorica ed Applicata 43/1-2, 53-78.

Price, N.J. & Cosgrove, J.W. 1990: Analysis of Geological Structures. Cambridge University Press, Cambridge.

Rahn, M.K., Hurford, A.J. & Frey, M. 1997: Rotation and exhumation of a thrust plane, apatite fission-track data from the Glarus Thrust, Switzerland. Geology 25/7, 599-602.

Ratschbacher, L., Frisch, W., Linzer, H.-G. & Merle, O. 1991a: Lateral extrusion in the Eastern Alps. Part 2: Structural analysis. Tectonics 10/2, 257-271.

Ratschbacher, L., Merle, O., Davy, P. & Cobbold, P. 1991b: Lateral extrusion in the Eastern Alps. Part 1: Boundary conditions and experiments scaled for gravity. Tectonics 10/2, 245-256.

Ratschbacher, L., Frisch, W., Neubauer, F., Schmid, S.M. & Neugebauer, J. 1989: Extension in compressional orogenic belts: The eastern Alps. Geology 17, 404-40.

Raymond, D., Defontaines, B., Fehri, A., Dorioz, J.M. & Rudant, J.P. 1996: Néotectonique dans la région sud-lémanique (Haute-Savoie, France): approche multisources (imagerie optique et hyperfréquences, analyse morphostructurale). Eclogae Geol. Helv. 89/3, 949-973.

Reasenberg, P.A. 1985: Second-order moment of Central California Seismicity. Journal of Geophysical Research, B, Solid Earth and Planets 90, 5479-5495.

Reinecker, J. & Schneider, G. 2002: Zur Neotektonik der Zollernalb: Der Hohenzollerngraben und die Albstadt-Erdbeben. Jber. Mitt. oberrhein. geol. Ver. 84, 391-417.

Roth, P., Pavoni, N. & Deichmann, N. 1992: Seismotectonics of the Eastern Swiss Alps and Evidence for Precipitation-Induced Variations of Seismic Activity. Tectonophysics 207/1-2, 183-197.

Rubin, C.M. 1996: Systematic underestimation of earthquake magnitudes from large intra-continental reverse faults: Historical ruptures break across segment boundaries. Geology 24/11, 989-992.

Sambeth, U. & Pavoni, N. 1988: A seismotectonic investigation in the Geneva Basin, southern Jura Mountains. Eclogae Geol. Helv. 81/2, 433-440.

Scandone, P. 1990: Structural Model of Italy. Consiglio Nazionale delle Ricerche, Florence, Italy.

Schaer, J.P., Reimer, G.M. & Wagner, G.A. 1975: Actual and ancient uplift rate in the Gotthard region, Swiss Alps: a comparison between precise levelling and fission track apatite age. Tectonophysics 29, 293-300.

Schindler, C., Beer, C., Mayer Rosa, D., Rüttener, E., Wagner, J.J., Jaquet, J.-M. & Frisch-knecht, C. 1996: Integrierte Auswertung von seismischen und bodenspezifischen Parametern: Gefährdungskarten im Kanton Obwalden. Geologische Berichte, Landeshydrologie und -geologie 19, 61.

Schlaefli, A. 1999: Geologie des Kantons Thurgau. In: Mitteilungen der Thurgauischen Natur-forschenden Gesellschaft 55, Frauenfeld, 102.

Schlunegger, F. & Hinderer, M. 2001: Crustal uplift in the Alps: why the drainage patterns matter. Terra Nova 13/6, 425-432.

PEGASOS PMT-TN-0135. WS-2 Summary SP1.

PEGASOS PMT-TN-0237. WS-3 Summary SP1.

Schmid, S.M., Aebli, H.R., Heller, F. & Zingg, A. 1989: The role of the Periadriatic Line in the tectonic evolution of the Alps. In: Alpine Tectonics (edited by Coward, M.P., Dietrich, D. & Park, R.G.) Special Publication No. 45. Geological Society London, Oxford, 153-171.

Schmid, S.M., Pfiffner, O.A., Schoenborn, G., Froitzheim, N. & Kissling, E. 1997: Integrated cross section and tectonic evolution of the Alps along the eastern traverse. In: Results of NRP 20 deep structure of the Swiss Alps (edited by Pfiffner, O.A., Lehner, P., Heitzmann, P., Mueller, S. & Steck, A.). Birkhäuser Verlag, Basel, 289-304.

Schmid, S.M. & Froitzheim, N. 1993: Oblique slip and block rotation along the Engadine line. Eclogae Geol. Helv. 86/2, 569-594.

Schneider, G. 1968: Erdbeben und Tektonik in Südwest-Deutschland. Tectonophysics 5/6, 459-511.

Schneider, G. 1972: Die Erdbeben in Südwestdeutschland als tektonisches Ereignis. Natur-wissenschaften 59/3, 112-119.

Schneider, G. 1973: Die Erdbeben in Baden-Württemberg 1963-1972. Landeserdbebendienst Baden-Württemberg, Stuttgart, Federal Republic of Germany.

Schneider, G. 1979: Earthquake in the Swabian Jura of 16 November 1911 and present concepts of seismotectonics. Tectonophysics 53/3-4, 279-288.

Schneider, G. 1993: Beziehungen zwischen Erdbeben und Strukturen der Süddeutschen Gross-scholle. Neues Jahrbuch für Geologie und Paläontologie, Abhandlungen 189/1-3, 275-288.

Schnellmann, M., Anselmetti, F.S., Giardini, D., McKenzie, J.A. & Ward, S.N. 2002: Pre-historic earthquake history revealed by lacustrine slump deposits. Geology 30/12, 1131-1134.

Schoenborn, G. 1992: Alpine tectonics and kinematic model of the central Southern Alps. Memorie di Scienze Geologiche 44, 229-393.

Schoenborn, G. 1999: Balancing cross sections with kinematic constraints: The Dolomites (northern Italy). Tectonics 18/3, 527-545.

Scholz, C.H. 1988: The brittle-plastic transition and the depth of seismic faulting. Geologische Rundschau 77, 319-328.

Schreiber, U. & Rotsch, S. 1998: Cenozoic block rotation according to a conjugate shear system in central Europe – indications from palaeomagnetic measurements. Tectono-physics 299/1-3, 111-142.

Schumacher, M.E. 1997: Geological interpretation of the seismic profiles through the Southern Alps (lines S1-S7 and C3-south). *In*: Results of NRP 20 deep structure of the Swiss Alps (edited by Pfiffner, O.A., Lehner, P., Heitzmann, P., Mueller, S. & Steck, A.). Birkhäuser Verlag, Basel, 101-114.

Sommaruga, A. 1997: Geology of the central Jura and the Molasse Basin: new insight into an evaporite-based foreland fold and thrust belt. Mémoire de la Société des Sciences naturelles de Neuchâtel 12, 145.

Sommaruga, A. 1999: Décollement tectonics in the Jura foreland fold-and-thrust belt. Marine and Petroleum Geology 16, 111-134.

Spicher, A. 1980: Tektonische Karte der Schweiz. Schweiz. Geol. Kommision.

Sue, C. 1998: Dynamique actuelle et récente des Alpes occidentales internes, approche struc-turale et sismologique. Unpubl. PhD thesis, Grenoble.

Sue, C., Grasso, J.R., Lahaie, F. & Amitrano, D. 2002: Mechanical behavior of western alpine structures inferred from statistical analysis of seismicity. Geophysical Research Letters 29/8, art. no. 1224.

Sue, C., Martinod, J., Tricart, P., Thouvenot, F., Gamond, J.F., Frechet, J., Marinier, D., Glot, J.P. & Grasso, J.R. 2000: Active deformation in the inner western Alps inferred from comparison between 1972-classical and 1996-GPS geodetic surveys. Tectonophysics 320/1, 17-29.

Sue, C., Thouvenot, F., Frechet, J. & Tricart, P. 1999: Widespread extension in the core of the western Alps revealed by earthquake analysis. Journal of Geophysical Research-Solid Earth 104/B11, 25611-25622.

Tardy, M., Deville, E., Fudral, S., Guellec, S., Ménard, G., Thouvenot, F. & Vialon, P. 1990: Interprétation structurale des données du profil de sismique réflexion profonde ECORS-CROP Alpes entre le front Pennique et la ligne du Canavese (Alpes occidentales). *In*: Deep Structure of the Alps (edited by Roure, F., Heitzmann, P. & Polino, R.) Mémoire 1. Société Géologique Suisse, 217-226.

Tate, R.F. 1959: Unbiased estimation: function of location and scale parameters. Ann. Math. Statist. 30, 331-366.

Thouvenot, F., Frechet, J., Tapponnier, P., Thomas, J.C., Le Brun, B., Menard, G., Lacassin, R., Jenatton, L., Grasso, J.R., Coutant, O., Paul, A. & Hatzfeld, D. 1998: The M-L 5.3 Epagny (French Alps) earthquake of 1996 July 15: a long-awaited event on the Vuache Fault. Geophysical Journal International 135/3, 876-892.

Toro, G. 2003: Technical note on the treatment of hypocentral depths and rupture-length effects for area sources in the FRISK88MP Software. PEGASOS Technical Note TP1-TN-0373.

Toro, G. 2003: Sensitivity of seismic hazard to the treatment of hypocentral depth. PEGASOS Technical Note TP4-TN-0360.

Trümpy, R. 1980: Geology of Switzerland – a guide-book. Part A: An outline of the geology of Switzerland. Part B: Geological excursions. Wepf, Basel, New York.

Turnovsky, J. & Schneider, G. 1982: The seismotectonic character of the September 3, 1978, Swabian-Jura earthquake series. Tectonophysics 83/3-4, 151-162.

Uhrhammer, R. 1986: Characteristics of northern and southern California seismicity. Earthquake Notes 57, 21.

Vigny, C., Chery, J., Duquesnoy, T., Jouanne, F., Ammann, J., Anzidei, M., Avouac, J.P., Barlier, F., Bayer, R., Briole, P., Calais, E., Cotton, F., Duquenne, F., Feigl, K.L., Ferhat, G., Flouzat, M., Gamond, J.F., Geiger, A., Harmel, A., Kasser, M., Laplanche, M., Le Pape, M., Martinod, J., Menard, G., Meyer, B., Ruegg, J.C., Scheubel, J.M., Scotti, O. & Vidal, G. 2002: GPS network monitors the Western Alps' deformation over a five-year period: 1993-1998. Journal of Geodesy 76/2, 63-76.

Wagner, J.J., Frischknecht, C., Rosset, P., Sartori, M., Schindler, C., Beer, C., Mayer-Rosa, D., Rüttener, E. & Smit, P. 2000: Contribution au zonage sismique dans la vallée du Rhône, entre Sion et Brigue. Landeshydrologie und -geologie, Geologische Berichte 25, 123.

Weichert, D.H. 1980: Estimation of the earthquake recurrence parameters for unequal observation periods for different magnitudes. Bull. Seis. Soc. Am. 70/4, 1337-1346.

Weidmann, M. 2002: Erdbeben in der Schweiz. Verlag Desertina, Chur.

Wells, D.L. & Coppersmith, K.J. 1994: New empirical relationships among magnitude, rupture length, rupture width, rupture area, and surface displacement. Bull. Seism. Soc. Am. 84/4, 974-1002.

Wenzel, F., Brun, J.P., Blum, R., Bois, C., Burg, J.P., Coletta, B., Duerbaum, H., Durst, H., Fuchs, K., Grohmann, N., Gutscher, M.A., Huebner, M., Karcher, T., Kessler, G., Kloeckner, M., Lucazeau, F., Lueschen, E., Marthelot, J.M., Meier, L., Ravat, M., Reichert, C., Vernassat, S. & Villemin, T. 1991: A deep reflection seismic line across the northern Rhine Graben. Earth and Planetary Science Letters 104/2-4, 140-150.

Wetzel, H.U. & Frantzke, H.J. 2001: Geologische Interpretation eines ESR-1 Radarmosaiks von Deutschland. Deutsche Gesellschaft für Photogrammetrie und Fernerkundung 10, 503-510.

Wiemer, S. 2002: Approaches to declustering earthquake catalogs. PEGASOS SP-2 Workshop (PEGASOS TP1-RF-0236).

Youngs, R.R. 2002: PLABD Computer Code. PEGASOS TP1-ASW-0021.

Youngs, R.R. 2003: PLFBAD Computer Code. PEGASOS TP1-ASW-0022.

Youngs, R.R., Swan, F.H., Power, M.S., Schwartz, D.P. & Green, R.K. 1987: Probabilistic analysis of earthquake ground shaking hazard along the Wasatch Front, Utah. *In:* Assessment of regional earthquake hazard and risk along the Wasatch Front, Utah, (edited by Glori, W.W. & Hays, P.L.), M1-M110.

Ziegler, P.A. 1982: Geological Atlas of Western and Central Europe. Shell Internationale Petroleum Maatschappij B.V., The Hague.

APPENDIX 1   EG1-HID-0033   HAZARD INPUT DOCUMENT FINAL MODEL, EXPERT TEAM EG1b

This document describes the final seismic source model developed by Expert Team EG1b. The data files associated with this seismic source model are located in the zip file EG1-HID-0033_EG1b_data.zip.

Seismic Source Zonation

Figure A-1 shows the overall logic tree for seismic source zonation. Two alternative zonations are considered.
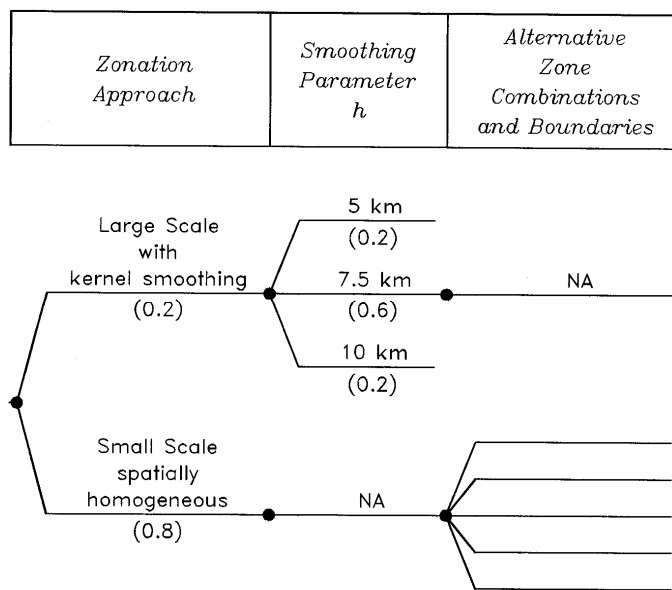
Fig. A-1:   Master logic tree for EG1b seismic source zonation

The first is termed 'large scale' and consists of 8 large regional zones, shown on Figure A-2. The zone polygon files are located in directory .\ZONES.LRG. Within each zone, seismicity is modeled by kernel smoothing with three alternative values of the kernel smoothing parameter h. The values are $h = 5$ km (weight 0.2), $h = 7.5$ km (weight 0.6), and $h = 10$ km (weight 0.2). The corresponding spatial seismicity grid files are designated by zone name and h value and are also located in directory .\ZONES.LRG.

The alternative approach is 'small scale' zonation in which the regional zones shown on Figure A-2 are subdivided. Figures A-3, A-4, A-5, A-6 and A-7 show the 'small scale' source zones. Seismicity within each 'small scale' zone is assumed to be spatially homogeneous. The zone polygon files for these zones are located in directory .\ZONES.SML.

As indicated on the master logic tree (Figure A-1), there are a number of alternative 'small scale' zone combinations and alternative boundaries. These are described in the following sections.
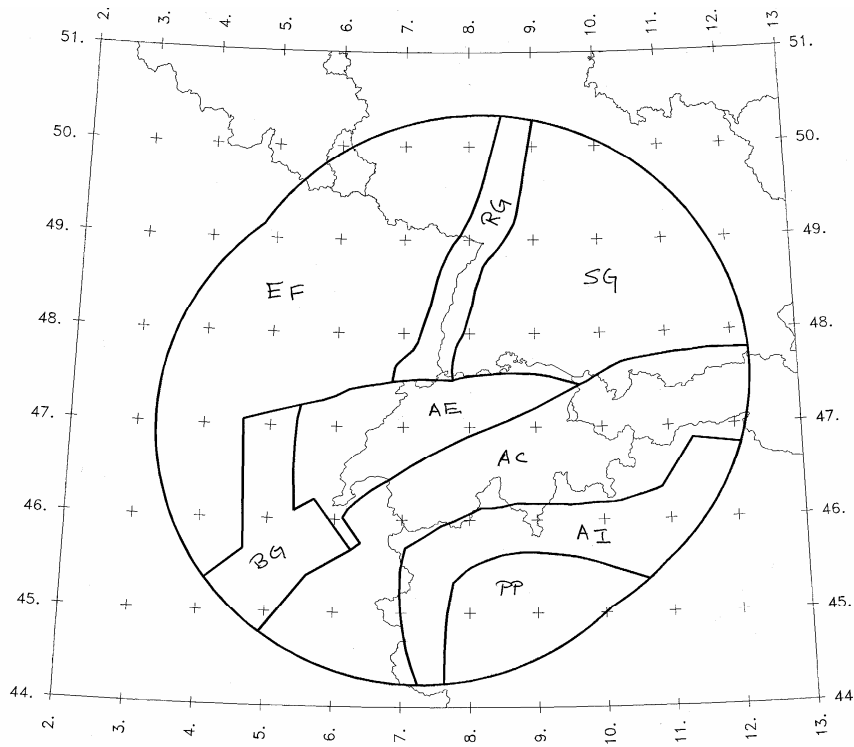
Fig. A-2:   Regional source zones in 'large scale' seismic source zonation
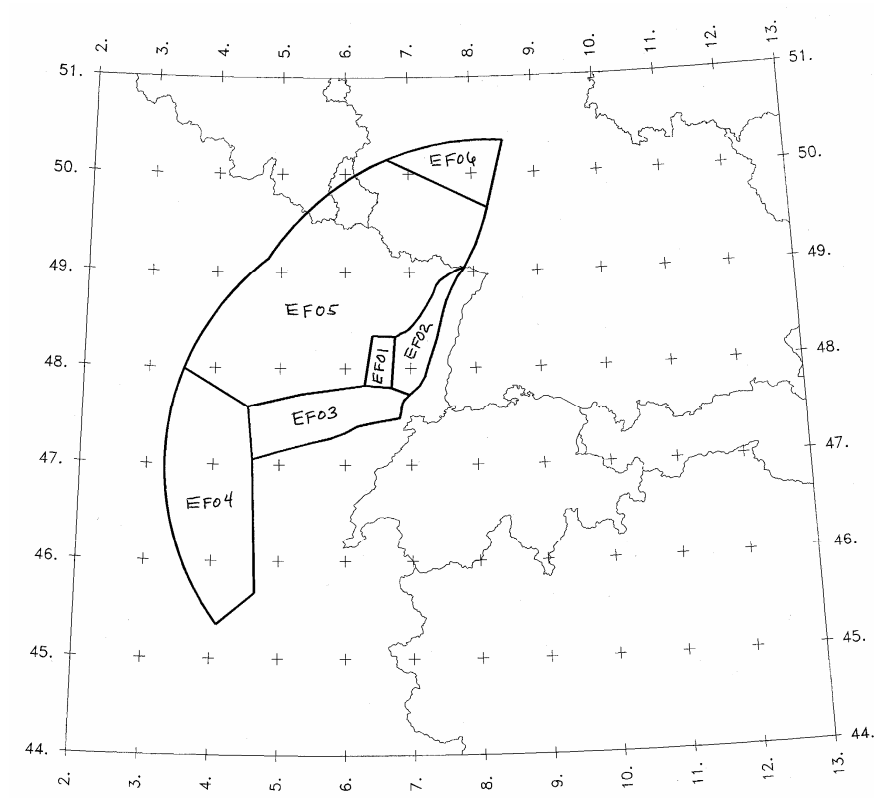
Fig. A-3:   Zonation of Eastern France (EF) in 'small scale' seismic source zonation
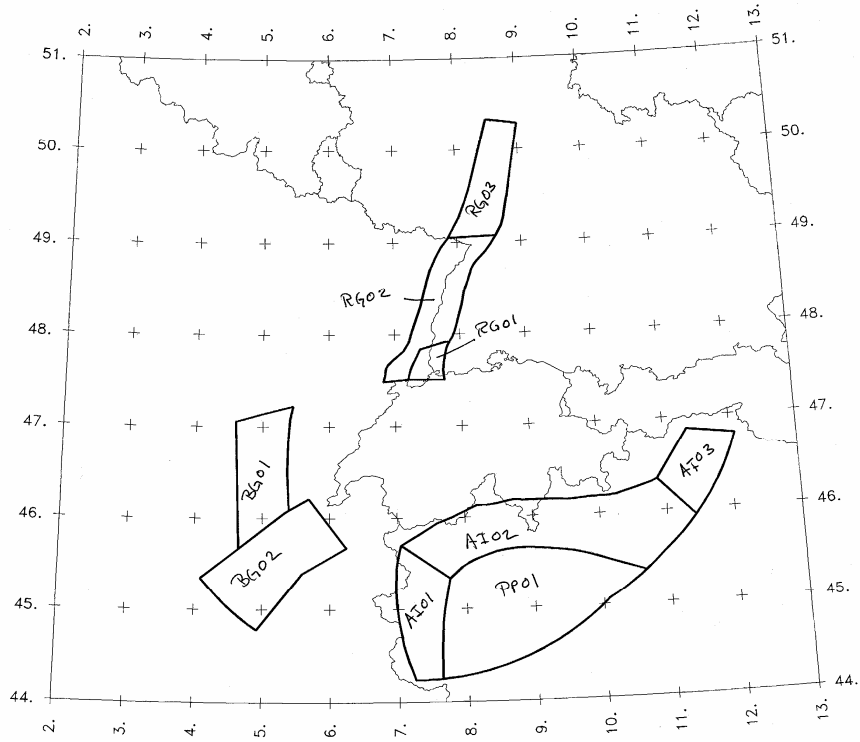
Fig. A-4:   Zonation of Bresse Graben (BG), Rhine Graben (RG), Alps Internal (AI), and Po-plain (PP) in 'small scale' seismic source zonation
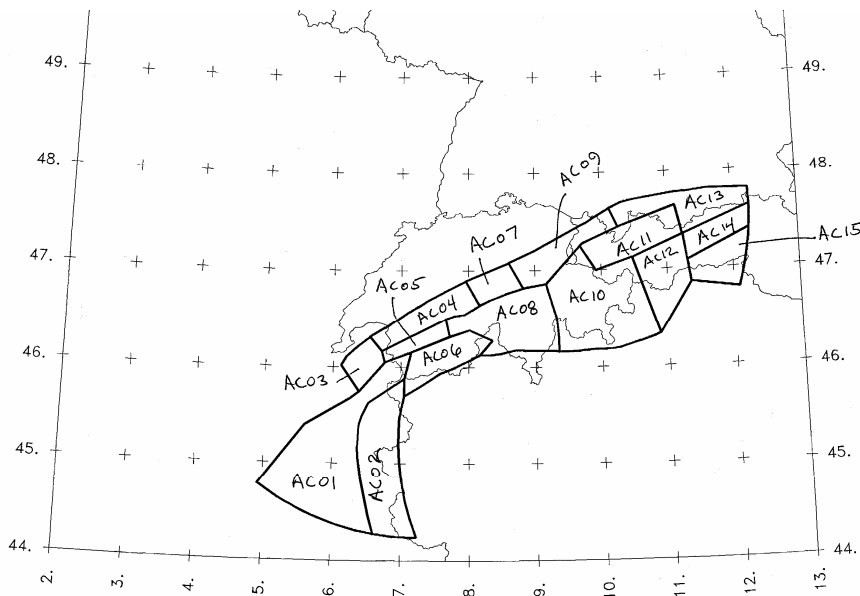
Fig. A-5:   Zonation of Alps Central (AC) in 'small scale' seismic source zonation
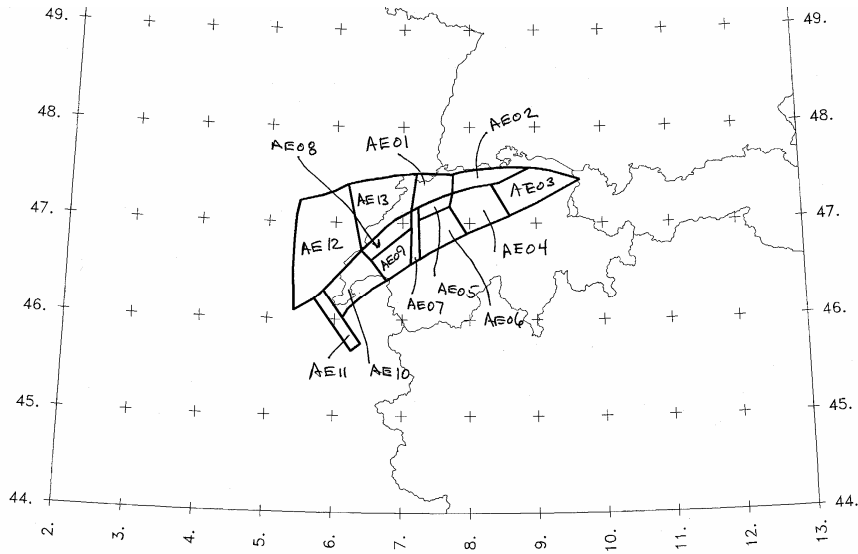
Fig. A-6: Zonation of Alps External (AE) in 'small zones' seismic source zonation
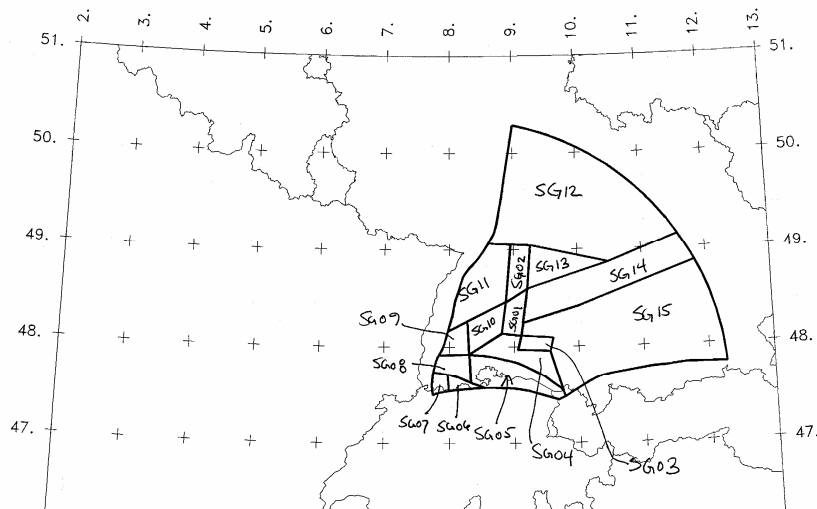
Fig. A-7: Zonation of South Germany (SG) in 'small scale' seismic source zonation

Zone Combinations within the 'Small Scale' model

There are three sets of alternative 'small scale' zone combinations that affect different areas. The first is the treatment of the Swabian Alps region. Figure A-8 shows the logic tree for these zones. Zones SG01 and SG02 are either considered to be separate, or are combined into a single zone SG1_2 (see Figure A-9).
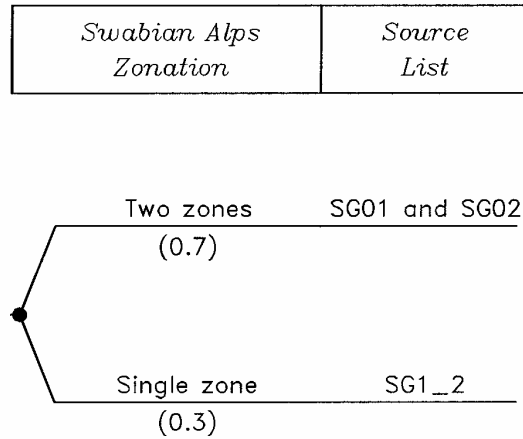
Fig. A-8:   Logic tree for Swabian Alps 'small scale' zonation
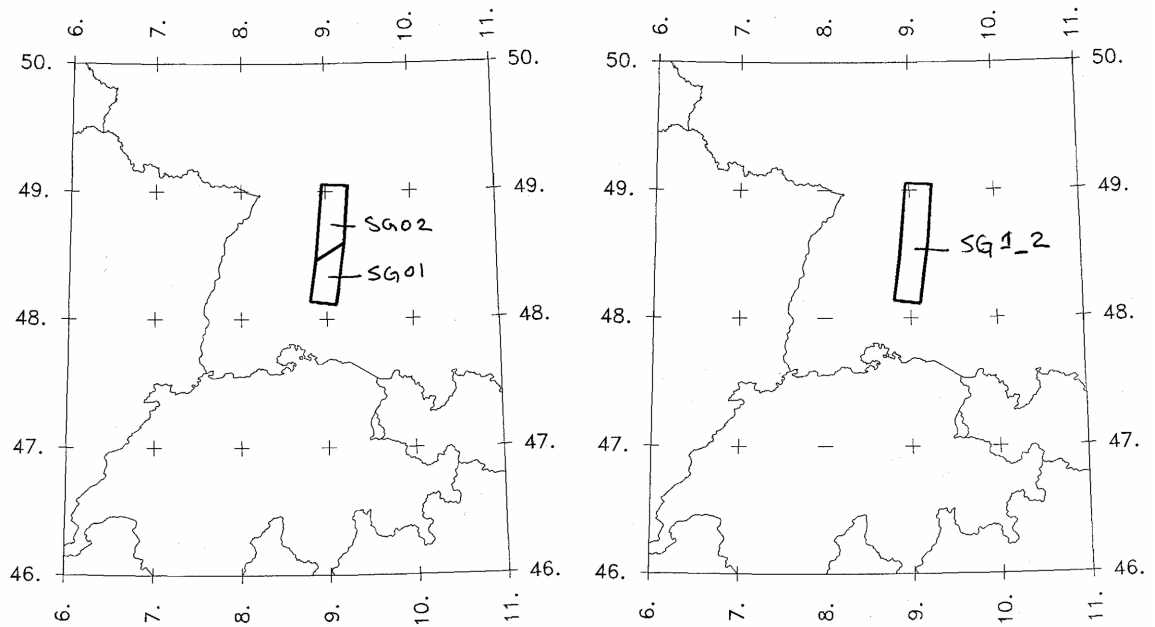
Fig. A-9:   Alternative zone combinations for the Swabian Alps in the 'small scale' seismic source zonation

Figure A-10 shows the logic tree for 'small scale' zonation in the Basel-Jura area. The first level addresses whether or not the Basel source extends into the Jura. If it does, then zones RG01 and AE01 are combined into zone RG1_AE1 (see Figure A-11). If the Basel source is separate from the Jura, then there are 4 alternative combinations of the Jura zones AE01, AE02, and AE13, as shown on Figures A-10 and A-11.

Basel–Jura Zonation	*Jura Zonation*	*Source List*

Southern
extension
of Basel
(0.5)   NA   RG1_AE1, AE02, and AE13

Basel
separate
from Jura
(0.5)

3 zones   RG01, AE01, AE02, and AE13
(0.7)

east+central   RG01, AE1_2, and AE13
(0.1)

west+central   RG01, AE1_13, and AE02
(0.1)

1 zone   RG01 and AE1_2_13
(0.1)
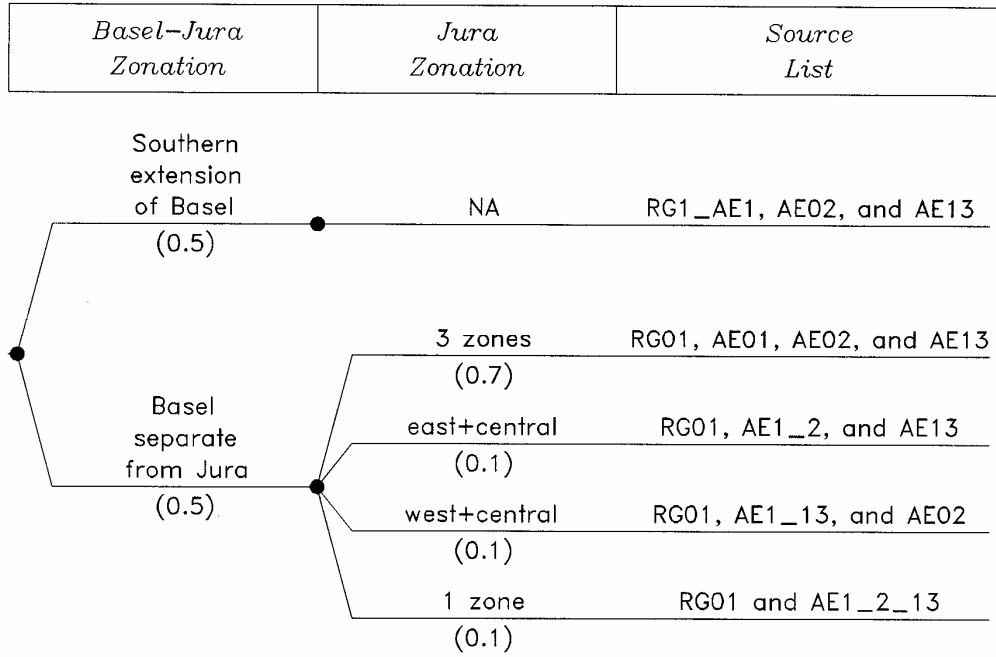
Fig. A-10:   Logic tree for Basel-Jura 'small scale' zonation
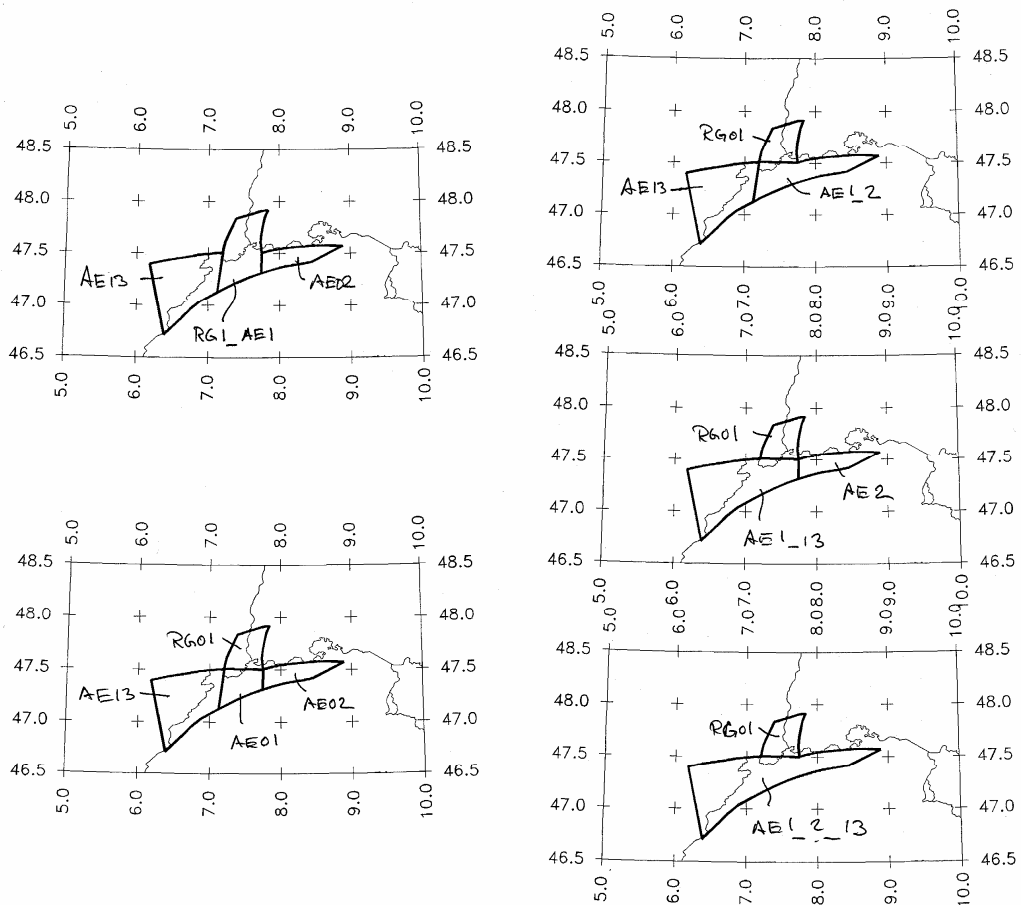
Fig. A-11:   Alternative zone combinations for Basel-Jura in the 'small scale' seismic source zonation

Figure A-12 shows the logic tree for 'small scale' zonation in the Dinkelberg-Bodensee area. The level addresses whether or not the Dinkelberg source (SG07) is separate from the rest of the area or is combined with zone SG06. The second level addresses the three alternative zone combinations conditional on the first branch. The resulting six sets of zones are listed on Figure A-12 and are shown on Figure A-13.

Dinkelberg – Bodensee Zonation	Bodensee Zonation	Source List
Dinkelberg separate from SG06 (0.8)	1 zone (0.6)	SG07 and SG5_6_8
	2 zones (0.2)	SG07, SG06, and SG5_8
	3 zones (0.2)	SG07, SG05, SG06, and SG08
Dinkelberg combined with SG06 (0.2)	1 zone (0.25)	SG5678
	2 zones (0.5)	SG6_7 and SG5_8
	3 zones (0.25)	SG6_7, SG05, and SG08
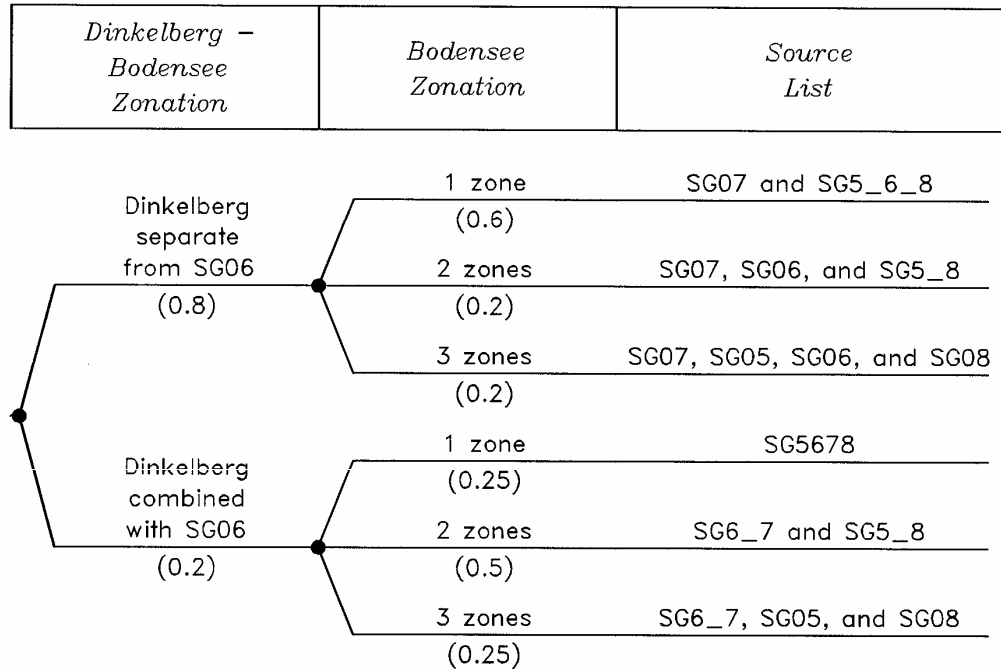
Fig. A-12:   Logic tree for Dinkelberg-Bodensee 'small scale' zonation
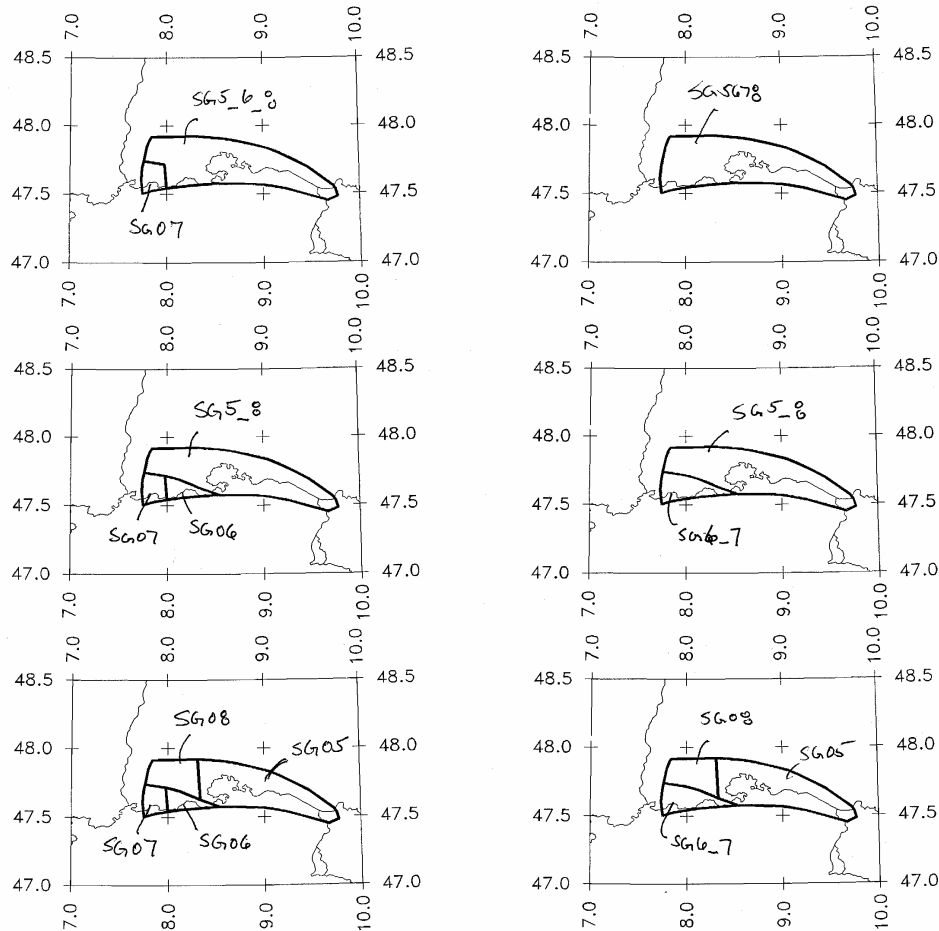
Fig. A-13:   Alternative zone combinations for the Dinkelberg-Bodensee area in the 'small scale' seismic source zonation

Polygons for all of the combined zones shown on the above figures are in directory .\ZONES.SML.

Uncertain Zone Boundaries within the 'Small Scale' model

There are two cases where the zone boundaries are considered to be uncertain in location ('soft'). The first is the eastern boundary of the Fribourg zone (AE07). Three alternatives are considered, as shown of Figure A-14. The change in boundary location affects zones AE07, AE05, and AE06. The central estimate is given the highest weight of 0.5. The two alternative locations are each given a weight of 0.25. The alternative zone polygon files are located in directory .\ZONES.SML. The zone boundary files for the preferred location have the extension *.ZON. The zone boundary files for the western location have the extension *.ZOW and those for the eastern location have the extension *.ZOE. These boundaries are completely dependent, all *.ZOW files are to be used together as one alternative and all *.ZOE files are to be used together as another alternative. Note that these alternative zonation boundaries are used *only* for the hazard computation. The zone seismicity parameters are obtained using the central location and are to be applied to all three geometries.
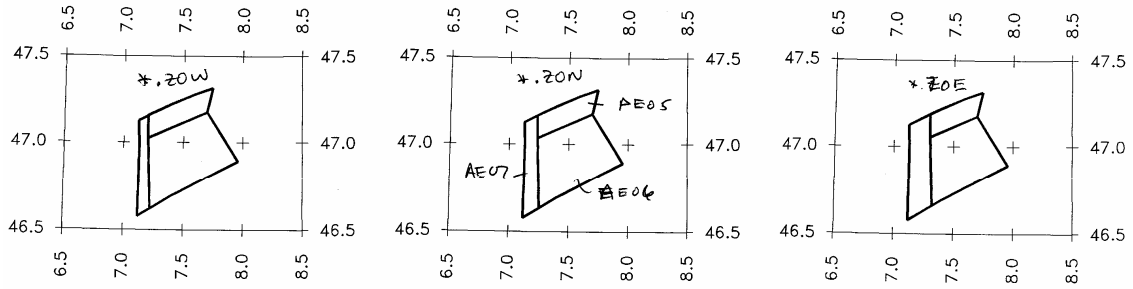
Fig. A-14: Alternative 'soft' eastern boundary for the Fribourg zone (AE07) and its neighboring zones in the 'small zones' seismic source zonation

The second case is the location of the northern and southern boundaries for the eastern Jura source AE02. As shown on Figure A-15, there are narrower and wider alternatives for this zone. The central estimate is given the highest weight of 0.5. The two alternative locations are each given a weight of 0.25. These alternative boundaries affect a number of the surrounding zones, as shown on Figures A-15 and A-16. The alternative zone polygon files are located in directory .\ZONES.SML. The zone boundary files for the preferred location have the extension *.ZON. The zone boundary files for the wide eastern Jura have the extension *.WZO and those for the narrow eastern Jura have the extension *.NZO. These boundaries are completely dependent, all *.WZO files are to be used together as one alternative and all *.NZO files are to be used together as another alternative. Again, note that these alternative zonation boundaries are used *only* for the hazard computation. The zone seismicity parameters are obtained using the central location and are to be applied to all three geometries. Please also note that this alternative width of the eastern Jura zone AE02 also interacts with the logic trees for the Basel-Jura area (Figures A-10 and A-11) and with the Dinkelberg – Bodensee area (Figures A-12 and A-13) to produce three alternatives for each.
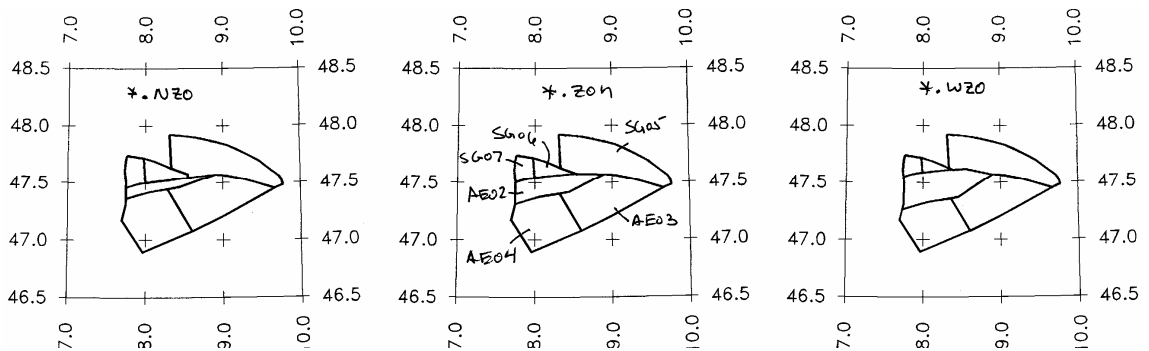
Fig. A-15: Alternative 'soft' boundaries for the eastern Jura zone AE02 and its neighboring zones in the 'small zones' seismic source zonation
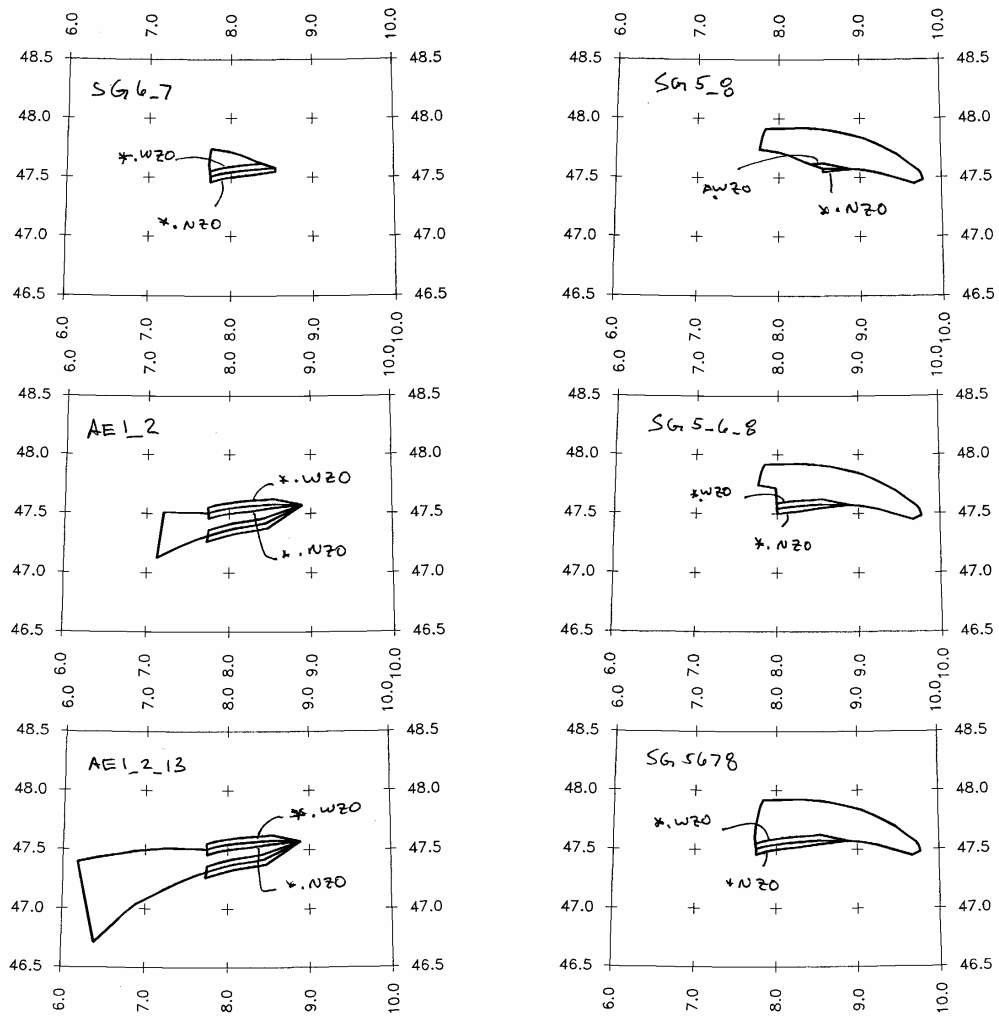
Fig. A-16: Alternative combined zone boundaries produced by the 'soft' boundaries for the eastern Jura zone AE02

Earthquake Rupture Geometry

The size of earthquake ruptures is defined by the relationship:

$$\text{Mean } \log_{10}(\text{rupture area}) = 1.02\,\text{M} - 4.15$$

$$\sigma_{\log 10(\text{rupture area})} = 0.24$$

Using the relationship for the expectation of a lognormal distribution, the mean (expected) rupture area is given by the relationship:

$$\text{mean rupture area} = 10^{(1.02\textbf{M} - 4.084)}$$

The relationship for the mean rupture area will be used in the hazard computations. The rupture length and width have an aspect ratio of 1:1 until the maximum rupture width for a source is reached. For larger earthquakes, the aspect ratio should change in order to preserve the rupture area. For the 'large scale' zones, earthquake epicenters are distributed according to the kernel density grids defined above. For the 'small scale zones' earthquake epicenters are uniformly distributed. Earthquake ruptures are located symmetrically on the epicenters (the epicenter is at the midpoint of the rupture). For those epicenters located closer than ½ rupture length to the source zone boundary, the ruptures are truncated at the source boundary, preventing them from coming closer to the site than the source boundary.

Table A-1 defines the relative frequency of the style of faulting for the individual sources. Three specific styles of faulting are considered, normal, strike-slip and reverse. For each style of faulting, there is a preferred direction of rupture and a preferred fault dip that should be used to model ruptures. The dip direction(s) are also given.

The depth distribution for small earthquakes for each zone is defined by a truncated normal distribution. The last three columns of Table A-1 list the peak of the distribution (the mean for an un-truncated distribution), the standard deviation (again for the un-truncated distribution) and the maximum depth that defines the lower limit of the distribution. The upper truncation point is zero depth. For larger earthquakes, a magnitude-dependent depth distribution is to be developed using the weighted approach outlined in Toro (2003, TP1-TN-0373) with T = 0.5 (hypocenter in lower half of rupture).

Earthquake Recurrence Parameters

Each source has a single distribution for maximum magnitude and a single distribution for earthquake recurrence parameters. Individual M_{max} distribution files for each source zone are contained in subdirectorys .\MMAX.LRG amd .\MMAX.SML. These distributions are limited to a minimum value of M_{max} of 5.5. The distributions have been truncated at the upper tail based on the minimum value resulting from two criteria: (1) the 95th cumulative probability of the posterior distribution produced using the EPRI approach, and (2) limiting magnitudes based on source dimensions.

The joint distributions for beta [b-value $\times \ln(10)$] and N (m $\geq$ 5) are contained in subdirectories .\REC.LRG and .\REC.SML. A truncated exponential earthquake recurrence relationship is used to define the relative frequency of earthquakes of different sizes.

Tab. A-1: Earthquake Rupture Parameters for EG1b

Label	Name	Style of faulting			Fault orientation									Depth (km)		
		[%]	[%]	[%]	Normal Fault			Strike Slip Fault			Thrust Fault					
		Normal	Strike Slip	Thrust	Strike	Dip	dip dir	Strike	dip	dip dir	Strike	dip	dip dir	max	peak	1σ
'Large Scale' Zones																
EF	Eastern France	0.15	0.8	0.05	150	60	NE, SW	0	90	-	60	45	NW, SE	15	10	3
RG	Rhine Graben	0.25	0.75	0	145	60	E,W	5	90	-	65	45	SE, NW	26	13	5
SG	South Germany	0.15	0.8	0.05	160	60	E,W	10	90	-	70	45	S,N	20	9	3
BG	Bresse Graben	0.4	0.6	0	160	60	E,W	10	90	-	70	45	S,N	30	15	15
AE	Alps external	0.1	0.8	0.1	150	60	NE, SW	0	90	-	60	30	SE	30	12	10
AC	Alps central	0.5	0.3	0.2	150	60	E,W	0	90	-	60	30	SE	15	9	4
AI	Alps internal	0	0.8	0.2	180	60	E,W	30	90	-	90	30	SE	37	18	10
PP	Po_Plain	0.333	0.334	0.333	random	60	-	random	90	-	random	45	-	20	10	8
'Small Scale' Zones																
EF01	Remiremont	0.15	0.8	0.05	150	60	NE, SW	0	90	-	60	45	NW, SE	15	10	3
EF02	Vosges	0.15	0.8	0.05	150	60	NE, SW	0	90	-	60	45	NW, SE	15	10	3
EF03	Dijon-Saône	0.15	0.8	0.05	150	60	NE, SW	0	90	-	60	45	NW, SE	15	10	3
EF04	Massif Central	0.15	0.8	0.05	150	60	NE, SW	0	90	-	60	45	NW, SE	15	10	3
EF05	Lorraine	0.15	0.8	0.05	150	60	NE, SW	0	90	-	60	45	NW, SE	15	10	3
EF06	Mainz	0.15	0.8	0.05	150	60	NE, SW	0	90	-	60	45	NW, SE	15	10	3
RG01	Basel	0.25	0.75	0	145	60	E,W	5	90	-	65	45	SE, NW	26	13	5
RG02	South Rhine Graben	0.25	0.75	0	145	60	E,W	5	90	-	65	45	SE, NW	26	13	5
RG03	North Rhine Graben	0.25	0.75	0	145	60	E,W	5	90	-	65	45	SE, NW	26	13	5
SG01	Schwäbische Alb	0.15	0.8	0.05	160	60	E,W	10	90	-	70	45	S,N	20	9	3
SG02	Stuttgart	0.15	0.8	0.05	160	60	E,W	10	90	-	70	45	S,N	20	9	3
SG03	Saulgau	0.15	0.8	0.05	160	60	E,W	10	90	-	70	45	S,N	20	9	3
SG04	Linzgau	0.15	0.8	0.05	160	60	E,W	10	90	-	70	45	S,N	20	9	3
SG05	Singen-Bodensee	0.15	0.8	0.05	160	60	E,W	10	90	-	70	45	S,N	20	9	3
SG06	Leibstadt	0.15	0.8	0.05	160	60	E,W	10	90	-	70	45	S,N	20	9	3
SG07	Dinkelberg	0.15	0.8	0.05	160	60	E,W	10	90	-	70	45	S,N	20	9	3
SG08	S Schwarzwald	0.15	0.8	0.05	160	60	E,W	10	90	-	70	45	S,N	20	9	3
SG09	W Schwarzwald	0.15	0.8	0.05	160	60	E,W	10	90	-	70	45	S,N	20	9	3
SG10	Rottweil	0.15	0.8	0.05	160	60	E,W	10	90	-	70	45	S,N	20	9	3
SG11	N Schwarzwald	0.15	0.8	0.05	160	60	E,W	10	90	-	70	45	S,N	20	9	3
SG12	Würzburg	0.15	0.8	0.05	160	60	E,W	10	90	-	70	45	S,N	20	9	3
SG13	Dreieck	0.15	0.8	0.05	160	60	E,W	10	90	-	70	45	S,N	20	9	3
SG14	Fränk.Alb	0.15	0.8	0.05	160	60	E,W	10	90	-	70	45	S,N	20	9	3
SG15	München	0.15	0.8	0.05	160	60	E,W	10	90	-	70	45	S,N	20	9	3
BG01	Bresse Graben	0.4	0.6	0	160	60	E,W	10	90	-	70	45	S,N	30	15	15
BG02	S_Bresse Graben	0.4	0.6	0	160	60	E,W	10	90	-	70	45	S,N	30	15	15

Tab. A-1: Continuation

Label	Name	Style of faulting			Fault orientation									Depth (km)		
		[%]	[%]	[%]	Normal Fault			Strike Slip Fault			Thrust Fault					
		Normal	Strike Slip	Thrust	Strike	Dip	Dip dir	Strike	Dip	Dip dir	Strike	Dip	Dip dir	max	peak	1σ
'Small Scale' Zones																
AE01	BaselJura	0.1	0.6	0.3	150	60	NE, SW	0	90	-	80	45	SE	30	12	10
AE02	E_Jura	0.1	0.7	0.2	150	60	NE, SW	0	90	-	80	45	SE	30	12	10
AE03	Zürich-Thurgau	0.2	0.7	0.1	150	60	NE, SW	0	90	-	70	45	SE	30	12	10
AE04	Aarau-Luzern	0.1	0.8	0.1	150	60	NE, SW	0	90	-	60	45	SE	30	12	10
AE05	Biel	0	0.8	0.2	155	60	NE, SW	5	90	-	65	45	SE	30	12	10
AE06	Napf	0.1	0.8	0.1	155	60	NE, SW	5	90	-	65	45	SE	30	12	10
AE07	Fribourg	0.05	0.9	0.05	155	60	NE, SW	5	90	-	65	45	SE	30	12	10
AE08	Neuchâtel Lake	0	0.8	0.2	155	60	NE, SW	5	90	-	65	45	SE	30	12	10
AE09	Vaud	0.1	0.8	0.1	155	60	NE, SW	5	90	-	65	30	SE	30	12	10
AE10	Geneva	0.1	0.8	0.1	130	60	NE, SW	160	90	-	70	30	SE	30	12	10
AE11	Vuache	0.05	0.8	0.15	130	60	NE, SW	160	90	-	70	30	SE	30	12	10
AE12	Jura West	0.1	0.8	0.1	130	60	NE, SW	160	90	-	70	30	SE	30	12	10
AE13	Jura Center	0.1	0.8	0.1	150	60	NE, SW	0	90	-	60	30	SE	30	12	10
AC01	Grenoble	0.5	0.3	0.2	150	60	E,W	0	90	-	60	30	SE	15	9	4
AC02	Briançon	0.5	0.3	0.2	150	60	E,W	0	90	-	60	30	SE	15	9	4
AC03	Arve	0.1	0.8	0.1	150	60	E,W	0	90	-	60	30	SE	15	9	4
AC04	Préalpes	0.1	0.8	0.1	150	60	E,W	0	90	-	60	30	SE	15	9	4
AC05	Wildhorn	0.2	0.8	0	80	60	S	80	90	-	-	-	-	15	9	4
AC06	Valais	0.6	0.4	0	100	60	N,S	70	90	-	-	-	-	15	9	4
AC07	Sarnen	0.1	0.8	0.1	150	60	E,W	0	90	-	60	30	SE	15	9	4
AC08	Ticino	0.5	0.3	0.2	150	60	E,W	0	90	-	60	30	SE	15	9	4
AC09	Walensee	0	0.8	0.2	150	60	E,W	0	90	-	60	30	SE	15	9	4
AC10	Graubünden	0.3	0.7	0	160	60	E,W	20	90	-	-	-	-	15	9	4
AC11	Vorarlberg	0.3	0.7	0	170	60	E,W	10	90	-	-	-	-	15	9	4
AC12	Glorenza	0.5	0.3	0.2	150	60	E,W	0	90	-	60	30	SE	15	9	4
AC13	Allgäu	0.5	0.3	0.2	150	60	E,W	0	90	-	60	30	SE	15	9	4
AC14	Inntal	0.3	0.7	0	150	60	E,W	70	90	-	-	-	-	15	9	4
AC15	Tauern	0.5	0.3	0.2	150	60	E,W	0	90	-	60	30	SE	15	9	4
AI01	DoraMaira	0	0.6	0.4	-	-	-	60	90	-	10	45	E	37	18	10
AI02	Alpi Sud	0.333	0.334	0.333	0	60	E,W	30	90	-	90	45	S	37	18	10
AI03	Bolzano	0.333	0.334	0.333	170	60	E,W	20	90	-	80	45	S	37	18	10
PP01	Po_Plain	0.333	0.334	0.333	random	60	-	random	90	-	random	45	-	20	10	8

Tab. A-1: Continuation

Label Name	Style of faulting			Fault orientation									Depth (km)		
	[%]	[%]	[%]	Normal Fault			Strike Slip Fault			Thrust Fault					
	Normal	Strike Slip	Thrust	Strike	Dip	dip dir	Strike	dip	dip dir	Strike	dip	dip dir	max	peak	1 σ
Regroupings of 'small scale' zones															
Dinkelberg Area: 'Tucan beak'															
SG5678	0.15	0.8	0.05	160	60	E,W	10	90	-	70	45	S,N	20	9	3
SG5_6_8	0.15	0.8	0.05	160	60	E,W	10	90	-	70	45	S,N	20	9	3
SG5_8	0.15	0.8	0.05	160	60	E,W	10	90	-	70	45	S,N	20	9	3
SG6_7	0.15	0.8	0.05	160	60	E,W	10	90	-	70	45	S,N	20	9	3
Basel area: 'Rhinozeros'															
RG1_AE1	0.15	0.6	0.25	145	60	E,W	5	90	-	80	45	SE	26	13	5
AE1_2	0.1	0.6	0.3	150	60	NE, SW	0	90	-	80	45	SE	30	12	10
AE1_2_13	0.1	0.65	0.25	150	60	NE, SW	0	90	-	75	45	SE	30	12	10
AE1_13	0.1	0.7	0.2	150	60	NE, SW	0	90	-	70	45	SE	30	12	10
Schwäbische Alb															
SG1_2	0.15	0.8	0.05	160	60	E,W	10	90	-	70	45	S,N	20	9	3
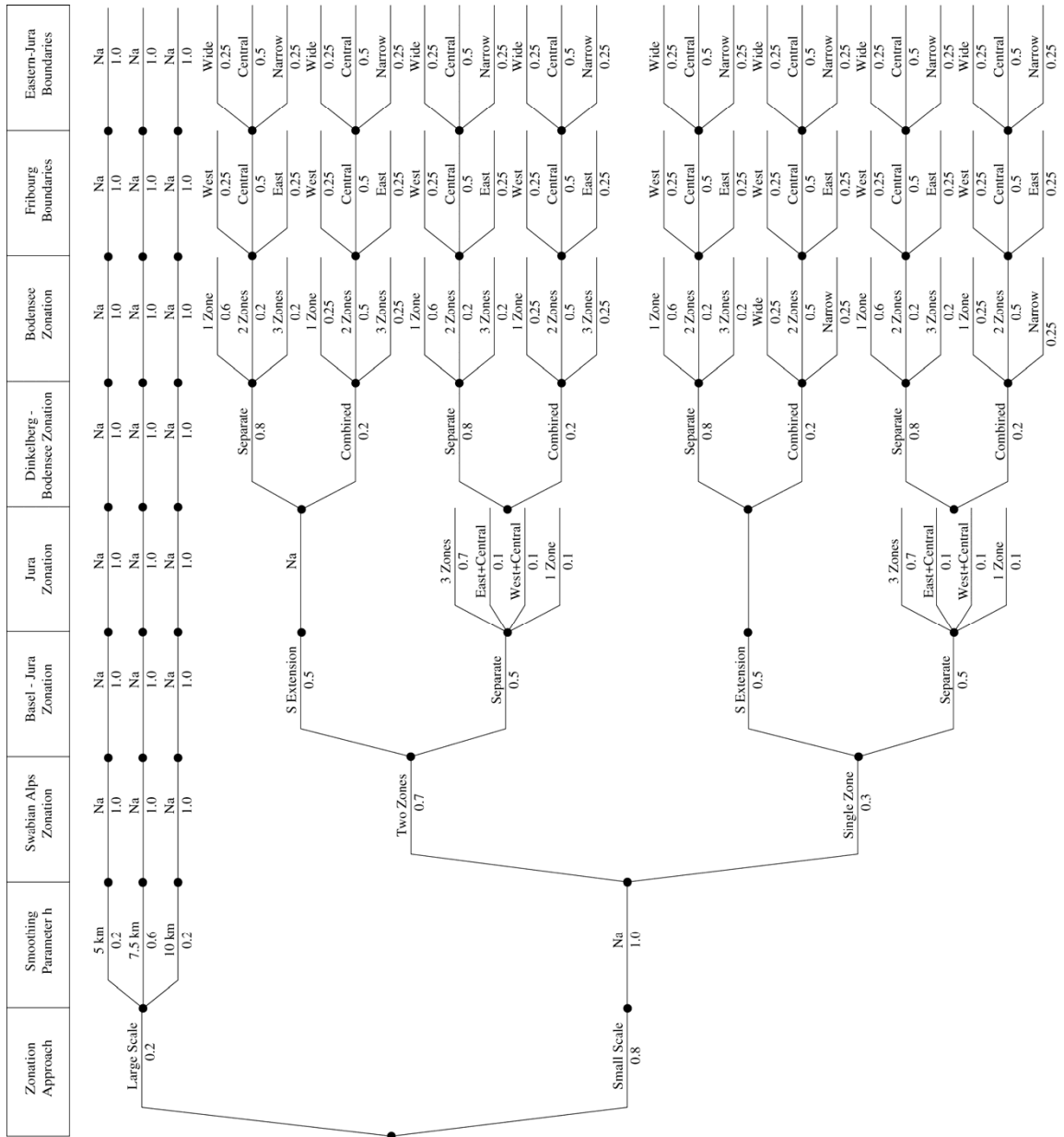
Fig. A-17:   Logic tree for EG1b

APPENDIX 2:   QA-CERTIFICATE FOR EG1-HID-0033

QA Certificate for Hazard Input Documents

LINULUANULN

2 1. Okt. 2003

PROSEIS AG

QA Certificate	**PEGASOS PROJECT**

Hazard Input Document (HID)

Expert group:	EG1b	**HID designation:**	**EG1-HID-0033**
Expert:		**Expert Model (EXM)**	EG1-EXM-0031

HID parameterisation of Expert Model:

TFI:	K. Coppersmith	**Hazard Input Specialist of TFI-team:**	B. Youngs

HID based on Elicitation Documents: ☒   EG1-ES-0045

HID based on Expert Assessments: ☐

Remarks on the HID model parameterisation in terms of hazard computation input:

The undersigned Hazard Input Specialist confirms that this HID includes all required (subproject specific) input information for hazard computations. No further interpretations of this input will be required and no simplifications except Algorithmic Pinching according to paragraph 2.9 of the QA-Guidelines will be applied to convert this HID into hazard software Input Files.

Signature:

HID acceptance by the Expert / Expert Group:

Date of HID review by the Expert / Expert group:

HID accepted: ☐   **HID not accepted:**   ☐

Reasons for non-acceptance of HID / Recommendations:

The undersigned Expert(s) accept(s) the parameterisation proposed in this HID as a faithful and adequate representation of his/their Expert Model. He/they confirm(s) that this HID is free of errors and agree(s) to its use as hazard computation input.

Signature Expert 1 / Expert:

Signature Expert 2:

Signature Expert 3:

QA-TN-0287 HID acceptanc form rev 02.doc

Part III: SP1 Seismic Source Characterisation, Elicitation Summary

Expert Team EG1c

Dr. Wolfgang Brüstle

Landesamt für Geologie, Rohstoffe und Bergbau Baden-Württemberg
Freiburg i. Breisgau – Germany

Dr. Roger M.W. Musson

British Geological Survey
Edinburgh – Great Britain

Dr. Souad Sellami

Schweizerischer Erdbebendienst / Institut für Geophysik ETHZ
Zürich – Switzerland

SP1 Seismic Source Characterisation

Elicitation Summary

Expert Team EG1c

Wolfgang Brüstle

Landesamt für Geologie, Rohstoffe und Bergbau Baden-Württemberg
Freiburg i. Breisgau – Germany

Roger M.W. Musson

British Geological Survey
Edinburgh – Great Britain

Souad Sellami

Schweizerischer Erdbebendienst / Institut für Geophysik ETHZ
Zürich – Switzerland

TABLE OF CONTENTS

LIST OF TABLES

LIST OF FIGURES

1   INTRODUCTION

This document describes the seismic source model prepared by team EG1c (Brüstle, Musson and Sellami) for the PEGASOS project. We begin with some account of the basic philosophy underlying our model, and continue by discussing the seismotectonic framework in more detail. This is followed by a description of the model itself on a zone-by-zone basis. This is followed by description of the details of the model in terms of the parameterisation of the individual zones.

This results in eight main sections, as follows:

1. Tectonic framework

2. Seismic source zonation

3. Catalogue declustering

4. Catalogue completeness

5. Maximum magnitude (M_{max}) estimation

6. Depth distribution

7. Earthquake rupture geometry and style of faulting

8. Earthquake recurrence parameters

The input files for the model are included as an appendix of the HID.

2   TECTONIC FRAMEWORK

There are various approaches to the task of partitioning any area into seismic sources. These may differ in terms of procedure, but we believe that the fundamental distinction is in terms of the basic conceptual model that underlies any source characterisation. The tools that are used to represent seismic sources may also seem misleadingly to represent different philosophies. Thus overmuch may be made of the distinction between the use of line sources, zone sources and smoothed seismicity in seismic source models. These are all means to an end, and it is fundamentally important to keep that end in view rather than to be too much distracted by the means. It is possible to construct a set of source zones that has a similar effect to a smoothed seismicity model, and a long thin area source can stand duty in some cases for a line source. But underlying any approach, there should be a conceptual model of the seismogenic processes that are at work. The decisions made as to how the model is implemented should ideally be decisions as to how best to express that conceptual model in practical terms. The application of any procedure in an automatic or unthinking way is essentially abrogating the role of the conceptual model, and leaves key decisions almost to chance.

2.1   Issues of Seismic Source Modelling

The issue of choice of approach to seismic source modelling nevertheless cannot be avoided. We therefore feel that at the outset it is helpful to establish some general principles that will be followed in the construction of this model.

The principal options that are available to the analyst are as follows:

1. The use of zones, as in the original Cornell (1968) procedure, that are assumed to be homogeneous with respect to seismicity.

2. The explicit modelling of individual fault structures.

3. Spatial smoothing of the seismicity data according to some algorithm (gridding, kernel smoothing).

One can posit a further type of source, the point source, but in practice this is not used, and in any case is equivalent to a very small zone. It also has to be borne in mind that seismicity exists in three dimensions, so a zone is not strictly an area source but a volume source, and a fault is not a line source but a plane. However, the use of the words "area" and "line" are so entrenched in common usage that they cannot be avoided.

There is also, of course, the possibility to use a combination of any of the above three, for example, as options within a logic tree structure. We start by considering the applicability of these different methods to the task in hand. We make the starting assumption that the use of a zone model is an appropriate way of modelling seismicity in the study area, and then consider whether the inclusion (partly or entirely) of fault sources and spatial smoothing would improve the model or not.

2.1.1   Modelling of Fault Structures

Conventional practice in PSHA includes explicit fault modelling for active faults, while seismicity for which the precise causative fault is not known is usually handled within the zone model. The explicit inclusion of individual faults has two important effects: (a) it enables the activity on this fault to be localised along its extent, possibly including a segmentation model; (b) it enables the effect of rupture dimensions to be included within the hazard estimation. The

word "explicit" is used judiciously; all earthquakes modelled in the PSHA process occur on faults. If a known fault is not modelled in detail, but is encompassed within some source zone, this does not mean that the fault is presumed not to be seismogenic. It means that the fault is not considered to be more hazardous than other faults within the same zone, which may or may not themselves be mapped. Some of the earthquakes that are implied to occur within the source zones will, in fact occur along the known fault in question. The absence of a specific fault source in the model simply implies that earthquakes will not preferentially occur on that fault rather than others in the same zone. It also implies that the rupture dimensions of earthquakes occurring on this fault are not significant to hazard. (And even this is not necessarily true, as some hazard code - including that used in the present project - treats a source as a set of pseudo-faults with known rupture behaviour.)

For a large source zone, it may well be true that rupture size is not significant to hazard. The assumption made in PSHA is that, for any zone, the epicentre of a future earthquake may be at any position with equal probability. However, the epicentre is in this context a notional point, and one could equally rephrase this as "the closest point of the rupture plane of a future earthquake projected to the surface may be at any position with equal probability". This is clearly not true for a small zone, the maximum dimension of which is only slightly larger than the projected rupture length of a large earthquake within the zone. But it may well be true for a large zone and small earthquakes.

The question now arises as to what constitutes an active fault, and which faults in the study area are active. Conventional definitions, largely developed in tectonic areas rather different from Switzerland, refer to any fault that has demonstrably moved in the past x years as active, where x is some large number extending certainly beyond historical times, usually back to the beginning of the Quaternary. It is common practice to examine known faults one by one, compare them to this definition, and decide if they are active or not. The number that meets this criterion indicates the number of "active faults"

We regard this process as unhelpful in a Central European context. The number of "active faults" can be more directly estimated by approaching the question from the other direction. All earthquakes occur on faults; there are approximately 2000 distinct epicentres in and around Switzerland; therefore there must be about 2000 active faults in Switzerland. Unfortunately, most cannot be identified or even guessed at.

This means that preferential modelling of those faults that can be guessed at can have a very undesirable consequence: it effectively changes the hazardousness of faults according to whether they have been mapped or not. Consider a case of a zone within which two earthquakes of magnitude 5 have occurred. One of these is close to a mapped fault and consistent with having occurred on that fault; the other one is not. It would be possible to identify the mapped fault as "active", model the seismicity along it on the basis of one observed event, and apportion the other event to the background of the whole zone. The effect of this is to concentrate hazard along the mapped fault, and the occurrence of the first earthquake has more impact (or at least, a different impact) on the hazard than the second one. Yet, seismologically, the two events are not different; both occur on faults. The only difference is the state of human knowledge concerning the two generating faults: one is mapped; the other is not. It is not satisfactory to have the distribution of hazard so much affected by this rather artificial distinction.

In the above example, it is assumed that both these faults are roughly similar structures that are old and have been reactivated in the present stress field. In such cases, there is no real reason why any neighbouring fault of similar orientation should not be reactivated. The fact that a particular fault has been reactivated once does not heavily prejudice one into believing that the next earthquake will occur on the same structure and not some other one.

However, some faults really are persistently active, such that one can state with certainty that future activity on these faults will occur at the same rate as past activity, and the slip rates can also be estimated. This occurs when faults are active because they are controlling recognisable

coseismic deformation. An example is the North Anatolian Fault - it is inevitable that seismicity will continue on this structure, for tectonic reasons that are very well understood. And as a result, it is true that seismicity is *preferentially* disposed to follow this structure because it controls deformation. In which case, it is essential to model it explicitly.

The question now becomes whether any such faults can be identified in Switzerland. Lacking any major active thrust features in the Alps, there appear to be five principal candidates: the Fribourg Fault, the Vuache Fault, the Reinach Fault, and the two master faults either side of the Rheingraben. These will be considered in turn.

2.1.1.1   The Fribourg Fault

As shown by Deichmann et al. (2000), there can be little doubt that the Fribourg earthquake of 14 February 1999 occurred along the Fribourg Fault. This structure is well known because it has been studied in detail, and can be contrasted with other faults in the same general area that have not been studied so well, cannot be characterised so well (if at all), and yet are probably equally dangerous. There is no tectonic reason why seismicity should occur preferentially along this fault, although, no doubt, it will reactivate again some time in the future. It seems inappropriate, therefore, to single this fault out for special treatment.

2.1.1.2   The Vuache Fault

This is a similar case to the Fribourg Fault; this fault produced a 5.3 ML earthquake on 15 July 1996 (Thouvenot et al. 1998). It is less significant than the Fribourg Fault because of its distance from the sites.

2.1.1.3   The Reinach Fault

A recent paper by Meghraoui et al. (2001) reports trenching across this fault south of Basel, with results that are held to show the fault rupture of the 1356 Basel earthquake as well as possible earlier events. If this evidence were correct, it could indicate a persistently active fault producing the largest regional events. However, normal faulting along this feature is an implausible hypothesis to explain the 1356 earthquake, as shown by Meyer et al. (1994). A much more probable explanation for the displacement seen on the Reinach Fault is simple slumping, which could be earthquake-triggered or not. In our view the probability that the Reinach Fault is significantly seismogenic is sufficiently small that according it special treatment is not required.

2.1.1.4   The Rheingraben Boundary Faults

The Rheingraben (Rhine Graben) is a major rift running roughly N-S, bounded by controlling faults on either side. If the graben were still subsiding, these boundary faults would be excellent examples of exactly the sort of fault for which special treatment as seismic sources would be required - faults the persistence of which can be assured because of their role in controlling contemporary deformation. Evidence suggests, however, that extension in the Upper Rheingraben ceased in Oligocene times. The significance of the bounding faults under the current tectonic regime is debatable. As will be discussed later, we conclude that these faults are not critical in controlling current seismicity.

2.1.1.5   Conclusion

We have not been able to identify any other candidate fault structures that require consideration, and cannot conclude that any of the faults discussed above merit special treatment within the seismic source model. We therefore decline to include individual faults in our seismic source model.

2.1.2   Spatial Smoothing

The use of spatial smoothing of seismicity as a means of modelling seismic hazard is currently a subject of much methodological discussion. The use of grids to smooth the observed earthquake pattern goes back in published studies at least as far as Jacob et al. (1994) and possibly before. It obtained some popularity through the work of Frankel et al. (1996), and the employment of kernel functions (Woo 1996) is also worthy of note.

All these methods are an attempt to remove the subjectivity involved in making decisions as to zone geometry, at the expense of abandoning any possible input from seismotectonics and geology. (There also remains some subjectivity in the choice of smoothing parameters.) The use of smoothed seismicity was aptly described by Perkins (1993, pers. comm.) as providing "a good quick first approximation to the hazard". It is certainly a useful tool for computing hazard (especially hazard maps, that will not be used for design purposes) in a hurry in areas where tectonic data are absent or hard to interpret. It can be viewed, for example, as a weapon of last resort.

As was discussed at PEGASOS SP1 Workshop 3, there is also an issue of spatial stationarity. The use of a large seismic source zone implies that future seismicity can be located anywhere within that zone with equal probability. The extreme opposed view would be that historically observed epicentres will repeat themselves exactly in the same places, over and over again. This latter view would amount to supposing that seismicity was, in a spatial sense, entirely stationary. Spatial smoothing, either of an entire catalogue, or selectively within broadly delimited zones, allows an intermediate position of partial stationarity - that earthquakes in future may occur anywhere, but with diminishing probability away from locations where they have not occurred in the past.

The use of spatial smoothing is not the only way to achieve the same effect. A model used by Musson and Winter (1996, 1997) and discussed in Musson (1997) overlays a series of broad seismic source zones with a second series of small ones concentrated around past historical epicentres.

At the first PEGASOS SP1 Interactive Meetings, an interesting discussion took place, which it may be helpful to recapitulate. The issue in question was whether it is correct to combine zoned and zoneless approaches in a logic tree. The argument against this is that a logic tree should confine itself to the expression of epistemic uncertainty (Abrahamson 2000), whereas a zoned approach and a zoneless approach represent a choice of tools, and not uncertainty about the nature of seismicity. To combine the two methods would be like attempting to combine probabilistic and deterministic hazard assessments within one logic tree.

The counter argument is that the primary epistemic uncertainty is in the conceptual models of seismicity that may be conceived by the analyst. Any procedural approach is a way of manifesting a conceptual model, and some models may be more easily expressed by one approach, and others more easily expressed by another. Hence, if one has two conceptual models of seismicity, one of which is more easily described by a set of zones, and the other by a set of smoothing parameters, then it makes perfect sense to combine both approaches in the same logic tree.

However, one does not formulate a conceptual model that seismicity follows some unknown pattern of zones, and then set out by trial and error to discover what those zones might be. Rather, one formulates a conceptual model that seismicity is higher in one place and lower in another place for certain reasons, and then uses a zone geometry as a tool to express this model. The concept of zonation has no practical meaning divorced from a real set of zones. Ultimately, a conceptual model does not follow the form of "seismicity is zoned", but rather "seismicity is zoned *in this way*".

The same is true of the zoneless approach. One's conceptual model cannot follow the form of "seismicity is smoothed" (in some unknown way), but should be "seismicity is smoothed *with*

these characteristics". Spatial smoothing becomes a useful tool to express a conceptual model that already contains a smoothing shape and wavelength. It cannot be sound practice to decide on a smoothing approach without any conception of the correct form of the smoothing parameters and then try and obtain these by trial and error (and with no means of judging what was error and what was not). This would no longer be the representation of a conceptual model.

In the case of the present study, we therefore ask ourselves whether our ideas about the distribution of hazard in the study area are more faithfully represented by a set of zone geometries that we can express, or a set of smoothing parameters that we can express. We find we have no way of judging the latter, but we can express our ideas in terms of the former. We therefore choose to reject the use of smoothed seismicity models in our approach to describing the seismicity of the study area. It can also be noted, from a technical perspective, that there is nothing that can be achieved using a spatial smoothing approach that cannot be more or less duplicated, in effect, by thoughtful application of source zones. This gives a further justification in restricting our approach to the use of source zones.

2.1.3   Towards the Construction of a Seismic Source Model

Our opinion is that the optimum way to construct a robust seismic source model follows three key stages, and this schema is what we have followed in this study.

The first stage involves the determination of the *kinematic model*. This is the basic element of the conceptual model of the seismic process at a sub-continental scale. The kinematic model describes, at the broadest scale, what is the relationship between large blocks in the Earth's crust in terms of relative movement. In a very simple case this might be stated as: Block A is subducting northwards under Block B, with resulting large thrust earthquakes at the interface and lesser amounts of intraplate seismicity within the two blocks in reaction to the stresses engendered by differential subduction. This describes the basic mechanisms for earthquakes that are to be expected in different parts of the area under examination.

The second stage refines the kinematic model into the *seismotectonic framework*. In this part of the process, the very broad divisions used in the kinematic model are looked at in more detail, with the aim of dividing them up into volumes of crust that are sufficiently structurally distinct that it is improbable that seismicity could be considered to be uniform across the boundaries of such divisions. At this stage, the key elements to be assessed do not include seismicity except in a rather broad sense. Rather, one is seeking to characterise areas that have a similar style of faulting, are experiencing a similar pattern of crustal stresses, and so on. In drawing up the seismotectonic framework one may start drawing basic crustal divisions that will ultimately form the outline of the seismic source model itself.

The third stage is the final construction of the *seismic source definition*. Here the final partition of the seismic source model is made from analysis of the seismotectonic framework together with the detailed pattern of observed seismicity and local geological structure.

By following this sequence of steps, we believe that an informed basis can be found for decision making about the detail of the model.

It should be noted from the outset that the model described in this report is designed equally for the four sites of concern to this study, but is *not* designed to be equally valid for all possible sites in the study area or even in all of Switzerland. At greater distances from the four sites, less detail was thought to be necessary in making partition of sources. Hazard at any site is totally insensitive to fine division of seismicity at large distances, and simple zones at long ranges are quite adequate.

How those decisions were taken in this study will now be described.

2.2 The Kinematic Model

In looking at the kinematics of crustal deformation in the area of study, a few key questions immediately arise. Firstly, what is the relationship between Alpine tectonics and seismicity? Can we see active seismicity along Alpine thrust structures indicating that mountain building is still in progress? Secondly, and clearly related, is the nature of the boundary between the Adriatic Plate and the European Plate. Thirdly, there are a number of contentious questions about the tectonics of the Alpine Foreland. We will take these topics in turn.

2.2.1 Alpine Tectonics

Although one might superficially expect the Alps to be similar to the Himalayas with respect to tectonics and seismicity, this is clearly not the case. With the Himalayas, the major active thrust planes (such as the Main Boundary Fault and Main Central Thrust) are easy to identify, and their activity is incontrovertible (Chandra 1978, Singh et al. 1990) even if the details are still subject to discussion.

The same is evidently not true in the Alps. There are no great earthquakes, and there is no apparent correlation between seismicity and major structural features. The rate of convergence and seismicity in the Himalayas is an order of magnitude greater than in the Alps.

While the Alps are still a young mountain range, it is clear, that the active orogenesis such as is seen in the Himalayas cannot be used as a model for the Alpine region.

2.2.2 The Adriatic-European Plate Boundary

Nevertheless, it is clear that the southern Alps mark a plate boundary between the Adriatic Plate and the European (Eurasian) Plate (Figure 1). The Adriatic Plate has been considered either to be part of the African Plate or an entity of its own; either way, it is not part of the European Plate and its interaction with that plate is clearly significant.

It has generally been accepted that the European Plate is subducting or has subducted under the Adriatic Plate, though the situation is far from clear. The "lithospheric root" discussed in Mueller (1997) can be interpreted as a broken-off slab, now almost vertical, though this seems to be controversial. Even more so would be a recent hypothesis, as yet unpublished, that the sense of subduction is reversed, and the Adriatic Plate is actually the under-riding plate (Schmid 2002 pers. comm.).
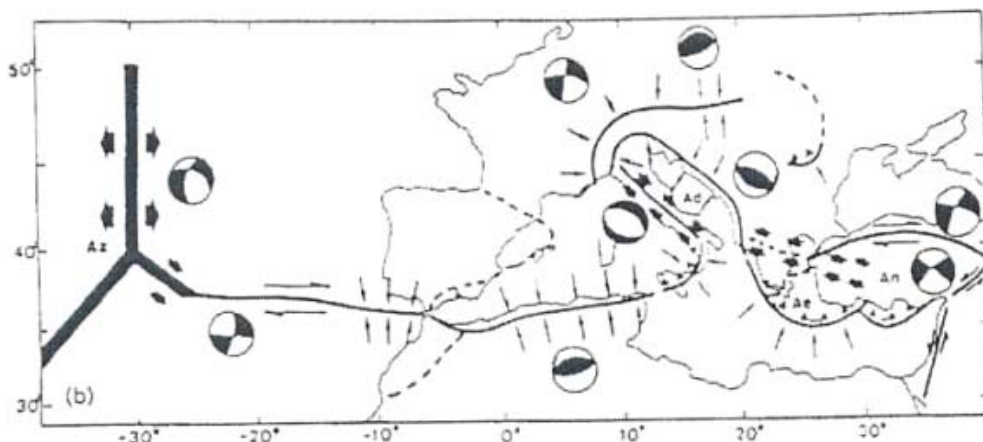
Fig. 1: South European tectonics

The role of the Adriatic Plate as a rigid indenter is significant and will be returned to frequently in the course of this report (Figure 2). On the one hand, the fact of continental-continental collision taking place (albeit at a relatively low rate) can be viewed as a driving force in terms of seismicity. Secondly, the nature of the collision, and the rotational movement involved (Meletti et al. 2000), can be seen to be strongly influencing the local stress field. The change in direction of maximum compressive stress from the Western Alps to the Eastern Alps is well documented, and has been interpreted since the work of Pavoni (1961, 1975) as due to this cause. The precise stress pattern in the Alpine region is suggested to be an interaction between the prevailing continental stress direction and the radial pattern resulting from the rotational collision of Adria and Europe (Kastrup et al. 2002).

Since the seismicity of Switzerland appears not to be interpretable in terms of active tectonic deformation along new features, the consensus of opinion is that the dominant cause of seismicity is the reactivation of old features in a typical intraplate manner. In this case, the radial stress pattern is rather important, as the distribution of seismicity is likely to be related to the interaction of stress direction and the availability of suitably oriented structures for reactivation.
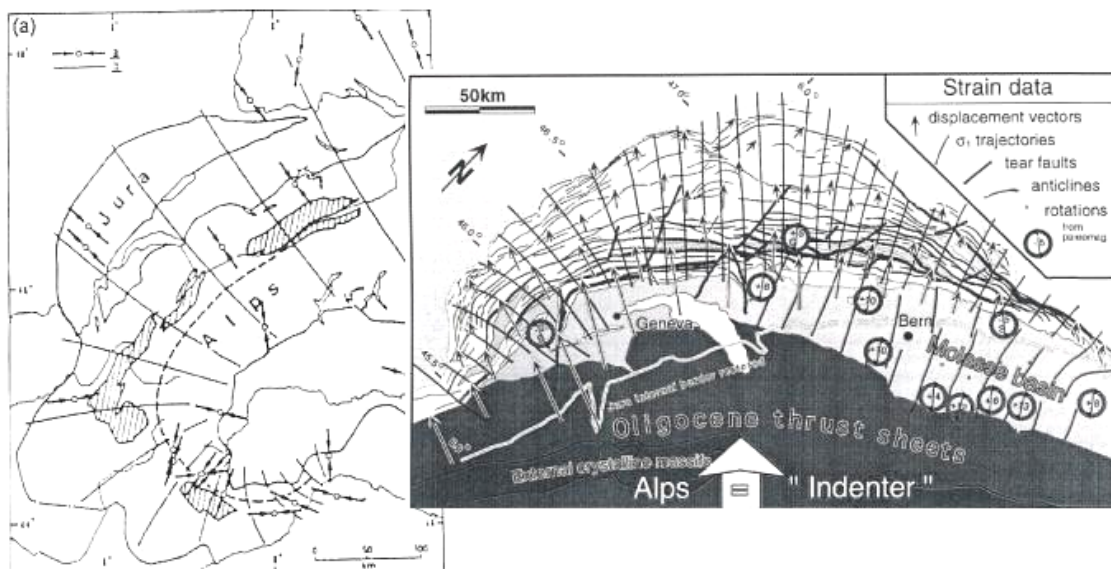
Fig. 2:   The Italian indenter

2.2.3   Alpine Foreland Tectonics

The recent tectonic history of the Alpine Foreland area, including the Molasse basins and the Jura, has long been a subject of controversy amongst geologists. The debate has been summed up recently by Sommaruga (1997). The basic dichotomy is between the schools of "thin-skinned" and "thick-skinned" tectonics (Figure 3). The former model states that northward movement has taken place of a crustal detachment over the whole Alpine Foreland area without involvement of the underlying basement. The thick-skinned model holds that major thrust structures in the Foreland region penetrate through the overlying detachment, and that the basement has also been affected by northward displacement.

The weight of contemporary geological opinion, we believe, generally favours the thin-skinned school. However, it is also clear from the earthquake catalogue that seismicity is far from being concentrated within the upper crustal detachment; nor is there any concentration of seismicity at the detachment-basement interface. In fact, seismicity appears to be more significantly concentrated within the basement.
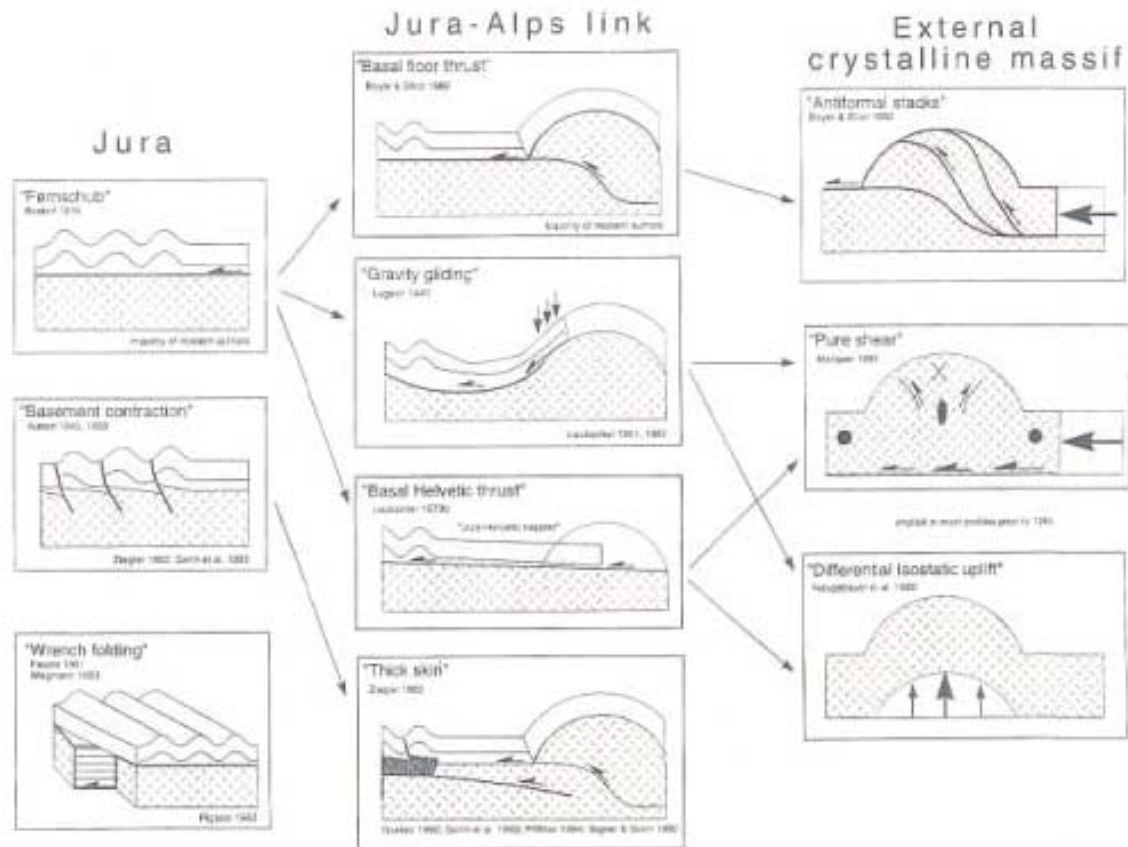
Fig. 3:   Thick-skin versus thin skin model (Sommaruga 1997)

The implication is that, whatever the dominant mode of deformation has been in the Alpine Foreland region in geologically recent times, currently, seismicity in the basement is more important. From this, it would appear that most geological data about the structure of the detachment is hardly relevant to the analysis of the seismicity. Most geological studies are principally concerned with the topmost 4 km of crust, where the seismicity is generally low. The structure of the basement between 5 – 15 km is not much known, yet this is where the majority of seismic energy is being released, even allowing for poor constraints on depth in the earthquake catalogue.

And yet, allowing for the fact that more seismicity seems to occur in this depth band than any other, the geographical pattern of seismicity in the basement and the detachment do not seem to be greatly different, apart from a pronounced absence of even small seismicity in a central part of the Molasse Basin in Switzerland at shallow depth (< 5 km). It seems paradoxical that, if there is no involvement of the basement in the shortening processes that occur in the detachment, there should nevertheless seem to be patterns of seismicity that persist in both, and perhaps even have some correlation with formations (such as the Jura) that exist only in the detachment. One senses that the domination of the thin-skinned school of explanations may not be wholly justified.

2.3   Seismotectonic Framework

Having established the broadest outline of the model, we now proceed to look for subdivisions within this, where we can discern reasons for supposing that the seismicity within certain volumes of crust is similar, and different from neighbouring volumes of crust. To start with, we

will summarise our thoughts about the different data sets that were examined and their relative importance to the task in hand.

2.3.1 Available Data

2.3.1.1 Earthquake Catalogue

This is a data set of primary importance, and to some extent the usefulness of other data sets is proportional to the extent to which they shed light on variations in seismicity. The depth distribution of seismicity is an important feature that is a function of the earthquake catalogue; particularly in the present case where major differences in depth distribution can be discerned from one area to another.

Maps of seismicity are useful both in showing the broader variations in seismicity that help to form the seismotectonic framework, and also in shaping the precise boundaries of individual zones later.

2.3.1.2 Topography

Topographical data is not of high importance, but equally, not to be ignored, as some important structures also have topographical expression (e.g. the Rheingraben, the Helvetic Front).

2.3.1.3 Geological Units

Geology needs to be considered in three dimensions; it is not probable that the distribution of surface outcrops will have a high significance, although sometimes, at least with the eye of faith, there appears to be some sort of correlation with seismicity (e.g. at the boundaries of the Jura). No general rules can be formulated; every case needs to be considered individually.

2.3.1.4 Faulting

The role of faults as individual sources has already been discussed. Even when approaching the modelling process entirely with a zoned approach, the use of fault data is important. In particular, one is interested in distinguishing areas where the faulting has similar characteristics. One would not normally group an area with a strong N-S trend of faulting with an adjacent area where the faulting was principally on a NW-SE trend, because it is unlikely that seismicity would be similar in both areas.

There is a separate problem, already alluded to, that the pattern of faulting seen at the surface may not be the same as that seen at depth. The thin-skinned model would seem to accentuate this for the Alpine Foreland.

In the model, observed faulting patterns (either mapped or from fault plane solutions, see below) were used to determine expected orientation of future earthquake ruptures. Observed faults were not used directly to restrict expected maximum rupture dimensions, which were derived from estimates of maximum magnitude. However, decisions on maximum magnitude were informed by the absence of suitable structures to host exceptionally large earthquakes.

2.3.1.5 Fault Plane Solutions

The distribution of fault plane solutions is useful for gaining insight into what seismic processes are taking place. They do relate partly to what faults are available for reactivation as much as general processes, which is why joint inversion is such a useful technique.

2.3.1.6   Stress Inversion

The practice of deriving stress inversions from groups of fault plane solutions overcomes any problems rising from vagaries within fault populations. Some excellent studies by Eva et al. (1997), Eva and Solarino (1998) and Kastrup (2002) show that conducting inversions for homogeneous earthquake populations can indicate the characteristic faulting type(s) and local stress field Figure 4. Attempting the same thing with heterogeneous sets of earthquakes gives conspicuously poor results. The very application of this method, therefore, serves to delineate areas where the seismicity is generally consistent, and then arrives at descriptions of that consistent character. We therefore accord this data a high priority in establishing the seismotectonic framework.
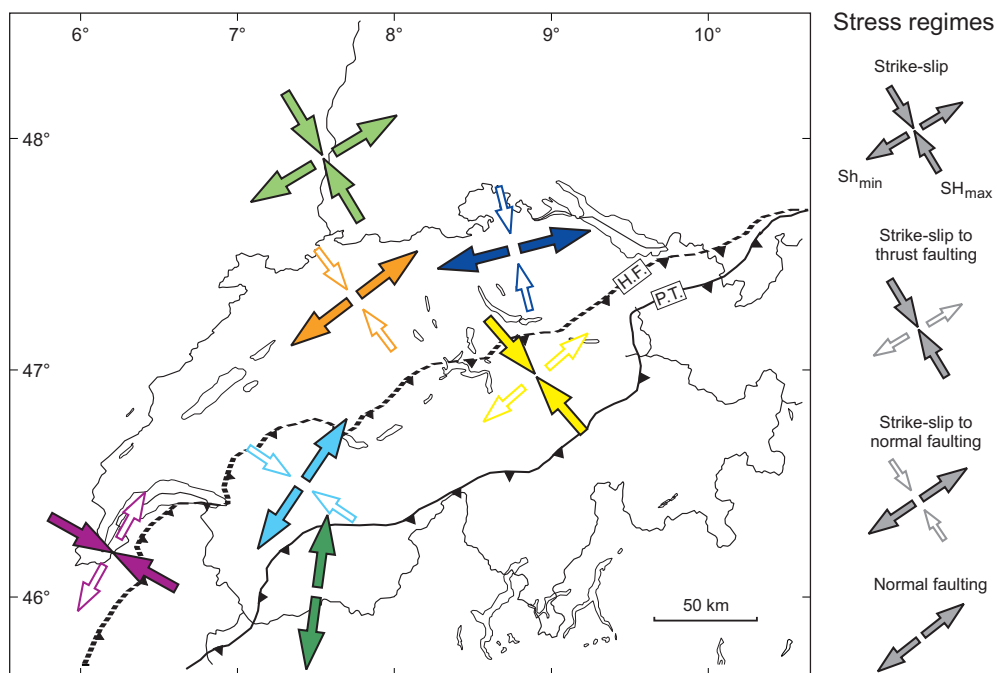
Fig. 4:   Stress inversion (Kastrup 2002)

2.3.1.7   b Values

The spatial variation of b values (the slope in the Gutenberg-Richter magnitude-frequency relationship) is a derivative of the earthquake catalogue, and hard to determine accurately. A preliminary attempt was made to investigate this, using a simple grid (in which, inevitably, some squares were under-populated with earthquakes). The results were hard to interpret, but did seem to show some areas where b values tended to be consistent; for example, values in the Western Alps tend to be around 0.65 while those in the Alpine Foreland tend to be around 0.9.

2.3.1.8   Depth to Moho

Maps showing depth to Moho show a smooth gradient over most of the study area. We do not consider this to be an important data set for informing the seismic source model in this project.

2.3.1.9   Depth of Mesozoic

We do not observe any patterns in this data set that appear to us to be significant for the purposes of this project.

2.3.1.10 Subsidence / Uplift

This data set is possibly significant, but hard to interpret, and needs to be taken into consideration alongside other factors.

2.3.1.11 In Situ Stress Measurements

These can be useful as corroborating evidence about local stress directions.

2.3.1.12 Palaeoseismic Data

While these data might be relevant to the assessment of single fault sources, they cannot be applied to the current task of building the seismotectonic framework, as they are very sparse in number and still debated as to their significance.

2.3.1.13 Macroseismic Field Data

This data set could indicate changes in crustal properties through variations in attenuation. The PEGASOS EXT-TB-0033 (2002) report does indicate that such a change does in fact take place across the Helvetic Front. Full study of this would, however, require investigations beyond the scope of source characterisation.

2.3.1.14 Maximum Intensity Map

Existing maps of maximum observed intensity (e.g. Rüttener 1995) were checked. These can really be considered more or less obsolete in the light of the data collected for PEGASOS EXT-TB-0033/35 (2002), which should form the basis for a new and improved map. No insights were obtained from the maps examined over and above what conclusions can be drawn from the catalogue data.

2.3.1.15 Gravity Data

The gravity data set is potentially useful. It needs to be checked in case it shows significant patterns that could be interpreted seismotectonically in the light of other data. It was checked. We did not discern anything of interest.

2.3.1.16 Magnetic Anomalies

The same remarks as in section 2.3.1.15 apply here also.

2.3.1.17 Thermal Springs

We did not consider this data set to be very useful.

2.3.1.18 Heat Flow

The same remarks as in section 2.3.1.15 apply here also. We now consider our basic framework.

2.3.2 Stress Inversion

As already mentioned, we find this data set of particular importance at this stage in the proceedings. Even a simple inspection of focal mechanisms in Switzerland shows differences in deformational style by area. The study by Kastrup (2002) found that acceptable stress inversions could be obtained by making about eight local groupings of events. The resulting analysis showed a range of stress regimes.

In the first place, it is clear that the direction of the maximum compressive stress shows a radial pattern, going from WNW-ESE around Geneva to NNW-SSE in the Zurich area. This confirms the pattern already discussed. This pattern, which follows the curve of the Alps, is only observed close to the mountain chain. As one moves away to the north, it gradually fades into the general European stress field arising from North Atlantic ridge push (Kastrup 2002).

In the second place, the predominant styles of faulting also change, from normal faulting in the Penninic Alps to strike-slip in the Rheingraben, with areas of strike-slip to thrust (e.g. Graubünden) contrasting with strike-slip to normal regimes (e.g. Zürich).

The existence of normal faulting is interesting in that it indicates that in the high Alps especially, deformation is no longer governed by compression (as one might expect in a collision-driven mountain belt) but extension is going on.

2.3.3   Major Crustal Boundaries

From Kastrup's (2002) study it also appears that lines marking major crustal boundaries are also significant in dividing different faulting regimes: in particular, the Helvetic Front (HF) and Peninnic Thrust (PT) appear to have this role (Figure 5). To these we would add the Insubric Line (IL), which appears to play a similar role in Eva et al. (1997).
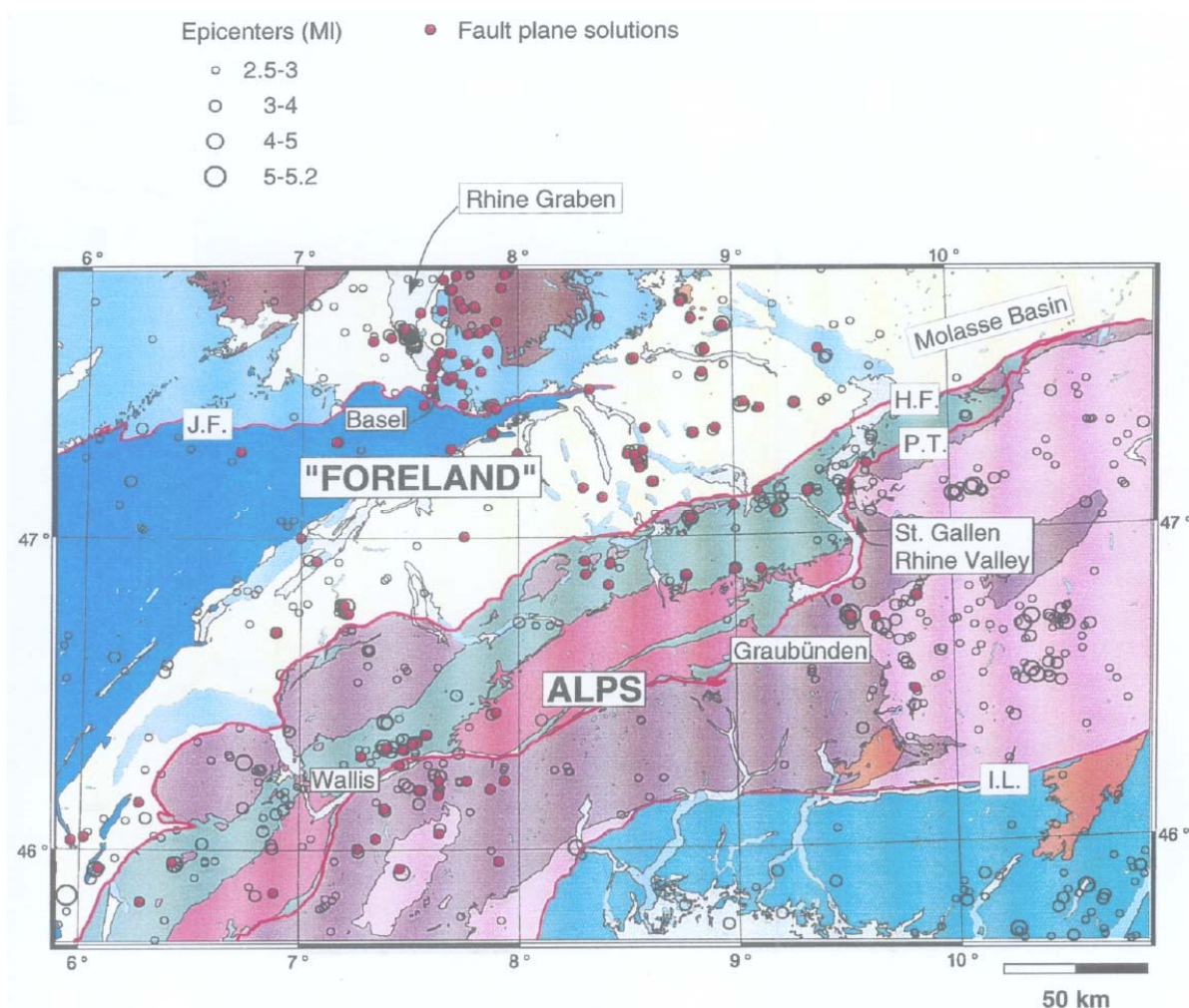
Fig. 5:   Tectonic structure (Kastrup 2002)

The significance of the Helvetic Front as a divider between areas of quite different seismogenic properties is underlined by the dramatic contrast in seismicity depth profiles to south and north of it, as shown by Deichmann et al. (2000). This boundary clearly separates volumes of crust with very different earthquake populations, and therefore cannot be ignored in the formulation of a seismic model.

We have not overlooked the fact that these lines are not vertical, and this is discussed further below in section 3.3.

2.3.4   Stress Patterns

It is rather striking, when considering the radial Alpine stress pattern, to note that precisely where the direction of maximum stress is perpendicular to the Helvetic Front (and also the important Hercynian trend) and parallel to the dip direction of the Moho, seismicity is conspicuously low both north and south of the Helvetic Front. Either side of this NW-SE band of low seismicity are bands of rather higher seismicity, again trending NW-SE, and beyond these, seismicity decreases again.

This may be a reflection of interaction between the direction of maximum compressive stress (which is radial) and the distribution of faults of given orientation (which probably isn't). In a very simple case (for example, imagine an Alpine Foreland populated exclusively with NE-SW trending vertical faults) one could postulate a pattern of sectors: low seismicity where the angle of stress to fault was very gentle or very steep, and high seismicity where the most favourable angle of 45 degrees was approached. Clearly such a simple case does not apply here, but it may be that something analogous may be taking place; we have not been able to test the hypothesis, however.

In discussions of this hypothesis at SP1 Workshop 3, it was objected that, supposing one did indeed have low seismicity in one radial zone and higher seismicity in the adjacent sectors, then, viewed kinematically, the deformation that is apparently not taking place in the "low" sector must still be taken up somehow. In other words, the deformation must simply be transferred further to the north. One could argue that this is actually observed, and use this as an explanation for the high seismicity in the Basel region, which is just to the north of the low seismicity "stable" sector running NW-SE through central Switzerland.

Also, in such discussions, it is uncertain how much weight to accord to rare large earthquakes. If one were to accept the hypothesis of Meyer et al. (1994) that the 1356 earthquake occurred as thrusting on a roughly E-W fault (even though such thrusting is not seen in this area in modern instrumental data), then it could be that one historical event actually took up, in one go, all the crustal shortening required for a substantial period of years longer than the present catalogue.

Whatever the explanation, the fact is that we do see a seismotectonic pattern in Switzerland that forms the basis of a seismic source partition, and, in simple terms, this consists of a series of dividing lines following the curve of the Alps, marking major crustal divisions, and a second series of dividing lines perpendicular to the first, following the direction of maximum compressive stress. The resulting pattern contrasts most strongly in seismicity rate as one moves from west to east, and contrasts most strongly in depth distribution (and possibly also b value) when moving from north to south.

2.3.5   Seismotectonics − Away From the Alps

While this pattern applies to the Alps and the Alpine Foreland, it is not applicable in the margins of the study area. However, the margins are relatively unimportant from the point of view of hazard and we feel it appropriate to treat them in less detail. For Northern Italy south of the Alps, our only concern has been to construct the model so that the right number of earthquakes appears at roughly the right distance. In the west, we consider the Bresse Graben to be a

significant structure, but we have not analysed it in any detail. Most of the territory of France that appears within the study area has been treated only in a very broad way.

The northern part of the study area is treated, so far as the seismotectonic framework is concerned, as three areas: a stable area in the east, a stable area in the west, and the Rheingraben separating them. The latter is a major structural weakness and is clearly the locus for most of the seismicity in that part of the study area north of the Alpine Foreland. The evolution of it is discussed comprehensively by Schumacher (2002), illustrating the shifting of the principal depocentres in geological time. The current regime is characterised as predominantly left-lateral strike-slip faulting with the central graben acting as a restraining bend. Young pull-apart basins are presumed to be forming in both the northern and southern graben segments. The detailed treatment of this in the zone model is discussed in the next section.

It is particularly noteworthy that there appears to be a rather higher level of seismic activity where the southern end of the Upper Rheingraben meets the Alpine Foreland. This area includes the largest earthquake in the study area (the 1356 Basel earthquake). The area will be discussed in more detail in the next section, but a word needs to be said from the point of view of the seismotectonic framework.

One possible explanation is that this enhanced seismicity results from the interaction between a major structure running roughly NNE-SSW (the Rheingraben) with structures having basically an E-W or ENE-WSW trend (in the Alpine Foreland). The influence of the two together could cause a critical zone of weakness.

A second possibility, already raised, is that the high seismicity in this area is related to the low seismicity between Basel and the Alps; that this block is relatively coherent and deformation is being transferred north in to the Basel area.

Both these ideas are, at present, rather speculative. However, they indicate that the increased seismicity at the southern end of the Rheingraben is not something that is inexplicable, and therefore probably not something arising from chance. Finding the precise form that the source zone model should take in this area is perhaps the hardest part of the source zone partitioning, which will now be described in detail.

3   THE SOURCE ZONATION

The zonation is based on a generalised kinematic schema, in which Italy is seen as a rigid indenter creating a radial stress pattern in the Alpine region. This creates a pattern of rings and sectors. The "rings" are progressively further from the Italian collision zone and are separated by major structural divisions (Penninic Thrust, Helvetic Front). The "sectors" are due to the rotation in the local stress regime, which interacts with the general structural grain (SW-NE), to produce a pattern of alternate zones of high and low seismicity.

The basic seismic source model consists of area source zones defined by simple polygons. Seismicity is assumed to be spatially homogeneous within these sources, with the exception of the distributed Basel source described below. The bulk of the model consists of a single set of unvarying polygonal source zones, defined in the conventional PSHA manner, the boundaries of which are firm divisions between different sets of seismicity parameters (i.e. most of the zone boundaries are not "soft" in the sense of allowing seismicity to percolate from one zone to adjoining territory).

In some source models, "soft" boundaries are used to indicate uncertainties in the location of the edges of source zones; particularly in cases where the model involves active sources surrounded by a matrix that is either discounted as aseismic or is modelled as a low-activity background area. Historically, this approach was first used to eliminate sharp "cliffs" from hazard maps (Bender and Perkins 1987), and its carry-over into site studies has not always found support (to judge from some informal conversations in the wider hazard community).

In this model, the source zones constitute a complete tessellation of the area under consideration, and we consider such an approach of less relevance, as it has the general effect of scattering earthquakes in both directions across any source zone boundary. To some extent many of the source boundaries have uncertainty inasmuch as we could postulate numerous minor variations in geometry; indeed, many such refinements were made in the course of the development of the model. Such variations would better express the uncertainty in the boundary positions than an ad hoc application of soft boundary methods; however, our consideration that incorporating such uncertainties would add hugely to the complexity of the model with very little actual benefit in terms of results.

All zones are given four-letter identification codes for ease of reference. These are generally contractions of geographical or geological terms, e.g. BAWU is from Baden-Württemberg. These codes are sometimes modified to refer to variants in different branches of the logic tree (e.g. BAW2).

3.1   Source Model Considered as a Logic Tree

In three areas there are important alternatives to cope with uncertainty in dealing with certain features. These three sets of alternatives are independent of one another. The probability of a choice in alternative two is not influenced by which choice is made for alternative one.

These alternatives make it difficult to portray the whole model in a single figure. Accordingly, the seismic source zonation for team EG1c is described in Figures 6 to 11. Figure 6 shows the logic tree structure for source zonation. The tree consists of three levels, according to the three sets of independent alternatives.

Rhine_Graben	Swabian_Jura	Permocarbon	Source_Set
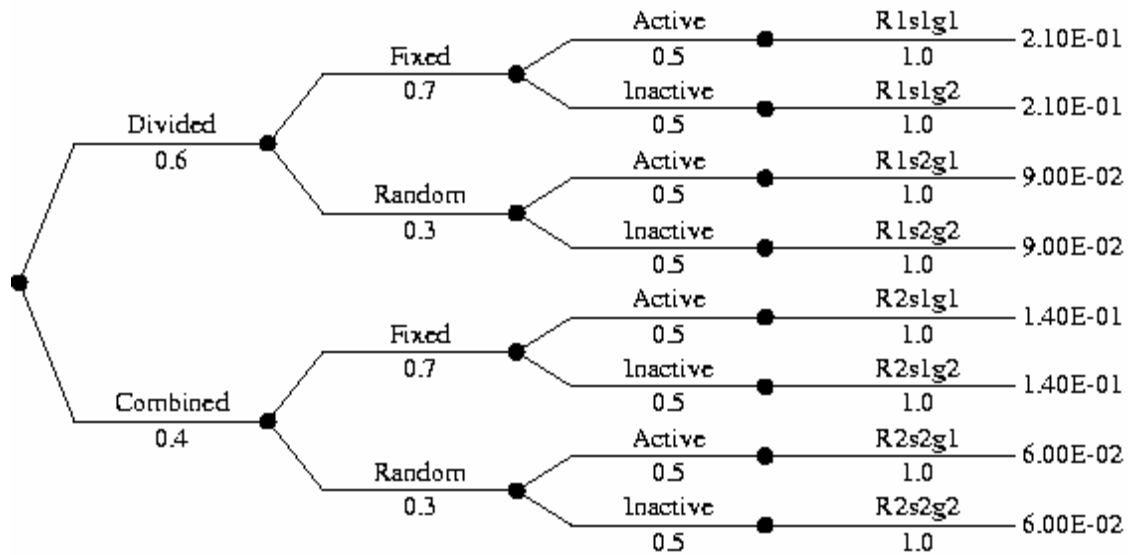
Fig. 6: Logic tree for EG1c seismic source zonation

3.1.1 The Rhine Graben

The first uncertainty concerns whether the Rhine Graben should be treated as a single source (RHEG) or divided into three sources (RHGN, RHGC, and RHGS). These alternative sources are shown on Figure 7. From a first order geological and tectonic approach the Upper Rhine graben is a unique feature with common features. Second order consideration suggests there is evidence for difference in at least two (separation North-South) and more likely three divisions (separation North-Central-South), as described in Section 2.3.5 above.
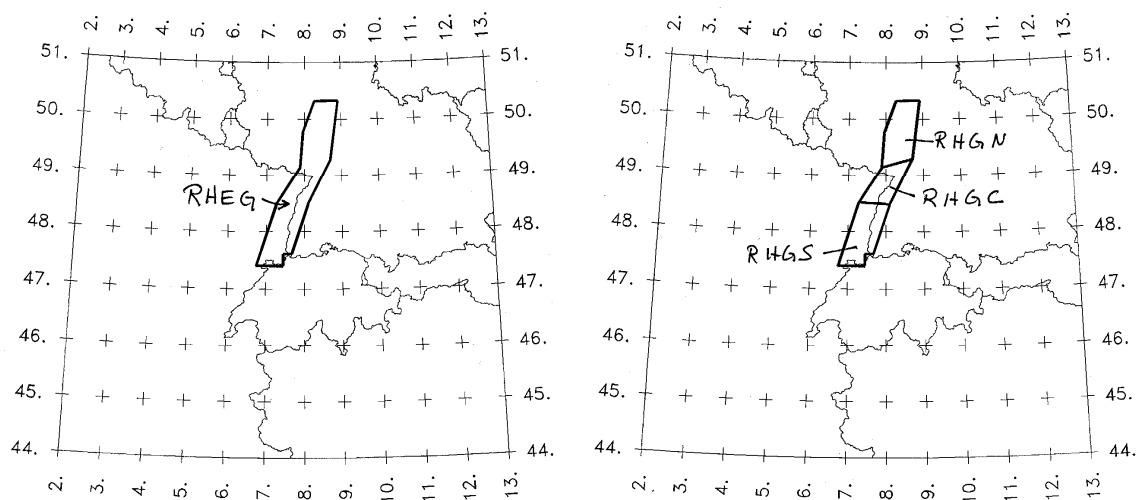
Fig. 7: EG1c alternative source zonations of the Rhine Graben

This relates both to observed seismicity, and changes in the geometry of faulting. The team weighted the model for the Upper Rhine Graben with 0.6 probability that the three-way divided model is preferable against 0.4 for the single zone model. A two-way divided model was not considered necessary. The basis for the weighting decision was that observations of differences in the seismicity in the three sections of the graben, allied to the change in the geometry from south to north, clearly indicated that the partitioned model should have the higher weight. However, the common features throughout the whole graben indicate that the weight for the unified zone should not be too low.

3.1.2 Permo-carboniferous Troughs

The second problem is whether or not the faulting connected with Permo-carboniferous troughs near the Swiss-German border is a significant active feature or not. The Permocarboniferous troughs in NW-Switzerland are best documented in Müller et al. (NTB 99-08, 2002), Beil. 2.4. ("Zentraler Nordschweizer Permokarbontrog") covering a region stretching East-West from Konstanz/D to at least Brugg/CH and possibly further to the West. In this region subsidence has been reported in the order of 0.1 mm/a, however not very convincingly throughout. If it is significant, then source NSPG is used as a source zone, the Zurich source has the configuration ZURI, and the area to the north comprising Baden-Württemberg and the Black Forest is modelled as BAWU (or BAWS, see next section), as shown on the bottom of Figure 8.
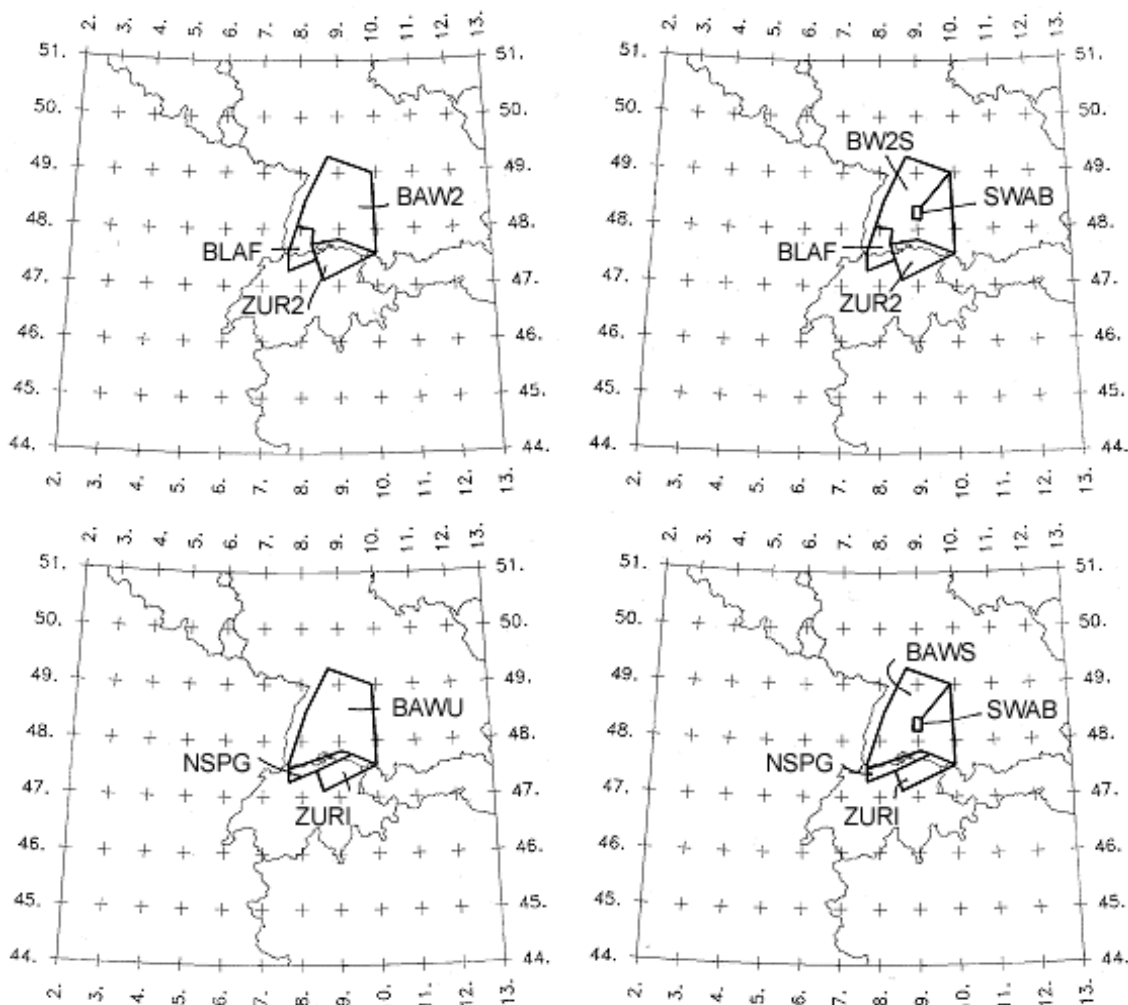
Fig. 8: EG1c alternative source zonations for the Swabian Jura and Permo-Carboniferous troughs

If it is not significant, then the Black Forest source BLAF is used as a source zone and the Zürich and Baden-Württemberg sources have configurations ZUR2, and BAW2, or (BW2S) as shown on the top of Figure 8. The zones BLAF and ZUR2, then coming into play, are designed on the basis of seismicity and on similarities of geological units.

Weighing all available arguments for and against the significance of the Permo-carboniferous troughs, and if they should be treated as a separate source zone or not, the team decided to assign equal weights to both alternatives. There seems to be little consensus in the literature to be guided by; on the one hand, from a structural point of view, these appear to be significant features that would be favourable for reactivation. On the other hand, there is no evident link with seismicity in the observed catalogue nor with the stress inversion data. Lacking any firm reason for a decision one way or the other, using equal weights appears to be the best way to resolve the situation.

3.1.3 The Swabian Jura

This branch in the logic tree addresses the treatment of the Swabian Jura active zone. The seismic activity within the Swabian Jura source (SWAB) as known from the catalogue rose slightly in about 1870, but then tremendously increased in the year 1911. Recurrence and M_{max} estimation in the SWAB source hence stems from the last 100 years only. Activity in all centuries before was just on the level of average of the surrounding BAWU region as a whole, as far as extent and completeness of the catalogue allows one to say. There is no clear tectonic or neotectonic evidence for the SWAB source known to date. (The Hohenzollern graben or trough, which crosses the SWAB source, is a surficial feature − depth extent about 1 km − of Pliocene age and is believed not to be in direct causal relation to the seismicity of the SWAB zone.) The question is therefore whether the observed strong seismicity in this area is due to a single, unique feature, or whether there are many other equivalent features any of which could be the locus of similar seismicity in the future.

In one model, the seismicity is confined to the distinct stationary source SWAB embedded in the larger zone BAWS or BW2S. These zones are shown on the right hand side of Figure 8. Zone files BAWS and BW2S were created to be simple polygons wrapping around zone SWAB. The alternative model considers the elevated seismicity in SWAB not to be a stationary source, but rather may occur anywhere within the larger BAWU zones. The EG1c team considers it a possibility that a source feature similar to that of SWAB appearing in the future at any place within the entire BAWU area with equal probability ("the SWAB source moving to a different position within BAWU, but is not duplicated"). This is equivalent to removing the zone SWAB and smoothing out the seismicity throughout the surrounding zone. As a result, just zones BAWU or BAW2 are used, as shown on the left of Figure 8.

The coding system used for the identifiers is that codes with an S (BAWS and BW2S) indicate the Swabian zone is fixed, those without (BAWU, BAW2) have it not fixed. Identifiers with a 2 (BAW2, BW2S) indicate that the Permo-Carboniferous grabens are not counted as an active source.

This possibility is given a weight of 0.3 as opposed to 0.7 for a stationary SWAB source. The weight of 0.3 is low, as an expression of the absence of reason why such an active feature should exist anywhere other than the one place where it clearly does exist at present. The continuation of activity in the same place is clearly the most likely future prospect after 100 years of elevated seismicity and several distinct and coherent characteristics regarding the source. However, given the lack of understanding of the active feature at this particular place, and the lack of assurance that such active features do *not* exist elsewhere in the larger BAWU area, indicates that this weight must not be too small.

3.1.4 The Unvarying Zones

In addition, there are 22 sources whose boundaries are unaffected by the alternatives discussed above. These are shown on Figure 9. The relation of the whole model to the seismotectonic plan can now be considered.
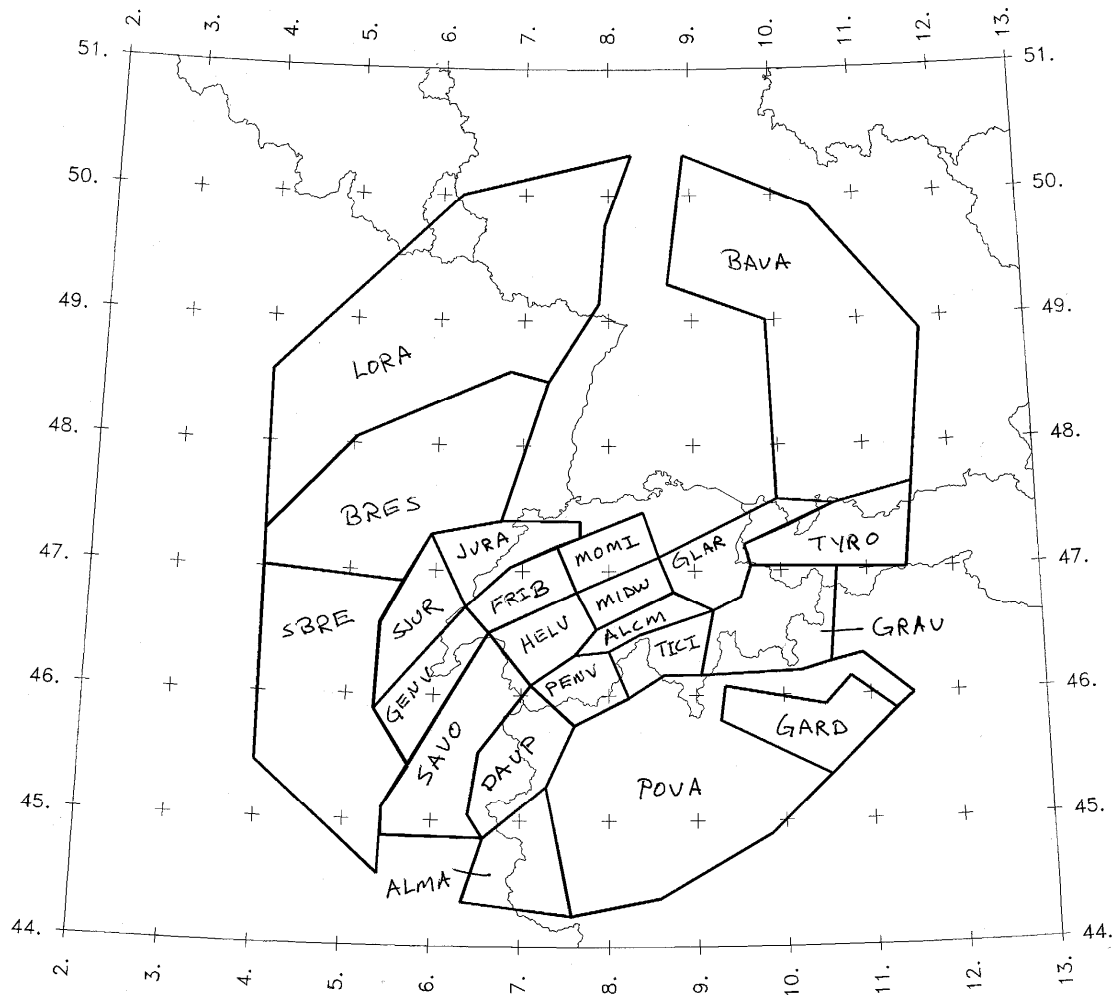
Fig. 9:   Source zones that do not change with the alternatives listed on Fig. 1

3.2   Discussion of the Zone Model

Zones can be divided into several groups for the purposes of discussion.

3.2.1   Group 1 – Molasse zones

These zones form the outermost ring of the kinematic model. Four zones are defined, alternating low – high – low – high seismicity from west to east. Divisions are made on a combination of stress inversion data and seismicity. From west to east the zones are:

GENV –   Geneva
FRIB   –   Fribourg
MOMI –   Swiss Molasse Mittelland
ZURI   –   Zürich (or ZUR2 when zone NSPG not present)

3.2.2   Group 2 − Helvetic zones

Distinct changes in crustal structures and seismicity occur across the Helvetic Front and between HF and PT. Therefore this area is structurally distinct, but can be further subdivided according to differences due to the rotation of stress axes due to the Italian indenter. The zone ALCM is due to the general aseismicity of crystalline massifs within the Alpine region (cf Western Alps). From west to east the zones are:

SAVO − Savoie
HELV − Helveticum
NIDW − Nidwalden
ALCM − Alpine crystalline massif
GLAR − Glarus

With respect to small magnitude seismicity, the zone NIDW is inhomogeneous. It was considered that this zone could be partitioned into two small zones of less seismicity (west) and more seismicity (east), or these two small zones could be added to ALCM and GLAR respectively. It was decided that there was insufficient justification for these modifications, given the generally low level of seismicity in this zone and a lack of larger events.

3.2.3   Group 3 − Penninic zones

As with the Helvetic zones, there are observed significant differences (from stress inversion) north and south of the Penninic Thrust. This area in the core of the Alps is bounded on the south by the Insubric Line, and can be divided similarly to the Helvetic area according to rotation of stress axes. These sectors again show alternating patterns of higher and lower seismicity. From west to east the zones are:

DAUP − Dauphine
PENN − Penninic Alps
TICI   − Ticino

3.2.4   Group 4 − Eastern Alps

To some extent this area is a continuation of the Alpine pattern observed further west, but there is a merging of structural units into the Austroalpine nappes. Structure is less clear at present. There may be a difference between the seismicity north and south in this area hence two source zones. There is at the very least an apparent discontinuity between the northern and southern seismicity.

GRAU − Graubünden
TYRO − Tyrol

3.2.5   Group 5 − Jura

In reviewing the discussions of thin-skinned and thick-skinned tectonics in the Jura it appears the thin-skinned model is more generally favoured. However, it seems clear that much of the seismicity occurs in the basement. This would imply that the seismicity is due to general intra-plate reactivation mechanisms and not due to active crustal shortening. While the boundary between Jura and Molasse is geologically very clear at the surface, it is less significant at seismogenic depths. However, the seismicity is less than in the corresponding Molasse zones, so the two groups cannot be combined. Two zones are defined on account of stress rotation.

JURA − Jura
SJUR − South Jura

3.2.6   Group 6 – Rheingraben

The Rheingraben (Rhine Graben) shows up very clearly as the locus of enhanced seismicity, but it is far from clear that any of this seismicity is associated with active graben subsidence or controlled by the master faults bounding the graben system. It seems more probable that the graben is simply acting as a zone of major weakness. The graben is modelled either as one or three zones, as already discussed.

The SW corner of the graben shows a very strong cluster of seismic activity, including the 1356 Basel earthquake. The reason for this focus is unclear; it may be due to this point being an inter-section of weaknesses (the N-S Rheingraben with ENE-WSW trending Permo-Carboniferous graben structures). It may also be exaggerated on account of the "migration" of historical epi-centres to an important city. This cluster has been modelled as a small zone, with a soft boundary.

This leads to the construction of a distributed Basel source. We define a source zone around the cluster of seismicity near Basel. However, we suggest that this concentration is at least partly due the process of recording historical earthquakes. It is well known that, especially for the early historical period, epicentres have a tendency to migrate towards important towns, since these are often the only place where the earthquake was reported. Most earthquake catalogues, given an event felt only in one town, will assign an epicentre under or near that town. In fact, the earthquake could have been some distance away, with closer reports from smaller settle-ments non-existent or lost. For this zone, therefore, we specify that the seismicity should be dispersed outward from the modelled source zone using a Gaussian decay in rate over a distance of 30 km, with a standard deviation of 10 km. The 30 km extent is estimated from the mean distance of Basel to other medieval towns in the vicinity of Basel (e.g. Zürich, Biel, Freiburg im Breisgau), to which historical earthquakes would otherwise have been assigned. The distributed Basel source is shown in Figure 10.

The decay of seismicity rate is described by a grid of longitude-latitude pairs with the fraction of the total rate for the source that is assigned to each grid point. Note that this spatial grid overlaps the adjacent sources by intent.

We consider that evidence for active faulting on the Reinach Fault is unconvincing. The inclu-sion of this feature as an explicit source in the model is of doubtful utility, since the seismicity in this area is already concentrated in quite a small zone. Since any earthquake occurring in a zone must occur on some fault within that zone, the existence of the zone already allows for some seismicity on this fault.

BASL –   Basel
RHEG –   Rheingraben

or

BASL –   Basel
RHGN –   Rheingraben North
RHGC –   Rheingraben Centre
RHGS –   Rheingraben South
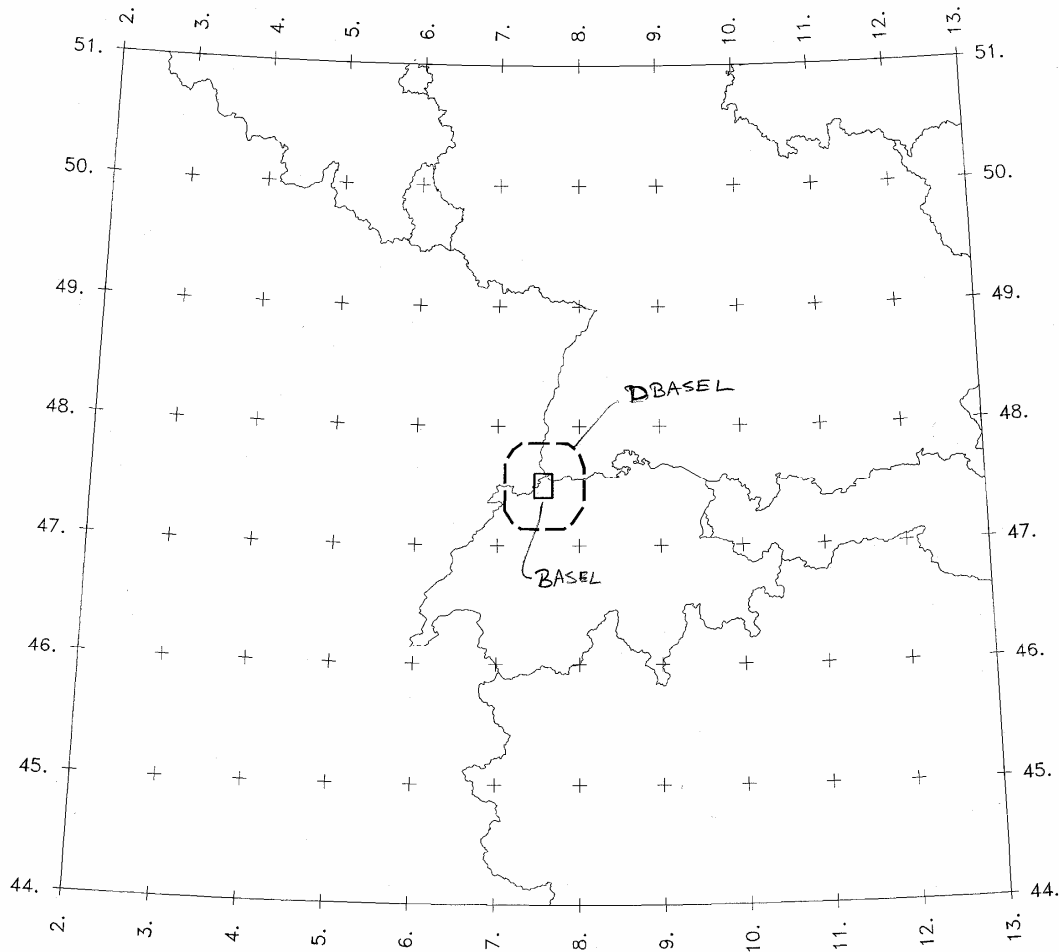
Fig. 10:   The nominal BASL polygon and the limits of the distributed source around it

3.2.7   Group 7 – Graben inversion

This group consists of a single zone. The existenc of graben inversion in this area is considered to be potentially significant in one iteration of the model.

NSPG – Nordschweizer Permo-Carboniferous Grabens

or

BLAF – Black Forest (part of Group 8). In this case, the geometry of ZURI and BAWU is also modified

3.2.8   Group 8 – SW Germany crustal unit

The area to the east of the Rheingraben has been taken to be a more or less coherent structure (the SW German crustal "plate"). The strong cluster of seismicity in the Swabian Jura has been modelled as a separate zone despite the fact that it has only been active since 1872 and mostly since 1911. The geological explanation for this is unknown. The alternative model removes this small zone and redistributes the seismicity.

BAVA – Bavaria
BAWS – Baden-Württemberg (or BW2S when zone NSPG not present)
SWAB – Swabian Jura

or

BAVA – Bavaria
BAWU – Baden-Württemberg (or BAW2 when zone NSPG not present)

3.2.9   Group 9 – French transpressional structures

Eastern France is treated rather broadly because of its distance from the sites, with a division into three zones, two of which are generally linked to the Bresse Graben, and divided as that structure changes direction. The northernmost zone is of low activity, except for mining seismicity.

LORA – Lorraine-Alsace
BRES – Bresse Graben
SBRE – South Bresse Graben

3.2.10   Group 10 – Southern background zones

The last three zones fill in the southernmost part of the area of interest. Their significance for the site hazard is very low, and little effort has been spent on precise definition.

ALMA – Alpes Maritimes
POVA – Po Valley
GARD – Garda

As indicated on the right hand side of Figure 6, the above alternative models lead to eight different source sets. These are listed in Table 1. The first row of the table lists the source set "UC" that includes the 22 zones shown on Figure 9 plus BASL. These sources do not change with the alternative zonations and are to be included in each set.

Tab. 1:   EG1c Seismic Source Sets

Source Set	Sources
UC (unchanging)	BASL, ALCM, ALMA, BAVA, BRES, DAUP, FRIB, GARD, GENV, GLAR, GRAU, HELV, JURA, LORA, MOMI, NIDW, PENV, POVA, SAVO, SBRE, SJUR, TICI, TYRO
R1S1G1	RHGN, RHGC, RHGS, SWAB, BAWS, NSPG, ZURI + UC
R1S1G2	RHGN, RHGC, RHGS, SWAB, BW2S, BLAF, ZUR2 + UC
R1S2G1	RHGN, RHGC, RHGS, BAWU, NSPG, ZURI + UC
R1S2G2	RHGN, RHGC, RHGS, BAW2, BLAF, ZUR2 + UC
R2S1G1	RHEG, SWAB, BAWS, NSPG, ZURI + UC
R2S1G2	RHEG, SWAB, BW2S, BLAF, ZUR2 + UC
R2S2G1	RHEG, BAWU, NSPG, ZURI + UC
R2S2G2	RHEG, BAW2, BLAF, ZUR2 + UC

3.3   Dipping zone boundaries

In the Alps the Penninic and Helvetic Nappes are thrust towards the north leading to crustal boundaries that dip southward. This is shown in cross sections interpreted from deep seismic profiles (Marchant and Stampfli 1997, Schmid and Kissling 2002).

The question arises as to whether the model should include dipping boundaries between some zones in this region. This could have the effect of exchanging seismicity between zones in the Penninic and Helvetic areas, or from the Helvetic to the Molasse basin. This is illustrated in cartoon form in Figure 11.
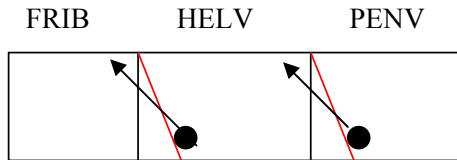
Fig. 11:   Possible migration of hypocentres between zones if major crustal boundaries are considered to be dipping

The argument against having dipping boundaries derives from the team's acceptance of the "thin skin" tetconic model; under the Alps earthquakes are considered rather shallow (less than 20 km and mostly less than 15 km), and from the geological cross sections, the dipping is very steep near the surface. The details of the layering of the nappes, which would produce some more subdivisions of the geological domains, seems not really to be relevant to the hazard. Moreover, in this part of the crust, the rupture is allowed to cross the source boundary if they exceed the source dimensions (see Section 8.1).

In conclusion, the team's opinion is that dipping boundaries are not useful to our model.

4   CATALOGUE DECLUSTERING

The declustered version of the earthquake catalogue used here is derived by a slightly modified version of the Reasenberg (1985) process. The main difference is that the Reasenberg algorithm processes an earthquake catalogue in chronological sequence from beginning to end. The process used here, which is described by Musson (1999, 2000), approaches a catalogue in magnitude space. The largest event in the catalogue is selected first. All subsequent events contained within a moving time window and stationary space window are flagged as being aftershocks. The size of the windows is predefined. If the length of the time window is t days, then an event within t days of either the mainshock or the last identified aftershock of the mainshock under consideration is considered to be an aftershock (as long as it is within r km of the mainshock epicentre, where r is the radius of the space window). The start of the time window is continuously reset until a point is reached where there are no events within t days of the last aftershock, within the space window. The same procedure is then run in the reverse direction (backwards in time from the main shock) in order to identify the foreshocks. Once all events in a sequence have been flagged, the next largest unflagged event in the catalogue is selected, and the process is run again. This continues until all events have been flagged as either mainshock, foreshock or aftershock. The mainshocks are then extracted to form the declustered catalogue.

The size of the windows was determined by an optimisation procedure. The rate at which the proportion of catalogue events defined as accessory shocks increased as a function of increasing t and r was examined. In an ideal case, the rate is first rapid as t and r increase from zero; the rate flattens as all accessory shocks are identified, and then increases again as events are wrongly identified as accessories. Making plots of such rate changes enables one to look for the values at which the flattening occurs, or failing that, at least a break in slope if the flat "ledge" cannot be identified. The resulting values were as follows:

pre-1970: radius 20 km, time (lag) window 28 days

post-1970: radius 15 km, time (lag) window 14 days

These parameters are derived from the catalogue itself and are regarded as being more trustworthy than prior values. Magnitude dependence for the radius could have been considered, but was considered not to be appropriate here because, in the bulk of historical events in the catalogue, the location inaccuracies are probably significantly larger than the source sizes.

These parameters identify 10355 events as main shocks, which is just over half the total PEGASOS catalogue. The cumulative moment, as well as the approximate cumulative seismic energy of the events thereby removed from further hazard investigation (9928 events) amounts to only about 3 % of the total (of which the M 6.2 1356 Basel foreshock alone is 1.5%).

Attempts were made to test further subdivisions of the pre-1970 catalogue, but the results were the same. Some specific cases were examined to test the results of the declustering procedure against the team members' personal expectations based on knowledge of these event sequences, and found to be satisfactory.

The team did not feel that it was necessary to use any different declustering of the catalogue in addition to the chosen one. The opinion in the team was that having such a variant catalogue would not result in any significant changes to hazard parameters. This conclusion is supported by tests made by Slejko (2002).

5   COMPLETENESS

The consideration of catalogue completeness is based on two different approaches. In the first case, one can consider the history of the earthquake service in Switzerland, and the development of the means by which data are recorded (Table 2); also the availability of historical information. Secondly, a statistical approach can be made, studying the plots of frequency distribution of different magnitudes in time, which are influenced by the fluctuation of the completeness of the seismic record with time.

Tab. 2:   Significant historical dates and their effect on interpretation of earthquake catalogue completeness

Year	Important events	NAGRA report	RUETTENER completeness	MECOS-DACH completeness	PEGASOS (ECOS) completeness
169	1st chronicle	1300-1754	1300 I ≥ 9 1600 I = 8	1300 I ≥ 8 1575 I = 7 1650 I = 6	1680 I = 8 (from 1300)
1755	Lisbon earthquake	1755-1878	1750 I = 6; 7		1750 I = 7 (from 1500)
1856	1st Catalogue in Switzerland				1850 I = 6 (from 1680)
1878	1st SED 'Jahresbericht'	1878-1941	1878 I = 4; 5	1875 I = 5; 4	1878 I = 5
1880	Earthquake commission				
1913	Installation of seismic stations				
1942	Additional station in Brig I and Ml	1942-1974			
1963	'Jahresbericht' Suspension until 1971				
1975	Installation of the seismic network				

5.1   Historical evaluation

In Switzerland, the level of completeness of historical data changes from canton to another. With reference to Figure 12, one can state that Region 1 (Basel, Zurich/Zg and Glarus: 4, 2 and 8) has the longest historical record, Region 2 (Be/West CH, Inner CH and Graubunden: 3, 1 and 7) has a shorter one, and Region 3 (Wallis and Ticino: 5 and 6), has the shortest record of all.
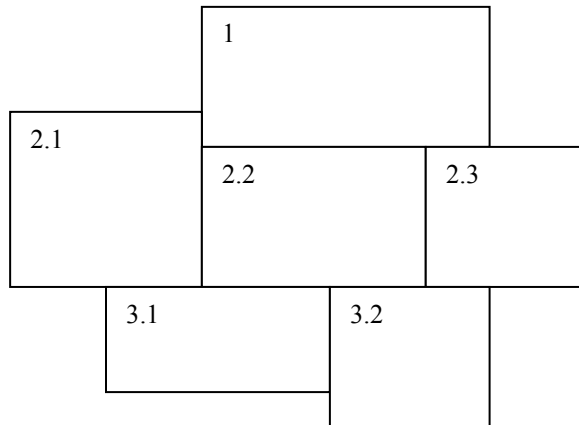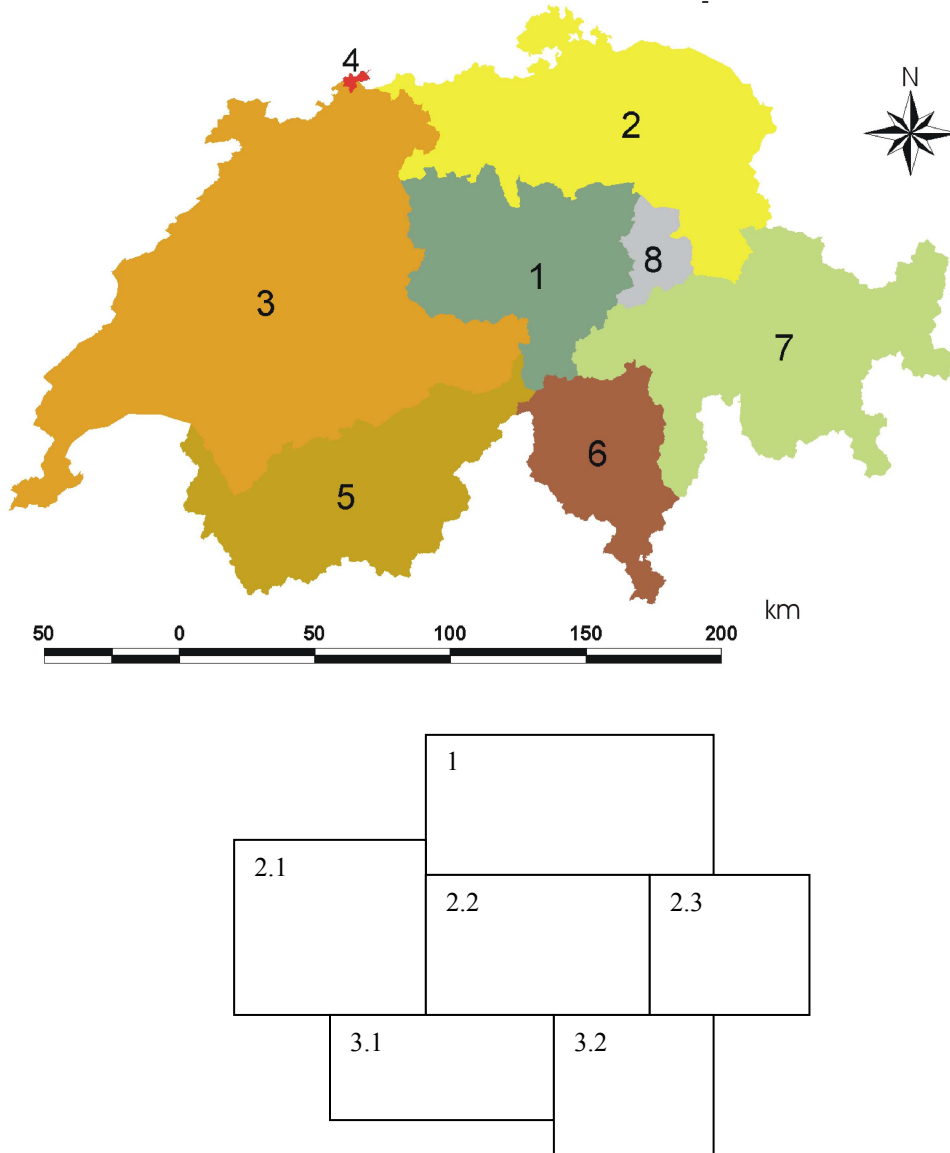
Fig. 12:   Regions in Switzerland for consideration of historical catalogue completeness

The lower part refers to the columns in Table 3.

Because the historical data are in intensities, we have to consider the conversion from intensity to magnitude, also. Figure 13 shows different previous relationships, and the equivalence used in the PEGASOS catalogue (MECOS Macroseismic Earthquake Catalogue of Switzerland). For most data intermediate values were used. So for Switzerland we have the intensity completeness thresholds shown in Table 3. For the zones outside Switzerland the values used in the DACH study (Grünthal et al. 1998) were taken, as shown in Table 4.
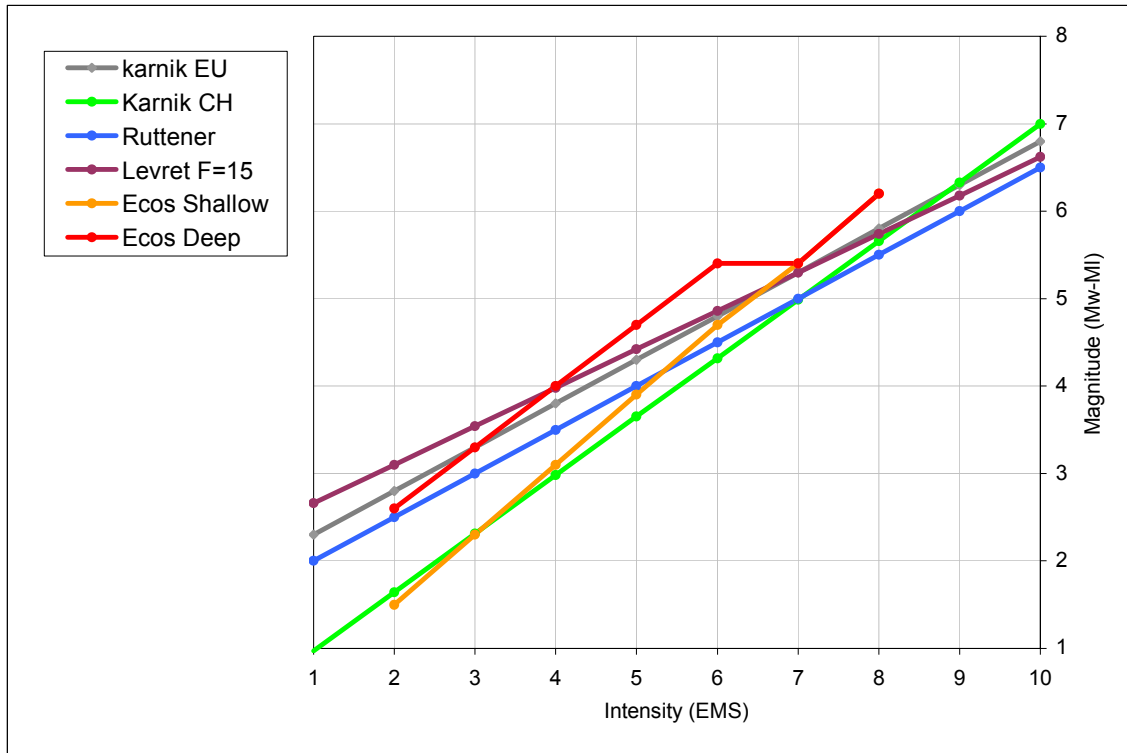
Fig. 13:   Comparative intensity-magnitude relationships

From Karník (1969, 1971), Rüttener (1995), Levret et al. (1994) and ECOS (PEGASOS 2002).

Tab. 3:   Completeness assumptions for Switzerland, by region (see Figure 12)

Mag All cat.	Eq. Int.	All CH	1.1	2.1	2.2	2.3	3.1	3.2
6	7-8	1600	1300	1600	1600	1600	1600	1600
5.5	7	1750	1300	1680	1680	1680	1750	1750
5	6	1850	1680	1750	1750	1750	1850	1850
4.5	5-6	1878	1800	1878	1878	1878	1878	1878
4	4-5	1878	1878	1878	1878	1878	1878	1878
3	3-4	1976	1964	1964	1964	1964	1964	1964
2.5	2-3	1980	1976	1976	1976	1976	1986	1986

This gives a start to deriving historical values, but it can also be considered that large earthquakes without a high Io value (for example, with an epicentre in a mountainous area) may perhaps still be identified because of the widespread effects.

To facilitate the analysis with respect to individual source zones, these were grouped into seven gross regions that were considered to be similar from the perspective of historical transmission of data (Figure 14). Analysis proceeded on the basis of each of these grouped zones, and completeness for each individual zone was then derived from its parent group.

Tab. 4:   Catalogue completeness (in terms of epicentral intensity) for regions outside Switzerland

Io	Austria SZ06	CH SZ01-04	Northern Italy SZ07	Germany Rhein SZ01	Germany other SZ06 / SZ01
10		1100			
9	1200	1300	1200	1250	
8	1550	1300	1200	1250	1625
7	1670	1575	1600	1500	1750
6	1850	1650	1750	1775	1875
5	1900	1875	1875	1825	1875
4	1900	1875	1875	1875	1925
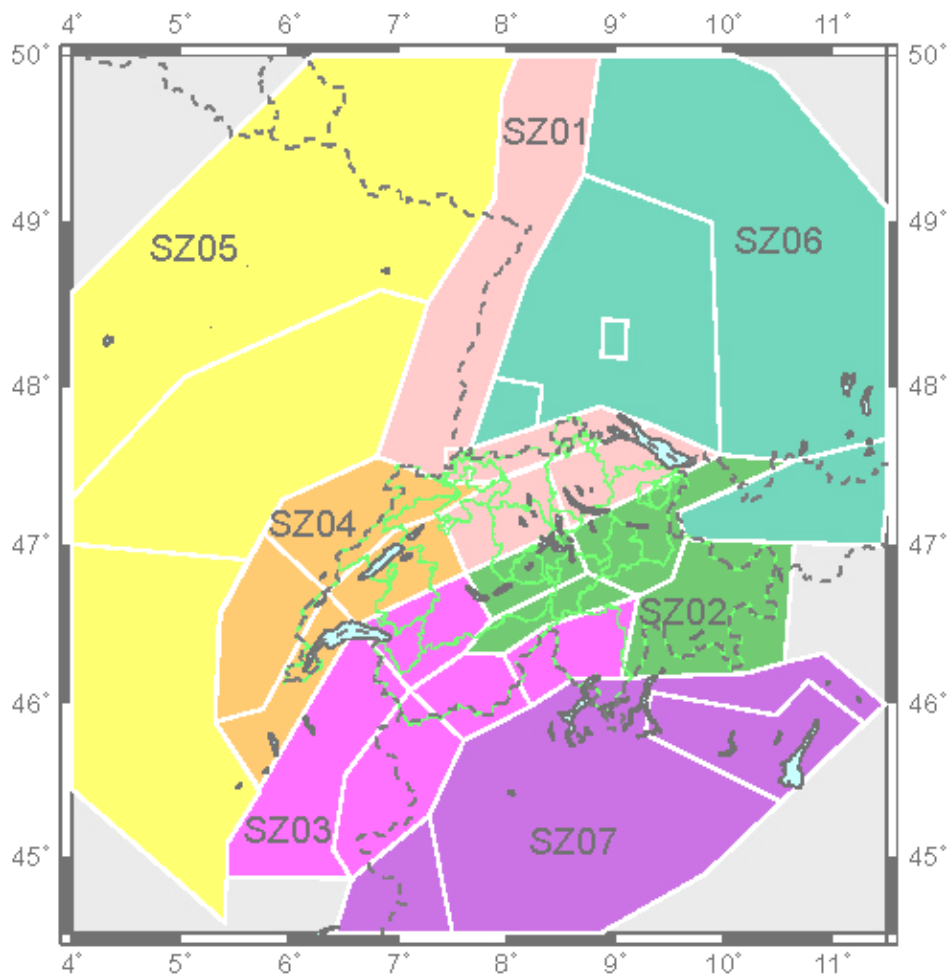
Fig. 14:   Groupings of zones used for final completeness analysis

5.2   Statistical evaluation

A number of statistical tests of earthquake catalogue completeness have been proposed (e.g. Musson 2000) but all of them are essentially variants of that introduced by Stepp (1972). The principle is that of plotting in some way the rate at which earthquakes occur over time. The average rate for a historical period for which the catalogue is incomplete will be less than for a period where the catalogue is complete. By identifying a rate change in the plot, typically some break in slope, one can detect roughly the limit of the complete part of the catalogue.

The completeness of the catalogue was studied using cumulative and non-cumulative plots for different magnitude threshold function of time, for the different grouped zones SZ01-07 as well as for individual sources. Two examples are shown: the zone ZURI and the grouped zone SZ003, which covers the western alpine area (Figure 15).
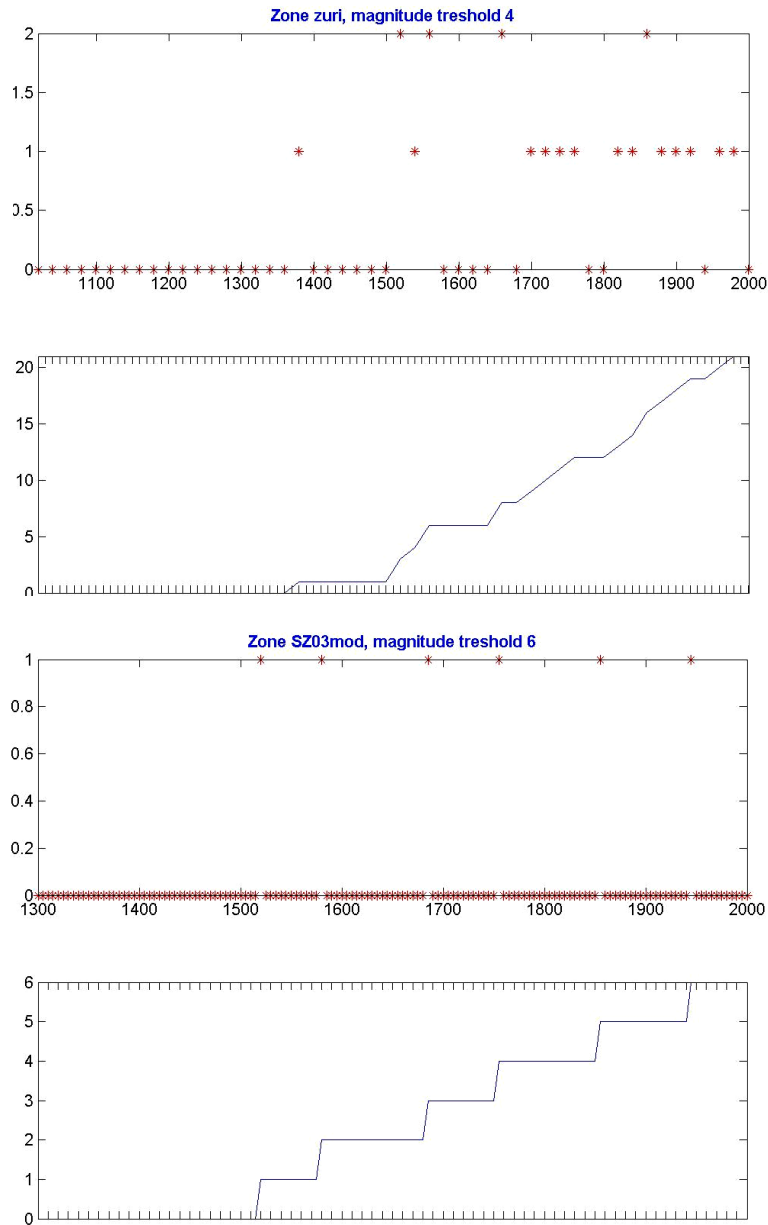
Fig. 15:   Sample completeness analysis graphs

5.3   Synthesis

Each member of the team made his or her own statistical evaluation of the completeness using whichever tool seemed most appropriate. The results were compared and interpreted in light of judgement about the historical data. In this way a single set of final completeness estimates was arrived at by a process of consensus. These are shown in Table 5.

Tab. 5:   Final assumptions as to earthquake catalogue completeness, by groups of source zones (see Figure 14)

Zone	SZ01	SZ02	SZ03	SZ04	SZ05	SZ06	SZ07
Mw	2000	2000	2000	2000	2000	2000	2000
3	1960	1976	1976	1976	1960	1976	1960
3.5	1920	1920	1940	1920	1920	1960	1960
4.0	1700	1750	1820	1810	1800	1870	1800
4.5	1650	1700	1750	1800	1550	1850	1750
5.0	1550	1700	1750	1750	1500	1650	1750
5.5	1350	1600	1670	1550	1500	1650	1750
6.0	1200	1270	1500	1500	1200	1200	1200
7.0	1100	1200	1200	1200	1100	1100	1100

Comparing the completeness estimation from statistical analysis of the catalogue with the completeness figures derived from historical information shows that the second method tends to be more pessimistic (shorter for the same range of magnitude); for example in the Wallis. This may be due to the high seismic activity of the area, or may simply show that sources are better than might be expected. This is an area that might repay further attention at some future time as a general subject of methodological interest (Musson 2002).

The completeness deduced from the statistical analysis of the catalogue may also be subject to fluctuation in seismic activity in some cases. This can lead to the contrary effect, of the historical judgement showing better completeness than shown by statistical analysis. The grouped zone SZ01, for example, is such a case. In such cases we preferred to choose the historical completeness values.

6   MAXIMUM MAGNITUDE ESTIMATION

Maximum magnitude is a necessary concept in seismic hazard analysis. The Gutenberg-Richter magnitude frequency curve cannot be extended indefinitely. There is not an infinitely small probability of an infinitely large earthquake. Therefore it is necessary to derive figures for a maximum possible magnitude (M_{max}) for each zone. It can be considered that there are particular geological or geophysical conditions and circumstances that prevent any earthquake in that zone to become larger than magnitude M_{max}. The reasons for this may be that:

− No structural lines/lineaments/fault lines/fracture zones/zones of weakness exist, which are longer than that to be associated with magnitude M_{max} ("no potential fault exists which could "host" earthquakes larger than M_{max}").

− Deformation rates are low to such an extent that the time for accumulating the total dislocation for an event larger than magnitude M_{max} is larger than the time, during which this amount of deformation can be sustained in the rock without being degraded by relaxation ("strain relaxation limit").

Data from regions with similar geological or seismological features may suggest from experience that a value M_{max} can be assigned which, in experience is never exceeded, and that such a value can be adopted in the region of interest as well.

There are a variety of methods available for deriving M_{max}, including a number of statistical analyses that can be applied to earthquake catalogues.

The distribution of historical observed values for M_{max} are shown in Figure 16, colour coded by zone. Note that a slight modification has been made to the epicentre of the 1295 earthquake, as discussed in section 9.0 below.

6.1   A Logic Tree for M_{max}

We approach this problem in several different ways, to cover the uncertainty as to the best approach to use (in addition to the uncertainty distribution that different methods produce), or, to put it another way, to cover the different conceptual approaches to M_{max} distribution. The logic tree we use combines methods for estimating M_{max} with methods for assessing seismicity rates; each branch contains one M_{max} technique and one seismicity rate/b value technique. These latter will be discussed more in a later section (9.2).

6.1.1   Global Approach

The first approach is to assess maximum possible magnitude M_{max} in a very general way. One can show a number of cases worldwide (especially in an intraplate environment) where approaches to estimating magnitude M_{max} have failed (or would have failed), because recent earthquakes have occurred with magnitude larger than what might have been previously assumed using geological or seismological indicators. To choose an example at random, a study by Al-Tarazi (1999) estimated a single maximum magnitude value for the Gulf of Aqaba of 5.7 ML, based on statistical analysis of an earthquake catalogue closing in 1993. In 1995 an earthquake of magnitude 7.2 Ms occurred in this locality.

We therefore start the logic tree with a branch for a set of "global" values for magnitude M_{max} being 6.5 Mw (weighted 0.2), 7.0 Mw (weighted 0.6) and 7.5 Mw (weighted 0.2). These values apply to all zones equally. So in this global branch it is believed that M_{max} is most likely 7.0 Mw anywhere in the region without taking into account the local features, and with a smaller

probability even as high as 7.5 Mw. Hence even a scenario such as that of the New Madrid earthquake in 1811, however unlikely in Switzerland, would be covered in this branch (taking into account latest revaluations of the New Madrid earthquakes, e.g. Hough et al. 2000; we do not believe these earthquakes were as large as magnitude 8 as many sources suggest).

The presence of this branch in the logic tree is intended to cover, even if only at low probabilities, the pessimistic possibility of an anomalously large event on some unknown feature that might strike anywhere.

It will be noted that one part of this branch supposes that *nowhere* in the study area will any earthquake exceed 6.5 Mw, which may seem strange when the PEGASOS catalogue includes an earthquake larger than this. We are taking into consideration the fact that the magnitude values of medieval earthquakes are inherently uncertain, and that the largest historical Swiss earthquake may perhaps not have been larger than 6.5 Mw whatever the "best-estimate" value in the catalogue is.

This approach to M_{max} is combined with a penalised maximum likelihood approach to seismicity parameters.
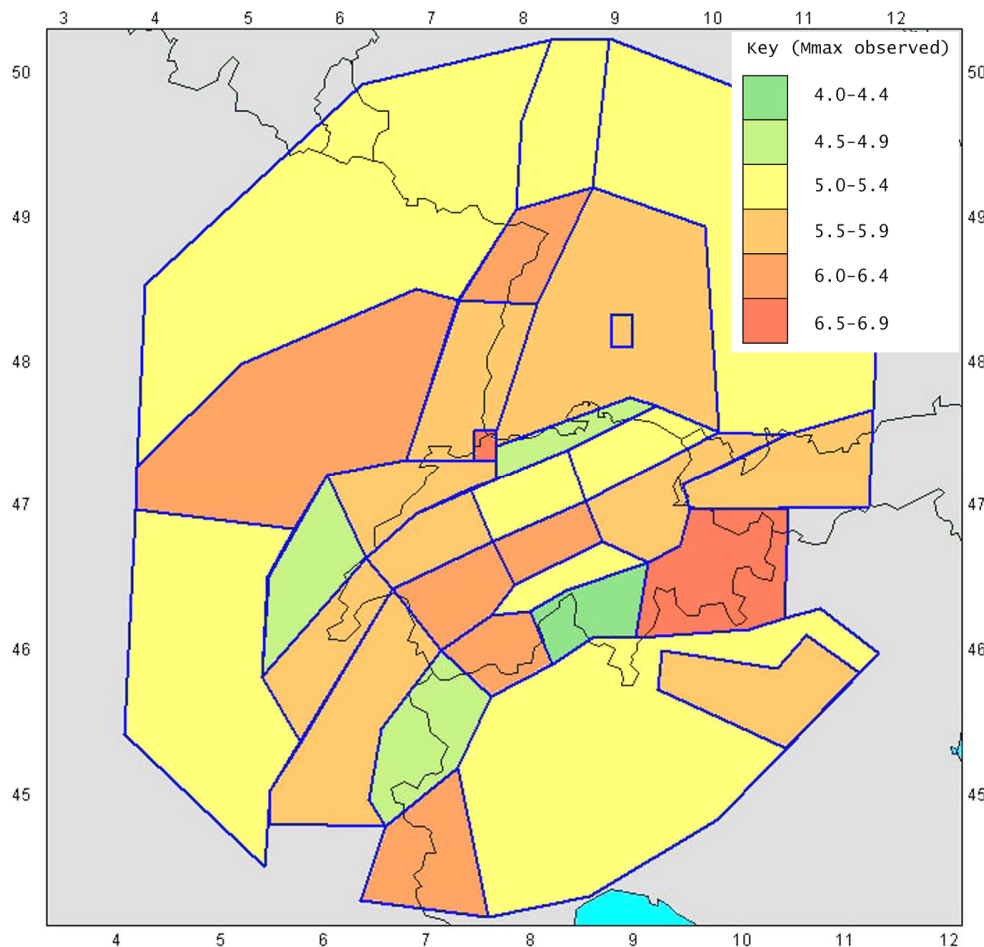
Fig. 16:   Distribution of historical observed M_{max} values by zone

         The 1295 earthquake (6.5 Mw) is considered to belong to zone GRAU, although the PEGASOS epicentre places it just inside zone GLAR.

6.1.2 Maximum likelihood approach

The two other branches of the logic tree present source-specific approaches to maximum possible magnitude; M_{max} is estimated in each source zone individually. Some general limits are set both in this branch and the next one. For each zone, M_{max} is never allowed to be less than 5.5 Mw or the largest historical earthquake in the zone (rounded up to the nearest half-magnitude), whichever is the larger. Also M_{max} is never allowed to be more than 7¼ Mw (it is regrettable to write this as 7.25; the decimal system has disadvantages when the inherent inaccuracy of data makes working in quarter-units necessary). This limit is based on a combination of a slight increase on the largest observed historical event, general judgement on maximum observed earthquakes in corresponding areas, and a lack of significant structures that would be reasonable to expect very large earthquakes to occur on. The slight *increase* on this limit in the first branch is specifically designed to provide an extra margin of conservatism to cover the small possibility of a larger earthquake in extreme circumstances (e.g. analogous to New Madrid 1811), and the fact that the largest possible events in the model only appear in one branch is a deliberate ploy to ensure that the overall weight assigned to these is low.

Within these limits, in this branch of the logic tree M_{max} is calculated using a simple maximum likelihood approach with no prior, taking into account the historical completeness values for the zone. This provides the distribution and weights.

Other studies that have used a maximum likelihood approach (e.g. Wahlström and Grünthal 2001) have usually restricted the results by using a prior derived from observations from similar crustal types. We prefer not to follow these examples; we prefer to rely entirely on the local data and accept the degree of uncertainty in the results that this decision entails. The imposition of an upper bound keeps the distribution of results within desired limits and preserves the desired shape.

In this branch, in which this approach to M_{max} is followed, seismicity parameters are estimated by the maximum likelihood method, but with strong priors for each zone (to be discussed later).

6.1.3 Joint determination approach

The final branch provides a joint determination of M_{max}, activity rate and *b* value. It will be explained in more detail in the discussion of seismicity parameters. The method relies on selecting possible seismicity parameters for a zone at random and attempting to generate synthetic earthquake catalogues (subject to the same historical completeness constraints) that match the real earthquake catalogue within an acceptable tolerance level. Values that give successful matches are noted, and the logic tree is ultimately compiled from this distribution.

In the case of M_{max}, a simplified explanation can be given. Suppose that activity rate and *b* value are known. Choose a value for M_{max} at random, generate a synthetic catalogue subject to historical constraints, and check whether an earthquake occurred larger than the maximum historical observed earthquake. If the historical maximum was not exceeded, note the M_{max} value. Proceed until 5,000 successes have been recorded. The distribution of M_{max} values for the logic tree is constructed from the distribution of 5,000 successful values.

Conceptually, this method is similar to the maximum likelihood approach with a flat prior (the same as no prior). It has the advantage that it estimates the seismicity parameters at the same time. Both our zone-specific approaches to maximum magnitude attempt to answer the same question, "Given the historical catalogue and the constraints upon it, what is the likelihood that events that are *x* magnitude units larger than the observed magnitude are possible, yet never happened in historical times?" One approach seeks to address this analytically, the other approach experimentally.

7   DEPTH DISTRIBUTION

Depth distribution can be a strong influence on seismic hazard estimates, especially in intraplate areas where the hazard is principally due to relatively small events that are unlikely to rupture all the way to the surface. In the case of this project, the issue is complicated by doubts held by the team as to the reliability of the hypocentral depth determination of individual events contained in the PEGASOS catalogue, and also about the significance of the depth errors specified.

Some broad conclusions about overall depth distribution can certainly be made. Figure 18 shows the depth distribution for well-located earthquakes from 1975 to 1999, overlapping Moho depth data from Waldhauser et al. (1998). The general trend is a shallower depth underneath the Alps. In this time period the earthquakes recorded are in the range of 2 to 4.5 Mw. The question arises if we can extrapolate this behaviour to larger earthquakes.

Considering that the few larger earthquakes that happened in the instrumental time in the Alps were rather shallow, we decided to have a broad distribution using the recent depth distribution as trends.

The depth distribution of hypocentres is defined by a trapezoidal distribution with the parameters listed in Table 6. Listed are the minimum and maximum depths and the upper and lower depths for the plateau in the trapezoidal distribution. Figure 17 shows a sample distribution.
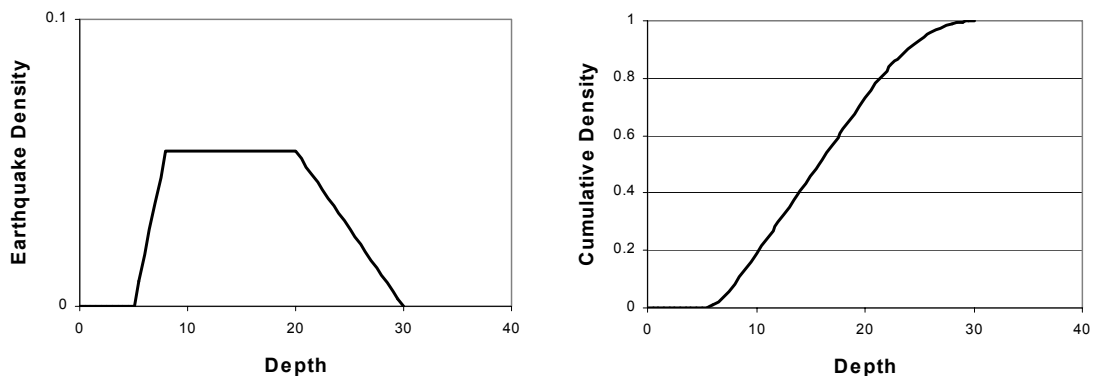
Fig. 17:   Example depth distribution with a minimum depth of 5, upper plateau depth of 8, lower plateau depth of 20, and a maximum depth of 30

Tab. 6:   Depth distributions used, by tectonic region

The zones BAWS and BW2S are not included, but are the same as BAWU and
BAW2 resp.

Tectonic Units	Group		Code	Prox.	Depth	Depth	min	plat. min	plat. max	max
								Depth distribution		
Basel	1	SZ01	BASL	Adj.	30	12	5	8	20	30
Rhine Graben	1	SZ01	RHEG	Adj.	30	12	5	8	20	30
Rhine Graben	1	SZ01	RHGC	Adj.	30	12	5	8	20	30
Rhine Graben	1	SZ01	RHGN	Adj.	30	12	5	8	20	30
Rhine Graben	1	SZ01	RHGS	Adj.	19	12	5	8	20	30
Graben Inv.	2	SZ01	NSPG	Adj.	24	9	3	8	20	30
SW Germany crustal str.	3	SZ06	BAVA	Adj.	30	9	5	8	15	30
SW Germany crustal str.	3	SZ06	BAWU	Adj.	30	9	5	8	15	30
SW Germany crustal str.	3	SZ06	BAW2	Adj.	30	9	5	8	15	30
SW Germany crustal str.	3	SZ06	SWAB	Far	30	9	5	8	15	30
SW Germany crustal str.	3	SZ08	BLAF	Adj.	24	15	5	8	15	30
Molasse	4	SZ01	MOMI	Adj.	30	12	5	8	20	30
Molasse	4	SZ01	ZURI	Adj.	30	15	5	8	25	30
Molasse	4	SZ01	ZUR2	Adj.	30	15	5	8	25	30
Molasse	4	SZ04	FRIB	Adj.	30	12	5	8	20	30
Molasse	4	SZ04	GENV	Far	30	9	5	8	20	30
Jura	5	SZ04	JUR	Adj.	6	6	5	8	15	20
Jura	5	SZ04	SJUR	Far	6	6	5	8	15	20
Helvetic	6	SZ02	ALCM	Far	10	6	3	6	12	20
Helvetic	6	SZ02	GLAR	Adj.	10	6	3	6	12	20
Helvetic	6	SZ02	NIDW	Adj.	10	6	3	6	12	20
Helvetic	6	SZ03	HELV	Adj.	7	6	3	6	12	20
Helvetic	6	SZ03	SAVO	Far	10	6	3	6	12	20
Penninic	7	SZ03	DAUP	Far	10	6	3	6	12	20
Penninic	7	SZ03	PENV	Far	10	6	3	6	12	20
Penninic	7	SZ03	TICI	Far	10	6	5	6	12	20
Eastern Alps	8	SZ02	GRAU	Far	6	6	3	6	12	20
Eastern Alps	8	SZ06	TYRO	Far	30	9	5	8	15	30
French. Transp. Structure	9	SZ05	BRES	Far	23	9	5	8	15	25
French. Transp. Structure	9	SZ05	LORA	Far	23	9	5	8	15	25
French. Transp. Structure	9	SZ05	SBRE	Far	23	9	5	8	15	25
South. Background zones	10	SZ07	ALMA	Adj.	64	9	5	8	15	50
South. Background zones	10	SZ07	GARD	Far	64	9	5	8	15	50
South. Background zones	10	SZ07	POVA	Far	64	9	5	8	15	50

Reproduziert mit Bewilligung des Bundesamtes für Landestopographie (BA002935)
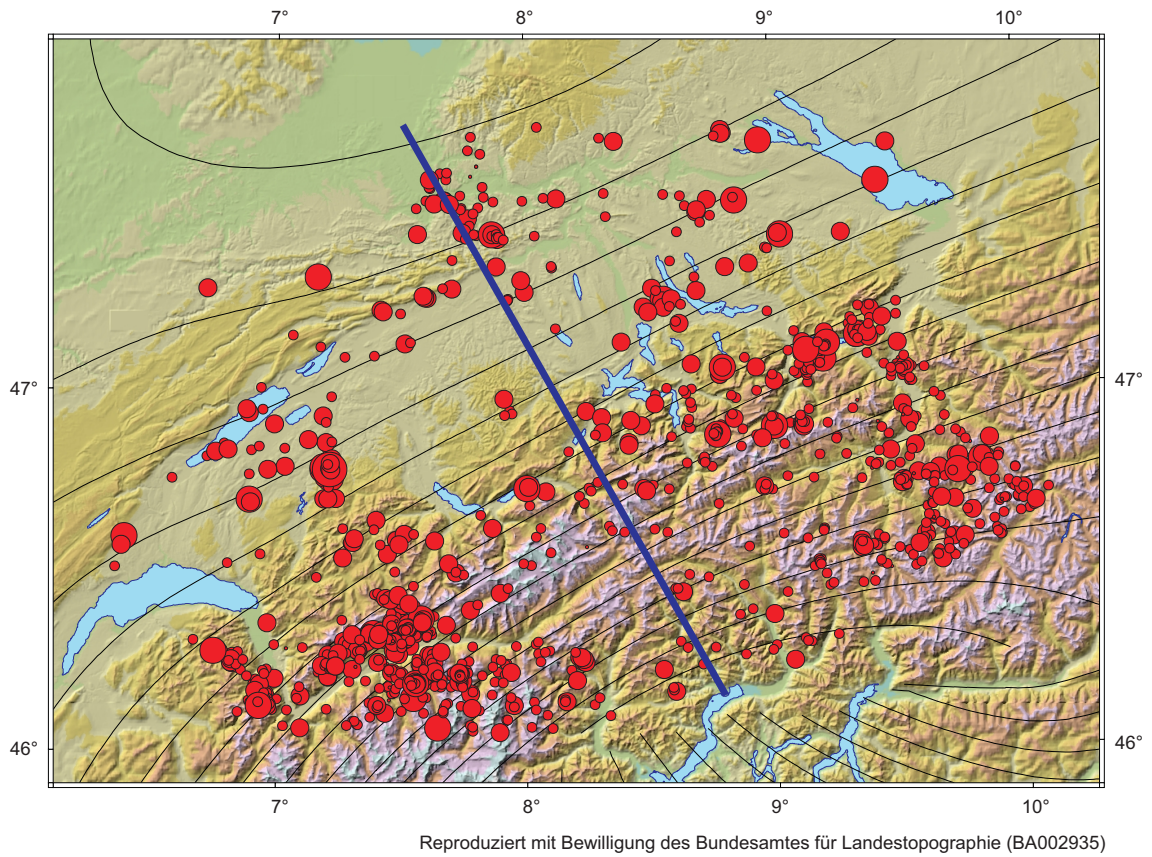
Magnitude

- 1.1 - 2.1
- 2.1 - 3.2
- 3.2 - 4.2
- 4.2 - 5.2

Moho
Äquidistanz: 2000 m

0   50 km
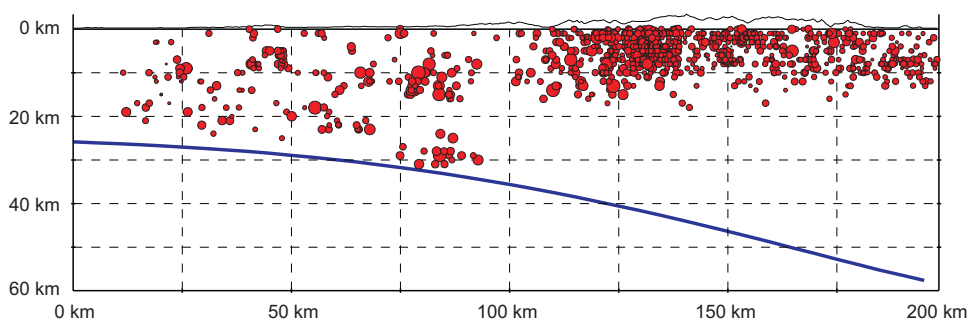
Fig. 18:   Depth profile across the seismicity of Switzerland

8   EARTHQUAKE RUPTURE GEOMETRY

Although the model presented here does not explicitly involve individual faults, the fault rupture properties are considered in the notional faults within any source zone that could be considered responsible for earthquakes that affect the hazard.

8.1   Rupture dimensions

We consider the size of such earthquake fault areas (noted as ruptures) to be defined according to the modified relationship from Wells and Coppersmith (1994):

$$\log_{10}(\text{rupture area in km}) = -4.31 + 1.04\ Mw \tag{8.1}$$

with $\sigma_{\log 10(\text{rupture area})} = 0.24$

The aspect ratio specifies the quotient of rupture length (assumed to be horizontally oriented) and rupture width. The aspect ratio in our model is considered to be 1.0, in the lack of any evidence to suggest the contrary. Ruptures are confined to the maximum allowed depth for the source zone, to be read from Table 6. Ruptures are considered to be uniformly distributed in the source (except for the distributed Basel source BASL) where a spatial density grid is provided.

If the rupture length exceeds the maximum source dimension in the direction of rupture, it may extend out of the source as long as it meets the restrictions indicated in Table 7. This is based on consideration of gross structural units. Thus, faulting initiating in LORA, BRES or SBRES may propagate into another of those three zones, but not out of the group. Although not explicitly stated in Table 7, the reverse restriction applies. Thus no fault initiating outside the LORA-BRES-SBRE group is allowed to cross into one of those three zones. This is demonstrated in Figure 19. Fault ruptures are not permitted to cross the heavy red lines. In practice, the same effect can be achieved, from the point of view of the sites of concern in this study, by making the boundaries of sources LORA, BRES, SBRE, RHEG, RHGS, BAVA and POVA impermeable to rupture propagation.

The one "wild card" is the BASL source. Ruptures from events associated with this source can extend anywhere, even across the red lines in Figure 19. This is intended to reflect the deep uncertainty about the mechanism of the large 1356 earthquake.

If the rupture area exceeds the depth interval between the earth's surface and the maximum depth specified for the respective zone (Table 6) then aspect ratio is lowered such that the rupture area fits into the depth range specified. Hence ruptures can reach the surface but cannot extent beyond the maximum depth specified in Table 6.

For the purpose of calculating hypocentres, we adopt the magnitude-dependent depth distribution using the weighted approach outlined in the PEGASOS Technical Note TP1-TN-0373 (Gabriel Toro, May 19, 2003) with T = 0.5 (hypocentre in lower half of rupture).

8.2   Fault style for large earthquakes

Table 7 also gives, for each zone, the probability that any large earthquake (> 5.5 Mw) is strike slip or reverse in fault type. The default, which is mostly applied, is that fault style is randomly determined (in other words, we have no strong opinion what sort of faulting is likely for large earthquakes in this zone).
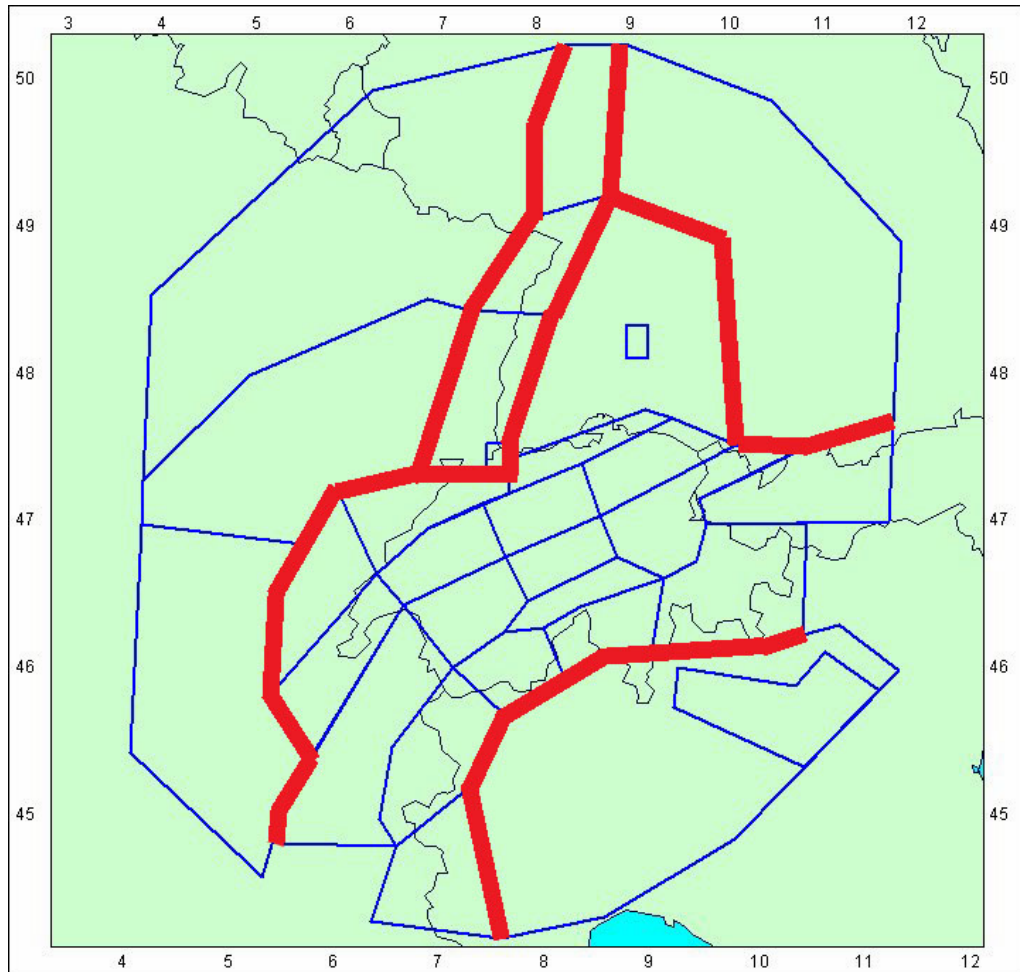
Fig. 19:   Restrictions on propagation of fault rupture

The red lines may not be crossed, except in the case of events originating from the BASL source

Well-determined data on contemporary earthquake mechanisms do not extent beyond earthquakes of 5.5 Mw. We consider, therefore, that the existing fault plane solution data do not carry enough information to infer fault type and orientation for larger events.

Hence for large earthquakes another approach is taken, based on inferring fault type and orientation according to regional tectonic and stress orientations. We took the most prominent structural lines present in the PEGASOS structural data base (all kinds of tectonic features, faults, lineaments, etc.) that are long enough to accommodate an earthquake of magnitude 6.5 to 7.5 Mw, then took the stress inversion data (combined PEGASOS stress data) and constructed the most likely fault type on it. This approach is the basis for Table 7.

Two specific styles of faulting are considered, strike-slip and reverse. Because of the overall stress field present today, which is roughly NW-SE horizontal compression, normal faulting is not considered here. The third condition specified in Table 7 is the specified fraction of earthquakes that are to be considered to have random orientation (uniform distribution for azimuth) and random style of faulting (equally likely to be strike-slip or reverse faulting). Table 7 also indicates those sources where ruptures are allowed to cross the source boundary if they exceed the source dimensions and which boundaries, as already discussed.

Tab. 7:   Rupture Orientation, style of faulting, and source boundary conditions

*First number is the relative frequency and second number is the rupture orientation. Note that strike-slip earthquakes have a dip of 90 degrees and reverse earthquakes have a dip of 45 degrees to the south, southeast, or east, depending on the strike.

Source	Strike Slip*	Reverse*	Random	Ruptures can cross Source Boundary
BASL	0.4, N20E	0.4, N75E	0.2	Yes
RHEG	1.0, N20E	0	0	No
RHGN	1.0, N20E	0	0	Only into RHGC
RHGC	1.0, N20E	0	0	Only into RHGN or RHGS
RHGS	1.0, N20E	0	0	Only into RHGC
LORA	0	0	1.0	Only into BRES
BRES	0	0	1.0	Only into LORA or SBRE
SBRE	0	0	1.0	Only into BRES
BAVA	0	0	1.0	No
SWAB	1.0, N10E	0	0	Yes
BAWU, BAW2, BAWS & BW2S	0	0	1.0	Not into RHEG or BAVA
BLAF	0	0	1.0	Not into RHEG or BAVA
NSPG	0	0.6, N75E	0.4	Yes
ZURI	0.1, N20E	0.4, N75E	0.5	Yes
ZUR2	0.1, N20E	0.4, N75E	0.5	Yes
MOMI	0.1, N20E	0.4, N60E	0.5	Yes
FRIB	0.1, N00E	0.4, N50E	0.5	Yes
JURA	0.1, N00E	0.4, N50E	0.5	Yes
SJUR	0.1, N10W	0.4, N40E	0.5	Yes
GENV	0.1, N10W	0.4, N40E	0.5	Yes
GLAR	0.1, N00E	0.6, N60E	0.3	Yes
NIDW	0	0.7, N60E	0.3	Yes
HELV	0	0.7, N50E	0.3	Yes
SAVO	0	0.7, N10E	0.3	Yes
GRAU	0	0	1.0	Yes
TICI	0	0	1.0	Yes
PENV	0	0	1.0	Yes

Source	Strike Slip*	Reverse*	Random	Ruptures can cross Source Boundary
DAUP	0	0	1.0	Yes
ALMA	0	0	1.0	Yes
ALCM	0	0	1.0	Yes
TYRO	0	0	1.0	Yes
GARD	0	0	1.0	Only into POVA
POVA	0	0	1.0	Only into GARD

8.3 Fault style for small earthquakes

For smaller magnitude earthquakes after about 1970, data from Kastrup (2002) can be used to estimate preferred type of faulting and preferred fault orientations with respect to the source zones. These findings are only assessed in an approximate way and are summarised in Table 8.

An overall distribution of strike-slip to normal-fault to thrust-fault components is given as "ss , nf , rf" with their respective weights. This is, of course, not the relation between pure strike-slip, normal-fault and thrust-fault types, but just percentages of respective ss, nf, and rf components taken from all events.

Table 8 further distinguishes between strike-slip, normal-fault and thrust-fault types "SS, NF, RF", which are called *predominant types* on one hand and *mixed types* "MU" on the other hand. The MU types are determined as those events with P or T axes having plunge angles very roughly between 30 and 60 deg. The reason is that only from the predominant types can fault orientations be inferred directly. The MU types are assumed to have strongly varying fault orientations, which are left undetermined and hence unrecognised.

Then from the predominant types, fault orientations are obtained (horizontal strike directions measured in degrees from N to E). These are named SS1-O_deg, with weight SS1-O for strike slip orientation, SS2-O_deg with weight SS2-O for alternative direction of strike slip, NF-O_deg with weight NF-O for normal fault orientation, and RF-O_deg with weight RF-O for reverse fault orientation. The rest are unspecified, and hence randomly oriented, with weight MU-O. Fault dip angles are assumed to be 90 deg (vertical) for SS, and 45 deg for NF and RF types (with dip towards S, SE and E depending upon strike), and again unspecified dip for MU.

By and large, we consider that fault style for smaller earthquakes is not critical for hazard, and that the procedure outlined in Section 8.2 can be used for all events. The effect of using Table 8 for smaller events would make a good sensitivity study.

Tab. 8:   Style of faulting and orientation to be used for smaller events (based on well determined events)

These values are to be used for events smaller than 5.5 Mw only. BAW2, BAWS and BW2S are as BAWU.

	ss	nf	rf	SS	SS1-O deg	SS1-O	SS2-O deg	SS2-O	NF	NF-O deg	NF-O	RF	RF-O deg	RF-O	MU	MU-O
LORA BRES SBRE															1	
RHEG RHG*	0.5	0.3	0.2	0.3	5	0.15	95	0.15	0.2	140	0.2	0.1	50	0.1	0.4	0.4
BAWU BLAF	0.5	0.3	0.2	0.3	5	0.15	95	0.15	0.2	140	0.2	0.1	50	0.1	0.4	0.4
BASL	0.5	0.3	0.2	0.3	5	0.15	95	0.15	0.2	140	0.2	0.1	50	0.1	0.4	0.4
NSPG	0.5	0.35	0.15	0.5	30	0.25	120	0.25	0.2	165	0.2	0			0.3	0.3
ZURI ZUR2	0.5	0.35	0.15	0.5	30	0.25	120	0.25	0.2	165	0.2	0			0.3	0.3
MOMI	0.6	0.3	0.1	0.6	15	0.3	105	0.3	0.1	150	0.1	0			0.3	0.3
FRIB	0.8	0.1	0.1	0.9	5	0.45	95	0.45	0			0			0.1	0.1
JUR	0.8	0.1	0.1													
GENV	0.7	0.1	0.2	0.8	340	0.4	70	0.4	0			0			0.2	0.2
SJUR	0.7	0.1	0.2													
GLAR	0.5	0.2	0.3	0.4	0	0.2	90	0.2	0.1	135	0.1	0.2	45	0.2	0.3	0.3
NIDW	0.5	0.2	0.3	0.4	0	0.2	90	0.2	0.1	135	0.1	0.2	45	0.2	0.3	0.3
HELV	0.6	0.25	0.15	0.7	350	0.35	80	0.35	0			0			0.3	0.3
SAVO																
GRAU	0.2	0.7	0.1	0.3	345	0.15	75	0.15	0.4	120	0.4	0			0.3	0.3
TICI																
PENV	0.3	0.6	0.1	0.2	320	0.1	50	0.1	0.5	95	0.5	0			0.3	0.3
DAUP																
ALMA																
SWAB	0.8	0.1	0.1	1	10	1			0			0			0	

9   EARTHQUAKE RECURRENCE PARAMETERS

Some discussion of this was initiated in the section on maximum magnitude. The logic tree for earthquake recurrence estimation is linked with that for maximum magnitude. It is shown in Figure 20. Three approaches are used, resulting in three sets of parameter distributions. *Note:* For all the analyses presented here, one small alteration was made in the earthquake catalogue. The earthquake of 4 September 1295 occurs on the border between zones GLAR and GRAU. It is technically within GLAR, but on account of its early date, the epicentre is very poorly determined. We consider it more likely to have occurred within zone GRAU and have moved it into that zone.

9.1   Seismicity model

For all zones we use a truncated linear Gutenberg-Richter model. Truncation is applied as a sharp cut-off. Examination of seismicity data did not suggest that there was evidence for seismicity in any zone not to follow this model.

Furthermore, the simulation method (Section 9.2.3 below) provides an inherent test of the applicability of the Gutenberg-Richter model. In cases where this model is not valid, it will simply not be possible (or only possible with extreme difficulty) to create a synthetic earthquake catalogue matching the historical catalogue using a linear model. The fact that synthetic catalogues *can* be generated, using a linear model, that match the historical distribution shows that the assumption of a linear model is a valid hypothesis.

Because of the world-wide experience with this model, we regard it to be the case that it is best to assume that the linear case is appropriate unless there is evidence to the contrary, which, in this model, there is not.

9.2   Seismicity parameters

The logic tree is summarised in Figure 20 and also presented in tabular form as Table 9. There are three main branches.
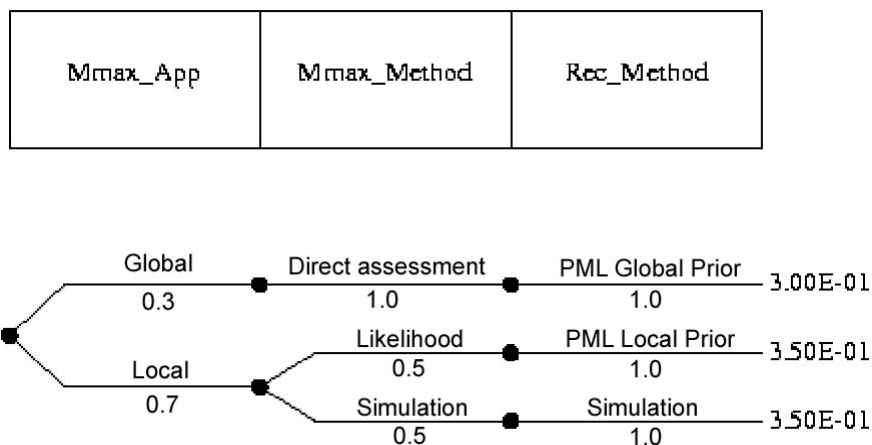

Fig. 20:   EG1c maximum magnitude and earthquake recurrence parameter logic tree

              PML = penalised maximum likelihood.

Tab. 9:   Logic tree for maximum magnitude and seismicity parameter estimation (see also
               Figure 20)

Branch	M_{max} approach	M_{max}	M_{max} method	Recurrence method	Weight
A	Global Distribution	M6.5	Direct assessment	Likelihood distribution	0.06
A	Global Distribution	M7.0	Direct assessment	Likelihood distribution	0.18
A	Global Distribution	M7.5	Direct assessment	Likelihood distribution	0.06
B	Local Distribution	from M5.5 or M_{max}-observed to 7.25	Likelihood function	Likelihood distribution	0.35
C	Local Distribution	from M5.5 or M_{max}-observed to 7.25	Joint simulation	Joint simulation	0.35

9.2.1   Penalised maximum likelihood

The first approach (Branch A in Table 9) consists of a directly assessed single distribution for maximum magnitude that is applied to all zones (see Section 6.1.1 above). The accompanying joint distributions for beta [b-value $\times \ln(10)$] and N (Mw ≥ 5) are determined using a maximum likelihood formulation for an exponential distribution and computing relative likelihood. The method used is essentially that of Veneziano & Van Dyck (1985). A prior of 0.9 (based on the global b value for the whole catalogue) was applied to all zones, with a weight of 50. The data analysed used the completeness figures from Table 5 for magnitudes 3.5 Mw and over.

This approach is presented as three sub-branches in Table 9, because, at least in principle, the resulting values are dependant on the M_{max} value chosen. In practice here, because the M_{max} values are all rather high compared to historical experience, there is no actual difference in the distributions computed for the different M_{max} values.

9.2.2   Least squares method

The second approach (Branch B) consists of individual source M_{max} distributions computed using a sample likelihood function as discussed in Section 6.1.2. The original intention was that the accompanying joint distributions for beta [b-value $\times \ln(10)$] and N (Mw ≥ 5) would be determined using a least-squares fit to the cumulative recurrence rates and computing relative probability distributions for the linear regression parameters. In practice, this method encountered problems.

The philosophy in designing branch A and B was as follows: it is generally considered that, from a mathematical point of view, estimating b values by maximum likelihood is more formally correct than using least squares. However, it is also frequently observed in practice (and was commented on at PEGASOS Workshop 4) that using maximum likelihood procedures often gives significantly lower b values than would be suggested from visual inspection, and there is some indication that the occurrence of large earthquakes is therefore overpredicted. By combining both procedures, a compromise could be reached that would be expressive of the uncertainties. However, the resulting joint distributions for beta and N proved unsatisfactory when obtained in this way.

As a compromise, the following solution was adopted. The distributions were computed using the same maximum likelihood as in Branch A, with this difference – instead of a moderate prior derived from the whole catalogue, strong (weight 100) local priors were used for each zone,

derived from the *b* value estimates that were obtained from the least squares analysis. The least squares analysis was undertaken earlier in the project using the program PLSREC11. The value for BASL (0.58) was not used as this is heavily influenced by the 1356 earthquake, the true return period of which is very poorly determined. A value of 0.77 was used as the prior for BASL (based on the rest of the seismicity in this zone).

Although it was expected that this branch would produce generally steeper *b* values than those in Branch A, this did not always happen in practice.

Tab. 10:   Least-squares recurrence parameters for the model

Source	mlb	mub	N(m ≥ 5)	sig_log[N]	b	sig_b
ALCM	3.0	5.0	0.1175E-02	0.356	-0.979	0.291
ALMA	4.0	6.0	0.1480E-01	0.274	-1.228	0.224
BASL	4.0	6.5	0.8643E-02	0.156	-0.578	0.103
BAVA	4.0	5.0	0.1138E-01	0.050	-0.707	0.077
BAW2	4.0	5.5	0.2367E-01	0.131	-0.922	0.140
BAWS	4.0	5.5	0.9236E-02	0.169	-0.766	0.181
BAWU	4.0	5.5	0.2428E-01	0.135	-0.950	0.144
BLAF	3.5	4.5	0.2696E-02	0.143	-0.914	0.222
BRES	4.0	6.0	0.3365E-02	0.250	-0.700	0.204
BW2S	4.0	5.5	0.8397E-02	0.144	-0.646	0.154
DAUP	3.5	4.5	0.3763E-02	0.181	-0.817	0.280
FRIB	4.0	5.5	0.1021E-01	0.192	-0.970	0.206
GARD	4.0	5.0	0.1685E-01	0.050	-1.013	0.078
GENV	4.0	5.5	0.9124E-02	0.046	-0.699	0.049
GLAR	4.0	6.5	0.9589E-02	0.227	-0.730	0.150
GRAU	4.0	5.0	0.1165E-01	0.148	-0.806	0.230
HELV	4.0	6.0	0.2510E-01	0.015	-0.489	0.012
JURA	4.0	5.5	0.5787E-02	0.181	-0.506	0.194
LORA	4.0	5.0	0.3977E-02	0.006	-0.664	0.009
MOMI	4.0	5.0	0.2591E-02	0.149	-0.705	0.231
NIDW	4.0	6.0	0.9209E-02	0.107	-0.683	0.087
NSPG	3.5	4.5	0.1451E-02	0.041	-1.154	0.063
PENV	4.0	6.0	0.2017E-01	0.016	-0.506	0.013
POVA	4.0	5.0	0.2670E-01	0.103	-1.091	0.160
RHEG	4.0	6.0	0.1441E-01	0.080	-0.991	0.065
RHGC	4.0	6.0	0.5682E-02	0.147	-0.811	0.120
RHGN	4.0	5.0	0.2587E-02	0.148	-1.180	0.229
RHGS	4.0	5.5	0.8065E-02	0.173	-0.781	0.185
SAVO	4.0	5.5	0.2501E-01	0.079	-0.745	0.085

Source	mlb	mub	N(m ≥ 5)	sig_log[N]	b	sig_b
SBRE	4.0	5.0	0.4242E-02	0.057	-1.001	0.088
SJUR	3.5	4.5	0.3109E-02	0.231	-0.619	0.357
SWAB	4.0	5.5	0.1461E-01	0.105	-1.057	0.112
TICI	3.0	4.0	0.6793E-03	0.384	-1.030	0.595
TYRO	4.0	5.5	0.1036E-01	0.090	-1.065	0.096
ZUR2	4.0	5.0	0.5345E-02	0.179	-1.000	0.278
ZURI	4.0	5.0	0.5260E-02	0.164	-0.811	0.253

9.2.3   Simulation method

The third approach (Branch C) consists of the results of a joint Monte Carlo simulation of $N(m \geq 5)$, b-value, and M_{max}. This was made by specifying a parameter search space for each zone (activity, b-value and M_{max}), choosing values at random within this space, generating a synthetic catalogue subject to the same historical completeness constraints, and comparing the result to the historical outcome. If the number of misfit events in the discrete (not cumulative) comparison of synthetic and historical catalogues exceeded a certain tolerance value, then that catalogue was rejected. The comparison was made by using bins at half a magnitude degree intervals, starting at a minimum magnitude value of 4.0 Mw. The permitted tolerance was 15 %, with the further modification that any synthetic catalogue with an event larger than the historical M_{max} was automatically rejected. So, for example, if the bin scores (number of events) for the historical catalogue were 8, 4, 1, 0, 1, the permitted margin of disagreement would be two events. A synthetic catalogue with bins of 7, 3, 1, 0, 1 would be considered a success, but 5, 4, 1, 0, 1, would be a failure. The process was continued until 5,000 successes were achieved, and the resulting 5,000 triplets of activity, b-value and M_{max} were themselves sorted into bins.

In some cases, the amount of data above magnitude 4.0 Mw was not enough for good estimates of parameters. If there were less than ten earthquakes for analysis, the lower magnitude threshold was reduced from 4.0 Mw to 3.0 Mw.

Activity rate was aggregated into ten bins spaced at intervals of 0.1 in Log N. The exact values for the activity rate search space were decided on a zone-by-zone basis with reference to simple regression results.

The b-values were aggregated at intervals of 0.1, from 0.7 to 1.1, except for the zone BASL, where the range was 0.5 to 0.9.

M_{max} was aggregated at intervals of a quarter of a magnitude degree, from the maximum observed value (or 5.5 Mw if the maximum observed is lower) up to 7¼ Mw. This has to be written as 7.25 Mw, but the use of two decimal places is not intended to indicate great accuracy, rather the reverse. The maximum observed value in each zone was considered to be uncertain, as historical magnitude values are not precise. This was studied by examining the magnitude history for each zone, as shown in Figure 21. In cases where the historical M_{max} was 5.5 or less, the lower bound for M_{max} was considered to be 5.5 with no uncertainty. For other cases, the lower bound was considered to be the historical M_{max} value ± 0.2 (normal distribution truncated at one standard deviation), except in cases where repeated events confirm the appropriateness of the given value, in which ± 0.1 was used (this only actually applied to zone GENV). In cases where the historical M_{max} event is a large earthquake occurring before 1750, the magnitude is considered to be very uncertain, and it is also considered that it is more likely that the magnitude reported is overestimated than underestimated. In such cases, uncertainty in the lower bound was modelled as a skewed normal distribution such that the true lower bound could be as

much as 0.5 magnitude units lower than the reported largest earthquake, but only 0.3 units larger. We considered the large earthquake of 250 AD so uncertain that it was discarded completely.

An advantage of this method is that it is entirely driven by the data, and results are based on what values are shown to be feasible parameters that could result in the historical outcome. Apart from the choice of the basic (linear) model, no assumptions are made about the shape of the distribution of uncertainties.

The analysis of each zone provides a set of logic-tree branches for M_{max}, b value and activity rate (i.e. one branch per triplet of values). The number of branches varied between 30 and 180 per zone. The number of branches is a function of the dispersion of the results. This itself is another attraction of the method. Normally, the number of branches to be used in any part of a logic tree is a subjective decision. Here, both the number of branches and the weights are simultaneously derived in a completely objective and transparent manner.

Examination of the results indicates that M_{max} has a low correlation with b-value, and thus the distribution for M_{max} can be considered essentially independent of that for $N(Mw \geq 5)$ and b-value. Accordingly, marginal distributions for M_{max} can be computed from the results in order to facilitate the hazard calculations.

One problem that was encountered concerned the zone BASL. It was found to be extremely difficult to find any adequate Gutenberg Richter fit to the data, given that it appears that not a single event has occurred with magnitude $4.0 \leq Mw < 4.5$ in the period for which this magnitude range is complete, i.e. the last 300 years. It will be recalled that, in our opinion, some events in this zone have been "gathered" towards Basel from neighbouring zones. In this case, one can conjecture that completeness for the BASL zone is actually significantly better than for the rest of the SZ01 area. For the purposes of this branch only, we treat the data set for BASL as if it were complete above 4.0 Mw since 1350. Examination of completeness charts for BASL, and of Figure 21, gives support to this conclusion. With this modification, it was possible to obtain the desired 5,000 simulations matching the data without difficulty.

9.3   Organisation of the logic tree

Since the three main branches of the logic tree link estimation of M_{max} with estimation of other seismicity parameters in a dependent way, it is necessary to say a few words about how these methods are paired.

Because the simulation method jointly determines M_{max} and recurrence parameters, the two necessarily share the last branch (C) of the logic tree.

The principal difference in approach between branches A and B relates to the difference between a least squares-approach and a maximum likelihood approach. The former treats all data points on a cumulative magnitude-frequency plot with equal weight, despite the fact that the low-magnitude points are based on more data (because the points are cumulative). The maximum likelihood approach, by contrast, is weighted by the more numerous lower-magnitude events. The distinction is between treating all earthquakes as of equal weight or all magnitude intervals as of equal weight.

Therefore, Branch A combines a global, conservative approach to maximum magnitude with a more generalised approach to recurrence (meaning, all earthquakes are considered equally weighted). Branch A also uses a slightly higher M_{max} than the other branches, and therefore "traps" the low possibility that a larger earthquake may occur than is supported by the other branches.

Branch B, on the other hand, represents an attempt to tackle each zone in a more precise and local-specific way, with individually determined maximum magnitude values, and recurrence

parameters estimated in a way that is relatively more sensitive to the occurrence of larger earthquakes in each zone.

Finally, Branch C treats all the zones in a way that is entirely driven by the local data, without preconceptions as to what the results "should" be, and completely accepting the uncertainty as to all the possible distributions of parameters.

Branches B and C constitute "local" approaches to the data in which, for each zone, the zone-specific data is allowed to speak for itself as much as possible. Branch A, on the other hand, is a more generalised approach intended to minimise the differences between the zones and emphasise the regional characteristics of the hazard (Figure 20). Because we consider the local approach to be generally more representative of the local hazard, we give this a significantly higher weight, 0.7, than the more regional approach. However, we have no clear reason to prefer Branch B over Branch C or vice versa, so these have equal weights, resulting in a final weighting system of 0.3, 0.35 and 0.35.

The results for the distribution of b values using the three branches can be compared, and these are shown in Figure 22. Only one version of the zone configuration is presented for simplicity (with SWAB and NSPG, and with the Rhine Graben partitioned). Zones are shown colour-coded for b value, with values less than 0.6 treated as 0.6. Because of the way the zones are coloured, some differences may be illusory: a difference between two zones between 0.99 and 1.01 will show as a colour change, whereas a difference between 0.91 and 0.99 will not. However, any difference of *two* colour grades is significant.

In the case of Branches A and B, the central (highest weighted) b value is plotted. The distribution of b values is symmetrical about this value. In the case of Branch C, the mean of all the results is plotted, since the uncertainty distributions may not be symmetrical.

What is striking is how different the three maps are. Some zones that stand out as having high values from one method are much lower given another, which is a good indication of the overall uncertainty in this parameter. Some of the results are predictable - Branch A has the least variation, which is as it should be considering that a global prior was applied to all zones. Similarly Branch B has the most extremes, reflecting the influence of the least squares method. It also has a tendency for lower b values overall. Branch C is particularly interesting, given that is perhaps the most objective.

Some things are consistent - the central Rhine Graben always comes out with a lower b value than the northern or southern zones, which strongly supports the interpretation to divide the Rhine Graben in this way. There is a general tendency for the Western Alps to show b values that are lower than average. BASL has a consistently low b value, and BAVA is always lower than BAWU. Otherwise there are many differences, although the overall trend is for values around 0.8-0.9.

The data values are all contained in the three appendices at the end of this report. Branch A is described in Appendix 1, Branch B in Appendix 2 and Branch C in Appendix 3.
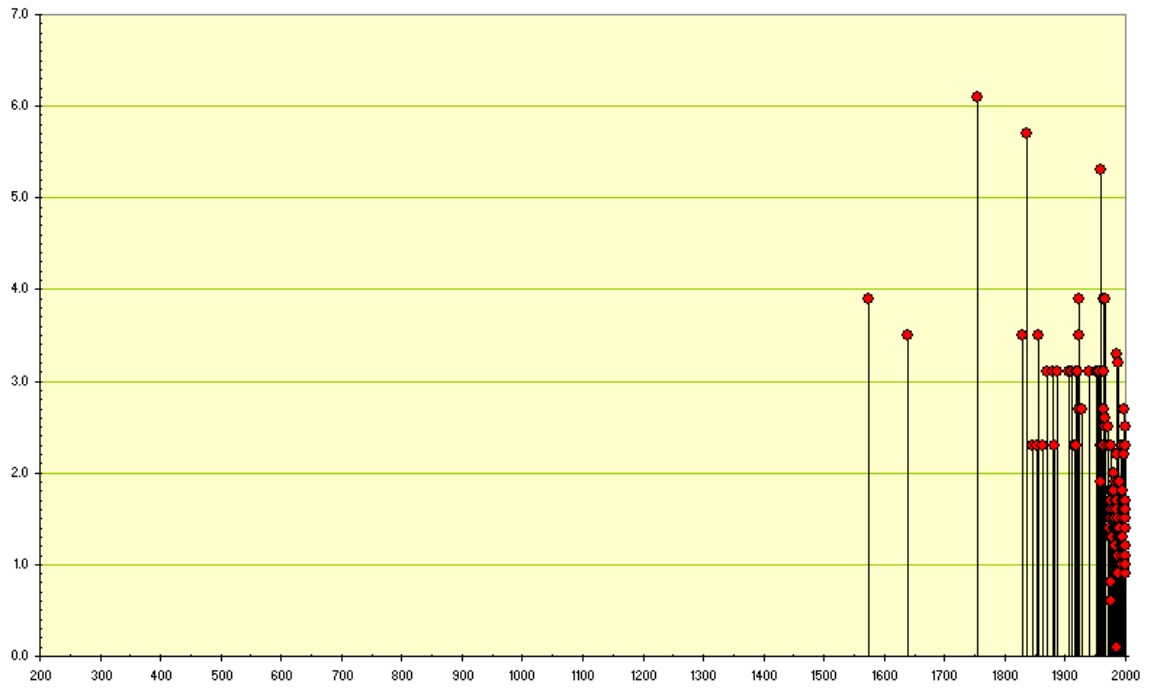
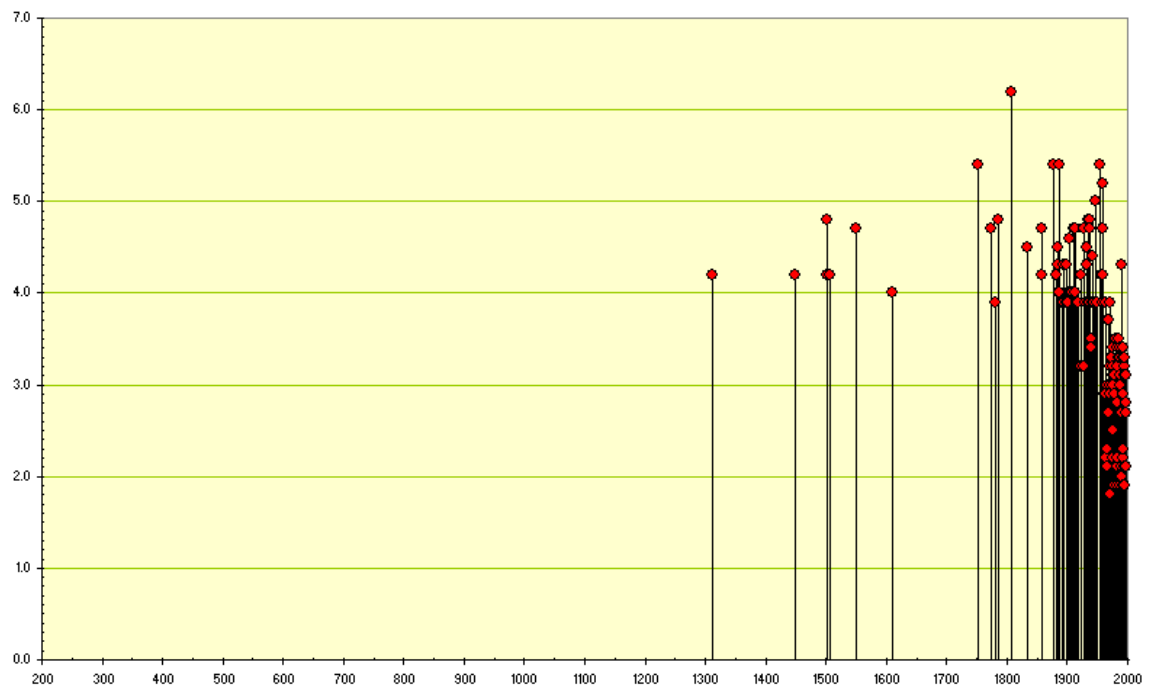Fig. 21a: Seismic history for zone ALCM

Fig. 21b: Seismic history for zone ALMA
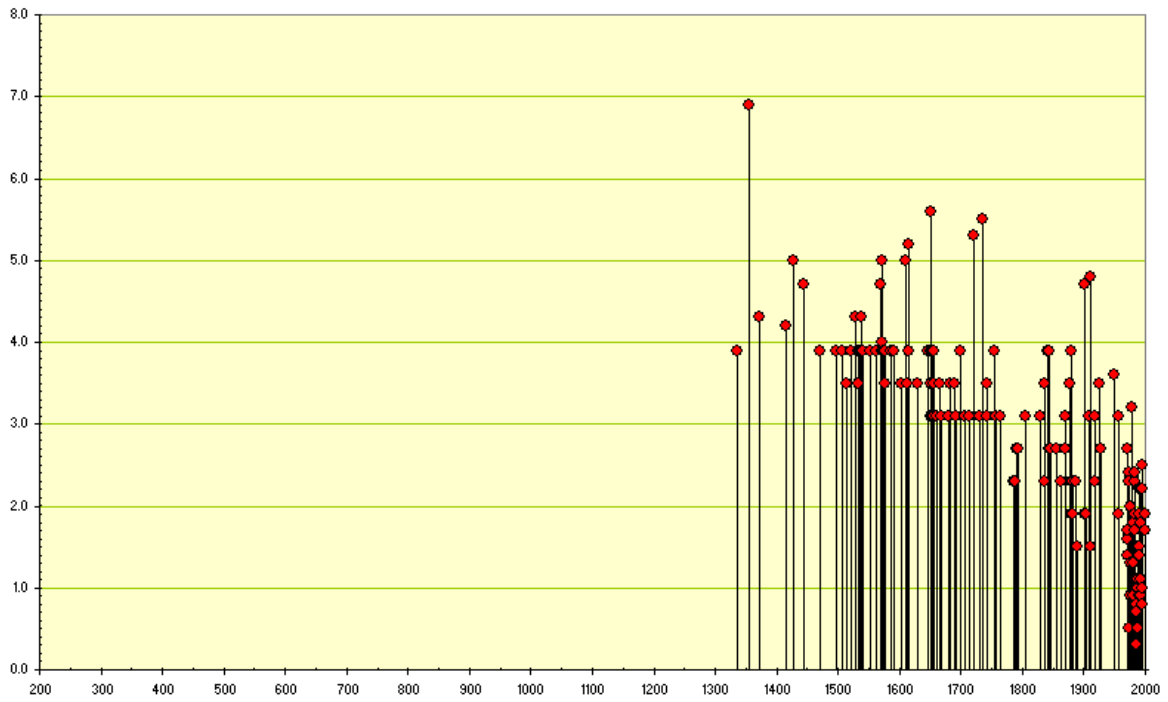
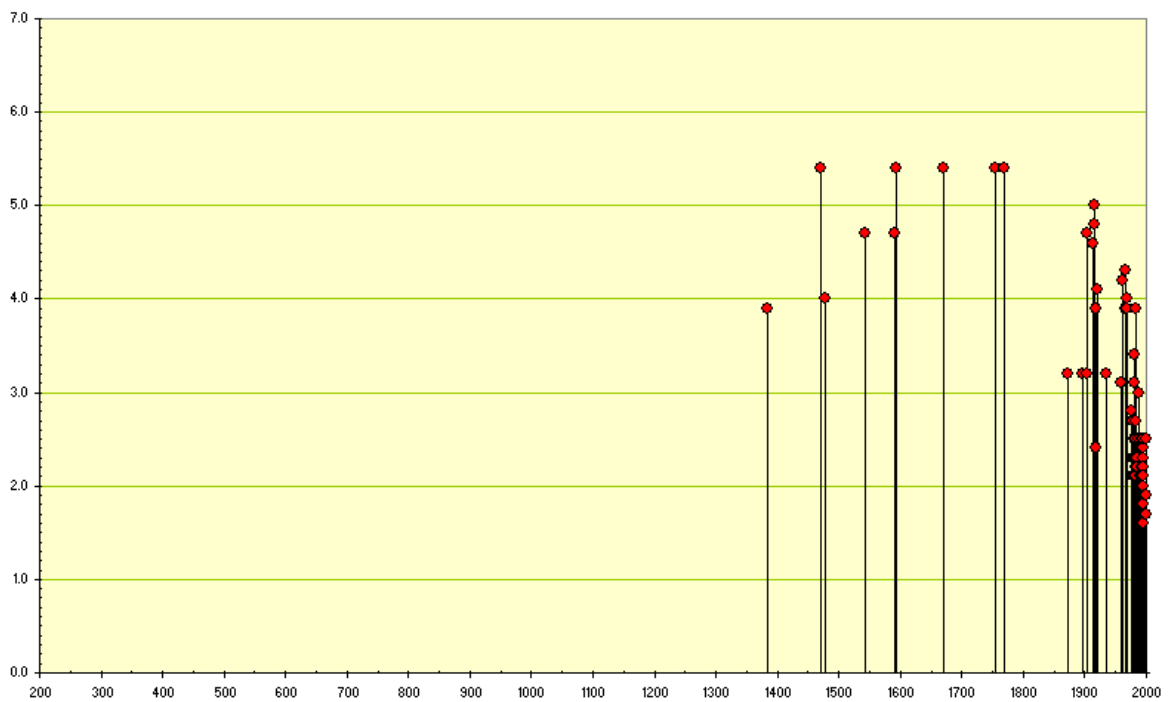Fig. 21c: Seismic history for zone BASL

Fig. 21d: Seismic history for zone BAVA
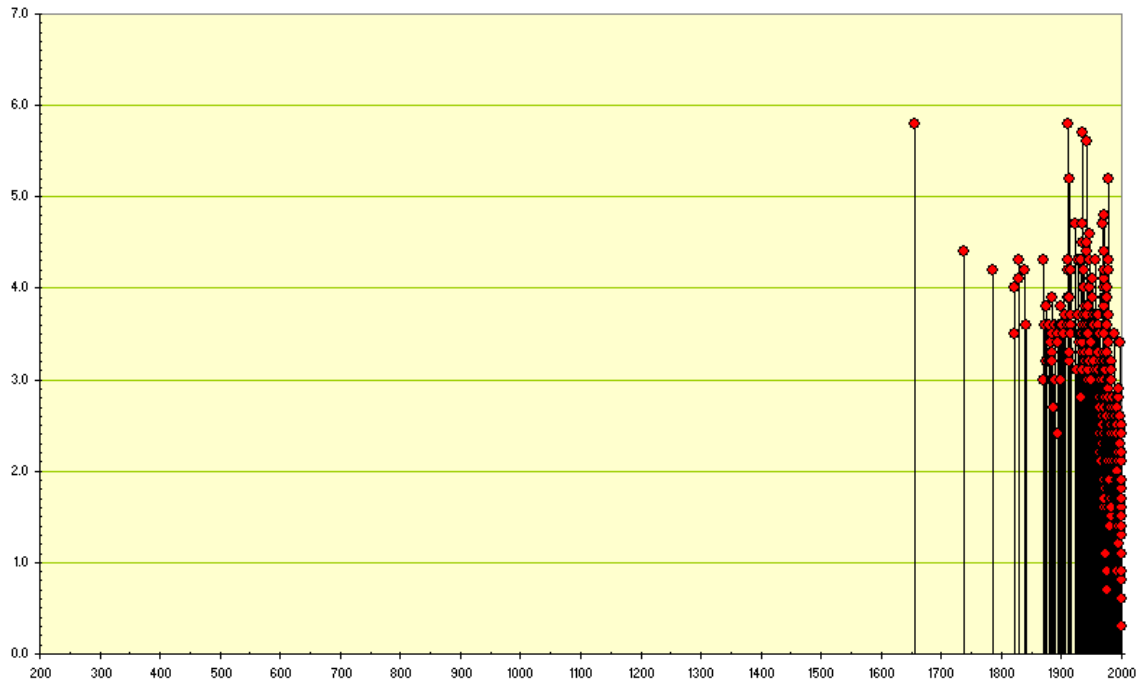
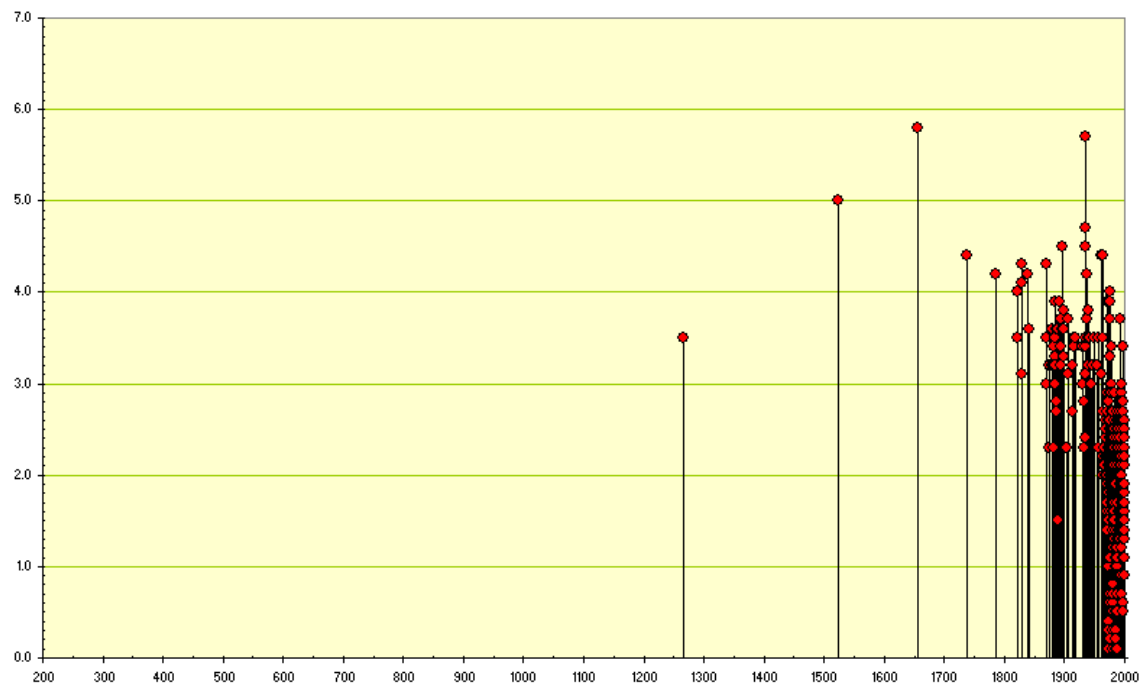Fig. 21e: Seismic history for zone BAW2

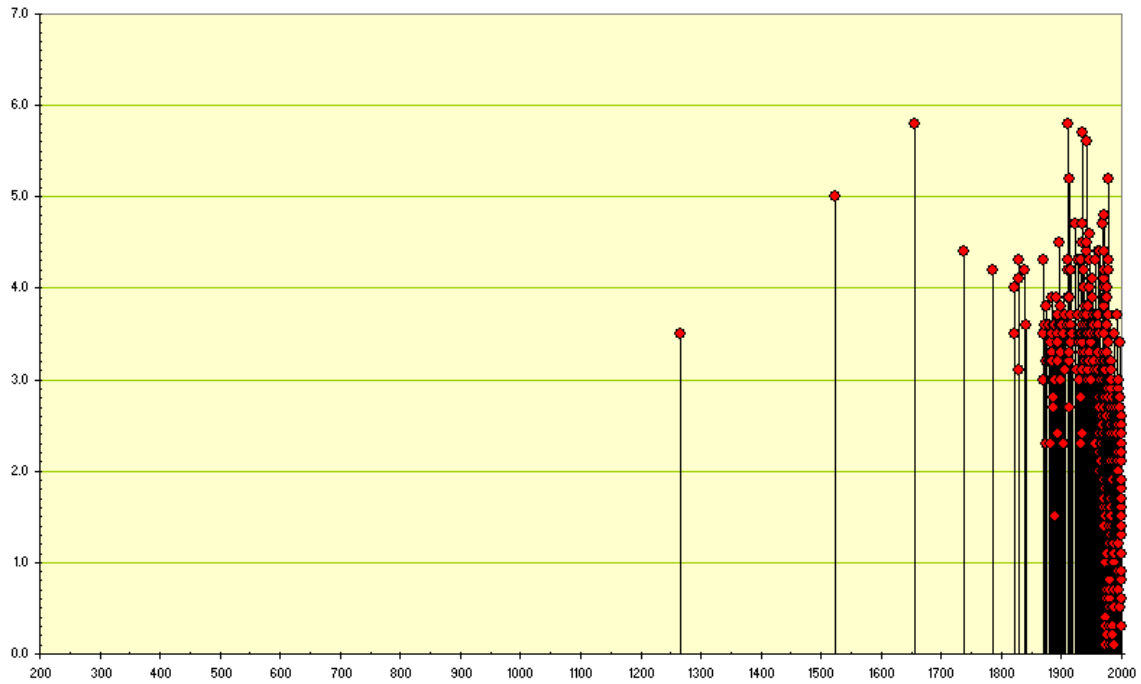Fig. 21f: Seismic history for zone BAWS

Fig. 21g: Seismic history for zone BAWU
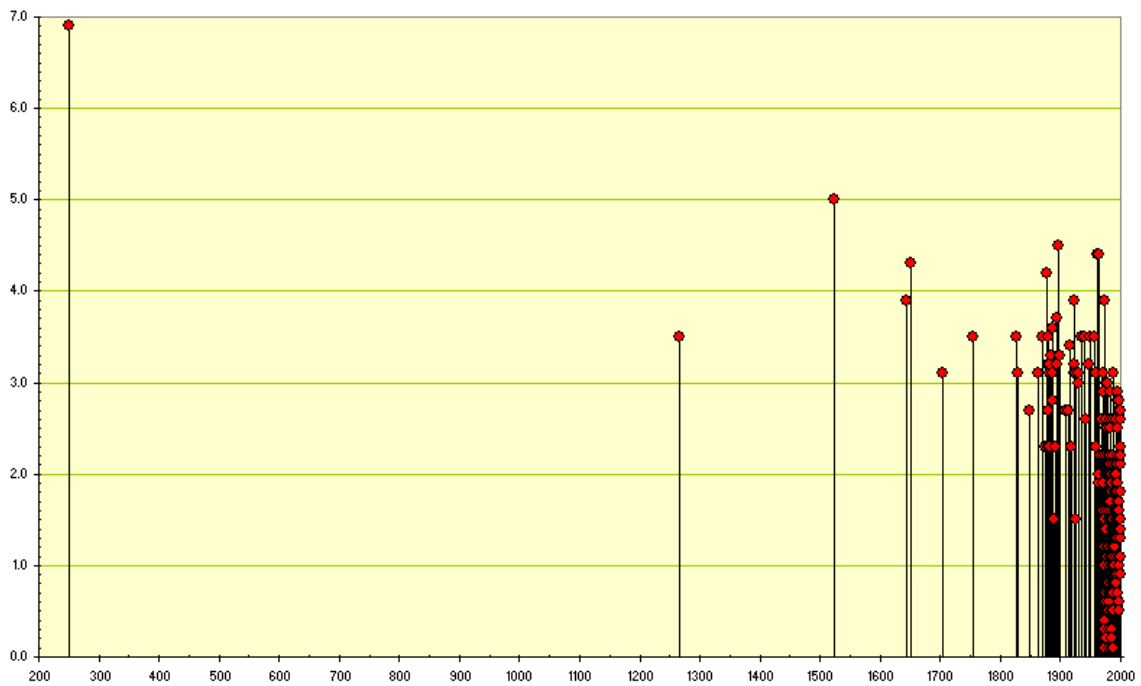

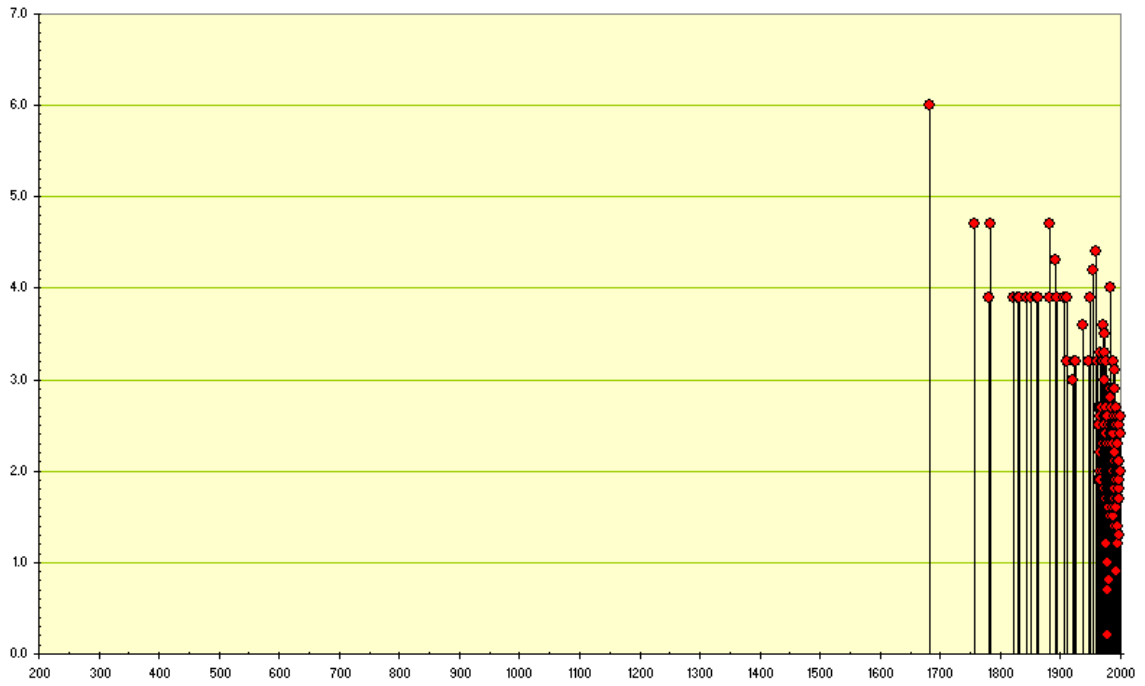Fig. 21h: Seismic history for zone BLAF

Fig. 21i: Seismic history for zone BRES

Fig. 21j: Seismic history for zone BW2S

Fig. 21k: Seismic history for zone DAUP

Fig. 21l: Seismic history for zone FRIB

Fig. 21m: Seismic history for zone GARD

Fig. 21n: Seismic history for zone GENV

Fig. 21o: Seismic history for zone GLAR
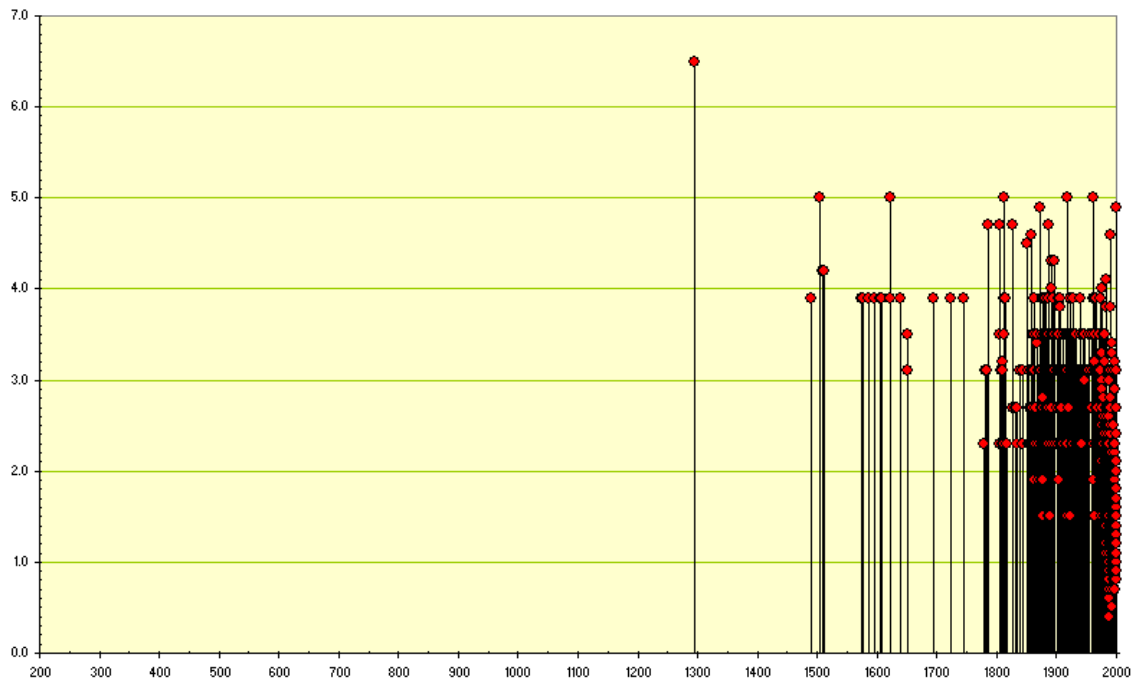
Fig. 21p: Seismic history for zone GRAU
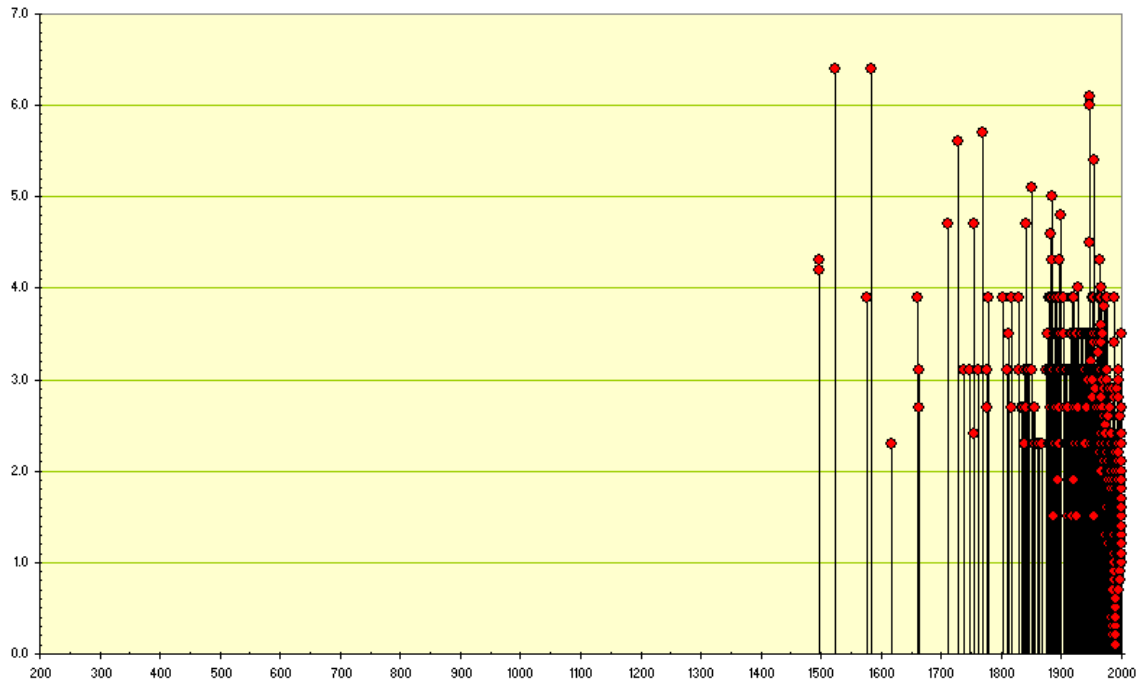
Fig. 21q: Seismic history for zone HELV
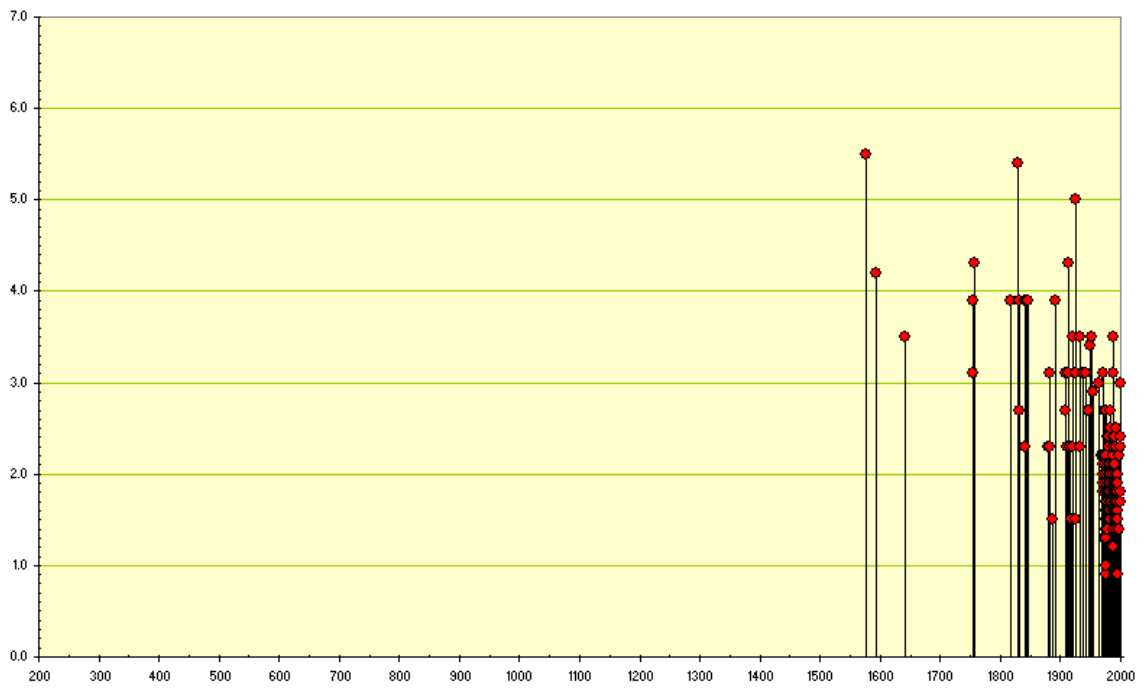
Fig. 21r: Seismic history for zone JURA
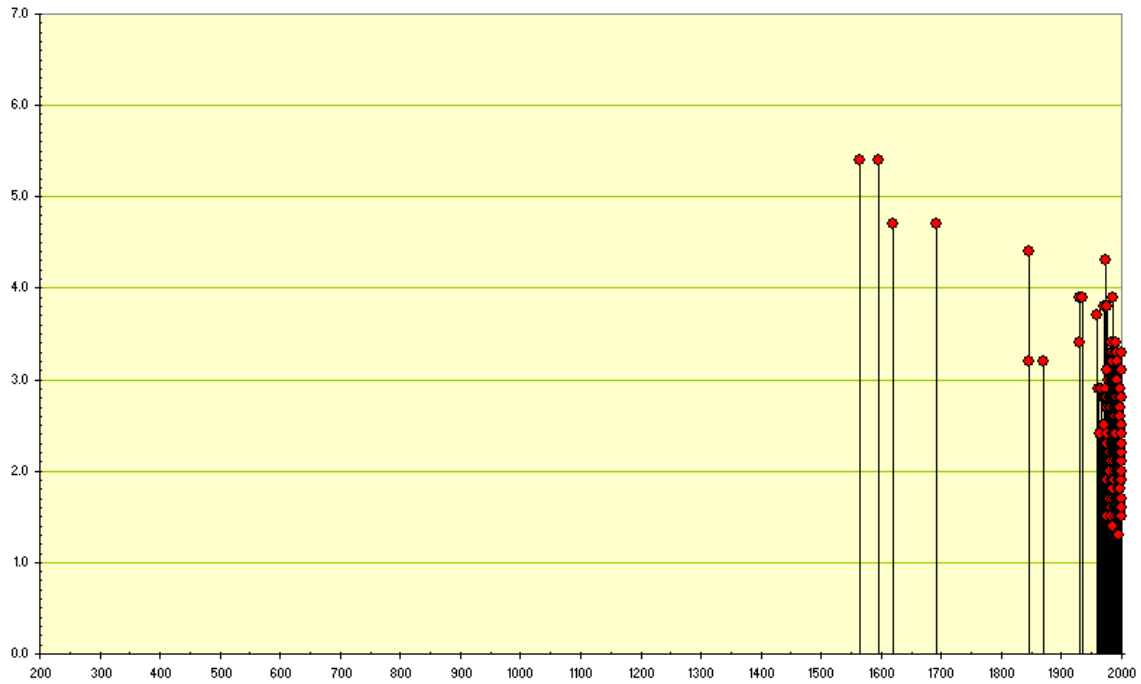
Fig. 21s: Seismic history for zone LORA
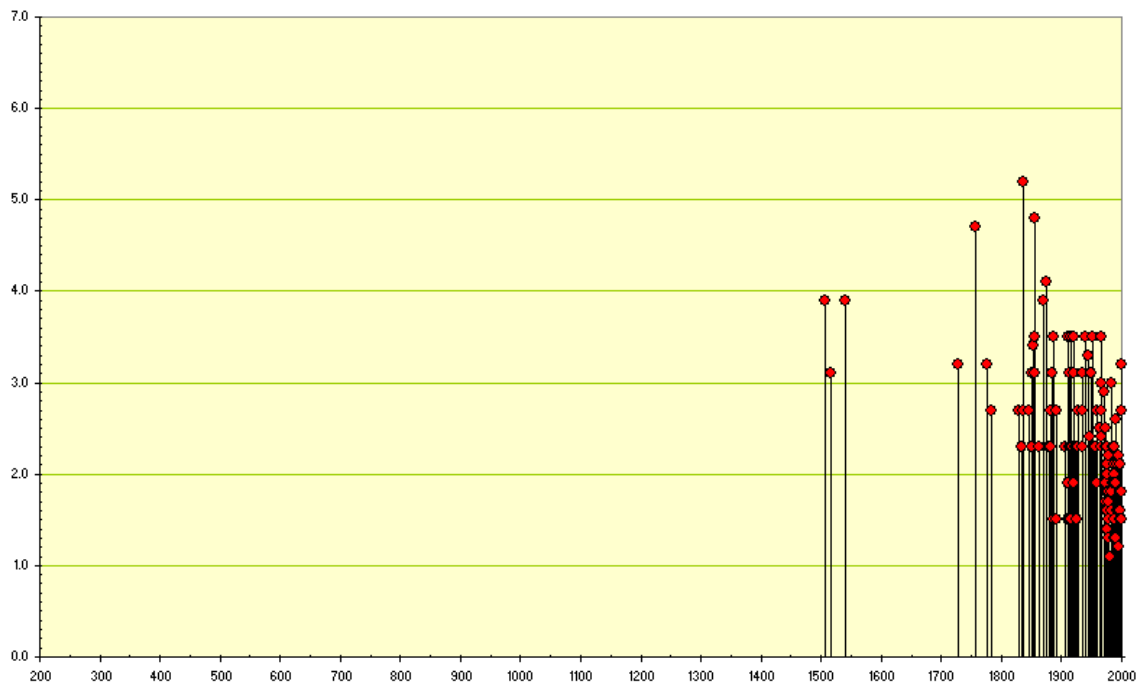
Fig. 21t: Seismic history for zone MOMI
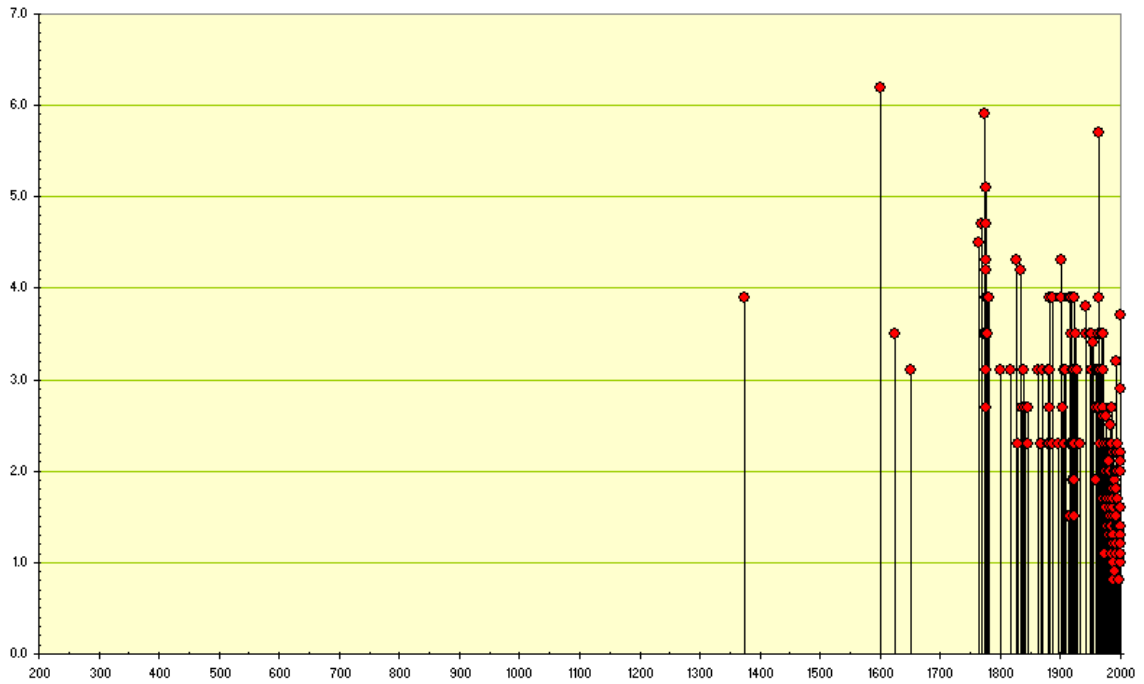
Fig. 21u: Seismic history for zone NIDW
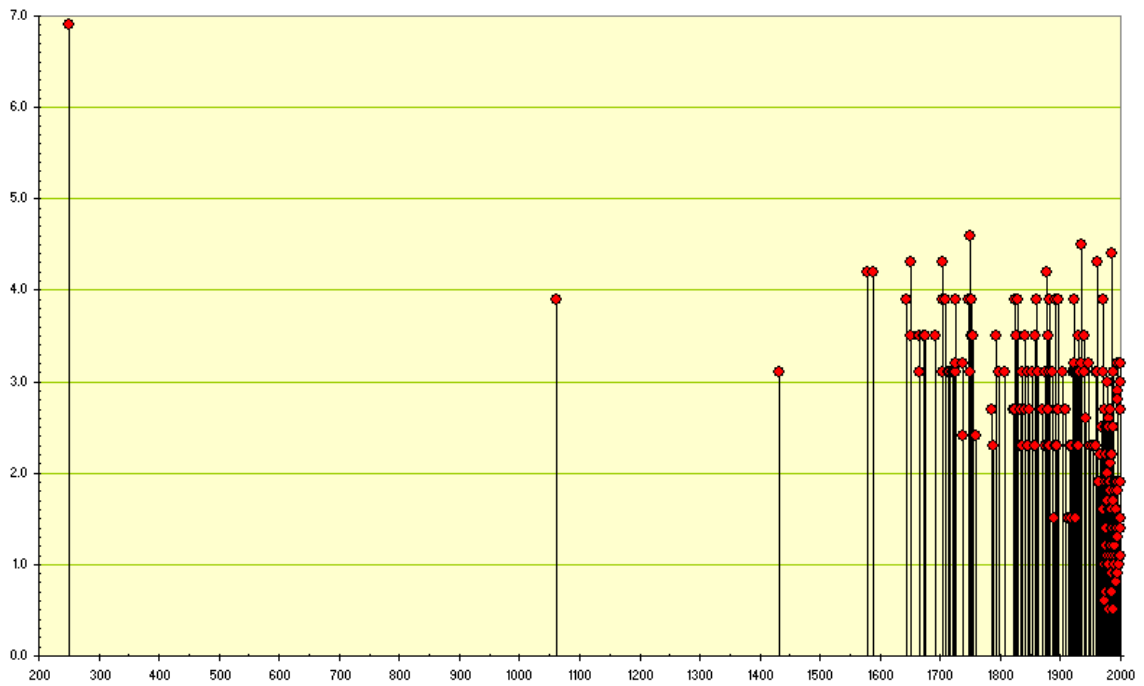
Fig. 21v: Seismic history for zone NSPG
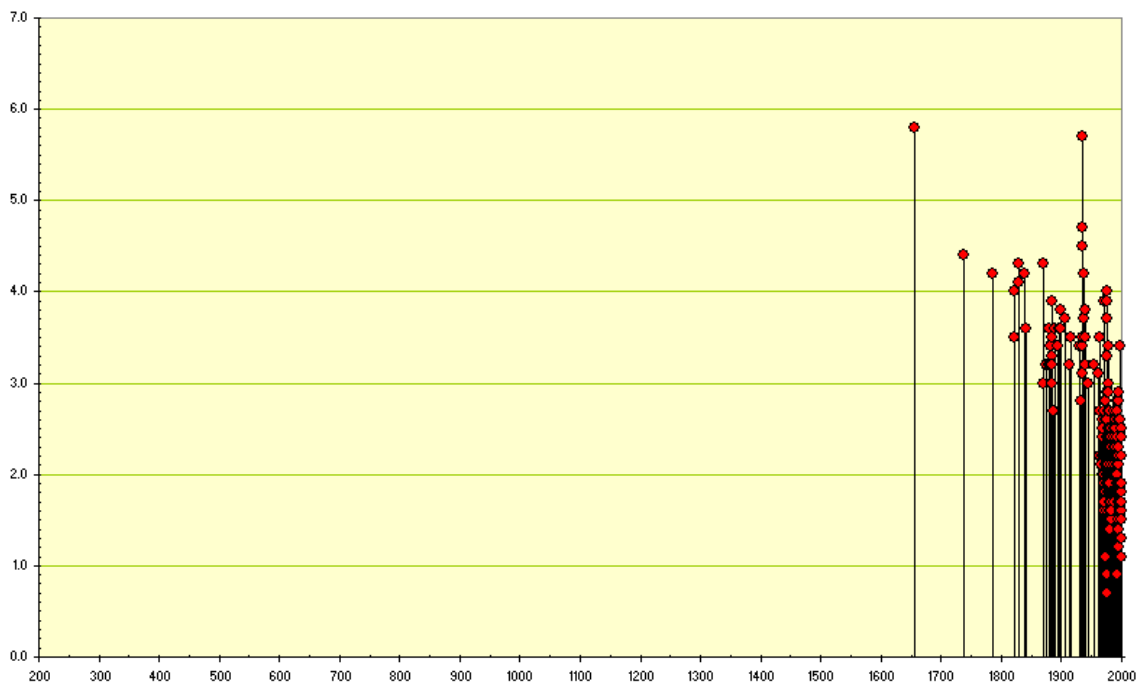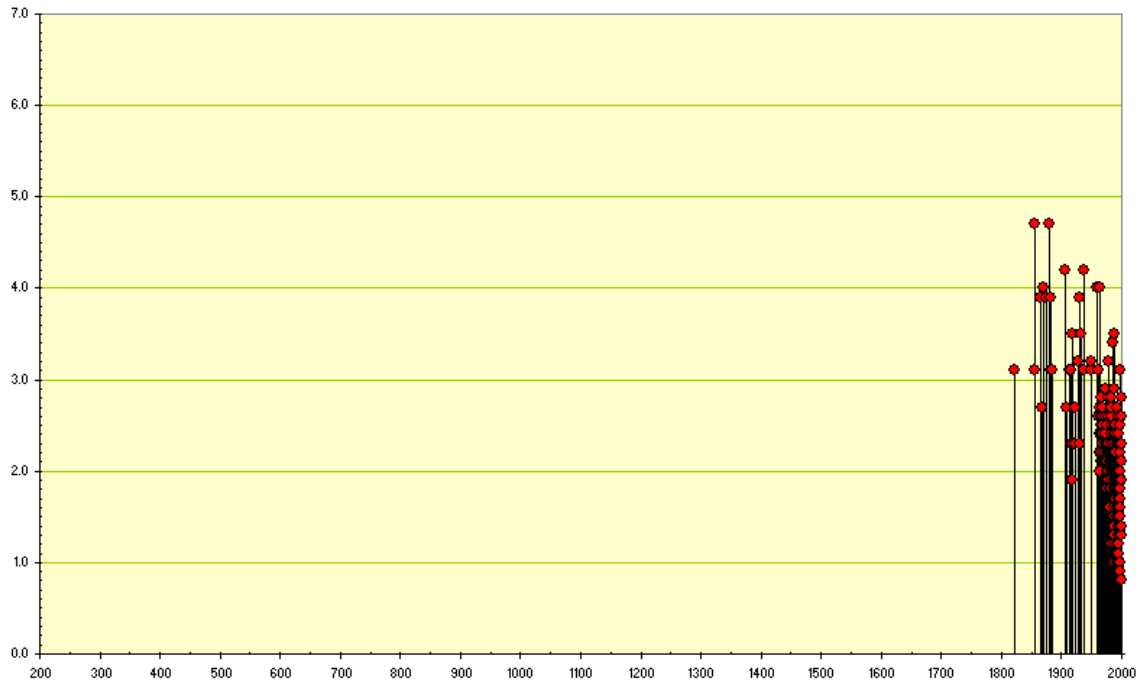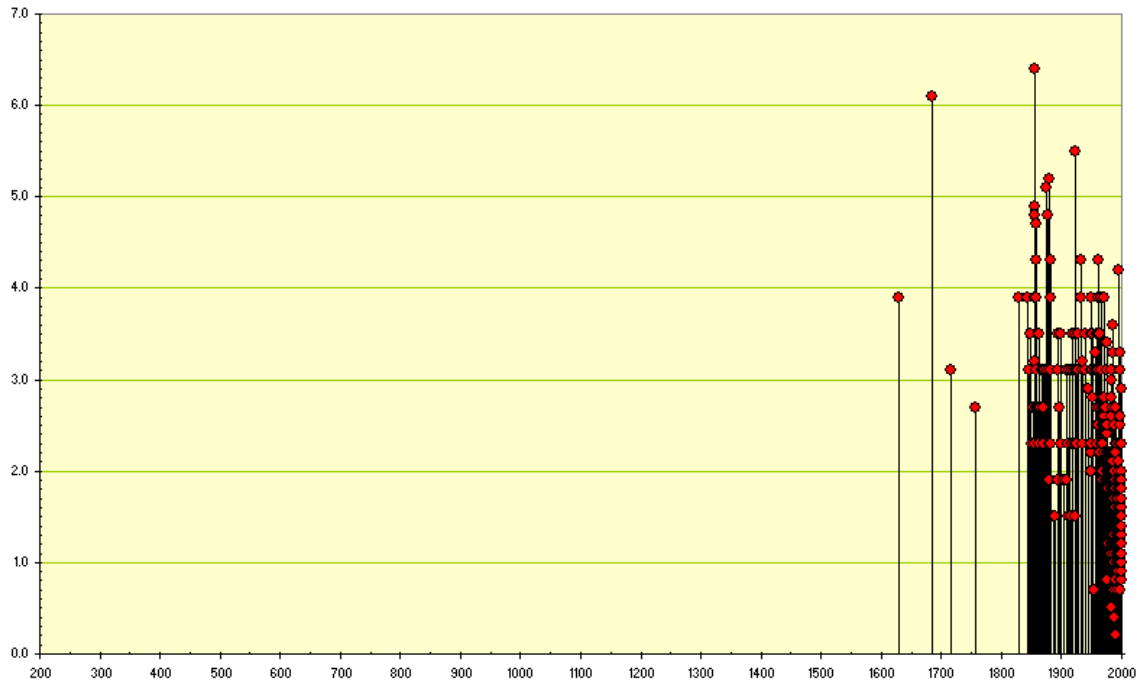
Fig. 21w: Seismic history for zone PENV
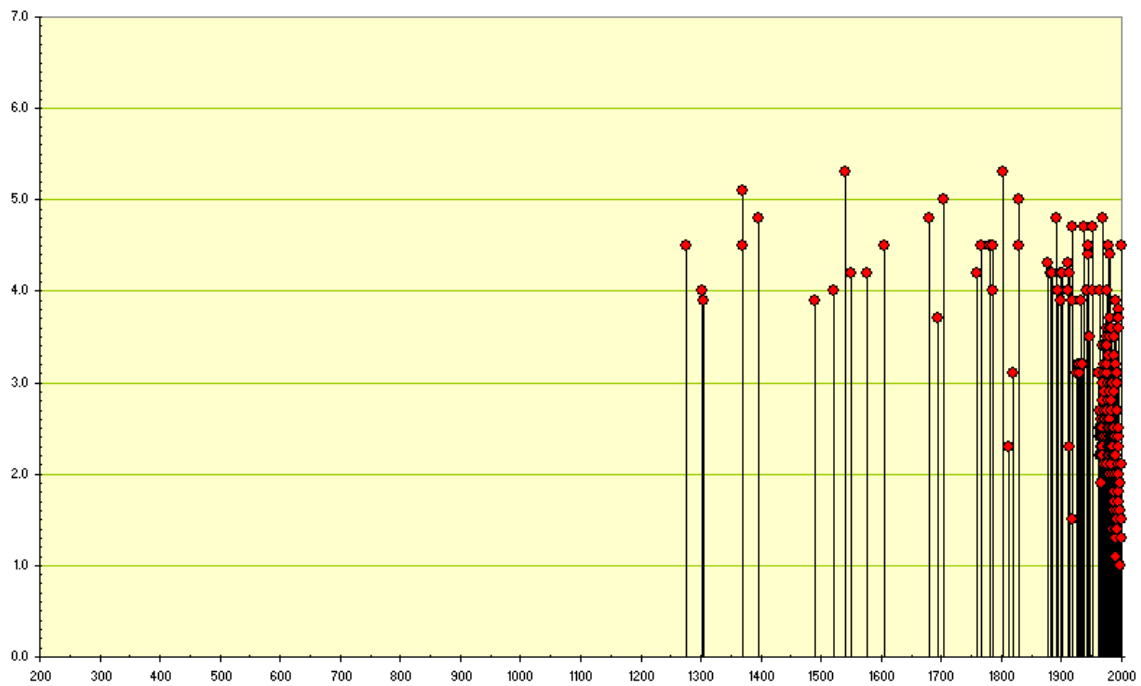
Fig. 21x: Seismic history for zone POVA
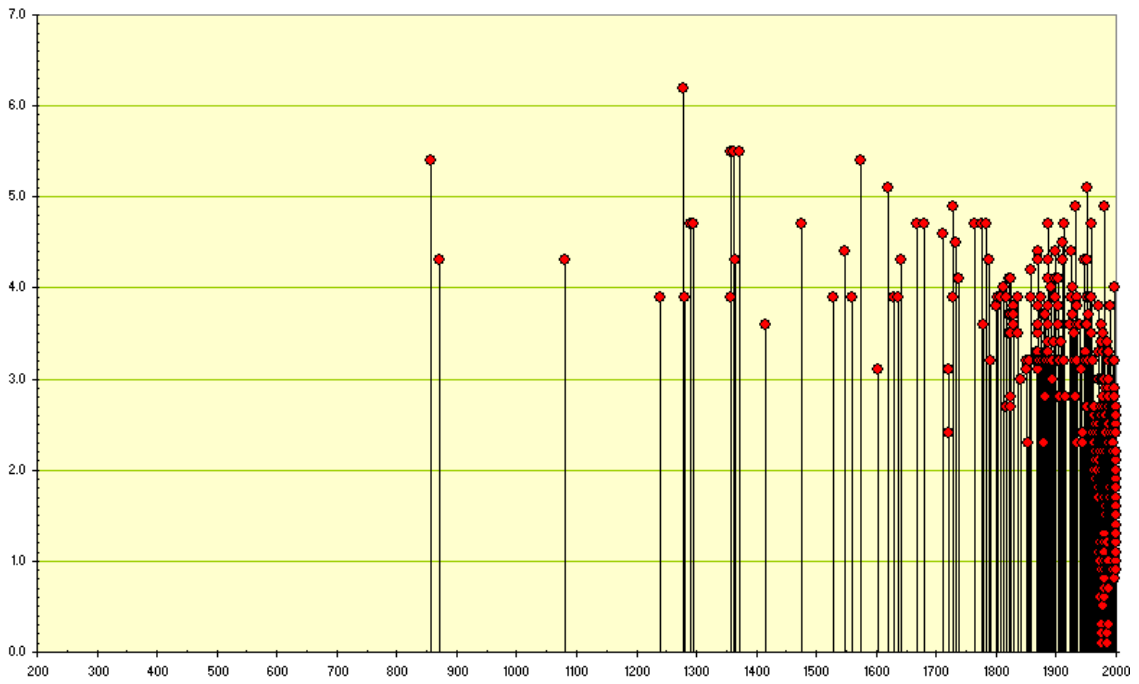
Fig. 21y: Seismic history for zone RHEG
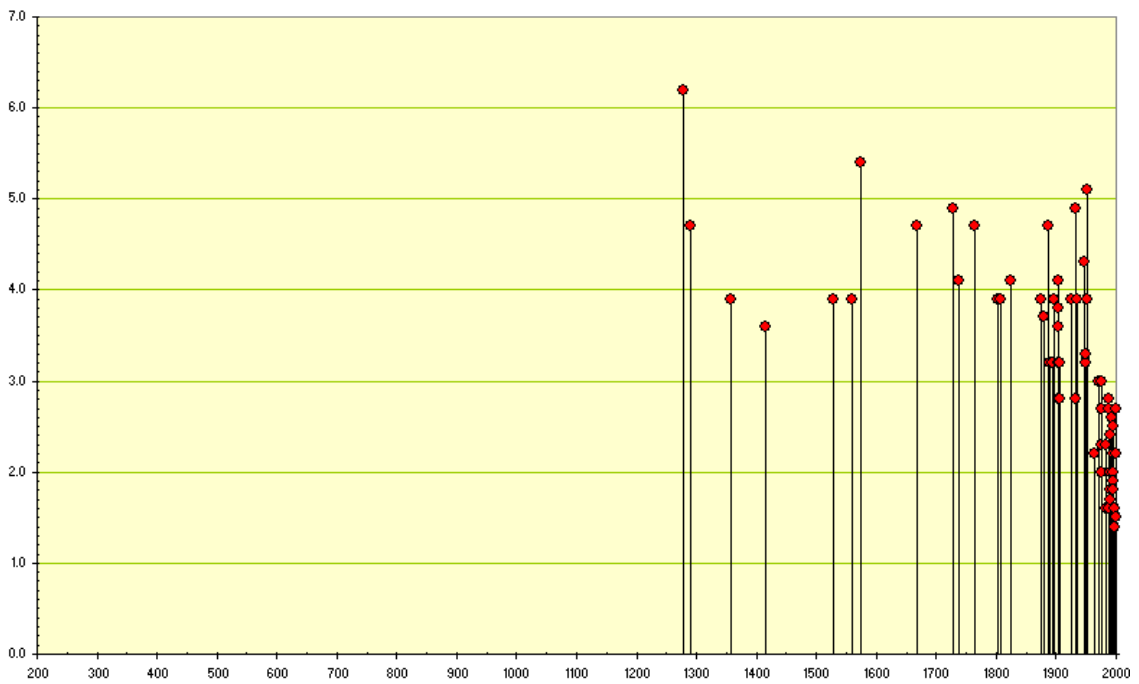
Fig. 21z: Seismic history for zone RHGC
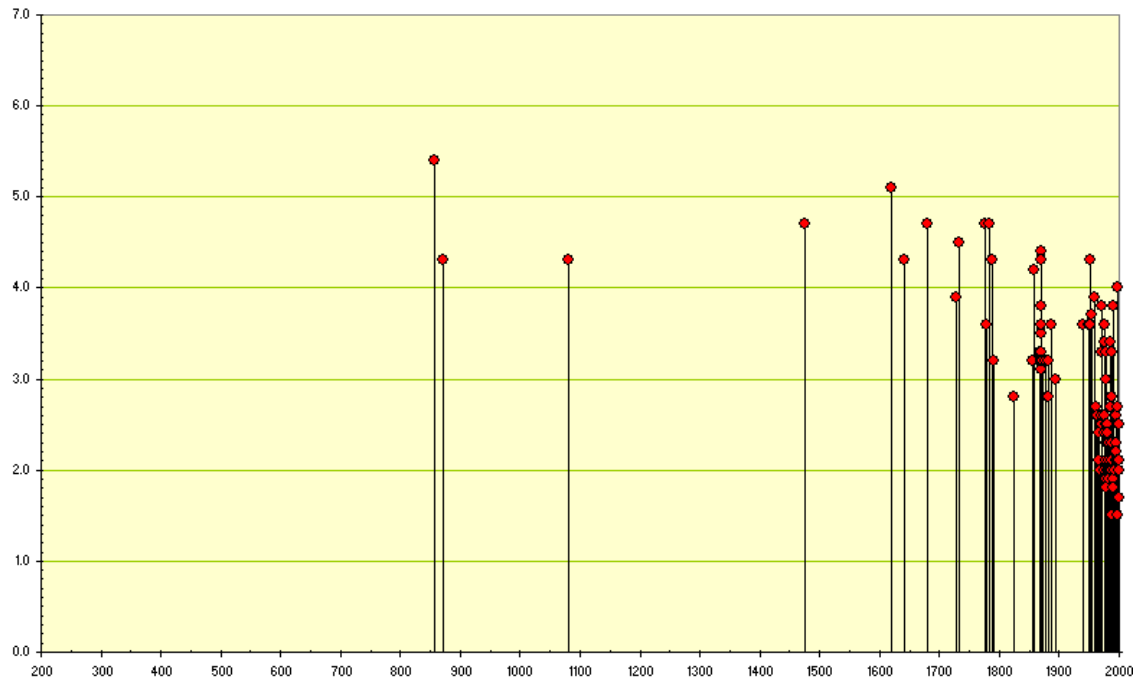
Fig. 21aa: Seismic history for zone RHGN
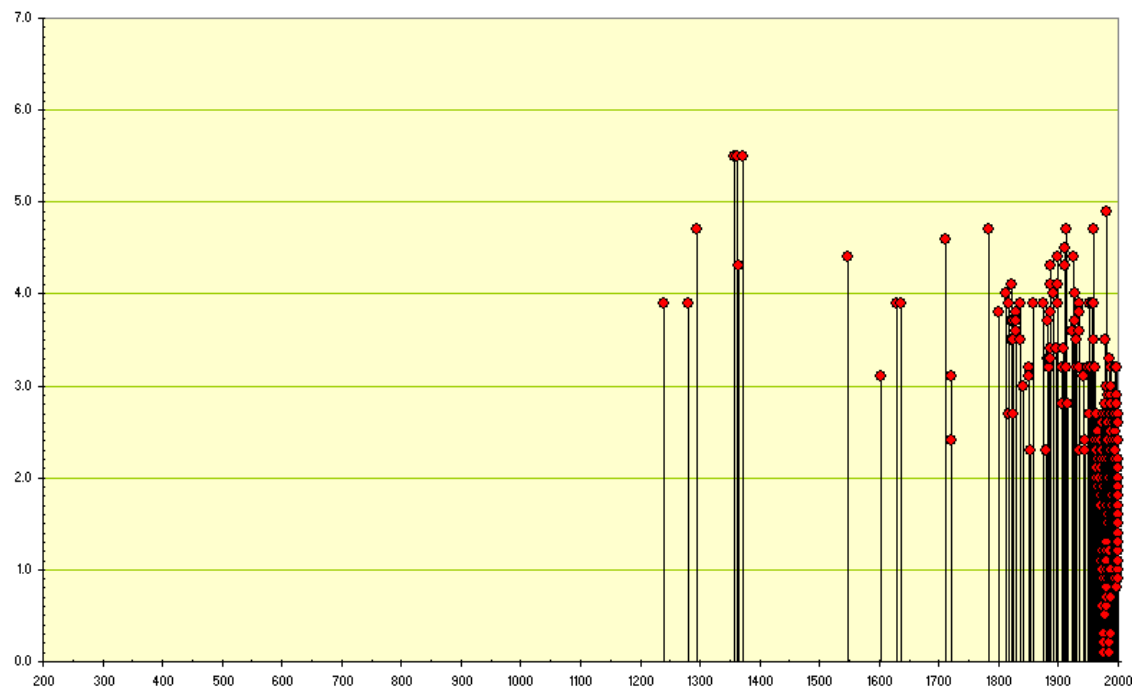
Fig. 21ab: Seismic history for zone RHGS
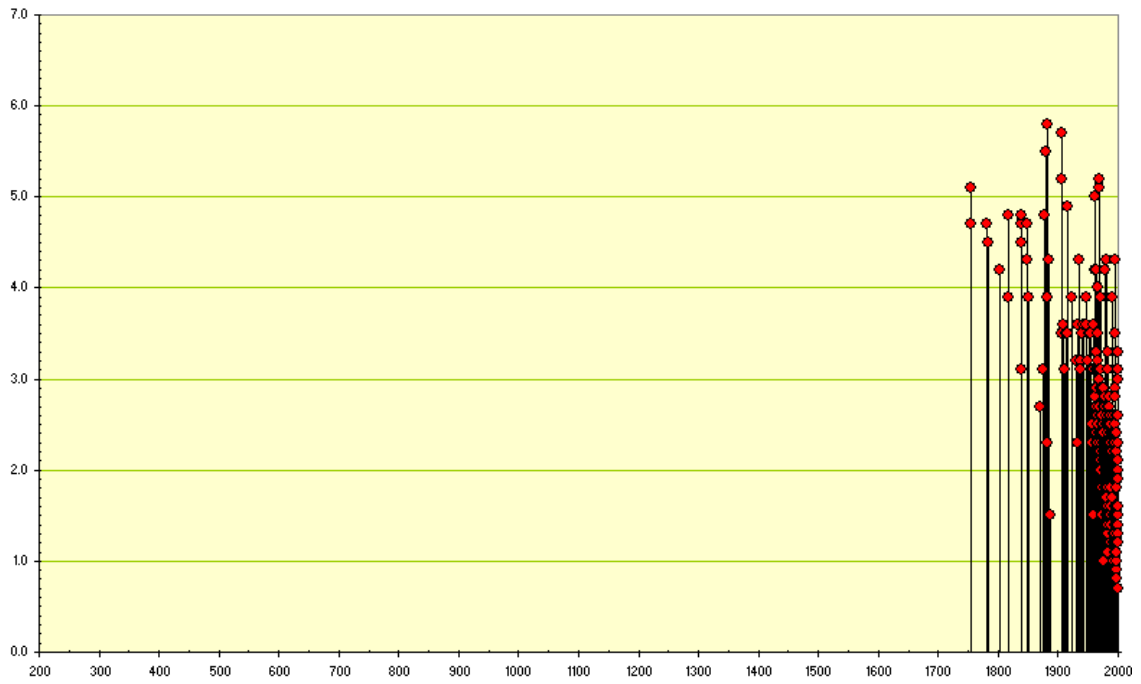
Fig. 21ac: Seismic history for zone SAVO
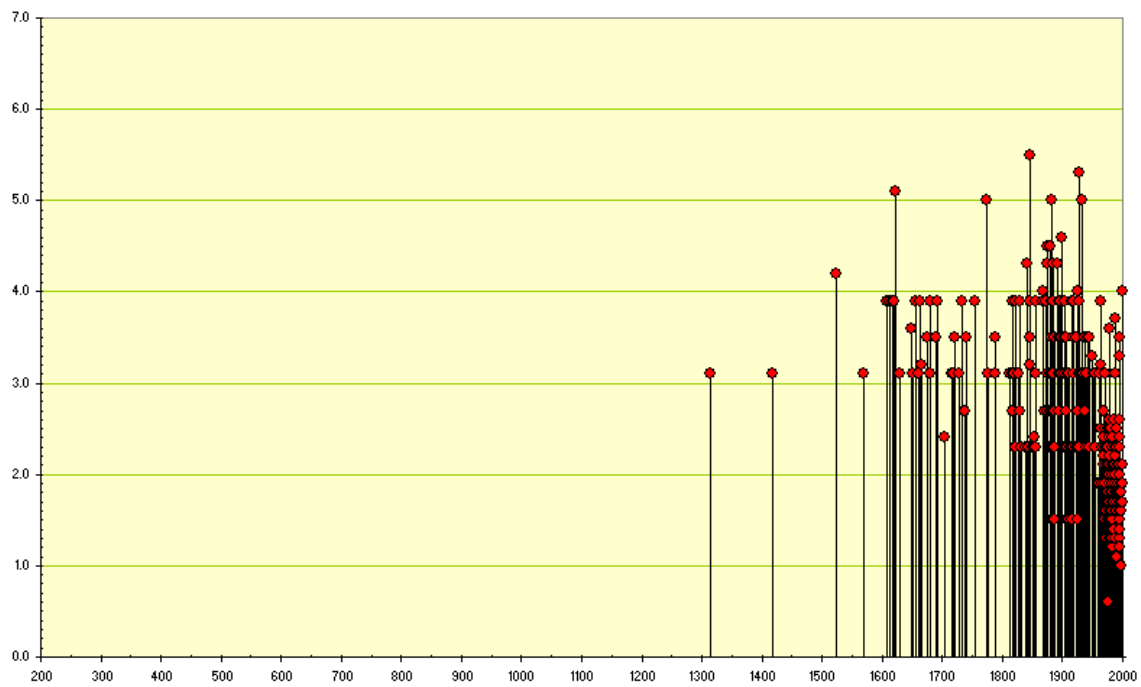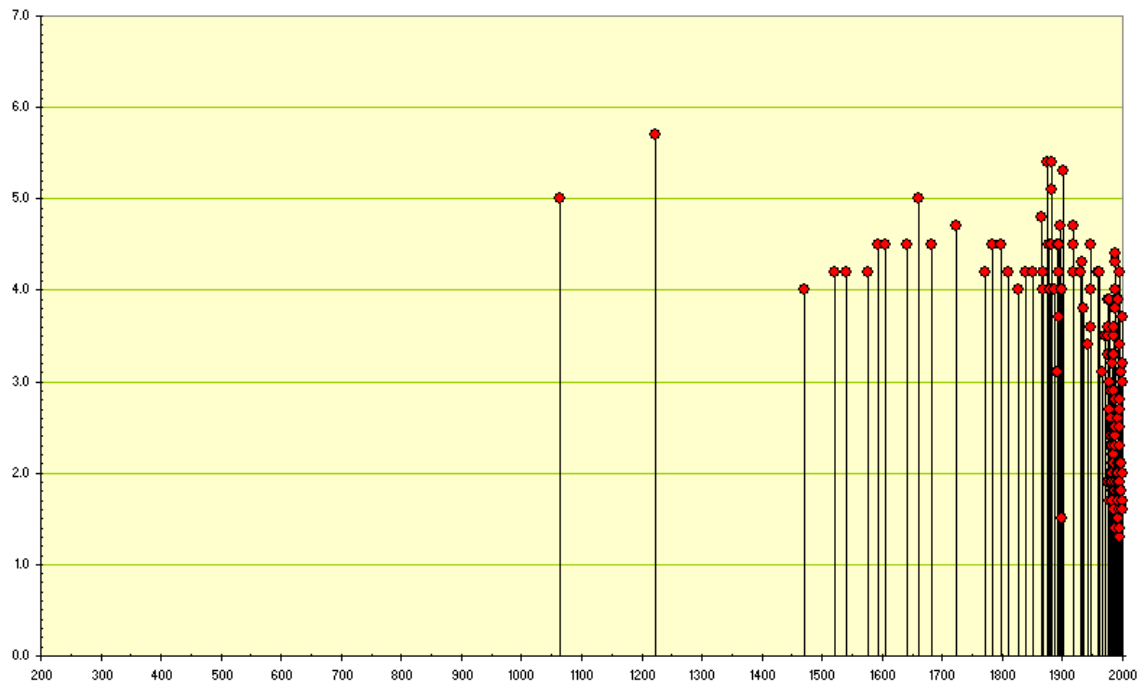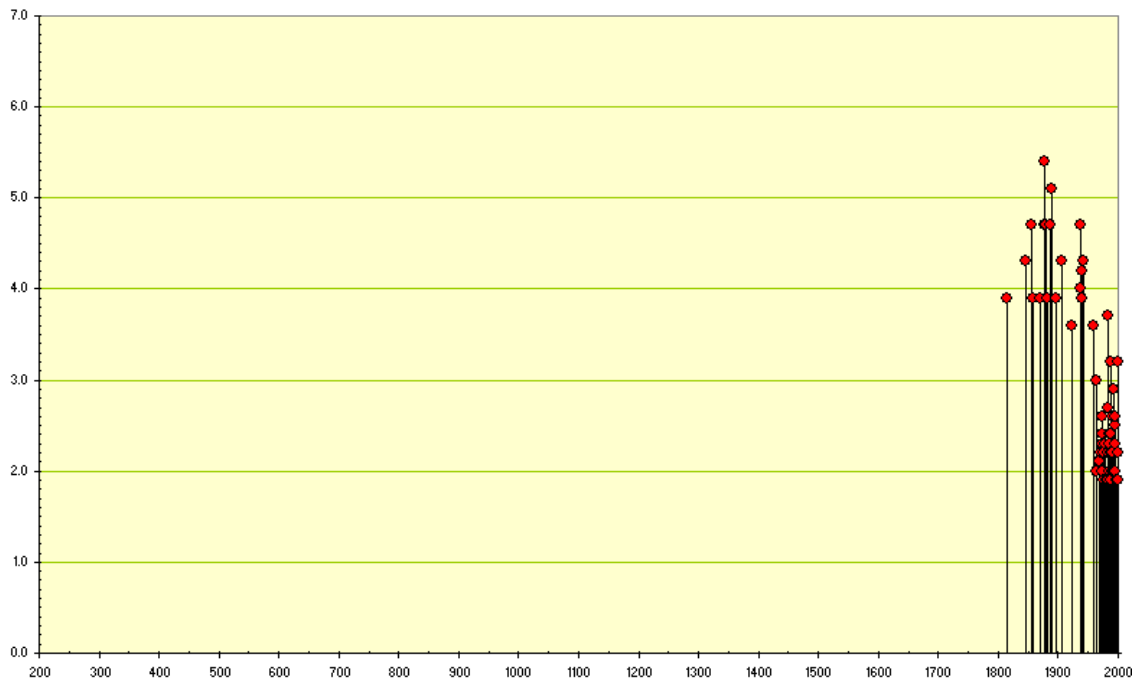

Fig. 21ad: Seismic history for zone SBRE
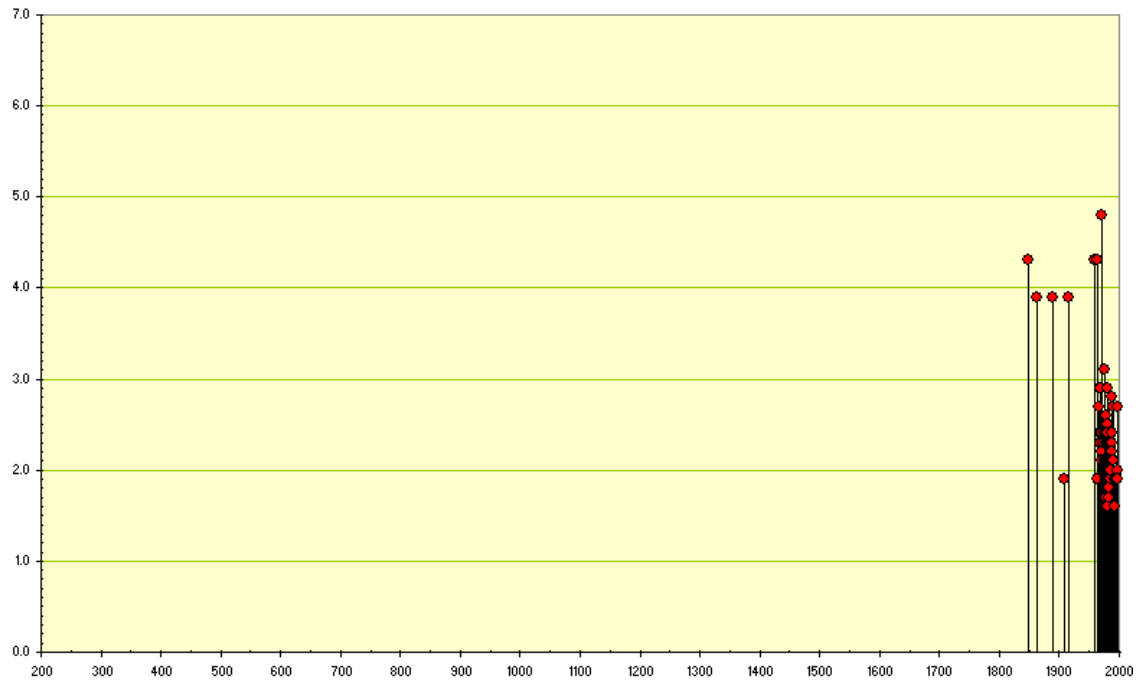
Fig. 21ae: Seismic history for zone SJUR
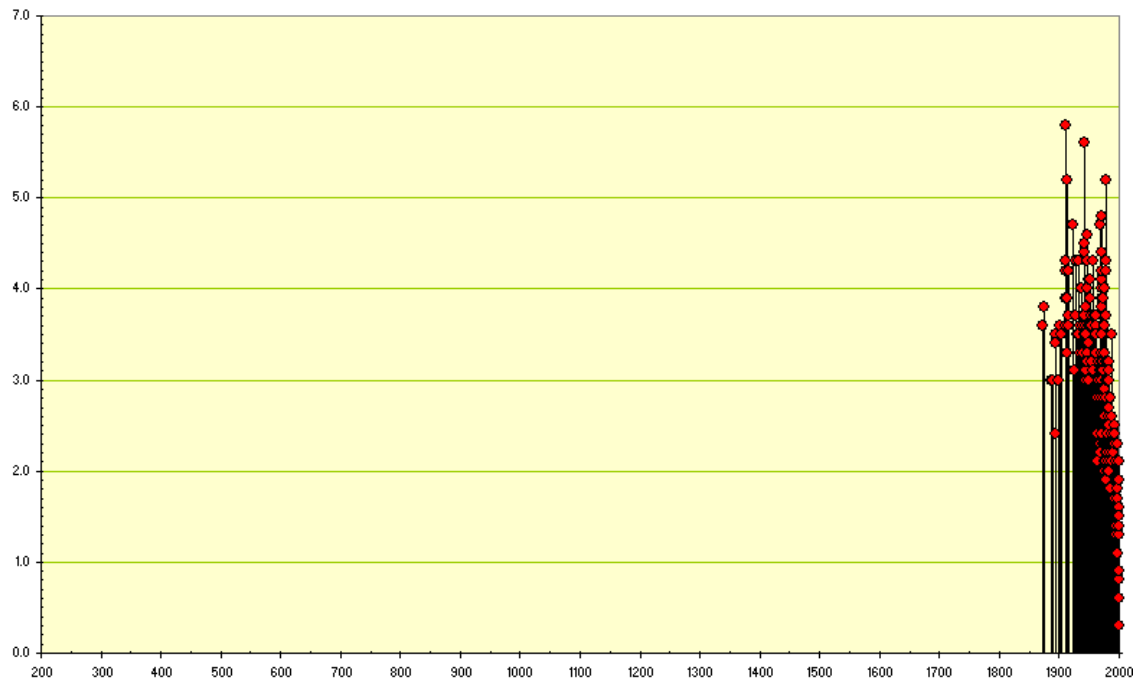
Fig. 21af: Seismic history for zone SWAB
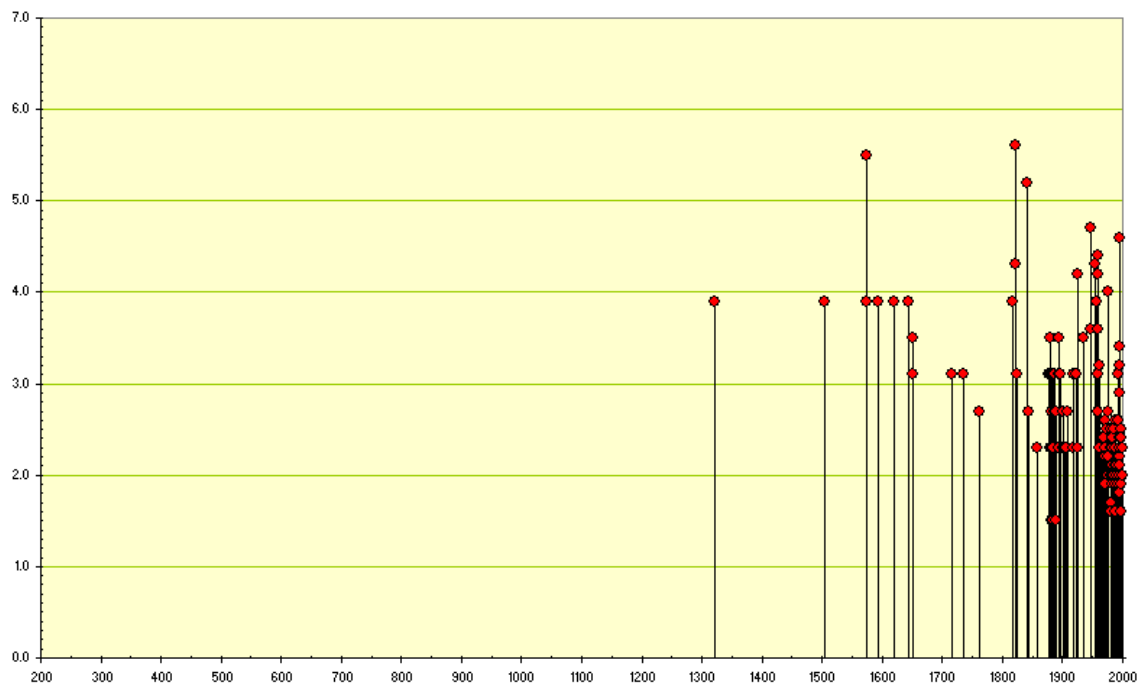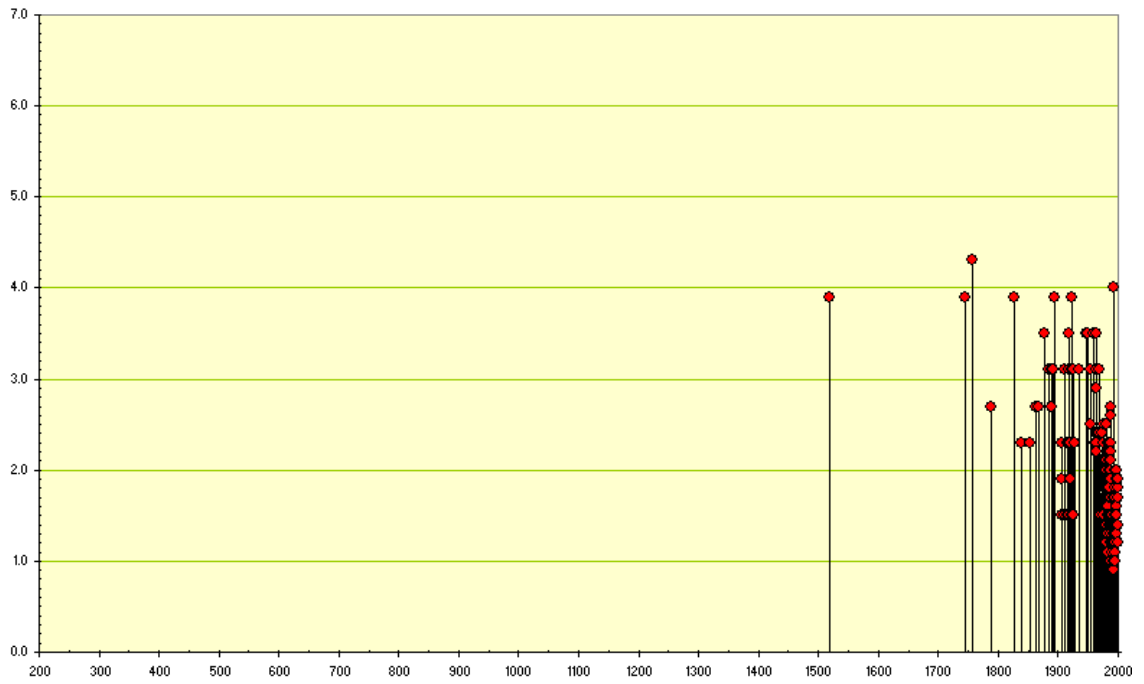
Fig. 21ag: Seismic history for zone TICI
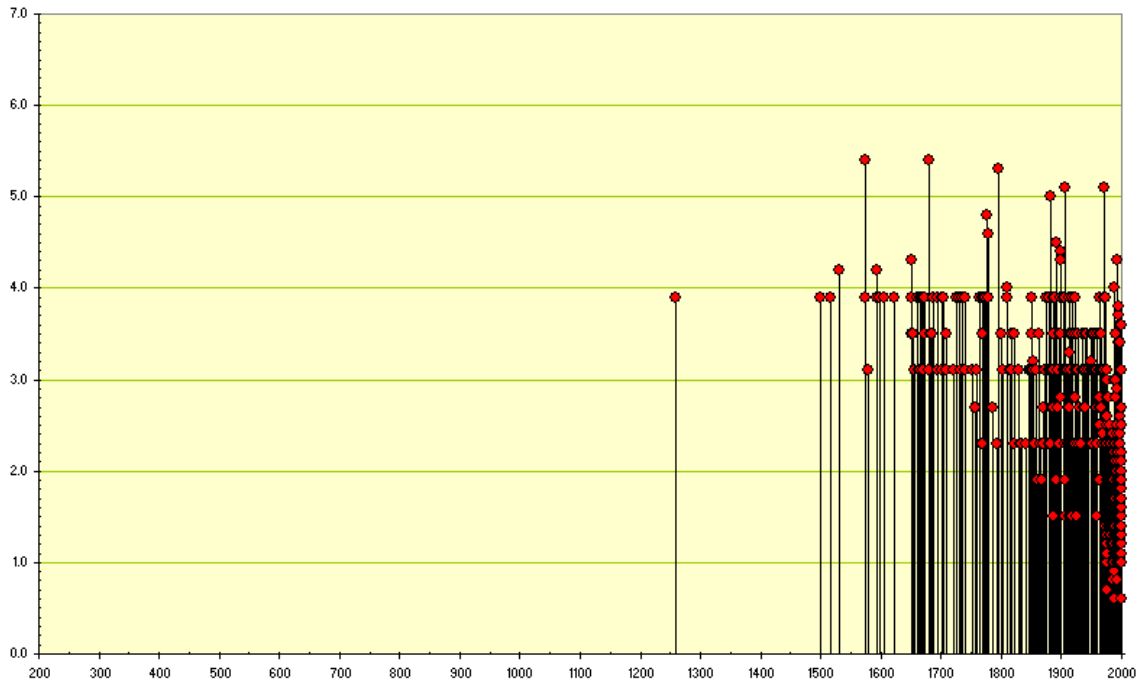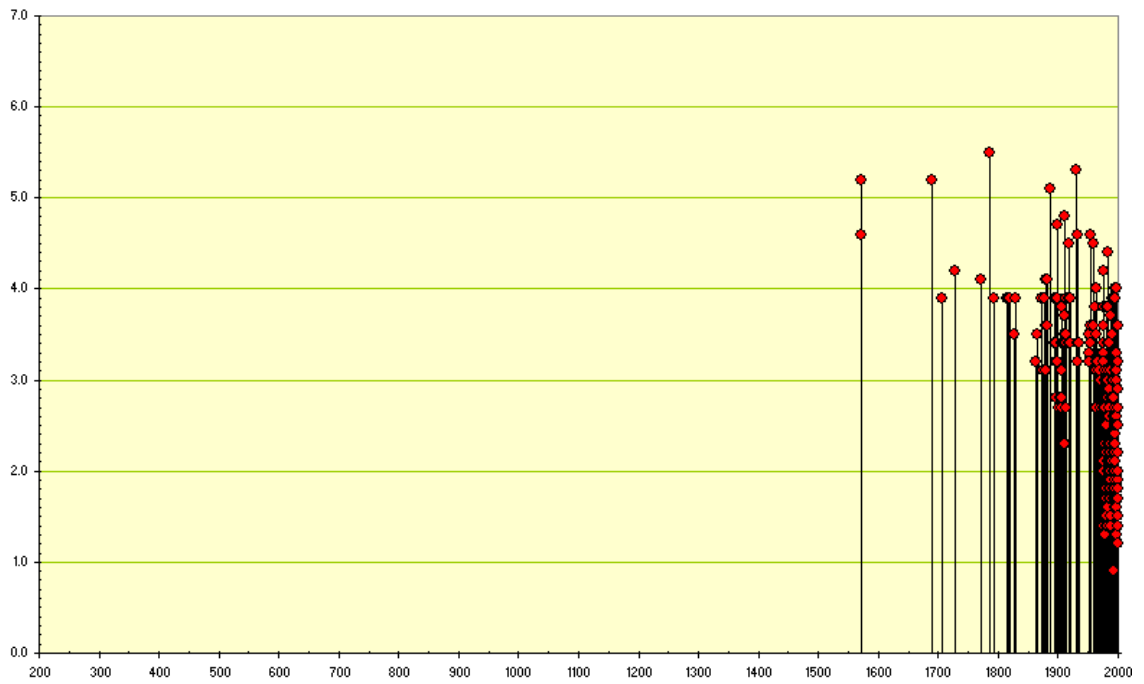

Fig. 21ah: Seismic history for zone TYRO
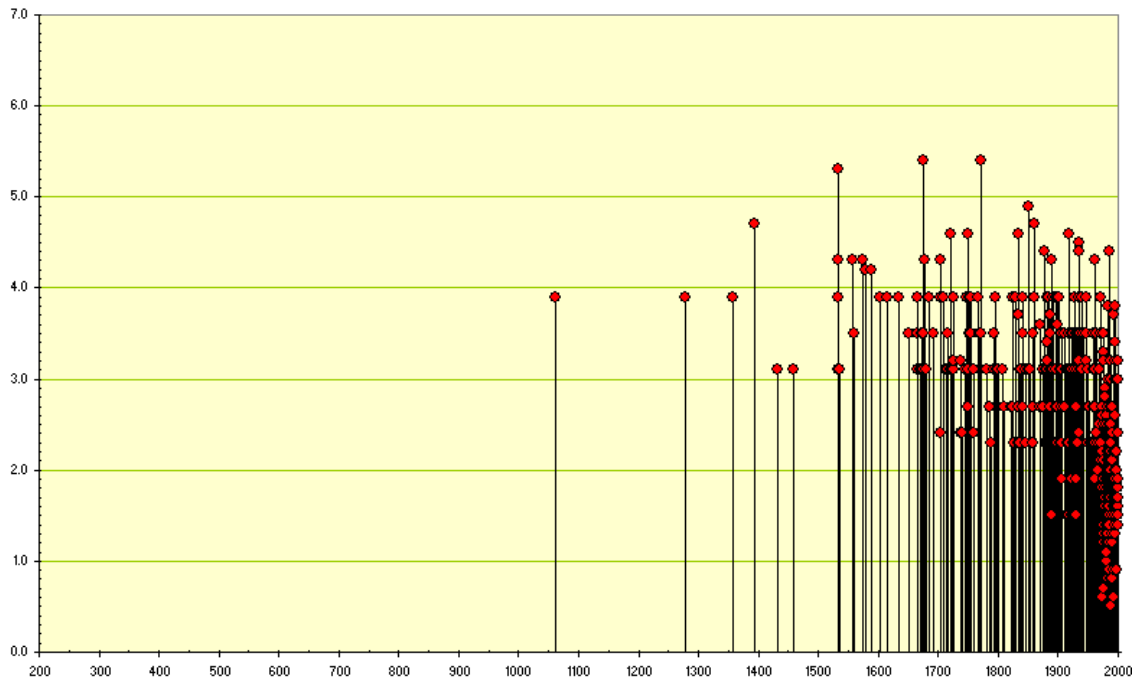
Fig. 21ai: Seismic history for zone ZUR2
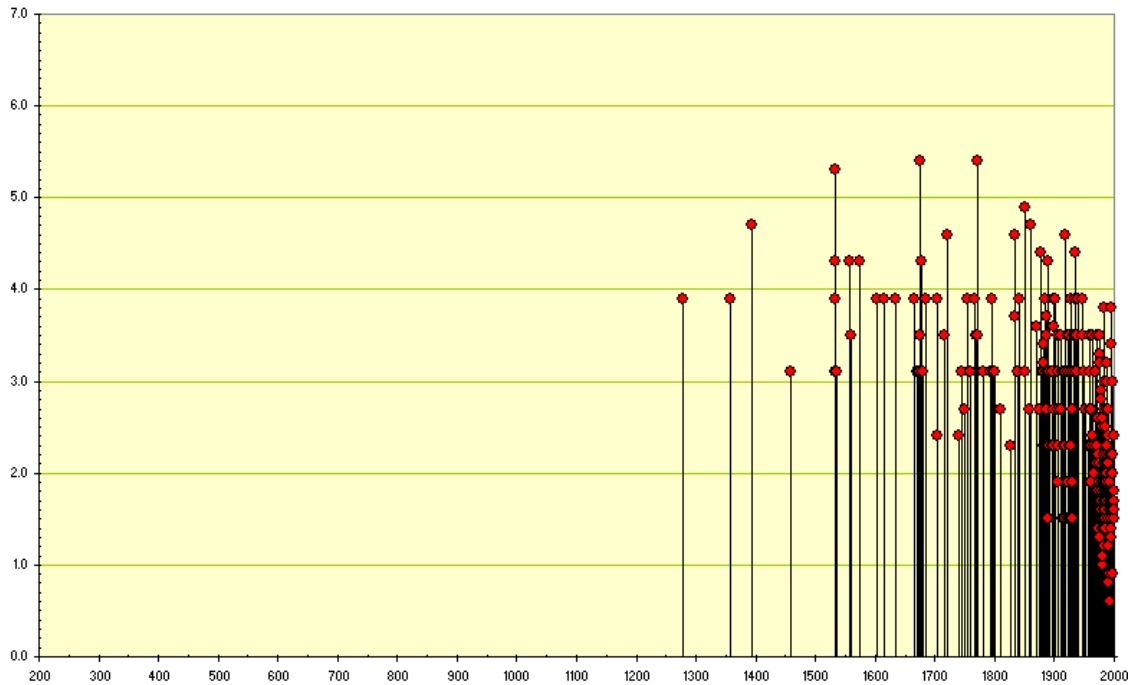
Fig. 21aj: Seismic history for zone ZURI
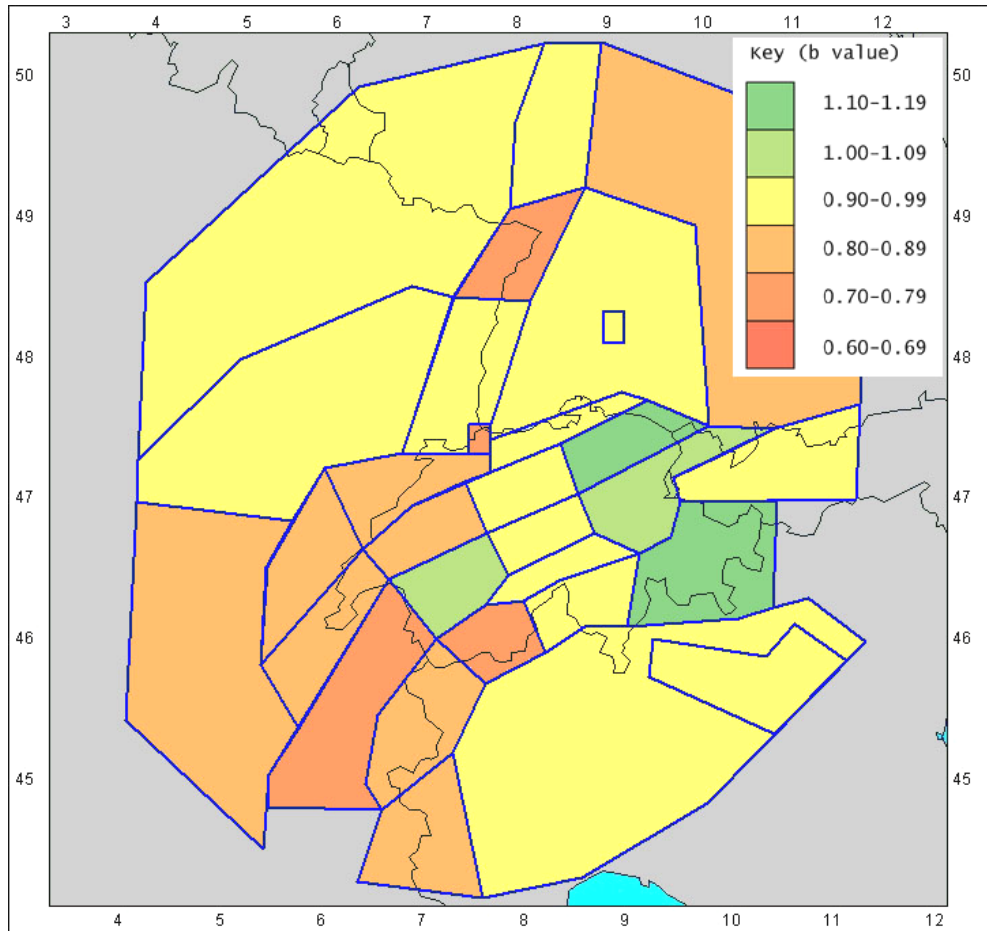
Fig. 22a: Distribution of *b* values for Branch A of the model
Only one zone configuration is shown.
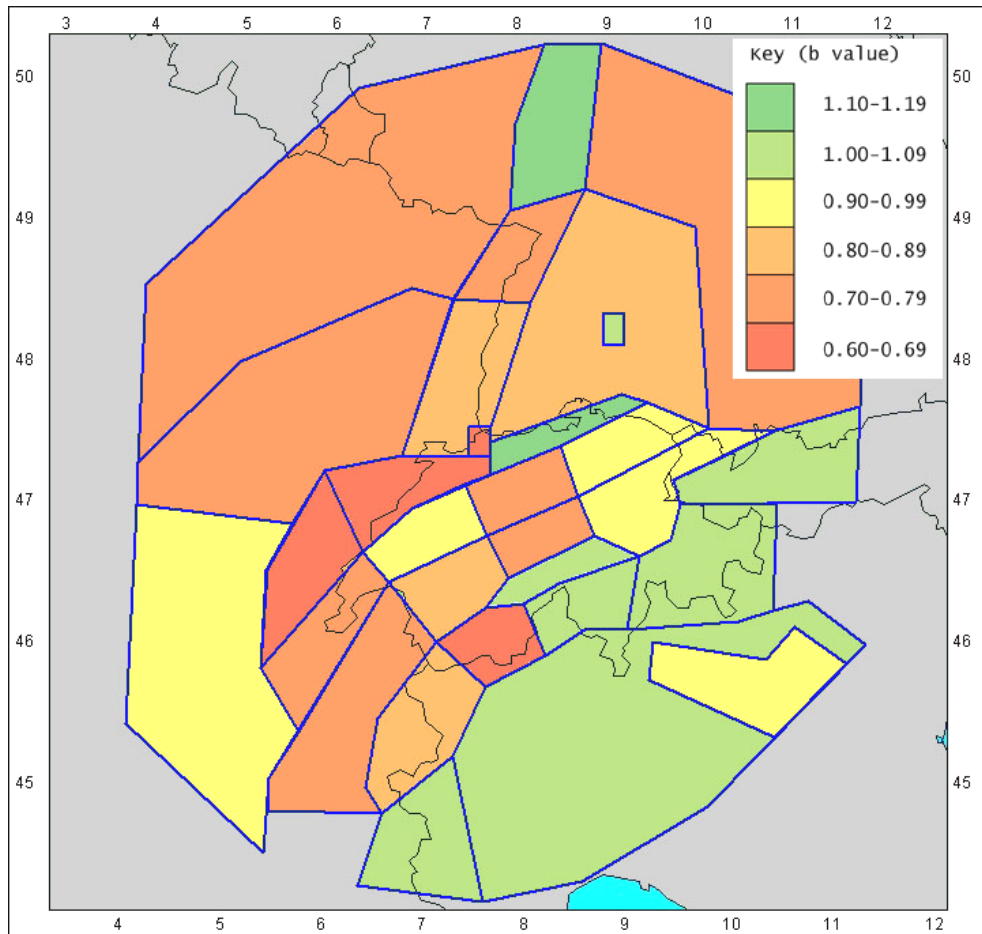
Fig. 22b: Distribution of *b* values for Branch B of the model

Only one zone configuration is shown. Values less than 0.6 are shown as 0.6.
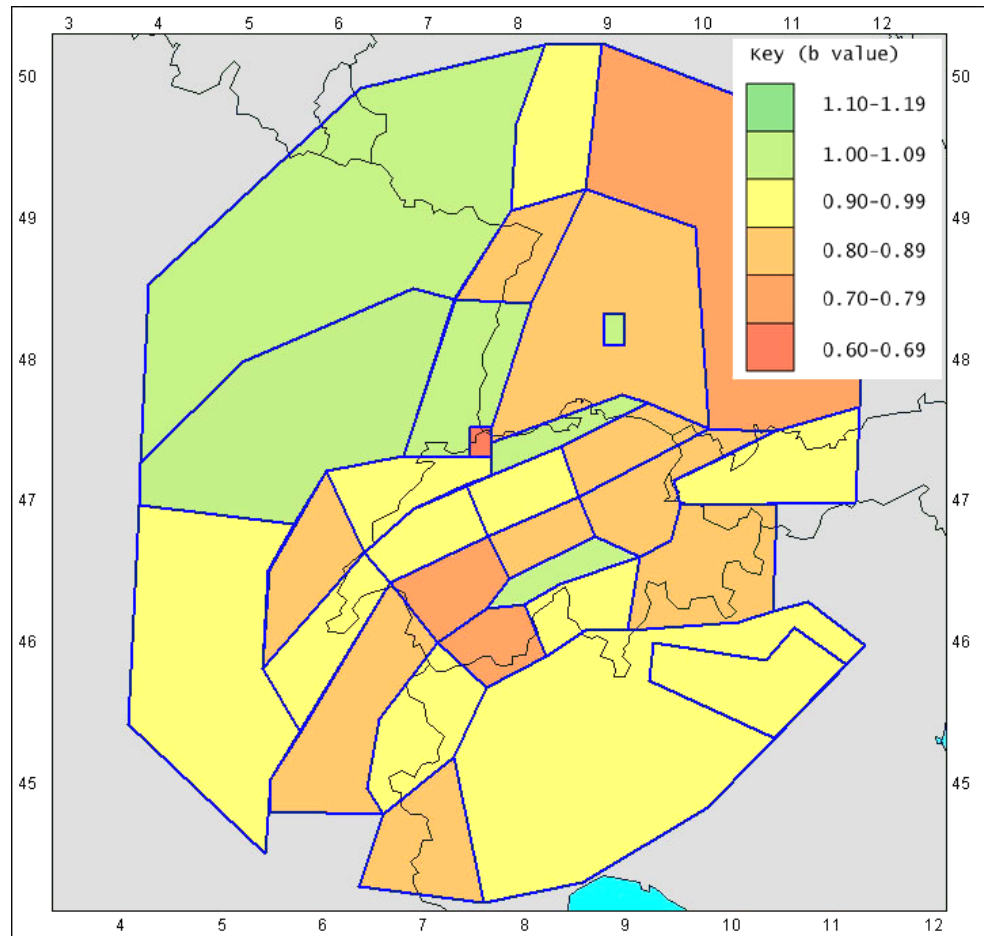
Fig. 22c: Distribution of *b* values for Branch C of the model

Only one zone configuration is shown. Values less than 0.6 are shown as 0.6.

10   ACKNOWLEDGEMENTS

11   REFERENCES

Abrahamson, N. 2000: State of the practice of Seismic Hazard Evaluation. Proc. GeoENG. 19-24 Nov 2000

Al-Tarazi, E. 1999: Regional seismic hazard study for the eastern Mediterranean (Trans-Jordan, Levant and Antakia) and Sinai region. Jnl. African Earth Sciences 28, 743-750.

Bender, B.K. & Perkins, D.M. 1987: SEISRISK III: a computer program for seismic hazard estimation. USGS Bulletin 1772.

Chandra, U. 1978: Seismicity, earthquake mechanisms and tectonics along the Himalayan mountain range and vicinity. Phys. Earth planet. Interiors 16, 109-131.

Cornell, C.A. 1968: Engineering seismic risk analysis, Bull. Seism. Soc. Am, 58, 1583-1606.

Deichmann, N., Baer, M., Braunmiller, J., Ballarin Dolfin, D., Bay, F., Delouis, B., Faeh, D., Giardini, D., Kastrup, U., Kind, F., Kradolfer, U., Kuenzle, W., Roethlisberger, S., Schler, T., Salichon, J., Sellami, S., Spuehler, E. & Wiemer, S. 2000: Earthquake in Switzerland and surrounding region during 1999. Eclogae Geol. Helv. 91/2, 395-406.

Eva, E., Solarino, S., Eva, C. & Neri, G. 1997: Stress tensor orientation derived from fault plane solution. Jnl. Geophys. Res. 102/B4, 8171-8185.

Eva, E. & Solarino, S. 1998: Variations of stress directions in the western Alpine Arc. Geophysical Journal International 135/2, 438-449.

Frankel, A., Mueller, C., Barnhard, T., Perkins, D., Leyendecker, E.V., Dickman, N. Hanson, S. & Hopper, M. 1996: National Seismic Hazard Maps: Documentation June 1996. U.S. Geological Survey Open-File Report 96-532, 44p.

Grünthal, G., Mayer-Rosa, D. & Lenhardt, W. 1998: Abschätzung der Erdbebengefährdung für die D-A-C-H-Staaten - Deutschland, Österreich, Schweiz. Bautechnik 10, 753-767.

Hough, S.E., Armbruster, J.G., Seeber, L. & Hough, J.F. 2000: On the Modified Mercalli intensities and magnitudes of the 1811-12 New Madrid earthquakes. J. Geophys. Res. 105, 23839-23864.

Jacob, K., Armbruster, J., Barstow, N. & Horton, S. 1994: Probabilistic ground motion estimates for New York: comparison with design ground motions in national and local codes. *In:* Proceedings of 5th U.S. National Conference on earthquake Engineering, Chicago III, 199-128.

Karnik, V. 1969 and 1971: Seismicity of the European Area, part I and II. D. Reidel Publishing Co., Dodrecht, Holland, 364p and 218p.

Kastrup, U. 2002: Seismotectonics and stress field variations in Switzerland. PhD Thesis ETHZ no. 14527, 153 p.

Kastrup, U., Zoback, M.L., Deichmann, N., Evans, K.F., Giardini, D. & Michael, A.J. 2004: Stress field variations in the Swiss Alps and the northern Alpine foreland derived from inversion of fault plane solutions. J. Geophys. Res. 109.

Levret, A., Backe, J.C & Cusching, M. 1994: Atlas of macroseismic maps for French earthquakes with their principal characteristics. Natural Hazard 10, 19-46.

Marchant, R.H. & Stampfli, G.M. 1997: Crustal and lithospheric structures of the Western Alps: geodynamic significance. *In:* Deep structure of the Swiss Alps – Results from NRP (Ed. by Pfiffner, O.A., Lehner, P., Heitzman, P.Z., Mueller, S. & Steck, A.). Birkhaueser AG., Basel, 326-337.

Meghraoui M., Delouis, B., Ferry, M., Giardini, D., Huggenberger, P., Spottke, I. & Granet, M. 2001: Active Normal Faulting in the upper Rhine Graben. Science 293, 2070-2073.

Meyer, B., Lacassin, R., Brulhet, J. & Mouroux, B. 1994: The Basel 1336 earthquake. Which fault produced it? Terra Nova 6, 54.

Meletti, C., Patacca E. & Scandone P. 2000: Construction of a Seismotectonic Model: The case of Italy. Pageoph 157, 11-35.

Mueller, S. 1997: The lithosphère-athenosphere System of the Alps. *In:* Deep structure of the Alps (Ed. By Pfiffner, O.A. et. al.). Birkhauser AG, Zürich, 338-347.

Mueller, W.H., Naef, H. & Graf, H.R. 2002: Geologische Entwicklung der Nordschweiz, Neotektonik und Langzeitszenarien Zürcher Weinland. Nagra Techn. Report NTB 99-08. Nagra, Wettingen, Switzerland.

Musson, R.M.W. 1997: Seismic Hazard studies in the U.K.: Source Specification Problems of Intraplate Seismicity. Natural Hazard 15, 105-119.

Musson, R.M.W. & Winter, P.W. 1996: Seismic hazard of the UK, AEA Technology Report No AEA/CS/16422000/ZJ745/005.

Musson, R.M.W. & Winter, P.W. 1997: Seismic hazard maps of the U.K. Natural Hazard 14/2-3, 141-154.

Musson, R.M.W. 1999: Probabilistic Seismic Hazard Maps for the North Balkan Region. Annali di Geofisica, GSHAP Special Volume 42/6, 1109-1124.

Musson, R.M.W. 2000: Generalised seismic hazard maps for the Pannonian Basin using probabilistic methods. Pageoph. 157, 147-169.

Musson, R.M.W. 2002: The significance of absent earthquakes: What is the weight of a historian's opinion? EOS Trans. AGU 83/47, Fall Meet. Suppl., pF1062.

Pavoni, N. 1961: Faltung durch Horizontal Verschiebung. Eclogae Geol. Helv. 54, 515-534.

Pavoni, N. 1975: Zur Seismotektonik des Westalpenbogens: Vermessung, Photogrammetrie. Kulturtechnik III/IV-75, 185-187.

PEGASOS EXT-TB-0033/35 2002: The PEGASOS Earthquake Catalogue (ECOS version 31.01.02).

Reasenberg, P. 1985: Second-order moment of Central Californian seismicity, 1969-1982. J. Geophys. Res. 90, 5479-5495.

Rüttener, E. 1995: Earthquake hazard evaluation for Switzerland. Matériaux pour la Géologie de la Suisse, Géophysique No 29 publié par la Commission Suisse de Géophysique. Schweizerischer Erdbebendienst, Zürich, 106 p.

Schmid, S.M. & Kissling, E. 2000: The arc of the western Alps in the light of geophysical data on deep crustal structure. Tectonics 19/1, 62-85.

Schumacher, M. 2002: Upper Rhine Graben: The Role of Pre-existing Structures Upper Rhine Graben: Role of preexisting structures during rift evolution. Tectonics 21/1.

Singh, R.P., Li, Q. & Nyland, E. 1990: Lithospheric deformation beneath the Himalayan region. Physics Earth planet. Interiors 61, 291-296.

Slejko, D. 2002: On the effect of different de-clustering methods on seismic parameter estimates. PEGASOS Technical note EG1-TN-0265.

Sommaruga, A. 1997: Geology of the central Jura and the molasses Basin. Mém. Soc. Neuch. SCc. Nat. XII. 176p.

Stepp, J.C. 1972: Analysis of completeness of the earthquake sample in the Puget Sound area and its effect on statistical estimates of earthquake hazard. International Conference on Microzonation, Proceedings 2, 897-910.

Thouvenot, F., Fréchet, J., Tapponnier, P., Thomas, J.-Ch., Le Brun, B., Ménard, G., Lacassin, R., Jenatton, L., Grasso, J.-R., Coutant, O., Paul, A. & Hatzfeld, D. 1998: The ML 5.3 Épagny (French Alps) earthquake of 1996 July 15: a long-awaited event on the Vuache fault. Geophys. J. Int. 135, 876-892.

Toro, G. 2003: Technical note on the treatment of hypocentral depths and rupture-length effects for area sources in the FRISK88MP Software. PEGASOS Technical Note TP1-TN-0373.

Veneziano, D. & Van Dyck, J. 1985: Seismic hazard methodology for nuclear facilities in the Eastern United States. EPRI Research Project Report P101-29.

Wahlström, R. & Grünthal, G. 2001: Probabilistic Seismic Hazard Assessment for Fennoscandia using the logic tree approach for regionalisation and non-regionalization models. Seis. Res. Lett. 72, 33-45.

Waldhauser, F., Kissling, E. Ansorge, J. & Mueller, S. 1998: 3D interface modeling with 2D seismic data: The Alpine crustal-mantle boundary. Geophys. J. Int. 135, 264-278.

Wells, D.L. & Coppersmith, K.J. 1994: New empirical relationships among magnitude, rupture length, rupture width, rupture area and surface displacement. Bull. Seism. Soc. Am., 84, 974-1002.

Woo, G. 1996: Kernel Estimation Methods for Seismic Hazard Area Sources. BSSA, 86, 2, 353-362.

APPENDIX 1:   EG1-HID-0040 HAZARD INPUT DOCUMENT, FINAL MODEL EXPERT TEAM Eg1c

This document describes the final seismic source model developed by Expert Team EG1c. The data files associated with this seismic source model are located in the zip file EG1-HID-0040_EG1c_data.zip.

A 1.1   Seismic Source Zonation

The basic seismic source model consists of areal source zones defined by simple polygons. Seismicity is assumed to be spatially homogeneous within these sources, with the exception of the distributed Basel source described below. The source zone files are located in directory: .\ZONES.

The seismic source zonation for team EG1c is described on Figures A1-1 through A1-5. Figure A1-1 shows the logic tree structure for source zonation. The tree consists of three levels. The first addresses whether the Rhine Graben should be treated as a single source (RHEG) or divided into three sources (RHGN, RHGC, and RHGS). These alternative sources are shown on Figure A1-2.

The second level addresses the treatment of the Swabian Jura active zone. In one model, the seismicity is confined to the distinct stationary source SWAB embedded in the larger zone BAWS or BW2S. These zones are shown on the right had side of Figure A1-3. Zone files BAWS and BW2S were created to be simple polygons wrapping around zone SWAB. The alternative model considers the elevated seismicity in SWAB not to be a stationary source, but rather may occur anywhere within the larger BAWU zones. As a result, just zones BAWU or BAW2 are used, as shown on the left of Figure A1-3. BAWU is equivalent to BAWS plus SWAB; BAW2 is equivalent to BW2S plus SWAB.

The third level addresses whether or not the permocarboniferous troughs are an active source zone or not. If they are an active, then source NSPG is used as a source zone and the Zurich and BAWU sources have configurations ZURI, BAWU or BAWS as shown on the bottom of Figure A1-3. If they are not an active, then the Black Forest source BLAF is used as a source zone and the Zurich and BAWU sources have configurations ZUR2, BAW2 or BW2S as shown on the top of Figure A1-3.

In addition, there are 22 sources whose boundaries are unaffected by the alternatives discussed above. These are shown on Figure A1-4.

The final source is the distributed Basel source. EG1c defined a source zone around the cluster of seismicity near Basel. However, they considered that the concentration was in part due the process of recording historical earthquakes and the seismicity should be dispersed outward from the modeled source zone using a Gaussian decay in rate over a distance of 30 km, with a standard deviation of 10 km. Polygon DBASL.ZON was created to encompass the distributed Basel source (Figure A1-5). The seismicity rate varies spatially within this source. File DBASL.XYG contains a grid of longitude-latitude pairs with the fraction of the total rate for the source that is assigned to each grid point. Note that this spatial grid overlaps the adjacent sources by intent.

As indicated on the right hand side of Figure A1-1, the above alternative models lead to eight different source sets. These are listed in Table A1-1. The first row of the table lists the source set "UC" that includes the 22 zones shown on Figure 4 plus DBASL. These sources do not change with the alternative zonations and are to be included in each set.

Tab. A1-1:   EG1c seismic source sets

Source Set	Sources
UC (unchanging)	DBASL, ALCM, ALMA, BAVA, BRES, DAUP, FRIB, GARD, GENV, GLAR, GRAU, HELV, JURA, LORA, MOMI, NIDW, PENV, POVA, SAVO, SBRE, SJUR, TICI, TYRO
R1S1G1	RHGN, RHGC, RHGS, SWAB, BAWS, NSPG, ZURI + UC
R1S1G2	RHGN, RHGC, RHGS, SWAB, BW2S, BLAF, ZUR2 + UC
R1S2G1	RHGN, RHGC, RHGS, BAWU, NSPG, ZURI + UC
R1S2G2	RHGN, RHGC, RHGS, BAW2, BLAF, ZUR2 + UC
R2S1G1	RHEG, SWAB, BAWS, NSPG, ZURI + UC
R2S1G2	RHEG, SWAB, BW2S, BLAF, ZUR2 + UC
R2S2G1	RHEG, BAWU, NSPG, ZURI + UC
R2S2G2	RHEG, BAW2, BLAF, ZUR2 + UC

Rhine_Graben	Swabian_Jura	Permocarbon	Source_Set
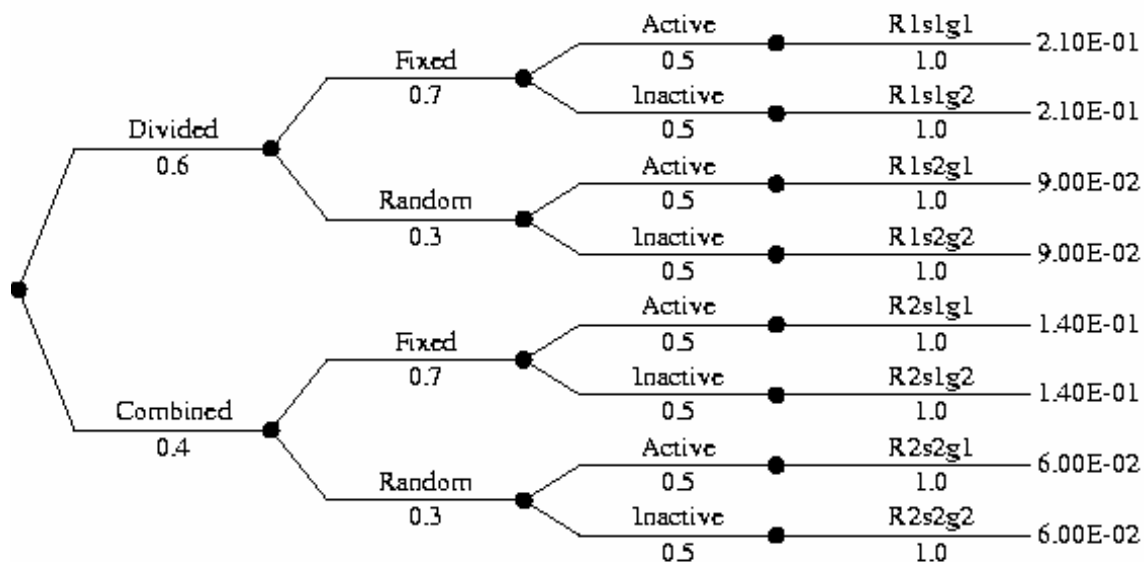
Fig. A1-1:   Logic tree for EG1c seismic source zonation
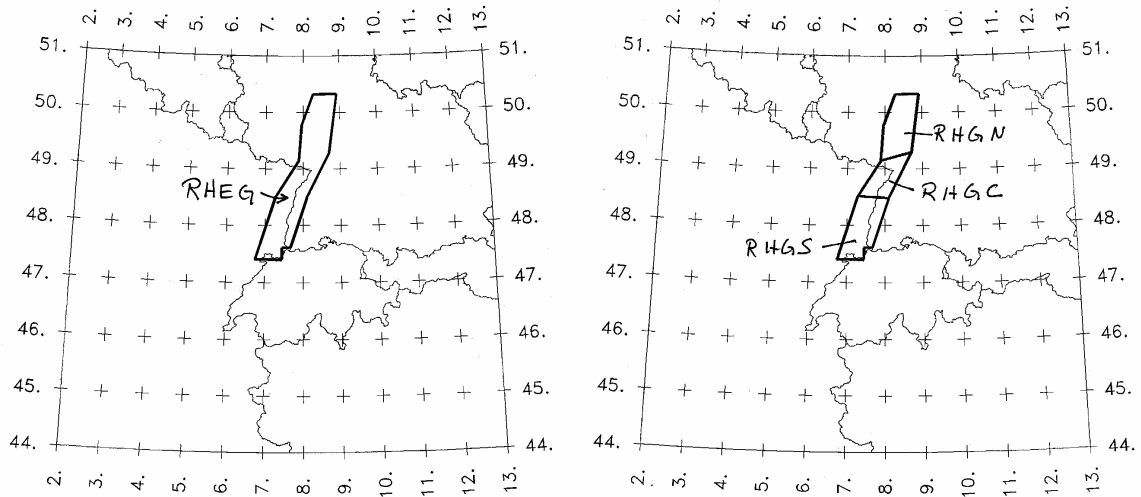
Fig. A1-2:   EG1c alternative source zonations of the Rhine Graben
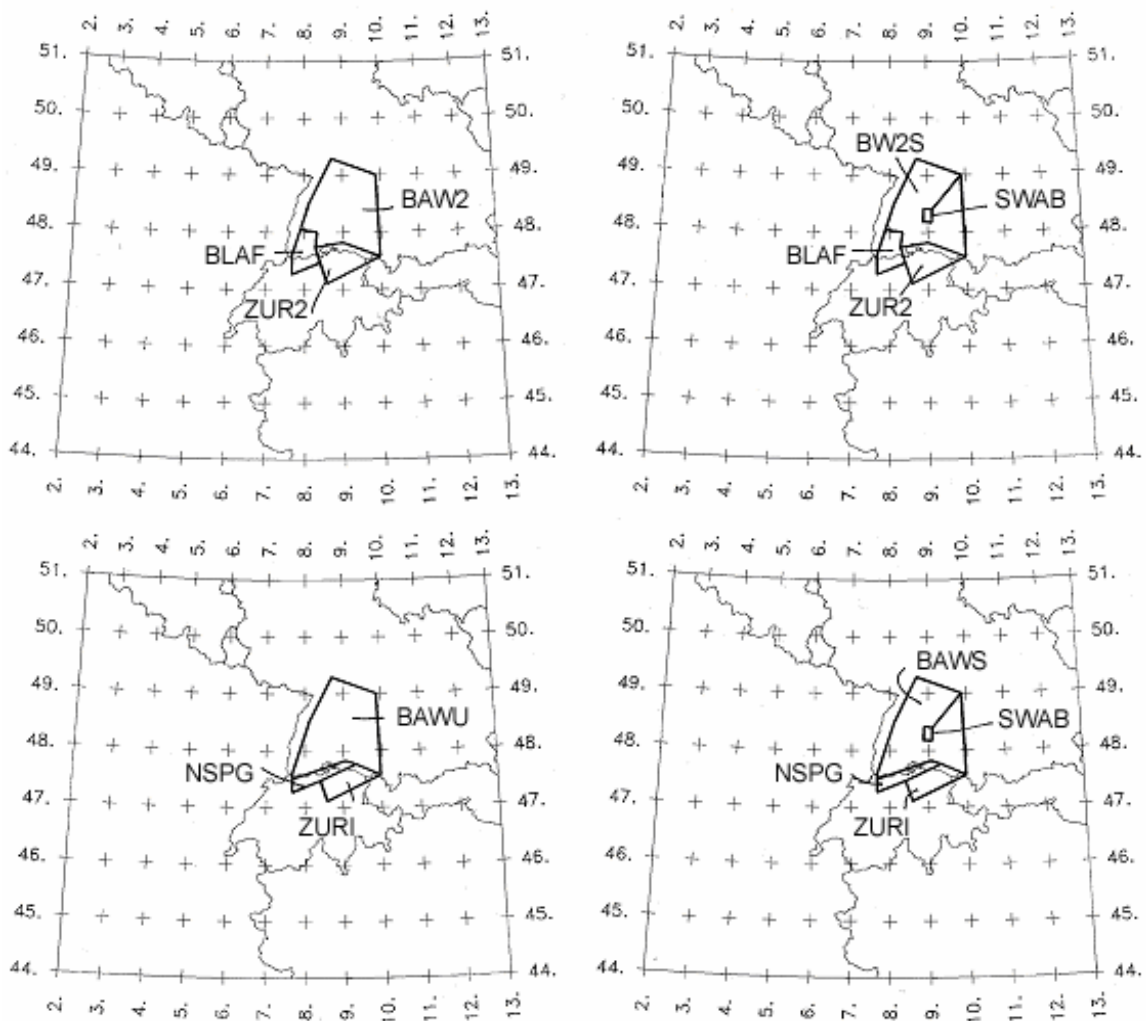
Fig. A1-3:   EG1c alternative source zonations for the Swabian Jura and Permo-Carboniferous troughs
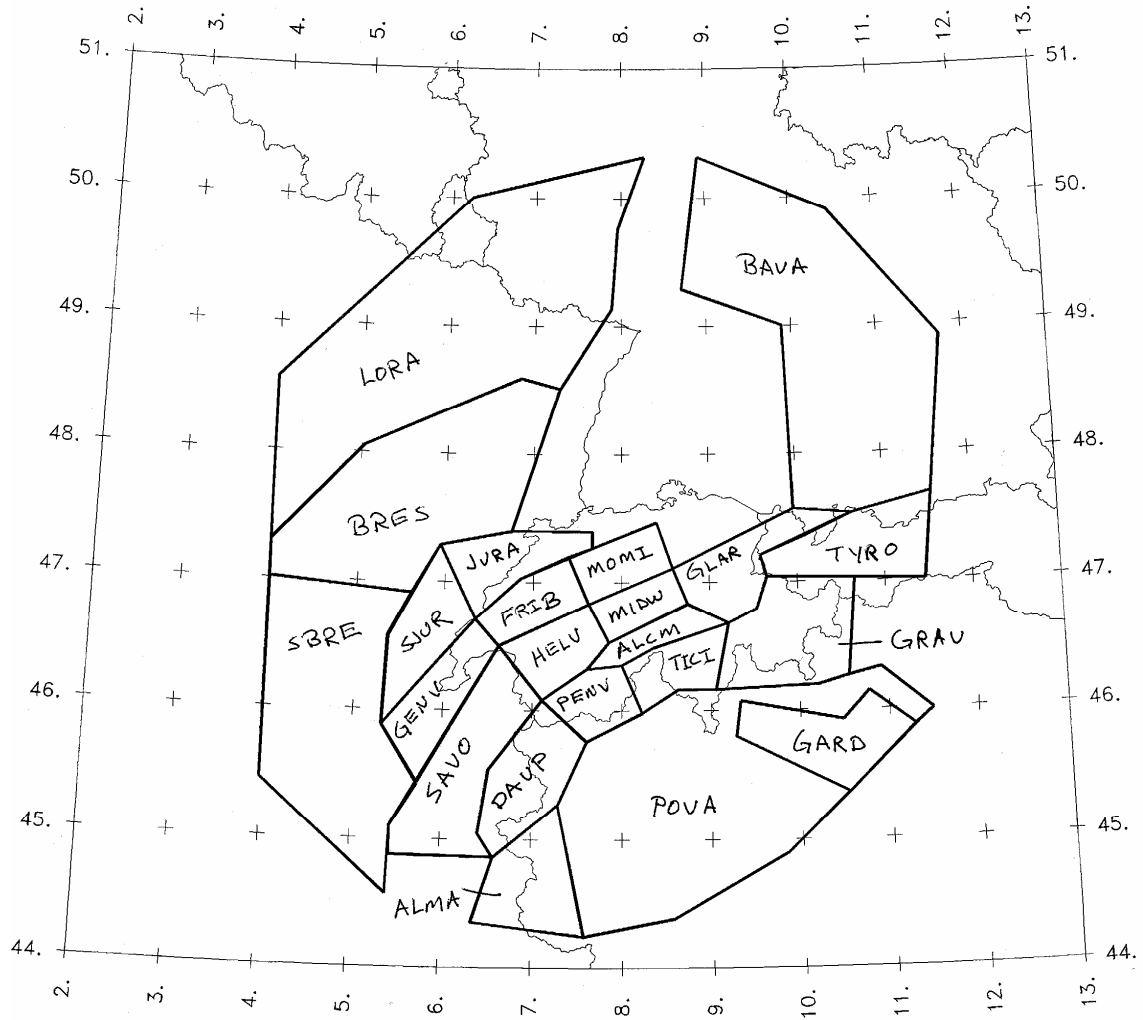
Fig. A1-4:   EG1c source zones that do not change with the alternatives listed on Figure A1-1
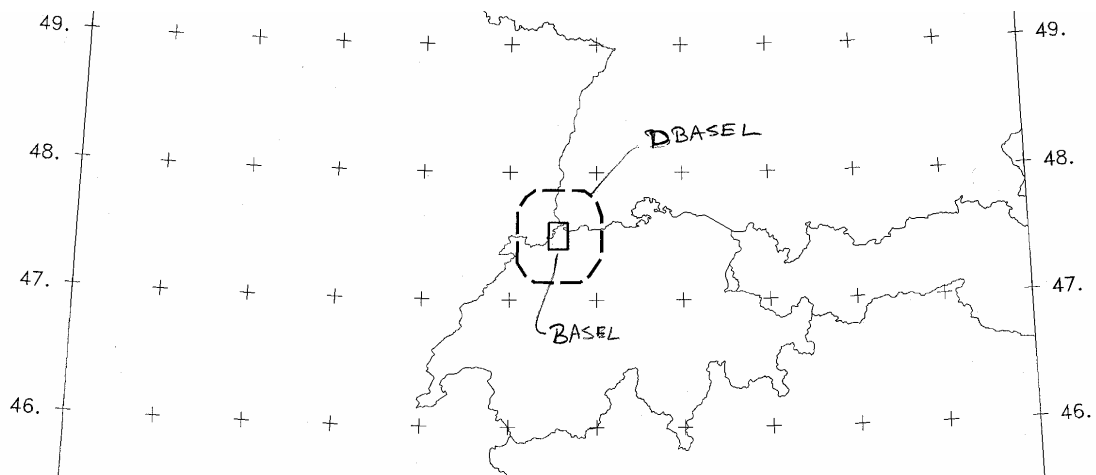
Fig. A1-5:   The nominal BASL polygon and the limits of the distributed Basel source, DBASL

A 1.2   Earthquake Rupture Geometry

The size of earthquake ruptures is defined by the relationship:

$$\text{Mean } \log_{10}(\text{rupture area}) = 1.04M\text{-}4.31$$

$$\sigma_{\log10(\text{rupture area})} = 0.24$$

Using the relationship for the expectation of a lognormal distribution, the mean (expected) rupture area is given by the relationship:

$$\text{mean rupture area} = 10^{(1.04M - 4.244)}$$

The relationship for the mean rupture area will be used in the hazard computations. The rupture length and width have an aspect ratio of 1:1 until the maximum rupture width for a source is reached. The maximum rupture width is determined on the basis of the maximum depth and fault dip, as defined below. For larger ruptures, the width is held constant at the maximum width and the length is obtained by dividing the rupture area by this width.

Earthquake epicenters are uniformly distributed within each source except for the distributed Basel source DBASL where a spatial density grid is provided. Earthquake ruptures are located symmetrically on the epicenters (the epicenter is at the midpoint of the rupture). For those epicenters located closer than ½ rupture length to the source zone boundary, the ruptures are allowed to extend beyond the source boundary except for the following cases. Figure A1-6 shows regional boundaries that ruptures cannot cross. Because the sites of interest are all located within the central region where ruptures can cross source boundaries, the objective of Figure A1-6 can be achieved by truncating ruptures at the source boundaries for sources RHEG, RHGS, BRES, SBRE, LORA, POVA, and BAVA. This will prevent ruptures originating outside of the central region from crossing the heavy boundaries on shown of Figure A1-6 and extending closer to the sites. The boundary condition for each source is listed in Table A1-2.

Table A1-2 defined the relative frequency of rupture orientations and styles of faulting for the individual sources. Two specific styles of faulting are considered for larger events (> M 5.5), strike-slip and reverse. A possible third condition may exist in which the specified fraction of earthquakes are to have random orientation (uniform distribution for azimuth) and random style of faulting (equally likely to be strike-slip or reverse faulting). The relative frequency of styles of faulting and rupture orientation for the larger earthquakes specified in Table A1-2 are to be used for all earthquakes.

The depth distribution of hypocenters for small events is defined by a trapezoidal distribution with the parameters listed in Table A1-3. Listed are the minimum and maximum depths and the upper and lower depths for the plateau in the trapezoidal distribution. Figure A1-7 shows an example distribution. For larger earthquakes, a magnitude-dependent depth distribution is to be developed using the weighted approach outlined in PEGASOS Technical Note TP1-TH-0373 (Gabriel Toro, May 19, 2003) with T = 0.5 (hypocenter in lower half of rupture).
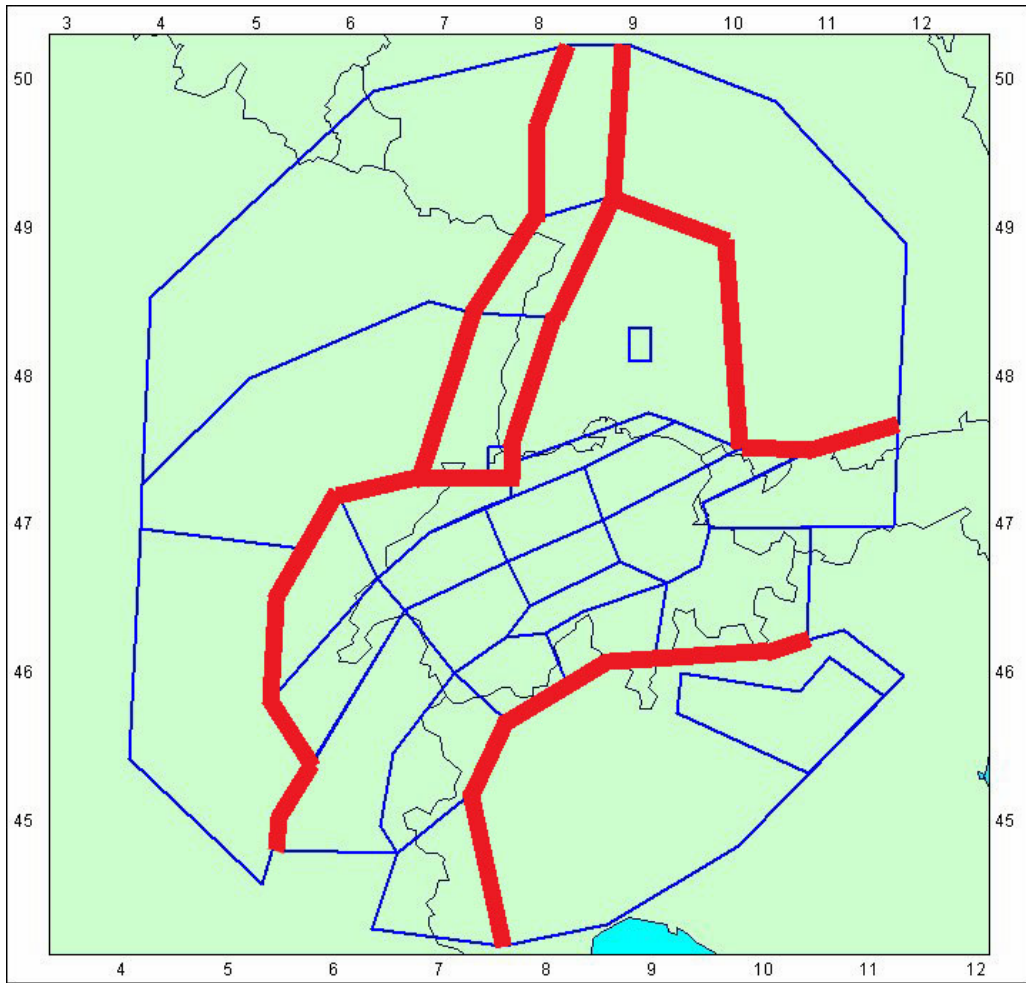
Fig. A1-6:   Restrictions on propagation of fault rupture

The darker blue sources have boundaries that may not be crossed by ruptures, except in the case of events originating from the BASL (DBASL) source.
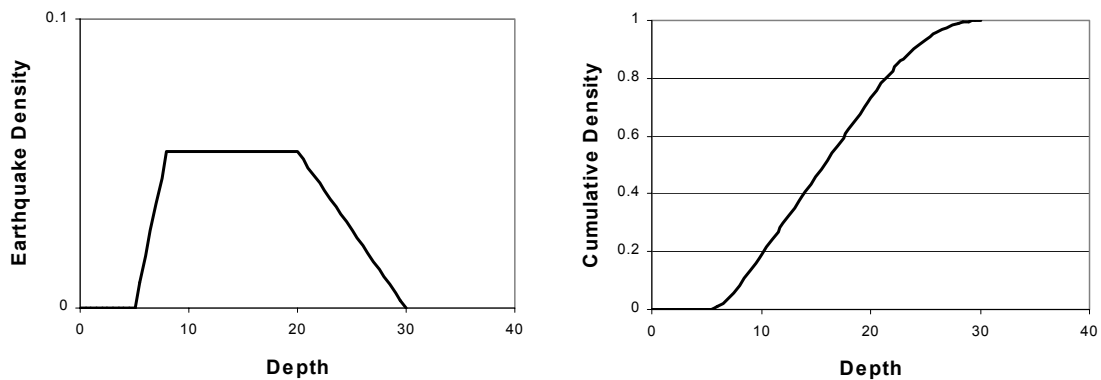
Fig. A1-7:   Example depth distribution with a minimum depth of 5, upper plateau depth of 8, lower plateau depth of 20, and a maximum depth of 30

Tab. A1-2:   Rupture orientation, style of faulting, and source boundary conditions

*First number is the relative frequency and second number is the rupture orientation. Note that strike-slip earthquakes have a dip of 90 degrees and reverse earthquakes have a dip of 45 degrees to the south, southeast, or east, depending on the strike.

Source	Strike Slip*	Reverse*	Random	Ruptures can cross Source Boundary
DBASL	0.4, N20E	0.4 N75E	0.2	Yes
RHEG	1.0, N20E	0	0	No
RHGN	1.0, N20E	0	0	Yes
RHGC	1.0, N20E	0	0	Yes
RHGS	1.0, N20E	0	0	No
LORA	0	0	1.0	No
BRES	0	0	1.0	No
SBRE	0	0	1.0	No
BAVA	0	0	1.0	No
SWAB	1.0, N10E	0	0	Yes
BAWU	0	0	1.0	Yes
BAW2	0	0	1.0	Yes
BAWS	0	0	1.0	Yes
BW2S	0	0	1.0	Yes
BLAF	0	0	1.0	Yes
NSPG	0	0.6, N75E	0.4	Yes
ZURI	0.1, N20E	0.4, N75E	0.5	Yes
ZUR2	0.1, N20E	0.4, N75E	0.5	Yes
MOMI	0.1, N20E	0.4, N60E	0.5	Yes
FRIB	0.1, N00E	0.4, N50E	0.5	Yes
JURA	0.1, N00E	0.4, N50E	0.5	Yes
SJUR	0.1, N10W	0.4, N40E	0.5	Yes
GENV	0.1, N10W	0.4, N40E	0.5	Yes
GLAR	0.1, N00E	0.6, N60E	0.3	Yes
NIDW	0	0.7, N60E	0.3	Yes
HELV	0	0.7, N50E	0.3	Yes
SAVO	0	0.7, N10E	0.3	Yes
GRAU	0	0	1.0	Yes
TICI	0	0	1.0	Yes

Source	Strike Slip*	Reverse*	Random	Ruptures can cross Source Boundary
PENV	0	0	1.0	Yes
DAUP	0	0	1.0	Yes
ALMA	0	0	1.0	Yes
ALCM	0	0	1.0	Yes
TYRO	0	0	1.0	Yes
GARD	0	0	1.0	Yes
POVA	0	0	1.0	No

Tab. A1-3: Hypocenter depth distribution parameters

Source	Minimum	Upper Plateau	Lower Plateau	Maximum
DBASL	5	8	20	30
RHEG	5	8	20	30
RHGN	5	8	20	30
RHGC	5	8	20	30
RHGS	5	8	20	30
NSPG	3	8	20	30
BAVA	5	8	15	30
BAWU	5	8	15	30
BAW2	5	8	15	30
BAWS	5	8	15	30
BW2S	5	8	15	30
SWAB	5	8	15	30
BLAF	5	8	15	30
MOMI	5	8	20	30
ZURI	5	8	25	30
ZUR2	5	8	25	30
FRIB	5	8	20	30
GENV	5	8	20	30
JURA	5	8	15	20
SJUR	5	8	15	20
ALCM	3	6	12	20
GLAR	3	6	12	20

Source	Minimum	Upper Plateau	Lower Plateau	Maximum
NIDW	3	6	12	20
HELV	3	6	12	20
SAVO	3	6	12	20
DAUP	3	6	12	20
PENV	3	6	12	20
TICI	5	6	12	20
GRAU	3	6	12	20
TYRO	5	8	15	30
BRES	5	8	15	25
LORA	5	8	15	25
SBRE	5	8	15	25
ALMA	5	8	15	50
GARD	5	8	15	50
POVA	5	8	15	50

A 1.3   Earthquake Recurrence Parameters

The alternatives for defining the maximum magnitude and earthquake recurrence parameters are shown on Figure A1-8. The approaches for assessing maximum magnitude and recurrence parameter distributions are linked as indicated in the logic tree, resulting in three sets of parameter distributions. Note that for all sources, a truncated exponential earthquake recurrence relationship is used to define the relative frequency of earthquakes of different sizes.

The first set consists of a directly assessed single distribution for maximum magnitude that is applied globally to all zones: M_{max} being 6.5 Mw (weighted 0.2), 7.0 Mw (weighted 0.6) and 7.5 Mw (weighted 0.2). Individual M_{max} distribution files for each source zone are contained in subdirectory .\RECMOD1.MMX. These individual source zone M_{max} distributions are dependent across all sources, that is M_{max} in all sources is simultaneously either 6.5, 7, or 7.5. The accompanying joint distributions for beta [b-value $\times \ln(10)$] and $N(m \geq 5)$ are determined using a maximum likelihood formulation for an exponential distribution with a global prior derived from the whole catalogue and computing relative likelihoods. Individual distribution files for each source zone are contained in subdirectory .\RECMOD1.ABD. The recurrence parameter distributions for each zone are independent. This set of parameters corresponds to the path through the logic tree (Figure A1-8) designated by "Global" for M_{max} approach, "Direct Assessment" for M_{max} method and "PML Global Prior" for recurrence method.

The second set consists of individual source M_{max} distributions computed using a sample likelihood function based on the maximum observed event and the number of earthquakes in the zone. The likelihood function is truncated at a maximum of 7.3 in order to generate a proper probability distribution. Individual M_{max} distribution files for each source zone are contained in subdirectory .\RECMOD2.MMX. The accompanying joint distributions for beta [b-value $\times \ln(10)$] and $N(m \geq 5)$ are determined using a maximum likelihood formulation but instead of a moderate prior derived from the whole catalogue (as in branch A), strong local priors were used for

each zone, derived from least-squares analysis. Individual distribution files for each source zone are in subdirectory .\RECMOD2.ABD. This set of parameters corresponds to the path through the logic tree (Figure 8) designated by "Local" for M_{max} approach, "Likelihood" for M_{max} method and "PML Local Prior" for recurrence method.

The third set consists of the results of a joint Monte Carlo simulation of $N(m \geq 5)$, *b*-value, and M_{max}. Examination of the results indicates that M_{max} has a low correlation with *b*-value, and can thus the distribution for M_{max} can be considered essentially independent of that for $N(m \geq 5)$ and *b*-value. Accordingly, marginal distributions for M_{max} were computed from the results. Individual M_{max} distribution files for each source zone are contained in subdirectory .\RECMOD3.MMX. The accompanying joint distributions for beta and $N(m \geq 5)$ are given in individual distribution files for each source zone in subdirectory .\RECMOD3.ABD. This set of parameters corresponds to the path through the logic tree (Figure A1-8) designated by "Local" for M_{max} approach and "Simulation" for the M_{max} and recurrence methods.

Mmax_App	Mmax_Method	Rec_Method
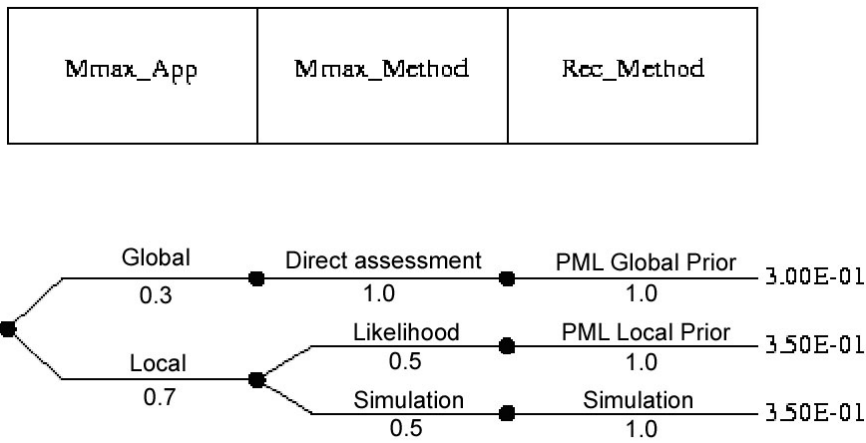
Fig. A1-8:   EG1c maximum magnitude and earthquake recurrence parameter logic tree
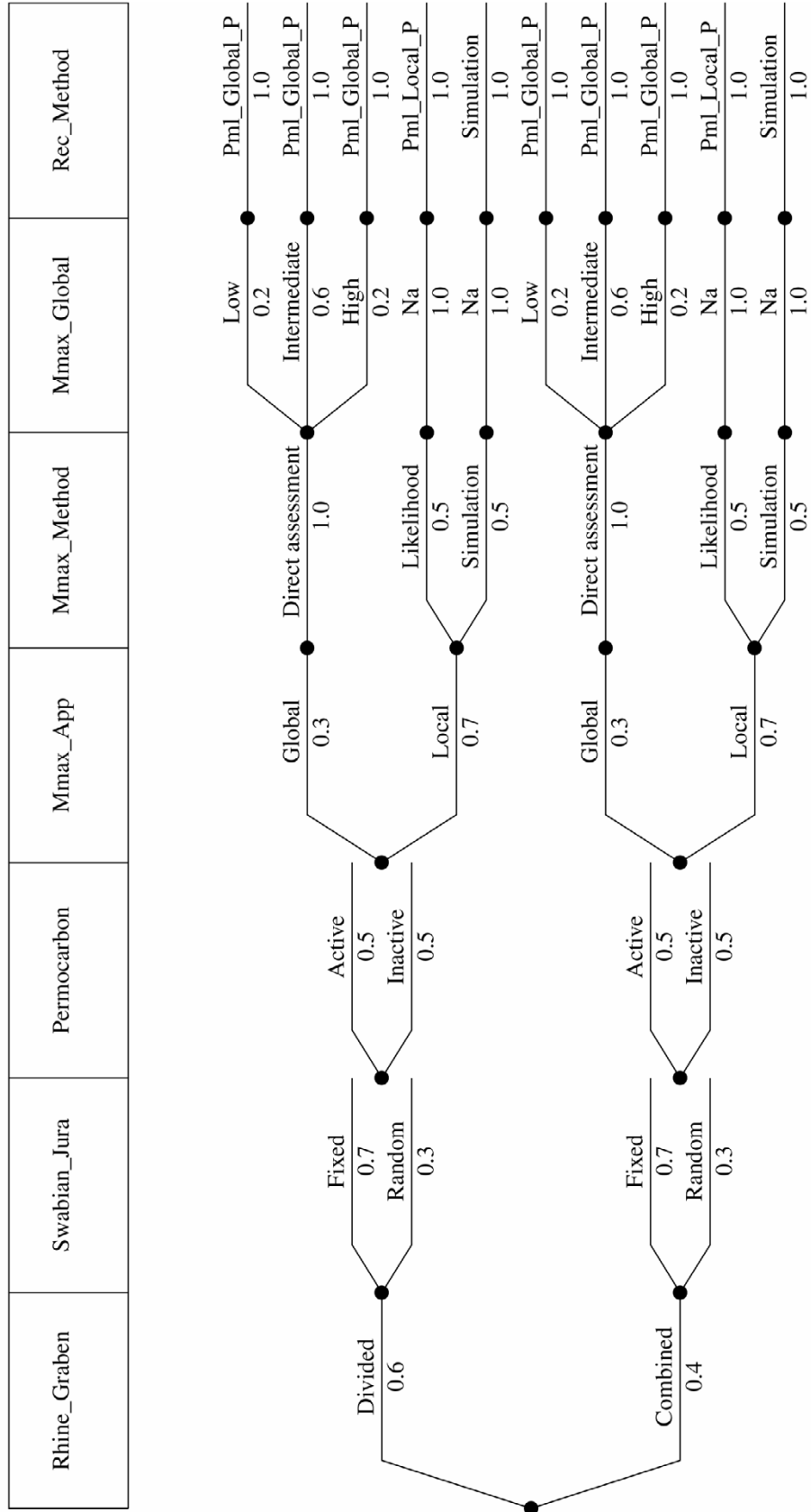
Fig. A1-9:   Logic tree for EG1c

APPENDIX 2: QA-CERTIFICATE FOR EG1-HID-0040

QA Certificate for Hazard Input Documents

QA Certificate | **PEGASOS PROJECT**

Hazard Input Document (HID)

Expert group:	EG1c	**HID designation:**	**EG1-HID-0040**
Expert:		**Expert Model (EXM)**	EG1-EXM-0026

HID parameterisation of Expert Model:

TFI: K. Coppersmith **Hazard Input Specialist of TFI-team:** B. Youngs

HID based on Elicitation Documents: ☒ EG1-ES-0040

HID based on Expert Assessments: ☐

Remarks on the HID model parameterisation in terms of hazard computation input:

This HID supercedes EG1-HID-0034_EG1c. The change is to make the Mmax distributions dependent across all sources for the global assessment branch (Figure 8)

The undersigned Hazard Input Specialist confirms that this HID includes all required (subproject specific) input information for hazard computations. No further interpretations of this input will be required and no simplifications except Algorithmic Pinching according to paragraph 2.9 of the QA-Guidelines will be applied to convert this HID into hazard software Input Files.

Signature: *Robert R Youngs*

HID acceptance by the Expert / Expert Group:

Date of HID review by the Expert / Expert group:

HID accepted: ☑   **HID not accepted:** ☐

Reasons for non-acceptance of HID / Recommendations:

The undersigned Expert(s) accept(s) the parameterisation proposed in this HID as a faithful and adequate representation of his/their Expert Model. He/they confirm(s) that this HID is free of errors and agree(s) to its use as hazard computation input.

Signature Expert 1 / Expert:

Signature Expert 2: *17.10.0*

Signature Expert 3:

QA-TN-0287 HID acceptanc form rev 02.doc

Part IV:

SP1 Seismic Source Characterisation, Elicitation Summary

Expert Team EG1d

Prof. Dr. Jean-Pierre Burg

Institute of Geology
ETH Zentrum NO G 46.1
Zürich – Switzerland

Dr. Mariano García-Fernández

Spanish Council for Scientific Research
Institute of Earth Sciences 'Jaume Almera'
Department of Geophysics and Tectonics
Barcelona – Spain

Dr. Stefan Wiemer

Swiss Seismological Service
Institute of Geophysics
ETH Hoenggerberg, HPP P,
Zürich – Switzerland

Probabilistische Erdbeben-Gefährdungs-Analyse für die KKW-Stand Orte in der Schweiz
(PEGASOS)

SP1 Seismic Source Characterisation

Elicitation Summary

Expert Team EG1d

Jean-Pierre Burg

Institute of Geology / ETH Zentrum
Zürich – Switzerland

Mariano García-Fernández

Spanish Council for Scientific Research / Institute of Earth Sciences 'Jaume Almera' /
Department of Geophysics and Tectonics
Barcelona – Spain

Stefan Wiemer

Swiss Seismological Service / Institute of Geophysics / ETH Hoenggerberg
Zürich – Switzerland

TABLE OF CONTENTS

LIST OF TABLES

LIST OF FIGURES

1 INTRODUCTION

In this elicitation summary, we develop one out of four seismogenic source models to be used by the PEGASOS project for site-specific probabilistic seismic hazard analysis at the Swiss nuclear power plant sites. The following elicitation summary takes in thorough consideration the requirement that all views expressed in the technical community and known to the EG1d team should be presented and balanced. However, while trying to weight alternative interpretations according to their scientific solidity, these interpretations inevitably reflect our own judgment. We tried to discuss in sufficient detail all relevant issues, such that our though processes is transparent to the reader. We pay particular attention to the treatment of uncertainties.

Before starting to develop our seismogenic model, the available sources of significant data were evaluated and prioritized with respect to their usefulness for source zonation in the framework of the PEGASOS project. We implemented the following data classification scheme:

− <u>A: Most Useful</u>. Immediately leads to specific source zones.

− <u>B: Moderately Useful</u>. Can aid in designing source zones and for consistency check of the zoning.

− <u>C: Marginally Useful</u>. Has little to no-value for source zonation in the framework of the PEGASOS project.

Below we classify the relevant data source accordingly, and we explain briefly the reasoning for our assessment (more details are given in the different sections of the Summary).

<u>Class A: Most Useful</u>

1. <u>Large-scale geological / rheological units</u>: Differences between crustal-scale units seem meaningful, since they coincide with differences in earthquake depth distribution (transition crystalline Alps – Alpine Foreland) (Deichmann 1992, Deichmann et al. 2000), differences in the density of earthquakes (PEGASOS TEP-CAT-0004, 0005, 0007 and PEGASOS EXT-TB-0043 2002), and differences in isostatic behavior (PEGASOS TP1-TEC-0004 and 0005). Major boundaries between these regions show no signs of recent activation in historical or geological data.

2. <u>Past Seismicity records</u>:

   − *Paleoseismicity:* 'Paleoseismic' events older than 3 Ma are considered to provide no pertinent information for current earthquake hazard. Younger, Holocene evidence is more critical.

Concerns:	Available paleoseismic evidence seems to be sparse, fragmented, incomplete, and uncertain in both space and magnitude (PEGASOS EXT-TB-0050 2002, Schmid 2002 TP1-RF-0162, Meghraoui et al. 2001, Becker et al. 2002). Owing to such drawbacks, we considered it to be of medium relevance for a country such as Switzerland at the present level of knowledge (reclassified as Class B).

- *Historical information:* While highly relevant, recurrence of large events remains difficult to establish based on the historical data due to the low to moderate level of seismic activity in the region. Uncertainty in magnitude and location is important and most likely large. While the available working catalogue (PEGASOS TP1-CAT-0004, PEGASOS EXT-TB-0043 2002) provides qualitative uncertainty values, these may not capture the aleatory and epistemic uncertainty entirely. In this context, the most relevant event in the Swiss catalogue, the 1356 Basel earthquake, does not seem to play any particular role regarding recurrence relationships and activity rates (e.g., to define characteristic earthquakes). We believe that the historical record is relatively too short to be relied upon solely in a region like Switzerland, which has a moderate to low seismicity with long recurrence intervals.

- *Instrumental seismicity*: Important to estimate depth distribution of seismicity (e.g., Deichmann et al. 2000), it is insufficient to obtain recurrence relationships and activity rates based only on the instrumental record, because there is no evidence that the activity of small earthquakes (most of the instrumental data) can define future large activity. It is also questionable to use the recent small events instrumentally recorded to define active faults with potential to generate large earthquakes in the future.

- *Focal mechanism*: The available focal mechanism solutions (Deichmann 2002a, PEGASOS EXT-TB-0042 and PEGASOS TP1-TEC-0010) are considered only as subsidiary information, because of open scaling questions (i.e. relationship between mechanism of small and large events), short record, non-unique correlation with faults, heterogeneity of the stress field (Kastrup et al. 2002), and uncertainties in the solutions. However, they can be useful to define potential for reactivation of existing faults, for general style-of-faulting, and to check consistency of zoning (reclassified as Class B).

Class B: Moderately useful

1. Hot springs (PEGASOS TP1-STR-0015): Hot springs inform on regions where water circulates deep and fast in the crust and their alignments across lithological boundaries are known to delineate major fracture zones, some of them going down to Moho depth. Their correlation with recent seismic activity is questionable, but such alignments are important for large-scale zoning because they point to crustal fractures, i.e. weak contacts prone to eventual reactivation. Still there is the problem of the interaction between fluids and seismicity, which remains unclear, or at least there is not a direct relationship. In addition, they do not yield a complete set of major fracture zones; other fracture zones, devoid of hot springs and water circulation, may exist.

2. Vertical movements, geodetic data, strain data (PEGASOS TP1-TEC-0004 and 0005): Geodetic data helps defining in our understanding broad regional patterns, unless specific and detailed measurements for individual faults exist, which is not the case in Switzerland. Yet, this information indicates seismic potential. In Switzerland and in neighboring areas, rates are homogeneous and overall very low (PEGASOS TP1-TEC-0004 and 0005), consistent with GPS measurements. Strain rates are low and do not yield evidence for strain localization on the surface: The average total convergence rate between Africa and Europe for the past 49 Ma is about 0.9 cm/a (Regenauer-Lieb & Petit 1997), which is in good agreement with the rate of 0.94 cm/a for the past 3 Ma, as implied by NUVEL-1 (DeMets et al. 1990). These numbers are reasonably consistent with long-term geological strain rates. Vertical movements are too small to distinguish isostatic due to post-glacial rebound from tectonic signals.

3. <u>Faults</u>: Numerous faults are identified on geological maps at all scales (e.g., PEGASOS TP1-STR-0003), which reveal an equal potential for earthquakes almost everywhere. In the literature, there is no convincing evidence for Quaternary movements that has offset topography and post-glacial features (e.g., Eckardt et al. 1983). Generally, these features do not correlate with observed seismicity. The Molasse Basin is less faulted than the Jura, a character that may indicate that Molasse sediments behave less brittle than surrounding rock units and a remark that we use for broad zoning. In fact, the fault distribution assigns the fracture potential to broad zones.

4. <u>Shallow seismic profiles</u> (TP1-STR-0006): Seismic lines help constraining the deformation ages if no signs of disturbance in the youngest sediments are time significant (thickness 2 sec, about 4 km, several Ma). An alternative is that fractures did not propagate upward into less brittle rocks, which brings some moderation to the previous assertion. From the existing information, the boundaries of the Carboniferous troughs appear to be important crustal discontinuities. <u>Problem:</u> Fragmented, limited information gives statistically biased view. The role of creep versus seismogenic deformation is unclear. Maps of basin depths are somewhat relevant for zooming, in that they show the distinction of late Paleozoic sediments – distribution of basement and sedimentary rocks. Thin-skin versus thick-skin faulting seems to us not immediately relevant for seismotectonic zonation, because its influence on hazard is not clear.

5. <u>Paleostress measurements</u>: Paleostress measurements have limited value because they are extremely imprecise in direction, shape of stress ellipsoid (hence stress regime) and age significance. In addition, stress fields older than the recent Quaternary are not pertinent to the project purposes. However, fault behaviors documented by paleostress studies were included in the general discussion on style-of-faulting with respect to stress directions (Homberg et al. 1994, Homberg et al. 1997).

6. <u>In situ stress measurements</u> (PEGASOS TP1-TEC-0002): In our assessment, there are relatively few data available, which are reasonably consistent with focal mechanisms. They show that the uppermost continental crust of Switzerland presently is mostly under nearly N-S compression. A broad stress field is consistent across the entire region, including the Rhine Graben, but different regions are dominated by different fault orientations. However, no local information is available for detailed zonation taking into account stress field variations. The lack of local information is limiting the relevance to broad scale zonation and for assessing the potential for reactivation under given stress regime.

7. <u>Deep seismic profiles, P- and S-wave velocity structure</u>: The regional velocity structure may in our assessment identify areas of potential deep activity. From tomographic studies and reflection / refraction seismology, a good knowledge of P-wave velocities down to the Moho exists (Husen et al. *in press*). The S-wave velocity structure, however, is largely unknown. In addition, it is not clear how these velocities relate to seismic potential, because ruptures can cut across velocity transients.

<u>Class C: Marginally useful</u>

1. <u>Moho depth</u> (PEGASOS TP1-STR-0004): The Moho surface in the study region is a regional feature that smoothly and regularly deepens southward. To the north of the Alps, it clearly is the bottom boundary of the seismogenic crust. However, it remains unclear how it can be used for zoning since in our assessment, there is no immediate correlation between seismic hazard and Moho depths. However, the Moho topography could play a significant role in the definition of regional attenuation models for Switzerland.

2. <u>Thickness of the sedimentary cover</u> (PEGASOS TP1-STR-0008 – 0012): The vertical distribution of seismic events indicates that the seismic behaviors of the sedimentary cover and the crystalline basement are grossly similar, with the exception of the Molasse basin, which seems to be less seismically active. In itself, the bathymetry of the sedimentary cover appears to have little value.

3. <u>Topography</u> (PEGASOS TP1-STR-0007): While topography in some regions of the world correlates weakly with seismic potential, it does in our assessment not provide a suitable basis for zonation in Switzerland that goes beyond an Alpine – Foreland – Rhine Graben classification. Therefore, we consider its value limited.

4. <u>Potential fields</u> (Gravimetry, Magnetism) (PEGASOS TP1-STR-0016, TP1-STR-0018 and TP1-STR-0019): Potential fields provide in our assessment regional, large-scale information. Their relevance for zonation is limited because the link between seismic hazard and potential fields is not clear. We attempted to integrate potential field for finding broad regional structures, however, they provided no additional constraints for our zonation efforts.

2   SEISMOTECTONIC FRAMEWORK

In this chapter, we briefly describe the seismotectonic framework that provides the guiding principles for our zonation.

−   Contemporary tectonic processes: The region of interest is characterized by localized deformation of brittle rock in the slow convergence zone (rates < 10 mm/a) between Europe and Adria. We are not in a 'pure' intraplate environment. The observed moderate to low seismicity rates, when compared to seismically much more active plate boundary interfaces, are consistent with the low deformation rate imposed by the tectonic system. This regime has been active for at least 1 Ma, probably 5 Ma or more, and we expect it to be similar for the foreseeable future. A high heat flow (thermal anomaly) underneath the crystalline Alps (PEGASOS TP1-STR-0014) restricts the seismogenic depth in this region to about 15 km (e.g., Deichmann et al. 2000).

−   Tectonic models: Several distinctive geological and rheological units are exposed to a broad regional stress / strain field. Within these large regions, seismic potential is, to a first order approximation, homogeneous, and seismicity is diffuse. Localized stress concentrations, fluid interactions, zones of weaknesses etc., give raise to persistent or temporary clusters of activity. In most cases, geological and geophysical reasons for clusters are unclear, and it is uncertain if historically observed activity centers will remain stationary.

−   Thin- versus thick-skinned structural interpretations: The concept is fundamentally geo-metrical and has essentially been applied to foreland fold-and-thrust belts to derive rules of thrusting (e.g., Boyer & Elliott 1982). Fold-and thrust belts are typical of most mountain belts and reflect shortening of the upper crust. However, deformation may involve basement (thick-skinned), or be limited to the sedimentary cover, which is detached from the base-ment (thin-skinned). In the Alps, the discussion has some importance concerning the bulk development of frontal zones such as the Jura Mountains, in which most of the deformation might be localized along a basal décollement, and in the post-Triassic sedimentary cover where thrust sheets deform internally by folding (e.g., Sommaruga 1999). The thin- versus thick-skin interpretation has consequences on the interpretation of the bulk shortening in Miocene to Pliocene times. It has less importance regarding the instantaneous, present-time deformation linked to seismicity. Recorded seismicity shows that the seismogenic defor-mation is equally distributed over the whole thickness of the European crust in the foreland area, and within the upper 15 km of the Alpine hinterland. Nowhere is the seismicity under-lining a preferred décollement plane. The geometrical concept is apparently irrelevant to seismogenic interpretations and it seems more reasonable to accept that seismicity in verti-cal sections reflects, as in map view, distributed strain of the brittle crust. The ductile crust, expected to underlay the hinterland, is not seismogenic because it is too warm, or because strain rates are too slow. The implication for source models is seismogenic homogeneity down to the lower seismogenic level.

−   Spatial distribution of seismicity: Spatial seismicity distribution (and related activity rates) clearly separates two regions: A higher seismic activity, shallow depths, in the crystalline zone in the south, and lower activity rates in the Molasse / Jura (e.g., Deichmann et al. 2000). Clusters of persistent activity exist within both zones, but these refer to a very short time period covering the last decades only. Assuming stationarity of seismicity, the past observed rates of seismicity are a guidance of the distribution of seismicity, but it is uncer-tain how stationarity can be expanded in future time. The Molasse rocks are poor in seismic events, in particular for high magnitudes. This observation fits rheological expectations as weak sediments dominate the bulk material. Conversely, basement faults, such as the Fribourg strike-slip fault (PEGASOS TP1-STR-0020), are reactivated and are potential

sources. The Fribourg fault is known thanks to its recorded activity over the last few decades yet is one structure of many of its sort that are inferred to exist by correlation with basement outcrops, or known to exist thanks to seismic surveys. The implication is that faults like the Fribourg one may begin activity at any time below the Molasse sediments and the Jura Mountains.

−   Focal mechanisms do in our assessment not particularly help in defining specific source zones, because they contain some imprecision in location, there is a limited sample, and the relationship or correspondence between small and large events is questionable. However, they provide some indication concerning local stress regimes under which the present seismic activity takes place and the orientation of faults that are activated today. Accordingly, focal mechanisms are useful guides to balance stress regimes and style-of-faulting likely to occur along given fault orientations (Deichmann 2002a, PEGASOS EXT-TB-0042 and PEGASOS TP1-TEC-0010), whether the moving fault planes are reactivated or created.

−   Usefulness of stresses / strains: Stress and strain measurements in the study region (PEGASOS TP1-TEC-0002, Regenauer-Lieb & Petit 1997) are important, because they provide constraints on maximum magnitude and total seismic energy release over the region. However, because of low strain rates, which are near the resolution limit of modern GPS based campaign, stress and stain measurements provide little insight into recurrence intervals or energy release of individual faults or fault zones. This is a major difference to active plate boundaries, where strain based model can provide important constraints on seismic hazard.

−   Assessment of reactivation of existing structures: Major fault boundaries are possible candidates to be reactivated, depending on their orientation to the general stress field and/or to local stress regimes. This point is highly relevant since the Fribourg strike slip fault demonstrates reactivation of old basement fractures (PEGASOS TP1-STR-0020, Müller et al. 2002). Reactivation potential concerns therefore any basement fault, and in particular the major transcurrent fault zones that bound Permo-Carboniferous trough identified from geophysical surveys below the Molasse basin (Neuchâtel, Northern Switzerland). It also concerns major faults that formed during the Alpine orogeny and Cenozoic extension responsible for both the Rhine and the Bresse graben on the European lithosphere (e.g., Schumacher 2002).

− M_{max}, b-values: In our assessment, we see no possibility for alternative zoning based on M_{max} or the magnitude-frequency distribution (b-value) on their own. M_{max}, is described later, is very uncertain and hence poorly suited for zonation. There is no accepted model of spatial b-value variations that are also stationary through time and which could be used for zonation.

3   SEISMIC SOURCE DEFINITION

3.1   Principles of zonation

Below, we outline the guiding principles we apply in our zonation.

The question of areal sources versus line sources: In our assessment, there is no convincing evidence for active faults and no slip rates on known faults in the study region. Consequently, we see no possibility to treat them separately. Major geological / rheological boundaries are not dramatically active faults at current, and may have not been especially active for 1 – 5 Ma. There is no reason to assume preferential activation of these structures in the immediate future.

Expert conclusion:	Therefore, areal sources capture best the diffuse nature of the observed seismicity in the studied region.

The question of stationarity: The most critical underlying questions for zoning is stationarity, the degree to which future seismicity will follow the past patterns. We are referring in this context to spatial stationarity, although spatial and temporal stationarity express themselves similarly in seismicity records. This determines largely which zoning strategy should be applied:

1. Large regional zones,
2. small source zones, or
3. a smoothed seismicity approach (also called 'historical approach').

We contend that the degree to which stationarity holds in general, and in the study region in particular, is unknown. The applicability of the stationarity approach also depends on the length of the forecast period: For short periods (days to years) stationarity may be more appropriate, for longer periods (millennia+) areal zoning may be the more accurate forecast. For the purpose of the PEGASOS project, we are looking for a forecast for the next 30 – 50 years, but at a low probability level.

The 'historical approach' versus the areal zonation: The strength of the historical approach ─ 'historical approach' in our use of the term is equivalent to a spatially smoothed seismicity, kernel smoothing, or 'Frankel method' (Veneziano et al. 1984, Frankel 1995, Frankel et al. 1997); however, similar results can be achieved using small areal sources and soft boundaries ─ is the development of a probabilistic forecast based on an optimal statistical representation of the past seismicity. Its main weakness is the underlying assumption of stationarity, and the reliance on a complete seismicity record. The strength of the areal zonation based on seismotectonic information (Cornell 1968, Giardini 1999) is the ability to integrate additional geological and geophysical knowledge. Its weakness is the possible ambiguity and subjectivity of the interpretations (Frankel 1995), and the main hypothesis of seismically homogeneous source zones, i.e. uniform distribution of seismicity. Both approaches have been widely used in PSHA studies, and are defendable in our case study. We believe both should be used in our source modeling as a way to express epistemic uncertainty in PSHA approaches, representing our aforementioned concepts of stationarity.

Expert decision:	Because the degree of spatial stationarity is unknown for the study region, it seems reasonable to represent different models of stationarity (from areal source zoning to spatially smoothed seismicity) as logic tree branches in order to capture the epistemic uncertainty introduced by the different models.

Expert decision:	We attempt to integrate alternative conceptual models regarding spatial stationarity into one model by designing broad source regions based mainly on seismotectonics and having variable degrees of smoothing within and across these regions.

Large scale versus small scale zonation: While it would be desirable to design small zones for higher resolution, individual zones not based solely on seismicity need to be based on reasonable and defendable assumptions. Smaller scale variations in seismicity are best represented using the historical approach.

Expert decision:	Our zonation relies mainly on large zones, which expresses our interpretation that in a setting of diffuse seismicity such as Switzerland, seismic potential over broad regions is comparable, and that fluctuations seen in earthquake density within zones may be a temporary fluctuation with limited predictive value.

Source boundary properties and their meaning: We preferred to define boundaries that have together a geological, a rheological, a geophysical (field gradients) and a seismic significance. As such, the zone boundaries delineate major contacts that can be identified in any geological map. Their attitude essentially refers to structural and geophysical information. Their dip has uncertainties that bear some importance in the boundary regions (for example, an epicenter may represent a focus deeper than the shallow dipping contact between the zone in which it plots and the neighboring, source zone). Other uncertainties are related to the interaction between zones, provoking some seismicity where accommodation problems between different geological / seismogenic zones stem.

Characterization of faults versus zones: Avoiding bias due to the use of known active faults was further motivation for large 'predictive' zones. There is in our opinion no convincingly demonstrated geomorphology that can be linked to any specific fault activity younger than the last glaciation event (with the possible exception of the Reinach fault), mostly because fractures associated with soil creeping or instability on steep mountain slopes can mimic fault traces. Consequently, none of the faults reported on geological maps and in the literature can be considered as potentially more seismogenic than the others. In the case of the Reinach Fault, recent, well-publicized work (Meghraoui et al. 2001) has drawn much attention that over-amplifies its real importance as a potential source, because several other recent faults mapped in the Basel area may also be the actual source of the 1356 Basel earthquake. Uncertainties in terms of location in both map view and depth do not allow identifying the actual location of this historical event.

Background probability: The role of background zones in our modeling is to express the general view that in the studied tectonic domain, moderate to large earthquakes (M 7) can occur anywhere with a small probability. This is true for any continental region, worldwide. Our model covers the entire map with no gaps; hence there is no need for a separate background zone.

Energy conservation: The summed moment release over the historic record, which is consistent with the observed geological strain rates in the study region, needs to be conserved over time.

<u>Uncertainty</u>: In geological structures and broad scale features, uncertainties are small, which results in little need for a range of models, i.e., hard boundaries. Exception: The Helvetic Front, whose surface trace coincides with the limit of the European foreland and the Alps, the two major domains characterized by a depth difference in seismicity: owing to its variable dips measured on the surface, the Helvetic Front is treated as a soft boundary (10 – 15 km width). Uncertainty in epicenters and hypocenters is more critical, but reasonably well quantified. Uncertainty in location and magnitude should be taken care of with a Monte Carlo approach in the rate and *b*-value computation.

<u>Faulting styles</u>: Faulting style includes relative movements along fault planes along with the predicted orientation of ruptures within each areal source zone. Therefore, faulting style should take into consideration the regional strain / stress field as well as its local perturbations. Focal mechanisms provide instantaneous information; yet, they do not give access to the integrated bulk pattern. This discrepancy in time scale on several mechanisms governing strain, thus seismogenic deformation, leaves open a broad uncertainty concerning faulting style. Concerning relative movements, the faulting style is simplified to three end members, i.e. thrusting, strike-slip and normal faulting. The three of them accommodate strain and may be coeval, depending on the fracture orientation, and may combine. Concerning the predicted orientation of ruptures, we assume that the local state of stress will tend to cause shear fracture in accordance with the Mohr-Coulomb criterion. In this case, the acute angle between conjugate faults is bisected by the greatest principal stress σ_1. The Mohr-Coulomb criteria implies that the yield envelope is a line of slope $\tan\phi$, with ϕ the angle of internal friction, then the angle between σ_1 and each fault plane is $45 - \phi/2$. Of paramount importance is the orientation of the greatest principal stress σ_1. Therefore, our assessment takes into consideration the focal mechanisms along with the dominant fault pattern reported in each area. Jura, Europe, Rhine Graben: Preferably strike slip (70 %). Overall 30 % normal in the Rhine Graben / Jura, 15 % thrusting and 15 % normal, south of the Helvetic Front. Table 1 offers a more detailed assessment of the faulting styles in the source zones designed by us.

Consequences:	We design regional zones based on large structures. Our zoning strategy is to separate zones only if convincing evidence demands it. Different degree of smoothing within regions / zones and across the boundaries represents the stationarity hypothesis.

Tab. 1:   Faulting styles for the source zones

Region	Strike slip [%]	Normal [%]	Thrust [%]
Europe (NEW, SWA, FKZ, TZ)	85	5	10
Southern Rhine Graben	75	20	5
Northern Rhine Graben	85	10	5
Jura (J)	75	5	20
Italy (SA)	70	10	20
Alps (SA, XWCA, XHHA, HA, XHA, XCA, XWA)	70	15	15

3.2 Areal source zone design

The zoning models are graphically presented in Appendix 1. Below we discuss the reasoning behind the decisions made.

1) Helvetic Front: Alpine Foreland and Alps proper: The major separation between the Alpine Foreland and the Alps proper is based on:

1. Depth distribution of events (Deichmann 1992, Deichmann et al. 2000) in Figures 1 and 2,
2. geological information (geological maps of Switzerland, PEGASOS TP1-STR-0001 and 0002), and
3. density of the seismic events.

This boundary, the Helvetic Front, is readily seen on any geological map with different rock units to the south and to the north, i.e. lithologies with different rheological / mechanical properties. The tectonic contact zone dips towards the south at an angle of 30 to 45°. A broad thermal anomaly (Jaboyedoff & Pastorelli 2003, and references herein) may limit the depth distribution of the seismic events since the seismogenic (brittle) crust is constrained to be about 20 km thick underneath the Alps proper, in contrast to the > 30 km seismogenic thickness to the north. The seismic activity along the Helvetic Front is apparently contained within the Alps proper rather than in the Foreland.

> Scientific conclusion: The Helvetic Front is a major crustal boundary that separates two distinctly different source zone environments.

Representation in the Source Model:

− The seismogenic depth differs, i.e. there are two separate depth profiles north and south of the Helvetic Front boundary. For computing the depth distribution, we used a relocated dataset of high quality hypocenters, provided by Husen (Husen et al. *in press*). The resulting depth distributions are listed in Table 2.

− We discussed two tree branches as end members:

a) Interface vertical, acceptably representing the thermal anomaly.
b) Interface dipping 30° S down to 30 km, the depth of the Moho surface documented in the region (PEGASOS TP1-STR-0004), seismicity is mostly within the southern block. However, because the boundary is far from the investigation sites, and because of subsequently discussed hypocenter uncertainty, smoothing of seismicity, and gradients applied to express boundaries (soft borders), this uncertainty is secondary and already expressed through these concepts.

> Expert decision: Therefore, from the discussion above, we decided to use vertical boundaries only.

Reproduziert mit Bewilligung des Bundesamtes für Landestopographie (BA002935)
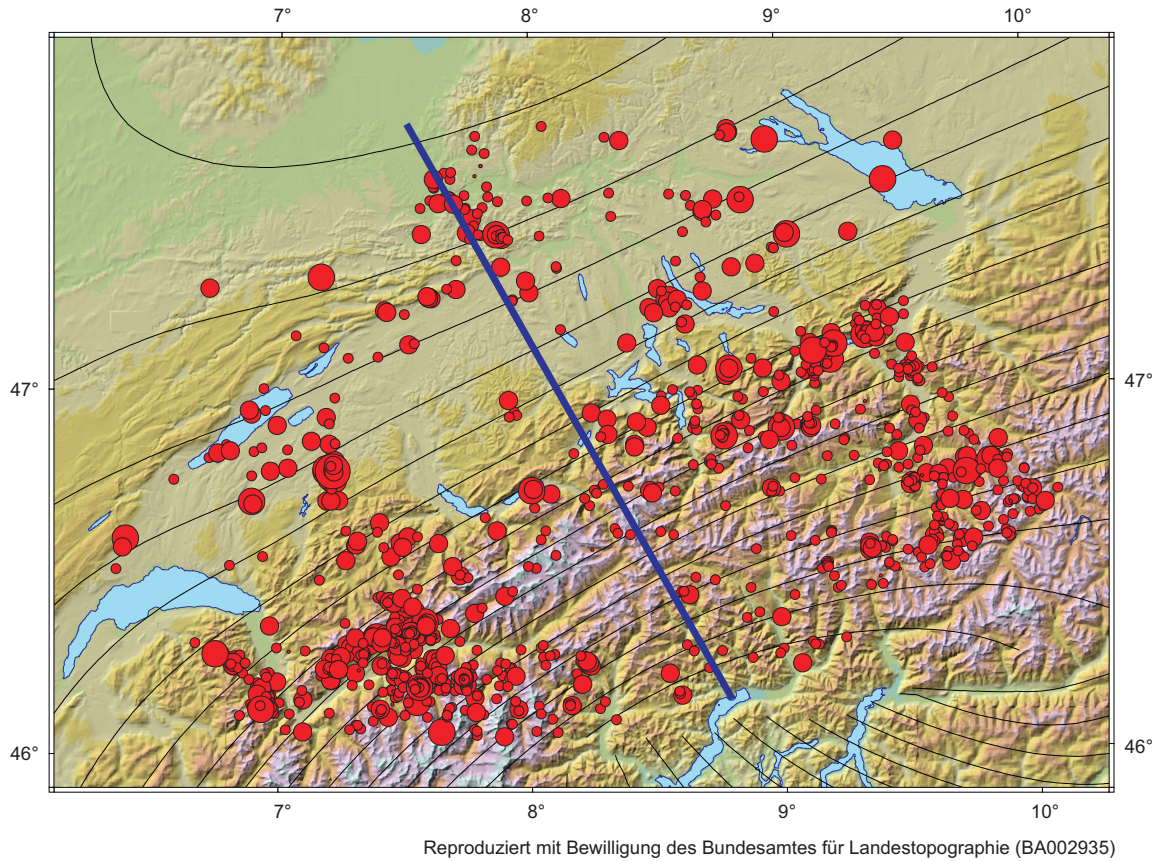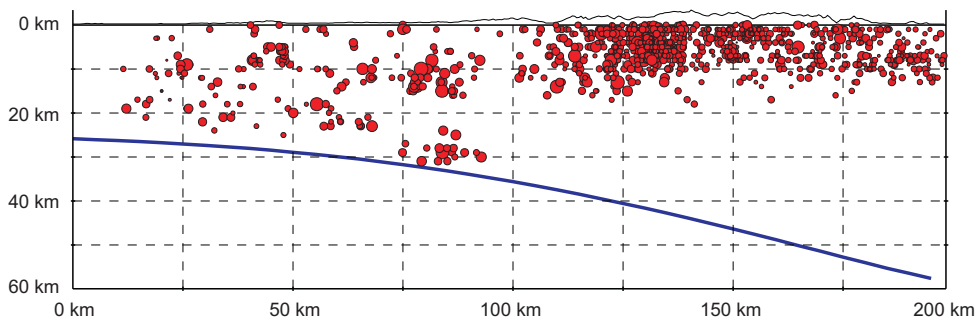
Fig. 1: Epicenter map (top), the thick black lines represent the location of the cross-section used in the bottom (from Deichmann et al. 2000)

Note the clear change of the depth distribution of seismicity between the Alps proper and the alpine foreland.
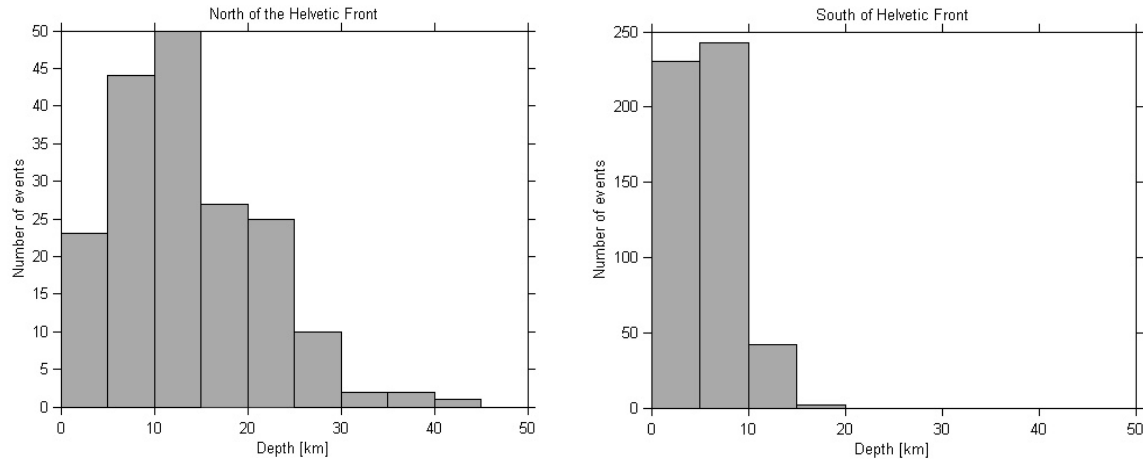
Fig. 2:   Histogram (in 5 km bins) of the depth distribution of seismicity North of the Helvetic Front (above) and south of it (below)

The data from this figure is taken from (Husen et al. *in press*).

Tab. 2:   Percentiles of earthquakes as a function of depth north and south of the Helvetic Front (HF)

Depth Range [km]	North of HF [percent]	South of HF [percent]
0 – 4.99	12.50	44.48
5 – 9.99	23.91	47.00
10 – 14.99	27.17	8.02
15 – 19.99	14.67	0.38
20 – 24.99	13.58	0.1
25 – 29.99	5.43	0
30 – 34.99	1.08	0
35 – 39.99	1.08	0
40 – 44.99	0.54	0
45 – 49.99	0	0

2) Insubric Line separating the Southern Alps from the Crystalline Alps: The Insubric (also called peri-Adriatic) Lineament is a long-known fundamental tectonic boundary in the Alps. A wealth of data provides several lines of evidence for different crustal characteristics on both sides of this fault: The Insubric Line separates the crystalline Alps, to the north, from the Southern Alps, to the south. The southern Alps were built on the Adria (Italy) microplate whereas the crystalline Alps derive from continental fragments that either belonged to the southern margin of Europe, or were isolated within the Tethys Ocean before collision between Adria and Europe (e.g., Schmid & Kissling 2000). The geophysical information confirms geological differences. Reflection seismology (Kissling 1993, Schmid et al. 1997, Ye et al. 1995), seismic behavior (less active towards the south), gravimetric (PEGASOS TP1-STR-7718), Moho depth (PEGASOS TP1-STR-7704). The Insubric Line is a nearly vertical and sharp contact.

Southern extend: Edge of 300 km circle.

Scientific conclusion: The Insubric Line is the second major crustal boundary that separates two distinctly different source zone environments.

Source Zones:

SA: Southern Alps

XWA: Crystalline Western Alps

XCA: Crystalline Central Alps

XHA: Crystalline Helvetic Alps

3) Penninic Front separating the Crystalline Alps (XWA, XCA sources) and the Helvetic Alps (HA, XHA sources): Geological maps show the Penninic Front as a major thrust placing the northern parts of the crystalline Alps over sediment-dominated allochthonous units (the Helvetic Alps). Crystalline and sedimentary rocks have marked rheological and behavior differences and their map occurrences point to upper crusts with different bulk compositions and behaviors on both sides of the Penninic Front. Based on geological information and seismic reflection profiles, this separation is well constrained as a south-dipping contact 30 ± 10 km, which is supported from seismicity evidence, and somewhat supported by stress directions. The pre-instrumental activity in the Wallis region may in our assessment possibly belong to the Helvetic Alps. The same is true for the St.Gallen-Rheintal activity, because of the dip of the structure. While we discussed to treat this boundary as a 3D structure, we ultimately decided that given its distance from the sites, and the aforementioned alternative mechanisms to express boundary uncertainty, to not do so.

Alternative interpretation: Is the Simplon Fault a subdivision between XWA and XCA? It is described as a major normal fault that was active about 5 Ma ago (Mancktelow 1985). This major fault does separate two regions, but its structural reality seems to have no expression in Quaternary tectonics. Furthermore, it does not mark any major separation between distinct seismogenic regions. On the one hand there is a major, crustal scale tectonic contact; on the other hand, there is no evidence for its recent and present day reactivation. Therefore, we consider a unique Crystalline Alps as equally likely as a divided one and thus treat them as two equally weighted branches in the logic tree (50 % to 50 %).

Alternative interpretation: Is there a separation between the XHA and HA? The seismic distribution suggests this possibility; however, lithologies and the general deformation and metamorphic history of both zones are the same. There is no clear-cut geological explanation for this anomaly in seismic distribution. This alternative is therefore an unlikely scenario that is treated as a logic tree branch with small weight (10 % probability).

Alternative interpretation: Subdividing the Wallis activity: We feel that the evidence for clustering is purely seismological: It is therefore best taken care by historical approach.

Alternative interpretation: Is the Engadine fault a source fault? We contend that there is currently no decisive geological evidence, only seismicity (historical: observed effects in the valley). Also, the faults would be far from the sites and hence of little interest.

4) Jura (J source): The Jura source zone is separated from other sources from the basis of rock composition and the existence of a shallow-dipping contact zone between the deformed sedimentary cover and the apparently less deformed basement (pre-Triassic rocks), i.e., 'décollement' (e.g., Burkhard 1990, Sommaruga 1999). We decided to put vertical boundaries to the N and W because they are reported to be subvertical strike-slip (for the N) and normal (for the W) faults (Truffert et al. 1990, Grellet et al. 1993). Individualizing this zone expresses the different activity rates of the Jura when compared to Europe (*E source*). However, this difference in strain and seismicity refers mostly to the near-surface of the Jura Mountains, which comes at

variance to the Molasse basin for which the near surface is nearly silent. The boundary between Jura and Molasse (*M source*) attempts to express in 3D this seismogenic difference. To the northeast, the border of the Molasse basin has no significance to zoning: It is stopped at Bodensee, where a NW-SE late-Paleozoic strike-slip fault runs against the Helvetic Front. The Molasse could be modeled as a 3D wedge with M_{max} of 4.0; however, given that the later on discussed weighted magnitude-dependent depth distribution produces a zone at the surface ~ 2 km thick in which no hypocenters occur, we feel that the Molasse source does not need separate treatment.

5) South Rhine Graben (SRG source): To express the Rhine Graben activity we first define a wide north-south trending zone that includes the Rhine Graben and its shoulders. Then, it was divided into a northern and a southern part along the Variscan suture zone (Lalaye-Lubine Fault in the Vosges to Baden-Baden in the Black-Forest, the Erstein Sill below the sedimentary infill of the Rhine Graben; Villemin et al. 1986, Sissingh 1998). This across-graben division is consistent with different temperature and composition characteristics of observed hot springs (PEGASOS TP1-STR-0015), and with the thermal anomalies (PEGASOS TP1-STR-0014). We also consider the possibility the northern part of the graben is an independent source *NRG*. To express these alternatives, we treat the existence of the NRG source as a logic tree branch with a 50 % weight. If it does not exist in the model, the area N of the suture zone is integrated into the Europe Zone (*E source*).

Alternative Models:

−   Specific sub-zone around Basel (*B source, weight 0.5*) separated from the remainder of the SRG source. The Basel region has experienced the largest earthquake in the study region in historical times, a magnitude 6.5 or larger event in 1356. Paleoseismic studies (Meghraoui et al. 2001) suggest that similar size events have taken place on the Reinach fault. There is evidence for at least three earthquakes, which occurred on that branch of the fault within the last 8500 years with vertical displacements ranging from 0.5 m to 0.8 m. To incorporate the special nature of the Reinach region into our model, we construct a small source zone that incorporates the Reinach fault. On the other hand, we believe that it is also possible that events such as the 1356 can occur anywhere within the SRG source. Therefore, we treat the Basel source as a logic tree branch with a 50 % weight. In addition, we note that by later on explicitly addressing the epicenter uncertainty, the 1356 Basel event will be probabilistically distributed over neighboring source zones.

−   South Rhine Graben Transfer Zone (*TZ source*) (Niviere & Winter, 2000). Northern-Jura border active fault system zone. Justification: This fault zone is geologically known to be an important fault zone probably initiated during the Carboniferous (e.g., Arthaud & Matte 1975), reactivated throughout the Mesozoic and in the Tertiary as a transfer between the Rhine and Bresse grabens (Villemin et al. 1986, Sissingh 2001). This fault zone has the potential to be reactivated under the current stress regime, consistent with focal mechanism, and difference in geodetic uplift behavior (PEGASOS TP1-TEC-0004 and 0005). There is in our assessment a small probability that the 1356 Basel event in fact took place on this structure. To address this potential that the TZ is active or reactivated, we incorporate it is a separate source, but with a small weight of 0.05, after the discussion above.

6) Europe (E source): Combined North-Eastern and North-Western Europe plus northern part of the Rhine Graben north of SRG up to about 50° N (inside the limits of the 300 km circles). This source represents the European background source (*E source*). Geological knowledge in this zone is generally more limited, because of lack of geological information in flat areas. Seismicity in the E source is generally low and diffuse in nature, with no specific centers of activity besides the ones discussed below.

7) Discussed additional and / or alternative zones:

Bresse Graben: The Bresse Graben is one of the Tertiary extensional basins that occurred within Europe (e.g., Sissingh 1998 and 2001, Ziegler 1992). It bounds the Jura Zone, to the West and stops, to the North, against the TZ Permo-Carboniferous trough that was reactivated during the Tertiary as a transfer zone between the Bresse and the Rhine grabens. Although it is geologically related to the Rhine Graben, we did not find pertinent to make a separate zone, as we do not individualize the Northern Rhine Graben in the basic zone model. This decision refers to both geological and seismological information (Truffert et al. 1990, Grellet et al. 1993). On a geological / structural point of view, the Bresse Graben expresses an amount of extension significantly smaller than that in the Rhine Graben; the Tertiary volcanism, quite voluminous in places of the Rhine Graben, is absent in the Bresse graben. Absence of volcanism emphasizes the difference in lithospheric history. Therefore, the Bresse Graben cannot be treated as the Rhine Graben. The Bresse Graben is only the northern segment of the Rhone – Golfe du Lyons extensional system that produced eastward drift of the Corsica – Sardinia Block from the Iberian Peninsula. The extensional deformation that could have differentiated the Bresse Basin from Europe concentrated in the new oceanic basin, leaving quickly the Bresse Graben as a part of continental Europe. Not surprisingly, the seism distribution does not display any difference in behavior between the Bresse Graben and adjacent parts of Europe. The distribution of other features such as hot springs also show that there is less difference between the Bresse Graben and the bulk of Europe than between the latter and the Northern Rhine Graben. Flat lying and undeformed Quaternary infill sediments suggest that seismicity eventually occurring in this structure would preferably take place on the boundary faults, the main boundary fault limiting the Jura Zone to the east, and the long, westward continuation of the Permo-Carboniferous trough to the North. Such seismogenic events can thus be integrated in the neighboring zones, which give less ground to make a very low probability, specific Bresse Graben Zone.

Expert decision:	The Bresse Graben does not deserve a special treatment with respect to the bulk Europe.

Freiburg Konstanz zone (includes Freiburg – Bonndorf – Bodensee Graben) (*FKZ source*): Inherited from Permian Carboniferous tectonics as a conjugate to TZ (Arthaud & Matte 1975). Its WNW-ESE strike has potential for reactivation under the present-day stress field and aligned hot springs show that this fracture zone may go relatively deep in the crust. However, there is no clear sign of current seismic activity. It is, however, visible from geodetic data (uplift). We decide to incorporate the possibility of re-activation of the FKZ as a logic tree branch, with a very low probability (weight: 0.05).

Swaebian Alb (*SWA source*): The Swaebian Alb (Schwäbische Alb) is a documented zone of episodic activity with consistent strike-slip focal mechanism propagating in a NS direction (PEGASOS TP1-TEC-0006, TP1-CAT-0004, TP1-TEC-0009). In our model, the clustered activity is incorporated by spatial smoothed model, which adequately expresses the current activity but also allows for migration of this activity, depending on the degree of stationarity. Despite the NS orientation of the recorded activity zone, we believe that there is a small probability that the active zone is not simply a Riedel direction highlighting the potential for localized activation of a larger, NW-SE trending zone, parallel to the FKZ. To address this possibility, which in itself is not adequately represented by smoothed seismicity, we define the SWA zone with a low weight of 10 %.

Summary of probability of subzones to exist:

1. Helvetic Front Boundary (50 %)
2. XWA and XCA (50 %)
3. HXA and HA (10 %)
4. B sub-zone (50 %)
5. TZ zone (5 %)
6. FKZ zone (5 %)
7. SWA1 (5 %)
8. SWA2 (5 %)

A map of all zones is shown in Figure 3. According to this main source zoning and the conditions of existence or not of some of the sources, our model ends up with seven decisions to be faced in the zoning domain. The implementation of the source zones in the hazard domain is summarized in Appendix 1 (see also PEGASOS document EG1d-HID-0006). Starting by a basic or start model (Figure 4), the different possibilities are developed. The names of the alternative sources are coded as follows:

The suffix '_nTZ' indicates that this source geometry is applicable when the source geometry 'TZ' does not exist. Ditto '_nSWA', '_nFKZ'

The suffix '_LG' corresponds to the large variant of the source geometry, applicable to the 'SRG' and 'B' zones when the zone 'TZ' does not exist. Conversely, the suffix '_SM' applies to the case where the zone 'TZ' does exist.

The suffix '_nps' indicates that this is the source geometry corresponding to the case where none of the sources with an existence probability of less than 1.0 are present. This is not precisely the case, as for example the source 'NWEE_nps' indicates that the sources geometries 'SWA', 'TZ', and 'FKZ' are not present, however the source geometry 'NRG' must exist in order to split the large source zone into 'NWEW' and 'NWEE' (see Figure 5).

When two source geometries are merged to form a single large geometry, the names are also merged, for example: 'XHA' + 'HA' becomes 'XHHA'.

Finally, the large source geometry 'NWE' has been sub-divided into 'NWE', 'NWEE', 'NWEN' & 'NWEW', depending on the presence or absence of the zones 'TZ' and 'NRG' which have a probability of existence of less than 1.0. (see Figure 5).
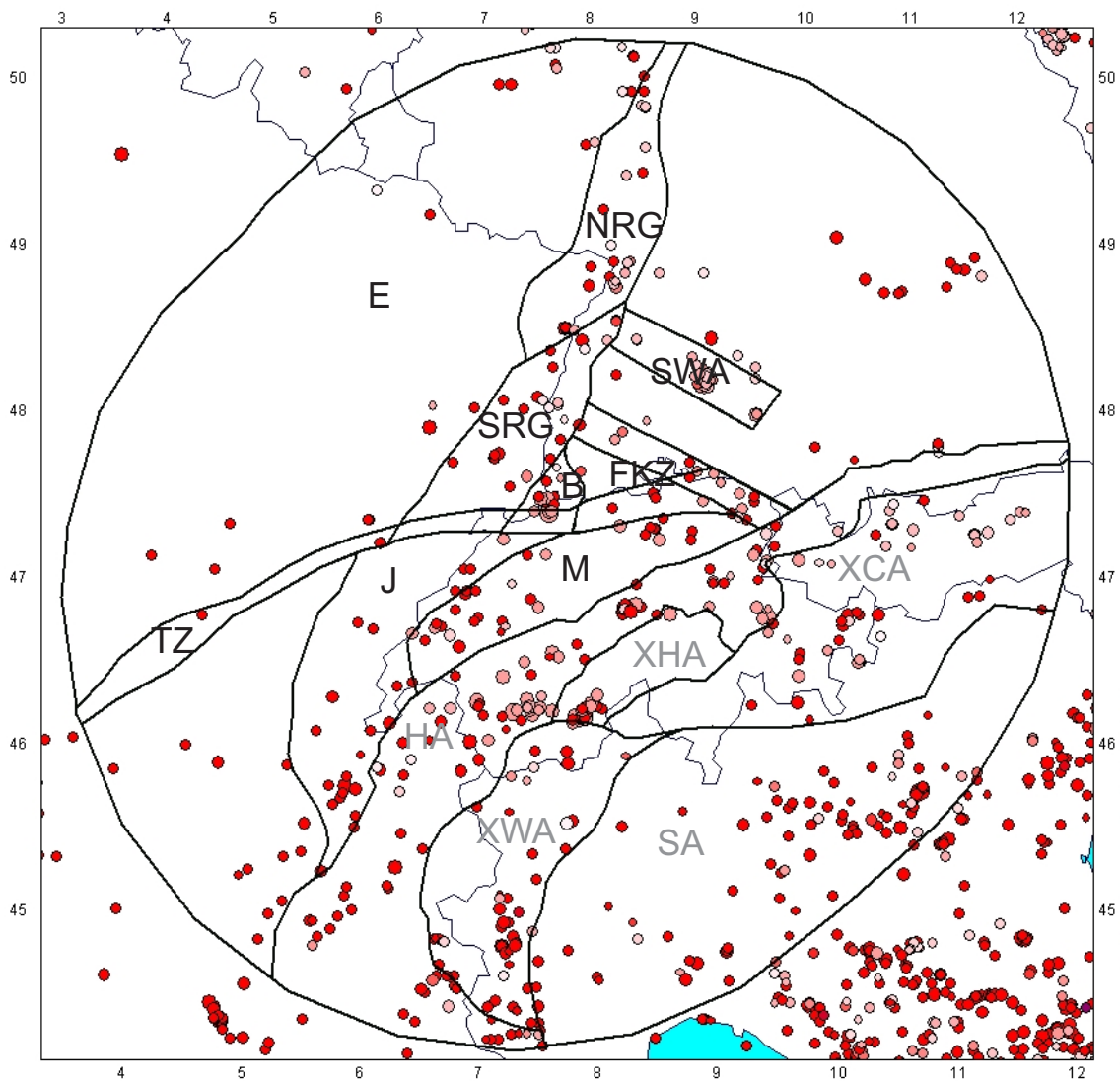
Fig. 3:   Map of the main source zones, different depth distributions of seismicity are
            assumed for the zones north and south of the Helvetic Front

            Shown on top is the seismicity M ≥ 4.0 from 1000 – 2001. Grey labels refer to
            zones south of the Helvetic Front, black ones to the north of it.
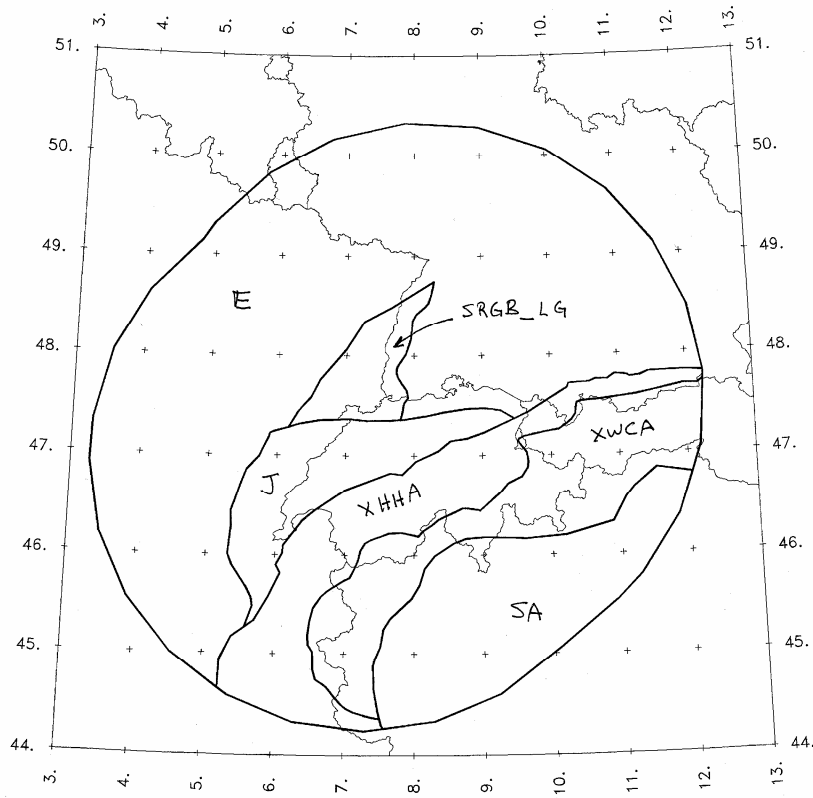
Fig. 4: Most basic (start) model for seismotectonical zonation

Fig. 5: Alternative models for the European background source

4   MAXIMUM EARTHQUAKE MAGNITUDES

Maximum magnitude (hereafter M_{max}) is recognized as a critical parameter with considerable influence on the final hazard. It is also the parameter most difficult to assess in the area scrutinized in the framework of the PEGASOS project, because the physical understanding of M_{max} is limited, and the database to derive this parameter is statistically very limited.

Expert conclusion:	Therefore, most importantly, Mmax has to be specified with a broad uncertainty.

We evaluated several techniques used in past evaluations of M_{max}, ranked below in order of descending significance in our opinion, although none of them provides a satisfying answer to the problem:

1. EPRI approach based on a global database (Johnston et al. 1994).
2. Strain data constraints (Regenauer-Lieb & Petit, 1997, DeMets et al. 1990).
3. Global statistical models (Kagan 1999, Kagan & Jackson 2000).
4. Seismotectonical constraints (Maximum available feature) (Wells & Coppersmith 1994).
5. Kijko numerical approach to assess M_{max} based on observed seismicity (Kijko & Graham 1998, Kijko et al. 2001).
6. 'One step beyond' method (e.g., Slejko et al. 1998).

Expert decision:	The 'one step beyond' technique, that was for example employed in Italy, does not seem appropriate for this study, because we are explicitly interested in low probability levels / long recurrence times and we are in a region with a low strain rate; therefore, the seismicity record of about 1000 years on the region may not offer insight into the maximum possible earthquake.

Kijko's approach (Kijko & Graham, 1998; Kijko et al. 2001), although interesting from the methodological point of view – it includes a non-parametric estimation that avoids any specific frequency-magnitude distribution – has a major drawback. In general, it requires knowing all the events with magnitude above a specific level of completeness, which represents a difficult task in regions like Switzerland with moderate to low seismic activity and no knowledge of the seismic cycle.

Expert decision:	The Kijko's method, especially the non-parametric approach, seems a robust technique when applied to complete catalogues that include at least one seismic cycle; i.e. from high activity regions, which it is not the case in Switzerland. For that reason we do not consider its application for this study.

Maximum available structure length (Wells & Coppersmith 1994) can be a powerful criterion, although it has been challenged in its usefulness as a predictive tool (D.D. Jackson, personal communication 2002). The main obstacle to applying it to Switzerland is that we have disputed and rather no information on active faults in the region. Even for the Basel region, exhumation of the Reinach fault offers little beyond the insight that the event had a magnitude of 6.5 ± 0.5. It remains unclear whether the Rheinach fault, for example, could in rare instances rupture much further along the Rhine Graben, resulting in a much larger earthquake.

Expert conclusion:	We retain that there is no identified active fault with rupture longer than about 30 km.

The lack of geological evidence of active structures larger than 30 km (capable of events of roughly M 6.5) is consistent with first-order strain rate consideration. To begin with, we can convert the seismic moments of the past 700 years into average annual strain, using a Kostrov model (Kostrov 1974). The main free parameters of such an analysis are the geometry of the deformation source region and its depth extent. Using 15 and 30 km depth extent, and a polygon that includes the region of the highest moment release (Basel), we computed values of shortening rate between 1.0 and 0.5 mm/a, respectively. These values are consistent with the deformation rates inferred for the past 3 Ma. In a second step, we can explore which strain rates would result from an assumed M_{max}, given the historically a-value (1.82) and b-value (0.75) and assuming a truncated Gutenberg Richter model.

As seen in Figure 6, a 1 mm/a strain rate (horizontal line) is compatible with a truncated Gutenberg Richter model with an assumed M_{max} of about 6.5. If M_{max} were to be 8.0, the required average deformation rate would be about 10 mm/a, which is not witnessed in the geological record or recent GPS surveys. While the strain rate analysis has many uncertainties, it can be interpreted as evidence that M_{max} much larger than 7 are not compatible with the observed geodetic strain rates.

Some purely statistical studies of M_{max} have been based on global instrumental datasets (Kagan 1999, Kagan & Jackson 2000). These studies suggest that there is little evidence to assume regional variations of M_{max}.

Expert conclusion:	There is only circumstantial evidence for events much larger than 7.0. Larger earthquakes (M 7.5 – M 8.0) are in some interpretations theoretically possible in all seismogenic regions but, given the tectonic / seismicity characteristics in the region, the chance of the M_{max} being as large as 8+ is essentially zero.

Although, as stated above, none of the available methods provides a satisfying answer to the M_{max} problem in the PEGASOS area, we favor the EPRI approach (Johnston et al. 1994) for the estimation of M_{max} as the most satisfying compromise option; specifically, we appreciate the resting broad uncertainty distribution of M_{max}. We consider the *prior distribution for extended continental crust* (Figure 7) appropriate for the study region because extension dominated the European crust in Permo-Carboniferous times (e.g., Burg et al. 1994) during the Mesozoic development of the Tethys passive margin (e.g., Ricou 1994) and during Tertiary extension (e.g., Ziegler 1992), and because the broader uncertainty distribution of extended crust expresses more accurately the notion that M_{max} is uncertain. Following the EPRI approach, M_{max} will be modified in each source zone to reflect the actually observed seismicity.

Expert statement:	We consider the occurrence of M 8+ events in the study region, as it has been proposed l in regions like for example New Madrid, USA, not possible, because the European lithosphere of the study area is younger and warmer than that of Eastern North America. Since we are also far away from subduction zones, where M 8+ events could be originated, we make the decision of limiting M_{max} to 8.0.

In order to reflect the evidence from estimated strain and maximum available rupture length that M >> 7 are highly improbable, and the expert statement limiting M_{max} to 8.0 from geodynamics considerations, we propose two models in which EPRI is to be applied:

1. *Truncated at an upper M_{max} bound of M 7.5*

2. *Truncated at an upper M_{max} bound of M 8.0*

We are fully aware that in some cases, the M_{max} in a source zone may result in a rupture zone considerably larger than the likely rupture dimension. This is accepted because we do not believe that our source zones have boundaries impermeable to rupture. This notion is embedded in our model when considering spatially smoothed seismicity rather than discreet source zones. Ruptures have been shown to be able to jump large distances (kilometers) from one fault to another, using static and dynamic stresses as the transport mechanism. We could envision such a scenario as one possibility on how ruptures can affect two or more source zones.

We cannot offer solid guidance on where the seismogenic structures for an M 8 event may be hidden in the crust. In our opinion, the minimal chance for such a large earthquake expresses also the fact that we may largely misunderstand the seismotectonics of the region. For example, could a large thrust event occur underneath Switzerland, within the strong, granulite facies lower crust without affecting the surface?
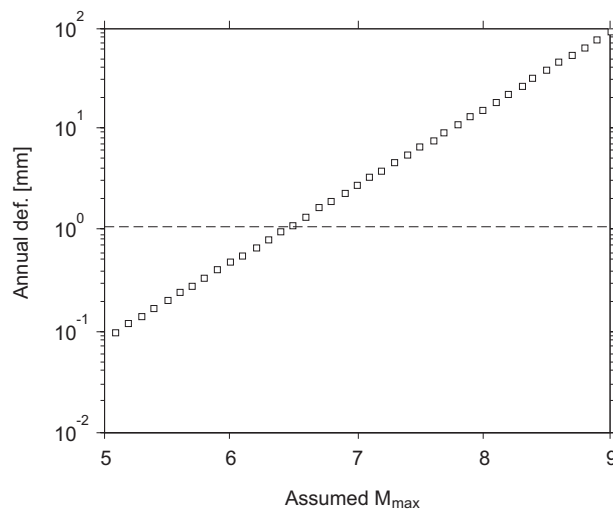
Fig. 6:   Given the observed *a*-value of 1.82 and a *b*-value of 0.75 for the Basel region, we compute the resulting average annual strain rate in [mm] for various assumed M_{max} (depth extend: 15 km)

The horizontal dashed line represents the approximate observed strain rate of 1 mm/a. Note that large M_{max} ($M_{max} > 8$) require strain rates of more than 10 mm/a.
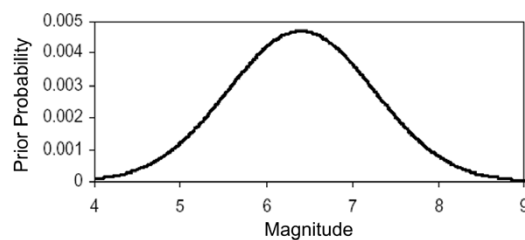
Fig. 7:   EPRI prior distribution for extended crust (mean = 6.4, std = 0.84)

5   EARTHQUAKE RECURRENCE RELATIONSHIPS AND LOGIC TREE DESIGN AND IMPLEMENTATION

In this chapter, we define the logic tree that allows the computation of earthquake recurrence relationship. It also discusses all necessary choices for rate computation, such as declustering, completeness, mining activity etc. Results from the sensitivity analysis from PEGASOS Sensitivity Results SP1 CD-ROM are also considered. In same cases they lead us to eliminating certain branches of the logic tree; however, we leave in the discussion of those branches to document our thought processes.

Our final logic tree consists of nine decision levels. The tree is shown in Figure 8. Below, we discuss each level in detail. To keep the writing focused, we refer to the Appendix in some cases for additional information.

5.1   Level 1: Input data

The PEGASOS (ECOS) Earthquake Catalogue (TP1-CAT-0004, accompanying report PEGASOS EXT-TB-0043 2002) contains events, which are qualified as 'questionable' or even uncertain (Field identifier: *cc*). These events have a small probability of actually having occurred (Faeh, personal communication 2002). Consequently, we believe that it would be inappropriate to use them for rate computation. Our subsequent analysis is based only on events classified in the PEGASOS database as certain (cc = 1).

Expert decision:	Remove 'questionable' and 'uncertain' events from database for purposes of recurrence calculations.

The PEGASOS catalogue also contains a number of identified explosions (Field identifier: *Type*). Explosions contaminate rate computation and *b*-value estimation and need to be excluded from the analysis. Only events with an identifier of 3 or higher should be used.

Nevertheless, more than 500 unidentified explosions remain in the data set, as detailed in *Appendix 2*. This is not surprising, because essentially all earthquake catalogues contain unidentified explosion events. Their identification based on waveform studies is extremely time-consuming and still ambiguous events will remain. In order to address the problem of quarries, we opt for a largely statistical identification and removal of events, as explained in *Appendix 2*. This removes about 1000 events from the PEGASOS catalogue. Their magnitudes are relatively small and they are all contained in the last 25 years of data.

Because of the uncertainty in the quarry identification, we treat both catalogues (original and 'dequarried') as input to subsequent calculations, forming the first two branches of our logic tree.

The feedback from PEGASOS Sensitivity Results SP1 CD-ROM shows clearly that de-quarrying has an insignificant effect on the hazard at the sites of interest (Figure 9). Therefore, de-quarrying shows no significant effect on the hazard. For final analysis, we prefer the de-quarried catalogue, including the removal of the French quarry region.

Expert decision:	Remove quarry blasts using a statistical criterion based on the day-night time ratio of events (Wiemer & Baer 2000). Remove French quarry region separately, to avoid influence on rate maps.
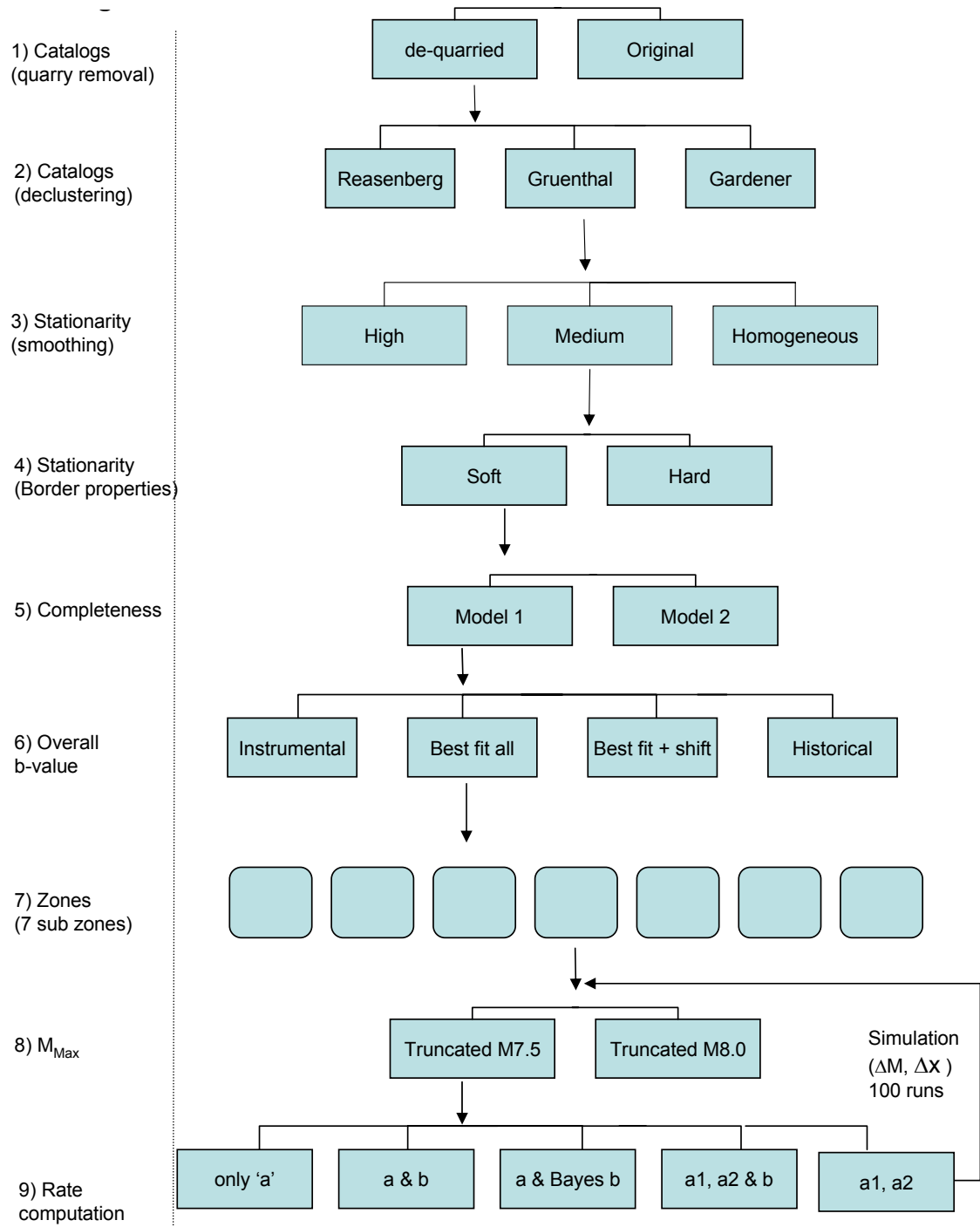
Fig. 8:   Eg1D model – Summary of logic tree flow
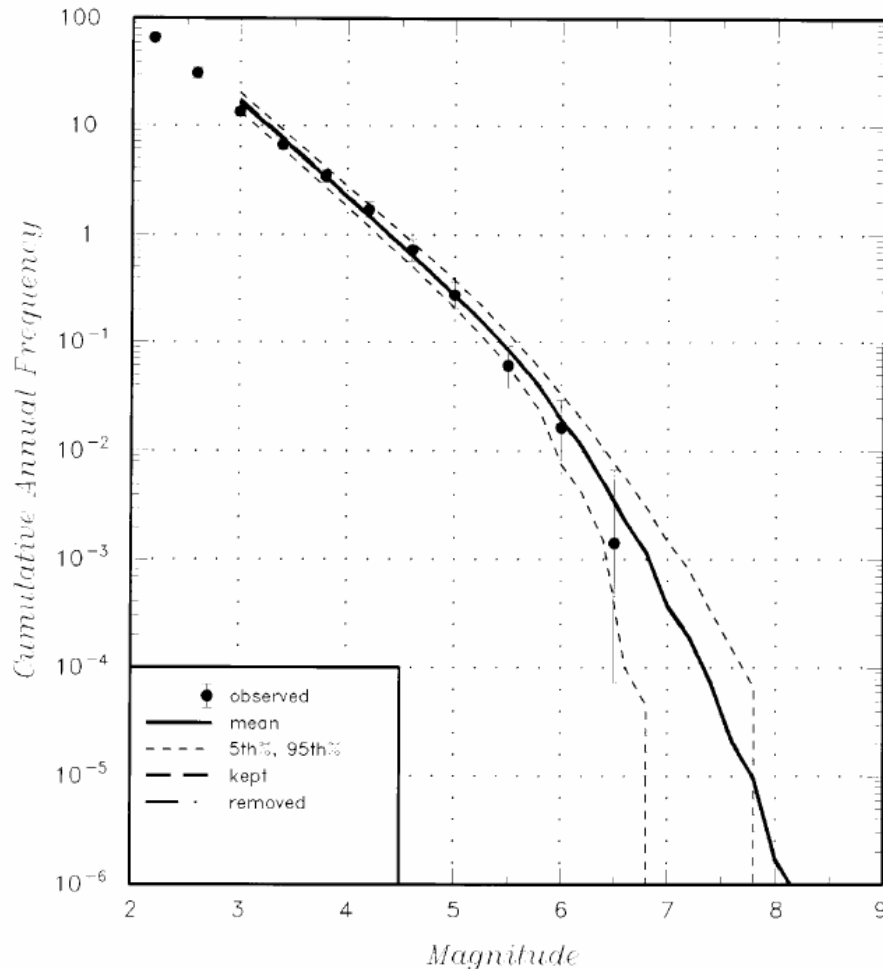
Fig. 9:   Predicted total regional recurrence rates showing the effect of removal of statistically identified quarry blasts

5.2   Level 2: Declustering

This branch expresses the epistemic and aleatory uncertainty of different declustering approaches. Declustering is necessary, because the assumption of a stationary poissonian process made in the subsequent hazard computations is not fulfilled in the original catalogue (Wiemer & Woessner 2002, PEGASOS TP1-TN-0266). It is our conclusion that no unique and generally accepted approach to declustering exists. To express the epistemic uncertainty of alternative connectional models of declustering, and alternative approaches to implementing these models, we apply two different methodologies: Reasenberg's physically-based declustering (Reasenberg 1985), and Gardner & Knopoff's fixed window declustering (Gardner & Knopoff 1974). These approaches are described in detail in Wiemer (2002, PEGASOS EXT-TN-0208).

To express the aleatory uncertainty in choosing the correct window parameters in Gardner's approach, we allow for two different setting: The original code proposed by Gardner & Knopoff (1974), and Gruenthal's modified parameters for Central Europe. As demonstrated in Wiemer (2002, PEGASOS EXT-TN-0208) and Deichmann (2002b, PEGASOS EG1-TN-0305), these algorithms result in considerably different numbers of events in the catalogue. It is, however,

questionable whether the algorithms have indeed an influence on the resulting rates and *b*-values for individual zones, or, even less likely, on the M_{max} estimation.

The sensitivity feedback from PEGASOS Sensitivity Results SP1 CD-ROM demonstrated that indeed the effect of the declustering on the final hazard is insignificant (Figure 10). Therefore, using only one declustered catalogue is sufficient. We prefer Gruenthal's windowing parameters because it is the only algorithm calibrated for the region and because of N. Deichmann's evaluations (Deichmann 2002b, PEGASOS EG1-TN-0305) on selected Swiss sequences.

Expert decision:	Use 'Gruenthal declustered' catalogue.
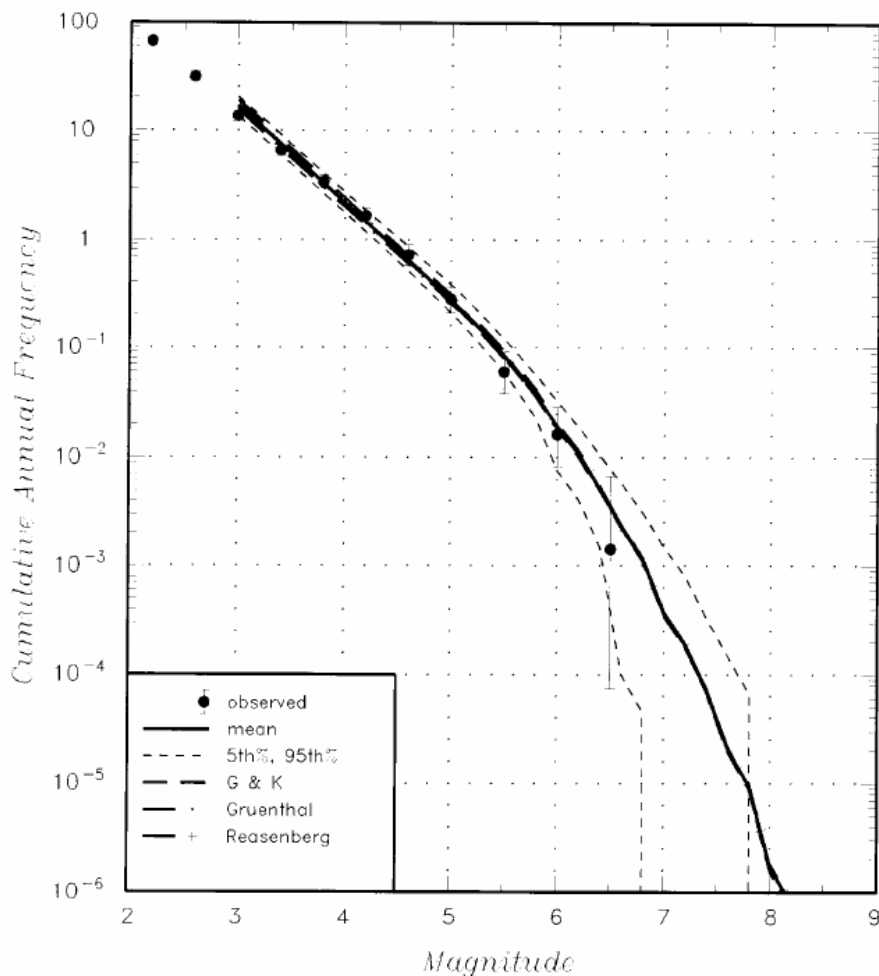
Fig. 10: Predicted total regional recurrence rates showing the effect of alternative declustering techniques

5.3   Level 3: Stationarity (smoothing)

This level and the subsequent level 4 both express the uncertainty in the degree of spatial stationarity of seismicity. We believe that the degree of stationarity is unknown and needs to be expressed as one of the principal uncertainties in the hazard assessment, as outlined Chapter 2.1. To represent this stationarity, we apply variable levels of spatial smoothing rates based on the observed seismicity within seismogenic areal zones.

Three levels of smoothing are considered:

1. *Homogeneous*: The rate of earthquakes is constant within an areal source region;

2. *High* (5 km kernel): The rate of earthquakes varies within area sources depending of the density of past earthquakes. The density distribution is obtained using Gaussian kernel smoothing with a kernel width that shows clusters of events to be reproduced.

3. *Medium* (15 km kernel): The rate of earthquakes varies within area sources depending of the density of past earthquakes. The density distribution is obtained using Gaussian kernel smoothing with a kernel width that shows the larger scale differences between regions to be reproduced.

Each branch receives equal weight. To decide which smoothing kernel represent the three conceptual levels of stationarity best, we evaluate 6 rate density maps, computed for kernels of 5, 10, 15, 20, 30, and 50 km (PEGASOS document TP1-SUP-0045). Rate density maps are computed based on a Reasenberg declustered catalogue (Wiemer 2002, PEGASOS EXT-TN-0208) cut roughly for completeness, based on the results by Ruettener (2002, PEGASOS TP1-RF-0158). Because rate density is a local feature, regional and temporal differences in completeness are nor critical in the estimation. The two kernels selected to represent high and medium stationarity (5 and 15 km, respectively) are shown in Figure 11 and 12. From these two maps, a smoothing matrix can be extracted for each zone. This matrix, normalized to one, will then be used to spatially distribute the *a*-value assigned to each zone.

Uncertainty in epicentral location is explicitly taken into account in the smoothing. This is accomplished by convolving the location uncertainty into the kernel operator. For a Gaussian kernel:

$$h\,(total) = sqrt\,(h\,(error)\,{}^\wedge 2 + h\,(kernel)\,{}^\wedge 2)$$

The uncertainties in epicentral error are given in Table 3.5.3 from the PEGASOS catalogue report (PEGASOS EXT-TB-0043 2002). We interpret the uncertainty bounds given in the PEGASOS catalogue as 2 sigma bounds, because in our opinion a box distribution makes no sense and was not intended by the SED (Giardini, personal communications 2002). Thus, the equivalent h(error) = 1/2 box width.
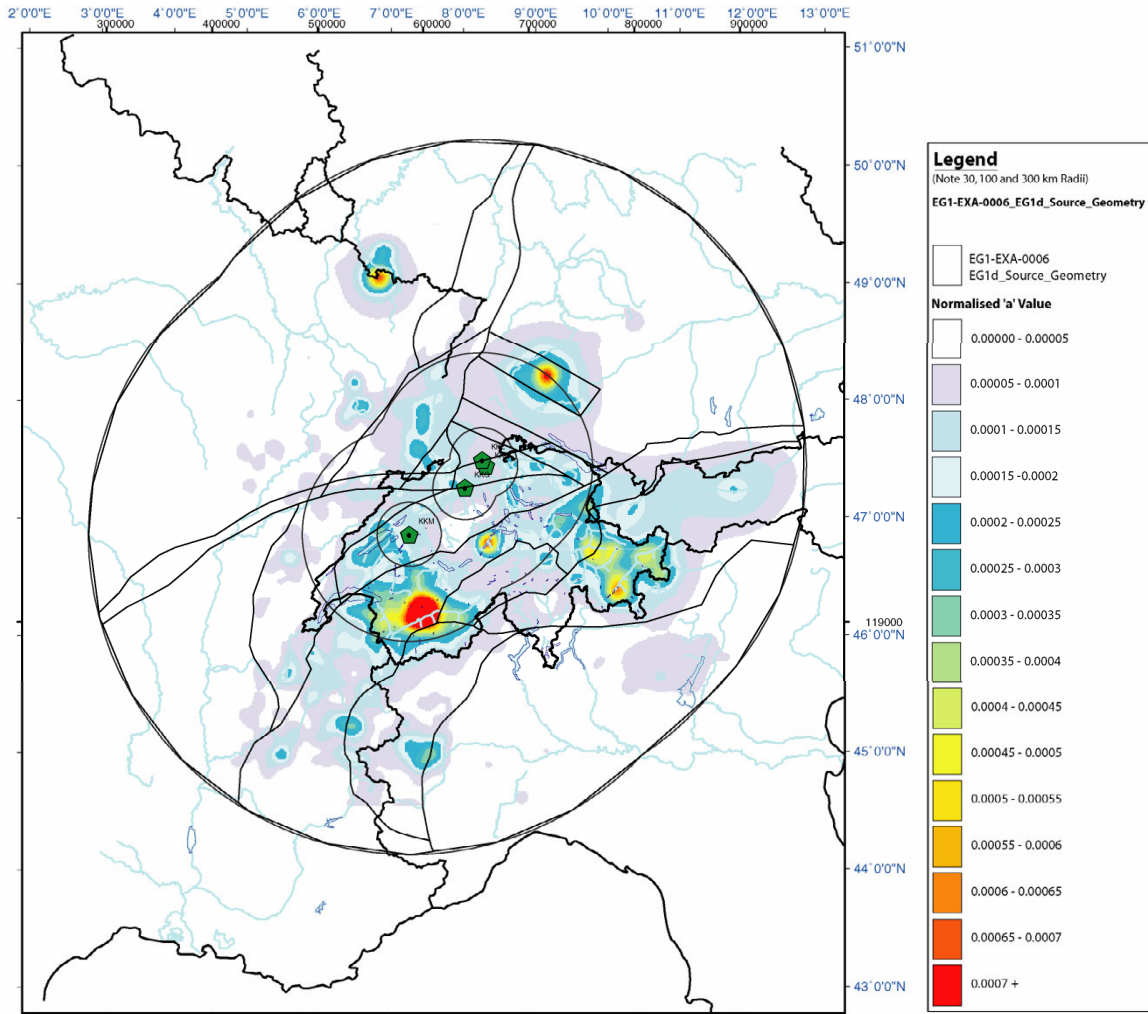
Fig. 11:   Map showing the density of seismicity, smoothed using a kernel of 5 km

For legend, see Figure 12. The analysis is based on a Reasenberg declustered catalogue, completeness is taken from Ruettener (2002, PEGASOS TP1-RF-0158) and applied to the entire region. Note that these figures are the preliminary smoothing masks, which are based on a catalogue that still contains explosion events.
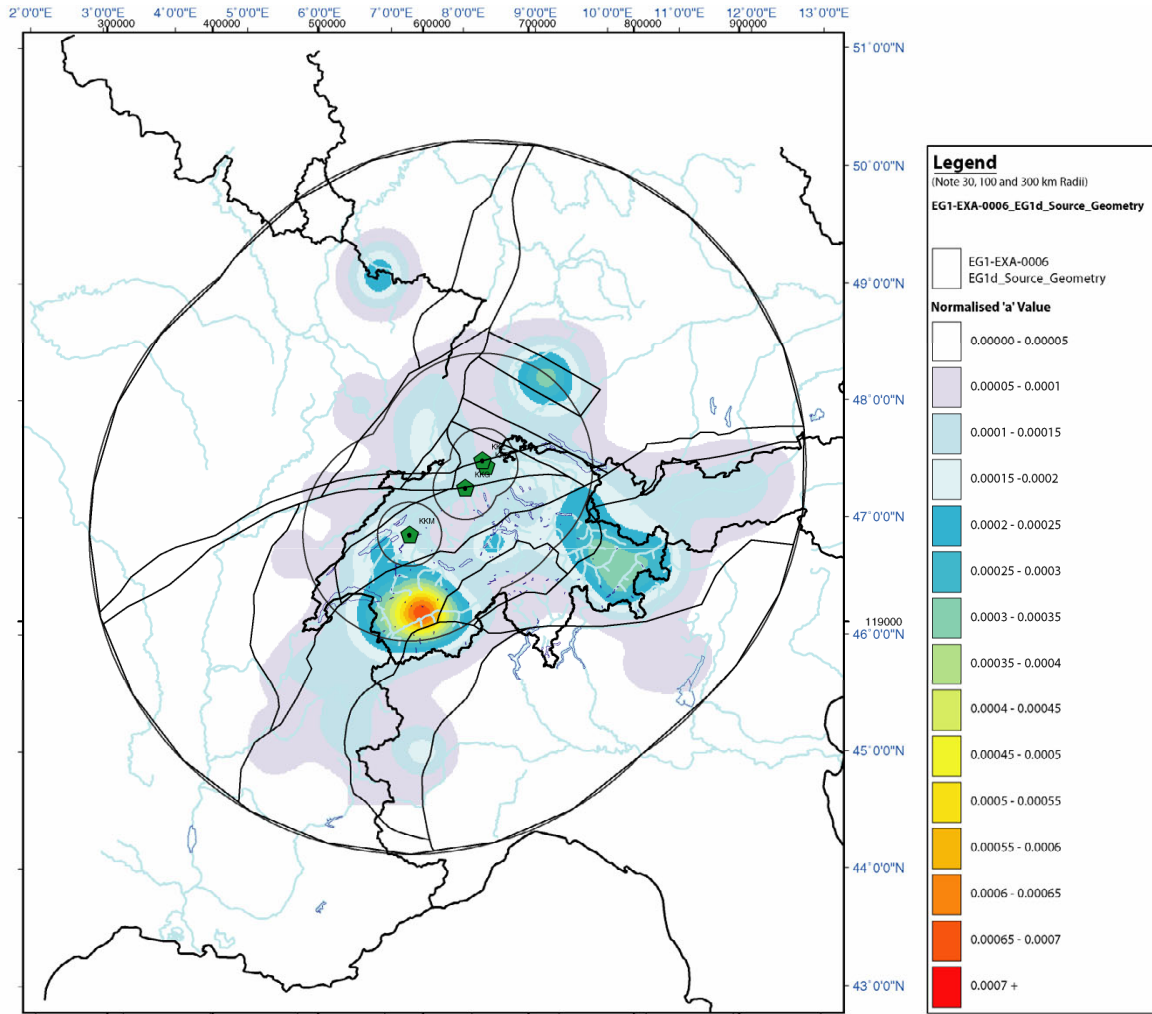
Fig. 12:   Map showing the density of seismicity, smoothed using a kernel of 15 km

The analysis is based on a Reasenberg declustered catalogue, completeness is taken from Ruettener (2002, PEGASOS TP1-RF-0158) and applied to the entire region. Note that these figures are the preliminary smoothing masks, which are based on a catalogue that still contains explosion events.

5.4   Level 4: Stationarity (boundary properties)

This level also expresses the uncertainty in the degree of stationarity, (level 3) but also the uncertainty in the exact location of boundaries and the idea that seismicity can interact across source zone boundaries. While these three concepts are different and could be expressed separately, we believe that they can all be satisfyingly expressed using a common decision tree level, considering that epicenter uncertainty is also taken into account.

In our model, areal source borders can have two properties:

1. *Hard*: Rates changes abruptly at borders of areal zones. This is based on the assumption that area zones borders are accurate and in essence impermeable for earthquake interaction.

2. *Soft*: A soft border allows a gradual transition of rates at zone borders. This is achieved by eroding the rate difference at the border, using a linear gradient with a total width of 5 km. (Figure 13). The overall rate (summed activity in both zones) should be conserved in this approach. Each branch receives equal weight. This decision level could be dropped if the project can show convincingly that for critical zones near the evaluation sites, the soft border has no effect on the resulting hazard.

The sensitivity feedback from PEGASOS Sensitivity Results SP1 CD-ROM (Figure 14) establishes that the choice of the boundary properties has a negligible effect on hazard. We therefore limit our analysis to hard borders.

Expert recommendation: Use hard borders only.
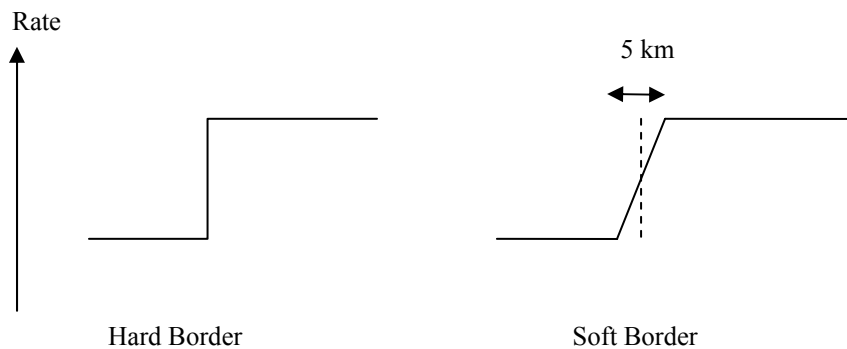
Fig. 13:   Schematic explanation of the soft boundary concept
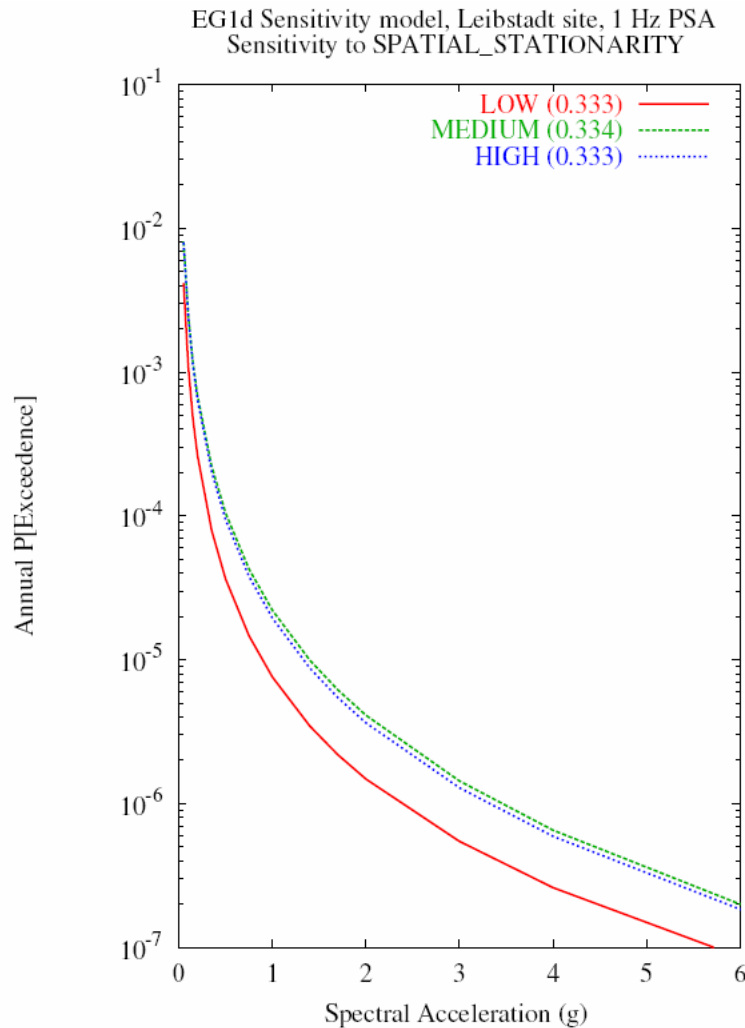
Fig. 14: Sensitively feedback (hazard) for site Leibstadt (from Toro 2003a, TP4-TN-0345)

Studied is the parameter 'stationarity'. Low and Medium / High hazard curves are clearly different.

5.5 Level 5: Completeness

Completeness in magnitude reporting is a critical parameter for rate computation. Small changes in assumed completeness can produce large changes in *b*-value and in extrapolated rates of moderate to large main-shocks (Rydelek & Sacks 1989, Wiemer & Wyss 2000, Wiemer & Wyss 2002). Completeness magnitude, Mc, however, is a complex function of space and time [Mc = Mc (x,y,t)], and can only be known with uncertainty. A Mc cut much too high, in order to be on the safe side, is not a satisfactory solution either, because it reduces the amount of available data for rate and *b*-value estimation. Smaller sample size then result again in larger uncertainties.

In order to express the aleatory uncertainty in Mc, we use two different models of Mc(x,y,t). Completeness is evaluated on a country-by-country scale. The details on Mc estimation are given in *Appendix 3*.

The sensitivity analysis to recurrence rates (Youngs 2003, PEGASOS TP1-TN-0339) confirms that indeed the choice of the completeness model influences the hazard in some zones signi-

ficantly (Figure 15). We keep both models to express this uncertainty. In our opinion, both models are based on reasonable assumptions and data, and we do not envision any hint to favor either. Therefore, we will use both, with equal weight, to express the uncertainty in Mc.

Expert decision:	Use two models of completeness as separate, equally weighted branches of the logic tree.
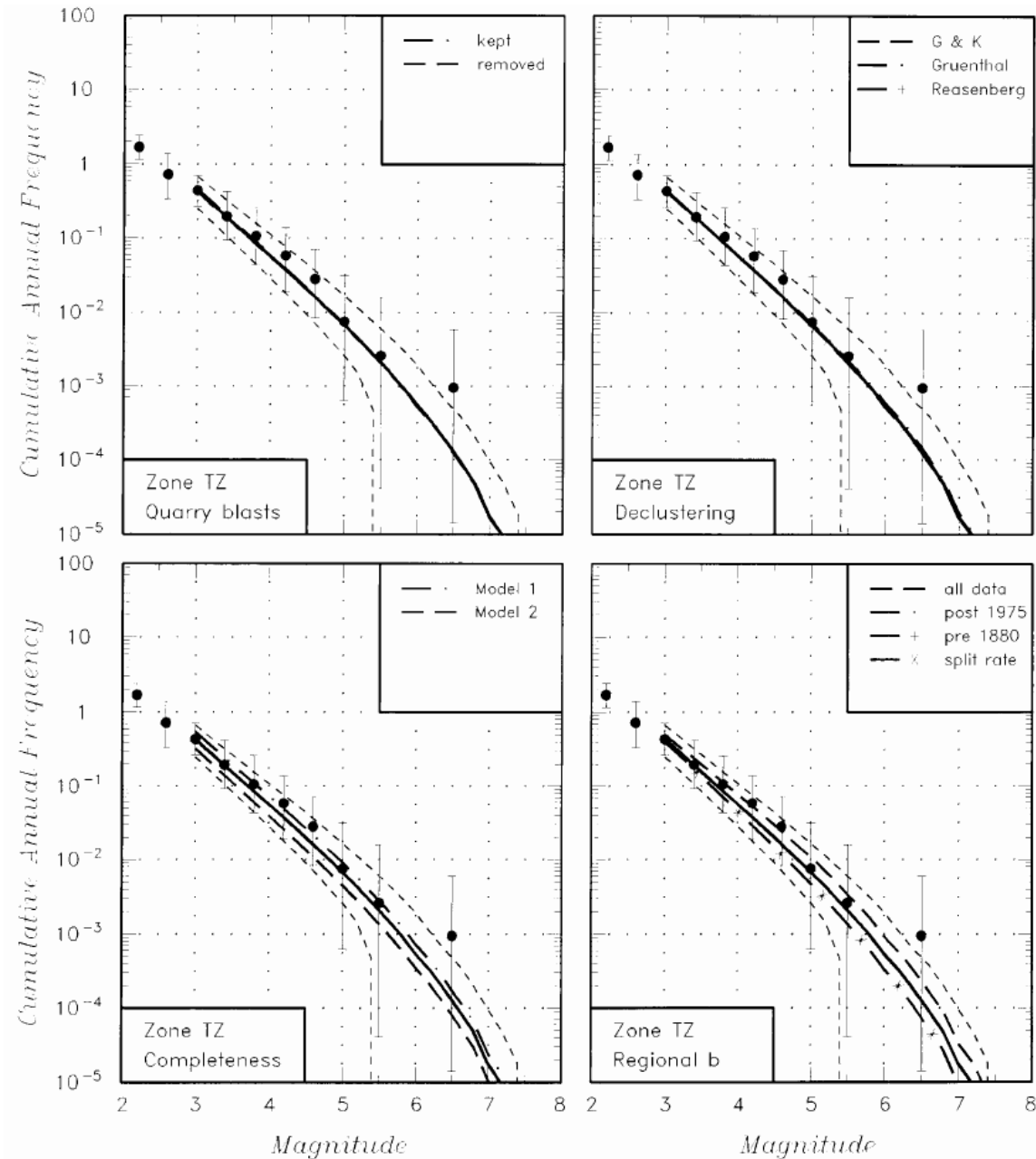
Fig. 15:   Sensitively feedback (recurrence rates) for zone TZ (from Youngs 2003, PEGASOS TP1-TN-0339)

Note, how quarry blasts removal or declustering does not change the final recurrence rate estimate, whereas completeness model or regional *b*-value choice does.

5.6   Level 6: Regional *b*-value

The regional *b*-value, b_0 is needed for the subsequent rate determinations for all models which allow an overall, constant *b*-value. b_0 has both aleatory and epistemic uncertainty. The aleatory uncertainty is best computed using bootstrapping of the sample for which b_0 is to be determined, and expressed as a standard deviation, Δb_0. This standard deviation is also later on needed for the Bayesian *b*-value estimation. In addition, there are systematic or model dependent differences for determining b_0. These different model assumptions are largely based on the fact that the relative weight of instrumental and historical data changes the b_0 estimation considerably. It also takes into account:

1. The possibility that intensities were systematically converted into too high magnitudes, particularly in the period 1880 – 1970, as described in *Appendix 4* (Giardini 2002a, PEGASOS EXT-TN-0145 and Giardini 2002b, PEGASOS EXT-TN-0296).

2. The possibility that rates changes naturally between different period, which (if completeness changes also) will bias the *b*-value estimation.

In each model, the *b*-value is computed using a maximum likelihood fit to a truncated Gutenberg Richter model (Bender 1983, Utsu 1999), corrected for the magnitude binning (0.1 or 0.5). Completeness varies as a function of space and time, as defined in level 5. The sampled volume for the overall *b*-value encompasses all events within 300 km from the sites. The four models selected to express the epistemic uncertainty in *b*-value estimation are:

1. *Instrumental b-value only*. This assumes that the *b*-value obtained from the data between 1975 and 2001 is the most reliable in terms of magnitudes, because it is based on instrumental data rather than macroseismic intensities.

2. *Best fit to all data*: This uses all available data (period 1300 – 2001) above the completeness threshold for computing the overall *b*-value.

3. *Historical only*: By using only the historical data, one avoids mixing two different data source with different properties. The *b*-value computed in this fashion avoids possible biases through mixing these two data sets. The *b*-value is computed using a maximum likelihood fit to the data from 1300 – 1880.

4. *Best fit to all data, allowing for a change in the a-value*. As discussed in *Appendix 4* (Giardini 2002a, PEGASOS EXT-TN-0145 and Giardini 2002b, PEGASOS EXT-TN-0296) activity rates vary between the historical data (particularly the period 1880 – 1970 and in the Wallis area) and the instrumental. This change in activity is in our belief caused by a mixture of natural rate fluctuations, and, possibly, some systematic shift due to the magnitude calibration used in the estimation of macroseismic magnitudes. Because this change in activity coincides with different completeness periods, it causes a systematically biased *b*-value (Figure 16). To avoid this bias, we determine through a joint maximum likelihood estimation the two rates of seismicity ('*a*-values') in the instrumental and historic period, respectively, and one single *b*-value.

Sensitivity feedback (Youngs 2003, PEGASOS TP1-TN-0339) shows that the regional *b*-value has some, albeit a small effect on the resulting recurrence rates for some zones, for example in zone TZ (Figure 15).

> Expert decision: Use four models to express the uncertainty on the overall *b*-value.
> We have no basis for preferring any model. Accordingly, they are
> assigned equal weight (0.25).
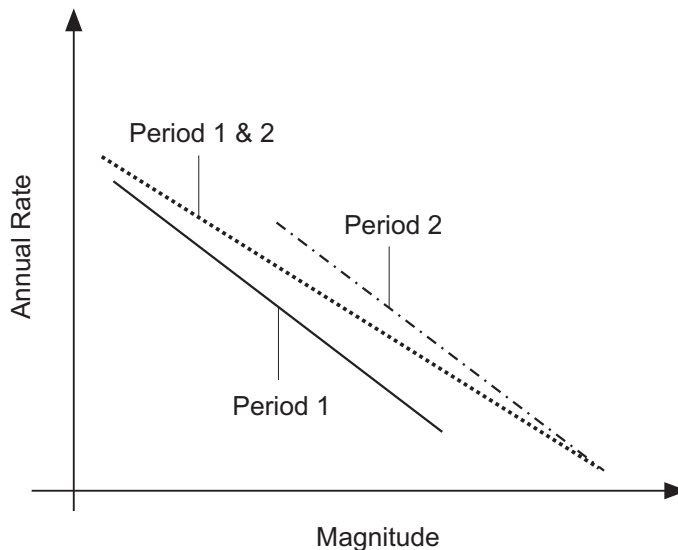
Fig. 16:   Schematic explanation of the influence of a temporal rate change on *a*- and *b*-values

The dashed line indicates the erroneous slope resulting from ignoring the fact that the rates of events in the two periods differ.

5.7   Level 7: Areal zoning

The reasoning for the applied zoning, the justification for each zone etc., are commented in Chapter 2. Our model ends up with seven decisions to be taken in the zoning domain, as explained in the aforementioned chapter. Implementation of all zones in the hazard domain is discussed in *Appendix 1*.

5.8   Level 8: M_{max} determination

The problem of maximum possible magnitude is discussed in Chapter 3. We capture the large epistemic and aleatory uncertainty in M_{max} using two logic tree branches based on the EPRI approach (see discussion in Chapter 3):

1. *EPRI approach for extended continental crust, truncated at M 8.0*

2. *EPRI approach for extended continental crust, truncated at M 7.5*

The advantage of the EPRI approach is that is built on an extensive global dataset of M_{max}. The resulting wide distribution of M_{max} expresses well the feeling of our group that M_{max} is indeed a very uncertain parameter in general and in particular in a region of low strain rate such as Switzerland. In those branches we use directly the EPRI approach, applied for each zone. Therefore, the prior distribution is modified using the observed M_{max} to create a posteriori

distribution with a long tail. This long tail is desired and expresses the possibility that even large earthquakes may in fact, with a small probability, occur in all seismogenic regions (e.g., statistical studies by Kagan 1999 and Kagan & Jackson 2000).

The branch with truncation at M 8.0 considers the expert statement limiting M_{max} to 8.0 from geodynamics considerations (see Chapter 3).

The branch with truncation at M 7.5 expresses the point of view that M >> 7.0 events are highly improbable in the study region. The main reasons for this interpretation are (see Chapter 3):

a) There is no evidence in the historical record of the past 2000 years, and paleoseismic record of the past 10'000 years of large earthquakes (M >> 7).

b) There are no structures of sufficient length available to support events with a magnitude M >> 7.

c) The average strain rate (Chapter 3) of the past 3 Ma is well explained with a maximum magnitude of about 7.0. Occasional events of M > 7.5 would have to be either very infrequent (less frequent than extrapolated from the observed *a*- and *b*-value), they would have to take place instead of more numerous smaller events, or they would require a sudden change in the average strain release.

Note, that this does not state that the M_{max} is 7.5 in all zones, because by using the EPRI approach we assign to each zone a distribution with a maximum allowed M_{max} of 7.5. We realize that the choice of 7.5 is somewhat arbitrary, but do not feel the need to assign an uncertainty to this value, given that the first branch of this level allows larger maximum M_{max}.

Each of the two branches is assigned an equal weight because we have no basis for preferring one model over the other, considering the arguments discussed above and in Chapter 3. To address the uncertainty in M_{max} estimation caused by the uncertainty in epicentral location and magnitude, we perform a simulation using the individual uncertainty values given for each event in the database. This simulation is described in more details below.

5.9   Level 9: Rate estimation

This final level addresses the epistemic and aleatory uncertainty in rate computation. The basic principles of our rate estimation are:

1. Objectivity and reproducibility: The rates should be computed in an automatic fashion.

2. Principle of simplicity: We will use a simple model with few parameters unless the data requires a different approach.

To achieve these goals, we develop a multi step scheme to assess the earthquake size distribution (*b*-value in the Gutenberg – Richter law, *log N = a – b M*, Gutenberg & Richter 1944) and activity rate (*a*-value). As described already in level 5 (overall *b*-value), assessing rates is complicated through the fact that the activity in certain regions (e.g., the Wallis) seems to change quite clearly with time.

We use the truncated exponential, which is the earthquake recurrence relationship most commonly used in PSHA (Cornell & Van Marke 1969). It is derived from the Gutenberg & Richter (1954) recurrence model by truncating the rate density of earthquakes at a maximum magnitude, m^u.

The truncated exponential model is given by the expression:

$$N(m) = N(m_0) \frac{e^{-\beta(m-m_0)} - e^{-\beta(m^u-m_0)}}{1 - e^{-\beta(m^u-m_0)}} \qquad (1)$$

where $N(m_0)$ is the annual frequency of earthquakes larger than magnitude m_0, and $\beta = b\ ln(10)$, the Gutenberg − Richter b-value. Other recurrence relationships, were considered, but ultimately rejected because:

1. There is little evidence for the validity of different recurrence laws in the literature,

2. Faults based, characteristic models are ill fit to the areal source zoning applied in our study.

We use the overall b-value determined in level 6, and assess the fit of five different models to the observed frequency-magnitude distribution (above the given completeness, which is defined as a function of space and time based on level 5) in each zone.

These models are:

1. Constant $b = b_0$, variable a-value determined on the entire observation period (taking into account the duration of each completeness period). b is computed using the maximum likelihood method. This model has one free parameter (the a-value).

2. Variable b and a: here we determine both the best fitting a- and b-value (in a maximum likelihood sense), hence the model has two free parameters.

3. Constant $b = b_0$ and two variable a-values (a_1 and a_2): one of the instrumental data (1975 − 2000), one for the historical period 1300 − 1975. The average a-value is then computed as the weighted (for the period length) average of the two a-values (two free parameters).

4. Variable b-value and two variable a-values: one of the instrumental data (1975 − 2000), one for the historical period 1300 − 1975. The average a-value is then computed as the weighted (for the period length) average of the two a-values (three free parameters).

5. Bayesian error weighted b-value, the weight between 0 and 1 is determined proportional to the uncertainties and sample sizes of the two b-values (between 1 and 2 free parameters).

$$bayes\_b = (err0\verb|^|2 / (err0\verb|^|2 + errb\verb|^|2 / N2)) * bwm\_2 + (errb\verb|^|2 / N2 / (err0\verb|^|2 + errb\verb|^|2 / 2)) * b_0$$

where *err0* is the one sigma uncertainty of the overall b-value, *errb* is the one sigma uncertainty of the b-value determined for this particular zone, *bwm_5* is the b-value determined in model 2, b_0 the overall b-value, and *N2* the number of samples. The degrees of freedom are then between 1 and 2, computed using the equation:

$$deg\_f = 1 + (err0\verb|^|2 / (err0\verb|^|2 + errb\verb|^|2 / N2))$$

The fit of each model to the observed data is given as a likelihood score; however, because the models have different degrees of freedom (i.e., free parameters), these likelihood sores cannot be compared directly. If two models have the same likelihood score, the one with fewer free

parameters should be the preferred model, because a simpler model tends to be more robust. In statistical terms, the decision which model to prefer at each node is based on the Akaike Information Criterion (*AIC*) score (Imoto 1991, Ogata 1999):

$$AIC_i = -2 * ln\,(likelihood) + 2 * K + (2 * K * (K + 1)) / (n - K - 1)$$

where K is the number of free parameters, and n the sample size. The model with the lowest *AIC* is the preferred model. This assures that a model with more free parameters (which implies reduced predictability) is only adopted when the data require doing so. For most zones in our whole-Switzerland model the first model is preferred (const $b = 0.9$ and variable a-value). In the Basel zone and in few other zones, a lower b-value is preferred. The *AIC* can also be used to obtain weighted alternative models in order to express the epistemic uncertainties in a logical tree approach. The best model is determined by examining their relative distance to the 'truth'. The first step is to calculate the difference between model with the lowest AIC and the others as:

$$\Delta_i = AIC_i - min\,AIC$$

where i is the difference between the AIC of the best fitting model and that of model I AIC_i is AIC for model i and *min AIC* is the minimum AIC value of all models. The relative weight can be described as:

$$w_i = \frac{exp(-0.5 * \Delta_i)}{\sum_{r=1}^{R} exp(-0.5 * \Delta_r)}$$

where w_i is known as *Akaike weights* for model I and the denominator is simply the sum of the relative likelihoods for all candidate models. An example of this kind of computation is shown in Figure 17.

The uncertainty in location is considered in the rate estimation through a simulation, as explained below. The uncertainty in magnitude could either be considered as part of the simulation or it could be integrated analytically as a bias adjustment for the rate, following Tinti & Mulargia (1985).
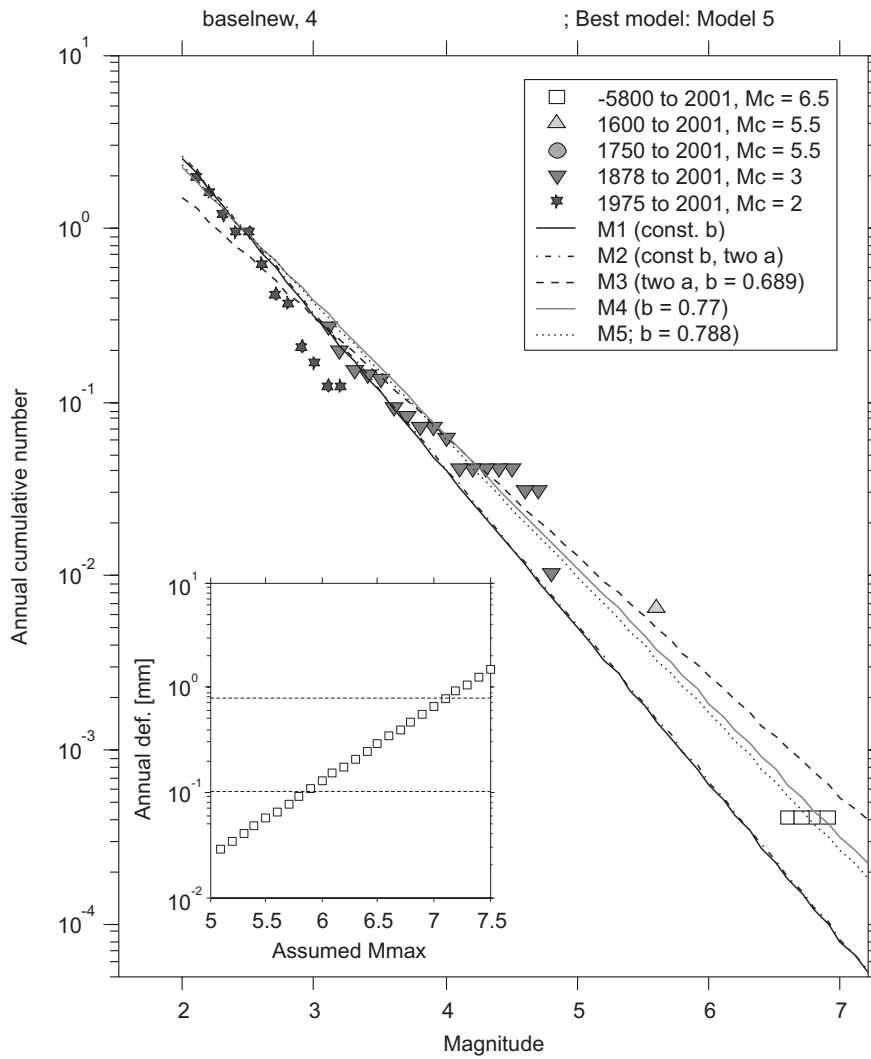
Fig. 17:   Cumulative annual rate of events as a function of magnitude for events in the Basel region

Symbols indicate five different completeness periods. The dashed and solid lines show the fit of five different models to the observation, the AIC score of each model is given in the bottom. The small inset displays the annual strain rate in [mm] as a function of assume M_{max}, using a Kostrov model with a 15 km depth extend of the seismogenic zone. The observed annual deformation from the last 7800 years of observations is about 0.2 mm/a, when using only the last 700 year, the rate is about 0.8 mm/a.

5.10 Treating the uncertainty in magnitude and hypocenter location

Hypocenters locations and magnitude are uncertain, and this uncertainty is known for each earthquake. In general, uncertainties in location and magnitude for events earlier in time are larger. Epicenter and magnitude uncertainties are important particularly for large historical event, because a given event could be associated with a number of zones.

In order to incorporate this epistemic uncertainty and quantify its influence on rates and b-values, we apply a Monte Carlo simulation to level 8 and 9. In each run of the simulation, a synthetic catalogue is created by randomly shifting each hypocenter and magnitude of individual events. The amount of random shift is based on the probability density function of the uncertainty. The uncertainties in epicentral and magnitude error are given in Table 3.5.3 from the PEGASOS report (PEGASOS EXT-TB-0043 2002). We interpret the uncertainty bounds given in the PEGASOS catalogue as 2 sigma bounds, because in our opinion a box distribution makes no sense and was not intended by the SED. Having created a randomized catalogue, the computation of M_{max} and rate in each areal source is repeated. By creating a large number of synthetic catalogues (> 100), the uncertainty in a-, b- and M_{max} based on magnitude and epicenter uncertainty is well resolved.

5.11 Depth distribution of seismicity

The depth distribution is explained in chapter 2, shown in Figure 2, and specified in Table 2. We use three different depth distributions:

1. South of the Helvetic Front (shallow activity)

2. North of the Helvetic Front (shallow and deep activity)

3. Molasse. For the Molasse we use the same depth distribution used in 2., modified such that the 3D volume of the Molasse, with a maximum depth of up to 5 km, remains aseismic.

5.12 Magnitude dependency of rupture depth

We are asked to assess the magnitude dependency of rupture depth. There is some evidence to suggest that the hypocenters of large earthquakes are located in the lower portion of the rupture, and that the aforementioned depth distribution for small events does not apply to large events. In our assessment, there is no specific data for Switzerland or Central Europe that addresses this issue. We therefore must rely on global studies (Stepp & Wong 1998). Two models are evaluated (Toro 2003b, PEGASOS TP4-TN-0360):

−   The *Weighted Approach,* which was used in the EPRI (1993) ground-motion study and in the Yucca Mountain study (Stepp & Wong 1998).

−   An alternative approach, the *Un-Weighted Approach,* has also been implemented.

Because of the hazard non-linearity, it is difficult for us to judge the relative importance of the magnitude-dependent depth dependency; consequently, we asked for a sensitivity analysis that illuminates the importance of this parameter. The results (Toro 2003b, PEGASOS TP4-TN-0360, Figure 18) show that sensitivity to the treatment of magnitude-dependent hypocentral depths for

area sources is very low. This has also implications for the treatment of the Molasse basin, which we consider not capable of supporting larger ruptures. The magnitude dependence of rupture depth expresses sufficiently our aforementioned opinion that M5+ events cannot originate in the Molasse; therefore, no special treatment of this zone is required. The sensitivity again confirms that this is not a critical decision for hazard.

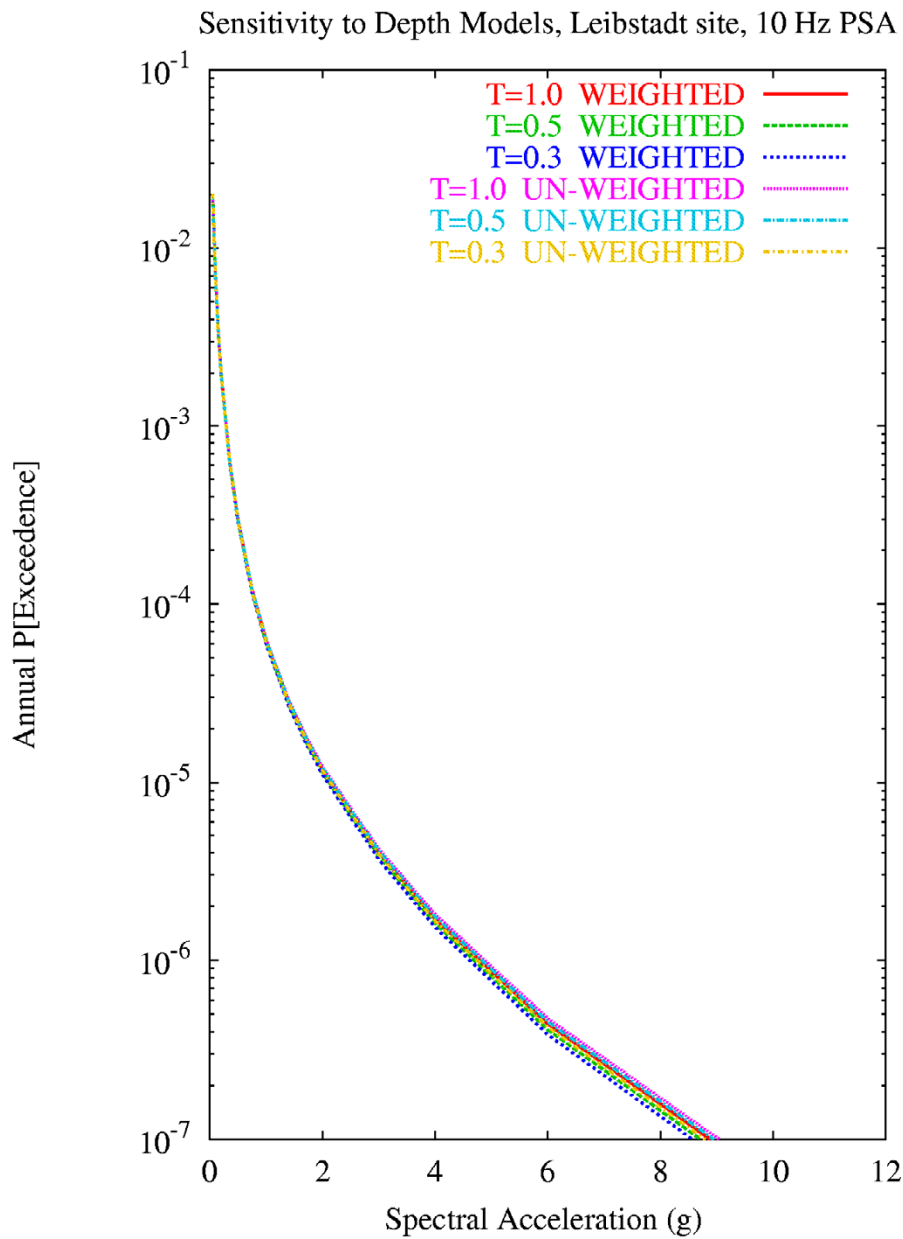|	
Expert conclusion:	Therefore, we feel confident in using an average value that has been used in the EPRI study: a magnitude-dependent depth distribution using the weighted approach outlined in Toro (2003c, PEGASOS TP1-TN-0373) with T = 0.5 (hypocenter in lower half of rupture).

Fig. 18:   Sensitivity of seismic hazard at Leibstadt site to assumptions regarding magnitude-dependent hypocentral depth: results for 10-Hz PSA (from Toro 2003b, PEGASOS TP4-TN-0360)

5.13   Earthquake rupture geometry

For the hazard computations, it is necessary to define the earthquake rupture geometry. To our knowledge, no specific relationships exist for Switzerland or Central Europe. Therefore, we resort to using globally establish relationships. We follow the Wells & Coppersmith (1994) approach. For defining the size of earthquake ruptures, we use the relationship:

$$\text{Mean } \log_{10}(\text{rupture area}) = 0.91 M - 3.49$$

$$\sigma_{\log10(\text{rupture area})} = 0.24$$

Using the relationship for the expectation of a lognormal distribution, the mean (expected) rupture area is given by the relationship:

$$\text{Mean rupture area} = 10^{(0.91 M - 3.424)}$$

The relationship for the mean rupture area will be used in the hazard computations. The rupture length and width have an aspect ratio of 2.5 : 1 until the maximum rupture width for a source is reached. The maximum rupture width is determined on the basis of the maximum depth and fault dip, as defined below.

For larger ruptures, the width is held constant at the maximum width and the length is obtained by dividing the rupture area by this width. Earthquake ruptures are located symmetrically on the epicenters (the epicenter is at the midpoint of the rupture). For those epicenters located closer than ½ rupture length to the source zone boundary, the ruptures are allowed to extend beyond the source boundary, as explained in Chapter 2.

We use the maximum depths in the distributions – 45 km, N of HF, and 25 km, S of HF – (Table 2) as a limit for the ruptures, to avoid unphysical deep ruptures.

The dip angle of ruptures is dependent on the faulting style, as defined in Table 2. We assume subvertical dip angles for strike slip ruptures, 60° dip for normal faulting, and 30° dip for thrusting. These values should be given a standard deviation of plus or minus 20° to remain consistent with the geological information.

5.14   Surface rupture versus surface faulting hazard

We discussed the issue of surface rupture versus surface faulting hazard. While we understand the potential implications of these distinctions for subsequent hazard assessments, we found ourselves unable to assert any rules for the occurrence or non-occurrence of surface rupture, as a function of earthquake magnitude.

6   REFERENCES

Note: We refer within the text extensively to archived data in the PEGASOS projectdata database (e.g. TP1-CAT-...., TP1-STR-.... etc.). These references are not included in this section; they can be retrieved from the PEGASOS archive.

Arthaud, F. & Matte, P. 1975. Les décrochements tardi-hercyniens du Sud-Ouest de l'Europe. Géométrie et essai de reconstitution des conditions de la déformation. Tectonophysics 25, 139-171.

Becker, A., Davenport, C.A. & Giardini, D. 2002: Paleoseismicity studies on end-Pleistocene and Holocene lake deposits around Basle, Switzerland. Geophys. J. Int. 149, 659-678.

Bender, B. 1983: Maximum likelihood estimation of b-values for magnitude grouped data. Bull. Seism. Soc. Am. 73, 831-851.

Boyer, S.E. & Elliott, D. 1982: Thrust systems. Bulletin of the American Association of Petroleum Geologists 66/9, 1196-1230.

Burkhard, M. 1990: Aspects of the large-scale Miocene deformation in the most external part of the Swiss Alps (Subalpine Molasse to Jura fold belt). Eclogae Geol. Helv. 83/3, 559-583.

Burg, J.-P., Van Den Driessche, J. & Brun, J.-P. 1994: Syn- to post-thickening extension in the Variscan Belt of Western Europe: Mode and structural consequences. Géologie de la France 3, 33-51.

Cornell, C.H. & Van Marke, E.H. 1969: The major influences on seismic risk. *In:* Proceedings of the Third World Conference on Earthquake Engineering, Santiago Chile A-1, 69-93.

Cornell, C.H. 1968: Engineering seismic risk analysis. Bulletin of the Seismological Society of America 58, 1583-1606.

Deichmann, N. 1992: Structural and rheological implications of lower crustal earthquakes below northern Switzerland. Phys. Earth. Plant. Inter. 69, 270-280.

Deichmann, N. 2002a: Focal mechanisms. Catalogue of fault-plane solutions of earthquakes, 15.04.02, PEGASOS EXT-TB-0042.

Deichmann N. 2002b: Performance of Declustering Methods. PEGASOS Technical Note EG1-TN-0305.

Deichmann, N., Baer, M., Braunmiller, J., Ballarin Dolfin, D., Bay, F., Delouis, B., Faeh, D., Giardini, D., Kastrup, U., Kind, F., Kradolfer, U., Kuenzle, W., Roethlisberger, S., Schler, T., Salichon, J., Sellami, S., Spuehler, E. & Wiemer, S. 2000: Earthquakes in Switzerland and surrounding regions during 1999. Eclogae Geol. Helv. 93.

DeMets, C., Gordon, R.G., Argus, D.F. & Stein, S. 1990: Current plate motions. Geophys. J. Int. 101, 425-478.

Eckardt, P., Funk, H.P. & Labhart, T. 1983: Postglaziale Krustenbewegungen an der Rhein-Rhone-Linie. Vermessung, Photogrammetrie, Kulturtechnik 2, 43-56.

EPRI 1993: Guidelines for Determining Design Basis Ground Motions, Vol. I: Early Site Permit Demonstration Program. Electric Power Research Institute, Palo Alto, CA, November.

Frankel, A. 1995: Mapping seismic hazard in the central and eastern United States. Seismo-logical Research Letters 66, 8-21.

Frankel, A., Mueller, C., Barnhard, T., Perkins, D., Leyendecker, E.V., Dickman, N., Hanson, S. & M. Hopper 1997: Seismic hazard maps for Califonia, Nevada and western Arizona/Utah. United States Geological Survey Open-File Report, 97-130, 1997.

Gardner, J.K. & Knopoff, L. 1974: Is the sequence of earthquakes in Southern California, with aftershocks removed, Poissonian? Bulletin of the Seismological Society of America 64, 1363-1367.

Grellet, B., Combes, P., Granier, T. & Philip, H. 1993: Séismotectonique de la France Métropolitaine. Mémoire de la Société géologique de France 164/1-2, 2 volumes.

Giardini, D. 1999: The Global Seismic Hazard Assessment Program (GSHAP) – 1992/1999. Annali de Geofisica 42, 957-974.

Giardini, D. 2002a: Answer to D. Slejko's and R. Musson's questions on TP1-CAT-0003. PEGASOS Technical Note EXT-TN-0145.

Giardini, D. 2002b: Supplementary SSS answers on the Rate Change Issue. PEGASOS Technical Note EXT-TN-0296.

Gutenberg, R. & Richter, C.F. 1944: Frequency of earthquakes in California. Bulletin of the Seismological Society of America 34, 185-188.

Homberg, C., Angelier, J., Bergerat, F. & Lacombe, O. 1994: New Tectonic Data in the External Jura – Contribution of Paleostress Reconstructions. Comptes Rendus De L'Academie Des Sciences Serie Ii 318/10, 1371-1377.

Homberg, C., Hu, J.C., Angelier, J., Bergerat, F. & Lacombe, O. 1997: Characterization of stress perturbations near major fault zones: Insights from 2-D distinct-element numerical modelling and field studies (Jura mountains). Journal of Structural Geology 19/5, 703-718.

Husen, S., Kissling, E., Deichmann, N., Wiemer, S., Giardini, D. & Baer, M. *in press*: Probabilistic Earthquake Location in Complex 3-D Velocity Models: Application to Switzerland. J. Geophys. Res. *in press*.

Imoto, M. 1991: Changes in the Magnitude Frequency B-Value Prior to Large (M-Greater-Than-or-Equal-to-6.0) Earthquakes in Japan. Tectonophysics 193/4, 311-325.

Jaboyedoff, M. & Pastorelli, S. 2003: Perturbation of the heat flow by water circulation in a mountainous framework: Examples from the Swiss Alps. Eclogae Geol. Helv. 96, 37-47.

Johnston, A.C., Coppersmith, K.J., Kanter, L.R. & Cornell, C.A. 1994: The Earthquakes of Stable Continental Regions: Vol. 1: Assessment of Large Earthquake Potential. Electric Power Research Institute EPRI TR-102261-V1.

Kagan, Y. 1999: Universality of the seismic moment-frequency relation. Pure and Applied Geophysics 155, 537-574.

Kagan, Y. & Jackson, D. 2000: Probabilistic forecasting of earthquakes. Geophysical Journal International 143, 438-453.

Kastrup, U., Zoback, M.-L., Deichmann, N., Evans, K., Michael, A.J. & Giardini, D. 2002: Stress field variations in the Swiss Alps and the Northern Alpine Foreland derived from inversion of fault plane solutions, submitted to J. Geophys. Res., Feb. 8, 2001 (PEGASOS EXT-RF-0030).

Kijko, A. & Graham, G. 1998: Parametric-historic procedure for probabilistic seismic hazard analysis – Part I: Estimation of maximum regional magnitude m(max). Pure and Applied Geophysics 152/3, 413-442.

Kijko, A., Lasocki, S. & Graham, G. 2001: Non-parametric Seismic Hazard in Mines. PAGEOPH 158/9-10, 1655-1675.

Kissling, E. 1993: Deep-Structure of the Alps – What Do We Really Know? Physics of the Earth and Planetary Interiors 79/1-2, 87-112.

Kostrov, B.V. 1974: Seismic moment and energy of earthquakes and seismic flow of rock, Izv. Acad. Sci. USSR Phys. Solid Earth, 1, 23-44, 1974.

Meghraoui, M., Delouis, B., Ferry, M., Giardini, D., Huggenberger, P., Spottke, I. & Granet, M. 2001: Active normal faulting in the Upper Rhine Graben and paleoseismic identification of the 1356 Basel earthquake. Science 293, 2070-2073.

Mancktelow, N. 1985: The Simplon Line: a major displacement zone in the Western Lepontine Alps. Eclogae Geol. Helv. 78, 73-96.

Niviere, B. & Winter, T. 2000: Pleistocene northwards fold propagation of the Jura within the southern Upper Rhine Graben: seismotectonic implications. Global and Planetary Change 27/1-4, 263-288.

Ogata, Y. 1999: Seismicity analysis through point-process modeling: A review. Pure and Applied Geophysics 155/2-4, 471-507.

PEGASOS EXT-TB-0043 2002: ECOS: Earthquake Catalogue of Switzerland. Final version, 16.04.02, SED-ETHZ.

PEGASOS EXT-TB-0050 2002: PALEOSEIS. Reconstructing the paleoseismological record in northern Switzerland. Final Report to HSK and NAGRA, 30.06.2002, SED-ETHZ.

Reasenberg, P.A. 1985: Second-order moment of Central California Seismicity. Journal of Geophysical Research 90, 5479-5495.

Regenauer-Lieb, K. & Petit, J.P. 1997: Cutting of the European continental lithosphere: Plasticity theory applied to the present Alpine collision. Journal of Geophysical Research-Solid Earth 102/B4, 7731-7746.

Ricou, L.-E. 1994: Tethys reconstructed: plates, continental fragments and their boundaries since 260 Ma from Central America to South-eastern Asia. Geodinamica Acta 7/4, 169-218.

Ruettener, E. 2002: Alternative source models for a PSHA in Switzerland, SP1 Workshop 2 (PEGASOS TP1-RF-0158).

Rydelek, P.A. & Sacks, I.S. 1989: Testing the completeness of earthquake catalogs and the hypothesis of self-similarity. Nature 337, 251-253.

Schmid, S.M. 2002: Trenching active fault-scarps in the Basle region, SP1 Workshop 2 (PEGASOS TP1-RF-0162).

Schmid, S.M. & Kissling, E. 2000: The arc of the western Alps in the light of geophysical data on deep crustal structure. Tectonics 19/1, 62-85.

Schmid, S.M., Froitzheim, N., Pfiffner, O.A., Schonborn, G. & Kissling, E. 1997: Geophysical-geological transect and tectonic evolution of the Swiss-Italian Alps (Vol. 15, p. 1036, 1996). Tectonics 16/1, 186-188.

Schumacher, M.E. 2002: Upper Rhine Graben: Role of preexisting structures during rift evolution. Tectonics 21, 10.1029/2001TC900022.

Sissingh, W. 1998: Comparative Tertiary stratigraphy of the Rhine Graben, Bresse Graben and Molasse Basin: correlation of Alpine foreland events. Tectonophysics 300/1-4, 249-284.

Sissingh, W. 2001: Tectonostratigraphy of the West Alpine Foreland: correlation of Tertiary sedimentary sequences, changes in eustatic sea-level and stress regimes. Tectonophysics 333, 361-400.

Slejko, D., Peruzza, L. & Rebez, A. 1998: Seismic hazard maps of Italy. Annali di Geofisica 41/2.

Sommaruga, A. 1999: Décollement tectonics in the Jura foreland fold-and-thrust belt. Marine and Petroleum Geology 16, 111-134.

Stepp, C. & Wong, I.G. (coordinating authors) 1998: Probabilistic Seismic Hazard Analysis for fault displacement and vibratory ground motion at Yucca Mountain, Nevada. Report to the U.S. Department of Energy by the CRWMS M&O Contractor.

Tinti, S. & Mulargia, F. 1985: Effects of magnitude uncertainties on estimating the parameters of the Gutenberg-Richter frequency-magnitude law. Bulletin of the Seismological Society of America 75, 1681-1697.

Toro, G. 2003a: Notes on Input files for EG1d Sensitivity Analyses. PEGASOS Technical Note TP4-TN-0345.

Toro, G. 2003b: Sensitivity of Seismic Hazard to the Treatment of Hypocentral Depth. PEGASOS Technical Note TP4-TN-0360.

Toro, G. 2003c: Technical Note on the Treatment of Hypocentral Depths and Rupture-Length Effects for Area Sources in the FRISK88MP Software. PEGASOS Technical Note TP1-TN-0373.

Truffert, C., Burg, J.-P., Cazes, M., Bayer, R., Damotte, B. & Rey, D. 1990: Structures crustales sous le Jura et la Bresse: contraintes sismiques et gravimétriques le long des profils ECORS Bresse-Jura et Alpes II. Mémoires de la Société Géologique de France 156, 157-164.

Utsu, T. 1999: Representation and analysis of the earthquake size distribution: A historical review and some new approaches. PAGEOP 155, 509-535.

Veneziano, D., Cornell, C.A. & O'Hara, C.A. 1984: Historical method of seismic hazard analysis. Electrical Power Research Institute Report NP-3438.

Villemin, T., Alvarez, F. & Angelier, J. 1986: The Rhinegraben – Extension, Subsidence and Shoulder Uplift. Tectonophysics 128/1-2, 47-59.

Wells, D.L. & Coppersmith, K.J. 1994: New Empirical Relationships among Magnitude, Rupture Length, Rupture Width, Rupture Area, and Surface Displacement. Bulletin of the Seismological Society of America 84/4, 974-1002.

Wiemer, S. 2002: Declustering the PEGASOS Earthquake Catalogue. PEGASOS Technical Note EXT-TN-0208.

Wiemer, S. & Baer, M. 2000: Mapping and removing quarry blast events from seismicity catalogs. Bulletin of the Seismological Society of America 90, 525-530.

Wiemer, S. & Woessner, J. 2002: Is the PEGASOS (ECOS) Earthquake Catalog Poissonian? PEGASOS Technical Note TP1-TN-0266.

Wiemer, S. & Wyss, M. 2000: Minimum magnitude of complete reporting in earthquake catalogs: examples from Alaska, the Western United States, and Japan. Bulletin of the Seismological Society of America 90, 859-869.

Wiemer, S. & Wyss, M. 2002: Mapping spatial variability of the frequency-magnitude distribution of earthquakes. Advances in Geophysics 45, 259-302.

Ye, S., Ansorge, J., Kissling, E. & Mueller, S. 1995: Crustal Structure beneath the Eastern Swiss Alps Derived from Seismic-Refraction Data. Tectonophysics 242/3-4, 199-221.

Youngs, R. 2003: Earthquake Recurrence Relationships Computed From Seismic Source Parameters Developed in Hazard Sensitivity Model of EG1d. PEGASOS Tehnical Note TP1-TN-0339.

Ziegler, P.A. 1992: European Cenozoic rift system. Tectonophysics 208, 91-111.

APPENDIX 1: SOURCE ZONE GEOMETRY AND LOGIC TREE

Start Model

SA
XWCA
XHHA
J
SRGB_LG
NWE_nps

Map of ecos$_a$ll3.mat; 1303.2 to 2001
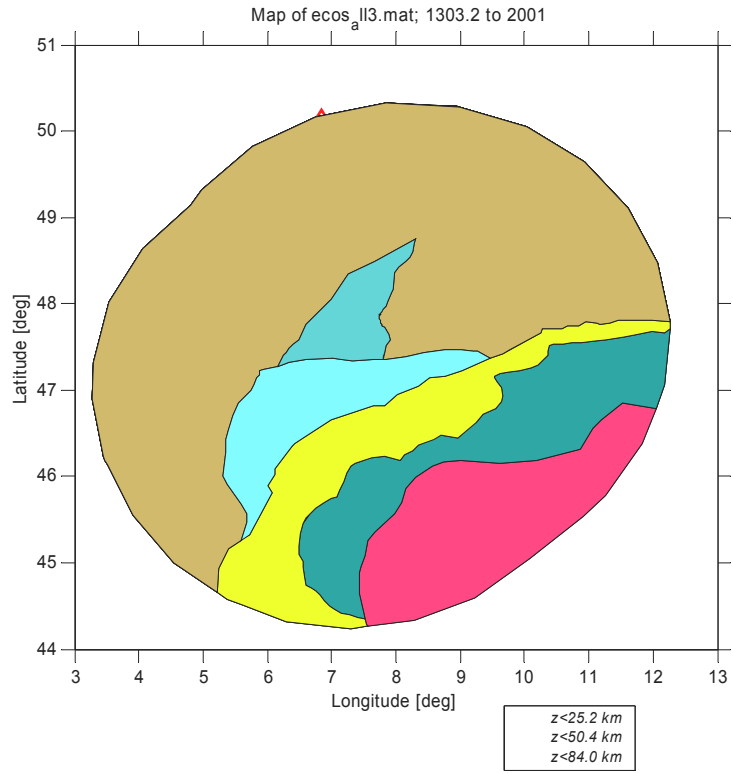
Decision 1

XHA exist (10 %)

→ Replace XHHA
with XHA and HA

Map of ecos$_a$ll3.mat; 1303.2 to 2001
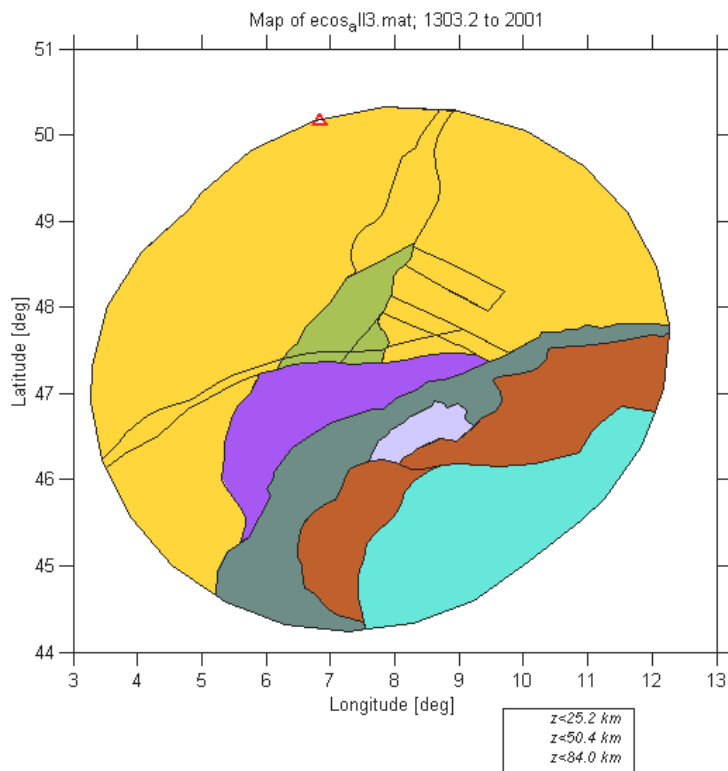
Decision 2

subdivide XWCA (50 %)
→ Replace XWCA
with XCA and XWA

Map of ecos$_a$ll3.mat; 1308.1 to 1986
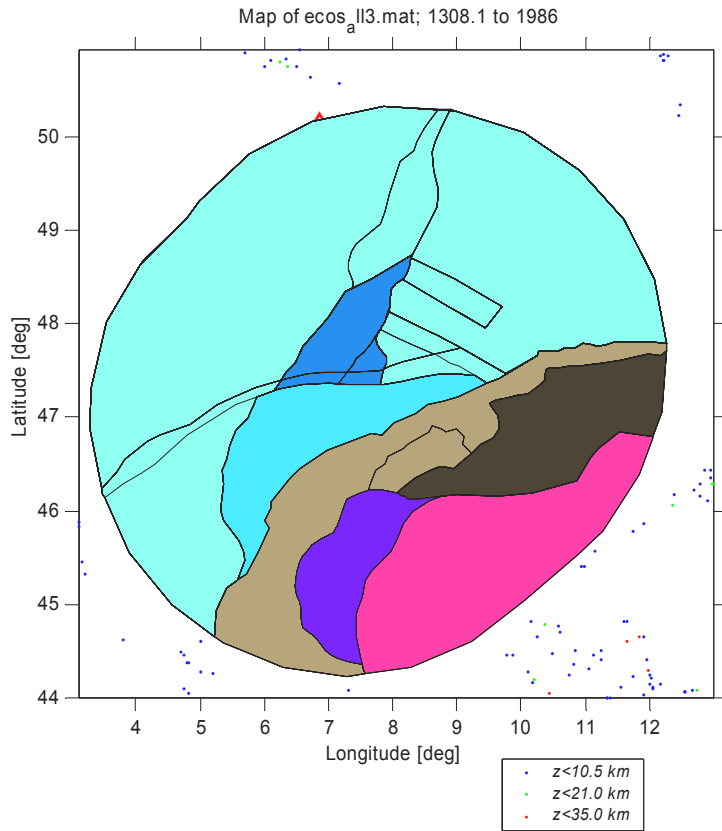
Decision 3

Basel subzone exists (50 %)
→ Replace SRGB_LG
with B_Lg and SRG_LG

Map of ecos$_a$ll3.mat; 1308.1 to 1986
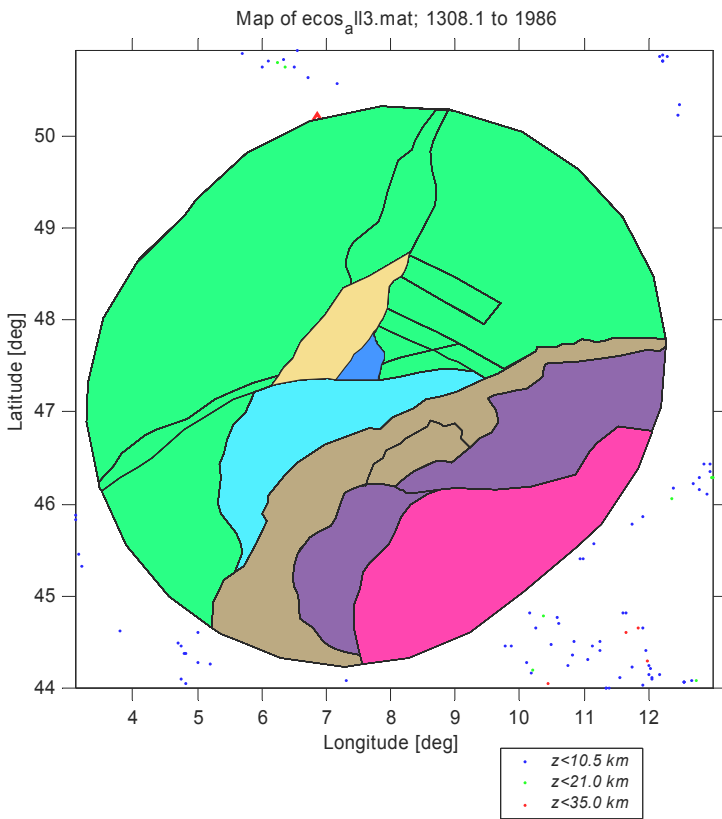
Decision 4

Swaebian Alb exists (10 %)
→ Replace NWE_nps
with SWA and
[NWE_nps minus SWA]

Map of ecos$_a$ll3.mat; 1308.1 to 1986
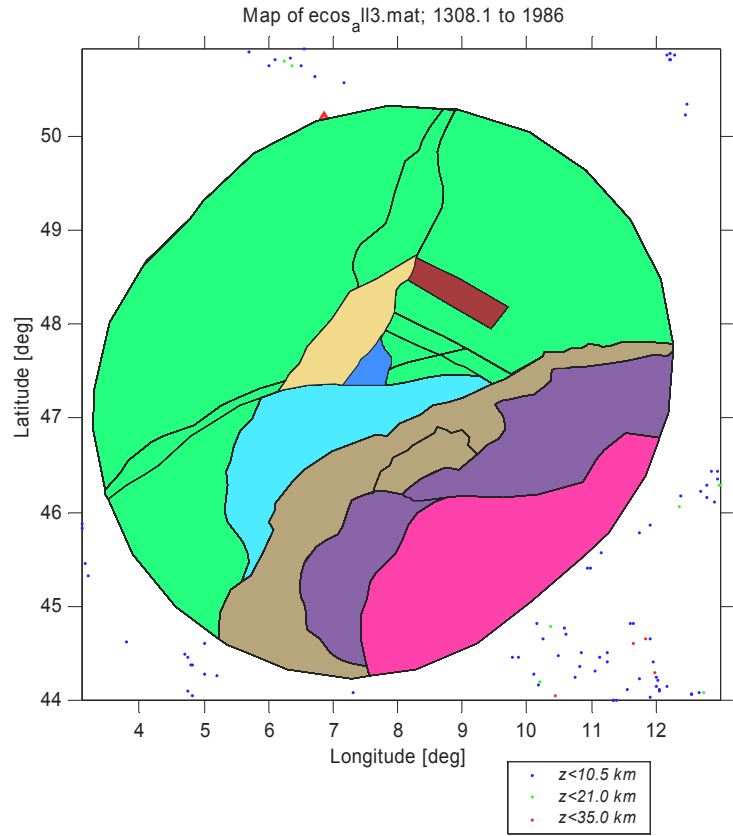
Decision 5

Northern Rhine Graben exists
(50 %)
→ Replace NWE_nps
with NRG and
[NWE_nps minus NRG]

Map of ecos$_a$ll3.mat; 1308.1 to 1986
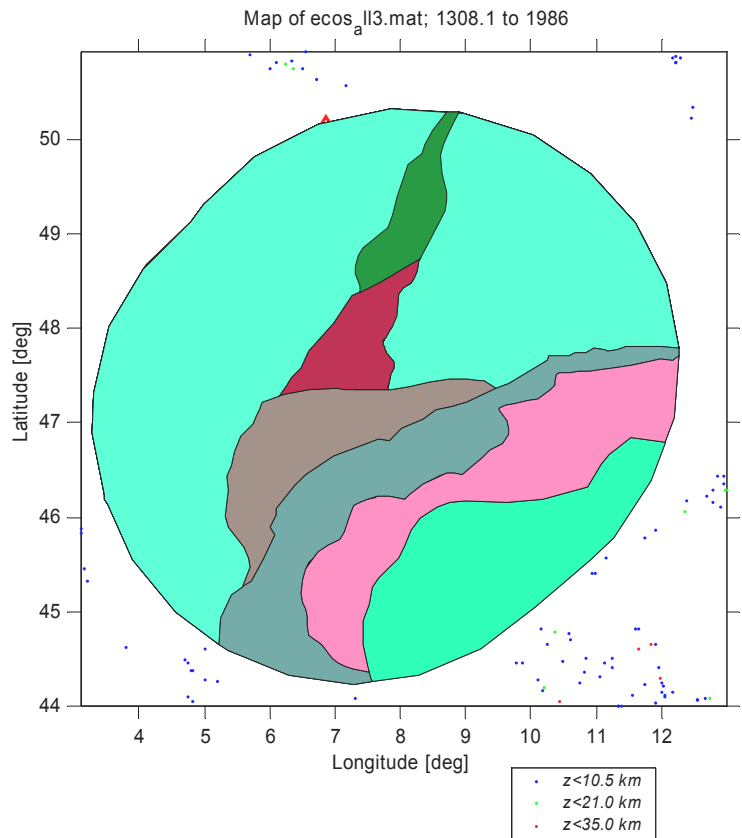
Decision 6

FKZ exist exists (5 %)
→ Replace NWE_nps
with FKZ and
[NWE_nps minus FKZ]

Map of ecos$_a$ll3.mat; 1308.1 to 1986

z<10.5 km
z<21.0 km
z<35.0 km
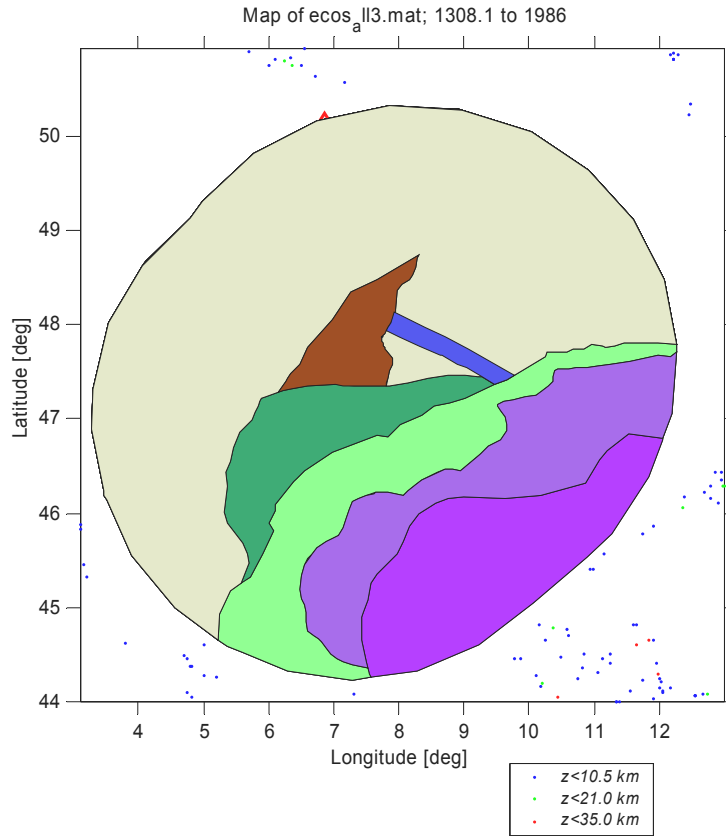
Decision 7

TZ exist exists (5 %)
→ Replace NWE_nps with TZ
and [NWE_nps minus TZ]
→ If B exists:
Replace B_LG
with B and
SRG_LG with SRG_SM
→ If FKZ exists:
Replace FKZ
with FKZ_no_TZ

Map of ecos$_a$ll3.mat; 1308.1 to 1986

z<10.5 km
z<21.0 km
z<35.0 km
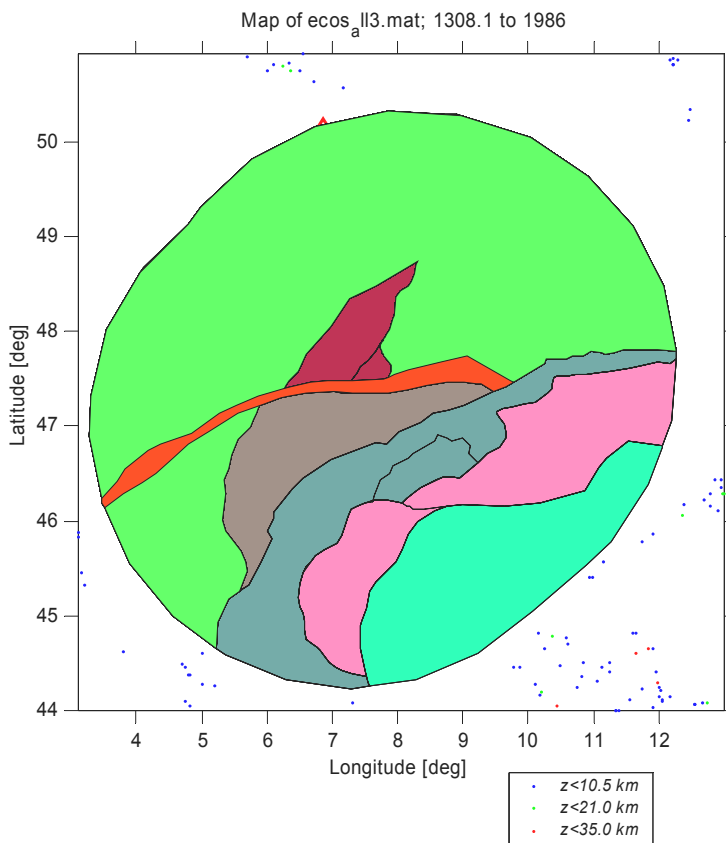
The most complex model possible is shown below:

Map of ecos$_a$ll3.mat; 250 to 1989.2
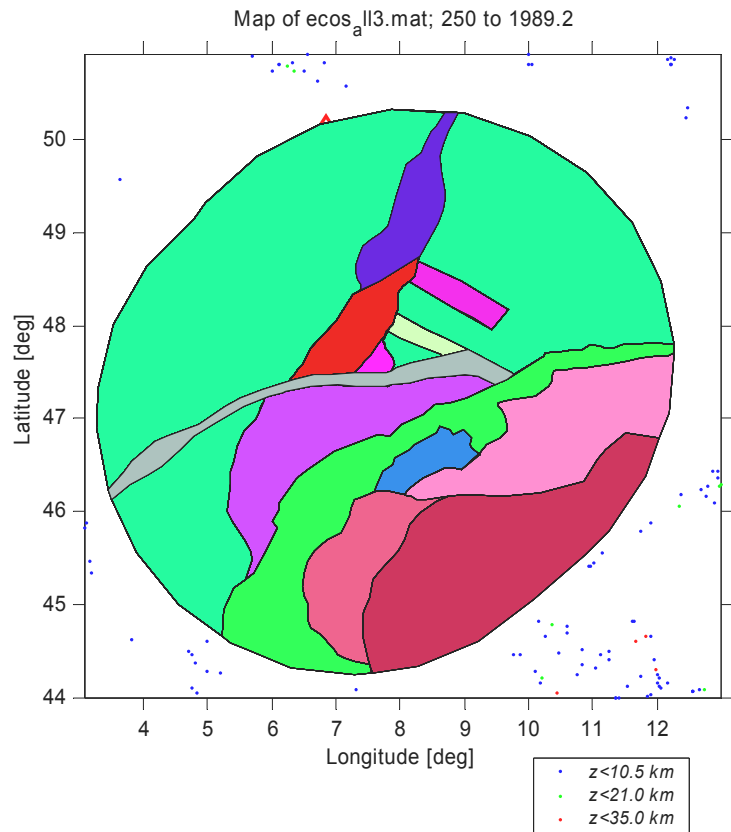
Note on choosing the correct European background:

The areal source 'Europe' is overlain by up to 4 independent source zones. Decision 4 – 7 all modify Europe. Therefore, a number of European backgrounds needs to be available, and I believe there may be 15 combinations:

1 (all four zones)
4 (all combination of 3 zones)
6 (all combination of 2 zones)
4 (only one zone)

Note that these zones are overlain, they do not separate the original zones they cut holes out of them. It might be best to digitize the 15 options, run through our 7 level decision tree outlined above, and find the 'right' Europe zones, depending on which of the element exist in this particular branch.

APPENDIX 2:   EXPLOSION CONTAMINATION OF THE PEGASOS CATALOGUE

The PEGASOS catalogue contains a certain number of unidentified explosion events. These events are largely contained in the most recent 30 year period of data. Their magnitudes are believed to be mostly smaller than M 3. Nevertheless, they significantly affect the smoothing and rate / b-value computation in some regions.

To estimate the amount of unidentified explosion, we plot a histogram of the time of the day of all unquestionable events not marked as explosion in the PEGASOS database (Figure A-1). This plots reveals a typical pattern for a quarry rich region (Wiemer & Baer 2000): Detection is best in the nighttime hours (Rydelek & Sacks 1989), therefore, more small events are found in these hours. The peak during daytime hours, however, is not explained by improved completeness, but caused by artifacts. From Figure A-1 we estimate that roughly 500 explosions are contained in the PEGASOS data.
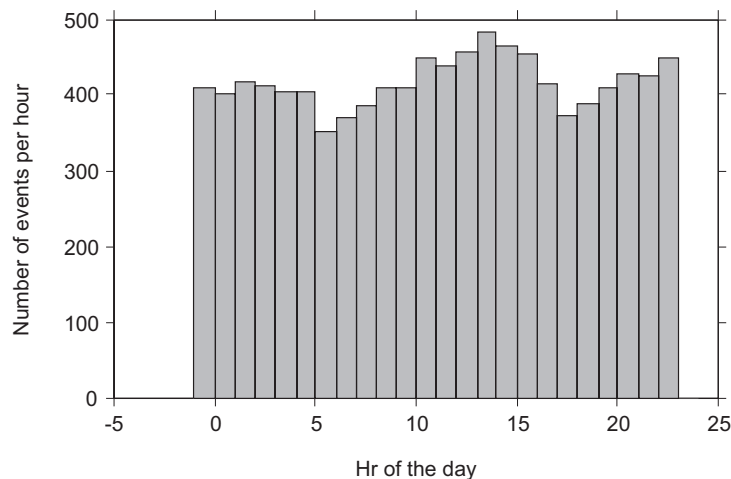
Fig. A-1:   Histogram of the hourly activity of the PEGASOS catalogue from 1970 – 2001

To learn more about these explosions, it is useful to map them out spatially (Wiemer and Baer 2000) (see also Baer, PEGASOS presentation, 2002). This map of the ratio of nighttime to daytime number of earthquakes pinpoints the location of quarries. The map in Figure A-2 was computed using sampling volumes of 60 events; therefore, ratios of > 2 plotted in blue to purple colors suggest a highly unusual distribution of seismicity (Wiemer & Baer, 2000). Unusually low ratios (red colors in Figure A-2) could also be indicative of man-made activity (e.g., nighttime underground mine activity), but is often less clear, because a similar ratio shift is caused by completeness. An example of the hourly distribution of events in an anomalous region is shown in Figure A-3, the 100 events near the 'Wallis anomaly' visible in Figure A-2.
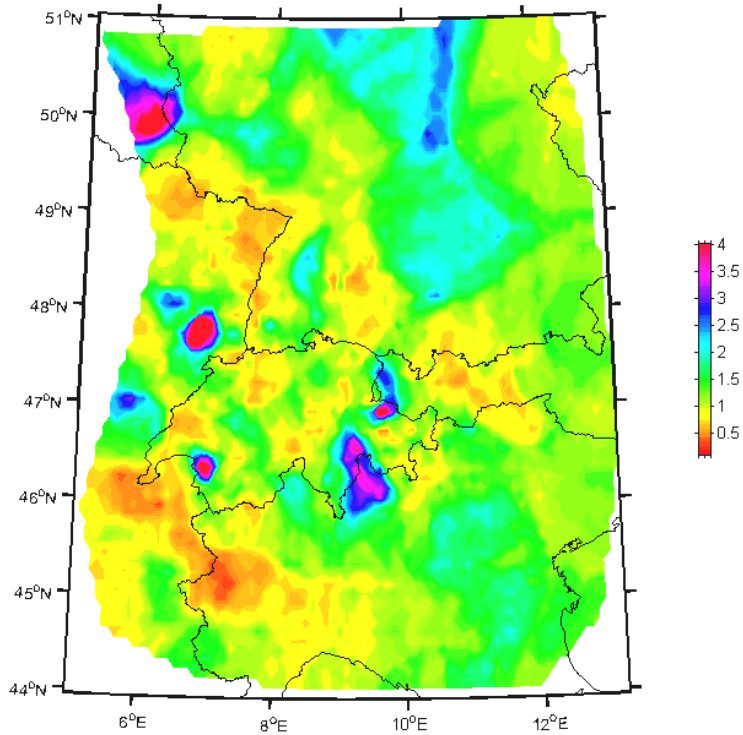
Fig. A-2:   Map of the daytime to nighttime ratio of events (daytime: 8:00 – 18:00 GMT)

High ratios (blue to purple colors) suggest the presence of explosion contamination in the data.
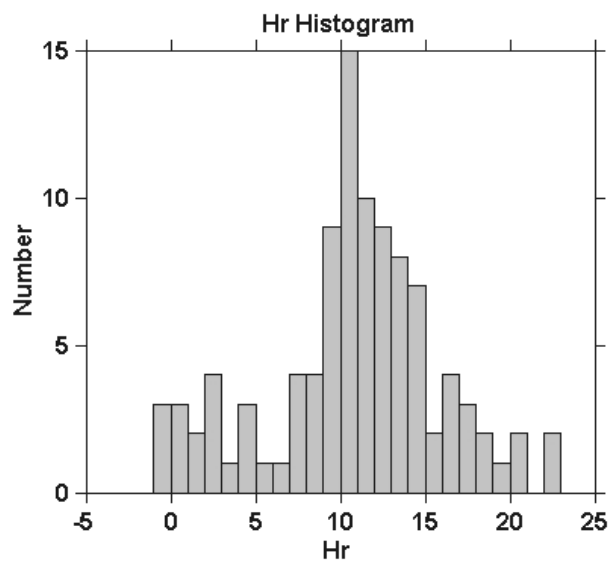
Fig. A-3:   Hourly histogram of events located near the 'Wallis anomaly' as seen in Figure A-2

While most explosions are comparatively small, they can reach up to magnitude 3 in general, and up to M4 in very selective regions. Therefore, even after cutting the catalogue at the respective completeness levels, the problem is not removed. In fact, after cutting it will before difficult to identify these fewer remaining events based on the simple statistical criterion used here. Cutting the catalogue at higher M that the M 1.8 lower bound proposed would be unsatisfactory, since it would reduce strongly the amount of available data. The effect of explosions is most critical for *b*-value estimations, because these artificial events of generally the same size results in an artificially high *b*-value and possibly a erroneously low return time for large events.

To address the problem of explosion contamination, we follow the iterative approach outlined in (Wiemer & Baer 2000). First, the most significant quarry anomaly in the entire data set is identified. Its extent is determined based on a maximization of the significance of the nighttime top daytime ratio. For this anomaly, all events in the daytime hour are removed. This process is repeated until no anomaly significant at 1 % remains.

The final 'dequarried' catalogue contains fewer events during daytime hours, because some real earthquakes are removed. However, because the removed real events are independent of magnitude, and presumably follow the true natural size distribution, the effect is only a reduction in rate for these volumes (Figure 5), limited to the instrumental data only. This unavoidable rate reduction is considerably less biasing than the original bias in rate, smoothing, and *b*-value caused by the numerous explosions.

In an additional step, we also remove manually events in the vicinity of a mining area in France. This region shows an anomalously low daytime to nighttime ratio, and a peculiar time distribution and magnitude size distribution of events (Figure A-4). The numerous seismicity events in these regions after 1980 corresponds almost exclusively with mine activity in the XXX region (Burg, personal communication 2002). Our final catalogue of possible quarry locations contains 1037 events in the period 1975 – 2001.

To incorporate the result of this computation into the hazard computation, we provide the project with an ASCII list (quarry_index.dat) of all event ID's (ECOS field identifier: *Catalogue_ID*) identified by this procedure.
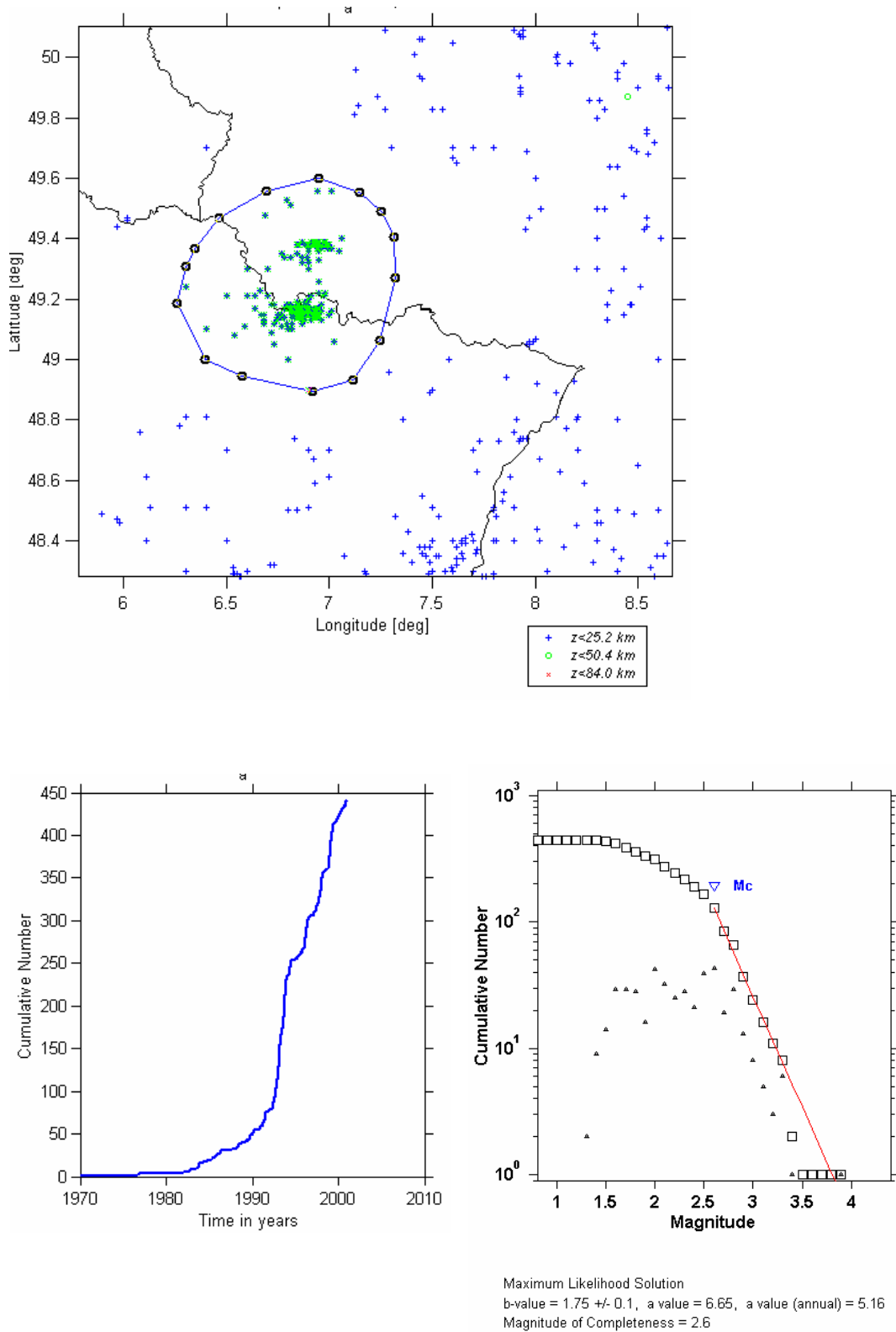
Fig. A-4: Map of seismicity, marked in green are events in the French mining area, also shown is their time and size distribution
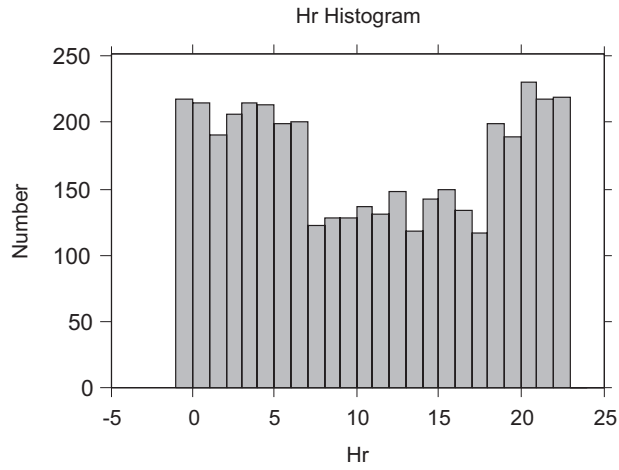
Fig. A-5:   Hourly distribution of events after 'dequarrying' the catalogue
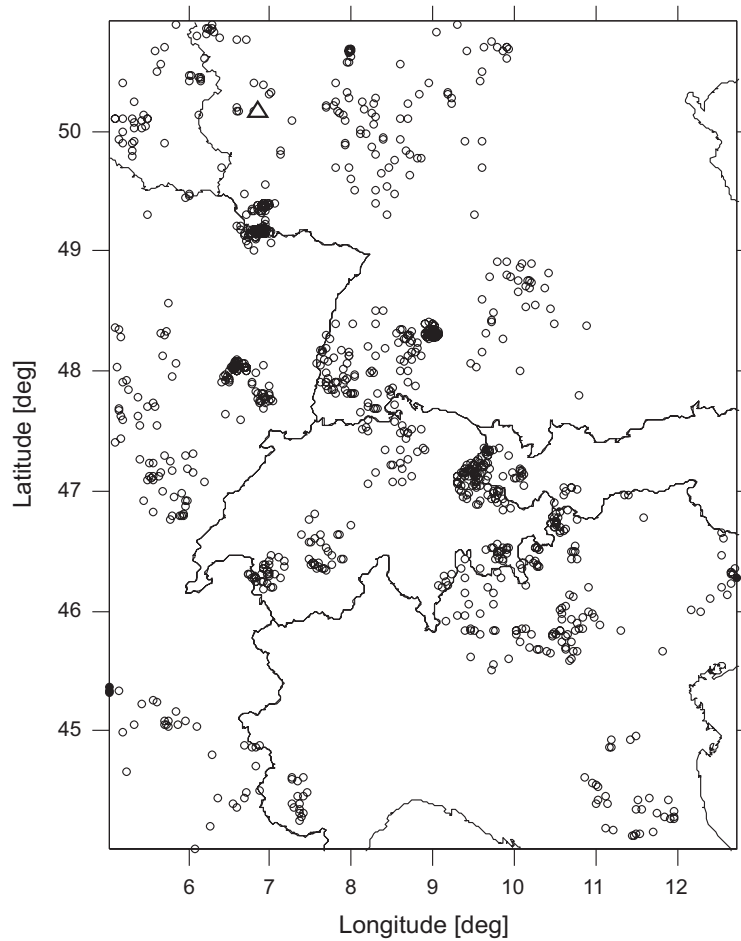
Fig. A-6:   Map of the events identified as possible quarry locations

APPENDIX 3:   COMPLETENESS ESTIMATION

General remarks: Completeness is estimated country by country, because differences between national catalogues are the first order boundaries in completeness. The completeness estimate is based on expert judgement, using various plots of the seismicity to appreciate Mc. The simplest plot of magnitude as a function of time gives a first overview of completeness. We then plot Stepp plots as well as frequency-magnitude distributions, and identify the major times of changes. This iterative process leads to a definition of completeness periods though time. In the case of Switzerland, results are then double-checked against historical estimations of completeness, as given in the ECOS catalogue. For the instrumental data, completeness is also computed using an algorithm developed for completeness mapping (Wiemer & Wyss 2000).

Completeness estimation, especially for historical data, is only possible with large uncertainties. To express this uncertainty, we define an alternative interpretation based on the assumption that historical data is less reliable; hence cutting at a higher Mc. Therefore, the alternative model gives relatively more weight to historical data.

Switzerland:

Period	Mc – Model 1 [Mw]	Mc – Model 2 [Mw]
1300 – 1600	6.0	6.0
1600 – 1750	5.5	5.7
1750 – 1880	4.7	5.0
1880 – 1977	3.0	4.2
1977 – 2001	1.8	1.9
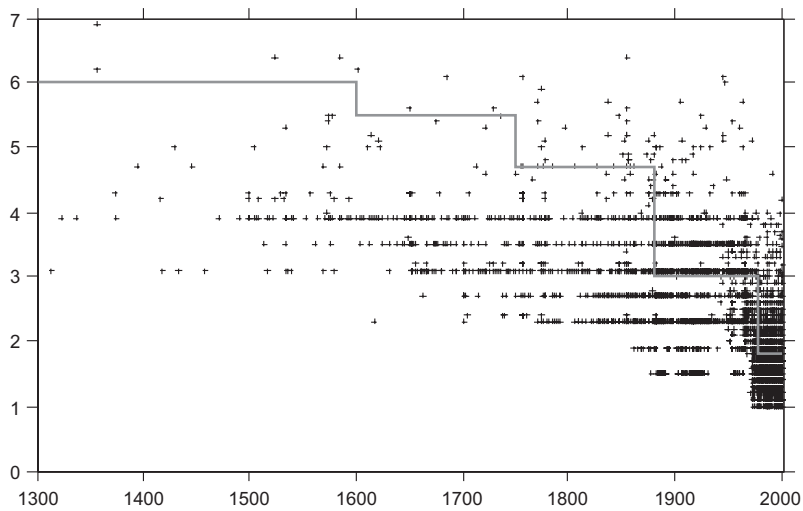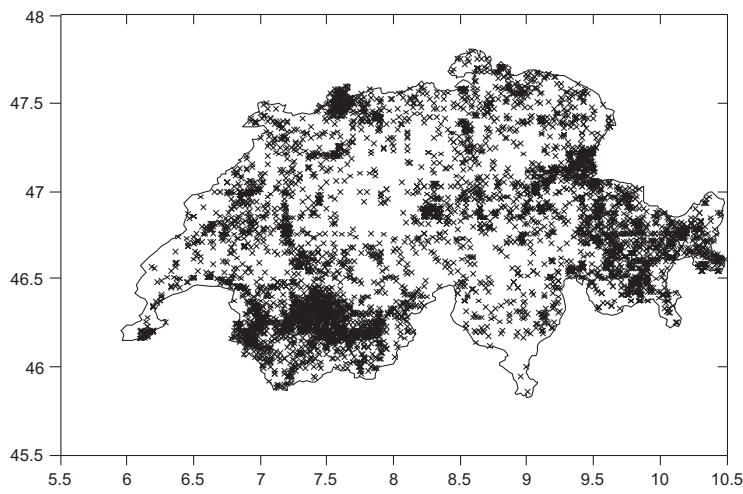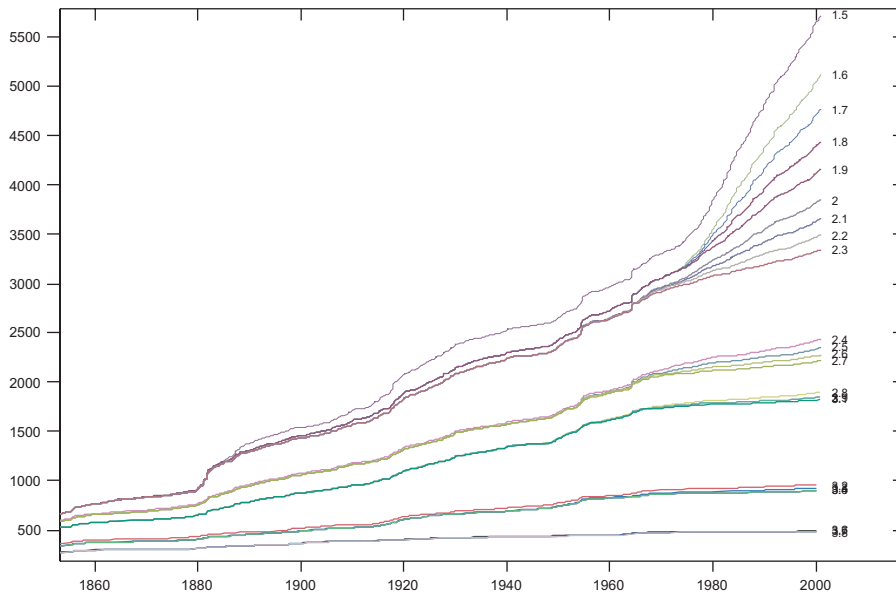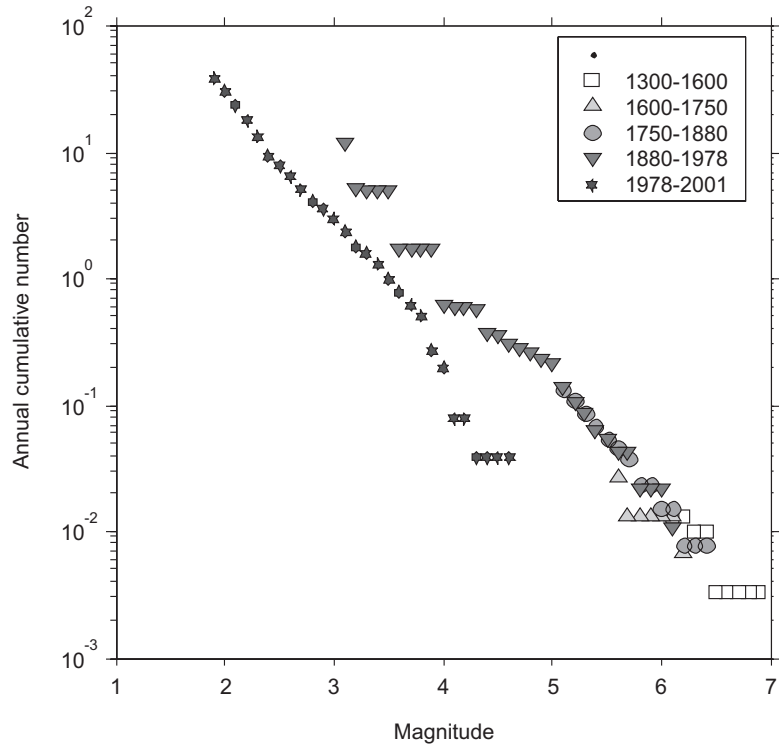
Germany

Period	Mc – Model 1 [Mw]	Mc – Model 2 [Mw]
1300 – 1620	6.0	6.5
1620 – 1870	5.4	5.6
1870 – 1980	3.1	3.5
1980 - 2001	3.0	3.1
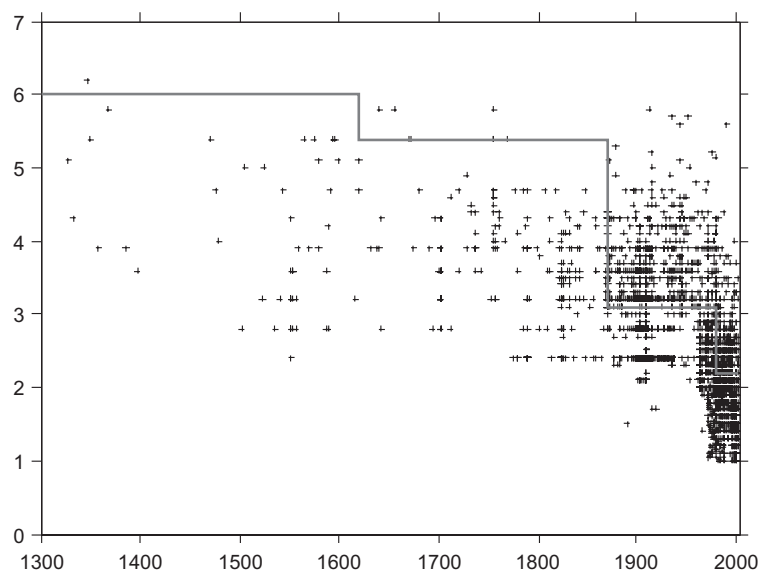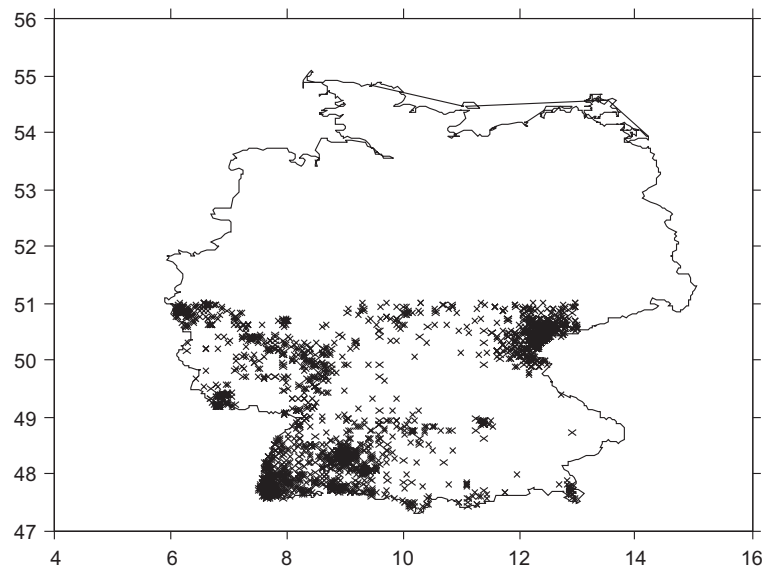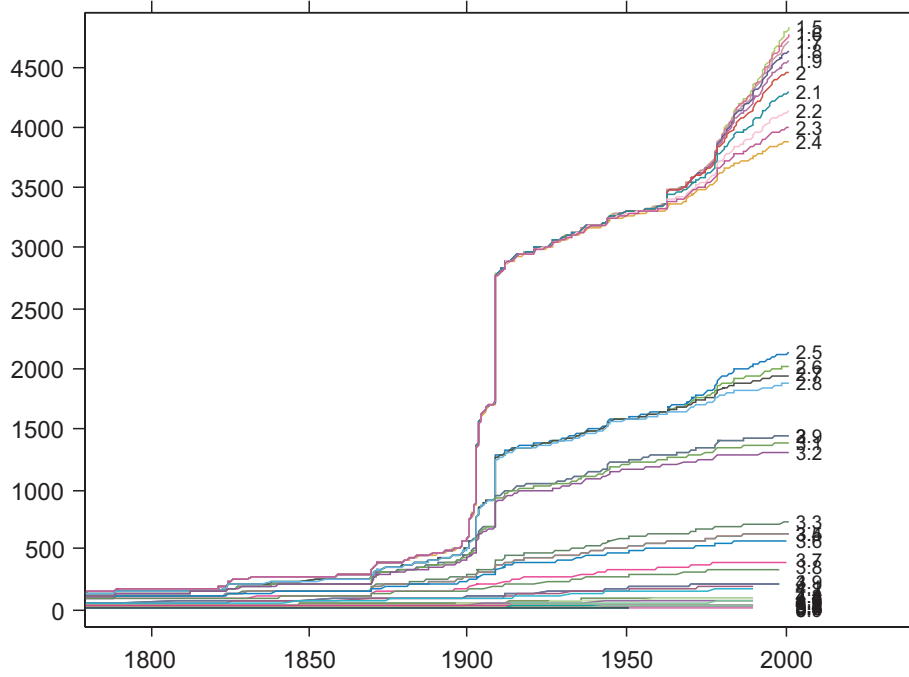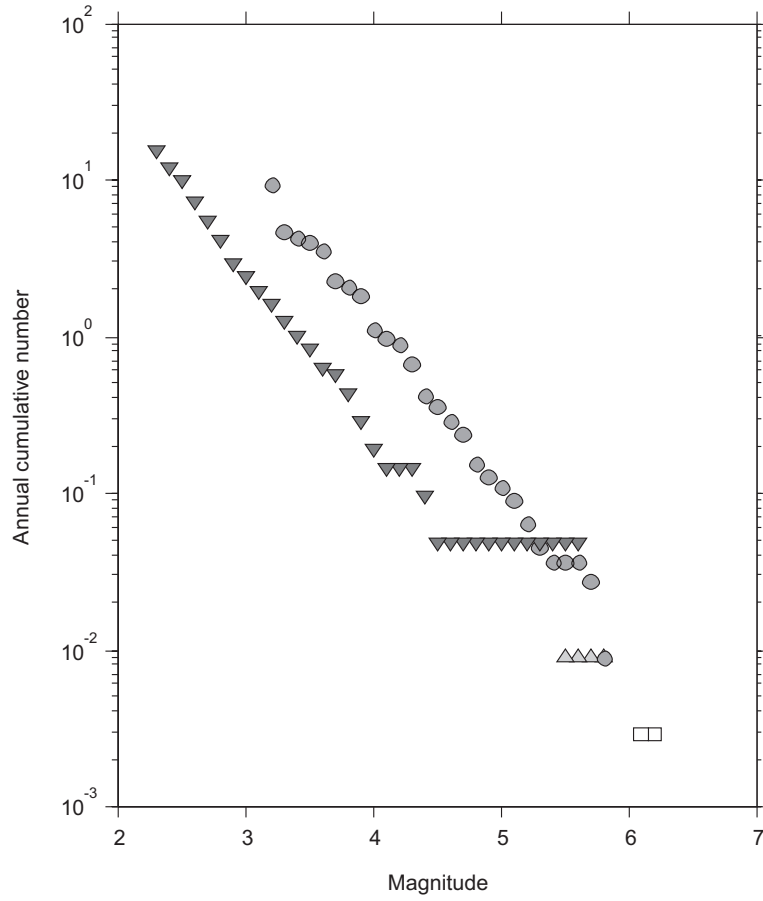
Austria

Period	Mc – Model 1 [Mw]	Mc – Model 2 [Mw]
1700 – 1896	5.5	6
1896 – 1978	3.1	3.3
1978 – 2001	2.5	2.5
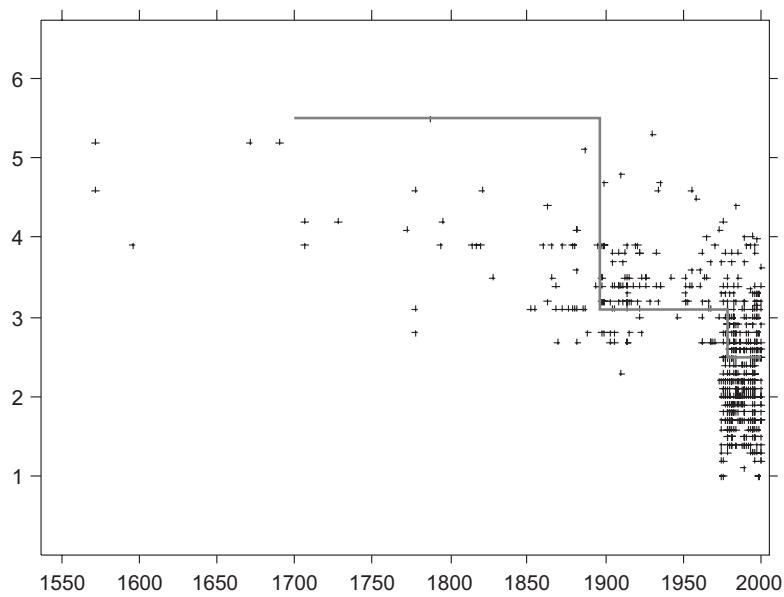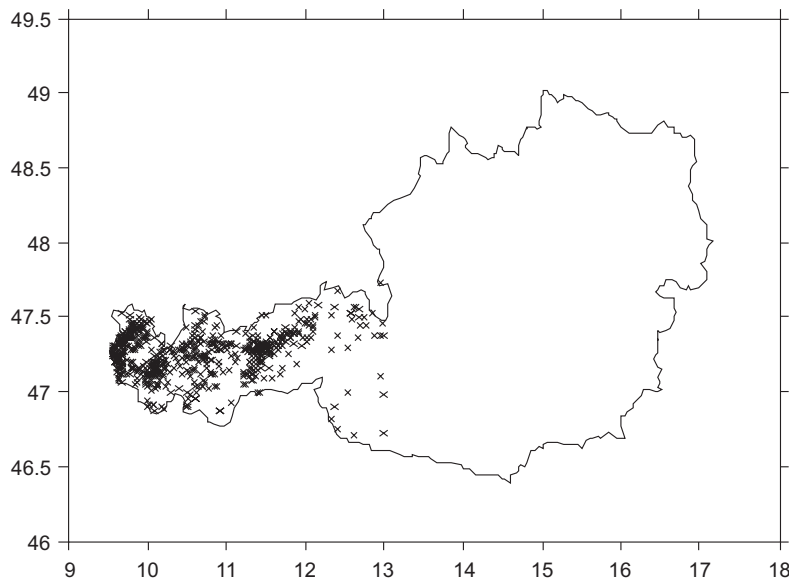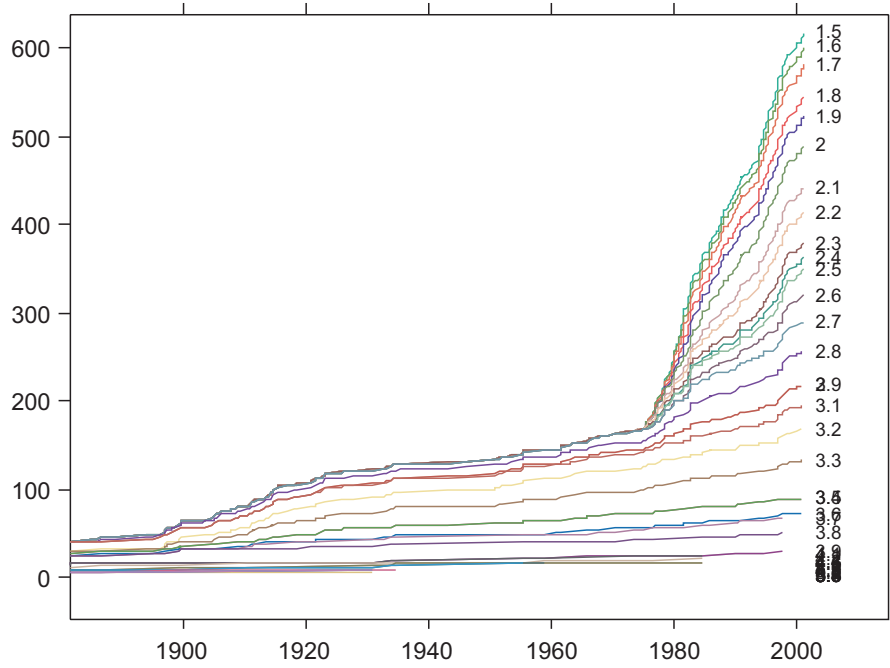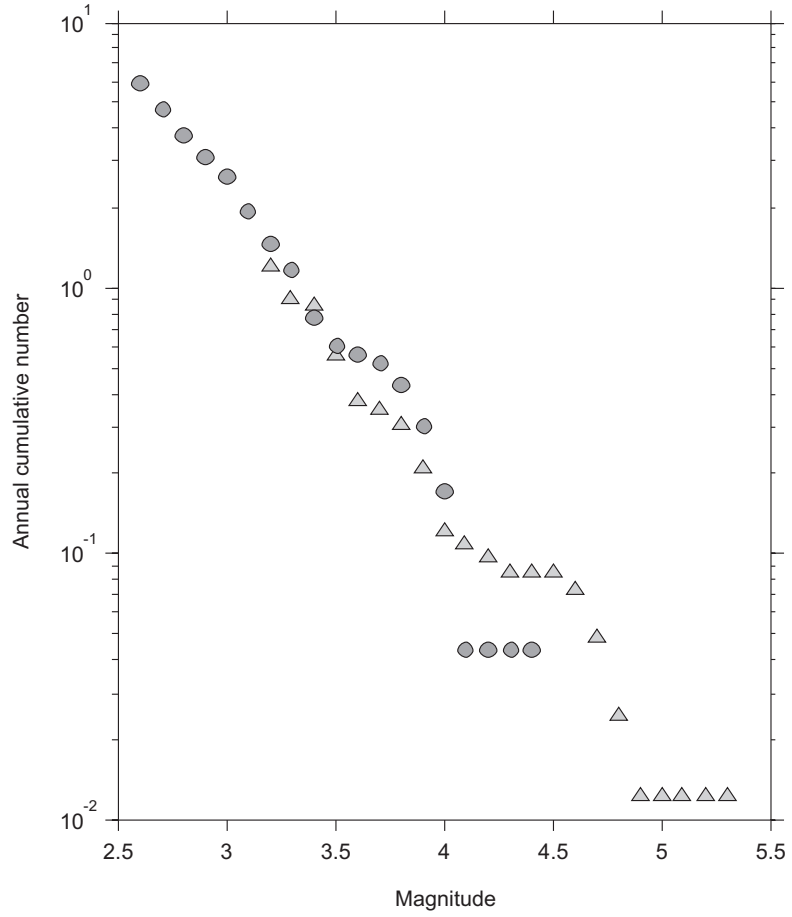
Italy

Period	Mc – Model 1 [Mw]	Mc – Model 2 [Mw]
1775 – 1880	5.5	5.7
1880- 1979	4.1	4.3
1979 – 2001	3.2	3.2
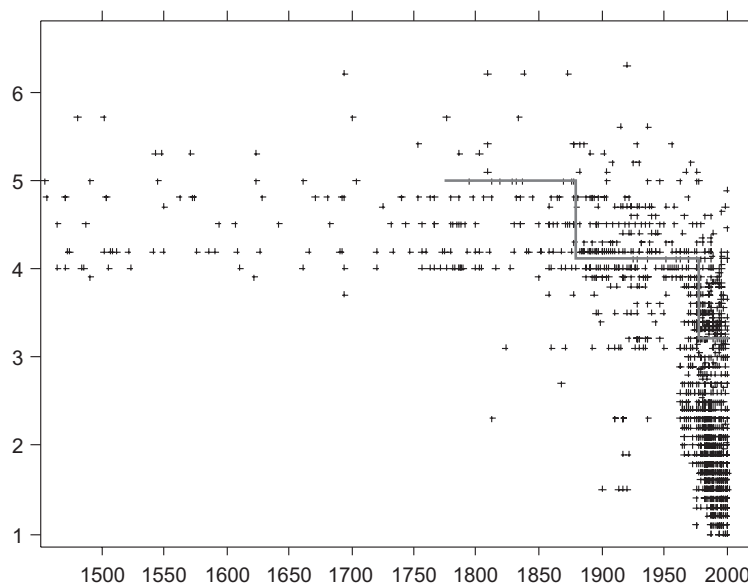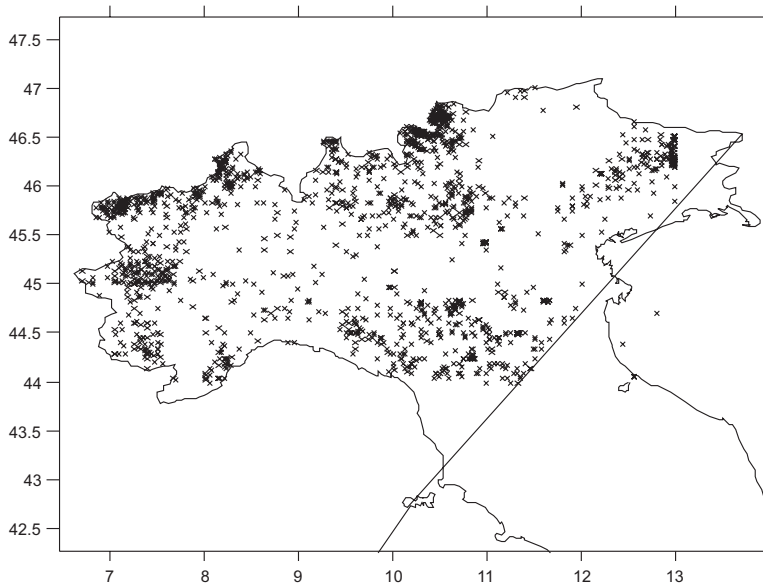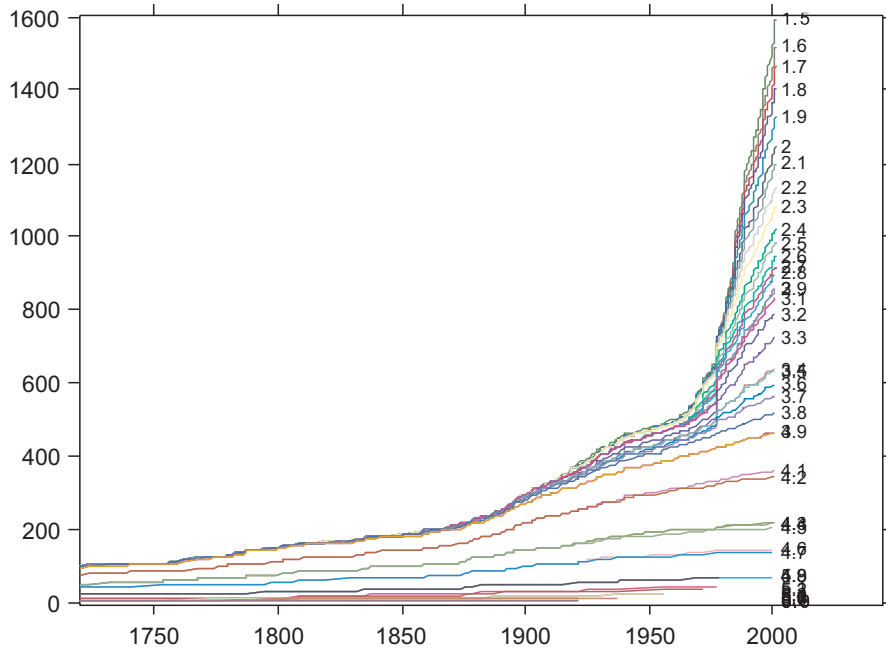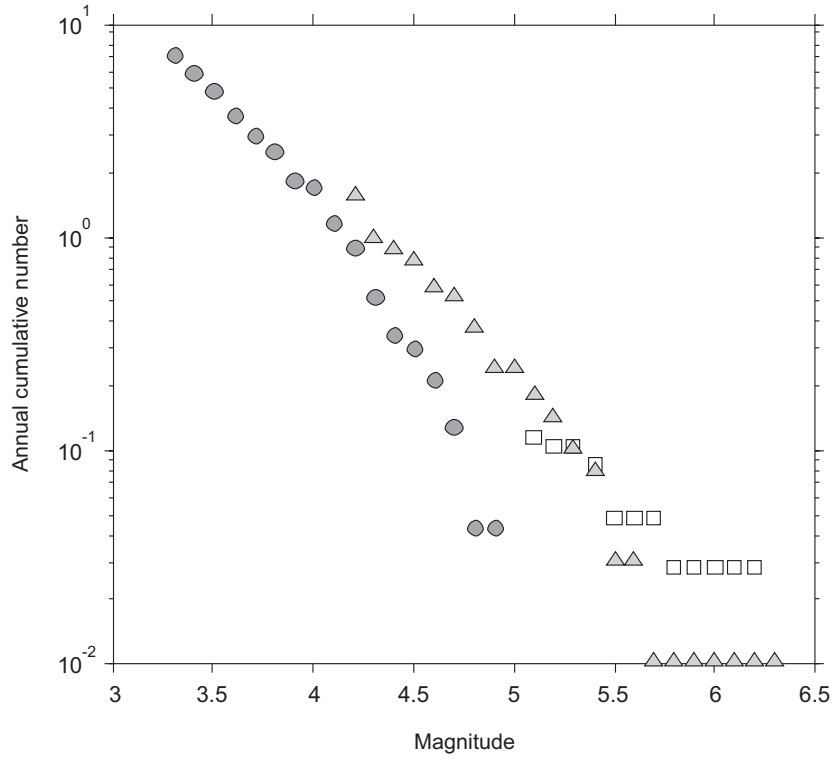
France:

Period	Mc – Model1 [Mw]	Completeness [Mw]
1700 - 1880	5.3	5.3
1880- 1978	3.7	4.0
1978 - 2001	2.2	2.2
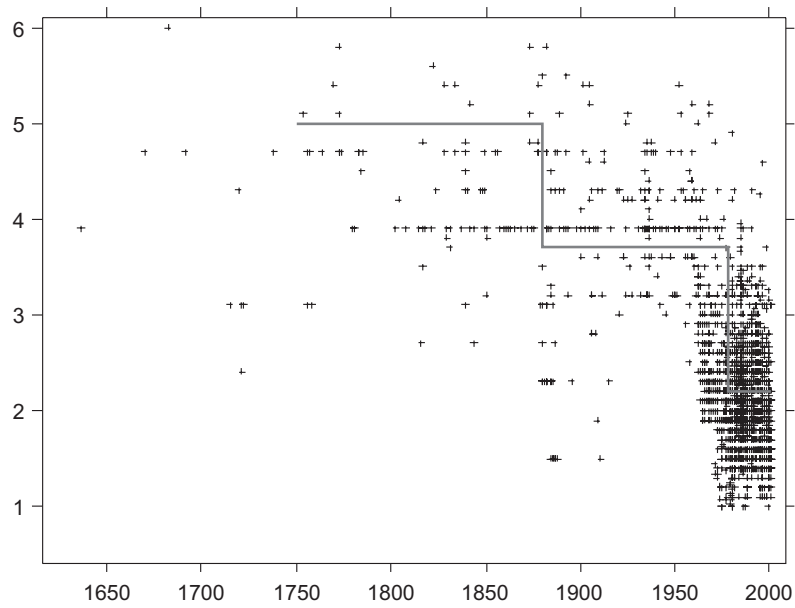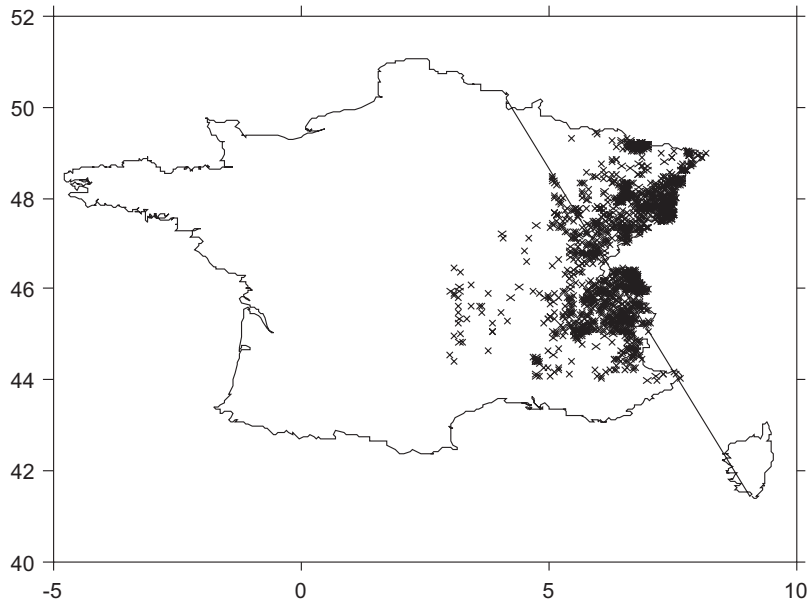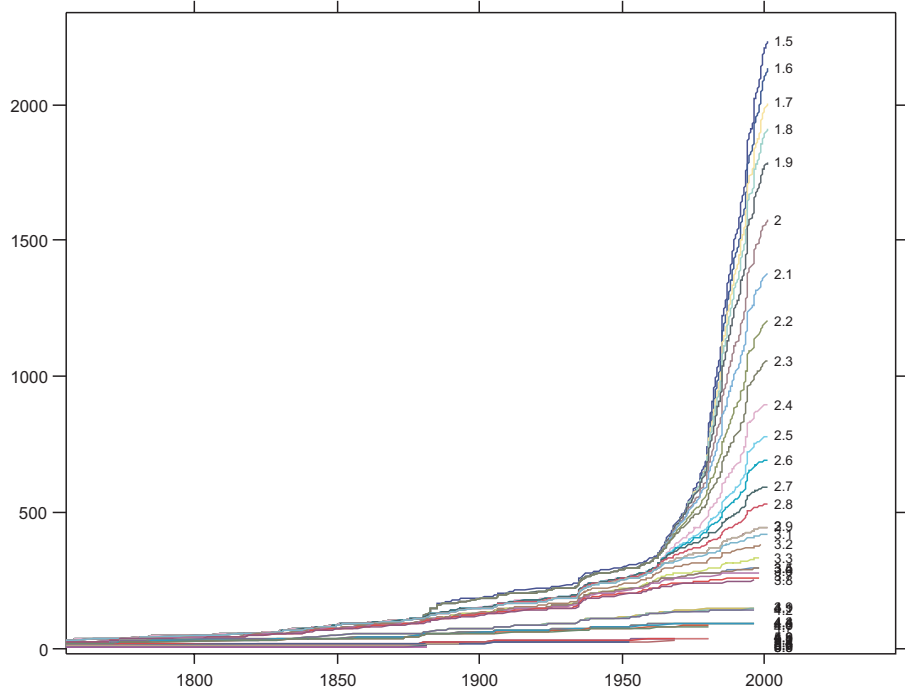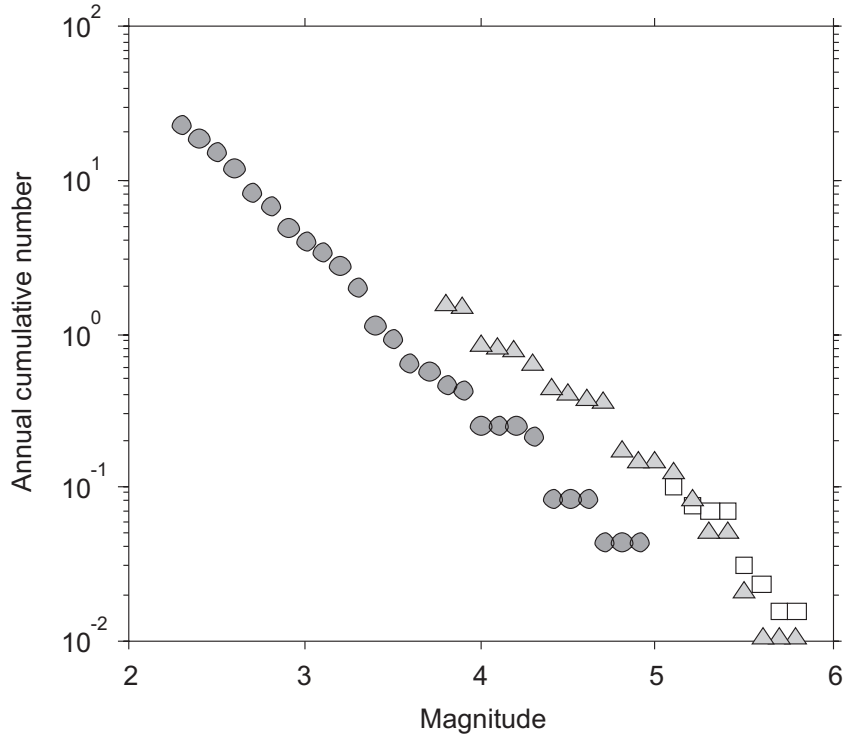
APPENDIX 4:   EVIDENCE FOR TEMPORAL CHANGES IN ACTIVITY

The following text is from a response by Stefan Wiemer to a question by Roger Musson regarding the possibility of an artificial shift between the instrumental and historical data.

Hello Roger:

I use the polygon listed below and the undeclustered dataset, to make sure that we talk about the same data. My FMD plot looks then a lot like yours, although it does look different in some of the details.
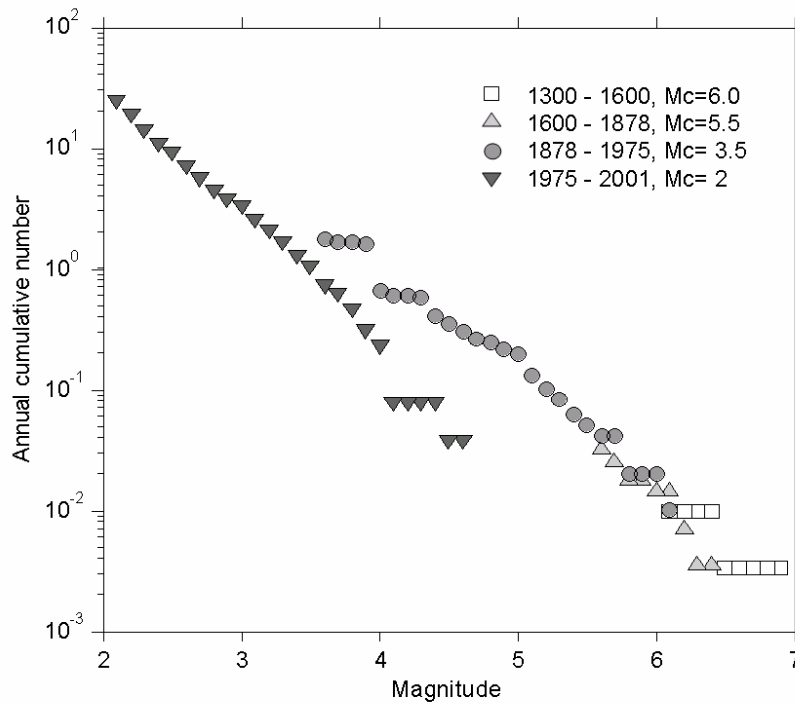
I would agree that from this plot, one might tempt to propose a general shift. Using the declustered dataset does not change the picture much. However, what is instructive is trying to spatially subdivide the data. For simplicity, I first simply look separately North and South of Latitude 47.0.
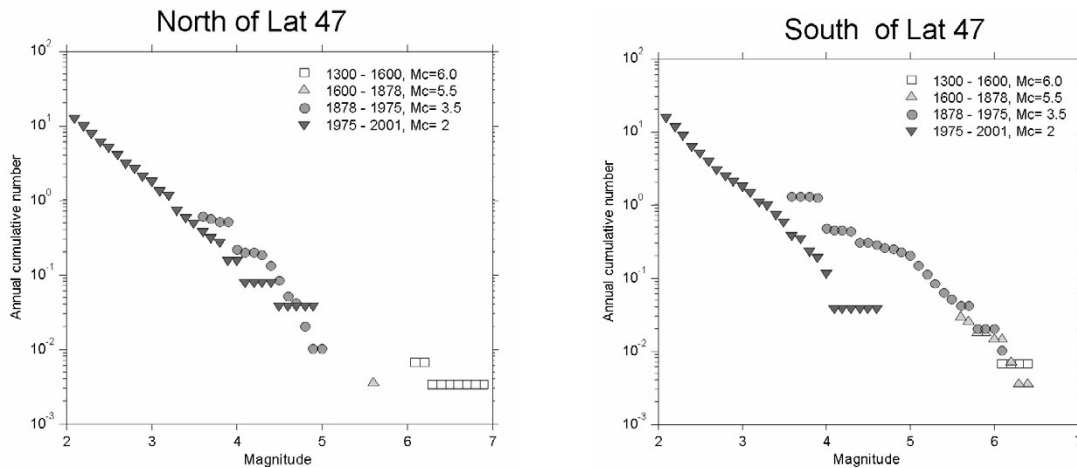
As you can see from the above Figure, the northern part shows little, if any, offset, whereas the southern does. To subdivide the south further, I looked East and West of Longitude 8.5.
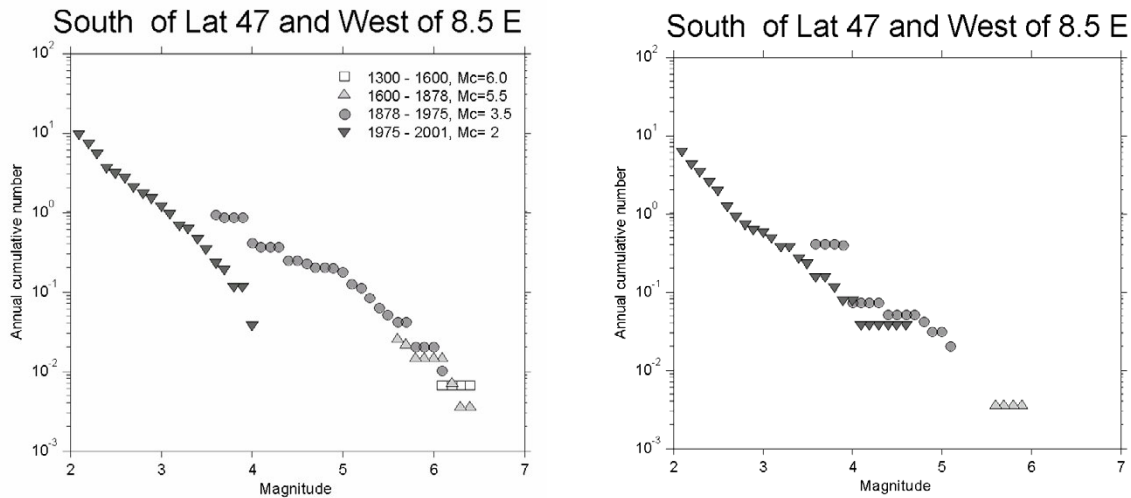
Again, only the Western part shows the shift. This region, of course is the greater Wallis area, and one could try to nail down the region a bit more, but it gets trickier with less data.

Therefore, if you believe a shift occurred in the PEGASOS catalogue then I think it is not correct to say it occurred in all of Switzerland and parts of Germany. It is really a sub region, the Wallis, which is affected. However, the Wallis is well known to have episodic periods of activity, and I believe this may be the more straightforward answer, with the possibility of a (small) added shift between epicentral intensities and magnitudes, as detailed in our write-up. If you force a fit to the Wallis data, you end up with an artificially low b-value, because a change in activity rate (under the presence of a completeness change) introduces a bias. In our (EG1d) rate computation, and in the Swiss hazard mapping effort, we allow for such a change in activity by allowing a model that fits in a maximum likelihood sense, two 'a' values to the seismicity but one b-value only.

In summary, I do not see evidence to change our assessment of the magnitude shift detailed in our report.

APPENDIX 5   EG1-HID-0035 HAZARD INPUT DOCUMENT FINAL MODEL, EXPERT TEAM EG1d

This document describes the final seismic source model developed by Expert Team EG1d. The data files associated with this seismic source model are located in the zip file EG1-HID-0035_EG1d_data.zip.

Seismic Zonation

Figure A-7 shows the global assessment that applies to modeling of the spatial distribution of seismicity. Three alternatives are considered. The first alternative is a low degree of stationarity in which seismicity is assumed to be homogeneously distributed with the boundaries of the seismic source zones. The second alternative is a moderate level of stationarity in which the spatial distribution of seismicity is modeled using a Gaussian kernel density function with the smoothing parameter $h = 15$ km. The third is a high level of stationarity in which the spatial distribution of seismicity is modeled using a Gaussian kernel density function with the smoothing parameter $h = 5$ km. These three alternatives are considered to be completely dependent across all sources.
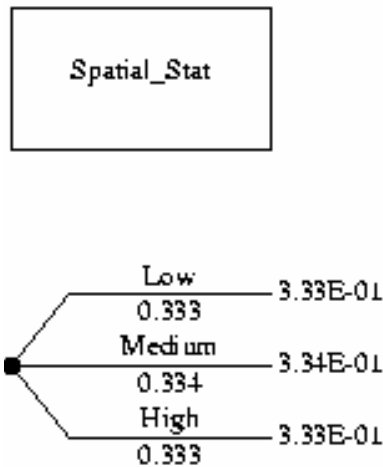
Fig. A-7:   Spatial stationarity logic tree for EG1d

The study region was divided into a number of large regional zones, as shown on Figure A-8. There are a number of alternative subdivisions of these zones as indicated on the logic trees shown on Figures A-9 and A-10.
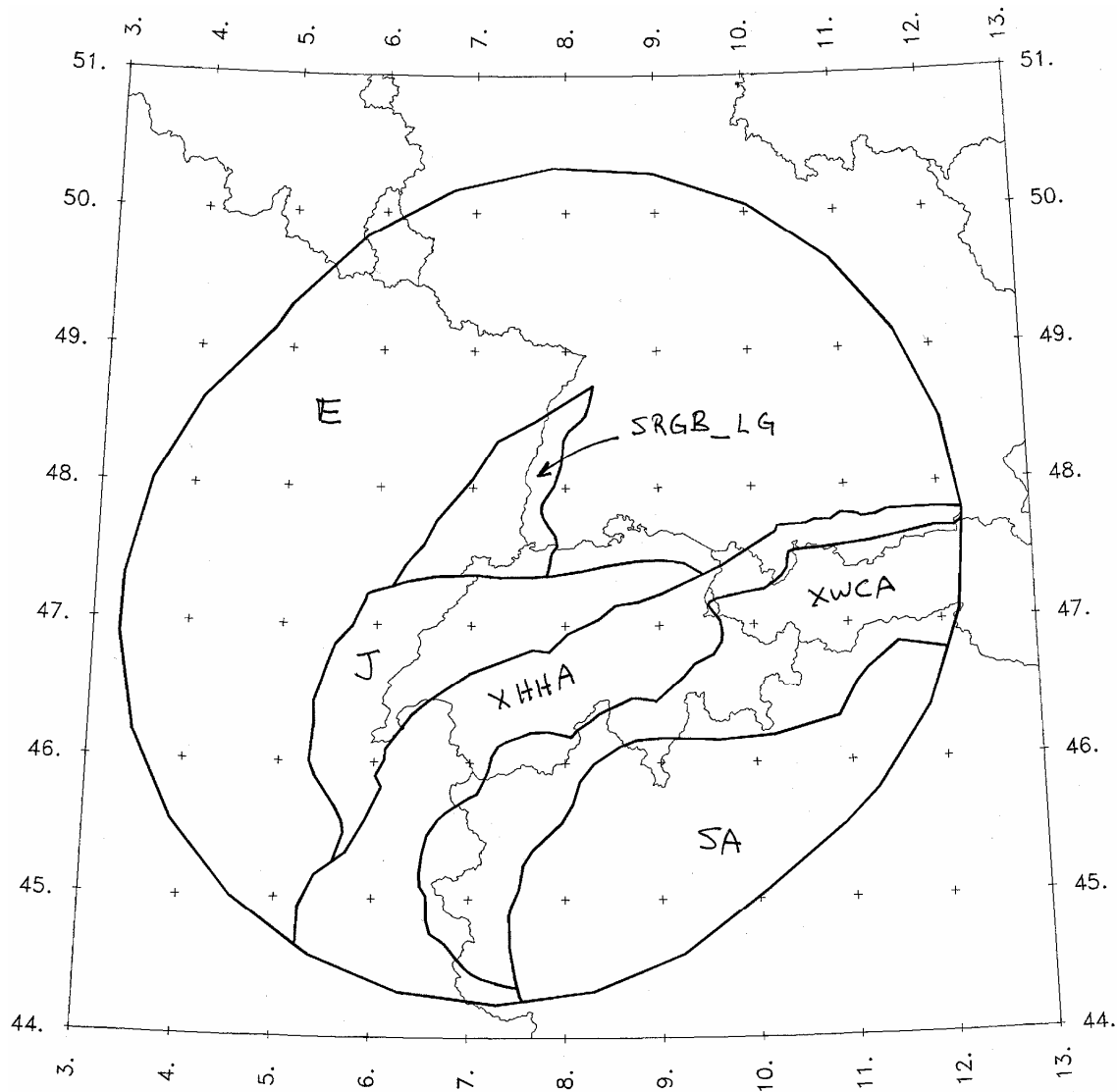
Fig. A-8: Regional zones for EG1d

Figure A-9 shows the logic tree for the alternative models for zones XHHA, XWCA, and SRGB_LG (and the related zone SRGB_SM). Zone XHHA is either treated as a single zone or is divided into two zones XHA and HA. These are shown in Figure A-11. Similarly, zone XWCA is either treated as a single zone or is divided into two zones XWA and XCA, shown in Figure A-11. The southern Rhine Graben source SRGB_LG is either a single zone, or the Basel region is a separate zone, B_LG from the rest of the southern Rhine Graben, SRG_LG. These alternatives are shown on the top of Figure A-12. If zone TZ (discussed below) is present, then the southern Rhine Graben sources have alternative geometries SRGB_SM, SRG_SM, and B_SM, as shown on the bottom of Figure A-12.
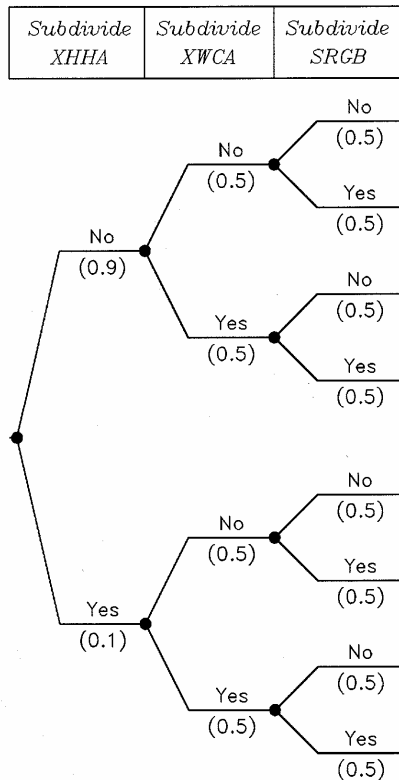
Fig. A-9:   Logic tree for alternative zonations of the Alps and the Rhine Graben

Figure A-10 shows the logic tree for zonation alternatives within northern Switzerland and southern Germany. The basic model consists of a large zone representing Europe north-north-west of the Alps and Jura (zone E in Figure A-8). Within this region, four alternative subzones are defined, SWA, NRG, FKZ, and TZ. The probabilities that each of these is present are independent. As a result, there are 16 alternative configurations for zone E. These are listed on the right-hand side off the logic tree in Figure A-10 and are shown on Figures A-13 through A-16. The alternatives for zone E are defined as simple polygons by wrapping the zone around narrow gaps between the other zones were necessary (for example between zones FKZ and SRG_LG).

The various logic tree branches produce 35 distinct source zone alternatives. Table A-1 lists the various combinations of sources corresponding to end branches of the logic trees shown in Figures A-9 and A-10. The zone files are located in directory .\ZONES. The spatial smoothing grid files are located in subdirectories within directory .\ZONES. These are named to identify the earthquake catalogue used to generate the kernel density function. These files have exten-sions *.h05 and *.h15 for h values of 5 and 15 km, respectively.
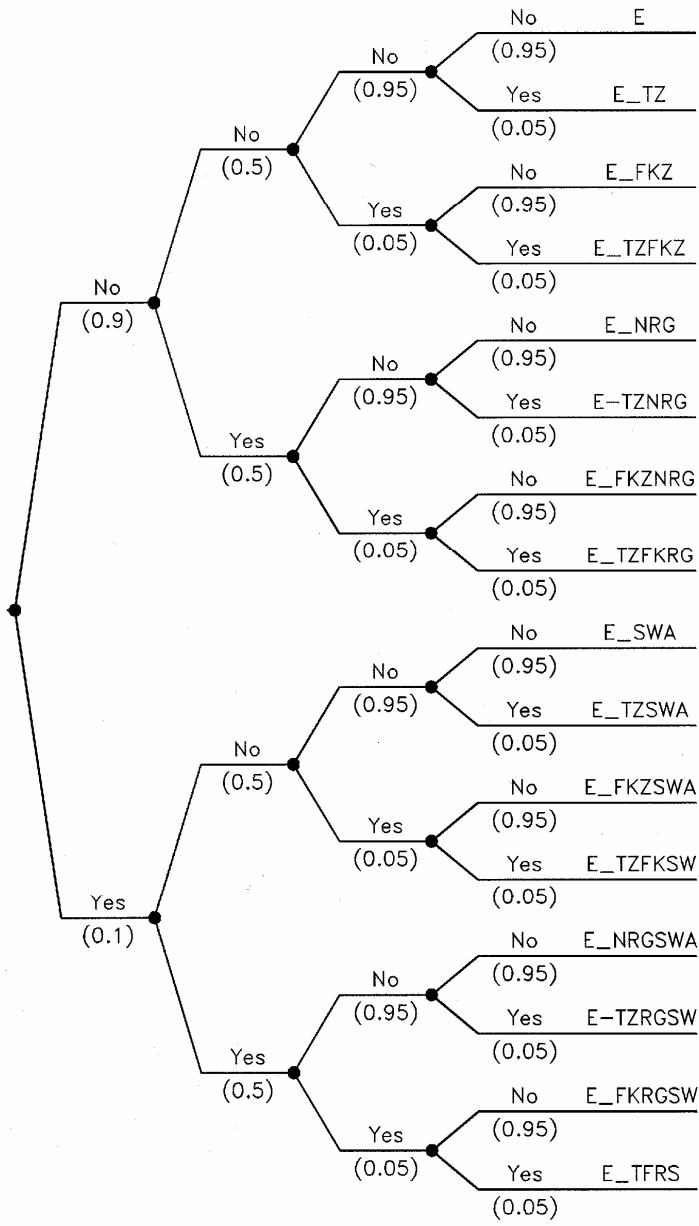
Fig. A-10: Logic tree for alternative sources within northern Switzerland and southern Germany
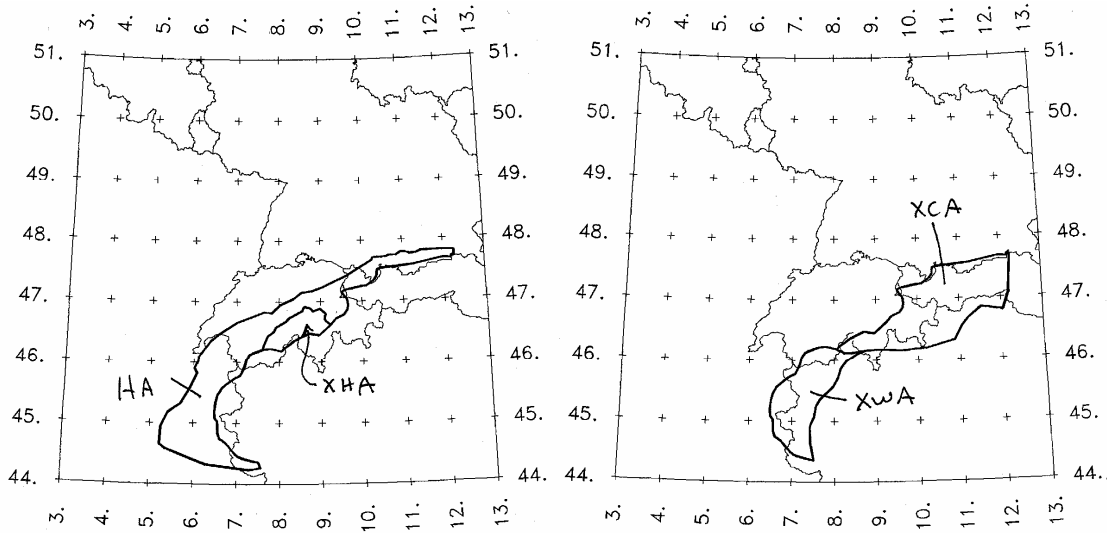
Fig. A-11:   Division of zone XHHA into XHA and HA (left), division of zone XWCA into XWA and XCA (right)
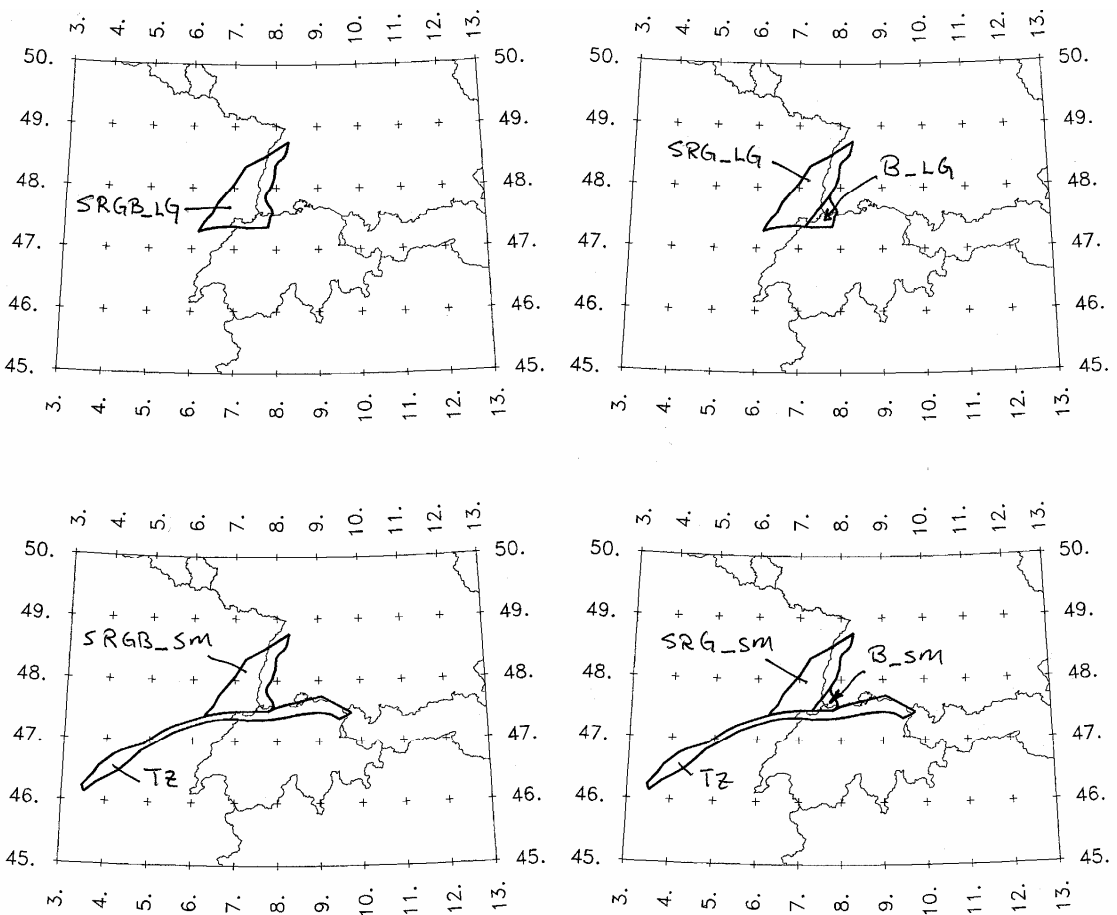
Fig. A-12:   Alternative models for SRGB zone: SRGB_LG (top left), division into SRG_LG and B_LG (top right), alternative geometry when zone TZ is present (as shown in bottom plots), sources SRG_LG and B_LG are replaced with SRG_SM and B_SM, respectively
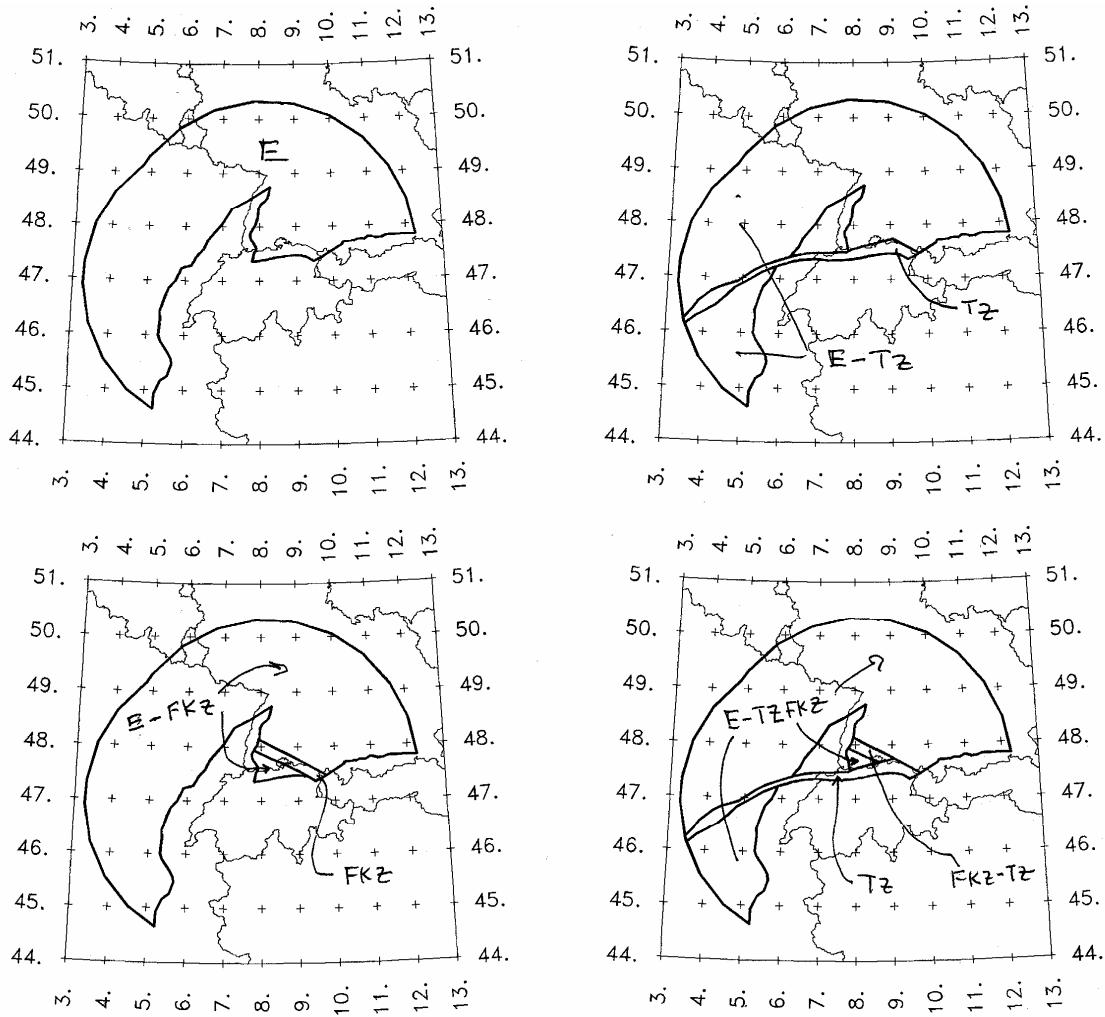
Fig. A-13: Alternative models of zone E reflecting the presence of zones TZ and FKZ
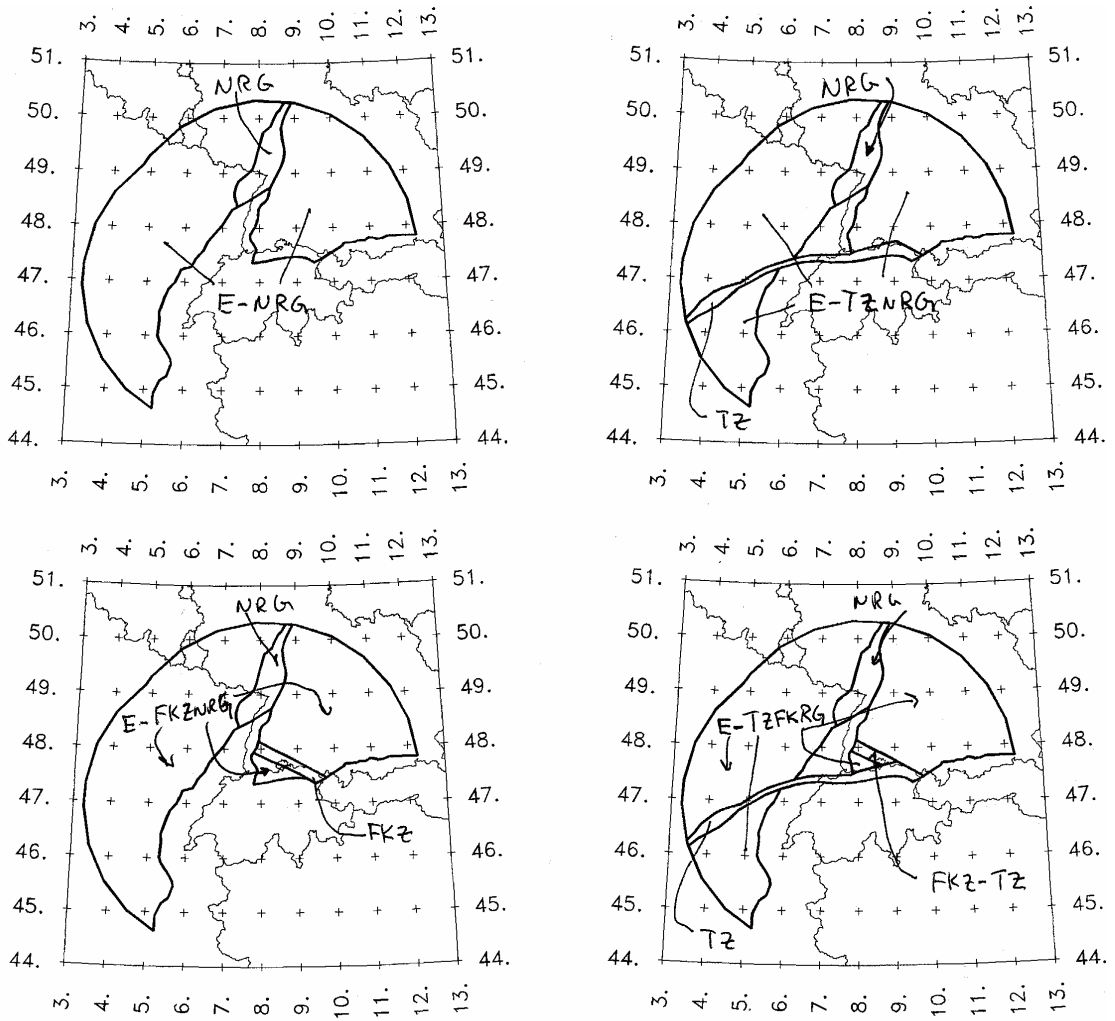
Fig. A-14: Alternative models of zone E reflecting the presence of zones NRG, TZ and FKZ
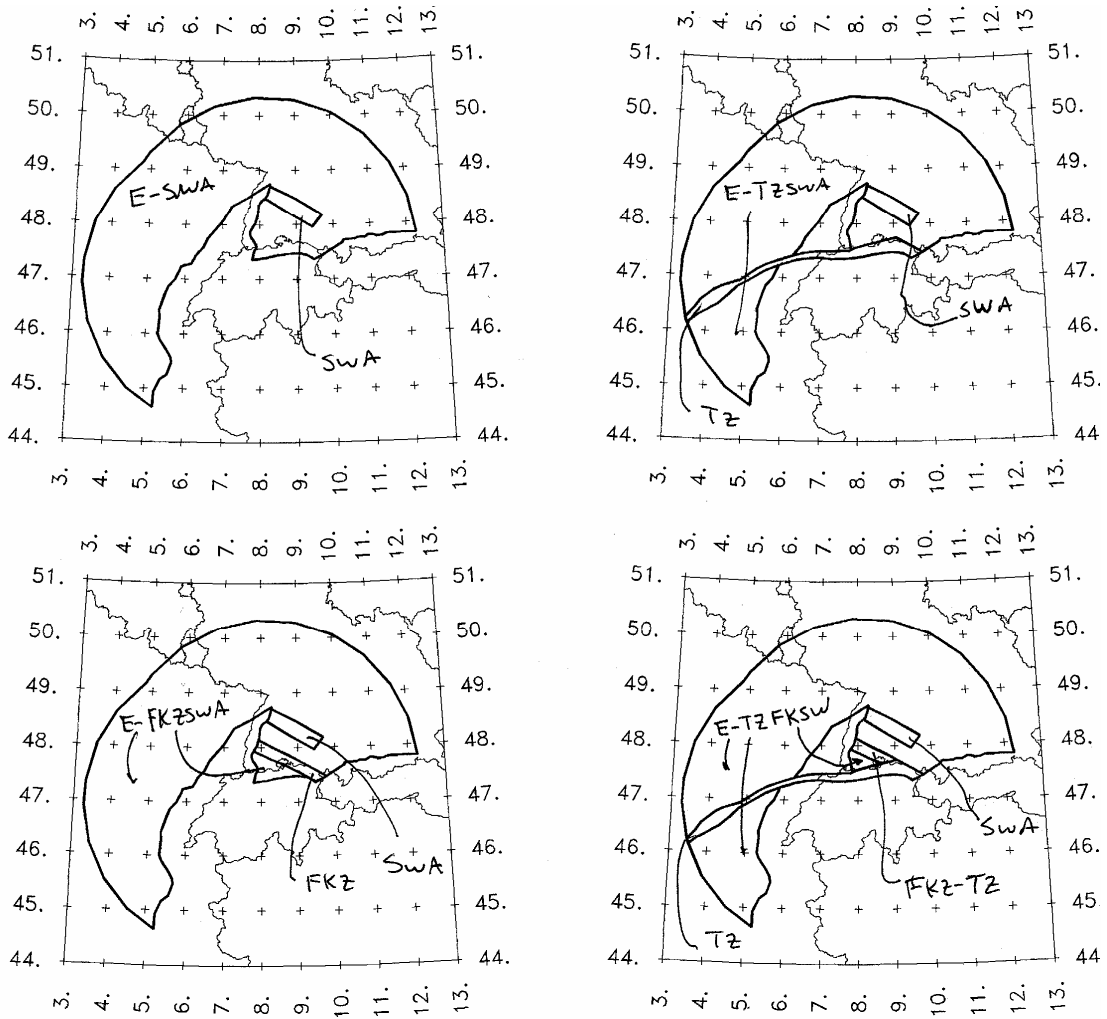
Fig. A-15: Alternative models of zone E reflecting the presence of zones SWA, TZ and FKZ
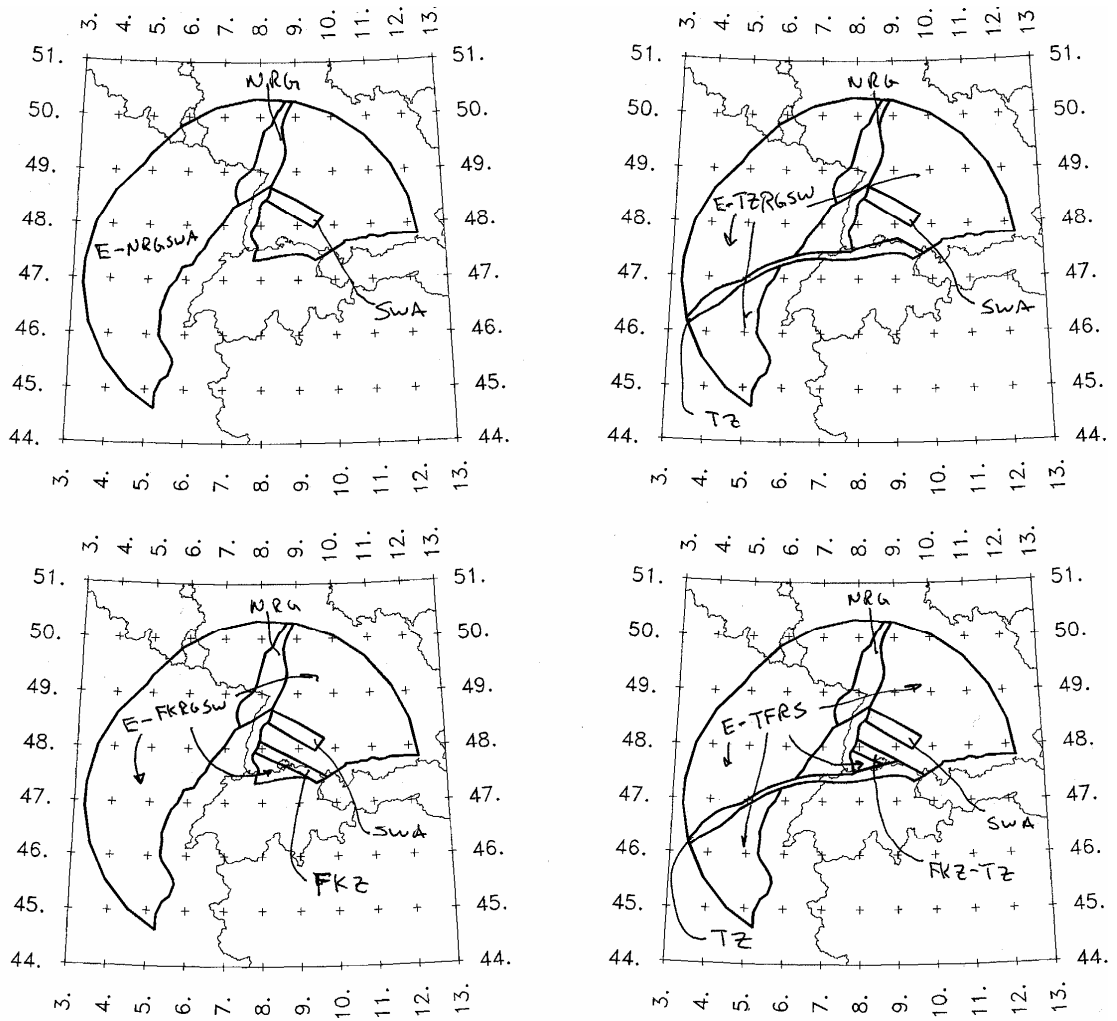
Fig. A-16:   Alternative models of zone E reflecting the presence of zones SWA, NRG, FKZ
             and TZ

Tab. A-1:   Source zone combinations for EG1d

Sub-divide XHHA	Sub-divide XWCA	Sub-divide SRGB	SWA Exists	NRG Exists	FKZ Exists	TZ Exists	Sources
No (0.9)	No (0.5)	No (0.5)	No (0.9)	No (0.5)	No (0.95)	No (0.95)	J, SA, XHHA, XWCA, SRGB_LG, E
No (0.9)	No (0.5)	No (0.5)	No (0.9)	No (0.5)	No (0.95)	Yes (0.05)	J, SA, XHHA, XWCA, SRGB_SM, TZ, E-TZ
No (0.9)	No (0.5)	No (0.5)	No (0.9)	No (0.5)	Yes (0.05)	No (0.95)	J, SA, XHHA, XWCA, SRGB_LG, FKZ, E-FKZ
No (0.9)	No (0.5)	No (0.5)	No (0.9)	No (0.5)	Yes (0.05)	Yes (0.05)	J, SA, XHHA, XWCA, SRGB_SM, TZ, FKZ-TZ, E-TZFKZ
No (0.9)	No (0.5)	No (0.5)	No (0.9)	Yes (0.5)	No (0.95)	No (0.95)	J, SA, XHHA, XWCA, SRGB_LG, NRG, E-NRG
No (0.9)	No (0.5)	No (0.5)	No (0.9)	Yes (0.5)	No (0.95)	Yes (0.05)	J, SA, XHHA, XWCA, SRGB_SM, TZ, NRG, E-TZNRG
No (0.9)	No (0.5)	No (0.5)	No (0.9)	Yes (0.5)	Yes (0.05)	No (0.95)	J, SA, XHHA, XWCA, SRGB_LG, FKZ, NRG, E-FKZNRG
No (0.9)	No (0.5)	No (0.5)	No (0.9)	Yes (0.5)	Yes (0.05)	Yes (0.05)	J, SA, XHHA, XWCA, SRGB_SM, TZ, FKZ-TZ, NRG, E-TZFKRG
No (0.9)	No (0.5)	No (0.5)	Yes (0.1)	No (0.5)	No (0.95)	No (0.95)	J, SA, XHHA, XWCA, SRGB_LG, SWA, E-SWA
No (0.9)	No (0.5)	No (0.5)	Yes (0.1)	No (0.5)	No (0.95)	Yes (0.05)	J, SA, XHHA, XWCA, SRGB_SM, TZ, SWA, E-TZSWA
No (0.9)	No (0.5)	No (0.5)	Yes (0.1)	No (0.5)	Yes (0.05)	No (0.95)	J, SA, XHHA, XWCA, SRGB_LG, FKZ, SWA, E-FKZSWA
No (0.9)	No (0.5)	No (0.5)	Yes (0.1)	No (0.5)	Yes (0.05)	Yes (0.05)	J, SA, XHHA, XWCA, SRGB_SM, TZ, FKZ-TZ, SWA, E-TZFKSW
No (0.9)	No (0.5)	No (0.5)	Yes (0.1)	Yes (0.5)	No (0.95)	No (0.95)	J, SA, XHHA, XWCA, SRGB_LG, NRG, SWA, E-NRGSWA
No (0.9)	No (0.5)	No (0.5)	Yes (0.1)	Yes (0.5)	No (0.95)	Yes (0.05)	J, SA, XHHA, XWCA, SRGB_SM, TZ, NRG, SWA, E-TZRGSW
No (0.9)	No (0.5)	No (0.5)	Yes (0.1)	Yes (0.5)	Yes (0.05)	No (0.95)	J, SA, XHHA, XWCA, SRGB_LG, FKZ, NRG, SWA, E-FKRGSW
No (0.9)	No (0.5)	No (0.5)	Yes (0.1)	Yes (0.5)	Yes (0.05)	Yes (0.05)	J, SA, XHHA, XWCA, SRGB_SM, TZ, FKZ-TZ, NRG, SWA, E-TFRS
No (0.9)	No (0.5)	Yes (0.5)	No (0.9)	No (0.5)	No (0.95)	No (0.95)	J, SA, XHHA, XWCA, SRG_LG, B_LG, E
No (0.9)	No (0.5)	Yes (0.5)	No (0.9)	No (0.5)	No (0.95)	Yes (0.05)	J, SA, XHHA, XWCA, SRG_SM, B_SM, TZ, E-TZ
No (0.9)	No (0.5)	Yes (0.5)	No (0.9)	No (0.5)	Yes (0.05)	No (0.95)	J, SA, XHHA, XWCA, SRG_LG, B_LG, FKZ, E-FKZ
No (0.9)	No (0.5)	Yes (0.5)	No (0.9)	No (0.5)	Yes (0.05)	Yes (0.05)	J, SA, XHHA, XWCA, SRG_SM, B_SM, TZ, FKZ-TZ, E-TZFKZ
No (0.9)	No (0.5)	Yes (0.5)	No (0.9)	Yes (0.5)	No (0.95)	No (0.95)	J, SA, XHHA, XWCA, SRG_LG, B_LG, NRG, E-NRG
No (0.9)	No (0.5)	Yes (0.5)	No (0.9)	Yes (0.5)	No (0.95)	Yes (0.05)	J, SA, XHHA, XWCA, SRG_SM, B_SM, TZ, NRG, E-TZNRG
No (0.9)	No (0.5)	Yes (0.5)	No (0.9)	Yes (0.5)	Yes (0.05)	No (0.95)	J, SA, XHHA, XWCA, SRG_LG, B_LG, FKZ, NRG, E-FKZNRG
No (0.9)	No (0.5)	Yes (0.5)	No (0.9)	Yes (0.5)	Yes (0.05)	Yes (0.05)	J, SA, XHHA, XWCA, SRG_SM, B_SM, TZ, FKZ-TZ, NRG, E-TZFKRG
No (0.9)	No (0.5)	Yes (0.5)	Yes (0.1)	No (0.5)	No (0.95)	No (0.95)	J, SA, XHHA, XWCA, SRG_LG, B_LG, SWA, E-SWA
No (0.9)	No (0.5)	Yes (0.5)	Yes (0.1)	No (0.5)	No (0.95)	Yes (0.05)	J, SA, XHHA, XWCA, SRG_SM, B_SM, TZ, SWA, E-TZSWA
No (0.9)	No (0.5)	Yes (0.5)	Yes (0.1)	No (0.5)	Yes (0.05)	No (0.95)	J, SA, XHHA, XWCA, SRG_LG, B_LG, FKZ, SWA, E-FKZSWA
No (0.9)	No (0.5)	Yes (0.5)	Yes (0.1)	No (0.5)	Yes (0.05)	Yes (0.05)	J, SA, XHHA, XWCA, SRG_SM, B_SM, TZ, FKZ-TZ, SWA, E-TZFKSW
No (0.9)	No (0.5)	Yes (0.5)	Yes (0.1)	Yes (0.5)	No (0.95)	No (0.95)	J, SA, XHHA, XWCA, SRG_LG, B_LG, NRG, SWA, E-NRGSWA

Tab. A-1:   Continuation

Sub-divide XHHA	Sub-divide XWCA	Sub-divide SRGB	SWA Exists	NRG Exists	FKZ Exists	TZ Exists	Sources
No (0.9)	No (0.5)	Yes (0.5)	Yes (0.1)	Yes (0.5)	No (0.95)	Yes (0.05)	J, SA, XHHA, XWCA, SRG_SM, B_SM, TZ, NRG, SWA, E-TZRGSW
No (0.9)	No (0.5)	Yes (0.5)	Yes (0.1)	Yes (0.5)	Yes (0.05)	No (0.95)	J, SA, XHHA, XWCA, SRG_LG, B_LG, FKZ, NRG, SWA, E-FKRGSW
No (0.9)	No (0.5)	Yes (0.5)	Yes (0.1)	Yes (0.5)	Yes (0.05)	Yes (0.05)	J, SA, XHHA, XWCA, SRG_SM, B_SM, TZ, FKZ-TZ, NRG, SWA, E-TFRS
No (0.9)	Yes (0.5)	No (0.5)	No (0.9)	No (0.5)	No (0.95)	No (0.95)	J, SA, XHHA, XCA, XWA, SRGB_LG, E
No (0.9)	Yes (0.5)	No (0.5)	No (0.9)	No (0.5)	No (0.95)	Yes (0.05)	J, SA, XHHA, XCA, XWA, SRGB_SM, TZ, E-TZ
No (0.9)	Yes (0.5)	No (0.5)	No (0.9)	No (0.5)	Yes (0.05)	No (0.95)	J, SA, XHHA, XCA, XWA, SRGB_LG, FKZ, E-FKZ
No (0.9)	Yes (0.5)	No (0.5)	No (0.9)	No (0.5)	Yes (0.05)	Yes (0.05)	J, SA, XHHA, XCA, XWA, SRGB_SM, TZ, FKZ-TZ, E-TZFKZ
No (0.9)	Yes (0.5)	No (0.5)	No (0.9)	Yes (0.5)	No (0.95)	No (0.95)	J, SA, XHHA, XCA, XWA, SRGB_LG, NRG, E-NRG
No (0.9)	Yes (0.5)	No (0.5)	No (0.9)	Yes (0.5)	No (0.95)	Yes (0.05)	J, SA, XHHA, XCA, XWA, SRGB_SM, TZ, NRG, E-TZNRG
No (0.9)	Yes (0.5)	No (0.5)	No (0.9)	Yes (0.5)	Yes (0.05)	No (0.95)	J, SA, XHHA, XCA, XWA, SRGB_LG, FKZ, NRG, E-FKZNRG
No (0.9)	Yes (0.5)	No (0.5)	No (0.9)	Yes (0.5)	Yes (0.05)	Yes (0.05)	J, SA, XHHA, XCA, XWA, SRGB_SM, TZ, FKZ-TZ, NRG, E-TZFKRG
No (0.9)	Yes (0.5)	No (0.5)	Yes (0.1)	No (0.5)	No (0.95)	No (0.95)	J, SA, XHHA, XCA, XWA, SRGB_LG, SWA, E-SWA
No (0.9)	Yes (0.5)	No (0.5)	Yes (0.1)	No (0.5)	No (0.95)	Yes (0.05)	J, SA, XHHA, XCA, XWA, SRGB_SM, TZ, SWA, E-TZSWA
No (0.9)	Yes (0.5)	No (0.5)	Yes (0.1)	No (0.5)	Yes (0.05)	No (0.95)	J, SA, XHHA, XCA, XWA, SRGB_LG, FKZ, SWA, E-FKZSWA
No (0.9)	Yes (0.5)	No (0.5)	Yes (0.1)	No (0.5)	Yes (0.05)	Yes (0.05)	J, SA, XHHA, XCA, XWA, SRGB_SM, TZ, FKZ-TZ, SWA, E-TZFKSW
No (0.9)	Yes (0.5)	No (0.5)	Yes (0.1)	Yes (0.5)	No (0.95)	No (0.95)	J, SA, XHHA, XCA, XWA, SRGB_LG, NRG, SWA, E-NRGSWA
No (0.9)	Yes (0.5)	No (0.5)	Yes (0.1)	Yes (0.5)	No (0.95)	Yes (0.05)	J, SA, XHHA, XCA, XWA, SRGB_SM, TZ, NRG, SWA, E-TZRGSW
No (0.9)	Yes (0.5)	No (0.5)	Yes (0.1)	Yes (0.5)	Yes (0.05)	No (0.95)	J, SA, XHHA, XCA, XWA, SRGB_LG, FKZ, NRG, SWA, E-FKRGSW
No (0.9)	Yes (0.5)	No (0.5)	Yes (0.1)	Yes (0.5)	Yes (0.05)	Yes (0.05)	J, SA, XHHA, XCA, XWA, SRGB_SM, TZ, FKZ-TZ, NRG, SWA, E-TFRS
No (0.9)	Yes (0.5)	Yes (0.5)	No (0.9)	No (0.5)	No (0.95)	No (0.95)	J, SA, XHHA, XCA, XWA, SRG_LG, B_LG, E
No (0.9)	Yes (0.5)	Yes (0.5)	No (0.9)	No (0.5)	No (0.95)	Yes (0.05)	J, SA, XHHA, XCA, XWA, SRG_SM, B_SM, TZ, E-TZ
No (0.9)	Yes (0.5)	Yes (0.5)	No (0.9)	No (0.5)	Yes (0.05)	No (0.95)	J, SA, XHHA, XCA, XWA, SRG_LG, B_LG, FKZ, E-FKZ
No (0.9)	Yes (0.5)	Yes (0.5)	No (0.9)	No (0.5)	Yes (0.05)	Yes (0.05)	J, SA, XHHA, XCA, XWA, SRG_SM, B_SM, TZ, FKZ-TZ, E-TZFKZ
No (0.9)	Yes (0.5)	Yes (0.5)	No (0.9)	Yes (0.5)	No (0.95)	No (0.95)	J, SA, XHHA, XCA, XWA, SRG_LG, B_LG, NRG, E-NRG
No (0.9)	Yes (0.5)	Yes (0.5)	No (0.9)	Yes (0.5)	No (0.95)	Yes (0.05)	J, SA, XHHA, XCA, XWA, SRG_SM, B_SM, TZ, NRG, E-TZNRG
No (0.9)	Yes (0.5)	Yes (0.5)	No (0.9)	Yes (0.5)	Yes (0.05)	No (0.95)	J, SA, XHHA, XCA, XWA, SRG_LG, B_LG, FKZ, NRG, E-FKZNRG
No (0.9)	Yes (0.5)	Yes (0.5)	No (0.9)	Yes (0.5)	Yes (0.05)	Yes (0.05)	J, SA, XHHA, XCA, XWA, SRG_SM, B_SM, TZ, FKZ-TZ, NRG, E-TZFKRG
No (0.9)	Yes (0.5)	Yes (0.5)	Yes (0.1)	No (0.5)	No (0.95)	No (0.95)	J, SA, XHHA, XCA, XWA, SRG_LG, B_LG, SWA, E-SWA

Tab. A-1:   Continuation

Sub-divide XHHA	Sub-divide XWCA	Sub-divide SRGB	SWA Exists	NRG Exists	FKZ Exists	TZ Exists	Sources
No (0.9)	Yes (0.5)	Yes (0.5)	Yes (0.1)	No (0.5)	No (0.95)	Yes (0.05)	J, SA, XHHA, XCA, XWA, SRG_SM, B_SM, TZ, SWA, E-TZSWA
No (0.9)	Yes (0.5)	Yes (0.5)	Yes (0.1)	No (0.5)	Yes (0.05)	No (0.95)	J, SA, XHHA, XCA, XWA, SRG_LG, B_LG, FKZ, SWA, E-FKZSWA
No (0.9)	Yes (0.5)	Yes (0.5)	Yes (0.1)	No (0.5)	Yes (0.05)	Yes (0.05)	J, SA, XHHA, XCA, XWA, SRG_SM, B_SM, TZ, FKZ-TZ, SWA, E-TZFKSW
No (0.9)	Yes (0.5)	Yes (0.5)	Yes (0.1)	Yes (0.5)	No (0.95)	No (0.95)	J, SA, XHHA, XCA, XWA, SRG_LG, B_LG, NRG, SWA, E-NRGSWA
No (0.9)	Yes (0.5)	Yes (0.5)	Yes (0.1)	Yes (0.5)	No (0.95)	Yes (0.05)	J, SA, XHHA, XCA, XWA, SRG_SM, B_SM, TZ, NRG, SWA, E-TZRGSW
No (0.9)	Yes (0.5)	Yes (0.5)	Yes (0.1)	Yes (0.5)	Yes (0.05)	No (0.95)	J, SA, XHHA, XCA, XWA, SRG_LG, B_LG, FKZ, NRG, SWA, E-FKRGSW
No (0.9)	Yes (0.5)	Yes (0.5)	Yes (0.1)	Yes (0.5)	Yes (0.05)	Yes (0.05)	J, SA, XHHA, XCA, XWA, SRG_SM, B_SM, TZ, FKZ-TZ, NRG, SWA, E-TFRS
Yes (0.1)	No (0.5)	No (0.5)	No (0.9)	No (0.5)	No (0.95)	No (0.95)	J, SA, XHA, HA, XWCA, SRGB_LG, E
Yes (0.1)	No (0.5)	No (0.5)	No (0.9)	No (0.5)	No (0.95)	Yes (0.05)	J, SA, XHA, HA, XWCA, SRGB_SM, TZ, E-TZ
Yes (0.1)	No (0.5)	No (0.5)	No (0.9)	No (0.5)	Yes (0.05)	No (0.95)	J, SA, XHA, HA, XWCA, SRGB_LG, FKZ, E-FKZ
Yes (0.1)	No (0.5)	No (0.5)	No (0.9)	No (0.5)	Yes (0.05)	Yes (0.05)	J, SA, XHA, HA, XWCA, SRGB_SM, TZ, FKZ-TZ, E-TZFKZ
Yes (0.1)	No (0.5)	No (0.5)	No (0.9)	Yes (0.5)	No (0.95)	No (0.95)	J, SA, XHA, HA, XWCA, SRGB_LG, NRG, E-NRG
Yes (0.1)	No (0.5)	No (0.5)	No (0.9)	Yes (0.5)	No (0.95)	Yes (0.05)	J, SA, XHA, HA, XWCA, SRGB_SM, TZ, NRG, E-TZNRG
Yes (0.1)	No (0.5)	No (0.5)	No (0.9)	Yes (0.5)	Yes (0.05)	No (0.95)	J, SA, XHA, HA, XWCA, SRGB_LG, FKZ, NRG, E-FKZNRG
Yes (0.1)	No (0.5)	No (0.5)	No (0.9)	Yes (0.5)	Yes (0.05)	Yes (0.05)	J, SA, XHA, HA, XWCA, SRGB_SM, TZ, FKZ-TZ, NRG, E-TZFKRG
Yes (0.1)	No (0.5)	No (0.5)	Yes (0.1)	No (0.5)	No (0.95)	No (0.95)	J, SA, XHA, HA, XWCA, SRGB_LG, SWA, E-SWA
Yes (0.1)	No (0.5)	No (0.5)	Yes (0.1)	No (0.5)	No (0.95)	Yes (0.05)	J, SA, XHA, HA, XWCA, SRGB_SM, TZ, SWA, E-TZSWA
Yes (0.1)	No (0.5)	No (0.5)	Yes (0.1)	No (0.5)	Yes (0.05)	No (0.95)	J, SA, XHA, HA, XWCA, SRGB_LG, FKZ, SWA, E-FKZSWA
Yes (0.1)	No (0.5)	No (0.5)	Yes (0.1)	No (0.5)	Yes (0.05)	Yes (0.05)	J, SA, XHA, HA, XWCA, SRGB_SM, TZ, FKZ-TZ, SWA, E-TZFKSW
Yes (0.1)	No (0.5)	No (0.5)	Yes (0.1)	Yes (0.5)	No (0.95)	No (0.95)	J, SA, XHA, HA, XWCA, SRGB_LG, NRG, SWA, E-NRGSWA
Yes (0.1)	No (0.5)	No (0.5)	Yes (0.1)	Yes (0.5)	No (0.95)	Yes (0.05)	J, SA, XHA, HA, XWCA, SRGB_SM, TZ, NRG, SWA, E-TZRGSW
Yes (0.1)	No (0.5)	No (0.5)	Yes (0.1)	Yes (0.5)	Yes (0.05)	No (0.95)	J, SA, XHA, HA, XWCA, SRGB_LG, FKZ, NRG, SWA, E-FKRGSW
Yes (0.1)	No (0.5)	No (0.5)	Yes (0.1)	Yes (0.5)	Yes (0.05)	Yes (0.05)	J, SA, XHA, HA, XWCA, SRGB_SM, TZ, FKZ-TZ, NRG, SWA, E-TFRS
Yes (0.1)	No (0.5)	Yes (0.5)	No (0.9)	No (0.5)	No (0.95)	No (0.95)	J, SA, XHA, HA, XWCA, SRG_LG, B_LG, E
Yes (0.1)	No (0.5)	Yes (0.5)	No (0.9)	No (0.5)	No (0.95)	Yes (0.05)	J, SA, XHA, HA, XWCA, SRG_SM, B_SM, TZ, E-TZ
Yes (0.1)	No (0.5)	Yes (0.5)	No (0.9)	No (0.5)	Yes (0.05)	No (0.95)	J, SA, XHA, HA, XWCA, SRG_LG, B_LG, FKZ, E-FKZ
Yes (0.1)	No (0.5)	Yes (0.5)	No (0.9)	No (0.5)	Yes (0.05)	Yes (0.05)	J, SA, XHA, HA, XWCA, SRG_SM, B_SM, TZ, FKZ-TZ, E-TZFKZ
Yes (0.1)	No (0.5)	Yes (0.5)	No (0.9)	Yes (0.5)	No (0.95)	No (0.95)	J, SA, XHA, HA, XWCA, SRG_LG, B_LG, NRG, E-NRG
Yes (0.1)	No (0.5)	Yes (0.5)	No (0.9)	Yes (0.5)	No (0.95)	Yes (0.05)	J, SA, XHA, HA, XWCA, SRG_SM, B_SM, TZ, NRG, E-TZNRG

Tab. A-1:   Continuation

Sub-divide XHHA	Sub-divide XWCA	Sub-divide SRGB	SWA Exists	NRG Exists	FKZ Exists	TZ Exists	Sources
Yes (0.1)	No (0.5)	Yes (0.5)	No (0.9)	Yes (0.5)	Yes (0.05)	No (0.95)	J, SA, XHA, HA, XWCA, SRG_LG, B_LG, FKZ, NRG, E-FKZNRG
Yes (0.1)	No (0.5)	Yes (0.5)	No (0.9)	Yes (0.5)	Yes (0.05)	Yes (0.05)	J, SA, XHA, HA, XWCA, SRG_SM, B_SM, TZ, FKZ-TZ, NRG, E-TZFKRG
Yes (0.1)	No (0.5)	Yes (0.5)	Yes (0.1)	No (0.5)	No (0.95)	No (0.95)	J, SA, XHA, HA, XWCA, SRG_LG, B_LG, SWA, E-SWA
Yes (0.1)	No (0.5)	Yes (0.5)	Yes (0.1)	No (0.5)	No (0.95)	Yes (0.05)	J, SA, XHA, HA, XWCA, SRG_SM, B_SM, TZ, SWA, E-TZSWA
Yes (0.1)	No (0.5)	Yes (0.5)	Yes (0.1)	No (0.5)	Yes (0.05)	No (0.95)	J, SA, XHA, HA, XWCA, SRG_LG, B_LG, FKZ, SWA, E-FKZSWA
Yes (0.1)	No (0.5)	Yes (0.5)	Yes (0.1)	No (0.5)	Yes (0.05)	Yes (0.05)	J, SA, XHA, HA, XWCA, SRG_SM, B_SM, TZ, FKZ-TZ, SWA, E-TZFKSW
Yes (0.1)	No (0.5)	Yes (0.5)	Yes (0.1)	Yes (0.5)	No (0.95)	No (0.95)	J, SA, XHA, HA, XWCA, SRG_LG, B_LG, NRG, SWA, E-NRGSWA
Yes (0.1)	No (0.5)	Yes (0.5)	Yes (0.1)	Yes (0.5)	No (0.95)	Yes (0.05)	J, SA, XHA, HA, XWCA, SRG_SM, B_SM, TZ, NRG, SWA, E-TZRGSW
Yes (0.1)	No (0.5)	Yes (0.5)	Yes (0.1)	Yes (0.5)	Yes (0.05)	No (0.95)	J, SA, XHA, HA, XWCA, SRG_LG, B_LG, FKZ, NRG, SWA, E-FKRGSW
Yes (0.1)	No (0.5)	Yes (0.5)	Yes (0.1)	Yes (0.5)	Yes (0.05)	Yes (0.05)	J, SA, XHA, HA, XWCA, SRG_SM, B_SM, TZ, FKZ-TZ, NRG, SWA, E-TFRS
Yes (0.1)	Yes (0.5)	No (0.5)	No (0.9)	No (0.5)	No (0.95)	No (0.95)	J, SA, XHA, HA, XCA, XWA, SRGB_LG, E
Yes (0.1)	Yes (0.5)	No (0.5)	No (0.9)	No (0.5)	No (0.95)	Yes (0.05)	J, SA, XHA, HA, XCA, XWA, SRGB_SM, TZ, E-TZ
Yes (0.1)	Yes (0.5)	No (0.5)	No (0.9)	No (0.5)	Yes (0.05)	No (0.95)	J, SA, XHA, HA, XCA, XWA, SRGB_LG, FKZ, E-FKZ
Yes (0.1)	Yes (0.5)	No (0.5)	No (0.9)	No (0.5)	Yes (0.05)	Yes (0.05)	J, SA, XHA, HA, XCA, XWA, SRGB_SM, TZ, FKZ-TZ, E-TZFKZ
Yes (0.1)	Yes (0.5)	No (0.5)	No (0.9)	Yes (0.5)	No (0.95)	No (0.95)	J, SA, XHA, HA, XCA, XWA, SRGB_LG, NRG, E-NRG
Yes (0.1)	Yes (0.5)	No (0.5)	No (0.9)	Yes (0.5)	No (0.95)	Yes (0.05)	J, SA, XHA, HA, XCA, XWA, SRGB_SM, TZ, NRG, E-TZNRG
Yes (0.1)	Yes (0.5)	No (0.5)	No (0.9)	Yes (0.5)	Yes (0.05)	No (0.95)	J, SA, XHA, HA, XCA, XWA, SRGB_LG, FKZ, NRG, E-FKZNRG
Yes (0.1)	Yes (0.5)	No (0.5)	No (0.9)	Yes (0.5)	Yes (0.05)	Yes (0.05)	J, SA, XHA, HA, XCA, XWA, SRGB_SM, TZ, FKZ-TZ, NRG, E-TZFKRG
Yes (0.1)	Yes (0.5)	No (0.5)	Yes (0.1)	No (0.5)	No (0.95)	No (0.95)	J, SA, XHA, HA, XCA, XWA, SRGB_LG, SWA, E-SWA
Yes (0.1)	Yes (0.5)	No (0.5)	Yes (0.1)	No (0.5)	No (0.95)	Yes (0.05)	J, SA, XHA, HA, XCA, XWA, SRGB_SM, TZ, SWA, E-TZSWA
Yes (0.1)	Yes (0.5)	No (0.5)	Yes (0.1)	No (0.5)	Yes (0.05)	No (0.95)	J, SA, XHA, HA, XCA, XWA, SRGB_LG, FKZ, SWA, E-FKZSWA
Yes (0.1)	Yes (0.5)	No (0.5)	Yes (0.1)	No (0.5)	Yes (0.05)	Yes (0.05)	J, SA, XHA, HA, XCA, XWA, SRGB_SM, TZ, FKZ-TZ, SWA, E-TZFKSW
Yes (0.1)	Yes (0.5)	No (0.5)	Yes (0.1)	Yes (0.5)	No (0.95)	No (0.95)	J, SA, XHA, HA, XCA, XWA, SRGB_LG, NRG, SWA, E-NRGSWA
Yes (0.1)	Yes (0.5)	No (0.5)	Yes (0.1)	Yes (0.5)	No (0.95)	Yes (0.05)	J, SA, XHA, HA, XCA, XWA, SRGB_SM, TZ, NRG, SWA, E-TZRGSW
Yes (0.1)	Yes (0.5)	No (0.5)	Yes (0.1)	Yes (0.5)	Yes (0.05)	No (0.95)	J, SA, XHA, HA, XCA, XWA, SRGB_LG, FKZ, NRG, SWA, E-FKRGSW
Yes (0.1)	Yes (0.5)	No (0.5)	Yes (0.1)	Yes (0.5)	Yes (0.05)	Yes (0.05)	J, SA, XHA, HA, XCA, XWA, SRGB_SM, TZ, FKZ-TZ, NRG, SWA, E-TFRS

Tab. A-1: Continuation

Sub-divide XHHA	Sub-divide XWCA	Sub-divide SRGB	SWA Exists	NRG Exists	FKZ Exists	TZ Exists	Sources
Yes (0.1)	Yes (0.5)	Yes (0.5)	No (0.9)	No (0.5)	No (0.95)	No (0.95)	J, SA, XHA, HA, XCA, XWA, SRG_LG, B_LG, E
Yes (0.1)	Yes (0.5)	Yes (0.5)	No (0.9)	No (0.5)	No (0.95)	Yes (0.05)	J, SA, XHA, HA, XCA, XWA, SRG_SM, B_SM, TZ, E-TZ
Yes (0.1)	Yes (0.5)	Yes (0.5)	No (0.9)	No (0.5)	Yes (0.05)	No (0.95)	J, SA, XHA, HA, XCA, XWA, SRG_LG, B_LG, FKZ, E-FKZ
Yes (0.1)	Yes (0.5)	Yes (0.5)	No (0.9)	No (0.5)	Yes (0.05)	Yes (0.05)	J, SA, XHA, HA, XCA, XWA, SRG_SM, B_SM, TZ, FKZ-TZ, E-TZFKZ
Yes (0.1)	Yes (0.5)	Yes (0.5)	No (0.9)	Yes (0.5)	No (0.95)	No (0.95)	J, SA, XHA, HA, XCA, XWA, SRG_LG, B_LG, NRG, E-NRG
Yes (0.1)	Yes (0.5)	Yes (0.5)	No (0.9)	Yes (0.5)	No (0.95)	Yes (0.05)	J, SA, XHA, HA, XCA, XWA, SRG_SM, B_SM, TZ, NRG, E-TZNRG
Yes (0.1)	Yes (0.5)	Yes (0.5)	No (0.9)	Yes (0.5)	Yes (0.05)	No (0.95)	J, SA, XHA, HA, XCA, XWA, SRG_LG, B_LG, FKZ, NRG, E-FKZNRG
Yes (0.1)	Yes (0.5)	Yes (0.5)	No (0.9)	Yes (0.5)	Yes (0.05)	Yes (0.05)	J, SA, XHA, HA, XCA, XWA, SRG_SM, B_SM, TZ, FKZ-TZ, NRG, E-TZFKRG
Yes (0.1)	Yes (0.5)	Yes (0.5)	Yes (0.1)	No (0.5)	No (0.95)	No (0.95)	J, SA, XHA, HA, XCA, XWA, SRG_LG, B_LG, SWA, E-SWA
Yes (0.1)	Yes (0.5)	Yes (0.5)	Yes (0.1)	No (0.5)	No (0.95)	Yes (0.05)	J, SA, XHA, HA, XCA, XWA, SRG_SM, B_SM, TZ, SWA, E-TZSWA
Yes (0.1)	Yes (0.5)	Yes (0.5)	Yes (0.1)	No (0.5)	Yes (0.05)	No (0.95)	J, SA, XHA, HA, XCA, XWA, SRG_LG, B_LG, FKZ, SWA, E-FKZSWA
Yes (0.1)	Yes (0.5)	Yes (0.5)	Yes (0.1)	No (0.5)	Yes (0.05)	Yes (0.05)	J, SA, XHA, HA, XCA, XWA, SRG_SM, B_SM, TZ, FKZ-TZ, SWA, E-TZFKSW
Yes (0.1)	Yes (0.5)	Yes (0.5)	Yes (0.1)	Yes (0.5)	No (0.95)	No (0.95)	J, SA, XHA, HA, XCA, XWA, SRG_LG, B_LG, NRG, SWA, E-NRGSWA
Yes (0.1)	Yes (0.5)	Yes (0.5)	Yes (0.1)	Yes (0.5)	No (0.95)	Yes (0.05)	J, SA, XHA, HA, XCA, XWA, SRG_SM, B_SM, TZ, NRG, SWA, E-TZRGSW
Yes (0.1)	Yes (0.5)	Yes (0.5)	Yes (0.1)	Yes (0.5)	Yes (0.05)	No (0.95)	J, SA, XHA, HA, XCA, XWA, SRG_LG, B_LG, FKZ, NRG, SWA, E-FKRGSW
Yes (0.1)	Yes (0.5)	Yes (0.5)	Yes (0.1)	Yes (0.5)	Yes (0.05)	Yes (0.05)	J, SA, XHA, HA, XCA, XWA, SRG_SM, B_SM, TZ, FKZ-TZ, NRG, SWA, E-TFRS

Earthquake Rupture Geometry

The size of earthquake ruptures is defined by the relationship:

$$\text{Mean } \log_{10}(\text{rupture area}) = 0.91M\text{-}3.49$$
$$\sigma_{\log10(\text{rupture area})} = 0.24$$

Using the relationship for the expectation of a lognormal distribution, the mean (expected) rupture area is given by the relationship:

$$\text{mean rupture area} = 10^{(0.91M - 3.424)}$$

The relationship for the mean rupture area will be used in the hazard computations. The rupture length and width have an aspect ratio of 2.5 : 1 until the maximum rupture width for a source is

reached. The maximum rupture width is determined on the basis of the maximum depth and fault dip, as define below. For larger ruptures, the width is held constant at the maximum width and the length is obtained by dividing the rupture area by this width. Earthquake epicenters are distributed within each source either uniformly or according to a kernel density function (Figure A-7). Earthquake ruptures are located symmetrically on the epicenters (the epicenter is at the midpoint of the rupture). For those epicenters located closer than ½ rupture length to the source zone boundary, the ruptures are allowed to extend beyond the source boundary.

Table A-2 defines the relative frequency of the style-of-faulting for the individual sources. Three specific styles of faulting are considered, normal, strike-slip and reverse. Rupture orientation should be uniformly distributed over the range of 0 to 360 degrees within each source (no preferred orientation of rupture). The dip angles for each style-of-faulting are specified by two (for strike-slip) or three (for dip slip) equally weighted angles representing aleatory variability in the dip of ruptures. These dip angles are: 70 (0,5), and 90 (0.5) degrees for strike-slip faulting; 40 (0.333), 60(0.333), and 80(0.333) degrees for normal faulting; and 10 (0.333), 30 (0.333), and 50 (0.333) degrees for thrust faulting.

Tab. A-2:   Styles of faulting for EG1d source zones

Region	Fraction [%] of earthquakes with style-of-faulting:		
	Strike Slip	Normal	Thrust
Europe (E, SWA, FKZ, TZ)	85	5	10
Southern Rhine Graben (SRG, SRGB, B)	75	20	5
Northern Rhine Graben (NRG)	85	10	5
Jura (J)	75	5	20
Italy (SA)	70	10	20
Alps (XWCA, XHHA, HA, XHA, XCA, XWA)	70	15	15

The depth distribution of small earthquakes for the sources is defined by the two distributions shown in Figure A-17 and listed in Table A-3. For larger earthquakes, a magnitude-dependent depth distribution is to be developed using the weighted approach outlined in Toro (2003c, PEGASOS TP1-TN-0373) with T = 0.5 (hypocenter in lower half of rupture).
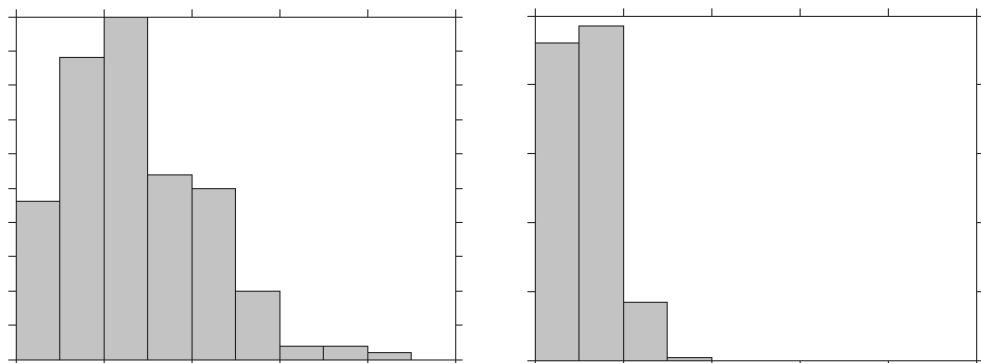
Fig. A-17:   Focal depth distributions

Tab. A-3:   Focal depth distributions

Depth Range [km]	North of HF [percent]	South of HF [percent]
0-4.99	12.50	44.48
5-9.99	23.91	47.00
10-14.99	27.17	8.02
15-19.99	14.67	0.38
20-24.99	13.58	0.1
25-29.99	5.43	0
30-34.99	1.08	0
35-39.99	1.08	0
40-44.99	0.54	0
45-49.99	0	0

The distribution labeled South of the Helvetic Front applies to sources SA, XHHA, XHA, HA, XWCA, XCA, and XWA. The distribution labeled North of the Helvetic Front applies to all other sources. Within each depth range, the distribution is assumed to be uniform.

Earthquake Recurrence Parameters

Figure A-18 shows the logic tree that defines the global alternatives for assessing earthquake recurrence parameters and maximum magnitudes. The global alternatives are dependent across all sources. The earthquake recurrence parameters are based on the PEGASOS catalogue (PEGASOS EXT-TB-0043) with all quarry blasts removes and declustered using the Gruenthal parameters. This is designated as the QGR catalogue. This catalogue was used to compute kernel density functions to model the spatial distribution of seismicity. Located within directory .\ZONES is subdirectory QGR.xy containing the spatial density grids developed using the QGR catalogue.

The first node of the logic tree (Figure A-18) addresses the assessment of catalogue completeness. Two alternative models, designated C1 and C2 are used for all assessments.

The second node of the logic tree shown on Figure A-18 addresses the alternatives for defining a regional b-value for use in maximum magnitude and recurrence parameter estimation. The four alternatives are: the use of all data (designated ba), the use of only post-1975 data (designated bi), the use of only historical data prior to 1880 (designated bh), and the use of all data allowing for a rate change in 1975 (designated bs). The result is 8 alternative data sets for maximum magnitude and recurrence parameter calculations. The results of these calculations are stored in subdirectories labeled by the three-letter catalogue designation QGR, C1 or C2 for the completeness model, and one of the four regional b-value designations. Table A-4 lists the 8 alternative data sets. These alternatives are dependent across all sources and all have equal weight.
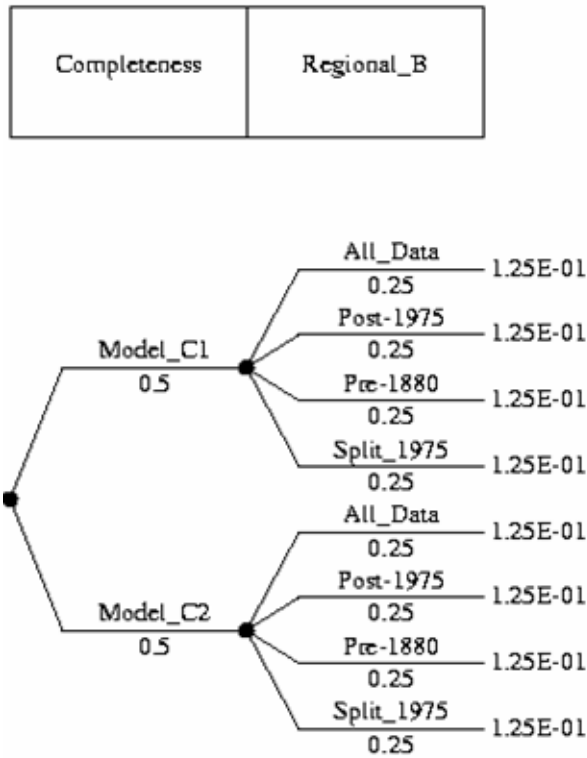
Fig. A-18:   Global catalogue and regional *b*-value alternatives

Tab. A-4:   Catalogue data sets used for maximum magnitude and recurrence parameter distributions

Completeness Model	Regional *b*-value	Catalogue Data Set
Model C1	All data	QGRC1-ba
Model C1	Post 1975	QGRC1-bi
Model C1	Pre 1975	QGRC1-bh
Model C1	Split at 1975	QGRC1-bs
Model C2	All data	QGRC2-ba
Model C2	Post 1975	QGRC2-bi
Model C2	Pre 1975	QGRC2-bh
Model C2	Split at 1975	QGRC2-bs

Maximum magnitude distributions were derived using the EPRI approach. Two global options are included for the upper tail truncated of the distributions, one at magnitude M 7.5 and one at M 8.0. The two global alternative truncation values have equal weight. The distribution files are located in directory .\MMAX in subdirectories that designate the 8 alternative data sets identified in Table A-4. The distributions for the individual sources are in separate files with the source name. The extensions *.mx7 correspond to the distributions truncated at M 7.5 and the extensions *.mx8 correspond to the distributions truncated at M 8.0.

Earthquake recurrence rates for each source are defined in terms of joint discrete distributions for $N(m \geq 5)$ and β $[b \ln(10)]$. Again, 8 sets of distributions were developed corresponding to the 8 data sets identified above. The distribution files are located in directory .\REC in sub-directories that designate the 8 alternative data sets listed in Table A-4.

Five alternative approaches were used to develop these distributions and five distribution files exist for each source and data set. The first approach is to use the regional b-value and its uncertainty to define the zone recurrence. The distribution file name s for this approach have the extension *.bx. The second approach is to fit the b-value to the local zone data. The distribution file names for this approach have the extension *.bf. The third approach is to again use the regional b-value, but allow for a rate change in 1975. The distribution file names for this approach have the extension *.bx2. The fourth approach is fit the b-value to the local zone data, allowing for a rate change in 1975. The distribution file names for this approach have the extension *.bf2. The fifth approach is to define a Bayesian-weighted b-value and use this to compute the recurrence parameter distribution. The distribution file names for this approach have the extension *.bb.

Relative weights for these five alternatives were developed on a zone-by-zone basis. The main directory .\REC contains files with the file name indicating the global data set and the extension *.wts. These files give the relative weight for the five alternative recurrence parameter distributions for each source zone.
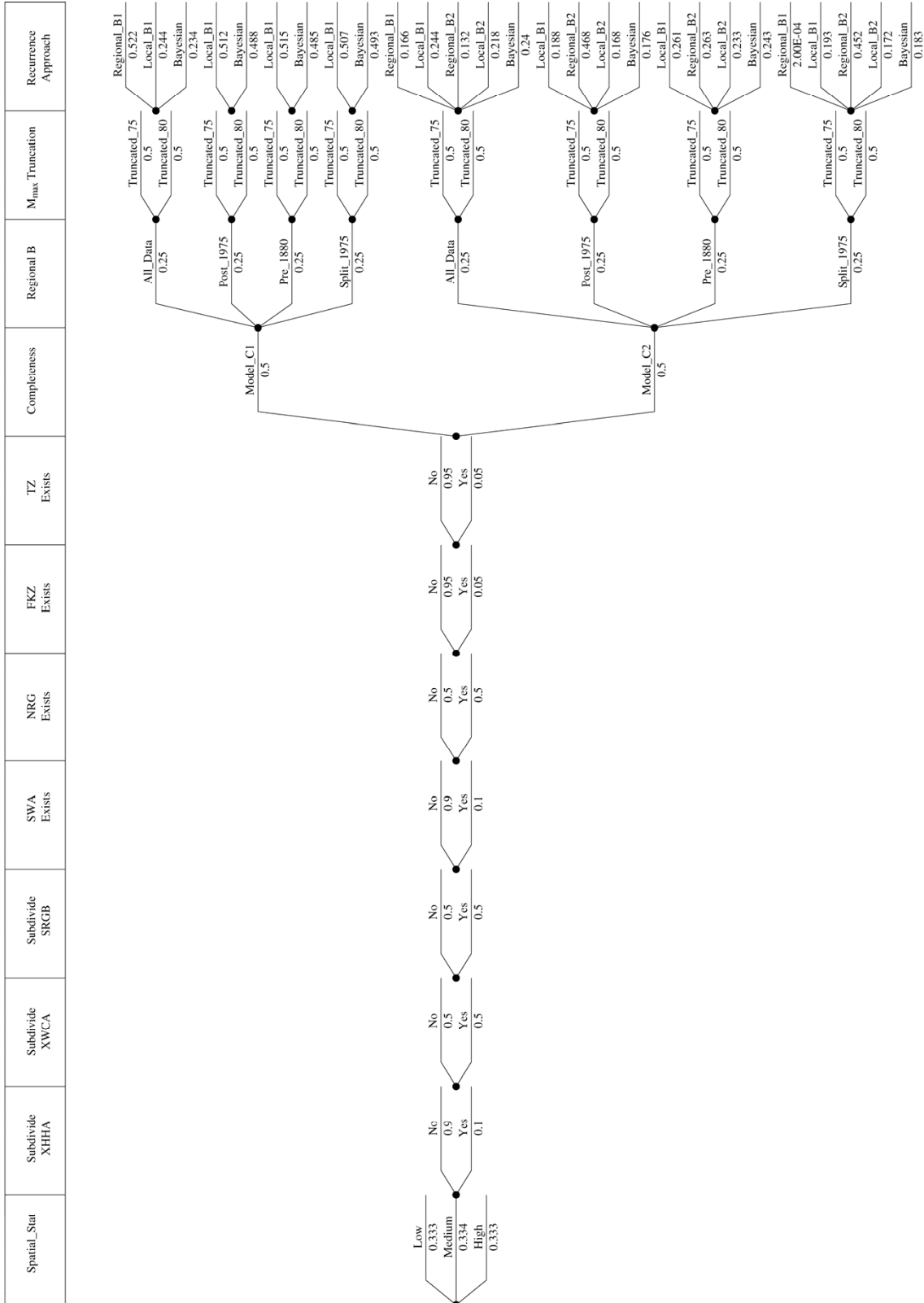
Fig. A-19: Logic tree for EG1d, source J, the trees for the other sources differ in the last global variable (Recurrence Approach)

APPENDIX 6:   QA-CERTIFICATE FOR EG1-HID-0035

QA Certificate for Hazard Input Documents

QA Certificate | PEGASOS PROJECT

Hazard Input Document (HID)

Expert group:	EG1d	**HID designation:**	**EG1-HID-0035**
Expert:		**Expert Model (EXM)**	EG1-EXM-0032

HID parameterisation of Expert Model:

TFI:	K. Coppersmith	**Hazard Input Specialist of TFI-team:**	B. Youngs
HID based on Elicitation Documents:	☒	EG1-ES-0046	
HID based on Expert Assessments:	☐		

Remarks on the HID model parameterisation in terms of hazard computation input:

The undersigned Hazard Input Specialist confirms that this HID includes all required (subproject specific) input information for hazard computations. No further interpretations of this input will be required and no simplifications except Algorithmic Pinching according to paragraph 2.9 of the QA-Guidelines will be applied to convert this HID into hazard software Input Files.

Signature:

HID acceptance by the Expert / Expert Group:

Date of HID review by the Expert / Expert group: 18/09/03

HID accepted: ☒   HID not accepted: ☐

Reasons for non-acceptance of HID / Recommendations:

The undersigned Expert(s) accept(s) the parameterisation proposed in this HID as a faithful and adequate representation of his/their Expert Model. He/they confirm(s) that this HID is free of errors and agree(s) to its use as hazard computation input.

Signature Expert 1 / Expert:

Signature Expert 2:

Signature Expert 3:

QA-TN-0287 HID acceptanc form rev 02.doc

Part V: Expert Biographies

Expert Group EG1a

Dr. Nicholas Deichmann received his first degree, a B.A. in philosophy, from McGill University, Montreal (Canada) in 1971, followed by a second degree in geophysics from the Federal Institute of Technology in Zurich (ETHZ) in 1977. In 1984, he obtained a Ph.D. in natural sciences, also from the ETHZ. He has been engaged since then as a seismologist with the Swiss Seismological Service and as a lecturer on seismotectonics and time series analysis with the ETHZ. In 1990, he was a visiting lecturer at the University of Genoa in Italy and, in 1995, a visiting scientist at the U.S. Geological Survey in Menlo Park, California. At present, he is Acting Director with responsibility for the Seismotectonics Group of the Swiss Seismological Service. A large part of his research interests have been dedicated to seismotectonics. In this context, he was, and continues to be, responsible for the seismological monitoring programs set up within the framework of Swiss radioactive waste disposal studies. He is also responsible for routine data analysis of the Swiss Seismological Service and for the publication of an annual report on the seismicity of Switzerland.

Dr. Dario Slejko graduated in mathematics from Trieste University in 1979. He has been working at the Istituto di Oceanografia e di Geofisica Sperimentale (OGS) of Trieste since 1972, firstly as a seismologist for the World Wide Standardized Seismographic Network (WWSSN) station and later as a researcher in seismology and engineering seismology. From 1996 to 2000, he was Director of the OGS seismological department and he currently holds the position of Research Director of the Institute He was chairman of the sub-commission on "Engineering Seismology" of the European Seismological Commission from 1996 to 2002 and director of the Italian "Gruppo Nazionale di Geofisica della Terra Solida" since 1998; he has also been active as a member of the scientific board of the Italian National Research Council's "Gruppo Nazionale per la Difesa dai Terremoti" (earthquake defense group). His teaching experience includes several courses at the universities of Udine and Padua. Most recently, he served as a referee for the seismic hazard map of Italy (2004). Dr. Slejko's main areas of interest have changed over the years, moving from regional seismicity and seismotectonics to engineering seismology and, more specifically, seismic hazard and risk. His studies in the field of seismotectonics have focused on the 1976 Friuli earthquakes, several historical earthquakes and definition of the seismogenic zones of the eastern Alps. His experience in seismic hazard studies has been wide-ranging, covering Italy, Greece, Cuba and Bulgaria. His work is documented in more than a hundred papers in Italian and international scientific journals. He has participated in several international geophysical expeditions and was involved in field data collection and interpretation for the 1980 Irpinia earthquake in southern Italy. Since 2000, he has been task leader on acceleration attenuation in NE Italy, as part of a project on the definition of damage scenarios in the Friuli - Veneto border region of Italy.

Prof. Dr. Stefan Schmid obtained both his Diploma in geology (1968) and his Ph.D. (1971) from the University of Zurich. After this, he spent six years as a post-doctoral fellow at the Federal Institute of Technology in Zurich (ETHZ), Imperial College in London, the Australian National University in Canberra and the Institute for Geophysics and Meteorology in Frankfurt. On returning to Switzerland, he held various positions at the ETHZ, culminating, in 1987, in a titular professorship at the Geological Institute. Since 1989, he has held the positions of Chair of Geology and Head of the Geological-Paleontological Institute at the University of Basel. During his career, he has received widespread recognition in his field, with awards including the "Landys & Gyr Prize in Earth Sciences". In 1997, he was nominated as a Fellow of the Geological Society of America. His main professional interest lies in the fields of structural geology and tectonics, experimental rock deformation and microfabrics and alpine geology. Notable among projects in which he has been a key contributor are a series of nationally funded studies on alpine geology and tectonics, metamorphic evolution and dating of orogeny in the

Italian-French Western Alps and the tectono-metamorphic evolution of the Italian-Swiss Central Alps. From 1990 to 2000, Professor Schmid was a member of the geological commission responsible for evaluating railway tunneling in the Swiss Alps on behalf of the Ministry of Transport. He has also been involved since 1999 as a co-investigator and main investigator on a number of European Union research projects on tectonics in the northern alpine foreland.

Expert Group EG1b

Dr. Gottfried Grünthal began his professional career with studies in geophysics at Leipzig University (1967-1971), where he later graduated with a Ph.D. in 1974. He then took up a position with the Central Institute for the Physics of the Earth (ZIPE) in Potsdam, in the area of deep seismic sounding research. In 1976, he conducted research in the fields of seismicity and seismic hazard, earthquake cataloguing, engineering seismology, seismotectonics, macroseismics and historical earthquakes later becoming Head of Department for engineering seismology and seismic hazard assessment at ZIPE. His current position is Head of the Research Section on Engineering Seismology at the GeoForschungsZentrum (Geosciences Research Centre), Potsdam. Dr. Grünthal and his group have wide experience in analyzing seismicity, seismotectonics and seismic hazard using the logic tree technique, as well as in the development of a modern macroseismic scale which is also used as a tool for seismic risk assessments. His work has wide relevance for engineering applications, for example in building codes. This is reflected in his membership, since 1991, of the German Committee on Seismic Building Codes and his eight-year membership of the Steering Committee of the German Society on Earthquake Engineering. His main professional interests relate to seismic hazard analysis, particularly in connection with determining reliable input data for probabilistic earthquake hazard assessments. This ranges from earthquake cataloguing, which is connected with historical earthquake studies and analysis of empirical relationships between earthquake strength parameters, through seismotectonics, stress and strain to engineering seismological parameters. Major projects in which Dr. Grünthal has been involved include updating of the European Macroseismic Scale EMS-98, which was developed under his chairmanship by an interdisciplinary international working group. This new scale not only meets the needs of seismologists but also of earthquake engineers. Within the Global Seismic Hazard Assessment Program (GSHAP, 1993-1999), he chaired a regional center aimed at creating a harmonized modern seismic hazard map for Central, North and NW Europe. In the final stage of GSHAP, his activities included compiling and harmonizing the GSHAP results from the different research groups active in the Mediterranean region, the Near and Middle East and Africa. More recently, he has been involved with the German Research Network on Natural Disasters (DFNK), where he was responsible for comprehensive seismic hazard assessments using complex logic trees. Within DFNK, he also chaired an interdisciplinary working group which carried out one of the first detailed comparative natural risk studies (for floods, storms and earthquakes). The target area for this comparative study was the city of Cologne.

Dr. Armando Cisternas has been active in the field of geophysics since qualifying as a mining engineer from the University of Chile in 1958. He received both his M.Sc. (1960) and Ph.D. (1965) from the California Institute of Technology (CALTECH). He was a Professor in the Department of Geophysics of the University of Chile from 1965 to 1973, followed by a two-year period as a Professor at the Astronomical and Geophysical Observatory, University of La Plata (Argentina). From 1975 to 1983, he held the position of "Maître des Conférences" at the Institut de Physique du Globe in Paris, before moving on to become "Physicien Titulaire" at the Institut de Physique du Globe in Strasbourg. In 2002, he moved to his current position of Visiting Professor at the Universidad Complutense de Madrid. His main scientific contributions have been in the area of the theoretical study of elastic wave propagation, linking, for the first

time, the ray representation with the mode representation in a spherical Earth and in determination of the average stress regime in a seismic region using microtectonic data and focal mechanisms from a population of earthquakes and inversion theory methods and application of this experience to tectonic regimes in the Caucasus, France, Spain, Colombia, Chile and other regions. He has also been involved in field studies of destructive earthquakes in Algeria, Armenia, Turkey and Chile using multidisciplinary methods, including aftershock recording, neotectonic observations, paleoseismology, deformation field etc. He is presently working on self-organization of the earthquake process using the generalized Tsallis entropy. Since 1962, he has published numerous papers in international journals, most recently on forecasting the end of a gap with reference to the large Antofagasta (northern Chile) earthquake of July 1995, seismic source studies of the Racha-Dzhava (Georgia) earthquake using aftershocks and broad-band teleseismic body wave records. In 2003, he published work on the Izmit Turkish earthquake of August 1999, covering previous seismicity, aftershocks and seismotectonics.

Prof. Dr. Martin Burkhard received a Diploma in geology from the Federal Institute of Technology in Zurich (ETHZ) in 1981 and a Ph.D. in geology from the University of Neuchâtel in 1986. He has held the position of Professor at the Institute of Geology of the University of Neuchâtel since 1993. His main professional interests lie in the areas of structural geology, tectonics, neotectonics, rock deformation, low grade metamorphism, fluid / rock interaction and alpine geology and tectonics. Since 1994, he has been involved in several major, nationally funded projects, including geomagnetism and electromagnetic sounding of the basement; determination of the contemporary state of stress in the Jura mountains and the Molasse basin using borehole slotter tests; tectonic and structural evolution of the NW alpine front and foreland basin from the Oligocene to the present, with particular emphasis on the formation of the arcuate Jura fold thrust belt and arc formation in fold thrust belts (the relationships between displacements and strain examined in the case of the Helvetic nappes). He has also been involved in several foreign studies, in Morocco (tectonics of the Anti Atlas), Egypt (magnetotelluric and seismicity studies along the high-risk seismic area of the Aswan Dam, Lake Nasser), the Canary Islands (audio-magnetotelluric and electromagnetic investigation of the Las Canadas Caldera, Tenerife) and China (rates and mechanisms of faulting and growth folding over 10ka to 20Ma timescales in the active southern Tienshan fold-and-thrust belt).

Expert Group EG1c

Dr. Wolfgang Brüstle received a Diploma in geophysics from the University of Munich in 1979, followed by a Ph.D. in seismology from the University of Frankfurt/Main, Germany, in 1985. He was a research associate with the German Science Foundation (DFG) from 1980 to 1984 and then worked for several years at the Gadjah-Mada University in Yogyakarta, Indonesia, where he was a lecturer, research scientist, consultant to the National Indonesian Earthquake Agency and expert of the German Technical Cooperation (GTZ). In 1989, he returned to Germany, to the University of Stuttgart, where he held the position of research scientist until 1993. Since then, he has been Head of the Baden-Württemberg Earthquake Survey for the State Bureau for Geology, Natural Resources and Mining (LGRB) in Freiburg, Germany. Dr. Brüstle's main professional interests lie in the areas of seismic recording and interpretation of volcanic tremors (Indonesia and Italy); design, installation and operation of seismic networks, seismic field surveys, seismic data analysis procedures and preparation of earthquake data catalogues; studies of seismicity and source parameters, fault mechanics, earthquake and volcano source investigations; source and site effects on seismic hazard, zonation and microzonation, strong motion and engineering seismology, seismic building codes.

He also has extensive teaching experience, having organized graduate courses in digital signal processing, mathematical methods in geophysics, inversion theory, seismic wave propagation and earthquake seismology. In terms of professional affiliations, he is a member of the German Geophysical Society, the German Working Group on Seismology and Seismic Observatory Practice, the German Earthquake Task Force Committee, the German Society of Earthquake Engineering and Structural Dynamics, the Committee on German Regulations for Earthquake Resistant Design of Structures, the Working Group for Earthquake Regulations of the German Federal Agency for Nuclear Safety and the Earthquake Engineering Research Institute. Major projects in which he has been involved include investigation of volcanic hazards associated with Indonesian and Italian volcanoes, classification of subsoil conditions for earthquake hazard zonation, a strong motion seismic network in the Upper Rhine Graben area in Germany and France and earthquake microzonation in the southern Upper Rhine Graben area.

Dr. Souad Sellami Leinen received a degree in engineering physics from the Swiss Federal Institute of Technology at Lausanne (EPFL) in 1985, which she followed with postgraduate studies on geological risks at the University of Geneva. She remained at Geneva to study for her Ph.D. in earth sciences, which she received in 1993. Since then, her professional experience has led her to hold a number of positions, including software engineer at the University of Geneva, research assistant at the Universities of Geneva and Lausanne, research assistant at the Swiss Federal Institute of Technology in Zurich (ETHZ), lecturer at the ETHZ and the "Hochschule für Technik und Wissenschaft" in Chur. She is also an independent geophysics consultant for the ETHZ, EPFL, Geowatt Zurich and the Swiss Geophysical Commission. She is a member of the Earthquake Engineering Research Institute, the Swiss Society for Earthquake Engineering and Structural Dynamics and the Swiss Association of Women Engineers (SVIN). Dr. Sellami's main professional interest is in the areas of programming, seismology, in particular seismic hazard; she also has wide experience in teaching geophysics. During the course of her career, Dr. Sellami has been involved in several major projects, including PNR 20: deep structure of the Alps, seismic reflection processing and laboratory measurements (as a Ph.D. student); the Gersco project, a seismic hazard study for the region of Cali in Colombia; the Maramara Poly-Project, a multi-disciplinary (geology, hydrogeology, geodesy, geothermy and seismology) study of the Maramara region of Turkey; the GSHAP Global Seismic Hazard Assessment Program on hazard mapping of the world (responsible for hazard in West Africa, Libya and the Middle East); SESAME, the seismic hazard assessment of the Mediterranean Region, and earthquake scenarios for Switzerland.

Dr. Roger Musson received his B.Sc. from Queen's University Belfast in 1975 and his Ph.D. from Edinburgh University in 1979. In 1980, he took up a position with the Institute of Geological Sciences, which later became the British Geological Survey (BGS) in 1984; he has continued to work for BGS ever since. Initially, he was involved in support work for seismic hazard projects and research into historical earthquakes in the UK, which eventually led to publication of the parametric UK earthquake catalogue (684-1993) in 1994. In 1987, he took over full responsibility for seismic hazard studies in BGS and, since then, has been project leader on many seismic hazard studies in the UK and worldwide. Other projects have involved site hazard calculations for nuclear power plants and other nuclear sites in the UK and for various engineering projects in the Caribbean, Mediterranean, Greece, Turkey, the Middle East, India, SE Asia and China. He has also worked on various international hazard projects such as the COPERNICUS Circum-Pannonian Basin project, GSHAP and SESAME. He is also author of the M3C probabilistic seismic hazard assessment program, as well as various programs in the field of hazard support software, notably the WIZMAP seismicity analysis program. Besides seismic hazard, his main interests are in the closely related fields of macroseismology and historical seismology. For many years, he was in charge of macroseismic investigations of UK earthquakes for BGS and was one of the editors of the European Macroseismic Scale, the revised version of the MSK intensity scale (1990-1998). Since 2002, he has been Chairman of

the ESC Sub-Commission on Engineering Seismology. He was also involved in the European project "Basic European Earthquake Catalogue and Database" and other historical earthquake studies in Europe, Africa and Asia. He was a co-director of the international workshop on historical seismology in Sicily in 2002, and is Chair of the IASPEI Working Group on Seismological Archives. He has also had some involvement in seismic attenuation studies, especially with respect to intraplate areas. Dr. Musson is a Fellow of the Geological Society, a Fellow of the Royal Astronomical Society and a Chartered Geologist.

Expert Group EG1d

Dr. Mariano Garcia-Fernandez began his academic studies in 1980 with a B.S. in Physics from the University Complutense of Madrid in Spain, where he remained for an M.S. in Geophysics in 1981. In 1986, he completed a Masters in Engineering Seismology and Structural Dynamics at the Technical University of Catalonia in Barcelona and went on to receive his Ph.D. in Physics from the University of Barcelona in 1989. From 1981 to 1983, he held a postgraduate scholarship with the Swiss Seismological Service at the ETH in Zurich. He was active, from 1984 to 1986, as a consultant on NPP reviews for the Spanish Nuclear Safety Council in Madrid. 1986 saw him back in Zurich as an Assistant Researcher for the Swiss Seismological Service, where he remained until 1991. He then took up his current position of Researcher for the Institute of Earth Sciences 'Jaume Almera' of the Spanish Research Council (ICTJA-CSIC) in Barcelona, Spain. His main professional interests lie in the areas of seismic hazard (regional hazard, hazard scenarios), seismic zonation and microzonation, engineering seismology (seismic wave attenuation, ground motion synthetics), seismic networks and earthquake location (regional, microseismicity, volcano monitoring), seismotectonics (intraplate, volcanic regions) and geodynamics (high precision gravimetry and GPS surveys). These interests are reflected in the major projects he has worked on over the years, including coordination of the Task Group 'Seismology and Hazard' of the project SERGISAI (SEismic Risk evaluation through integrated use of Geographical Information Systems and Artificial Intelligence techniques). for the European Commission; coordination of the Ibero-Maghreb region Working Group for the Global Seismic Hazard Assessment Program (GSHAP) and co-direction of the SESAME project (Seismotectonics and Seismic Hazard Assessment of the Mediterranean Basin). He is presently co-director of the IUGS-UNESCO project 'Basement volcanoes interplay and human activities' (2001-2005), a member of the review panel for compilation of the seismic hazard map of Italy and director of the project 'Earthquake Hazard Scenarios for Integrated Seismic Risk Assessment Systems: Optimal Design of an Integrated System for the Vega Baja, Alicante. In addition to these activities, he has also found the time to hold a number of other positions: he is currently Secretary General of the European Seismological Commission, a member of the Board of Directors of ORFEUS (Observatories and Research Facilities for European Seismology) and a member of the Advisory Committee of the Strategic Leadership Council, Global Alliance for Disaster Reduction.

Dr. Stefan Wiemer received an M.S. from the Ruhr University at Bochum in Germany in 1992 and went on to complete a Ph.D. in geophysics at the Geophysical Institute of the University of Alaska (Fairbanks, USA) in 1996. He remained in Alaska as a post-doctoral researcher at the Institute until 1997, when he took up a post as Fellow of the Alexander von Humboldt Foundation in Germany. He then moved to Japan at the end of 1997 to carry out post-doctoral research with the Seismological and Volcanological Research Department of the Japan Meteorological Agency in Tsukuba. Since 1999, he has been a research scientist with the ETH Zurich (ETHZ), Deputy Director of the Swiss Seismological Service and Head of the Earthquake Statistics Group. In terms of career orientation, his main interests lie in the areas of

statistical seismology, seismicity analysis and earthquake prediction research, volcano-seismology, seismotectonic analysis of volcanic regions, probabilistic seismic and volcanic hazard and risk assessment, particularly time-dependent hazard assessment and quality and consistency of earthquake catalogues. Major projects in which he has been involved include an ETHZ project on improving seismic hazard assessment in the near-field of seismogenic faults and statistical approaches to seismicity monitoring; Regional Earthquake Likelihood Models (RELM) for Southern California (time-dependent hazard models); SEISWATCH: real-time monitoring of seismicity in Japan; Humboldt Foundation/Japan Science and Technology Agency fellowship research project on quantitative approaches to seismicity analysis and a National Earthquake Hazard Reduction Program (NEHRP) project on seismicity parameters for seismic hazard assessment in Alaska.

Prof. Dr. Jean-Pierre Burg began his career in geosciences with a doctorate from the University of Montpellier in France in 1983. He was a Reader in structural petrology at the University from August to December 1976 and was employed as a lecturer for extended periods up to 1993. In the interim period, between 1983 and 1986, he was a Research Fellow at Melbourne University in Australia. Since 1993, he has held the position of Professor at the Geological Institute of the Swiss Federal Institute of Technology in Zurich (ETHZ). Professor Burg's contribution in his field has been widely recognized by a number of professional awards, from the Australian Society of Educational Technology, the Prix Henri Becquerel of the Académie des Sciences de Paris, Doctor Honoris Causa of Sofia University, Fellowship of the Pakistan Academy of Geological Sciences, Fellowship of the Japan Society for the Promotion of Science, the Gibson Distinguished Visiting Professorship at the University of Minnesota and the Prix Viquesnel 2001 of the Société Géologique de France. He is also a member of several professional societies, including the European Union of Geosciences, the European Geophysical Society, the Geological Society of France and the Geological Society of Switzerland. His professional interest lies mainly in the area of structural geology, particularly natural and experimental deformation of rocks. In terms of research, he has focused on field-based problems with strong complementary theoretical and laboratory research in the areas of rock fabrics, numerical and analogue modeling and experimental rock deformation. Over the years he has been involved in numerous key projects, including experimental determination of physical properties of rocks under high temperature, confining and pore pressure conditions (Swiss National Science Foundation (SNF) project), rheology and microfabric evolution during simple shear of quartz and olivine: high temperature torsion experiments and electron backscatter diffraction (SNF project), thermo-mechanical conditions of collision syntaxes: structural and metamorphic development of the Namche-Barwa syntaxis (Eastern Himalayas) (ETH project) and collision zone tectonics in orogenic syntaxial regions and the along-strike evolution of the Indus suture in NE Pakistan (ETH project).